UNIVERSITY OF SOUTHAMPTON

PREDICTION AND CONTROL OF VIBRATIONAL POWER TRANSMISSION BETWEEN COUPLED STRUCTURAL SYSTEMS

by

Yong - Khiang KOH

Thesis submitted for the degree of
Doctor of Philosophy

FACULTY OF ENGINEERING AND APPLIED SCIENCE

INSTITUTE OF SOUND AND VIBRATION RESEARCH

December 1992

UNIVERSITY OF SOUTHAMPTON

ABSTRACT

FACULTY OF ENGINEERING AND APPLIED SCIENCE
INSTITUTE OF SOUND AND VIBRATION RESEARCH

Doctor of Philosophy

PREDICTION AND CONTROL OF VIBRATIONAL POWER TRANSMISSION BETWEEN COUPLED STRUCTURAL SYSTEMS

by

Yong - Khiang KOH

Vibration transmission from resiliently mounted machines to flexible seating structures has, in the past, often been studied by over-simplified mass-spring models coupled to rigid foundations. It has been recognised that a more detailed model for the study of machine-induced vibration problems, considering resonance responses of the coupled systems as well as the interactions among governing degrees-of-freedom is necessary. This study examines in detail, using the unifying concept of time-averaged vibrational power, the problem of vibration transmission from a machine source to flexible beam and plate-like seating structures via the translational and rotational motions as well as the coupling between these motions, for the case when the seating structures are subjected to co-located simultaneously acting sinusoidal force and moment excitations.

The driving point mobility functions of uniform beams and rectangular plates are obtained analytically based on the classical theories for beams and plates in flexural vibration. For linear structures subjected to simultaneously acting force and moment excitations, the driving point coupling mobility functions always exist, except for the special situation when the excitation point coincides with a point of mode shape symmetry of beams and plates with symmetric boundary conditions. These coupling mobility functions contribute to vibrational power components input to the structures as importantly as the direct force and/or moment mobility functions. Because of the contributions from the coupling terms, cancellation of vibrational power components input to the seating structures is possible, which is the basis of the novel vibration control technique proposed and investigated in this study.

Based on the mobility coupling approach, the problem of vibration transmission between a multi-point mounted flexible source-isolator-receiver system is also studied in terms of the vibrational power input, transmission and dissipation in the structures. Vibrational power, being a single quantity which embodies both the force and velocity as well as their phase relationship at the point of concern on the structure, offers a better insight into the problem than the conventional force or motion transmissibility analysis.

The novel vibration control technique, as mentioned above, is proposed to reduce the unwanted machine-induced vibration levels on the seating structure, at a specific frequency, by controlling the ratio of the applied moment to the applied force via suitably designed force and moment seatings attached to the mounting points. This control technique is most suitable for the case of a low to medium constant speed machine mounted on a flexible seating structure.

These theoretical findings have all been validated by laboratory experimental results.

ACKNOWLEDGEMENTS

A research study spanning over a period of three years would not have been made possible without the help, support and encouragement of many parties. I would like to thank the Defence Research Agency and the former Procurement Executive, Ministry of Defence for their support of the unclassified contract under which this research work was carried out.

Personally, I wish to express my warmest gratitude to Professor R.G. White, my supervisor, for offering me the opportunity to conduct this research and for his guidance, supervision and encouragement throughout the course of the work. His substantial advice given in the preparation of Technical Reports and the manuscript of this thesis is gratefully acknowledged.

I would also like to thank many colleagues in ISVR for their friendly cooperation and assistance, particularly to :

my friend and former colleague, Dusan Lednik for his assistance in data acquisition system and computing needs;
Mike Bartlett, Dave Edwards and all the members of mechanical workshop, for fabrication of the test rigs;
Dennis Howell, for his assistance in problems related to instrumentation;
Jon Hall and Gill Jewell, for their assistance in problems related to programming;
John Mason, for lending the electric motor; and
Terry Vass, Julie Lees and Sally Abrams for much assistance pertaining to administrative matters.

Acknowledgement is also given to Dr Ben Dobson for many stimulating discussions and help provided during the initial phase of this work and to Professor D.J. Mead for introducing me to the 'art' of Structural Dynamics.

Finally, I would like to thank my wife, Quee Lee, for her love, patience, understanding and sacrifice, and for sharing all the good and bad moments. Without her full support and encouragement, this thesis would not have been brought to completion. I dedicate this thesis to her, and to our sons Thong Meng and Thong En.

CONTENTS

Chapter 7 : VIBRATIONAL POWER TRANSMISSION PREDICTION AND MEASUREMENT

PART III : VIBRATION CONTROL VIA POWER INPUT TO FLEXIBLE SEATING STRUCTURES

Chapter 8 : VIBRATION CONTROL USING THE CONCEPT OF VIBRATIONAL POWER FLOW

Chapter 9 : VIBRATION CONTROL OF AN UNBALANCED ROTATING MOTOR VIA THE FORCE AND MOMENT SEATING

Chapter 10 : PARAMETRIC STUDY OF THE FORCE AND MOMENT SEATING DESIGN

LIST OF SYMBOLS

General

f	Frequency in Hertz
j	Complex operator ($\sqrt{-1}$)
t	Time (sec)
x,y,z	Cartesian coordinates
A	Cross-sectional area (m^2)
E	Modulus of Elasticity (Nm^{-2})
F	Amplitude of the transverse harmonic point force excitation (N)
I	Second moment of area of cross-section (m^4)
K	Spring stiffness (Nm^{-1})
η	Loss factor of material (hysteretic losses)
ρ	Density (kgm^{-3})
ω	Excitation frequency ($rad.sec^{-1}$)
$Re\{\ \}$	Real part of a complex quantity
$Im\{\ \}$	Imaginary part of a complex quantity

Superscripts

c	Complex quantity
*	Complex conjugate of a complex quantity

Chapter 2

a	Moment arm (m)
k	Flexural wavenumber (m^{-1})
w	Displacement in the Z direction (m)
$\dot{w}$	Velocity in the Z direction ($msec^{-1}$)
A_2	Near field wave amplitude (m)
A_4	Propagating wave amplitude (m)

B_1, B_2, B_3, B_4	Integration constants
$F(t)$	Transverse harmonic point force excitation (N)
$M(t)$	Harmonic moment excitation (Nm)
M, M'	Bending moments (Nm)
P_F	Time-averaged vibrational power input due to force and translational velocity components (Watts)
P_M	Time-averaged vibrational power input due to moment and rotational velocity components (Watts)
P_{force}	Time-averaged vibrational power input due to the force excitation only (Watts)
P_{moment}	Time-averaged vibrational power input due to the moment excitation only (Watts)
$P_{coupling}$	Time-averaged vibrational power input due to the coupling mobility (Watts)
P_T, P_{total}	Resultant time-averaged vibrational power input due to simultaneously acting force and moment excitations (Watts)
S, S'	Shear forces (N)
W	Displacement amplitude function in the z direction (m)
Y_{FF}	Driving point force mobility (mN^{-1} sec^{-1})
Y_{FM}	Driving point coupling mobility (N^{-1} sec^{-1})
Y_{MF}	Driving point coupling mobility ($rad.N^{-1}$ sec^{-1})
Y_{MM}	Driving point moment mobility ($rad.(Nm\ sec)^{-1}$)
α	Phase angle (degree)
θ	Rotation of beam (rad.)
$\dot{\theta}$	Rotational velocity of beam ($rad.sec^{-1}$)
$\mathcal{L}$	Length of beam (m)
$\mathcal{P}$	Power reduction index, P_{total} / P_{force}
$\{F\}$	Applied force vector
$\{\dot{w}\}$	Velocity vector
$[J]$	Dynamic stiffness matrix of a uniform beam in flexural vibration
$[R]$	Receptance matrix of a uniform beam in flexural vibration
$[Y]$	Driving point mobility matrix
C-F	Uniform beam with one end clamped, the other free
C-SS	Uniform beam with one end clamped, the other simply supported
C-C	Uniform beam with both ends fully clamped
SS-SS	Uniform beam with both ends simply-supported

Chapter 3 and 4

a,b	Plate edge lengths (m)
a_x, a_y	Moment arms (m)
h	Plate thickness (m)
k_{xm}, k_{yn}	Flexural wavenumbers (m^{-1})
m,n,r,s	Mode (integer) numbers
u,v,w	Displacements in X-, Y- and Z-directions, respectively (m)
$\dot{u}$, $\dot{v}$, $\dot{w}$	Velocities in X-, Y- and Z-directions, respectively (m sec^{-1})
x_0	X-coordinate of excitation point
y_0	Y-coordinate of excitation point
B_{1m}, B_{2m} etc	Integration constants
C_{1n}, C_{2n} etc	Integration constants
D	Plate flexural rigidity (Nm)
G	Shear modulus (Nm^{-2})
J_{mm}, J_{nn}	Definite integrals
JJ_{mr}, JJ_{ns}	Definite integrals
JJJ_{mr}, JJJ_{ns}	Definite integrals
M_x, M_y	Bending moments or amplitudes of the harmonic moment excitations (Nm)
M_{xy}, M_{yx}	Twisting moments (Nm)
$P(x,y)f(t)$	Lateral load per unit area (Nm^{-2})
P_F	Time-averaged vibrational power input due to force and translational velocity components (Watts)
P_{force}	Time-averaged vibrational power input due to force excitation only (Watts)
P_{M_x}, P_{M_y}	Time-averaged vibrational power input due to moment and rotational velocity components (Watts)
P_T, P_{total}	Resultant time-averaged vibrational power input due to simultaneously acting force and moment excitations (Watts)
S_x, S_y	Shear forces (N)
T	Plate kinetic energy (J)
U	Plate strain energy (J)
$X_m(x)$	Characteristic beam functions in the X direction
$Y_n(y)$	Characteristic beam functions in the Y direction
Y_{11}	Driving point force mobility function ($mN^{-1}sec^{-1}$)
Y_{21}, Y_{31}	Driving point coupling mobility functions ($N^{-1}sec^{-1}$)

Y_{32}	Driving point coupling mobility functions (rad.(Nmsec)$^{-1}$)
Y_{22}, Y_{33}	Driving point moment mobility functions (rad.(Nmsec)$^{-1}$)
$Y_{F\infty}$	Driving point force mobility of infinite plate (mN^{-1}sec^{-1})
$Y_{M\infty}$	Driving point moment mobility of infinite plate (rad.(Nmsec)$^{-1}$)
α	Phase angle (degree)
ε	An arbitrary small quantity
$\varepsilon_x, \varepsilon_y$	Direct strains
γ_{xy}	Shear strain
θ_x, θ_y	Plate edge rotations (rad.)
$\dot{\theta}_x$, $\dot{\theta}_y$	Plate rotational velocities (rad.sec^{-1})
$\sigma_x, \sigma_y, \sigma_z$	Direct stresses (Nm^{-2})
τ_{xy}, τ_{yx}	Shear stresses (Nm^{-2})
μ	Mass per unit area (kgm^{-2})
ν	Poisson's ratio
$\omega_\Lambda, \omega_{xm}, \omega_{yn}$	Eigenfrequencies (rad.sec^{-1})
δ	Kronecker delta function
$\Psi_\Lambda(x,y)$	Eigenfunctions
ξ_Λ	Definite integral
$\zeta_{mn}(t)$	Unknown arbitrary functions
$\{\zeta_{mn}\}$	Unknown function vector
$\{Q_{rs}\}$	Generalised force vector
$[K]$	Plate stiffness matrix
$[M]$	Plate mass matrix
$[\chi_{rsmn}]$	Plate dynamic matrix
$[\lambda_{mnrs}]$	Inverse of matrix $[\chi_{rsmn}]$
$[Y]$	Driving point mobility matrix
SSSS	Rectangular plate with all edges simply supported
CFSF	Rectangular plate with the edge along x=0 fully clamped, the edge along x=a simply supported, and both edges along y=0 and y=b free

Chapter 5, 6 and 7

h	Isolator edge length (m)
m	Number of sinusoidal excitations
n	Total number of co-ordinates (degrees-of-freedom)
k_l	Longitudinal wavenumbers (m^{-1})

$\dot{g}, \dot{t}, \dot{u}, \dot{v}, \dot{w}$	Translational and rotational velocities ($msec^{-1}$) or ($rad.sec^{-1}$)
F	Excitation forces (N) and moments (Nm)
K_r	Rotational spring stiffness ($Nm(rad.)^{-1}$)
L	Length of isolator or spring (m)
N	Number of resilient mounts
P,Q,R,S	Transmitted forces (N) and Moments (Nm)
G_{ff}	Power spectral density function of input force excitation
G_{uu}, G_{vv}	Power spectral density function of velocity responses
G_{fv}	Cross spectral density function between force and velocity
G_{vu}	Cross spectral density function between two velocities
M	Driving Point Mobility function ($mN^{-1}sec^{-1}$)
M_1, M_2	Transfer mobility functions ($mN^{-1}sec^{-1}$)
$M_{\theta 1}, M_{\theta 2}$	Transfer mobility functions of rotational response ($rad.N^{-1}sec^{-1}$)
M_x,M_y	Bending moments or amplitudes of the harmonic moment excitations (Nm)
$\alpha_{11},\alpha_{12},\alpha_{21},\alpha_{22}$	Dynamic transfer properties (four pole parameters) of isolator
$\beta_{11},\beta_{12},\beta_{21},\beta_{22}$	Dynamic transfer properties (four pole parameters) of isolator with end plates
γ	Scaling factor
η_m	Loss factor of isolator
$\dot{\theta}$	Rotational velocity ($rad.sec^{-1}$)
$\dot{\theta}_x$, $\dot{\theta}_y$	Plate rotational velocities ($rad.sec^{-1}$)
$\boldsymbol{E}$	Isolator effectiveness
$\boldsymbol{P}$	Time-averaged vibrational power (Watts)
$\boldsymbol{P}_{in}$	Time-averaged vib. power input to source beam (Watts)
$\boldsymbol{P}_{iso}$	Time-averaged vib. power transmitted to an isolator (watts)
$\boldsymbol{P}_{plt}$	Time-averaged vib. power transmitted to receiver at a mounting point (Watts)
$\boldsymbol{P}_{tr\text{-}iso}$	Time-averaged vib. power transmitted to all isolators (Watts)
$\boldsymbol{P}_{tr\text{-}plt}$	Total time-averaged vib. power transmitted to receiver (Watts)
$\boldsymbol{P}_{dis\text{-}bm}$	Time-averaged vib. power dissipated in source beam (Watts)
$\boldsymbol{P}_{dis\text{-}iso}$	Time-averaged vib. power dissipated in all isolators (Watts)
$\boldsymbol{TR}$	Force transmissibility
$\{\dot{g}\},\{\dot{t}\},\{\dot{u}\},$ $\{\dot{v}\},\{\dot{w}\}$	Translational and rotational velocity vectors
$\{F\}$	Excitation force and moment vector
$\{P\},\{Q\},\{R\},\{S\}$	Transmitted force and moment vectors
$[A],[B],[C],[D]$	Dynamic transfer property matrices of isolator

$[X]$	Generalised mobility matrix of vibrating machine
$[Y]$	Generalised mobility matrix of seating structure

Chapter 8

a	Moment arm (m)
a_x, a_y	Moment arms of rectangular plate (m)
a_c	Controlled moment arm (m)
d	Distance between a force couple (m)
$F_a(t)$	Primary applied force excitation (N)
$F_c(t)$	Secondary force excitation (N)
$M_a(t)$	Primary applied moment excitation (Nm)
$M_c(t)$	Secondary moment excitation (Nm)
α,β,γ	Coefficients of a quadratic function
ξ	Ratio of applied force to applied moment (m^{-1})

Subscripts

a	Primary applied excitation
c	Secondary (controlled) excitation
f	Force control scheme
fr	Frequency of interest
m	Moment control scheme
opt	Optimal value
p	Passive approach of vibration control

Chapter 10

a	Moment arm (m)
d	Distance from the fixed end of cantilever beam (m)
h	Thickness of rectangular block (m)
m	Mass (kg)
w	Displacement in the Z direction or deflection of beam (m)
$\dot{w}$	Velocity in the Z direction ($msec^{-1}$)
F_A, F_B	Applied end forces of beam segment (N)
F_C	Transmitted force on coupled plate (N)

I_m	Mass moment of inertia (kgm^2)
$K_{c,stat}$	Static coupling stiffness ($Nrad.^{-1}$ or N)
$K_{r,stat}$	Static rotational stiffness ($Nmrad.^{-1}$)
$K_{t,stat}$	Static translational stiffness (Nm^{-1})
L	Length of rectangular block (m)
M_A, M_B	Applied end moment of beam segment (Nm)
M_C	Transmitted moment on coupled plate (Nm)
θ_y	Rotation or slope of deflection curve of beam (rad.)
$\dot{\theta}_y$	Rotational velocity of beam ($rad.sec^{-1}$)
[R]	Driving point receptance matrix
[Y]	Driving point mobility matrix

CHAPTER 1

INTRODUCTION

1.1 BACKGROUND TO THE STUDY

Machinery installations on board ship or in a building usually consist of a source of vibration (an operating machine), mounted on resilient mounts (isolators) and attached to a seating structure (receiver). Vibration transmission takes place from the source through the isolators to the receiver. Vibration transmission can also be taken place from the machine through the connecting pipes to the surrounding structures. This study concerns vibration transmission in the former case. Vibration transmission through a source-isolator-receiver system and the associated sound radiation from the vibrating structures, especially in the frequency range where both the source and the receiver are non-rigid, has been a subject of continuing interest.

Modern engineering practices aim at designing machines that rotate at relatively high speeds to compete for better performance and the construction of lightweight machines and transportation equipment, such as automobiles, ships and aeroplanes, to save costs and fuel. Such structures have more resonance frequencies and are more sensitive to vibration environments than massive structures. Vibration control has thus continued to be a challenging task for many design engineers.

The classical single degree-of-freedom vibration isolation model which considers the vibrating machine as a rigid mass, the resilient mounts as lumped, massless damped springs and the seating structure as an infinitely stiff foundation, is generally of limited application to the study of low frequency vibration isolation. It is known that this simple model is inadequate for predicting high frequency vibration isolation and noise reduction performance [1,2]. In the high frequency regime, resonances of the machine and seating structure are likely to occur and 'wave effects' could also be present in the mounts. All of these high frequency phenomena are not accounted for in the classical simplified model. A more representive multi-directional, multi-point coupled source-isolator-receiver model has long been sought.

On the other hand, machine structures are generally complex and with the combined sources of the vibratory output of a machine (e.g. unbalanced forces, combustion processes, friction, fluid flow, etc.) the resulting machinery motions are inherently multi-directional in nature. Furthermore, due to the finite area of mechanical connection, the coupling of the isolators to the seating structure and the machine may cause forces and moments to act, which in turn, produce velocities in all three co-ordinate axes and rotations about these axes. The motion at the attachment point of the isolator to the seating structure is therefore generally complicated. In a completely generalised model, vibration transmission via the translational motions in all three co-ordinate axes and rotational motions about these axes need to be considered. Detailed estimation of vibration transmission to the seating structure would require a more thorough description of the force, moment and coupling mobility functions at the point of interest.

In the study of a machine isolation system, especially when the source and/or receiver are non-rigid, [2-6] conventionally only the translational motion normal to the surface of the seating has usually been considered. However, it is known that vibrational power input to a beam or a plate due to moment excitation, by virtue of flexural wave motion, is more severe in the high frequency region compared to the power input due to force excitation [1,7]. Recent studies by Petersson and Gibbs [8,9] have shown that for contact points between a source and receiver located at positions at or close to discontinuities, moment excitation plays a vital role in vibration transmission even at low frequencies. It was proposed that for machine sources installed or to be installed close to discontinuities to assume combined moment and force excitation in the analyses of sound and vibration transmission problems. In these studies, it was shown that the phase shift between the moment and force played a critical role. However, contributions from the coupling between different degrees-of-freedom were not considered. Hence, there remains a need to examine the vibration transmitted to flexible seating structures subjected to simultaneously acting force and moment excitations, and in particular, the interactions between the force excitation and the rotational motion or the moment excitation and the translational motion.

In the past two decades, many researchers have attempted to study the problem of multi-directional vibration transmission between coupled machine source - isolator - receiver systems. Although a multi-directional theoretical model has been developed based on linear multi-terminal mechanical network theory by Soliman and Hallam [10], and Sykes [11], and also an experimental procedure for determining the multi-

directional blocked transfer impedances of the isolator has been developed by Verheij [12-14], direct comparison of the predicted and measured results has not been made. A set of multi-directional blocked transfer impedances of typical vibration mounts was presented by Verheij [14], but their relative contribution to the overall sound transfer characteristics was not directly comparable because of incompatibility of units. A more detailed review of the multi-directional vibration transmission between coupled systems is given in Section 1.2.

The difficulty of comparing the effects of multi-directional vibration transmission in an isolation system due to incompatible units of the transfer functions, for example translational mobilities and rotational mobilities, can be overcome if one expresses these quantities in terms of time-averaged vibrational power [1,7,15]. This unifying concept of vibrational power not only facilitates direct comparison of the translational and rotational transfer functions but also has the potential to enable vibration transmission via different degrees-of-freedom to be ranked according to their relative contribution to the total vibrational power input to the seating structure, especially the contribution from the coupling between different degrees-of-freedom.

1.2 LITERATURE REVIEW

Soliman and Hallam [10] combined the mobility matrices describing the dynamic characteristics of the machine and foundation and the transfer matrix of the isolators to calculate the overall response for systems containing any number of isolators when the machine and foundation are both non-rigid. Although a multi-directional, multi-point coupling model was presented, the numerical examples investigated were essentially unidirectional and the isolator was assumed to be spring-like. The machine and foundation were represented by a free-free beam and two simply-supported beams respectively. The effects of various types of isolators, an undamped spring , a spring in parallel with a dashpot and a spring in parallel with a series spring-dashpot element, on the force transmissibilities, the motions of the foundation and at the machine driving point were studied. However, no comparison with experimental results was made.

Sykes [11] applied multi-terminal mechanical network theory to derive expressions describing the multi-directional, multi-point coupled vibration transmission problem. The machine and supporting structure were modelled as nonrigid structures, and vibration mounts were modelled as arbitrary two-terminal structures with six degrees-of-freedom at each terminal. The coupling method is essentially identical to that used by

Soliman and Hallam [10]. This investigation was purely theoretical, no numerical or experimental results were provided.

Verheij [12-14] developed an experimental procedure for determining the vibration transfer through the resilient mountings underneath shipboard machinery. The theoretical approach was essentially the same as that adopted by Soliman and Sykes [10,11], i.e. based on linear mechanical network theory, and took into account six degrees-of-freedom for the motions at the top of a mounting and for the excitaton of the seating underneath. Under the assumption of a large impedance mismatch at the mounting / seating interface, the resilient mountings were characterised by transfer functions for a 'blocked' terminal on the seating side. The force acting on the seating for a given velocity at the top of the mounting was determined by the blocked transfer impedance of the mounting, and was independent of the seating impedance. A set of multi-directional blocked transfer impedances of typical vibration mounts, such as a rubber isolator, helical steel spring, air spring, bellows and flexible shaft coupling with rubber elements, was measured using the proposed method. However, their relative contribution to the overall vibration transfer characteristics was not directly comparable because of their incompatibility of units. The work was solely experimental, no comparison was made with the theoretical predictions.

Petersson and Plunt [16] investigated the structure-borne sound power transmission between an engine and a foundation using the concept of an effective point mobility for each mounting point, which took into account the interaction between different points and different directions, or an effective overall mobility which was a space averaged mobility over all excitation points, to simplify the calculations of the total transmitted sound power. The concept of effective mobilities was originally proposed by Popkov [17]. In Petersson and Plunt's work, the motions with different components were assumed to be uncoupled or only weakly coupled, thus, different directions of motion could be treated separately (i.e. one direction was treated at a time). However, the experimental determination of mobilities was limited to the vertical direction only.

Goyder and White [18] studied the vibrational power flow through the isolators and into the supporting foundation of a machine. The elements of the machine and isolator were modelled as masses and springs respectively. The foundation was assumed to be flexible and its mobility modulus spectral was represented by straight line approximations when plotted on log-log scales. These approximations only gave an overall nature of the mobility spectra, no account was given to the resonance effects of the foundation. Both one and two stage isolation of machines with internal force or velocity

sources were considered. The purpose of the isolation method presented was to minimize the power flowing into the structure by optimizing the isolator design with respect to source and receiver characteristics so that the power available for subsequent vibration and radiation was a minimum.

Pinnington and White [19,20] also investigated analytically and experimentally the vibrational power transmission between machine sources and substructures via spring-like vibration isolators. The machine or source structure was modelled as a simple mass element for low frequency vibration transmission and as a free-free beam for high frequency transmission. The seating structure was modelled by a beam with one end free and the other with an arbitrary termination. The coupling of the source and isolator to the seating structure was applied to the free end. Practical methods of measuring vibrational power input at a point on the seating structure and the power transmission through a spring-like isolator from a rigid mass were studied. The vibrational power transmission from a DC electric motor mounted upon a heavily damped beam stiffened plate via four vibration isolators was also investigated [20,21]. These investigations resulted in various methods for measuring vibrational power transmission through vibration isolators via the vertical translational degree-of-freedom only, which was considered to be the dominant motion.

Jacobsen and Ohlrich [22] also studied vibrational power transmission from multi-point mounted machinery to the supporting structure. In their experimental work, coupling between different directions of motion and between motions at neighbouring mounting points was ignored. Only two sets of coordinates : translation in the vertical direction and translation in the lateral direction were considered.

Reviews of the above studies concerning the vibrational power transmission through the machine isolation system show that they were either mainly focused on the power transmission via the vertical translational degree-of-freedom or the interactions between different degrees-of-freedom were considered to be secondary or neglected, thus each degree-of-freedom was treated separately. However, machines mounted on an isolation system are likely to apply both force and moment to the seating structure due to finite areas of their mechanical connections. It is also known from theory that, for flexural vibration in beam-like structures, the motions induced by bending moments are equally important to those caused by shear forces. Hence, there remains a need to examine the relative importance of the vibrational power transmission due to each possible degree-of-freedom and the interaction between different degrees-of-freedom.

1.3 THE SCOPE AND AIMS OF THIS STUDY

This study has an overall objective of predicting and controlling vibration transmission from resiliently mounted shipboard machinery to flexible seating structures by using the concept of vibrational power flow. With the common unit of power (in Watts), the study aims to evaluate the relative importance of the vibrational power transmitted to the seating structures due to the translational and the rotational motions, as well as the coupling between these motions. The study also aims to control or reduce the unwanted vibration level of the structures by minimising the vibrational power input to the structures.

The study begins with the analyses of the vibrational power input to flexible beam and plate-like seating structures when subjected to simultaneously acting force and moment excitations. To facilitate these analyses, the driving point mobility functions of these structures are derived analytically based on the classical theories of beams and rectangular plates in flexural vibration. The contributions from the translational and the rotational degrees-of-freedom as well as those from the coupling between these degrees-of-freedom are compared using the unifying term of vibrational power.

With the mobility functions and the experimentally measured dynamic transfer properties of resilient mounts, the study then proceeds with the analysis of the vibrational power transmission between coupled structural systems. The vibrational power input to a source beam, and the subsequent power transmitted to the resilient mounts and the receiver plate, as well as the power dissipation in these structures are examined for different sets of resilient mount properties.

Finally, based on the vibrational power contributed from the coupling terms, a potential novel approach for controlling vibration transmitted to a flexible seating structure from a source, at a specific frequency, e.g. the fundamental unbalance frequency of a rotating machine, is proposed.

1.4 OVERVIEW OF THE THESIS

This thesis is divided into three parts. Part I consists of Chapters 2, 3 and 4 which form the bases of the study. It has the objectives of examining the vibrational power input to flexible beam and plate-like structures which are subjected to simultaneously acting force and moment excitations, the relative contributions of the force and moment

excitations, and in particular, the interaction or the coupling between the force and a rotational velocity or the moment and a translational velocity.

In Chapter 2, theoretical expressions for the driving point mobility functions of a semi-infinite beam and finite beams with clamped-free (C-F), clamped-simply supported (C-SS), clamped-clamped (C-C), and simply supported- simply supported (SS-SS) boundary conditions, subjected to simultaneously acting force and moment excitations are derived. Expressions for the time-averaged vibrational power input to the beam-like structures due to both force and moment excitations are also given. Analytical results for the vibrational power input to the semi-infinite and finite beams with various boundary conditions are compared. Particular attention is drawn to the conditions in which the cancellation of the vibrational power components occurs in both the semi-infinite and finite beams.

Chapter 3 extends the analyses performed for the beam-like seating structures (in Chapter 2) to rectangular flat plates. For rectangular plates with all edges simply supported (i.e. a SSSS plate), the mobility functions are obtained from the well-known Eigenfunction Expansion Theorem. For rectangular plates with combined clamped, free and simply supported boundary conditions where exact solutions of the governing equation of motion do not exist, the mobility functions are obtained by the Rayleigh - Ritz method with appropriate characteristic beam functions as the assumed functions.

Chapter 4 describes an approximate method for experimental determination of the driving point mobility functions of a rectangular plate with one edge clamped, the opposite edge simply supported and the other pair of edges free (i.e. a CFSF plate). The measured mobility functions are compared with the predicted mobility functions obtained in Chapter 3.

Part II of the thesis consists of Chapters 5, 6 and 7. The study presented in this Part examines the time-averaged vibrational power transmission in a multi-point mounted flexible source - isolator - receiver system. Unlike the conventional approach of studying vibration isolation problems in terms of force or motion transmissibility, vibration transmission between the coupled structures is expressed in terms of the vibrational power input and dissipation in the structures. Vibrational power is preferred as it is a single quantity which embodies both the force and velocity at the points of concern on the structures. It also facilitates a direct comparison of the translational and rotational transfer functions.

Chapter 5 describes a generalised multi-directional model for vibrational power transmission between a multi-point mounted flexible source - isolator - receiver system. Following the mobility coupling approach for linear structures used by Soliman and Hallam [10], expressions for the time-averaged vibrational power input to a source beam and the subsequent power transmitted to the resilient mounts and the receiver plate are derived. Various simplifications of the generalised model are also discussed.

Chapter 6 gives a detailed description of the point, coupling and transfer mobility functions of a free-free beam and a CFSF plate. The flexible source is modelled as a free-free beam and the flexible receiver is a rectangular plate with CFSF boundary conditions. The point, coupling and transfer mobility functions of these structures are obtained from the analytical methods described in Chapters 2 and 3. The dynamic transfer properties (four-pole parameters) of the resilient mounts are obtained experimentally based on the 'Long Rod' model of the isolator. The experimental set-up for measuring these properties is also described in this chapter.

In Chapter 7, the vibrational power input to the source beam and subsequently transmitted to the resilient mounts and receiver plate as well as the power dissipation in these structures are examined for various sets of isolator properties. Contributions of the vibrational power input to the receiver plate from adjacent mounting points and from the rotational degrees-of-freedom are also studied. The experimental arrangement for measuring the velocity responses and vibrational power transmission between a corresponding coupled system subjected to a random force excitation on the source beam is also described in this chapter. Comparisons between the measured and the predicted results are made.

Part III of the thesis consists of Chapters 8, 9 and 10. This part of the thesis examines the potential approaches of controlling the vibration transmitted to the receiver from a source by combined force and moment excitations. In Chapter 8, various 'active' vibration control schemes using either a secondary controlled force or moment in addition to the primary applied force are analysed for beam-like seating structures. A passive approach for controlling vibration transmission at a specific frequency from a source to a seating beam or plate-like structure is also examined. Expressions for optimal moment arms or the ratio of applied moment to applied force in order to minimise the resultant vibrational power input to flexible beam and plate-like structures are derived. The experiment arrangement and validation of the passive approach of vibration control via a force and moment seating are also discussed in this chapter.

Chapter 9 begins with a summary of the design procedures for designing a set of force and moment seatings at the pre-selected mounting points in order to reduce the vibrational response of the seating structure at the frequency of interest. The experimental arrangement for an unbalanced motor, resiliently mounted at four corners, to the CFSF plate is described. The vibrational responses of the CFSF plate caused by the unbalanced motor with and without the attachment of the force and moment seatings at each mounting point are measured and compared.

Chapter 10 describes the parametric study of the force and moment seating design. The effects of seating plate properties, such as damping, thickness and the mounting locations on the optimal moment arms and the reduction in the vibrational power components input to the seating plate are analysed. The effect of resonances of the force and moment seating on the cancellation of vibrational power components is also discussed. Finally, some practical simplified design formulae for the optimal moment arms are also obtained for specified frequency ranges.

Chapter 11 is the concluding chapter. The main findings from this study and their practical implications are discussed and recommendations for further work are given in this chapter.

1.5 ASSUMPTIONS AND LIMITATIONS OF THE STUDY

The assumptions and limitations of the study are given in the appropriate sections in this thesis. Only the main assumptions are summarised in this section.

The analytical models and solutions described in Chapters 2, 3 and 5 are valid only for linear systems. Hence, the primary assumption of the study is that all the structures or systems considered e.g. beams, rectangular plates and the coupled source - isolator - receiver systems are linear systems. Under this assumption, the theorem of superposition of forced responses and the reciprocity principle can then be applied. The driving point mobility matrices derived for the beams and rectangular plates are symmetric matrices.

The material of the beam and plate-like structures is assumed to be elastic, homogeneous and isotropic. Thus, geometric and material non-linearity are not included in this study. Damping caused by internal hysteretic losses (i.e. material damping) is accounted for by a loss factor defined as the ratio of the imaginary part to the real part of the complex Modulus of Elasticity (Young's Modulus) of the material.

This loss factor is assumed to be constant for all flexural modes for the beam and plate-like structures.

For the semi-infinite and finite beams considered, the assumptions of Euler - Bernoulli Beam theory are applied, i.e. the rotary inertia and shear deformation of beam sections are neglected. Although the higher order beam theory such as the Timoshenko Beam theory can be adapted, it is not included in this study as the primary frequency range of interest is from 1 to 1000Hz, which in most cases does not warrant to do so. For the rectangular plates considered in Chapter 3, the assumptions for small deflections of thin plates are applied which are described in details in Section 3.2.1.

The degrees-of-freedom considered in this study are those associated with flexural vibration of the seating beam and plate-like structures. This is because studies related to the radiation of sound from vibrating structures [23,24], has shown that flexural wave motion induced in the seating structures is usually the dominant sound radiation mechanism in the low to medium frequency range, compared with the in-plane shear and longitudinal wave motions. However, it must be mentioned that for stiffened plates or built-up seating structures, the effect of in-plane shear and longitudinal vibrations can be significant in a lower frequency range [25].

In the theoretical solutions of forced response, the forcing function is assumed to vary sinusoidally with time. Other forcing types, such as random excitation or transient forces are not considered in this study.

This study assumes a direct relationship between the applied force and moment excitations, i.e. the applied moment is equal to the applied force multipled by a moment arm which is the horizontal offset of the line of action of the vertical applied force to the centre of the seating block (see figure 2.6 for illustration). The phase relationships between the force and moment excitations are examined for two limiting cases by the positive and negative moment arms, which correspond to the in-phase and 180 degrees out-of-phase conditions, respectively, between the applied force and moment excitations. This is because one of the main objectives of this study is to control or reduce the unwanted vibration level transmitted from a source to the seating structure, only these two limiting cases can be simply applied by a force and moment seating design without introducing other complications, such as to incorporate a specific phase shift between the excitations.

1.6 DEFINITIONS OF TERMINOLOGY

The most essential terminology in association with this study are defined in the following paragraphs :

Degrees-of-freedom : The number of degrees of freedom of a vibrational system is the number of independent spatial co-ordinates required to specify completely the displacement of the system. For a vibrating structure, the number of modes of vibration in which the structure can respond is equal to the number of degrees-of-freedom.

Vibrational Power : The vibrational power input to a structure by a point excitation force is generally defined as the product of the excitation force and the resulting velocity at that point. For a vibrating structure subjected to a point sinusoidal force excitation of $F(t)$ Newton with an excitation frequency of ω radians per second, resulting in a velocity response of $\dot{w}$ metres per second at the point of excitation, the time-averaged vibrational power, P, input to the structure is the nett power input to the structure over a period of vibration (i.e. $2\pi / \omega$), which is given as :

$$P = \frac{1}{2} Re\{ F \dot{w}^* \} \tag{1.1}$$

In general, F and $\dot{w}$ are complex quantities as all physical structures dissipate vibrational energy in one form or another, and $\dot{w}^*$ is the complex conjugate of the velocity response.

Mobility function : The mobility function of a mechanical vibrational system can generally be defined as the frequency response function formed by the ratio of the velocity response to the excitation force. The term *driving point mobility function* refers to the mobility function formed by the velocity response and the excitation force or moment in the same direction and at the same point on the structure.

> Driving point force mobility function refers to the mobility function formed by the ratio of the translational velocity to the excitation force, at the same location and in the same direction, which has the unit of metres per Newton second.

Driving point moment mobility function refers to the mobility function formed by the ratio of the rotational velocity to the excitation moment, at the same location and about the same axis, which has the unit of radians per Newton metre second.

Driving point coupling mobility function refers to the mobility function formed by either the ratio of the translational velocity to the excitation moment or the ratio of the rotational velocity to the excitation force or the ratio of the rotational velocity to the excitation moment, at the same location but about two different axes, which has the unit of metres per Newton metre second or radians per Newton second or radians per Newton metre second respectively.

The term *transfer mobility function* is generally referred to the mobility function formed by the ratio of the velocity response to the excitation force or moment at two different locations on the structure.

PART I

VIBRATIONAL POWER INPUT TO FLEXIBLE BEAM AND PLATE-LIKE STRUCTURES

CHAPTER 2

VIBRATIONAL POWER INPUT TO BEAM-LIKE SEATING STRUCTURES

2.1 INTRODUCTION

The study of time-averaged vibrational power input to an infinite or a semi-infinite beam subjected to a sinusoidal transverse force has received detailed study in the past [19,20]. A uniform beam having an infinite extent in its length is the simpliest, one-dimensional model of a continuous system, compared to the lumped mass discrete system, and is often used as the basic system to generate sufficient insight into the understanding of a particular problem of interest. This chapter, as is the usual practice, begins with the study of the vibrational power input to a semi-infinite beam subjected to simultaneously acting sinusoidal force and moment excitations at one end of the beam. The study then proceeds with the study of uniform beams of finite length with various boundary conditions.

For simultaneously acting force and moment excitations, one needs to consider more than one degree-of-freedom at the same time and the coupling between these degrees-of-freedom. Hence, one needs to derive the driving point mobility matrix at the excitation point to describe the dynamic characteristics of the structures and the power input to the structures [24]. The interactions or the relative contributions of the force and moment excitations and the coupling between the force and a rotational velocity or the moment and a translational velocity can then be analysed and compared using the unifying term of time-averaged vibrational power.

The driving point mobility matrix for a semi-infinite beam was obtained by the flexural wave motion approach. For finite beams with clamped - free, clamped - simply supported, clamped - clamped, and simply supported - simply supported boundary conditions, the driving point mobility matrix was obtained from consideration of appropriate boundary conditions, the requirements of motion continuity and force

equilibrium conditions at the excitation point, and the use of the receptance matrix and the dynamic stiffness matrix for a uniform beam in flexural vibrations. Throughout this analysis, the assumptions of Euler - Bernoulli beam theory are applied and only flexural vibration of uniform beams is considered.

2.2 DRIVING POINT MOBILITY MATRIX OF A SEMI-INFINITE BEAM

Consider a semi-infinite beam of length extending from $x=0$ to $x=\infty$ which is excited at $x=0$ by simultaneously acting harmonic force, $F(t)$ and moment, $M(t)$ excitations. The force is assumed to be perpendicular to the beam axis and the moment is about an axis perpendicular to that of the beam. The force and the moment excitations generate a near field wave (A_2 wave) and a propagating wave (A_4 wave) towards the right, as illustrated in figure 2.1.

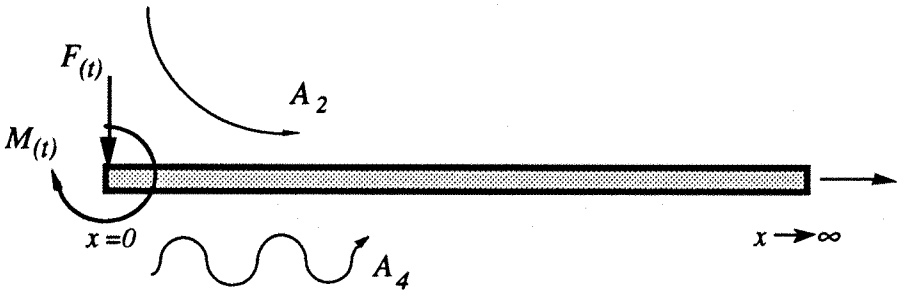

Figure 2.1 : A semi-infinite beam with simultaneously acting force and moment excitations at one end and the resulting flexural wave fields.

Assuming that the Euler-Bernoulli beam theory is valid, i.e. neglecting the rotary inertia and the shear deformation of the beam section, the equation of motion of the beam in free flexural vibration can be written as:

$$E I \frac{\partial^4 w}{\partial x^4} + \rho A \frac{\partial^2 w}{\partial t^2} = 0 \qquad (2.1)$$

where $E I$ is the flexural stiffness of the beam, (E is the Modulus of Elasticity , I is the relevant second moment of area of the cross-section); and ρA is the mass per unit length, (ρ is the density and A is the cross-sectional area).

The transverse displacement function $w(x,t)$ is a function of time, t, and distance, x, along the length of the beam, and is generally expressed as:

$$w(x,t) = A_2 e^{-kx} e^{j\omega t} + A_4 e^{j(\omega t - kx)} \tag{2.2}$$

where A_2 and A_4 are the integration constants (for flexural waves propagating to the right only), j denotes the complex operator $\sqrt{-1}$, ω is the circular frequency in radians per second and k is the flexural wavenumber which is given by :

$$k = \sqrt[4]{\frac{\omega^2 \rho A}{E I}} \tag{2.3}$$

The first and second terms on the right of eqn. (2.2) correspond to the near field and the propagating waves respectively.

The sign conventions of the transverse displacements and angular rotations are that displacements are positive if the beam deflects downwards and the rotations are positive if the beam rotates clockwise. The sign conventions of the applied forces and moments are that they are positive if they act in the positive directions of displacements and rotations.

The sign conventions of the induced shear forces and bending moments acting on an element of the beam section by virtue of the flexural vibration are those usually employed. The positive shear forces, S and S', and the positive bending moments, M and M' are shown in figure 2.2.

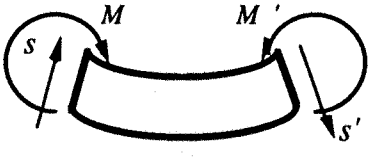

Figure 2.2: The sign conventions of positive shear forces and bending moments.

With this set of sign conventions, the expressions for the shear force and bending moment can be written as [26]:

$$M = -EI\frac{\partial^2 w}{\partial x^2} \tag{2.4}$$

$$S = -EI\frac{\partial^3 w}{\partial x^3} \tag{2.5}$$

The boundary conditions of the semi-infinite beam subjected to simultaneously acting force and moment excitations at $x=0$ are that the induced shear force and bending moment at $x=0$ are equal to the applied force and moment. Thus,

$$F(t) = -S = EI\left(\frac{\partial^3 w}{\partial x^3}\right)_{x=0} \tag{2.6}$$

$$M(t) = M = -EI\left(\frac{\partial^2 w}{\partial x^2}\right)_{x=0} \tag{2.7}$$

For harmonic force and moment excitations, the time dependent factor $e^{j\omega t}$ can be omitted for simplicity and on substituting eqn. (2.2) into eqns. (2.6) and (2.7), the A_2 and A_4 terms can be expressed as :

$$A_2 = -\frac{1}{2EIk^3}\left[(1+j)F + (1-j)Mk\right] \tag{2.8}$$

$$A_4 = -\frac{1}{2EIk^3}(1+j)\left[F - Mk\right] \tag{2.9}$$

The transverse velocity and angular velocity at the excitation point ($x=0$) are :

$$\dot{w} = \left(\frac{dw}{dt}\right)_{x=0} = \left(j\omega w\right)_{x=0} \tag{2.10}$$

$$\dot{\theta} = \left(\frac{d^2 w}{dxdt}\right)_{x=0} = \left(j\omega\frac{dw}{dx}\right)_{x=0} \tag{2.11}$$

Substituting the expressions for A_2 and A_4 into eqn. (2.2), and from eqns. (2.10) and (2.11), the transverse velocity and angular velocity at the excitation point are:

$$\dot{w} = \frac{(1-j)\omega}{EIk^3}F - \frac{\omega}{EIk^2}M \tag{2.12}$$

$$\dot{\theta} = -\frac{\omega}{EIk^2}F + \frac{(1+j)\omega}{EIk}M \tag{2.13}$$

Equations (2.12) and (2.13) can be written in matrix form as :

$$\begin{Bmatrix} \dot{w} \\ \dot{\theta} \end{Bmatrix} = \begin{bmatrix} \frac{(1-j)\omega}{EIk^3} & -\frac{\omega}{EIk^2} \\ -\frac{\omega}{EIk^2} & \frac{(1+j)\omega}{EIk} \end{bmatrix} \begin{Bmatrix} F \\ M \end{Bmatrix} \tag{2.14}$$

or simply, $\{ \dot{w} \} = [Y] \{ F \}$ (2.15)

where $[Y] = \begin{bmatrix} Y_{FF} & Y_{FM} \\ Y_{MF} & Y_{MM} \end{bmatrix}$ (2.16)

in which, $Y_{FF} = \frac{(1-j)\omega}{EIk^3}$, $Y_{FM} = Y_{MF} = -\frac{\omega}{EIk^2}$, $Y_{MM} = \frac{(1+j)\omega}{EIk}$

is the driving point mobility matrix. Y_{FF} is the driving point force mobility of the semi-infinite beam due to the applied force only; Y_{MM} is the driving point moment mobility due to the applied moment only; Y_{FM} and Y_{MF} are the coupling mobilities due to the simultaneously acting force and moment excitations. The presence of these coupling terms can be explained physically that for the semi-infinite beam in flexural vibration caused by simultaneously acting force and moment excitations, the resulting translational response (i.e. velocity, displacement or acceleration) at a particular point or at the excitation point is partly due to the force excitation and partly due to the moment excitation. The part resulting from the moment excitation constitutes the coupling mobility function Y_{FM}. Likewise for the resulting rotational response due to the simultaneously acting force excitation and the coupling mobility function Y_{MF} of the beam.

However, these coupling mobility functions cannot exist on their own, which means that a point force excitation acting on a linear structure will not result in a rotational response without translational motion in the direction of the force. This remark also applies to a point moment excitation and the resulting translational response without rotational motion. On the other hand, it will be shown in later that under certain conditions, the coupling mobility functions do not exist or are negligibly small even for the case of simultaneously acting force and moment excitations.

From the above expressions it can be seen that the coupling mobilities are identical, hence, the mobility matrix is a symmetric matrix. As the flexural wavenumber, k, is proportional to the square-root of frequency, the coupling mobilities are independent of frequency. However, the driving point mobilities of the semi-infinite beam due to the force alone, Y_{FF}, or the moment alone, Y_{MM}, are frequency dependent : Y_{FF} is

inversely proportional to the square root of frequency and Y_{MM} is proportional to the square root of frequency.

2.3 RECEPTANCE MATRIX OF A UNIFORM BEAM IN FLEXURAL VIBRATION

For free flexural vibration of a uniform beam, the transverse displacement function is a harmonic function of time, which can be written as :

$$w(x,t) = W(x)\ sin\ (\omega t + \alpha) \tag{2.17a}$$

or

$$w(x,t) = W(x)\ e^{j\omega t} \tag{2.17b}$$

where $W(x)$ is the transverse displacement amplitude function, ω is the circular frequency in radians per second and α is the phase angle. In dealing with the flexural vibration of a uniform beam of finite length, it is more convenient to express the transverse displacement amplitude function of the beam as a function of transcendental terms rather than exponential terms. The equation of motion of the beam for free flexural vibration (i.e. eqn. (2.1)) can be rewritten as :

$$E I \frac{d^4W}{dx^4} - \rho A \omega^2 W = 0 \tag{2.18}$$

The general solution of eqn (2.18) or the transverse displacement amplitude function $W(x)$ is :

$$W(x) = B_1 sin\ kx + B_2\ cos\ kx + B_3\ sinh\ kx + B_4\ cosh\ kx \tag{2.19}$$

where B_1, B_2, B_3 and B_4 are the integration constants whose values depend on the boundary conditions of the beam. Consider a uniform beam of length ℓ subjected to applied end forces, $F_A(t)$ and $F_B(t)$, and the applied end moments, $M_A(t)$ and $M_B(t)$, as shown in figure 2.3:

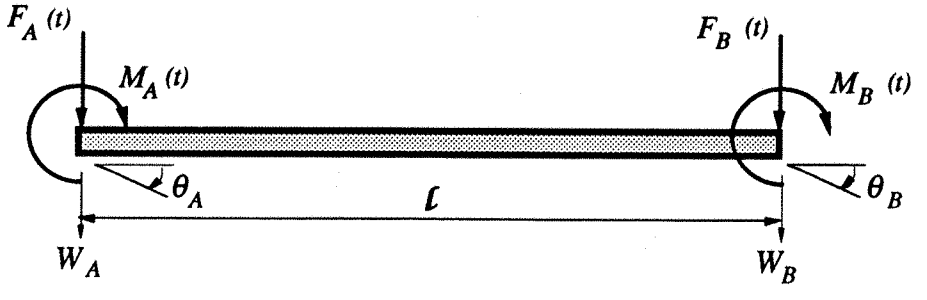

Figure 2.3 : A uniform beam subjected to the applied end forces and moments.

The end displacements, W_A and W_B and the end rotations, θ_A and θ_B of the beam are :

$$W_A = W_{x=0} = B_2 + B_4 \tag{2.20a}$$

$$W_B = W_{x=\ell} = B_1 \sin k\ell + B_2 \cos k\ell + B_3 \sinh k\ell + B_4 \cosh k\ell \tag{2.20b}$$

$$\theta_A = \left(\frac{dW}{dx}\right)_{x=0} = kB_1 + kB_3 \tag{2.20c}$$

$$\theta_B = \left(\frac{dW}{dx}\right)_{x=\ell} = kB_1 \cos k\ell - kB_2 \sin k\ell + kB_3 \cosh k\ell + kB_4 \sinh k\ell \tag{2.20d}$$

These end displacements and rotations can be expressed in matrix form as :

$$\begin{Bmatrix} W_A \\ W_B \\ \theta_A \\ \theta_B \end{Bmatrix} = \begin{bmatrix} 0 & 1 & 0 & 1 \\ \sin k\ell & \cos k\ell & \sinh k\ell & \cosh k\ell \\ k & 0 & k & 0 \\ k\cos k\ell & -k\sin k\ell & k\cosh k\ell & k\sinh k\ell \end{bmatrix} \begin{Bmatrix} B_1 \\ B_2 \\ B_3 \\ B_4 \end{Bmatrix} \tag{2.21}$$

The applied end forces and moments can also be expressed in terms of the end displacements and rotations by equating them to the appropriate shear forces and bending moments acting at the ends of the beam, i.e.

$$M_A(t) = -EI\left(\frac{d^2W}{dx^2}\right)_{x=0} \tag{2.22a}$$

$$M_B(t) = EI\left(\frac{d^2W}{dx^2}\right)_{x=\ell} \tag{2.22b}$$

$$F_A(t) = EI\left(\frac{d^3W}{dx^3}\right)_{x=0} \tag{2.22c}$$

$$F_B(t) = -EI\left(\frac{d^3W}{dx^3}\right)_{x=\ell} \tag{2.22d}$$

Substituting for the transverse displacement amplitude function, $W(x)$ from eqn (2.19) into eqn. (2.22) and re-arranging for the integration constants (B_1,B_2,B_3 and B_4) to be expressed in terms of the applied end forces and moments, one obtains :

$$\begin{Bmatrix} B_1 \\ B_2 \\ B_3 \\ B_4 \end{Bmatrix} = \begin{bmatrix} Q_{11} & Q_{12} & Q_{13} & Q_{14} \\ Q_{21} & Q_{22} & Q_{23} & Q_{24} \\ Q_{31} & Q_{32} & Q_{33} & Q_{34} \\ Q_{41} & Q_{42} & Q_{43} & Q_{44} \end{bmatrix} \begin{Bmatrix} F_A \\ F_B \\ M_A \\ M_B \end{Bmatrix} \tag{2.23}$$

where Q_{ij} $(i=1,2,3,4;\ j=1,2,3,4)$ are transcendental functions of frequency. The expressions for each of these terms are given in Appendix A.

Substituting for B_i *(i=1,2,3,4)* into eqn. (2.21), one obtains the receptance matrix *[R]* of the uniform beam in flexural vibration. Thus,

$$\{ W \} = [R] \{ F \} \tag{2.24}$$

where $\{ W \}^T = \{ W_A \; W_B \; \theta_A \; \theta_B \}$

$\{ F \}^T = \{ F_A \; F_B \; M_A \; M_B \}$

and the receptance matrix :

$$[R] = \begin{bmatrix} R_a & R_b & R_c & R_d \\ R_b & R_a & -R_d & -R_c \\ R_c & -R_d & R_e & R_f \\ R_d & -R_c & R_f & R_e \end{bmatrix} \tag{2.25}$$

in which

$$R_a = H (\cosh k\ell \sin k\ell - \sinh k\ell \cos k\ell)$$

$$R_b = H (\sin k\ell - \sinh k\ell)$$

$$R_c = H k (- \sin k\ell \sinh k\ell)$$

$$R_d = H k (\cos k\ell - \cosh k\ell)$$

$$R_e = H k^2 (\cosh k\ell \sin k\ell + \sinh k\ell \cos k\ell)$$

$$R_f = H k^2 (\sinh k\ell + \sin k\ell)$$

$$H = \frac{1}{E I k^3 (\cos k\ell \cosh k\ell - 1)}$$

The receptance matrix *[R]* of a uniform beam of finite length in flexural vibration is also symmetric.

2.4 DRIVING POINT MOBILITY MATRIX OF FINITE BEAMS

Consider a uniform beam of length, $\ell = \ell_1 + \ell_2$ which is excited at $x = \ell_1$ by simultaneously acting force, *F(t)*, and moment, *M(t)* excitations, as shown in figure 2.4. The boundary conditions of the beam considered here are:

(1) both ends simply-supported;
(2) both ends fully clamped;
(3) one end fully clamped, the other free;
(4) one end fully clamped, the other simply-supported.

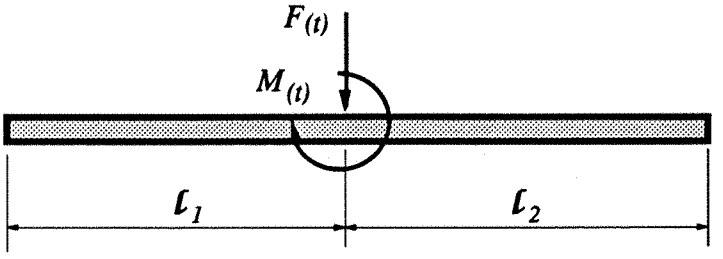

Figure 2.4 : A uniform beam of finite length subjected to simultaneously acting force and moment excitations at an arbitrary point along the length.

The beam is divided into two segments AB and CD of length ℓ_1 and ℓ_2 respectively. The end displacements and rotations, and the applied end forces and moments are shown in figure 2.5.

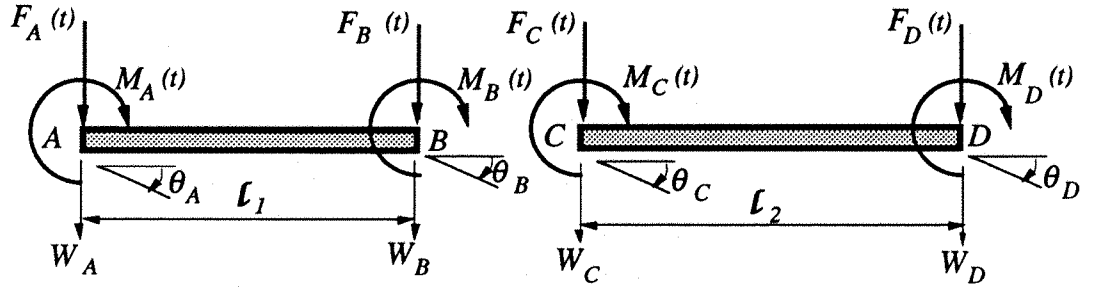

Figure 2.5 : Beam segments AB and CD subjected to applied end forces and moments.

The continuity conditions require that :

$$W_B = W_C \tag{2.26}$$

and

$$\theta_B = \theta_C \tag{2.27}$$

and the equilibrium conditions require that :

$$F_B(t) + F_C(t) = F(t) \tag{2.28}$$

$$M_B(t) + M_C(t) = M(t) \tag{2.29}$$

The boundary conditions are :

for case (1) :
$$W_A = M_A = W_D = M_D = 0 \tag{2.30}$$

for case (2) :
$$W_A = \theta_A = W_D = \theta_D = 0 \tag{2.31}$$

for case (3) :
$$W_A = \theta_A = F_D = M_D = 0 \tag{2.32}$$

for case (4) :
$$W_A = \theta_A = W_D = M_D = 0 \tag{2.33}$$

The end displacements and rotations of these beam segments are related to the appropriate end forces and moments by the receptance matrix *[R]*. Introducing the subscripts 1 for the beam segment AB and 2 for the beam segment CD, these relationships are :

$$\begin{Bmatrix} W_A \\ W_B \\ \theta_A \\ \theta_B \end{Bmatrix} = \begin{bmatrix} R_{a1} & R_{b1} & R_{c1} & R_{d1} \\ R_{b1} & R_{a1} & -R_{d1} & -R_{c1} \\ R_{c1} & -R_{d1} & R_{e1} & R_{f1} \\ R_{d1} & -R_{c1} & R_{f1} & R_{e1} \end{bmatrix} \begin{Bmatrix} F_A \\ F_B \\ M_A \\ M_B \end{Bmatrix} \tag{2.34}$$

and

$$\begin{Bmatrix} W_C \\ W_D \\ \theta_C \\ \theta_D \end{Bmatrix} = \begin{bmatrix} R_{a2} & R_{b2} & R_{c2} & R_{d2} \\ R_{b2} & R_{a2} & -R_{d2} & -R_{c2} \\ R_{c2} & -R_{d2} & R_{e2} & R_{f2} \\ R_{d2} & -R_{c2} & R_{f2} & R_{e2} \end{bmatrix} \begin{Bmatrix} F_C \\ F_D \\ M_C \\ M_D \end{Bmatrix} \tag{2.35}$$

where the expressions for the elements of the receptance matrices are given in eqn. (2.25) with length ℓ replaced by ℓ_1 and ℓ_2 for beam segments AB and CD respectively. For a beam of uniform cross-section, the constants E, I, ρ and A and the flexural wavenumber k are the same for both beam segments AB and CD.

2.4.1 Uniform Beam with Both Ends Simply-supported

Applying the boundary conditions, eqn. (2.30) and from eqns. (2.34) and (2.35) :

$$W_B = R_{b1} F_A + R_{a1} F_B - R_{c1} M_B \tag{2.36}$$

$$\theta_B = R_{d1} F_A - R_{c1} F_B + R_{e1} M_B \tag{2.37}$$

$W_A = 0$ gives,
$$R_{a1} F_A + R_{b1} F_B + R_{d1} M_B = 0 \tag{2.38}$$

$W_D = 0$ gives,
$$R_{b2} F_C + R_{a2} F_D - R_{d2} M_C = 0 \tag{2.39}$$

Hence,
$$F_A = \frac{1}{R_{a1}} \left[-R_{b1} F_B - R_{d1} M_B \right] \tag{2.40}$$

$$F_D = \frac{1}{R_{a2}} \left[-R_{b2} F_C + R_{d2} M_C \right] \tag{2.41a}$$

From the equilibrium conditions, eqns. (2.28) and (2.29),

$$F_D = \frac{1}{R_{a2}} \left[-R_{b2} (F - F_B) + R_{d2} (M - M_B) \right] \tag{2.41b}$$

From the continuity conditions, eqns. (2.26) and (2.27),

$W_B = W_C$ gives,

$$R_{b1} F_A + R_{a1} F_B - R_{c1} M_B = R_{a2} F_C + R_{b2} F_D + R_{c2} M_C \tag{2.42}$$

$\theta_B = \theta_C$ gives,

$$R_{d1} F_A - R_{c1} F_B + R_{e1} M_B = R_{c2} F_C - R_{d2} F_D + R_{e2} M_C \tag{2.43}$$

Using the equilibrium conditions and substituting for F_A and F_D into eqns.(2.42) and (2.43) and rearranging for F_B, M_B, F and M in matrix form, one obtains :

$$\begin{bmatrix} T_{11} & T_{12} \\ T_{21} & T_{22} \end{bmatrix} \begin{Bmatrix} F_B \\ M_B \end{Bmatrix} = \begin{bmatrix} U_{11} & U_{12} \\ U_{21} & U_{22} \end{bmatrix} \begin{Bmatrix} F \\ M \end{Bmatrix} \tag{2.44}$$

or

$$[T] \begin{Bmatrix} F_B \\ M_B \end{Bmatrix} = [U] \begin{Bmatrix} F \\ M \end{Bmatrix}$$

in which,

$$\begin{aligned} T_{11} &= R_{a1} R_{a2} + R_{a2} R_{a2} - R_{b2} R_{b2} - \frac{R_{a2} R_{b1} R_{b1}}{R_{a1}} \\ T_{12} &= R_{a2} R_{c2} - R_{a2} R_{c1} + R_{b2} R_{d2} - \frac{R_{a2} R_{b1} R_{d1}}{R_{a1}} \\ T_{21} &= R_{a2} R_{c2} - R_{a2} R_{c1} + R_{b2} R_{d2} - \frac{R_{a2} R_{b1} R_{d1}}{R_{a1}} \\ T_{22} &= R_{a2} R_{e1} + R_{a2} R_{e2} - R_{d2} R_{d2} - \frac{R_{a2} R_{d1} R_{d1}}{R_{a1}} \end{aligned} \tag{2.44a}$$

$$\begin{aligned} U_{11} &= R_{a2} R_{a2} - R_{b2} R_{b2} \\ U_{12} &= R_{a2} R_{c2} + R_{b2} R_{d2} \\ U_{21} &= R_{a2} R_{c2} + R_{b2} R_{d2} \\ U_{22} &= R_{a2} R_{e2} - R_{d2} R_{d2} \end{aligned} \tag{2.44b}$$

Notice that $T_{12} = T_{21}$ and $U_{12} = U_{21}$, thus, the $[T]$ and $[U]$ matrices are symmetric. From eqn. (2.44):

$$\begin{Bmatrix} F_B \\ M_B \end{Bmatrix} = [T]^{-1} [U] \begin{Bmatrix} F \\ M \end{Bmatrix} \tag{2.45}$$

where $[T]^{-1}$ is the inverse of matrix $[T]$. Substituting for F_A, eqn.(2.40) into eqns. (2.36) and (2.37), and rearranging in matrix form, one obtains :

$$\begin{Bmatrix} W_B \\ \theta_B \end{Bmatrix} = \begin{bmatrix} S_{11} & S_{12} \\ S_{21} & S_{22} \end{bmatrix} \begin{Bmatrix} F_B \\ M_B \end{Bmatrix} = [S] \begin{Bmatrix} F_B \\ M_B \end{Bmatrix} \tag{2.46}$$

in which,

$$\begin{aligned} S_{11} &= R_{a1} - \frac{R_{b1} R_{b1}}{R_{a1}} \\ S_{12} &= -R_{c1} - \frac{R_{b1} R_{d1}}{R_{a1}} \\ S_{21} &= -R_{c1} - \frac{R_{b1} R_{d1}}{R_{a1}} \\ S_{22} &= R_{e1} - \frac{R_{d1} R_{d1}}{R_{a1}} \end{aligned} \tag{2.46a}$$

As $S_{12} = S_{21}$, the *[S]* matrix is also symmetric. From eqns. (2.45) and (2.46), one obtains the driving point receptance matrix *[R]*, for a uniform beam with both ends simply-supported, i.e.:

$$\begin{Bmatrix} W_B \\ \theta_B \end{Bmatrix} = [S]\,[T]^{-1}\,[U] \begin{Bmatrix} F \\ M \end{Bmatrix}$$

and

$$[R] = [S]\,[T]^{-1}\,[U] \tag{2.47}$$

From eqn. (2.17b), the corresponding velocity and angular velocity at the end B are :

$$\begin{aligned} \dot{W}_B &= \frac{dW_B}{dt} = j\omega W_B(x) \\ \dot{\theta}_B &= \frac{d\theta_B}{dt} = j\omega \theta_B(x) \end{aligned}$$

which can be written in matrix form as :

$$\begin{Bmatrix} \dot{W}_B \\ \dot{\theta}_B \end{Bmatrix} = j\omega \begin{Bmatrix} W_B \\ \theta_B \end{Bmatrix} = j\omega\,[S]\,[T]^{-1}\,[U] \begin{Bmatrix} F \\ M \end{Bmatrix} \tag{2.48}$$

The driving point mobility matrix *[Y]* for a uniform beam with both ends simply-supported is thus given as :

$$[Y] = j\omega\,[S]\,[T]^{-1}\,[U] \tag{2.49}$$

where the elements of the *[S]* , *[T]* and *[U]* matrices are given in eqns. (2.46a), (2.44a) and (2.44b) respectively.

The same procedures can be applied to derive the driving point mobility matrix of the uniform beam with simultaneously acting force and moment excitations for the other

three combinations of boundary conditions. However, as these three sets of boundary conditions have one end which is fully clamped, a further simplification can be obtained if one makes use of the receptance matrix and the dynamic stiffness matrix of a uniform beam in flexural vibration.

The dynamic stiffness matrix *[J]* also relates the end displacements and rotations of the beam with the applied end forces and moments. This relationship can be written as :

$$\{ F \} = [J] \{ W \} \tag{2.50}$$

where the transposes of *{F}* and *{W}* are given in eqn. (2.24) and the dynamic stiffness matrix *[J]* can be derived in an identical manner as shown in the previous section.

The dynamic stiffness matrix as given in [26] is :

$$[J] = \begin{bmatrix} J_a & J_b & J_c & J_d \\ J_b & J_a & -J_d & -J_c \\ J_c & -J_d & J_e & J_f \\ J_d & -J_c & J_f & J_e \end{bmatrix} \tag{2.51}$$

in which,

$$\begin{aligned} J_a &= - G k^3 (\cos k\ell \sinh k\ell + \sin k\ell \cosh k\ell) \\ J_b &= G k^3 (\sin k\ell + \sinh k\ell) \\ J_c &= - G k^2 \sin k\ell \sinh k\ell \\ J_d &= G k^2 (\cos k\ell - \cosh k\ell) \\ J_e &= G k (\cos k\ell \sinh k\ell - \sin k\ell \cosh k\ell) \\ J_f &= G k (\sin k\ell - \sinh k\ell) \\ G &= \frac{E I}{\cos k\ell \cosh k\ell - 1} \end{aligned}$$

2.4.2 Uniform Beam with Both Ends Fully Clamped

Using the dynamic stiffness matrix, eqn. (2.51) and the boundary conditions, eqn. (2.31), one obtains :

$$\begin{aligned} F_B &= J_{a1} W_B - J_{c1} \theta_B \\ M_B &= - J_{c1} W_B + J_{e1} \theta_B \\ F_C &= J_{a2} W_C + J_{c2} \theta_C \\ M_C &= J_{c2} W_C + J_{e2} \theta_C \end{aligned}$$

Applying the equilibrium conditions eqns. (2.28) and (2.29) and the continuity conditions eqns. (2.26) and (2.27), one obtains :

$$(J_{a1} + J_{a2})\, W_B + (J_{c2} - J_{c1})\, \theta_B = F$$
$$(J_{c2} - J_{c1})\, W_B + (J_{e1} + J_{e2})\, \theta_B = M$$

or
$$\begin{bmatrix} (J_{a1} + J_{a2}) & (J_{c2} - J_{c1}) \\ (J_{c2} - J_{c1}) & (J_{e1} + J_{e2}) \end{bmatrix} \begin{Bmatrix} W_B \\ \theta_B \end{Bmatrix} = \begin{Bmatrix} F \\ M \end{Bmatrix} \tag{2.52}$$

Hence,
$$\begin{Bmatrix} W_B \\ \theta_B \end{Bmatrix} = \begin{bmatrix} R_{FF} & R_{FM} \\ R_{MF} & R_{MM} \end{bmatrix} \begin{Bmatrix} F \\ M \end{Bmatrix} \tag{2.53}$$

in which,
$$R_{FF} = \frac{1}{\Delta_1}(J_{e1} + J_{e2})$$
$$R_{FM} = \frac{1}{\Delta_1}(J_{c1} - J_{c2})$$
$$R_{MF} = \frac{1}{\Delta_1}(J_{c1} - J_{c2})$$
$$R_{MM} = \frac{1}{\Delta_1}(J_{a1} + J_{a2})$$

and
$$\Delta_1 = (J_{a1} + J_{a2})(J_{e1} + J_{e2}) - (J_{c2} - J_{c1})^2$$

For harmonic response, the velocity and angular velocity at the end B are :

$$\begin{Bmatrix} \dot{W}_B \\ \dot{\theta}_B \end{Bmatrix} = j\omega \begin{Bmatrix} W_B \\ \theta_B \end{Bmatrix} = j\omega \begin{bmatrix} R_{FF} & R_{FM} \\ R_{MF} & R_{MM} \end{bmatrix} \begin{Bmatrix} F \\ M \end{Bmatrix} \tag{2.54}$$

The driving point mobility matrix *[Y]* for a uniform beam with both ends fully clamped is:

$$[Y] = \begin{bmatrix} Y_{FF} & Y_{FM} \\ Y_{MF} & Y_{MM} \end{bmatrix} = j\omega \begin{bmatrix} R_{FF} & R_{FM} \\ R_{MF} & R_{MM} \end{bmatrix} \tag{2.55}$$

2.4.3 Uniform Beam with One End Fully Clamped and the Other Free

Consider the beam segment AB, from the dynamic stiffness matrix and using the boundary conditions ($W_A = \theta_A = 0$), one obtains :

$$F_B = J_{a1} W_B - J_{c1} \theta_B$$
$$M_B = -J_{c1} W_B + J_{e1} \theta_B$$

Consider the beam segment CD, from the receptance matrix and using the boundary conditions ($F_D = M_D = 0$), one obtains :

$$W_C = R_{a2} F_C + R_{c2} M_C$$
$$\theta_C = R_{c2} F_C + R_{e2} M_C$$

Using the continuity and equilibrium conditions and from the above four equations obtained by satisfying the boundary conditions, after some manipulation, the driving point mobility matrix of the beam can be written as :

$$[Y] = \begin{bmatrix} Y_{FF} & Y_{FM} \\ Y_{MF} & Y_{MM} \end{bmatrix} = j\omega \begin{bmatrix} R_{FF} & R_{FM} \\ R_{MF} & R_{MM} \end{bmatrix} \tag{2.56}$$

in which,

$$R_{FF} = \frac{1}{\Delta_2} [R_{a2} + J_{e1} (R_{a2} R_{e2} - R_{c2} R_{c2})]$$
$$R_{FM} = R_{MF} = \frac{1}{\Delta_2} [R_{c2} + J_{c1} (R_{a2} R_{e2} - R_{c2} R_{c2})]$$
$$R_{MM} = \frac{1}{\Delta_2} [R_{e2} + J_{a1} (R_{a2} R_{e2} - R_{c2} R_{c2})]$$

and

$$\Delta_2 = (1 + R_{a2} J_{a1} - R_{c2} J_{c1})(1 + R_{e2} J_{e1} - R_{c2} J_{c1}) - (R_{c2} J_{e1} - R_{a2} J_{c1})(R_{c2} J_{a1} - R_{e2} J_{c1})$$

2.4.4 Uniform Beam with One End Fully Clamped and the Other Simply-supported

Using the boundary conditions, the continuity and equilibrium conditions, and the dynamic stiffness and receptance matrices of a uniform beam in flexural vibration, the driving point mobility matrix of the beam with one end fully clamped and the other simply-supported can be shown to be :

$$[Y] = \begin{bmatrix} Y_{FF} & Y_{FM} \\ Y_{MF} & Y_{MM} \end{bmatrix} = j\omega \begin{bmatrix} R_{FF} & R_{FM} \\ R_{MF} & R_{MM} \end{bmatrix} \tag{2.57}$$

in which, $R_{FF} = \frac{1}{\Delta_3} [R_{a2} (R_{a2} R_{a2} - R_{b2} R_{b2}) - J_{e1} (R_{a2} R_{c2} + R_{b2} R_{d2})^2 + J_{e1} (R_{a2} R_{a2} - R_{b2} R_{b2})(R_{a2} R_{e2} - R_{d2} R_{d2})]$

$$R_{FM} = \frac{1}{\Delta_3}\left[R_{a2}\left(R_{a2}R_{c2} + R_{b2}R_{d2}\right) - J_{c1}\left(R_{a2}R_{c2} + R_{b2}R_{d2}\right)^2 + J_{c1}\left(R_{a2}R_{a2} - R_{b2}R_{b2}\right)\left(R_{a2}R_{e2} - R_{d2}R_{d2}\right)\right]$$

$$= R_{MF}$$

$$R_{MM} = \frac{1}{\Delta_3}\left[R_{a2}\left(R_{a2}R_{e2} - R_{d2}R_{d2}\right) - J_{a1}\left(R_{a2}R_{c2} + R_{b2}R_{d2}\right)^2 + J_{a1}\left(R_{a2}R_{a2} - R_{b2}R_{b2}\right)\left(R_{a2}R_{e2} - R_{d2}R_{d2}\right)\right]$$

and

$$\Delta_3 = \left[R_{a2} + J_{a1}\left(R_{a2}R_{a2} - R_{b2}R_{b2}\right) - J_{c1}\left(R_{a2}R_{c2} + R_{b2}R_{d2}\right)\right] x \left[R_{a2} - J_{c1}\left(R_{a2}R_{c2} + R_{b2}R_{d2}\right) + J_{e1}\left(R_{a2}R_{e2} - R_{d2}R_{d2}\right)\right] - \left[J_{e1}\left(R_{a2}R_{c2} + R_{b2}R_{d2}\right) - J_{c1}\left(R_{a2}R_{a2} - R_{b2}R_{b2}\right)\right] x \left[J_{a1}\left(R_{a2}R_{c2} + R_{b2}R_{d2}\right) - J_{c1}\left(R_{a2}R_{e2} - R_{d2}R_{d2}\right)\right]$$

2.5 VIBRATION ANALYSIS WITH DAMPING

All physical structures dissipate energy, in one way or the other, when they vibrate. Hence, to obtain a realistic resonance response level or to predict the resonance displacement amplitude, damping must be included in the analysis. The inherent material damping can be accounted for in the analysis by replacing the Modulus of Elasticity, E, by a complex Modulus of Elasticity, E^c, which is defined as :

$$E^c = E(1 + j\eta) \tag{2.58}$$

where η is the loss factor in this hysteretic mechanism.

With the inclusion of the complex Modulus of Elasticity, the flexural wavenumbers become complex. The receptance and the dynamic stiffness matrices also become complex matrices, and the corresponding end displacements and rotations are complex quantities. The trigonometric and hyperbolic functions in these matrices thus have complex arguments.

As the inherent material loss factor for common metallic materials, such as steel and aluminium alloys is in the order of 10^{-4} to 10^{-3}, for such a small material loss factor, the trigonometric and hyperbolic functions with complex arguments may be approximated by the following expressions as given in [26] :

$$
\begin{aligned}
k^c &= k\left(1 - j\frac{\eta}{4}\right) \\
\sin k^c \ell &= \sin k\ell - j\frac{\eta k\ell}{4}\cos k\ell \\
\cos k^c \ell &= \cos k\ell + j\frac{\eta k\ell}{4}\sin k\ell \\
\sinh k^c \ell &= \sinh k\ell - j\frac{\eta k\ell}{4}\cosh k\ell \\
\cosh k^c \ell &= \cosh k\ell - j\frac{\eta k\ell}{4}\sinh k\ell
\end{aligned}
\tag{2.59}
$$

2.6 VIBRATIONAL POWER INPUT TO BEAM-LIKE STRUCTURES SUBJECTED TO SIMULTANEOUSLY ACTING FORCE AND MOMENT EXCITATIONS

The translational velocity and the rotational velocity of a structure at the excitation point can be expressed in terms of the applied force, and the applied moment, by the mobility matrix as follows :

$$
\begin{Bmatrix} \dot{w} \\ \dot{\theta} \end{Bmatrix} = \begin{bmatrix} Y_{FF} & Y_{FM} \\ Y_{MF} & Y_{MM} \end{bmatrix} \begin{Bmatrix} F \\ M \end{Bmatrix} \tag{2.60}
$$

The time-averaged power input to a structure by a point harmonic force can be shown [24] to be :

$$
P_F = \frac{1}{2}\, Re\, \{ F\ \dot{w}^* \} \tag{2.61}
$$

where $\dot{w}^*$ is the complex conjugate of the velocity response $\dot{w}$ at the excitation point, and $Re\{\ \}$ denotes the real part of the complex quantity. The time-averaged power input to a structure due to an applied moment can also be shown [24] to be :

$$
P_M = \frac{1}{2}\, Re\, \{ M\ \dot{\theta}^* \} \tag{2.62}
$$

where $\dot{\theta}^*$ is the complex conjugate of the angular velocity response $\dot{\theta}$ at the excitation point.

For a beam-like structure subjected to simultaneously acting force and moment excitations, the translational and rotational velocities are given as (from eqn. (2.60)) :

$$
\dot{w} = Y_{FF}\, F + Y_{FM}\, M \tag{2.63a}
$$

$$
\dot{\theta} = Y_{MF}\, F + Y_{MM}\, M \tag{2.63b}
$$

The complex conjugates of these two quantities are respectively :

$$\dot{w}^* = Y^*_{FF}\, F^* + Y^*_{FM}\, M^* \tag{2.64a}$$

$$\dot{\theta}^* = Y^*_{MF}\, F^* + Y^*_{MM}\, M^* \tag{2.64b}$$

The time-averaged vibrational power input to the beam-like structure due to the force component is :

$$\begin{aligned} P_F &= \frac{1}{2}\, Re\{ F\ \dot{w}^* \} \\ &= \frac{1}{2}\, Re\{ F\, Y^*_{FF}\, F^* + F\, Y^*_{FM}\, M^* \} \\ &= \frac{1}{2}\, |F|^2\, Re\{Y^*_{FF}\} + \frac{1}{2}\, Re\{F\ Y^*_{FM}\, M^*\} \end{aligned} \tag{2.65}$$

and the time-averaged vibrational power input to the beam-like structure due to the moment component is :

$$\begin{aligned} P_M &= \frac{1}{2}\, Re\{ M\ \dot{\theta}^* \} \\ &= \frac{1}{2}\, Re\{ M\, Y^*_{MF}\, F^* + M\, Y^*_{MM}\, M^* \} \\ &= \frac{1}{2}\, |M|^2\, Re\{Y^*_{MM}\} + \frac{1}{2}\, Re\{M\, Y^*_{MF}\, F^*\} \end{aligned} \tag{2.66}$$

For a practical excitation system, both the applied force and moment are real quantities, the time-averaged vibrational power input to the beam-like structure therefore becomes :

$$\begin{aligned} P_F &= \frac{1}{2}\, F^2\, Re\{Y^*_{FF}\} + \frac{1}{2}\, F\, M\, Re\{Y^*_{FM}\} \\ &= \frac{1}{2}\, F^2\, Re\{Y_{FF}\} + \frac{1}{2}\, F\, M\, Re\{Y_{FM}\} \end{aligned} \tag{2.67}$$

$$\begin{aligned} P_M &= \frac{1}{2}\, M^2\, Re\{Y^*_{MM}\} + \frac{1}{2}\, M\, F\, Re\{Y^*_{MF}\} \\ &= \frac{1}{2}\, M^2\, Re\{Y_{MM}\} + \frac{1}{2}\, M\, F\, Re\{Y_{MF}\} \end{aligned} \tag{2.68}$$

The resultant time-averaged vibrational power input to the beam-like structure subjected to simultaneously acting force and moment excitations is the sum of the power inputs due to the force and the moment components. Thus,

$$
\begin{aligned}
P_T &= P_F + P_M \\
&= \frac{1}{2} F^2 \, Re\{Y_{FF}\} + \frac{1}{2} F M \, Re\{Y_{FM}\} + \\
&\quad \frac{1}{2} M^2 \, Re\{Y_{MM}\} + \frac{1}{2} M F \, Re\{Y_{MF}\} \\
&= \frac{1}{2} F^2 \, Re\{Y_{FF}\} + \frac{1}{2} M^2 \, Re\{Y_{MM}\} \\
&\quad + F M \, Re\{Y_{FM}\}
\end{aligned} \tag{2.69}
$$

In the expression for the resultant power input, eqn. (2.69), the first two terms on the right correspond to the time-averaged vibrational power inputs to the beam-like structure due to the force and the moment components as if they were acting alone. The third term corresponds to the additional power input attributed to the coupling mobilities resulting from the simultaneously acting force and moment excitations.

2.7 ANALYTICAL RESULTS AND DISCUSSION

Based on the theoretical expressions for the driving point mobility matrix for the semi-infinite and finite beams, the time-averaged vibrational power inputs to various beam configurations subjected to simultaneously acting force and moment excitations have been studied. The aim of this analysis is to study the variations of the vibrational power input to flexible beam-like structures subjected to the changes in the moment arm, the damping of the structures, the excitation locations and the boundary conditions. In particular, the interaction among the coupling, force and moment mobilities on the resultant vibrational power input to the structures. In the calculation of the vibrational power, damping of the beam-like structures was taken into consideration. The material and geometric properties of the beam used in the analysis were :

Modulus of Elasticity, E	=	207×10^9	Nm^{-2}
Density of material, ρ	=	7850.0	kgm^{-3}
Material loss factor, η	=	0.005	
Length of beam, ℓ	=	0.585	m
Width of beam	=	0.04	m
Thickness of beam	=	0.004	m

The applied moment is taken to be equal to the applied force multiplied by a moment arm,a, which is the horizontal offset of the line of action of the vertical force to the centre of the mounting, as illustrated in figure 2.6. Hence, for a given value of the

applied force, the applied moment is proportional to the moment arm. For simplicity, the seating block was assumed to be massless and infinitely stiff. The resonance effects of the seating block on the resultant vibrational power input to the seating structures are studied later in Chapter 10, Section 10.4.

The applied force is assumed to be sinusoidal having a magnitude of 1 N. The moment arm and the point of excitation along the beam (except for the case of the semi-infinite beam, the excitation is applied at one end) are the parameters of analysis. The frequency range of the analyses carried out was from 1Hz to 1000Hz with a resolution or frequency increment of 2Hz.

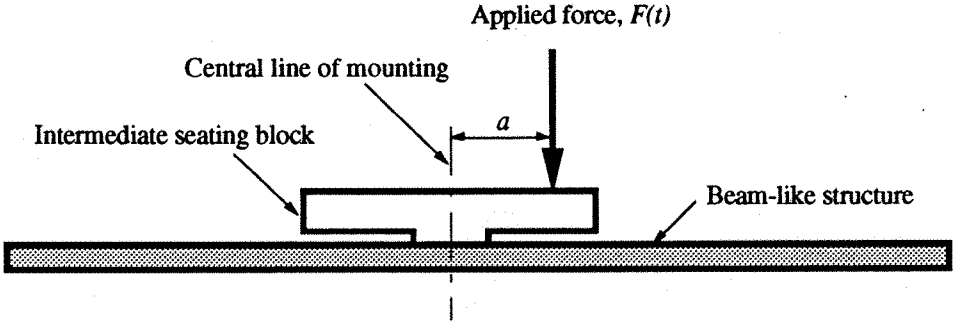

Figure 2.6 : Simultaneously acting force and moment excitations on a beam-like structure.

The notations P_{force} , P_{moment}, $P_{coupling}$ and P_{total} used in the figures for illustration denote the time-averaged vibrational power inputs to the beam due to the force acting alone, the moment acting alone, the coupling mobilities and the resultant of the combined force and moment respectively. The expressions for these vibrational powers can be obtained from eqn. (2.69) :

$$P_{force} = \frac{1}{2} F^2 \, Re \{ Y_{FF} \} \tag{2.70}$$

$$P_{moment} = \frac{1}{2} M^2 \, Re \{ Y_{MM} \} \tag{2.71}$$

$$P_{coupling} = \frac{1}{2} F M \, Re \{ Y_{FM} \} \tag{2.72}$$

$$\begin{aligned} P_{total} &= \frac{1}{2} F^2 \, Re \{ Y_{FF} \} + \frac{1}{2} M^2 \, Re \{ Y_{MM} \} \\ &\quad + F M \, Re \{ Y_{FM} \} \\ &= P_{force} + P_{moment} + 2 P_{coupling} \end{aligned} \tag{2.73}$$

The vibrational power contributed from the coupling mobility functions, Y_{FM} and Y_{MF}, is denoted here as a separate power component, $P_{coupling}$, for ease of accountability and explanation. The physical meaning of the coupling mobility functions and the condition for their existence, as given in Section 2.2, must always be

borne in mind. This implies that $P_{coupling}$ will be zero if either P_{force} or P_{moment} is zero. The relationships of these terms with those given in eqns. (2.67), (2.68) and (2.69) are :

$$\begin{aligned} P_F &= P_{force} + P_{coupling} \\ P_M &= P_{moment} + P_{coupling} \\ P_T &= P_{total} \end{aligned} \tag{2.74}$$

2.7.1 Vibrational Power Input to a Semi-infinite Beam

a. The Effect of Moment Arm

The variations of the time-averaged power inputs to the semi-infinite beam versus frequency for given values of the force and moment are shown in figures 2.7(a) to 2.7(d). The plots given in these figures correspond to values of the moment arm, *a,* of 0.02m, 0.05m, 0.169m and - 0.169m respectively. The value of 0.169m corresponds to a minimum P_{total} value at the frequency of 33 Hz, a typical firing frequency of diesel engines. The negative moment arm, by definition, gives rise to a negative moment, i.e. anticlockwise moment according to the sign convention.

It can be seen from these figures that :

(1) P_{force} decreases linearly with increasing frequency on a log-log scale;

(2) P_{moment} increases linearly with increasing frequency on a log-log scale;

(3) $P_{coupling}$ is a constant value, (i.e. independent of frequency) which is negative for given positive applied force and moment arm;

(4) P_{total} has a minimum value at the cross-over frequency of the P_{force} line and the P_{moment} line, which depends on the value of the moment arm or the ratio of the applied moment to the applied force. For a given force, the larger the value of the moment arm the lower is the frequency at which the minimum occurs.

(5) For the positive moment arms (figures 2.7(a) to 2.7(c)), the minimum of P_{total} is very much lower than either the P_{force} or the P_{moment} value at that frequency. This result implies that there appears to be some cancellation effects on the resultant power input to the beam.

(6) For the negative moment arm (figure 2.7(d)), the P_{total} line is above both the P_{force} and the P_{moment} lines. Thus, there is an increase in the resultant power input to the beam if the moment acts in the negative direction.

The cancellation effect in the resultant time-averaged vibrational power input to the semi-infinite beam subjected to simultaneously acting force and moment excitations, is attributed to the coupling mobilities. Ignoring the damping terms and from the expressions given in eqn. (2.16), the real parts of the force mobility, Y_{FF}, and the moment mobility, Y_{MM}, are positive, whereas the real parts of the coupling mobilities, Y_{FM} and Y_{MF} , are negative. The resultant time-averaged vibrational power input, from eqn. (2.69), is:

$$P_T = \frac{1}{2} F^2 \left(\frac{\omega}{EIk^3}\right) + \frac{1}{2} M^2 \left(\frac{\omega}{EIk}\right) + F M \left(-\frac{\omega}{EIk^2}\right)$$

$$= \frac{1}{2} \left(\frac{\omega}{EIk^3}\right) \left[F^2 + (kM)^2 - 2F(kM) \right] \qquad (2.75)$$

The first two terms on the right of the above expression correspond to P_{force} and P_{moment} respectively. As the flexural wavenumber, k, is proportional to the square-root of frequency, P_{force} is thus inversely proportional to the square-root of frequency and P_{moment} is proportional to the square-root of frequency, which confirms the relationships observed in points (1) and (2) above. The third term corresponds to twice the magnitude of $P_{coupling}$, which is independent of frequency as noted in point (3) above. The vibrational power input due to moment excitation becomes more important with increasing frequency.

Equation (2.75) also shows that, for the case of an undamped beam, there exists a condition in which P_{total} is zero . This condition is :

$$F = k M \qquad (2.76)$$

As $M = F a$, eqn. (2.76) can also be written as :

$$k a = 1 \qquad (2.77)$$

Hence, for given material and geometric properties of the beam, and for a given force, the larger the moment arm the lower is the frequency at which the cancellation effect occurs. However, if the moment arm is negative, then from eqn. (2.75), the three terms on the right of the expression are additive and the cancellation effect ceases to exist.

This condition of zero resultant time-averaged vibrational power input to the semi-infinite beam due to simultaneously acting force and moment excitations can also be explained from the expression for the propagating A_4 wave (eqn. (2.9)), as for $F=k\,M$, the A_4 term vanishes, which corresponds to the condition of no propagating wave in the beam, except the exponentially decaying near field wave, a condition which was also highlighted by Cremer, Heckl and Ungar [24].

The above discussion gives a mathematical explanation for the cancellation effect in the total vibrational power input to the semi-infinite beam. Physically, this means that the A_4 propagating waves generated from the force and moment excitations respectively are equal in magnitude but opposite in phase and thus cancel each other.

b. The Effect of Damping

The hysteretic loss factor, η used in the previous cases was 0.005. It is of interest to study the effect of material damping on the time-averaged vibrational power inputs to the beam, and in particular, the cancellation effect as noted above. Figures 2.8(a) and 2.8(b) show the time-averaged power inputs to the semi-infinite beam for loss factors of 0.1 and 0 respectively, the moment arm for these two cases is 0.169m. A comparison of P_{total}, for η = 0.1, 0.005 and 0 is shown in figure 2.8(c). This set of results shows that the higher the material damping, the smaller is the cancellation effect.

2.7.2 Vibrational Power Input to Finite Beams

a. The Effect of Boundary Conditions

The effect of the boundary conditions, i.e. clamped - free; clamped - simply supported; clamped - clamped and simply supported at both ends, on the time-average vibrational power inputs to finite beams subjected to simultaneously acting force and moment excitations at the mid-span are shown in figures 2.9(a) to 2.9(d). These figures show comparisons of P_{total}, P_{force} and P_{moment}. The moment arm for these analyses was constant at 0.02m.

It can be seen that with symmetric boundary conditions and the excitation at mid-span, the resonance peaks due to the force and the moment components are well separated (figures 2.9(c) and 2.9(d)). This corresponds to the special case in which the point of excitation coincides with a point of mode shape symmetry, i.e. at the excitation point, the translational degree of freedom (transverse velocity) only occurs for the odd

numbered modes and the rotational degree of freedom (angular velocity) only occurs for the even numbered modes. There is no coupling mobility, which can be seen from eqn. (2.53) with $J_{c1} = J_{c2}$ for the case of clamped - clamped boundary conditions. The resultant vibrational power input to the beams is the sum of these two components (i.e. P_{force} and P_{moment}).

For unsymmetric boundary conditions, especially the clamped - simply supported condition, the resonance peaks due to the force and the moment components occur at the same frequency, as depicted in figure 2.9(b). The coupling terms in the driving point mobility matrix exist. These coupling mobilities in combination with the given positive values of force and moment result in a reduction of the resultant vibrational power input to the beam at certain frequencies, such as the fourth resonance frequency as shown in the figure.

The cancellation effect for finite beams due to the coupling mobilities can be explained from the expression of P_{total} as given in eqn. (2.73) and the values of the real parts of Y_{FF}, Y_{MM} and Y_{FM}. Figures 2.10(a), 2.10(b) and 2.10(c) show the real parts of Y_{FF}, Y_{MM} and Y_{FM} respectively for the clamped - simply supported beam. As the real parts of Y_{FF} and Y_{MM} are always positive and the real part of Y_{FM} can be positive or negative depending on the particular mode shapes, for a positive moment arm and a positive applied force, the product $F\,M$ is positive, thus, the effect of cancellation occurs when the real part of Y_{FM} is negative. Figure 2.10(c) shows that the second and fourth resonance peaks are negative. Hence, in combination with the given force and the positive moment arm, they contribute to the cancellation of the resultant power input to the beam. The reduction in the second resonance peak is not obvious because of the smaller contribution of $Re\,\{\,Y_{FM}\,\}$ compared to that of the fourth resonance peak. This amount of reduction can be increased by increasing the moment arm for a given applied force, as will be shown later for the case of larger moment arm of 0.0438m (figure 2.15(b)).

b. <u>The Effect of Excitation Location</u>

The effect of different excitation locations on the resultant time-averaged vibrational power input to the clamped - simply supported beam has been examined. Figure 2.11 shows the variation of P_{total} with frequency for excitation locations at the mid-span ($\ell/2$) , and at a distance of $\ell/4$ and $3\ell/8$ from the clamped end. The moment arm, a, used in the analysis was 0.02 m. With this positive moment arm and for a given applied force, these plots show different magnitudes of the resonance peaks for excitations

applied at different locations. This is due to different values of the real parts of driving point force, moment and coupling mobilities. This set of results indicates that whilst a given combination of applied force and moment at a specific location may be favourable in reducing the resultant vibrational power input to the beam at a specific frequency, it may not be the case for another location along the beam.

c. The Effect of Moment Arm

Figure 2.12 shows the variation of P_{total} of the clamped - simply suppported beam for three values of the moment arm, a : 0.02m, 0.169m and - 0.169m. The excitation was located at the mid-span. As for a given applied force, the moment excitation is directly proportional to the moment arm, it is expected that more vibrational power must be injected into the finite beam for the cases of larger moment arms. However, it can be seen that for the moment arm of -0.169m, the peak at the third resonance frequency is the smallest and that at the fifth resonance frequency is comparable to the peak for the 0.02m moment arm. These reductions in the resultant vibrational power input for the case of a negative moment arm are due to the positive peaks at the third and fifth resonance frequencies of the real part of the coupling mobility, Y_{FM} as depicted in figure 2.10(c).

d. The Effect of Damping

Increase in material damping has been shown to reduce the cancellation effect for the case of a semi-infinite beam. The effect of material damping on the time-averaged vibrational power input to the finite beam was analysed for the clamped - simply supported beam with the excitation located at the mid-span and a 0.02m moment arm. Comparisons of P_{force} , P_{moment} and P_{total} of the clamped - simply supported beam for loss factors of 0.005 and 0.1 are shown in figures 2.13(a), 2.13(b) and 2.13(c) respectively. These plots show that increase in material damping reduces the power input at the resonance peaks but it also widens the peaks and raises the power input in between the resonance peaks. The net result may be that more vibrational power is injected into a finite beam for a specific frequency bandwidth.

e. Comparison with the Semi-infinite Beam Results

Comparisons of P_{force} and P_{moment} for the semi-infinite beam with those for the finite beam with various boundary conditions, such as clamped - free, clamped - simply supported, clamped - clamped and simply supported at both ends are shown in figures

2.14(a) to 2.14(d) respectively. For these analyses, the moment arm was 0.02m and the excitation was located at the mid-span for finite beams. The results indicate that the trends of the vibrational power input to the finite beams are in agreement with those of the semi-infinite beam. The vibrational power input to beam-like structures due to the moment excitation is more critical at higher frequencies.

For the case of a semi-infinite beam, it was shown in Section 2.7.1 (a) that a condition exists in which the resultant time-averaged vibrational power input to an undamped beam is zero. In an attempt to analyse whether such a condition for the semi-infinite beam could be used to predict or reduce the vibrational power input to an identical but finite beam, additional analyses were carried out on the clamped - simply supported beam.

The theoretical fourth resonance frequency of the chosen beam is 491.6 Hz. The corresponding moment arm, a, in order to minimise the resultant vibrational power input to an identical but semi-infinite beam at this frequency is 0.0438m (from eqn. (2.77)). The analytical results obtained with this value of moment arm are shown in figures 2.15(a) to 2.15(c).

Figure 2.15(a) shows the comparison of P_{force} and P_{total} for the semi-infinite beam and figure 2.15(b) shows the corresponding comparison for the clamped-simply supported beam. It can be seen that whilst there is an obvious reduction in P_{total} for the semi-infinite beam at frequencies around 490Hz, the fourth resonance peak of the finite beam does not reduce. However, there is a reduction in P_{total} for the second resonance peak as depicted in figure 2.15(b).

If one defines a Power Reduction index, $\mathcal{P}$, as the ratio of P_{total} to P_{force}, i.e.

$$\mathcal{P} = \frac{P_{total}}{P_{force}} \tag{2.78}$$

then a value of $\mathcal{P}$ less than unity indicates a reduction in the resultant time-averaged vibrational power input to the beam-like structure as a result of introducing a simultaneously acting moment excitation to the beam.

A comparison of power reduction index spectra for the semi-infinite and the clamped-simply supported beams is shown in figure 2.15(c). It can be seen that whilst the power reduction index spectrum of the semi-infinite beam is below the unity (10^0) line throughout the whole frequency range of analysis, the power reduction index spectrum

of the finite beam is below the unity line only for frequencies close to the second resonance peak. Hence, the reduction in the resultant time-averaged vibrational power input to the clamped-simply supported beam due to simultaneously acting force and moment excitations is limited to a specific frequency bandwidth. This comparison also shows that the condition of minimum power input to the semi-infinite beam cannot be directly applied for a corresponding finite length beam.

2.8 SUMMARY

The time-averaged vibrational power input to beam-like structures subjected to simultaneously acting force and moment excitations has been studied and the interactions between the driving point force, moment and coupling mobilities of a semi-infinite beam and finite beams with various boundary conditions have been examined analytically. The analytical results have also been reported in [27]. Some of the important conclusions from this study are summarised as follows :

(1) for a semi-infinite beam excited by simultaneously acting force and moment excitations at one end, a condition exists for which the resultant time-averaged vibrational power input to the beam is a minimum. Increase in material damping will diminish this cancellation effect.

(2) For beams of finite length subjected to simultaneously acting force and moment excitations, reduction in the resultant time-averaged vibrational power input is observed for frequencies around some resonance frequencies. This reduction is attributed to the negative real parts of the coupling mobility function for positive force and moment excitations.

(3) For finite beams with symmetric boundary conditions, the coupling mobility functions do not exist if the excitation location coincides with a point of mode shape symmetry.

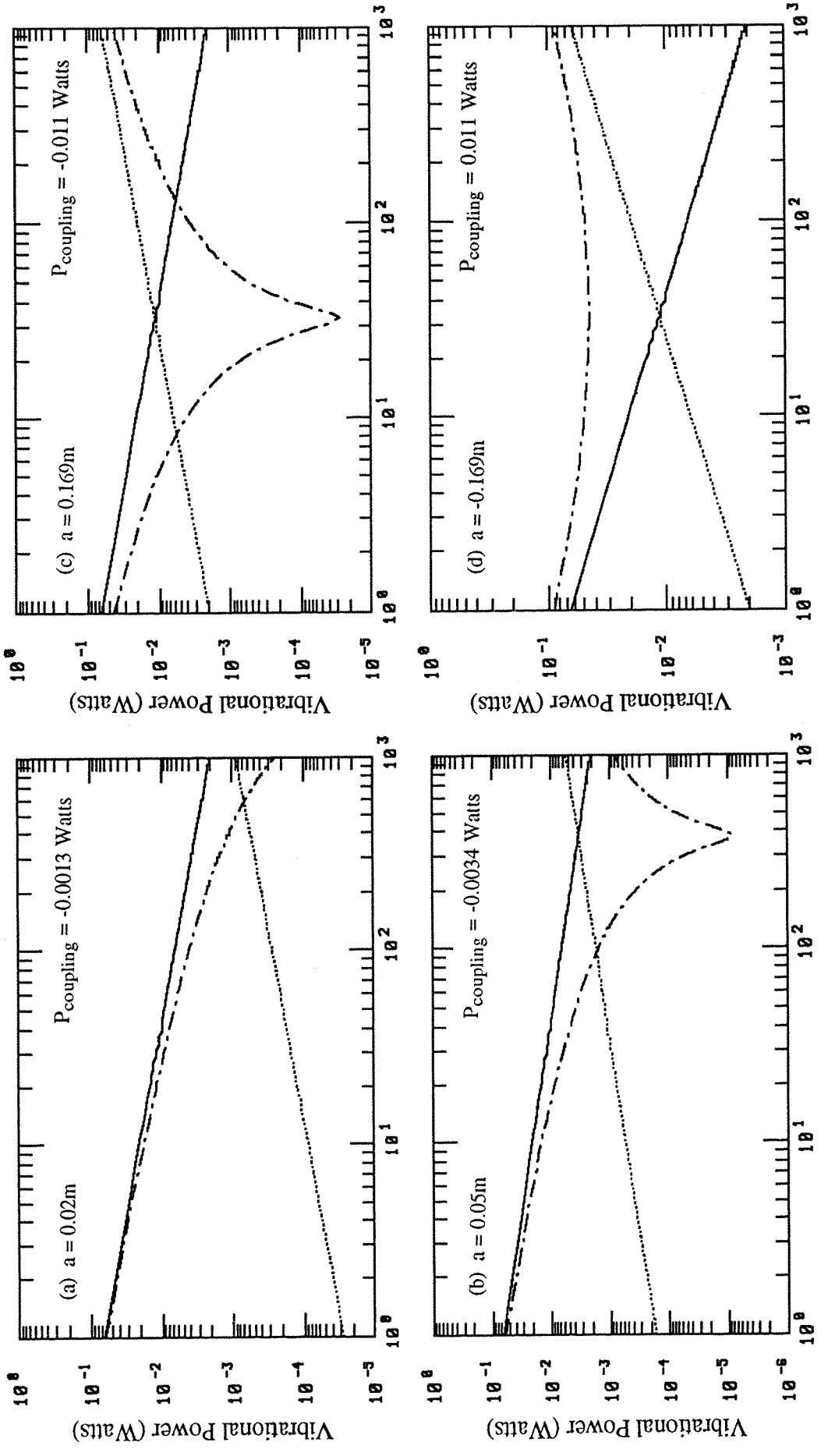

Figure 2.7 : Vibrational power inputs to a semi-infinite beam for various values of moment arms : (a): a = 0.02m, (b): a = 0.05m, (c): a = 0.169m and (d): a = –0.169m; ——— P_{force}, ... P_{moment}, -·-·- P_{total} (force amplitude = 1N, loss factor = 0.005).

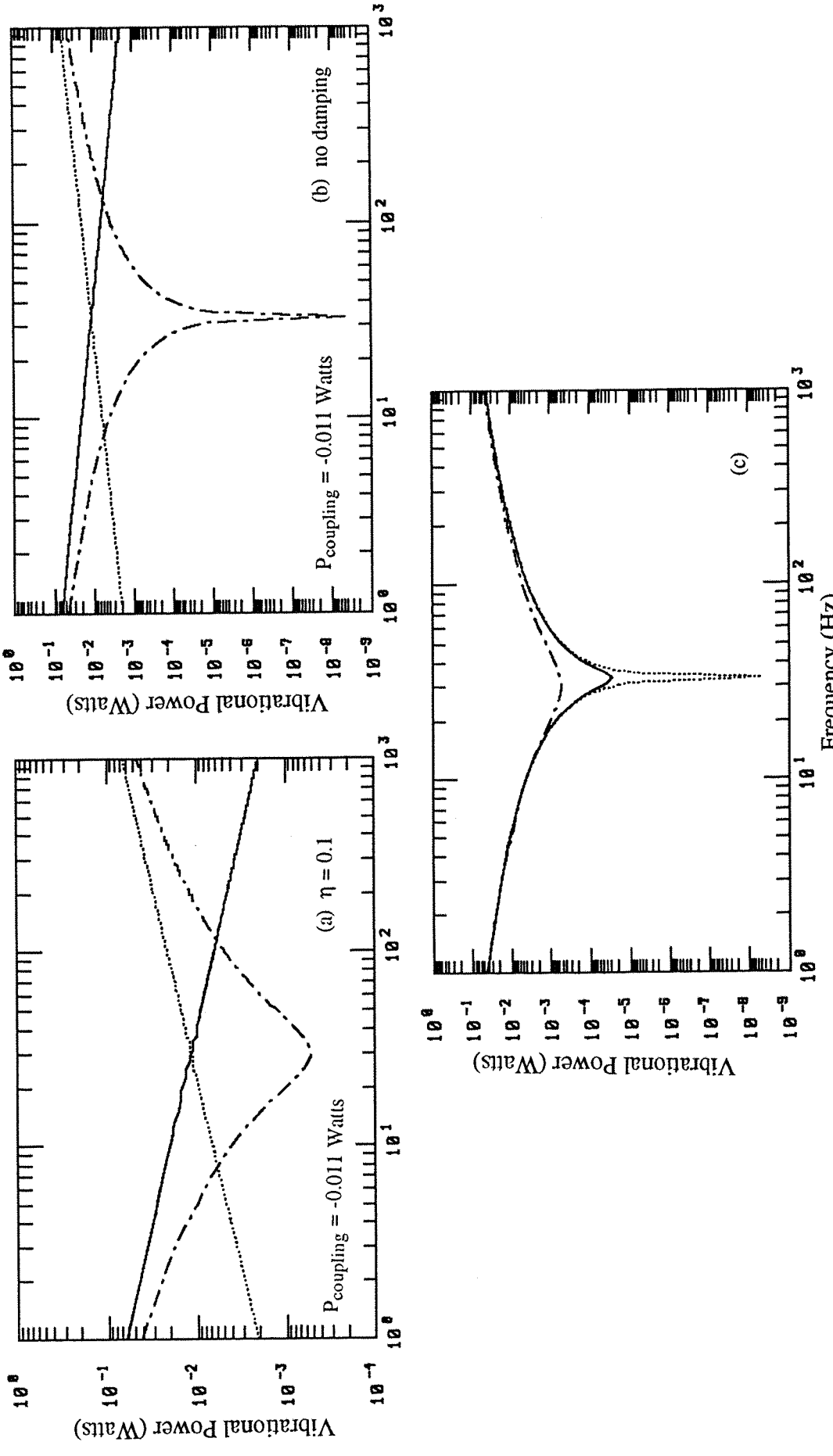

Figure 2.8 : Vibrational power inputs to a semi-infinite beam for various values of loss factor : (a): $\eta = 0.1$, (b): no damping, (c): variations of P_{total} for various values of loss factor : ——— P_{force}, ... P_{moment}, -·-·- P_{total}, ——— $\eta = 0.1$, ——— $\eta = 0.005$, ... no damping (force amplitude = 1N, moment arm = 0.169m).

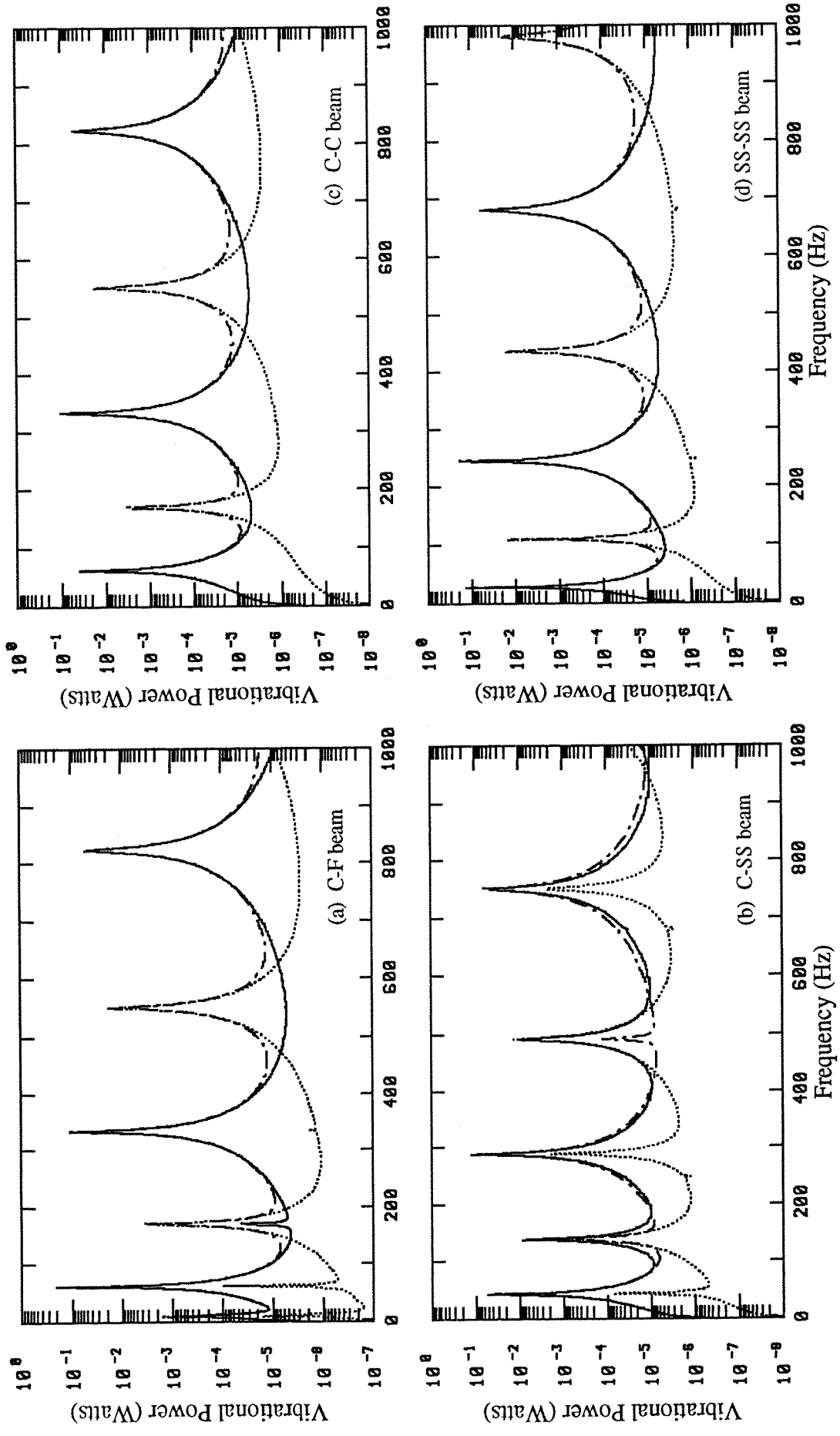

Figure 2.9 : Effects of boundary conditions on the vibrational power inputs to uniform beams of finite length : (a) C-F beam, (b): C-SS beam, (c): C-C beam and (d) SS-SS beam; ——— P_{force}, ... P_{moment}, —·—·— P_{total} (force amplitude = 1N, moment arm = 0.02m, loss factor = 0.005).

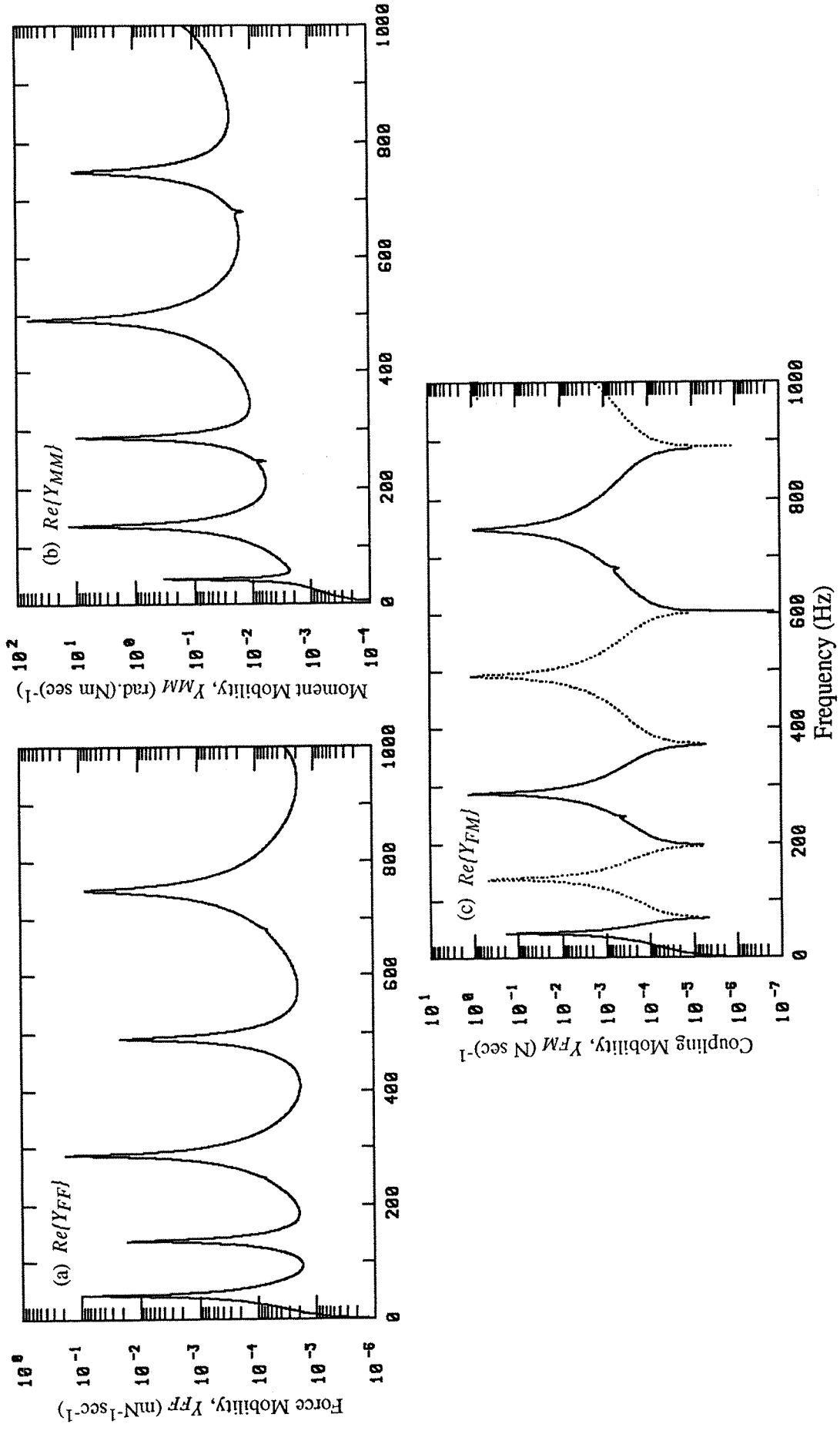

Figure 2.10 : Real parts of the driving point mobility functions for the clamped -simply supported beam : (a): Y_{FF}, (b): Y_{MM} and (c): Y_{FM} ; ——— positive values, ... negative values (force amplitude = 1N, moment arm = 0.02m, loss factor = 0.005).

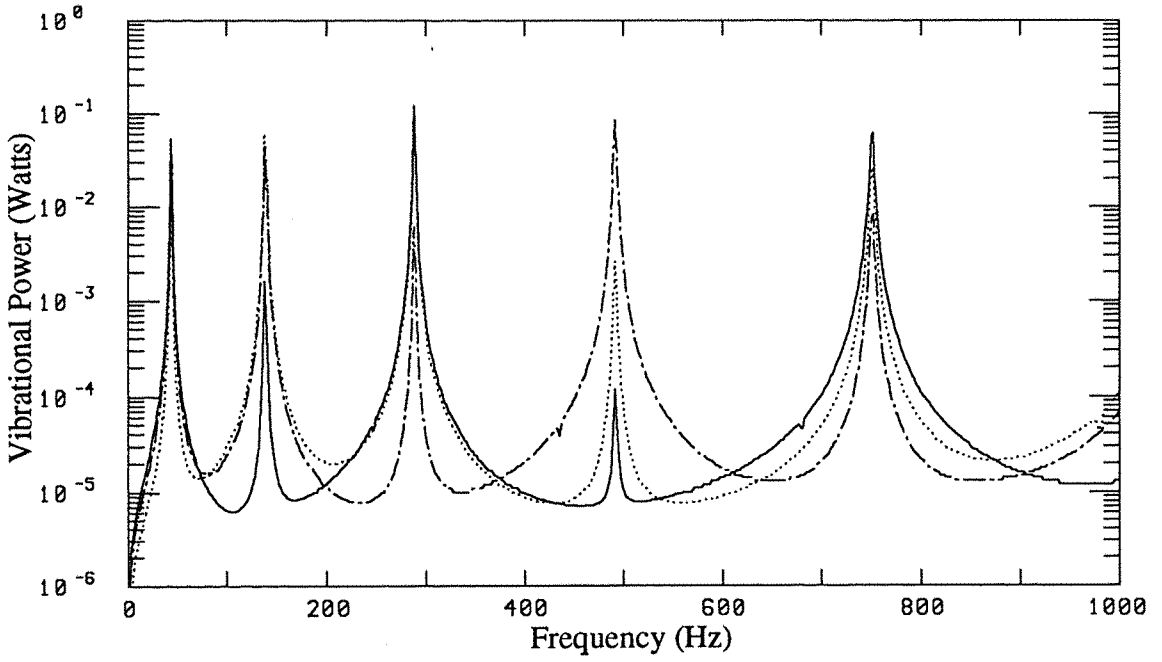

Figure 2.11 : Comparison of P_{total} of the clamped - simply supported beam for various locations of excitation : ——— ℓ/2, ····· ℓ/4 and —·—·— 3ℓ/8 (force amplitude = 1N, moment arm = 0.02m, loss factor = 0.005).

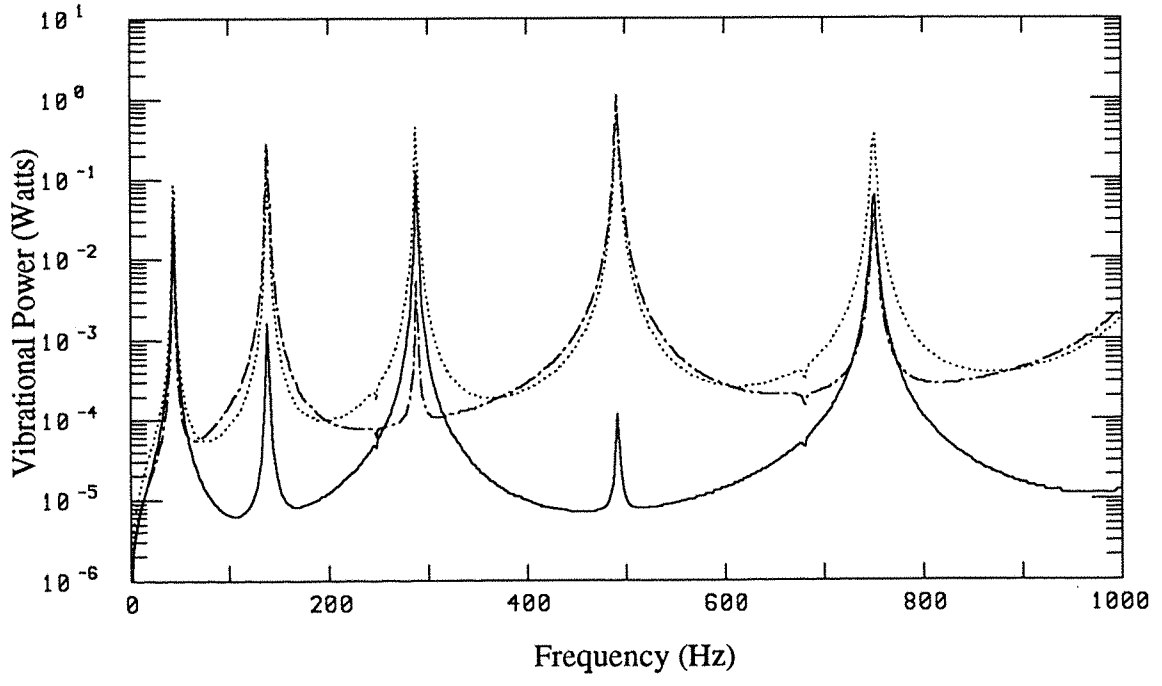

Figure 2.12 : Comparison of P_{total} of the clamped - simply supported beam for various values of moment arm : ——— 0.02m, ····· 0.169m and —·—·— –0.169m (force amplitude = 1N, loss factor = 0.005).

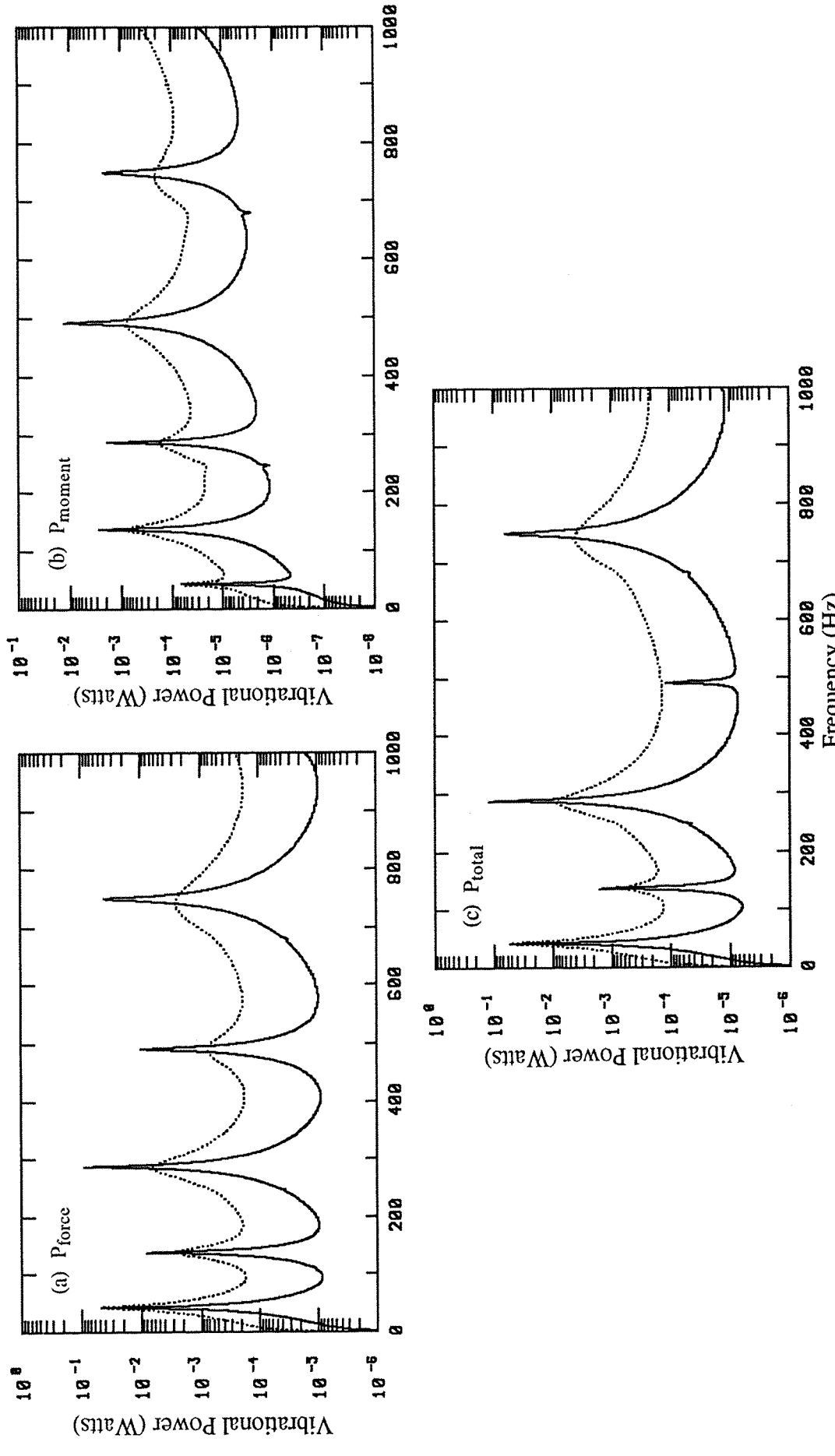

Figure 2.13 : Effects of damping on the vibrational power inputs to the clamped -simply supported beam : (a): P_{force}, (b): P_{moment} and (c): P_{total}; ——— $\eta = 0.005$, ... $\eta = 0.1$ (force amplitude = 1N, moment arm = 0.02m).

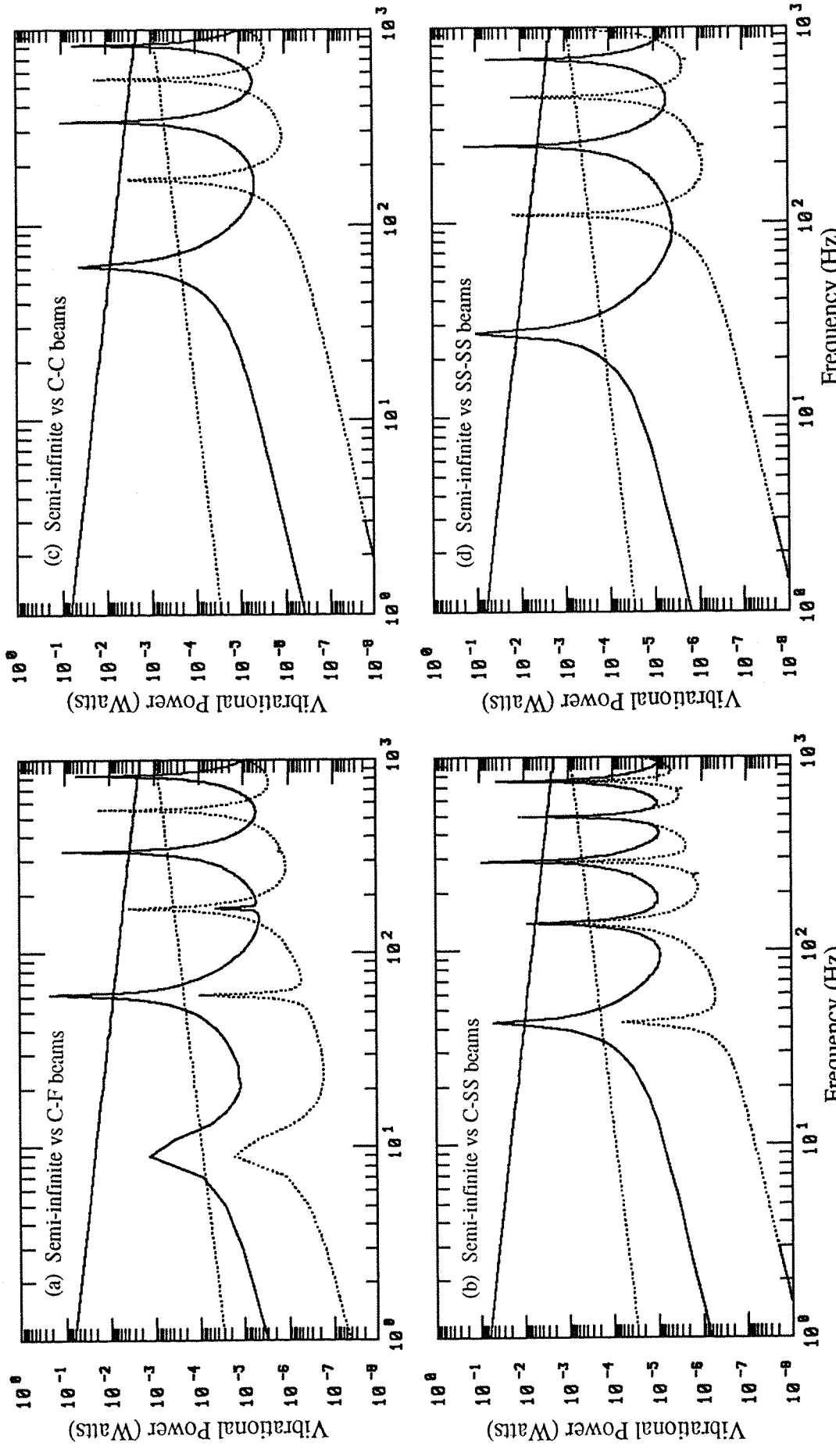

Figure 2.14 : Comparisons of the vibrational power inputs to a semi-infinite beam and finite beams with various boundary conditions : (a) C-F beam, (b): C-SS beam, (c): C-C beam and (d) SS-SS beam; ——— P_{force}, ... P_{moment}, (force amplitude = 1N, moment arm = 0.02m, loss factor = 0.005).

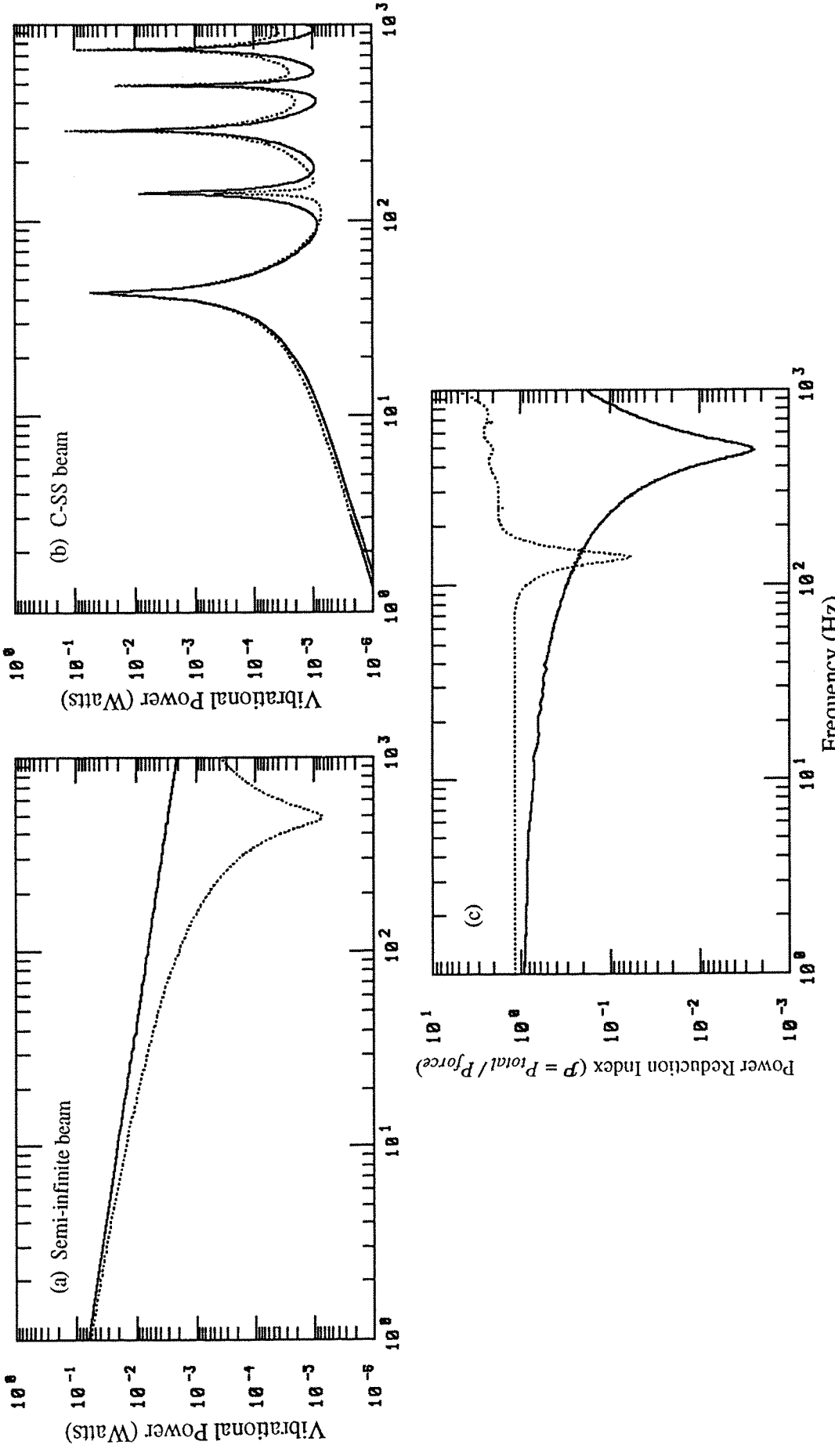

Figure 2.15 : (a) and (b): Comparisons of P_{force} and P_{total} for a semi-infinite beam and a clamped - simply supported beam respectively with moment arm = 0.0438m : ——— P_{force}, ... P_{total}, (force amplitude = 1N, loss factor = 0.005). (c): Comparison of the corresponding power reduction index spectra : ——— semi-infinite beam, ... C-SS beam.

CHAPTER 3

VIBRATIONAL POWER INPUT TO PLATE-LIKE SEATING STRUCTURES

3.1 INTRODUCTION

The use of the unifying term of vibrational power has resulted in some interesting findings concerning the power input to beam-like seating structures subjected to simultaneously acting force and moment excitations [27]. This chapter extends those analyses to flexible plate-like seating structures. Rectangular plates were used to represent flexible seating structures and the study considered only the governing degrees-of-freedom associated with flexural vibration of rectangular plates.

Unlike the theoretical calculation of the undamped natural frequencies and mode shapes of rectangular plates, there are very few publications on the forced response of rectangular plates and virtually no publications on the driving point mobility matrix of rectangular plates, especially for those combinations of simple boundary conditions where exact solutions of the governing equation of motion do not exist.

This chapter begins with the derivation of the driving point force, moment and coupling mobility functions for rectangular plates in flexural vibration and satisfying small deflections and thin plate theory. For rectangular plates with all edges simply supported, (i.e. a SSSS plate), the mobility functions were obtained from the well-known Eigenfunction Expansion Theorem. For rectangular plates with combined clamped, free and simply supported boundary conditions where exact solutions of the governing equation of motion do not exist, the mobility functions were obtained by the Rayleigh - Ritz method.

The driving point mobility functions of a SSSS plate and those of a plate with one edge fully clamped, the opposite edge simply-supported and the other pair of edges free (i.e. a CFSF plate) are presented. The time-averaged vibrational power input to the SSSS plate and the CFSF plate subjected to simultaneously acting sinusoidal force and

moment excitations has also been studied. The cancellation of the vibrational power components resulting from the coupling mobility functions has also been demonstrated for these rectangular plates. The 'CFSF' boundary conditions correspond to the boundary conditions of the model structure used to support an electric motor and in the experimental work reported upon in Chapters 4, 8 and 9.

3.2 TRANSVERSE VIBRATION OF RECTANGULAR PLATES

3.2.1 Classical Theory and Assumptions

Consider a thin rectangular plate acted upon by a lateral load in the Z-direction of $P(x,y)f(t)$ per unit area. The undeformed middle surface of the plate is defined as OXY with the X- and Y-axes parallel to the edges of the plate, the Z-axis is taken as positive downward, as shown in figure 3.1. The length of the edges along the X- and Y-axes are a and b respectively.

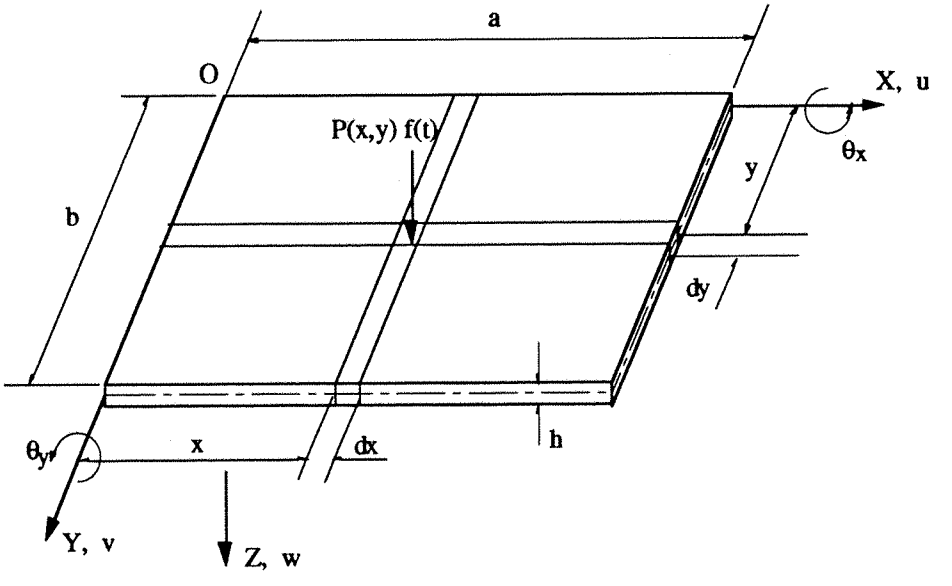

Figure 3.1 : Laterally loaded rectangular plate.

The material of the plate is assumed to be elastic, homogeneous and isotropic. The assumptions for small deformations of thin plates are assumed to be valid for the following analyses. These assumptions which can be found in most of the text books on the vibration of plate structures, such as [26,28], are :

(1) the plate is thin and of uniform thickness h ; thus the free surfaces of the plate are the planes $z = \pm \frac{1}{2} h$.

(2) The direct stress in the transverse direction σ_z is zero. This stress must be zero at the free surfaces, and provided that the plate is thin, it is reasonable to assume that it is zero at any section z.

(3) Stresses in the middle plane of the plate (in-plane or membrane stresses) are neglected, i.e. transverse forces are supported by bending stresses, as in flexure of a beam. For membrane action not to occur, the displacements must be small compared with the thickness of the plate.

(4) Plane sections that are initially normal to the middle plane remain plane and normal to it, which implies that deformation due to transverse shear is neglected. Thus with this assumption the shear strains γ_{xz} and γ_{yz} are zero.

(5) The deflection of the plate is produced by displacement of points of the middle surface normal to its initial plane.

The external and internal forces and the deflection components u,v and w are considered positive when they point toward the positive direction of the co-ordinate axes X,Y and Z. The positive internal moments produce tension in the fibres located below the middle surface of the plate, as used in general engineering practice.

Consider an elemental parallelepiped cut out of the plate, as shown in figure 3.2. The positive internal forces and moments are assigned to the near faces BDHF and CDHG. To satisfy the equilibrium of the element, negative internal forces and moments must act on its far sides: ACGE and ABFE.

The first subscript of the internal forces indicates the direction of the surface-normal relevant to the section on which the force or the moments acts. The element of the plate is subjected to a bending moment M_x, a twisting moment M_{xy} and a transverse shear force S_x per unit length of the middle surface on the face ACGE. On the face ABFE, there are a bending moment M_y, a twisting moment M_{yx} and a shear force S_y (per unit length).

The bending moments M_x and M_y are the resultant moments due to the direct stresses σ_x and σ_y, respectively, after integrating through the thickness of the plate. Similarly, the twisting moments M_{xy} and M_{yx} are the resultant moments due to the shear stresses τ_{xy} and τ_{yx} respectively (for equilibrium, $\tau_{xy} = \tau_{yx}$), and the transverse shear forces

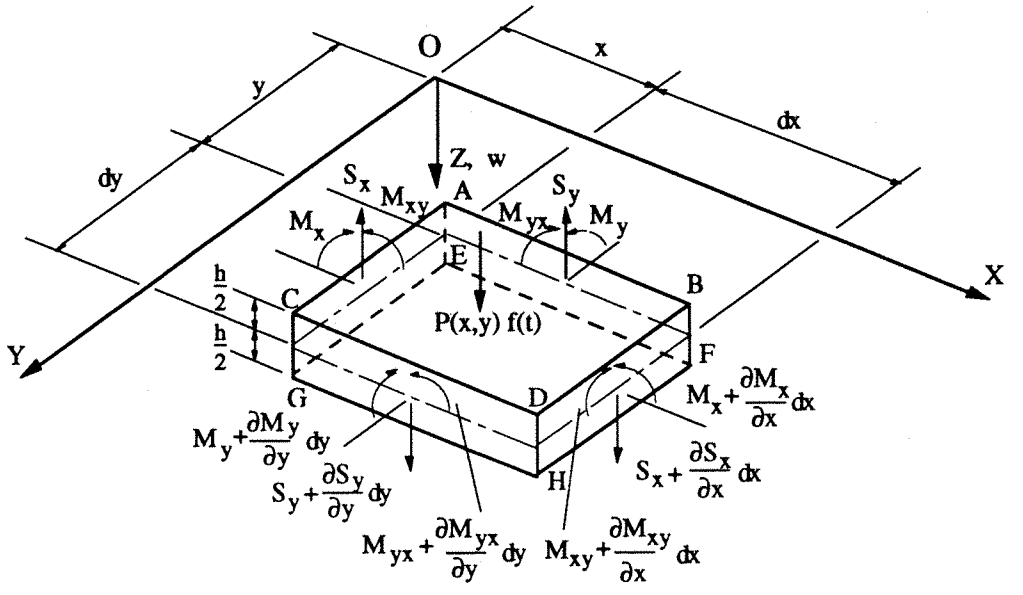

Figure 3.2 : Forces and moments acting on a plate element in flexure.

S_x and S_y are resultant forces due to the transverse shear stresses τ_{xz} and τ_{yz} respectively. These internal moments are :

$$M_x = \int_{-h/2}^{h/2} \sigma_x \, z \, dz \tag{3.1}$$

$$M_y = \int_{-h/2}^{h/2} \sigma_y \, z \, dz \tag{3.2}$$

$$M_{xy} = M_{yx} = \int_{-h/2}^{h/2} \tau_{xy} \, z \, dz \tag{3.3}$$

The internal forces and moments with incremental quantities (in the form of a truncated Taylor's series) are shown in figure 3.2 acting on the faces of BDHF and CDHG. In addition to these internal forces and moments and the lateral load *P(x,y)f(t)* per unit area, there is an inertia force per unit area, $\rho h \frac{\partial^2 w}{\partial t^2}$ in the Z-direction.

3.2.2 Equation of Motion and Boundary Conditions

Consider the external forces and the internal forces and moments acting on the plate element as shown in figure 3.2, the equilibrium equations of the plate element can be obtained by resolving the forces in the Z-direction and taking moments about the Y- and X-axes. After some manipulation, one obtains:

$$\frac{\partial^2 M_x}{\partial x^2} + 2\,\frac{\partial^2 M_{xy}}{\partial x \partial y} + \frac{\partial^2 M_y}{\partial y^2} + P(x,y)f(t) = \rho h \frac{\partial^2 w}{\partial t^2} \tag{3.4}$$

From the generalised Hooke's Law, the stress and strain relations for the plate element are :

$$\sigma_x = \frac{E}{1-\nu^2}\,(\varepsilon_x + \nu\,\varepsilon_y) \tag{3.5}$$

$$\sigma_y = \frac{E}{1-\nu^2}\,(\varepsilon_y + \nu\,\varepsilon_x) \tag{3.6}$$

$$\tau_{xy} = \tau_{yx} = G\,\gamma_{xy} = \frac{E}{2(1+\nu)}\,\gamma_{xy} \tag{3.7}$$

In these equations, E, G and ν are the elastic constants: Young's modulus, shear modulus and Poisson's ratio respectively of the plate material.

By considering the geometry of a deflected plate section for small displacements, one obtains the following strain - displacement relations [26,28]:

$$\varepsilon_x = -\,z\,\frac{\partial^2 w}{\partial x^2} \tag{3.8}$$

$$\varepsilon_y = -\,z\,\frac{\partial^2 w}{\partial y^2} \tag{3.9}$$

$$\gamma_{xy} = -\,2\,z\,\frac{\partial^2 w}{\partial x \partial y} \tag{3.10}$$

From the above stress - strain and the strain - displacement relations and after subsitituting these relations in eqns (3.1) to (3.3) and integrating with respect to z, one obtains the following relations between the internal moments and the z-displacement :

$$M_x = -\,D\left(\frac{\partial^2 w}{\partial x^2} + \nu\frac{\partial^2 w}{\partial y^2}\right) \tag{3.11}$$

$$M_y = -D\left(\frac{\partial^2 w}{\partial y^2} + \nu\frac{\partial^2 w}{\partial x^2}\right) \tag{3.12}$$

$$M_{xy} = -D(1-\nu)\frac{\partial^2 w}{\partial x \partial y} \tag{3.13}$$

where $D = \dfrac{E h^3}{12(1-\nu^2)}$ represents the bending or flexural rigidity of the plate.

Substituting of eqns (3.11), (3.12) and (3.13) into eqn (3.4) yields the governing differential equation for the forced transverse vibration of the plate :

$$D\left[\frac{\partial^4 w}{\partial x^4} + 2\frac{\partial^4 w}{\partial x^2 \partial y^2} + \frac{\partial^4 w}{\partial y^4}\right] + \rho h\frac{\partial^2 w}{\partial t^2} = P(x,y)f(t) \tag{3.14}$$

An exact solution for transverse vibration of a rectangular plate must simultaneously satisfy the above differential equation and the prescribed boundary conditions of the plate. The standard simple boundary conditions consist of simply supported, clamped and free conditions. Consider the edge of the plate along $x=0$, the expressions for these boundary conditions are :

(1) simply supported :
$$\left.\begin{aligned}(w)_{x=0} &= 0\\ (M_x)_{x=0} &= 0\end{aligned}\right\} \tag{3.15}$$

(2) clamped :
$$\left.\begin{aligned}(w)_{x=0} &= 0\\ \left(\frac{\partial w}{\partial x}\right)_{x=0} &= 0\end{aligned}\right\} \tag{3.16}$$

(3) free :
$$\left.\begin{aligned}(M_x)_{x=0} &= 0\\ (Q_x)_{x=0} &= 0\end{aligned}\right\} \tag{3.17}$$

where Q_x is the effective shear force which is a combination of the torsional moment M_{xy} and the transverse shear force S_x [26,28]. The expressions for the boundary conditions along the $x=a$ edge are obtained by simply replacing $x=0$ by $x=a$. Those along the $y=0$ and $y=b$ edges are obtained by interchanging x by y.

3.2.3 Forced Response of Finite Systems

In general, the forced response of finite systems whose eigenfunctions satisfy the orthogonality relationship can be obtained from the well known Eigenfunction Expansion Theorem [24], which states that *the response of a system to any arbitrary*

excitation can be expressed in terms of the system's eigenfunctions and eigenfrequencies. Thus, for a damped system subjected to a sinusoidal force excitation of $P(x,y)\sin\omega t$ per unit area, the velocity amplitude function $\dot{w}(x,y)$ can be shown to be [24] :

$$\dot{w}(x,y) = \sum_{\Lambda=1}^{\infty} \frac{\psi_\Lambda(x,y)}{\left[\omega_\Lambda^2 (1+j\eta) - \omega^2\right] \xi_\Lambda} \int_A j\omega P(x,y)\, \psi_\Lambda(x,y)\, dxdy \qquad (3.18)$$

and $$\xi_\Lambda = \int_A \mu\, \psi_\Lambda^2(x,y)\, dxdy$$

where $\psi_\Lambda(x,y)$ are the eigenfunctions of the system satisfying the free vibration differential equation and the prescribed boundary conditions, ω_Λ are the eigenfrequencies or the undamped natural frequencies of the system, η is the loss factor which characterises the damping of the system, ω is the excitation frequency (in radians per sec), μ is the mass per unit area and A is the entire area of the system.

For a practical system, damping may arise from internal dissipation of energy (i.e. hysteretic losses), from losses resulting from structural joints and boundaries and from external dissipation to the surrounding fluid media. For simplicity, only the hysteretic losses are considered in this study. Hence, η is introduced through the complex Modulus of Elasticity of the material. This hysteretic loss factor is defined as the ratio of the imaginary part to the real part of the complex modulus, which in general, is assumed to be constant for all flexural modes.

3.3 DRIVING POINT MOBILITY MATRIX OF RECTANGULAR PLATES

3.3.1 General Expressions for Driving Point Mobility Matrix

The driving point mobility matrix *[Y]* of a system relates the applied excitations to the system and the resulting velocity responses at the excitation point. For transverse vibration of rectangular plates, the three degrees of freedom are the lateral displacement, w, and the angular rotations about the X- and Y-axes, denoted by θ_x and θ_y respectively. These angular rotations are positive if they rotate about the positive X- and Y-axes. The three possible types of excitation are the lateral force $F(t)$, and the moments about the X- and Y- axes, $M_x(t)$ and $M_y(t)$ respectively. The relationship between these excitations and the resulting velocity responses : $\dot{w}$, $\dot{\theta}_x$ and $\dot{\theta}_y$ can be written as :

$$\begin{Bmatrix} \dot{w} \\ \dot{\theta}_x \\ \dot{\theta}_y \end{Bmatrix} = \begin{bmatrix} Y_{11} & Y_{12} & Y_{13} \\ Y_{21} & Y_{22} & Y_{23} \\ Y_{31} & Y_{32} & Y_{33} \end{bmatrix} \begin{Bmatrix} F \\ M_x \\ M_y \end{Bmatrix} \tag{3.19}$$

where $[Y] = \begin{bmatrix} Y_{11} & Y_{12} & Y_{13} \\ Y_{21} & Y_{22} & Y_{23} \\ Y_{31} & Y_{32} & Y_{33} \end{bmatrix}$ is the driving point mobility matrix of the plate.

For a thin rectangular plate bounded by four edges : $x=0$, $x=a$, $y=0$ and $y=b$ and of uniform thickness h, density ρ, the transverse velocity amplitude function, due to a sinusoidal lateral load of $P(x,y)\sin\omega t$ can be written (from eqn (3.18)) as:

$$\dot{w}(x,y) = \sum_{\Lambda=1}^{\infty} \frac{\psi_\Lambda(x,y)}{[\omega_\Lambda^2 (1+j\eta) - \omega^2]\,\xi_\Lambda} \int_0^a \int_0^b j\omega\, P(x,y)\, \psi_\Lambda(x,y)\, dxdy \tag{3.20}$$

and $$\xi_\Lambda = \int_0^a \int_0^b \rho\, h\, \psi_\Lambda^2(x,y)\, dxdy$$

For the case of a point force with force amplitude F acting at location $x = x_0$ and $y = y_0$, the forcing function can be written as :

$$P(x,y)\sin\omega t = F\, \delta(x-x_0)\, \delta(y-y_0)\sin\omega t \tag{3.21}$$

where $$\delta(x-x_0) = \begin{cases} 0 & \text{if } x \neq x_0 \\ 1 & \text{if } x = x_0 \end{cases}$$

is the Dirac delta function [26,29].

The velocity amplitude function at any point on the plate is thus :

$$\dot{w}(x,y) = j\omega F \sum_{\Lambda=1}^{\infty} \frac{\psi_\Lambda(x,y)}{[\omega_\Lambda^2 (1+j\eta) - \omega^2]\,\xi_\Lambda} \psi_\Lambda(x_0,y_0) \tag{3.22}$$

At the excitation point, the velocity response is obtained by substituting the co-ordinates of the point into the above equation. One thus obtains the driving point force mobility function :

$$Y_{11} = \frac{\dot{w}(x_0,y_0)}{F} = j\omega \sum_{\Lambda=1}^{\infty} \frac{\psi_\Lambda^2(x_0,y_0)}{[\omega_\Lambda^2 (1+j\eta) - \omega^2] \xi_\Lambda} \tag{3.23}$$

In the co-ordinate system for the rectangular plate as shown in figure 3.1, the angular rotations are defined as :

$$\theta_x = \frac{\partial w}{\partial y} \tag{3.24}$$

$$\theta_y = -\frac{\partial w}{\partial x} \tag{3.25}$$

Thus from the general velocity response expression, eqn (3.22), and the above equations, one obtains the driving point coupling mobility functions between rotational degrees-of-freedom and the applied force :

$$Y_{21} = \frac{\dot{\theta}_x(x_0,y_0)}{F} = j\omega \sum_{\Lambda=1}^{\infty} \frac{\left[\frac{\partial}{\partial y} \psi_\Lambda(x,y)\right]_{x_0\, y_0}}{[\omega_\Lambda^2 (1+j\eta) - \omega^2] \xi_\Lambda} \psi_\Lambda(x_0,y_0) \tag{3.26}$$

$$Y_{31} = \frac{\dot{\theta}_y(x_0,y_0)}{F} = -j\omega \sum_{\Lambda=1}^{\infty} \frac{\left[\frac{\partial}{\partial x} \psi_\Lambda(x,y)\right]_{x_0\, y_0}}{[\omega_\Lambda^2 (1+j\eta) - \omega^2] \xi_\Lambda} \psi_\Lambda(x_0,y_0) \tag{3.27}$$

For moment excitation on the plate, the approach used by Cremer, Heckl and Ungar [24] by considering the plate as being excited by two equal and opposite point forces, F and $-F$, applied at two neighbouring points of distance $2\,\varepsilon$ apart where ε is a sufficiently small quantity was adopted. Thus, the resulting moment is $M = 2\,\varepsilon F$ and the resultant force vanishes.

Hence, for moment excitation, M_x applied at location (x_0, y_0) is replaced by two equal and opposite point forces, F and $-F$ applied at $(x_0, y_0+\varepsilon)$ and $(x_0, y_0-\varepsilon)$ respectively. Similarly, for moment excitation M_y at location (x_0, y_0), the locations for the two point forces, F and $-F$, are $(x_0-\varepsilon, y_0)$ and $(x_0+\varepsilon, y_0)$, as shown in figure 3.3.

The transverse velocity response of the plate subjected to moment excitations can then be obtained by summing the responses due to the exciting forces based on the superposition theorem for linear systems.

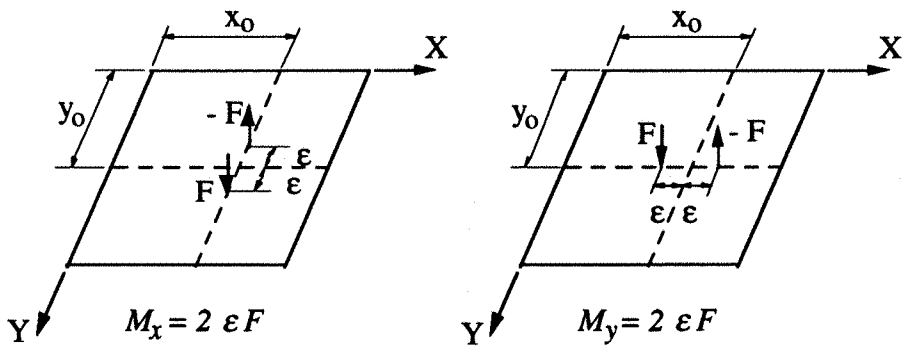

Figure 3.3 : Representations of moment excitations.

Thus for M_x acting at location (x_0, y_0) and from eqn (3.22), one obtains :

$$\dot{w}(x_0,y_0) = j\omega F \sum_{\Lambda=1}^{\infty} \frac{\psi_\Lambda(x_0,y_0)}{[\omega_\Lambda^2 (1+j\eta) - \omega^2]\,\xi_\Lambda} [\psi_\Lambda(x_0,y_0+\varepsilon) - \psi_\Lambda(x_0,y_0-\varepsilon)] \quad (3.28)$$

For the rotational degrees-of-freedom, one obtains :

$$\dot{\theta}_x(x_0,y_0) = j\omega F \sum_{\Lambda=1}^{\infty} \frac{\left[\frac{\partial}{\partial y}\psi_\Lambda(x,y)\right]_{x_0\,y_0}}{[\omega_\Lambda^2 (1+j\eta) - \omega^2]\,\xi_\Lambda} [\psi_\Lambda(x_0,y_0+\varepsilon) - \psi_\Lambda(x_0,y_0-\varepsilon)] \quad (3.29)$$

$$\dot{\theta}_y(x_0,y_0) = -j\omega F \sum_{\Lambda=1}^{\infty} \frac{\left[\frac{\partial}{\partial x}\psi_\Lambda(x,y)\right]_{x_0\,y_0}}{[\omega_\Lambda^2 (1+j\eta) - \omega^2]\,\xi_\Lambda} [\psi_\Lambda(x_0,y_0+\varepsilon) - \psi_\Lambda(x_0,y_0-\varepsilon)] \quad (3.30)$$

By the same analogy, for moment excitation, M_y at location (x_0, y_0), the required velocity and angular velocity responses can be obtained by simply replacing the locations of the exciting forces in the above expressions from $(x_0, y_0+\varepsilon)$ to $(x_0-\varepsilon, y_0)$ and $(x_0, y_0-\varepsilon)$ to $(x_0+\varepsilon, y_0)$.

3.3.2 Driving Point Mobility Matrix of a Rectangular Plate with All Edges Simply-supported

For a thin rectangular plate with all edges simply supported, the eigenfunctions satisfying the boundary conditions, eqn (3.15), and the homogeneous differential equation of the plate can be written as [24,26,28] :

$$\psi_{m,n}(x,y) = \sin\frac{m\pi x}{a} \sin\frac{n\pi y}{b} \quad (3.31)$$

where m,n are integers which range from 1 to ∞. The eigenfrequencies are :

$$\omega_{m,n} = \sqrt{\frac{D}{\rho h}} \left[\left(\frac{m\pi}{a}\right)^2 + \left(\frac{n\pi}{b}\right)^2 \right] \tag{3.32}$$

The driving point force mobility function of the plate is obtained from eqns (3.23) and (3.31) with the integer Λ replaced by m and n, and $\xi_{m,n}$ replaced by $\frac{1}{4}\rho h a b$.

$$Y_{11} = \frac{\dot{w}(x_0,y_0)}{F} = \frac{4j\omega}{\rho hab} \sum_{m=1}^{\infty} \sum_{n=1}^{\infty} \frac{\sin^2 \frac{m\pi x_0}{a} \sin^2 \frac{n\pi y_0}{b}}{\left[\omega_{mn}^2 (1+j\eta) - \omega^2\right]} \tag{3.33}$$

From eqns (3.26) and (3.27), after the differentiation and manipulation, one obtains the driving point coupling mobility functions :

$$Y_{21} = \frac{\dot{\theta}_x(x_0,y_0)}{F} = \frac{4j\omega\pi}{\rho hab^2} \sum_{m=1}^{\infty} \sum_{n=1}^{\infty} \frac{n \sin^2 \frac{m\pi x_0}{a} \sin\frac{n\pi y_0}{b} \cos\frac{n\pi y_0}{b}}{\left[\omega_{mn}^2 (1+j\eta) - \omega^2\right]} \tag{3.34}$$

$$Y_{31} = \frac{\dot{\theta}_y(x_0,y_0)}{F} = -\frac{4j\omega\pi}{\rho ha^2 b} \sum_{m=1}^{\infty} \sum_{n=1}^{\infty} \frac{m \sin\frac{m\pi x_0}{a} \cos\frac{m\pi x_0}{a} \sin^2 \frac{n\pi y_0}{b}}{\left[\omega_{mn}^2 (1+j\eta) - \omega^2\right]} \tag{3.35}$$

For moment mobility functions, if one uses the small angle approximation (i.e. $\sin\theta \approx \theta$ if θ is small), it can be shown that :

$$\psi_\Lambda(x_0,y_0+\varepsilon) - \psi_\Lambda(x_0,y_0-\varepsilon) \approx 2 \frac{n\pi\varepsilon}{b} \sin\frac{m\pi x_0}{a} \cos\frac{n\pi y_0}{b} \tag{3.36}$$

$$\psi_\Lambda(x_0-\varepsilon,y_0) - \psi_\Lambda(x_0+\varepsilon,y_0) \approx -2 \frac{m\pi\varepsilon}{a} \cos\frac{m\pi x_0}{a} \sin\frac{n\pi y_0}{b} \tag{3.37}$$

Hence, from eqns (3.28), (3.29), (3.30), (3.36) and (3.37), one obtains :

$$Y_{12} = \frac{\dot{w}(x_0,y_0)}{M_x} = \frac{4j\omega\pi}{\rho hab^2} \sum_{m=1}^{\infty} \sum_{n=1}^{\infty} \frac{n \sin^2 \frac{m\pi x_0}{a} \sin\frac{n\pi y_0}{b} \cos\frac{n\pi y_0}{b}}{\left[\omega_{mn}^2 (1+j\eta) - \omega^2\right]}$$

$$= Y_{21} \tag{3.38}$$

$$Y_{22} = \frac{\dot{\theta}_x(x_0,y_0)}{M_x} = \frac{4j\omega\pi^2}{\rho h a b^3} \sum_{m=1}^{\infty}\sum_{n=1}^{\infty} \frac{n^2 \sin^2\frac{m\pi x_0}{a} \cos^2\frac{n\pi y_0}{b}}{[\omega_{mn}^2(1+j\eta) - \omega^2]} \tag{3.39}$$

$$Y_{32} = \frac{\dot{\theta}_y(x_0,y_0)}{M_x} = -\frac{4j\omega\pi^2}{\rho h a^2 b^2} \sum_{m=1}^{\infty}\sum_{n=1}^{\infty} \frac{m\,n \sin\frac{m\pi x_0}{a} \cos\frac{m\pi x_0}{a} \sin\frac{n\pi y_0}{b} \cos\frac{n\pi y_0}{b}}{[\omega_{mn}^2(1+j\eta) - \omega^2]} \tag{3.40}$$

Similarly, for M_y excitation, one obtains :

$$Y_{13} = \frac{\dot{w}(x_0,y_0)}{M_y} = -\frac{4j\omega\pi}{\rho h a^2 b} \sum_{m=1}^{\infty}\sum_{n=1}^{\infty} \frac{m \sin\frac{m\pi x_0}{a} \cos\frac{m\pi x_0}{a} \sin^2\frac{n\pi y_0}{b}}{[\omega_{mn}^2(1+j\eta) - \omega^2]}$$

$$= Y_{31} \tag{3.41}$$

$$Y_{23} = \frac{\dot{\theta}_x(x_0,y_0)}{M_y} = -\frac{4j\omega\pi^2}{\rho h a^2 b^2} \sum_{m=1}^{\infty}\sum_{n=1}^{\infty} \frac{m\,n \sin\frac{m\pi x_0}{a} \cos\frac{m\pi x_0}{a} \sin\frac{n\pi y_0}{b} \cos\frac{n\pi y_0}{b}}{[\omega_{mn}^2(1+j\eta) - \omega^2]}$$

$$= Y_{32} \tag{3.42}$$

$$Y_{33} = \frac{\dot{\theta}_y(x_0,y_0)}{M_y} = \frac{4j\omega\pi^2}{\rho h a^3 b} \sum_{m=1}^{\infty}\sum_{n=1}^{\infty} \frac{m^2 \cos^2\frac{m\pi x_0}{a} \sin^2\frac{n\pi y_0}{b}}{[\omega_{mn}^2(1+j\eta) - \omega^2]} \tag{3.43}$$

Hence, the driving point mobility matrix *[Y]* of a rectangular plate with all edges simply supported is a symmetric matrix.

3.3.3 Driving Point Mobility Matrix of a Rectangular Plate with Simple Boundary Conditions where Exact Solutions Do Not Exist

It is well known that for transverse vibrations of thin rectangular plates, exact solutions to the differential equation can be obtained only if one pair of opposite edges are simply supported, which includes the case of all edges simply supported as considered in the previous section. For other boundary conditions approximate methods of solution must be adopted. A brief description and comparison of nine approximate analytical methods for the solution of plate bending problems was given by Leissa, Clausen, Hulbert and Hopper [30].

In the following analysis of the driving point mobility matrix of rectangular plates with combined clamped, free and simply supported boundary conditions where exact

solutions of the governing equation of motion do not exist, the Rayleigh - Ritz method similar to the approach used by Warburton [26,29] was adopted.

a. The Rayleigh - Ritz Method

Consider a rectangular plate whose geometry is as shown in figure 3.1. The transverse displacement of the plate is assumed to be expressed by the following finite series :

$$w(x,y,t) = \sum_{m=1}^{M} \sum_{n=1}^{N} X_m(x)\, Y_n(y)\, \zeta_{mn}(t) \tag{3.44}$$

where $X_m(x)$ and $Y_n(y)$ are known as assumed functions which, respectively, are functions of x and y co-ordinates only, and $\zeta_{mn}(t)$ are arbitrary functions which are assumed to be harmonic for calculation of natural frequencies and response to sinusoidal forced excitation.

For the Rayleigh - Ritz method, each assumed function $X_m(x)$ must satisfy all geometric boundary conditions at the edges $x=0$ and $x=a$; each function $Y_n(y)$ must satisfy the geometric boundary conditions at the edges $y=0$ and $y=b$. In the following analyses, these assumed functions are approximated by the characteristic beam functions with boundary conditions similar to those of the plate. The characteristic beam functions for various boundary conditions can be found in [31].

For a CFSF plate, the boundaries are rigidly clamped along the edge $x=0$, simply supported along the edge $x=a$, and free along both edges $y=0$ and $y=b$. Hence, $X_m(x)$ are the characteristic functions of a clamped - simply supported beam of length a, and $Y_n(y)$ are the characteristic functions of a free - free beam of length b. These characteristic beam functions are expressed in the following general forms :

$$X_m(x) = B_{1m}e^{jk_{xm}x} + B_{2m}e^{-jk_{xm}x} + B_{3m}e^{k_{xm}x} + B_{4m}e^{-k_{xm}x} \tag{3.45}$$

$$Y_n(y) = C_{1n}e^{jk_{yn}y} + C_{2n}e^{-jk_{yn}y} + C_{3n}e^{k_{yn}y} + C_{4n}e^{-k_{yn}y} \tag{3.46}$$

where $k_{xm} = \sqrt[4]{\frac{\omega_{xm}^2\, \rho\, A}{E\, I}}$ are the flexural wavenumbers, ω_{xm} are the undamped natural frequencies (in radians per sec) associated with the beam functions in the X-direction, and B_{1m}, B_{2m} ... etc. are coefficients whose values depend on the boundary conditions. Similar definitions are defined for k_{yn}, ω_{yn} and C_{1n}, C_{2n} ... etc.

The integers, m and n, denote the mode numbers of the beam functions in the X- and Y-directions respectively.

The characteristic beam functions used have the following orthogonal and normalised properties :

$$\int_0^a X_m(x)\, X_r(x)\, dx = \begin{cases} 0 & \text{if } m \neq r \\ a & \text{if } m = r \end{cases} \tag{3.47}$$

$$\int_0^b Y_n(y)\, Y_s(y)\, dy = \begin{cases} 0 & \text{if } n \neq s \\ b & \text{if } n = s \end{cases} \tag{3.48}$$

The strain energy, U, and the kinetic energy, T, expressions for the plate in flexure are [26,29]:

$$U = \frac{D}{2} \int_0^a \int_0^b \left[\left(\frac{\partial^2 w}{\partial x^2} \right)^2 + \left(\frac{\partial^2 w}{\partial y^2} \right)^2 + 2\nu \left(\frac{\partial^2 w}{\partial x^2} \right)\left(\frac{\partial^2 w}{\partial y^2} \right) + 2(1-\nu) \left(\frac{\partial^2 w}{\partial x \partial y} \right)^2 \right] dy\, dx \tag{3.49}$$

$$T = \frac{1}{2} \rho h \int_0^a \int_0^b \left(\frac{\partial w}{\partial t} \right)^2 dy\, dx \tag{3.50}$$

Following Warburton's approach, i.e. by substituting the transverse displacement function, eqn (3.44) into the above energy expressions and applying the Lagrange equation with respect to the functions ζ_{mn}, one obtains the following set of simultaneously linear equations for the plate subjected to sinusoidal force excitation :

$$[\chi_{rsmn}]\, \{\zeta_{mn}\} = \{Q_{rs}\} \tag{3.51}$$

where $[\chi_{rsmn}] = [\, [K] - \omega^2 [M] + j\, \eta\, [K]\,]$ is a MN by MN matrix ($r=1,...,M$; $s=1,...,N$; $m=1,...,M$ *and* $n=1,...,N$) representing the dynamic properties of the plate, in which, $[K]$ is the stiffness matrix, $[M]$ is the mass matrix, η is the hysteretic loss factor, and ω is the excitation frequency (in radians per sec); $\{\zeta_{mn}\}$ is a MN by 1 function vector whose values are to be determined and $\{Q_{rs}\}$ is a MN by 1 generalised force vector. A typical term of the generalised force vector is :

$$Q_{rs} = \int_0^a \int_0^b P(x,y)\, f(t)\, X_r(x)\, Y_s(y)\, dy\, dx \tag{3.52}$$

For a uniform plate of constant thickness, the expression for the elements of the mass matrix is :

$$M_{rsmn} = \rho h \int_0^a X_r X_m \, dx \int_0^b Y_s Y_n \, dy \tag{3.53}$$

The stiffness matrix obtained from the strain energy expression is more complicated with the diagonal terms ($r = m, s = n$) given by :

$$K_{mnmn} = D \Big[b k_{xm}^4 J_{mm} + a k_{yn}^4 J_{nn} + 2 \nu k_{xm}^2 k_{yn}^2 JJ_{mm} JJ_{nn} + 2 (1-\nu) k_{xm}^2 k_{yn}^2 JJJ_{mm} JJJ_{nn} \Big] \tag{3.54}$$

and the off-diagonal terms ($r \neq m, s \neq n$) are :

$$K_{rsmn} = D \Big[\nu \left(k_{xr}^2 k_{yn}^2 JJ_{rm} JJ_{ns} + k_{xm}^2 k_{ys}^2 JJ_{mr} JJ_{sn} \right) + 2 (1-\nu) k_{xr} k_{xm} k_{ys} k_{yn} JJJ_{rm} JJJ_{sn} \Big] \tag{3.55}$$

where

$$J_{mm} = \int_0^a {}_2X_m \; {}_2X_m \; dx \tag{3.56}$$

$$JJ_{mr} = \int_0^a {}_2X_m \; X_r \; dx \tag{3.57}$$

$$JJJ_{mr} = \int_0^a {}_1X_m \; {}_1X_r \; dx \tag{3.58}$$

$${}_1X_m(x) = j B_{1m} e^{jk_{xm}x} - j B_{2m} e^{-jk_{xm}x} + B_{3m} e^{k_{xm}x} - B_{4m} e^{-k_{xm}x} \tag{3.59}$$

$${}_2X_m(x) = -B_{1m} e^{jk_{xm}x} - B_{2m} e^{-jk_{xm}x} + B_{3m} e^{k_{xm}x} + B_{4m} e^{-k_{xm}x} \tag{3.60}$$

J_{nn}, JJ_{ns} and JJJ_{ns} are obtained from the expressions for J_{mm}, JJ_{mr} and JJJ_{mr} respectively by replacing X, x, a, m and r by Y, y, b, n and s, respectively. A typical expression for the above definite integrals is given in Appendix B.

For any excitation frequency ω, the transverse displacement function of the plate is obtained by solving the set of simultaneously linear equations (eqn (3.51)) for the unknown functions ζ_{mn}, and substituting these functions in eqn (3.44).

b. The 'Rigid-Body' Beam Functions

In addition to the free - free beam functions in the Y-direction, two additional 'rigid-body' beam functions were used as the assumed functions. These beam functions are the translational and the rotational beam deflections with no curvature. The expressions used were the normalised forms as given in [32] :

Translational 'rigid-body' beam function : $Y_{-1}(y) = 1$ (3.61)

Rotational 'rigid -body' beam function : $Y_{-2}(y) = \frac{2\sqrt{3}}{b}\left(y - \frac{b}{2}\right)$ (3.62)

The expressions for the definite integrals involving these 'rigid-body' beam functions and the flexural beam functions are given in Appendix C.

c. The Driving Point Mobility Matrix

For a thin rectangular plate subjected to a point sinusoidal force of amplitude F acting at location $x = x_0$ and $y = y_0$, the amplitude of the generalised force reduces to:

$$Q_{rs} = F\, X_r(x_0)\, Y_s(y_0) \tag{3.63}$$

The solution to eqn (3.51) can be expressed in matrix form as :

$$\{\zeta_{mn}\} = [\lambda_{mnrs}]\,\{Q_{rs}\} \tag{3.64}$$

where $[\lambda_{mnrs}] = [\chi_{rsmn}]^{-1}$ is the inverse of matrix $[\chi_{rsmn}]$.

or $$\zeta_{mn} = F \sum_{r=1}^{M} \sum_{s=1}^{N} \lambda_{mnrs}\, X_r(x_0)\, Y_s(y_0) \qquad \text{for } m = 1,2...M;\ n = 1,2...N \tag{3.65}$$

The transverse displacement response at any point on the plate is thus :

$$w(x,y) = F \sum_{m=1}^{M} \sum_{n=1}^{N} \sum_{r=1}^{M} \sum_{s=1}^{N} \lambda_{mnrs}\, X_r(x_0)\, Y_s(y_0)\, X_m(x)\, Y_n(y) \tag{3.66}$$

Following the same procedures used for the SSSS plate, the driving point mobility functions are :

$$Y_{11} = \frac{\dot{w}(x_0,y_0)}{F} = j\omega \sum_{m=1}^{M}\sum_{n=1}^{N}\sum_{r=1}^{M}\sum_{s=1}^{N} \lambda_{mnrs} X_r(x_0) Y_s(y_0) X_m(x_0) Y_n(y_0) \tag{3.67}$$

$$Y_{21} = \frac{\dot{\theta}_x(x_0,y_0)}{F} = j\omega \sum_{m=1}^{M}\sum_{n=1}^{N}\sum_{r=1}^{M}\sum_{s=1}^{N} \lambda_{mnrs} X_r(x_0) Y_s(y_0) X_m(x_0) \left(\frac{dY_n}{dy}\right)_{y_0} \tag{3.68}$$

$$Y_{31} = \frac{\dot{\theta}_y(x_0,y_0)}{F} = -j\omega \sum_{m=1}^{M}\sum_{n=1}^{N}\sum_{r=1}^{M}\sum_{s=1}^{N} \lambda_{mnrs} X_r(x_0) Y_s(y_0) \left(\frac{dX_m}{dx}\right)_{x_0} Y_n(y_0) \tag{3.69}$$

For moment excitations, the responses due to two closely spaced equal and opposite point forces are superimposed as was done in the case of a SSSS plate, thus

$$Y_{12} = \frac{\dot{w}(x_0,y_0)}{M_x} = \frac{j\omega}{2\varepsilon} \sum_{m=1}^{M}\sum_{n=1}^{N}\sum_{r=1}^{M}\sum_{s=1}^{N} \lambda_{mnrs} X_r(x_0)\left[Y_s(y_0+\varepsilon) - Y_s(y_0-\varepsilon)\right] X_m(x_0) Y_n(y_0) \tag{3.70}$$

$$Y_{22} = \frac{\dot{\theta}_x(x_0,y_0)}{M_x} = \frac{j\omega}{2\varepsilon} \sum_{m=1}^{M}\sum_{n=1}^{N}\sum_{r=1}^{M}\sum_{s=1}^{N} \lambda_{mnrs} X_r(x_0)\left[Y_s(y_0+\varepsilon) - Y_s(y_0-\varepsilon)\right] X_m(x_0)\left(\frac{dY_n}{dy}\right)_{y_0} \tag{3.71}$$

$$Y_{32} = \frac{\dot{\theta}_y(x_0,y_0)}{M_x} = -\frac{j\omega}{2\varepsilon} \sum_{m=1}^{M}\sum_{n=1}^{N}\sum_{r=1}^{M}\sum_{s=1}^{N} \lambda_{mnrs} X_r(x_0)\left[Y_s(y_0+\varepsilon) - Y_s(y_0-\varepsilon)\right]\left(\frac{dX_m}{dx}\right)_{x_0} Y_n(y_0) \tag{3.72}$$

$$Y_{13} = \frac{\dot{w}(x_0,y_0)}{M_y} = \frac{j\omega}{2\varepsilon} \sum_{m=1}^{M}\sum_{n=1}^{N}\sum_{r=1}^{M}\sum_{s=1}^{N} \lambda_{mnrs} \left[X_r(x_0-\varepsilon) - X_r(x_0+\varepsilon)\right] Y_s(y_0) X_m(x_0) Y_n(y_0) \tag{3.73}$$

$$Y_{23} = \frac{\dot{\theta}_x(x_0,y_0)}{M_y}$$
$$= \frac{j\omega}{2\varepsilon}\sum_{m=1}^{M}\sum_{n=1}^{N}\sum_{r=1}^{M}\sum_{s=1}^{N}\lambda_{mnrs}\left[X_r(x_0-\varepsilon) - X_r(x_0+\varepsilon)\right] Y_s(y_0)\, X_m(x_0)\left(\frac{dY_n}{dy}\right)_{y_0} \tag{3.74}$$

$$Y_{33} = \frac{\dot{\theta}_y(x_0,y_0)}{M_y}$$
$$= -\frac{j\omega}{2\varepsilon}\sum_{m=1}^{M}\sum_{n=1}^{N}\sum_{r=1}^{M}\sum_{s=1}^{N}\lambda_{mnrs}\left[X_r(x_0-\varepsilon) - X_r(x_0+\varepsilon)\right] Y_s(y_0)\left(\frac{dX_m}{dx}\right)_{x_0} Y_n(y_0) \tag{3.75}$$

Using the small angle approximation, it can be shown that :

$$\left[Y_s(y_0+\varepsilon) - Y_s(y_0-\varepsilon)\right] \approx 2k_{ys}\varepsilon\left[j C_{1s} e^{jk_{ys}y_0} - j C_{2s} e^{-jk_{ys}y_0} + C_{3s} e^{k_{ys}y_0} - C_{4s} e^{-k_{ys}y_0}\right]$$
$$= 2\varepsilon\left(\frac{dY_s}{dy}\right)_{y_0} \tag{3.76}$$

$$\left[X_r(x_0-\varepsilon) - X_r(x_0+\varepsilon)\right] \approx 2k_{xr}\varepsilon\left[-j B_{1r} e^{jk_{xr}x_0} + j B_{2r} e^{-jk_{xr}x_0} - B_{3r} e^{k_{xr}x_0} + B_{4r} e^{-k_{xr}x_0}\right]$$
$$= -2\varepsilon\left(\frac{dX_r}{dx}\right)_{x_0} \tag{3.77}$$

Substituting these two approximate expressions into eqns (3.70) to (3.75), it can be shown that the driving point mobility matrix of the plate with general boundary conditions is also a symmetric matrix.

3.4 VIBRATIONAL POWER INPUT TO RECTANGULAR PLATES SUBJECTED TO SIMULTANEOUSLY ACTING FORCE AND MOMENT EXCITATIONS

For a rectangular plate subjected to simultaneously acting force and moment excitations, the translational and rotational velocities at the excitation point can be expressed in terms of the driving point mobility functions and the applied excitations, as from eqn(3.19) :

$$\dot{w}(x_0,y_0) = Y_{11} F + Y_{12} M_x + Y_{13} M_y \tag{3.78}$$
$$\dot{\theta}_x(x_0,y_0) = Y_{21} F + Y_{22} M_x + Y_{23} M_y \tag{3.79}$$
$$\dot{\theta}_y(x_0,y_0) = Y_{31} F + Y_{32} M_x + Y_{33} M_y \tag{3.80}$$

Expressions for the time-averaged vibrational power input to a structure by a point harmonic force, $F(t)$ and a point harmonic moment, $M(t)$ have been given in eqns. (2.61) and (2.62) respectively. The time-averaged vibrational power input to the rectangular plate due to the force and the moment components are :

$$P_F = \frac{1}{2} F^2 Re\{Y_{11}\} + \frac{1}{2} F M_x Re\{Y_{12}\} + \frac{1}{2} F M_y Re\{Y_{13}\} \tag{3.81}$$

$$P_{M_x} = \frac{1}{2} M_x^2 Re\{Y_{22}\} + \frac{1}{2} F M_x Re\{Y_{21}\} + \frac{1}{2} M_x M_y Re\{Y_{23}\} \tag{3.82}$$

$$P_{M_y} = \frac{1}{2} M_y^2 Re\{Y_{33}\} + \frac{1}{2} F M_y Re\{Y_{31}\} + \frac{1}{2} M_x M_y Re\{Y_{32}\} \tag{3.83}$$

where F, M_x and M_y are the amplitudes of the force and moment excitations. The resultant time-averaged vibrational power input to the plate subjected to simultaneously acting sinusoidal force and moment excitations is the sum of the power inputs due to the force and moment components :

$$\begin{aligned} P_T &= P_F + P_{M_x} + P_{M_y} \\ &= \frac{1}{2} F^2 Re\{Y_{11}\} + \frac{1}{2} M_x^2 Re\{Y_{22}\} + \frac{1}{2} M_y^2 Re\{Y_{33}\} \\ &\quad + F M_x Re\{Y_{21}\} + F M_y Re\{Y_{31}\} + M_x M_y Re\{Y_{32}\} \end{aligned} \tag{3.84}$$

3.5 ANALYTICAL RESULTS AND DISCUSSION

Based on the theoretical expressions given in the previous sections, a FORTRAN computer program was written to calculate the driving point mobility functions of rectangular plates subjected to various combinations of clamped, free and simply supported boundary conditions. The flow diagram showing the computation algorithms of the program is given in Appendix D. The program runs interactively on a micro-computer with a small number of characteristic beam functions (typically up to 1kHz). For large matrix size (i.e. more beam functions of up to 4kHz), the solution has to be submitted as a batch job in the IBM 3090 main frame computer.

In the calculation of the transverse displacements of the plate based on the Rayleigh - Ritz method, the number of terms used in the finite series approximation (eqn. 3.44) are determined by a user-defined frequency multiplication factor and the highest frequency range of interest. For instance, if the highest frequency range of interest is 1kHz and a frequency factor of 4.0 has been specified, then all the characteristic beam

functions of frequencies up to 4kHz will be used in the calculation of the mobility functions of the plate. A typical set of input parameters is given in Table D-1 of Appendix D. The results of the calculation from the program are the real and imaginary parts of the six driving point mobility functions which are stored in six separate files for plotting.

In the following discussion, the six driving point mobility functions (i.e. Y_{11}, Y_{22}, Y_{33}, Y_{32}, Y_{21} and Y_{31}) of a SSSS plate and a CFSF plate in flexural vibrations are presented. These analytical results were obtained for a rectangular plate having a uniform thickness of 4.1mm and dimensions of a = 585mm and b = 390mm for the edges parallel to the X- and Y- axes respectively. The Modulus of Elasticity, density and Poisson's ratio of the plate material were assumed to be 207 x 10^9 Nm^{-2}, 7850.0 kgm^{-3} and 0.3 respectively. The hysteretic loss factor used in the calculation was 0.001 to represent a lightly damped structure and the frequency resolution of the mobility spectra was 1Hz, unless stated otherwise.

3.5.1 Driving Point Mobility Functions of a SSSS Plate

The modulus spectra of the six driving point mobility functions of a rectangular plate with all edges simply supported are shown in figures 3.4 to 3.9 for excitations at an off-centre location: x = 0.22a and y = 0.62b. In figures 3.4 to 3.6, modulus spectra of the force and moment mobility functions (i.e. Y_{11}, Y_{22} and Y_{33}) of the plate for excitations at the plate centre: x = 0.5a and y = 0.5b are also given. It can be seen that there are fewer resonance peaks in the force and moment mobility plots at the central location and there are no coupling mobility functions (i.e. $Y_{21} = Y_{31} = Y_{32} = 0$) for this special case of symmetric boundary conditions and with the excitations at the centre of the plate. The reason that the coupling mobility functions do not exist for this special case is because the point of excitation coincides with the point of mode shape symmetry, which has been identified and discussed for the cases of a uniform beam with both ends clamped or simply supported and with the excitations at the mid-span.

3.5.2 Driving Point Mobility Functions of a CFSF Plate

The modulus spectra of the six driving point mobility functions for the CFSF plate are given in figures 3.10 to 3.15 for excitations at the same off-centre location (i.e. x=0.22a, y=0.62b). The modulus spectra of Y_{11}, Y_{22} , Y_{33} and Y_{31} of the plate for excitations at the plate centre are given in figures 3.10, 3.11, 3.12 and 3.15 respectively for comparison with the off-centre results. The coupling mobility

functions: Y_{21} and Y_{32} for excitations at the plate centre are of very small quantities (typically from 10^{-12} to 10^{-8} rad(Nsec)$^{-1}$ or rad(Nmsec)$^{-1}$) as the plate has a pair of symmetric boundary conditions (free-free) along the edges parallel to the X-axis and the excitation point coincides with the point of mode shape symmetry of the characteristic beam functions in the Y-direction.

3.5.3 Comparison with Infinite Plate Solutions

Theoretical expressions for the driving point force and monent mobility functions of an infinite plate have been derived by Cremer, Heckl and Ungar [24]. The driving point force mobility of an infinite plate is real and independent of frequency, and is given by :

$$Y_{F\infty} = \frac{1}{8\sqrt{D\rho h}} \tag{3.85}$$

The real part of the driving point moment mobility of an infinite plate is proportional to frequency and is given by :

$$Re\{ Y_{M\infty} \} = \frac{\omega}{16\,D} \tag{3.86}$$

Comparison of the real parts of the force and moment mobility functions between the SSSS plate with excitations at the centre of the plate and an infinite plate of the same thickness are shown in figures 3.16 to 3.18. Figures 3.19 to 3.21 give the similar comparison for the CFSF plate. It can be seen from these comparisons that :

(1) the logarithmic mean values of the real parts of the driving point force mobility function of finite plates seem to be constant (i.e independent of frequency) toward the high frequency region, and appear to converge to the infinite plate solution.

(2) The logarithmic mean values of the real parts of the driving point moment mobility functions of finite plates are proportional to frequency and also appear to converge to the infinite plate solution.

(3) At low frequencies, below the first resonance frequency, both the real parts of the force and moment mobility functions of the finite plates are 'spring-like' in nature (i.e. mobility functions increase with increasing frequency). However, as the real part of the driving point force mobility of an infinite plate is

independent of frequency, it is thus unable to represent the 'spring-like' nature of constrained finite plates below the first resonance frequency as shown in figures 3.16 and 3.19.

(4) Increase in the hysteretic loss factor from 0.001 to 0.1 has significant effects on the real parts of the mobility functions. The logarithmic mean values of the real parts of the mobility functions converge to the straight line solutions of the infinite plate with increasing loss factor. Whereas, as would be expected, the loss factor affects only the resonance peaks and the anti-resonance dips of the modulus of the mobility functions.

3.5.4 The Effect on the Number of Terms Used in the Solution for Plate Response

The theoretical expressions for the driving point mobility functions of finite rectangular plates assume a combination of very large number of terms of either the exact eigenfunctions or the appropriate characteristic beam functions in order to obtain the exact solutions. There are naturally limits on the computing resource and effort pertaining to the number of terms used in the solution. The effect on the number of terms used in the solution has been studied. Figures 3.22 to 3.27 show the modulus spectra of the six mobility functions of the SSSS plate respectively using mxn = 10x10, 25x25 and 50x50 terms of exact eigenfunctions (eqn (3.31)). The frequency resolution of these spectra was 5Hz instead of the 1Hz resolution presented in previous sections.

It can be seen that the number of terms used in the solution has significant effect on the moment mobility functions (Y_{22} and Y_{33}) : the greater the number of terms used in the solution the greater are the off-resonance moduli of the moment mobility functions. For the force mobility function (Y_{11}), the effect is less significant and is only important at high frequencies. Surprisingly, the number of terms used has no significant effect on the coupling mobility functions (Y_{21}, Y_{31} and Y_{32}) in the frequency range investigated.

The influence of the number of terms used on the driving point mobility functions can be explained if one examines the expressions for these mobility functions as given in equations 3.33, 3.34, 3.35, 3.39, 3.40 and 3.43. The moment mobility functions are affected the most as the numerator within the summation series consists of three squared terms, whereas the force mobility function has only two squared terms and the coupling mobility functions have each a product of an odd (sine) and an even (cosine) function terms.

The real parts of the driving point mobility functions are important functions which determine directly the vibrational power input to the seating structure. The influence of the number of terms used on the real parts of the moment mobility functions has therefore also been studied and is shown in figures 3.28 and 3.29. It can be seen that for lightly damped structures, the number of terms used in the solution does not have a significant influence on the real parts of moment mobility functions compared to the moduli of these functions, in the frequency range studied.

Similar effects of the number of terms used for the solution of the driving point mobility functions for the CFSF plate by the Rayleigh - Ritz method were noted. Although the same number of terms such as 25x25 and 50x50 cannot be used without having to solve the inverse of a large matrix size (i.e. 625 and 2500), these effects were compared for relatively smaller number of terms : $m \times n = 9 \times 7$ versus 11 x 9 of the characteristic beam functions (corresponding to the frequency factors of 2.5 and 4.0 respectively).

An implication from this analysis is that in order to predict the driving point moment mobility functions reliably, one needs to use relatively more terms of the exact eigenfunctions or the appropriate characteristic beam functions than the number of terms required for the force or coupling mobility functions.

3.5.5 Validation of the Solution Routines

In view of the complexity of the driving point mobility functions for the rectangular plates, an attempt was made to validate the solution routines used to calculate the mobility functions derived from the Rayleigh - Ritz method. The validation was performed for the SSSS plate with the mobility functions obtained from the Eigenfunction Expansion Theorem and the Rayleigh - Ritz method.

It can be shown that when applying the Rayleigh - Ritz method to the SSSS plate, the expression for the displacement amplitude function $w(x,y)$ of the plate is identical to the expression obtained using the Eigenfunction Expansion Theorem, eqn (3.33). The derivation of the expression is given in Appendix E.

Comparisons of the modulus spectra of the six driving point mobility functions for the SSSS plate with excitations at an off-centre location : x = $0.22a$ and y = $0.62b$ obtained from the two methods are shown in figures E-1 to E-6. These two sets of

results match extremely closely which also indirectly verifies the written solution routines.

3.5.6 Vibrational Power Input to Rectangular Plates

From the study of the vibrational power input to beam-like structures (Chapter 2, [27]), it was shown that due to the contribution of the vibrational power components resulting from the coupling mobility functions, the resultant vibrational power input to the structures subjected to simultaneously acting force and moment excitations, at certain frequencies, could be smaller than the vibrational power input resulting from the force alone. In the following sections, similar analyses are performed for the SSSS and the CFSF plates.

a. Vibrational Power Input to a SSSS Plate

Figure 3.30 shows a comparison between the vibrational power input to the SSSS plate for the force acting alone (P_{force}) and the resultant vibrational power (P_{total}) due to simultaneously acting force and moment excitations at the same off-centre point : x=0.22a and y=0.62b. The force amplitude was constant at 1 N and the moment arms (a_x and a_y) for the latter case were constant at 0.02m. The expression for P_{force} is given in eqn. (2.70), in which Y_{FF} is replaced by Y_{11} (i.e. the driving point force mobility function), and the expression for P_{total} is the same as eqn (3.84).

It can be seen that there is a significant vibrational power reduction in the 580 to 720 Hz frequency range for this specific value of moment arms and the particular location on the plate. The reduction in the resultant input power is due to the cancellation effect of the coupling mobility functions, as was discussed in the finite beam analysis.

The power reduction index (as defined in eqn. (2.78)) spectrum of the SSSS plate for the specific moment arms and location is given in figure 3.31, which shows significant power reduction (i.e. below the unity line) in the 580 to 720 Hz frequency range.

b. Vibrational Power Input to a CFSF Plate

A similar comparison of P_{force} and P_{total} for the CFSF plate is given in figure 3.32. The moment arms used for the calculation of P_{total} were : $a_x = -0.1m$ and $a_y = 0$. These moment arms were chosen to minimise the vibrational power input to the plate in

the low frequency region as shown in figure 3.32 and the corresponding power reduction index spectrum (figure 3.34).

A cumulative power plot, figure 3.33, clearly shows the reduction of vibrational power to the plate at low frequencies of up to about 500 Hz as a result of introducing the simultaneously acting moment. At frequencies above 500 Hz, the vibrational power increases due to the additional power input caused by the moment excitation.

3.6 SUMMARY

The driving point mobility matrix of rectangular plates in transverse vibration has been derived based on the Eigenfunction Expansion Theorem for plates with all edges simply supported and the Rayleigh - Ritz method for plates with combined clamped, free and simply supported boundary conditions where exact solutions of the governing equation of motion do not exist. Based on the driving point force, moment and coupling mobility functions, the time-averaged vibrational power input to a SSSS plate and a CFSF plate subjected to simultaneously acting sinusoidal force and moment excitations have also been studied. The main findings from this study are :

(1) for rectangular plates of symmetric boundary conditions and with the excitation location coinciding with a point of mode shape symmetry, the driving point coupling mobility functions do not exist, a condition which has been identified for uniform beams.

(2) The high frequency trends of the real parts of the force and moment mobility functions are in good agreement with the infinite plate solution published elsewhere. Increase in hysteretic loss factor of the plates clearly shows the convergence of the real parts of the force and moment mobility functions to the infinite plate values.

(3) The number of terms of the exact eigenfunctions or the characteristic beam functions used in the solution has significant effects on the predicted moment mobility functions. However, the number of terms affects the force mobility function only at high frequencies and there is no significant effect on the coupling mobility functions in the frequency range investigated.

(4) In the case of simultaneously acting force and moment excitations, the cancellation of the vibrational power components resulting from the coupling mobility functions occurs for rectangular plates in a similar manner as has been previously demonstrated for beams.

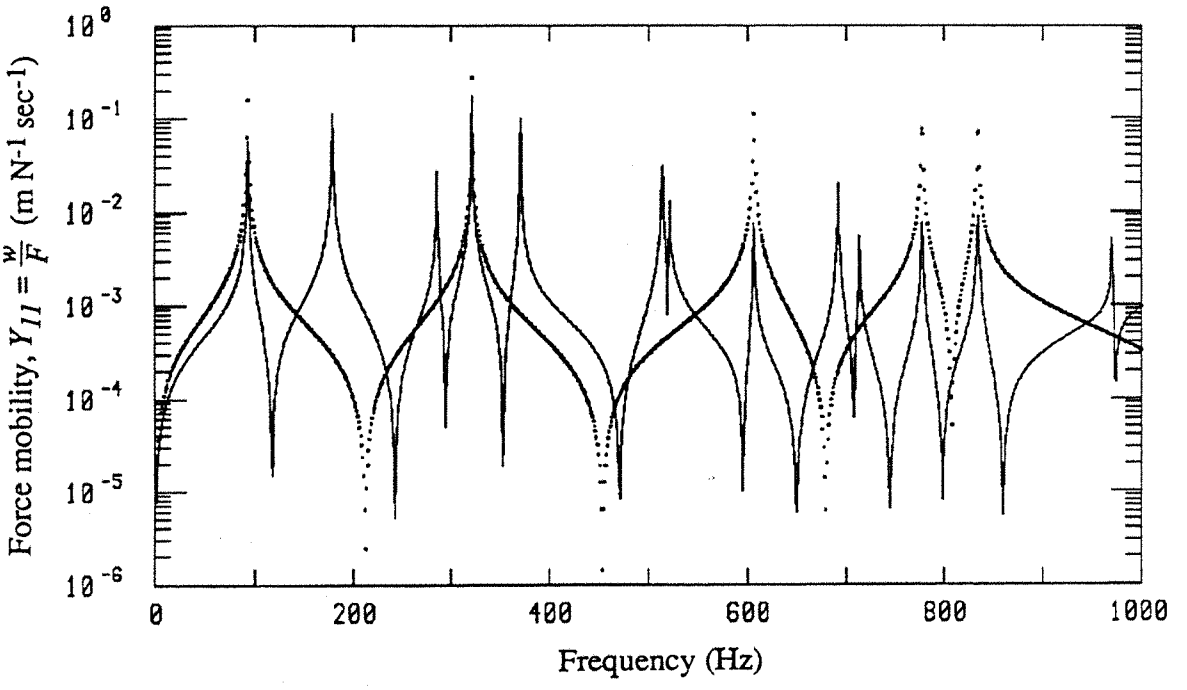

Figure 3.4 : Comparison of the modulus spectra of the force mobility, Y_{11} for the SSSS plate : ····· at the plate centre (x=0.5a , y=0.5b), —— at an off-centre point (x=0.22a , y=0.62b).

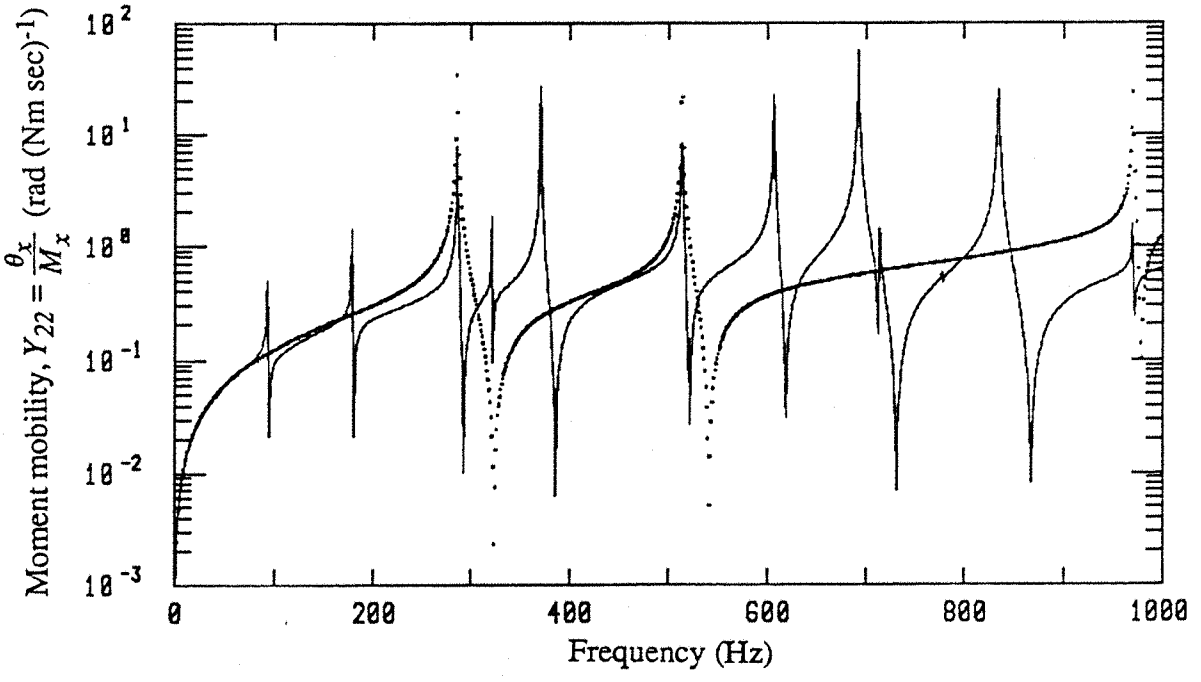

Figure 3.5 : Comparison of the modulus spectra of the moment mobility, Y_{22} for the SSSS plate : ····· at the plate centre (x=0.5a , y=0.5b), —— at an off-centre point (x=0.22a , y=0.62b).

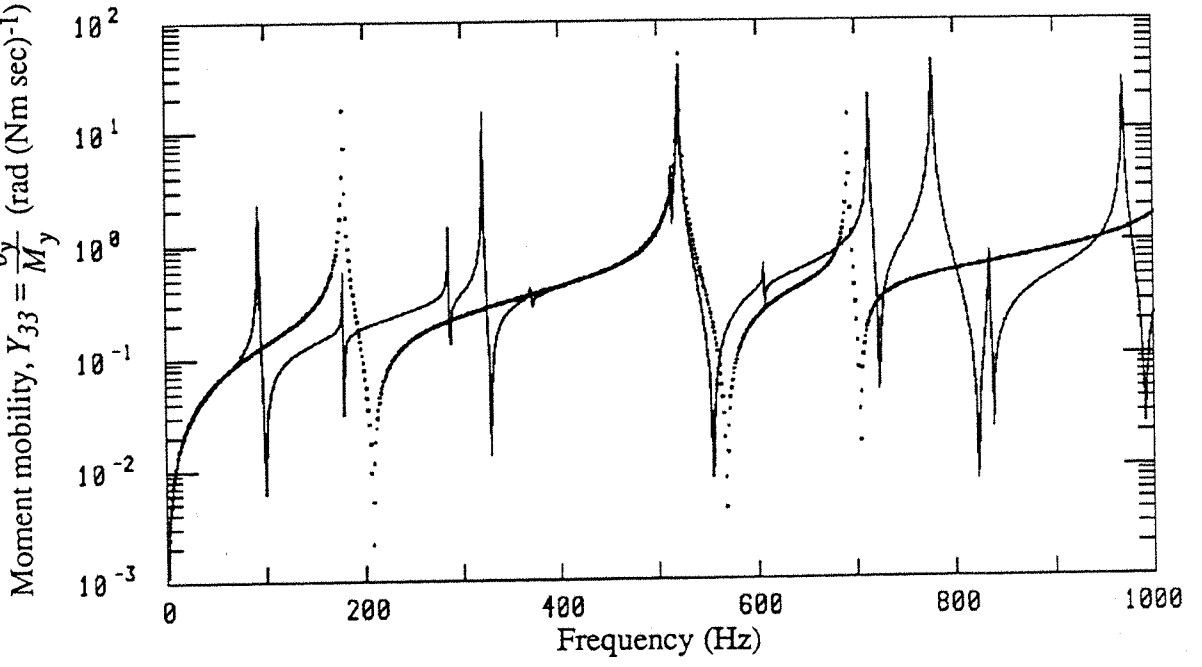

Figure 3.6 : Comparison of the modulus spectra of the moment mobility, Y_{33} for the SSSS plate : ····· at the plate centre (x=0.5a , y=0.5b), —— at an off-centre point (x=0.22a , y=0.62b).

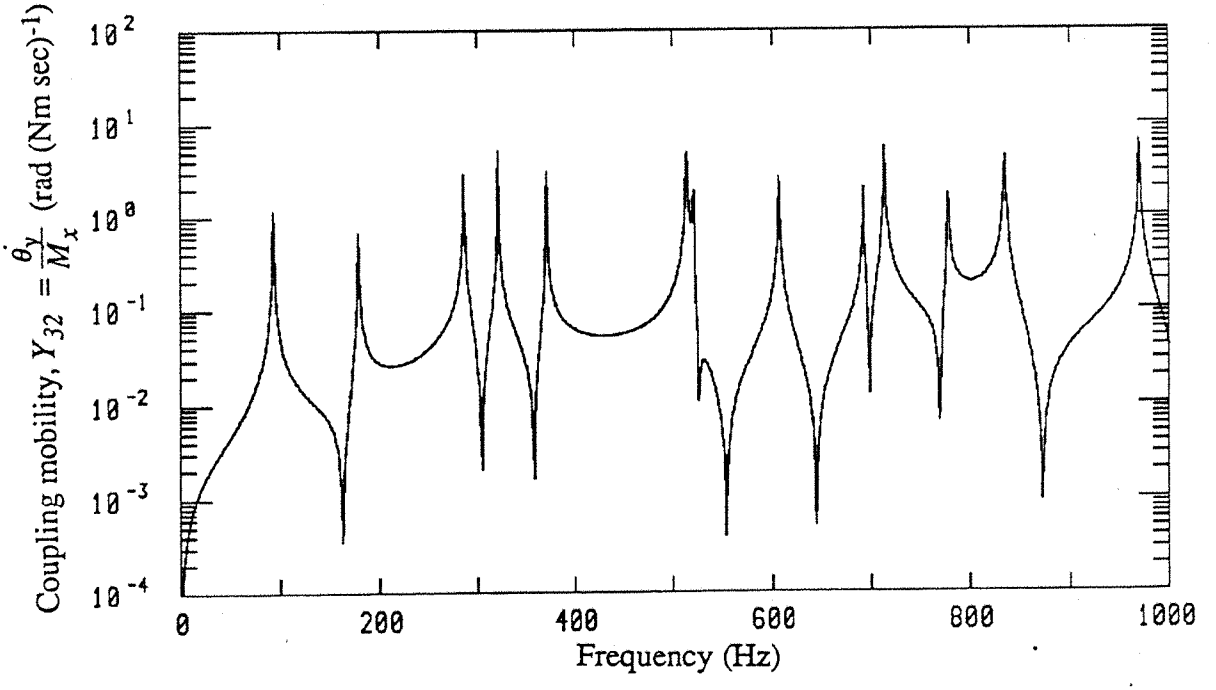

Figure 3.7 : Modulus spectrum of the coupling mobility, Y_{32} for the SSSS plate at an off-centre point (x=0.22a , y=0.62b).

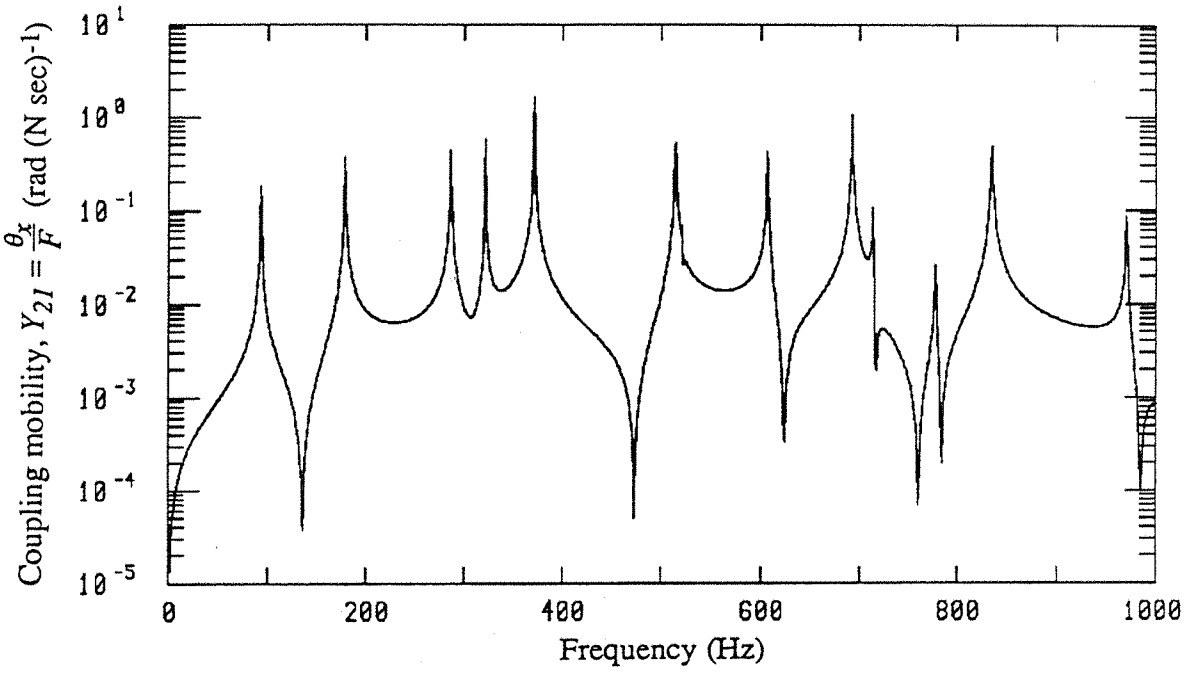

Figure 3.8 : Modulus spectrum of the coupling mobility, Y_{21} for the SSSS plate at an off-centre point (x=0.22a , y=0.62b).

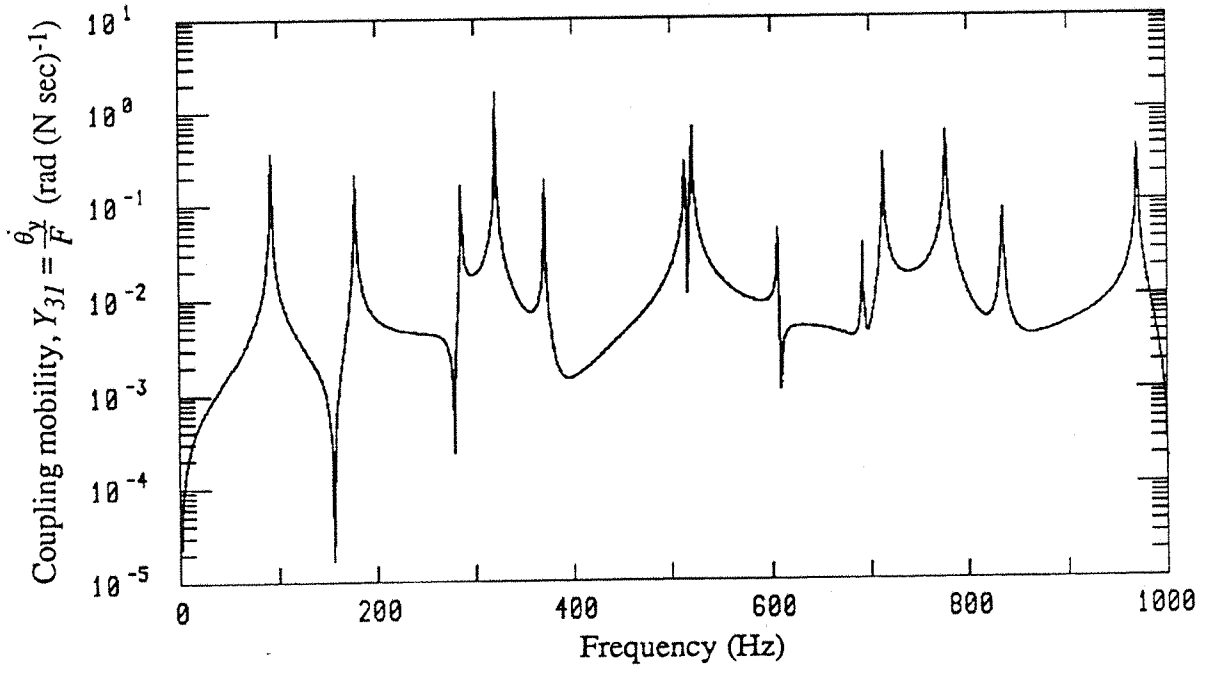

Figure 3.9 : Modulus spectrum of the coupling mobility, Y_{31} for the SSSS plate at an off-centre point (x=0.22a , y=0.62b).

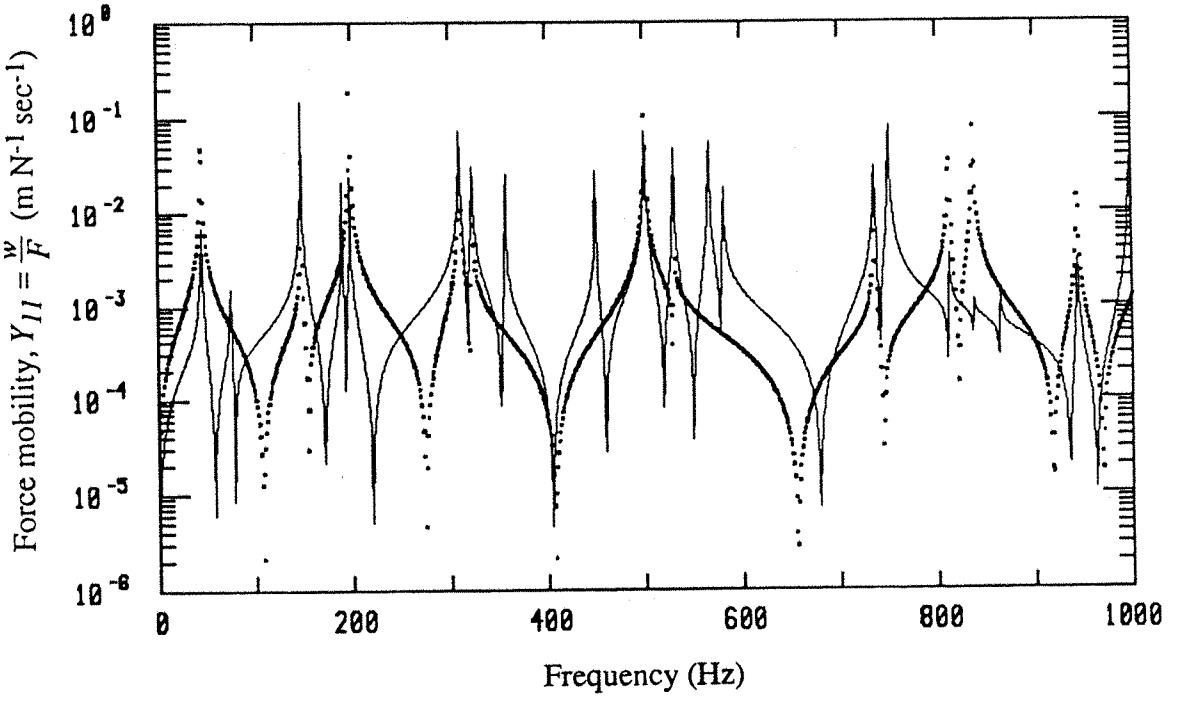

Figure 3.10:Comparison of the modulus spectra of the force mobility, Y_{11} for the CFSF plate : ····· at the plate centre (x=0.5a , y=0.5b), —— at an off-centre point (x=0.22a , y=0.62b).

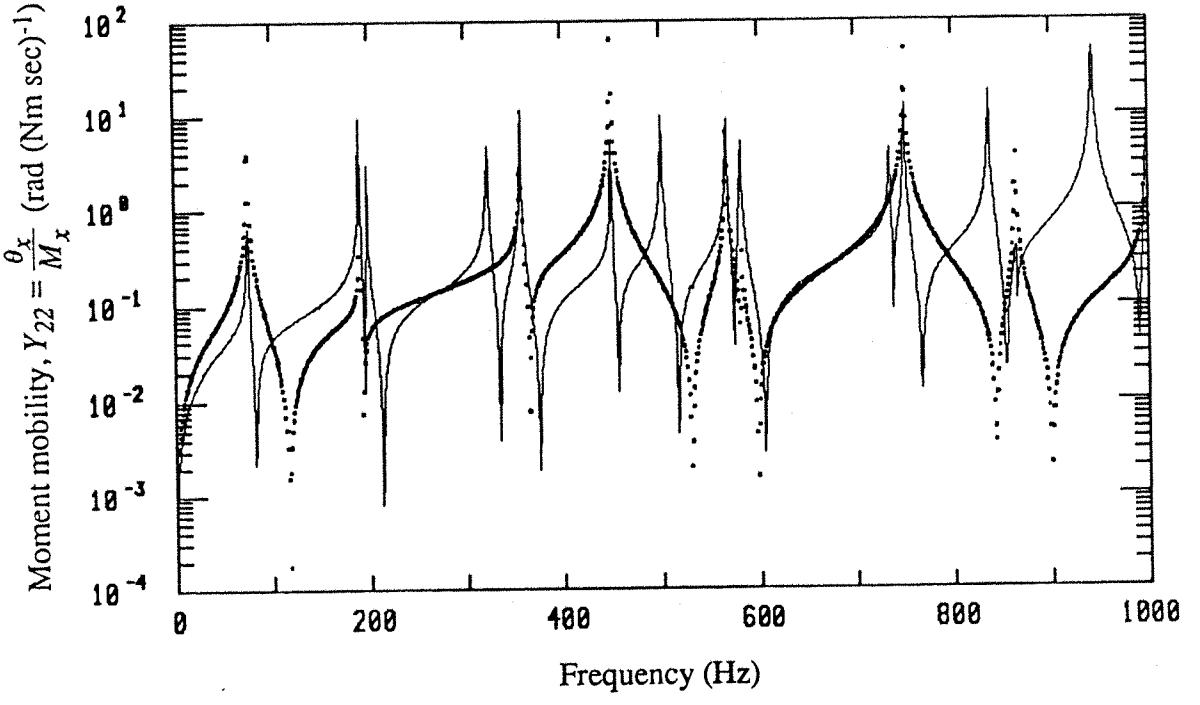

Figure 3.11:Comparison of the modulus spectra of the moment mobility, Y_{22} for the CFSF plate : ····· at the plate centre (x=0.5a , y=0.5b), —— at an off-centre point (x=0.22a , y=0.62b).

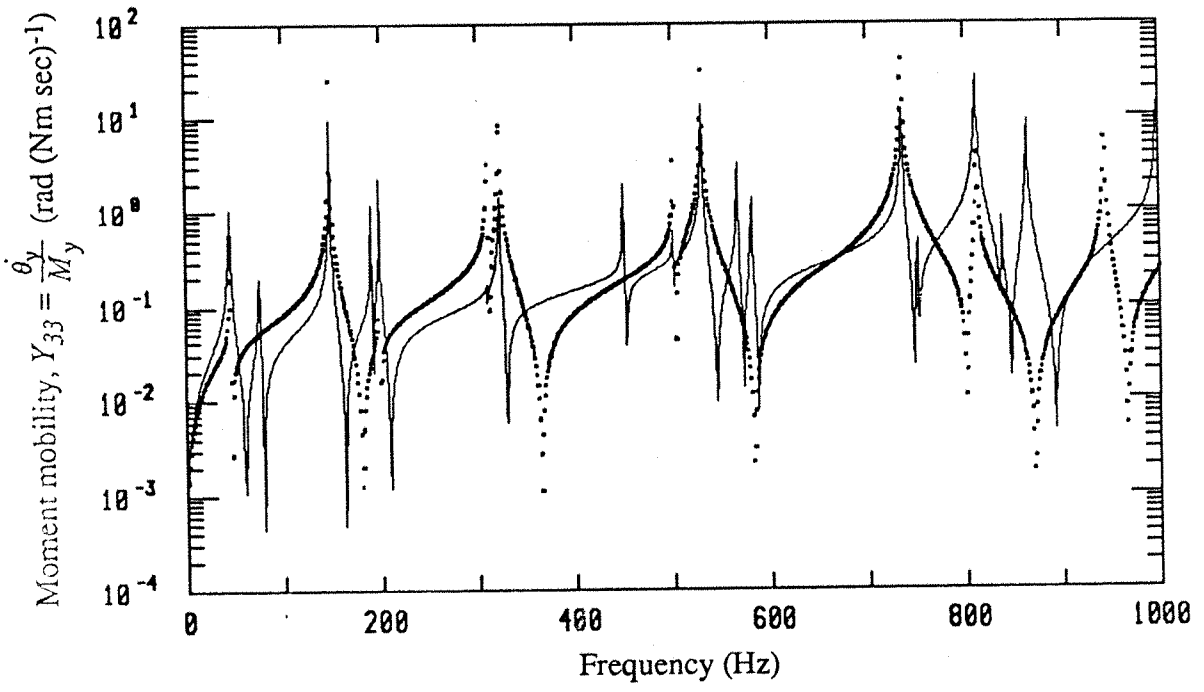

Figure 3.12:Comparison of the modulus spectra of the moment mobility, Y_{33} for the CFSF plate : ····· at the plate centre (x=0.5a , y=0.5b), —— at an off-centre point (x=0.22a , y=0.62b).

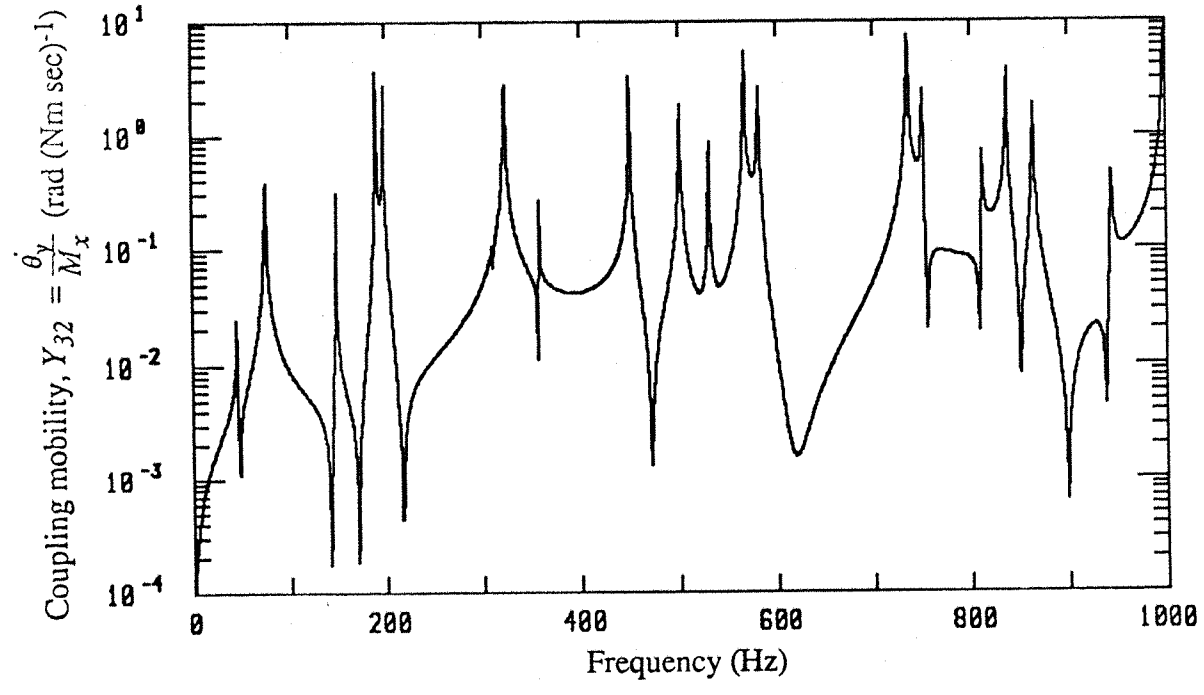

Figure 3.13 : Modulus spectrum of the coupling mobility, Y_{32} for the CFSF plate at an off-centre point (x=0.22a , y=0.62b).

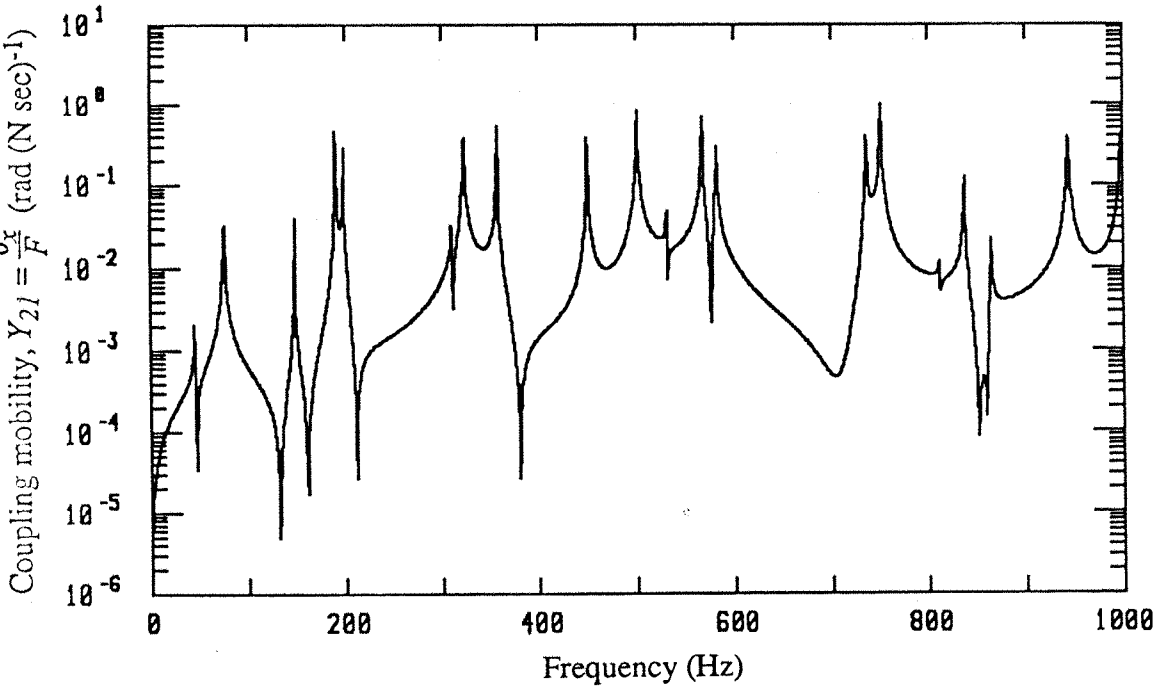

Figure 3.14 : Modulus spectrum of the coupling mobility, Y_{21} for the CFSF plate at an off-centre point (x=0.22a , y=0.62b).

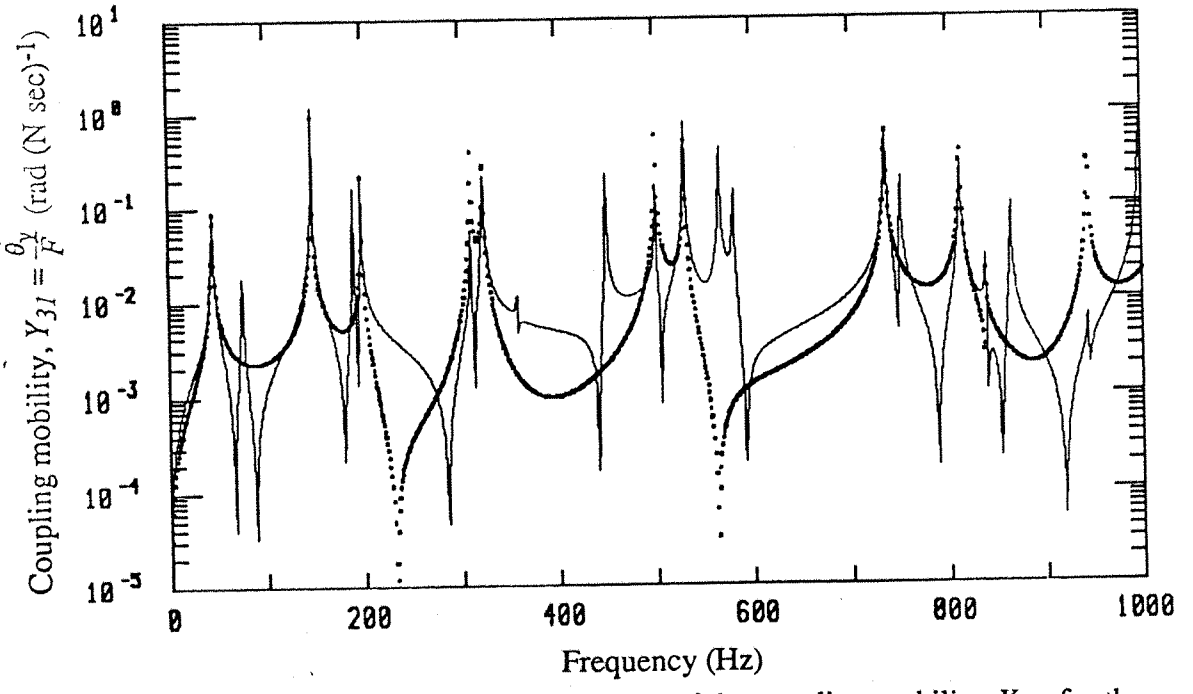

Figure 3.15 : Comparison of the modulus spectra of the coupling mobility, Y_{31} for the CFSF plate : ····· at the plate centre (x=0.5a , y=0.5b), —— at an off-centre point (x=0.22a , y=0.62b).

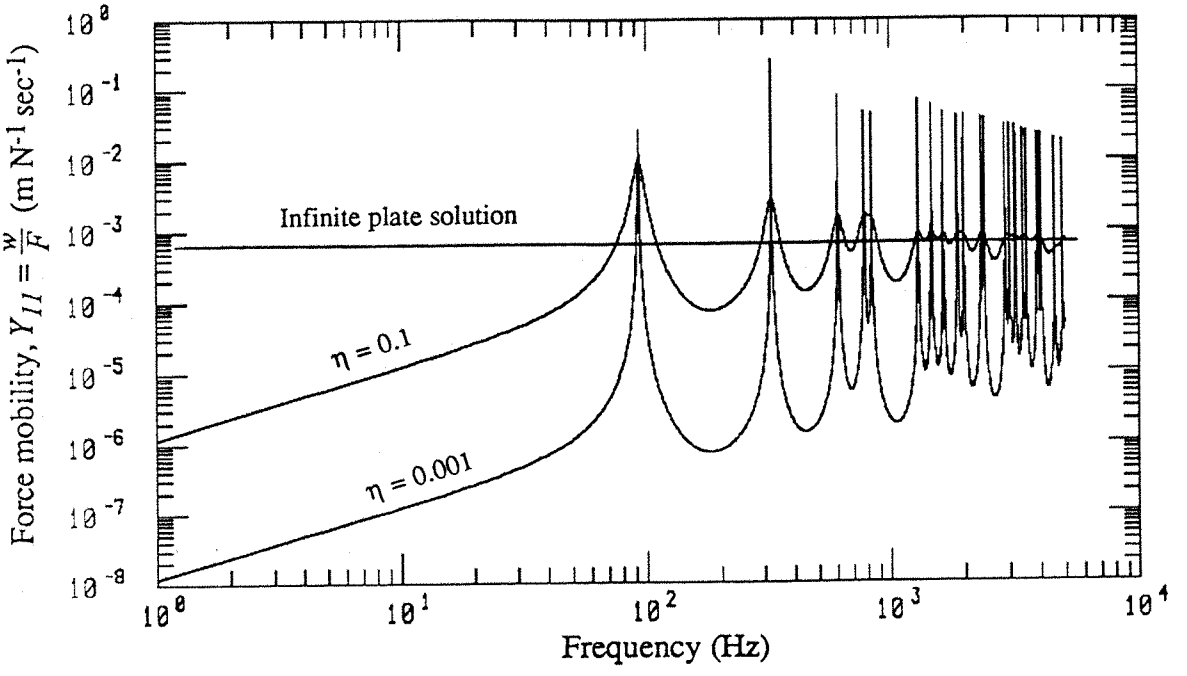

Figure 3.16 : Comparison of the real parts of the force mobility,Y_{11} between the infinite plate and the SSSS plate with excitations at the plate centre.

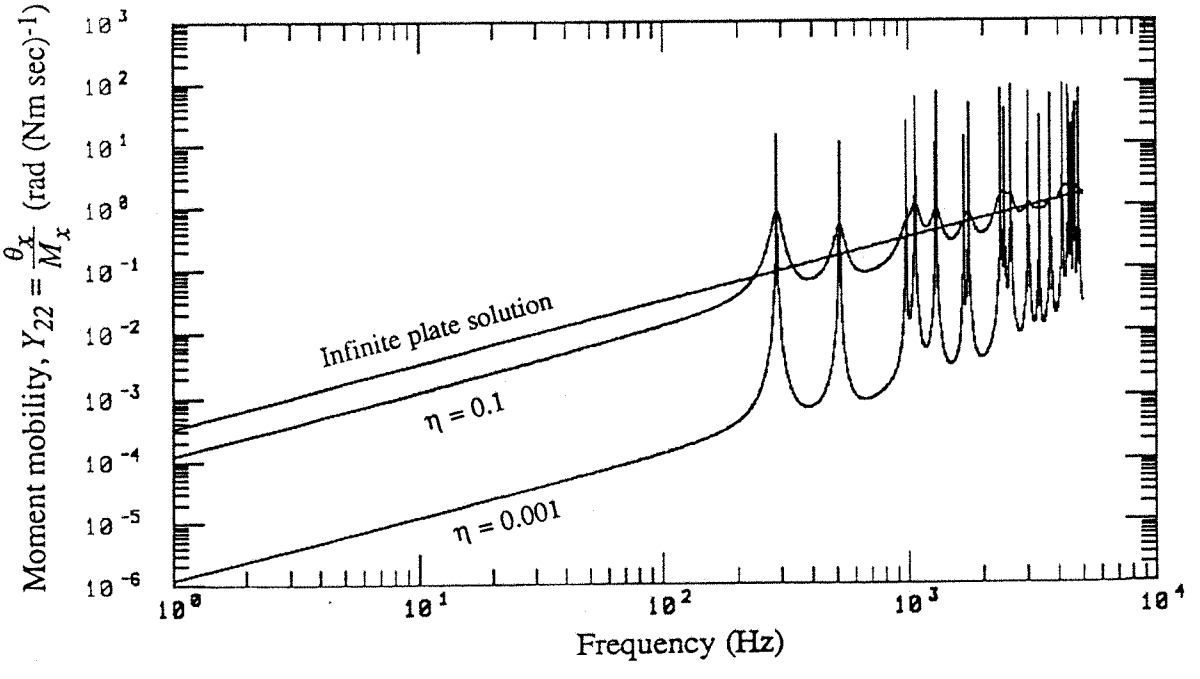

Figure 3.17 : Comparison of the real parts of the moment mobility,Y_{22} between the infinite plate and the SSSS plate with excitations at the plate centre.

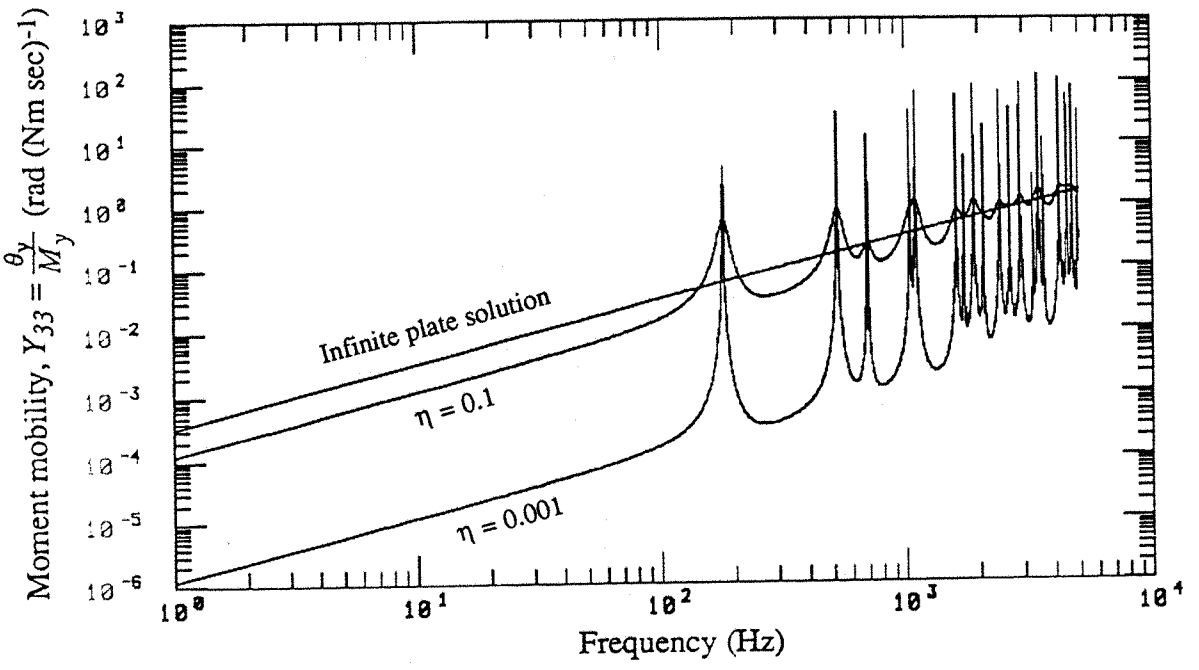

Figure 3.18 : Comparison of the real parts of the moment mobility,Y_{33} between the infinite plate and the SSSS plate with excitations at the plate centre.

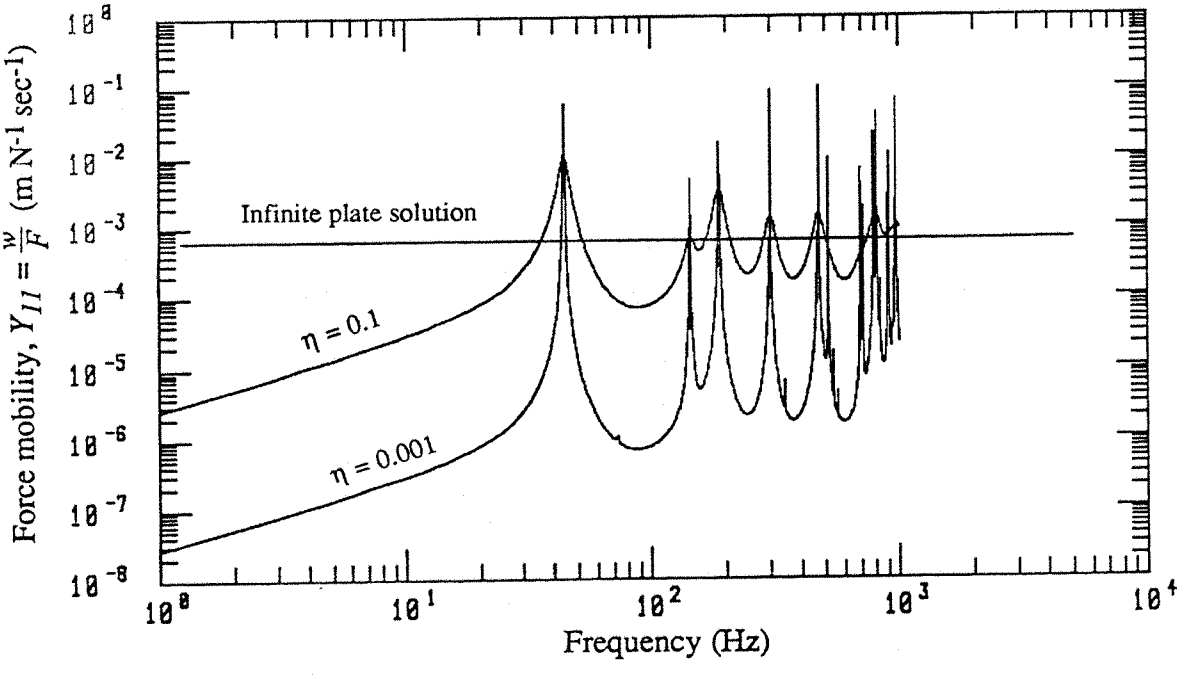

Figure 3.19 : Comparison of the real parts of the force mobility,Y_{11} between the infinite plate and the CFSF plate with excitations at the plate centre.

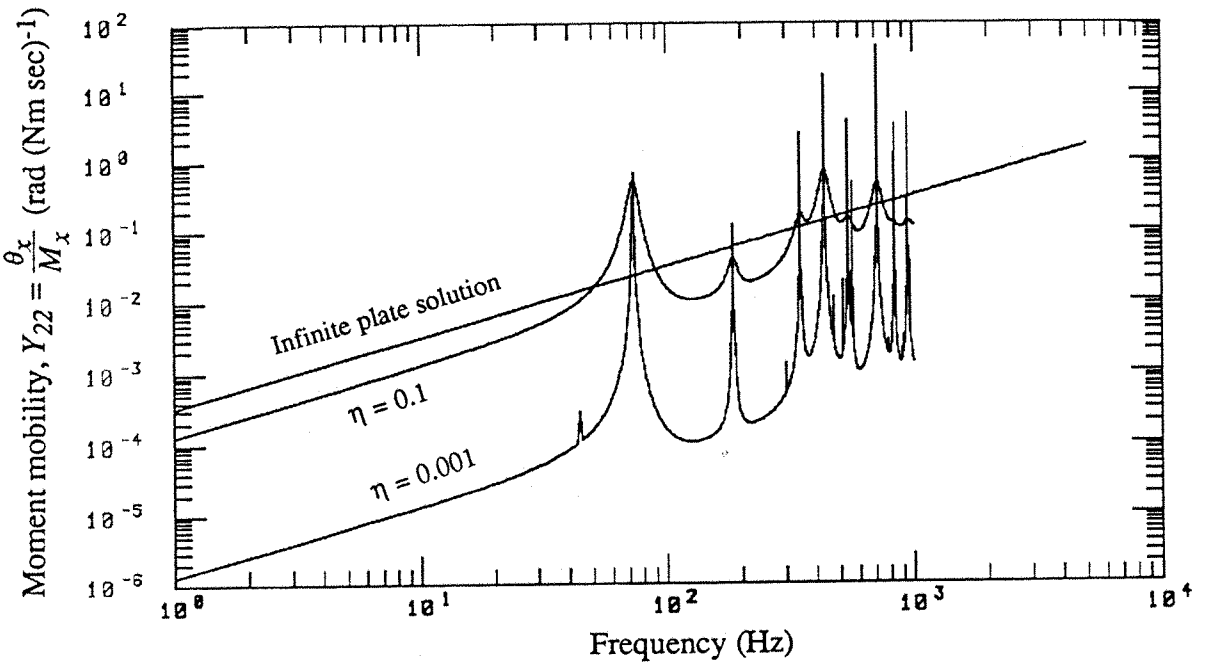

Figure 3.20 : Comparison of the real parts of the moment mobility,Y_{22} between the infinite plate and the CFSF plate with excitations at the plate centre.

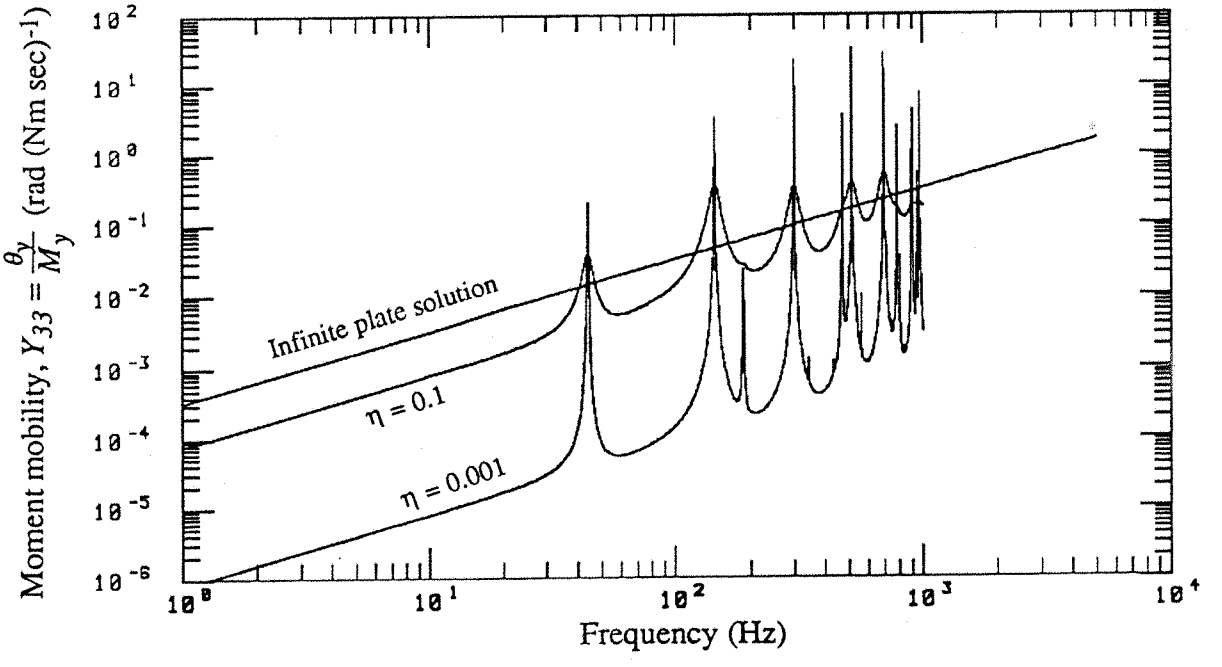

Figure 3.21 : Comparison of the real parts of the moment mobility,Y_{33} between the infinite plate and the CFSF plate with excitations at the plate centre.

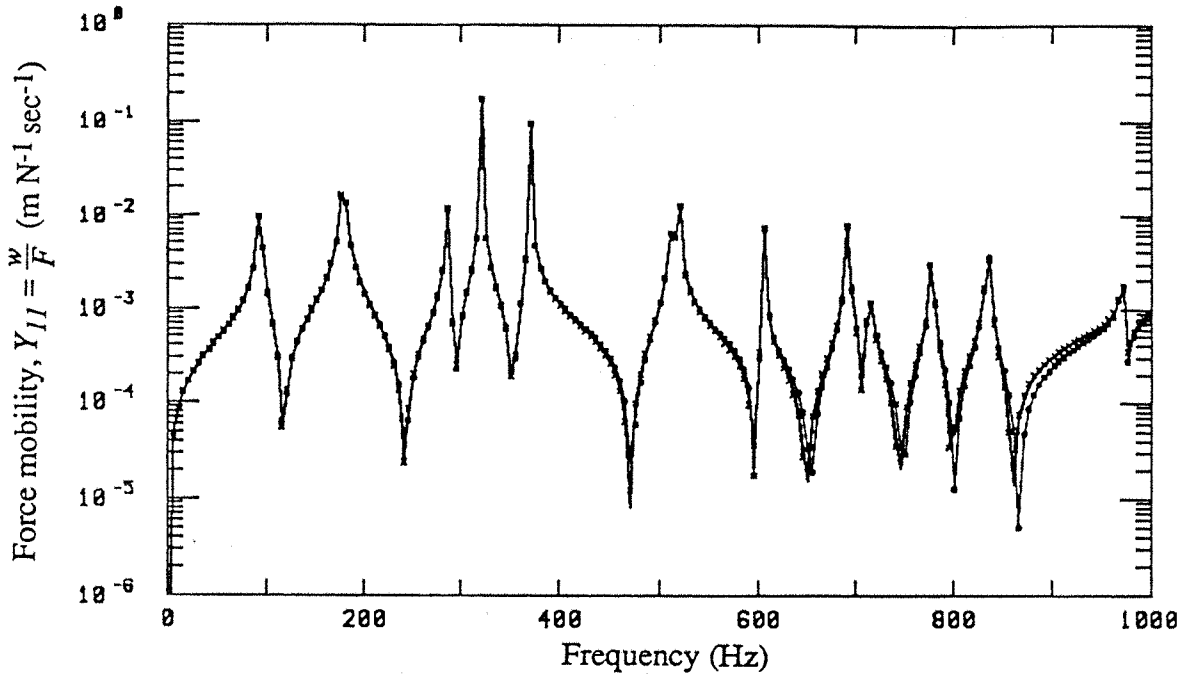

Figure 3.22 : Comparison of the modulus spectra of the force mobility, Y_{11} for the SSSS plate for various numbers of terms (mxn) :
⋯⋯ 10x10, —— 25x25 and ⋆⋆⋆⋆ 50x50.

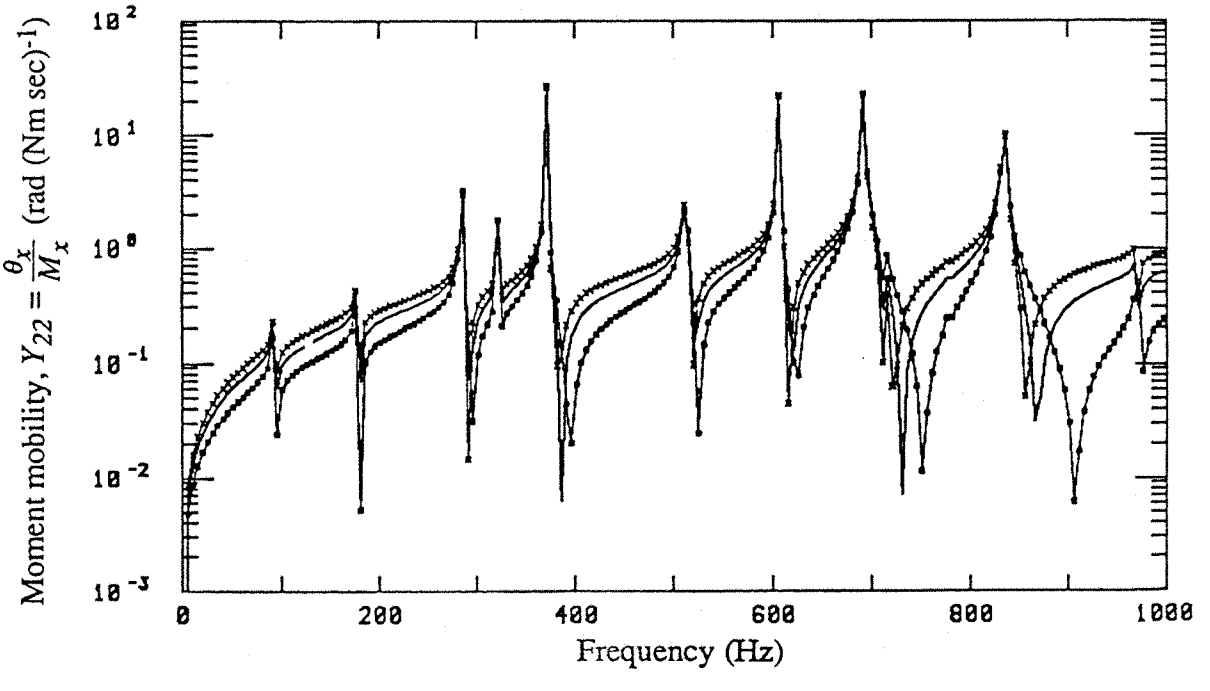

Figure 3.23 : Comparison of the modulus spectra of the moment mobility, Y_{22} for the SSSS plate for various numbers of terms (mxn) :
⋯⋯ 10x10, —— 25x25 and ⋆⋆⋆⋆ 50x50.

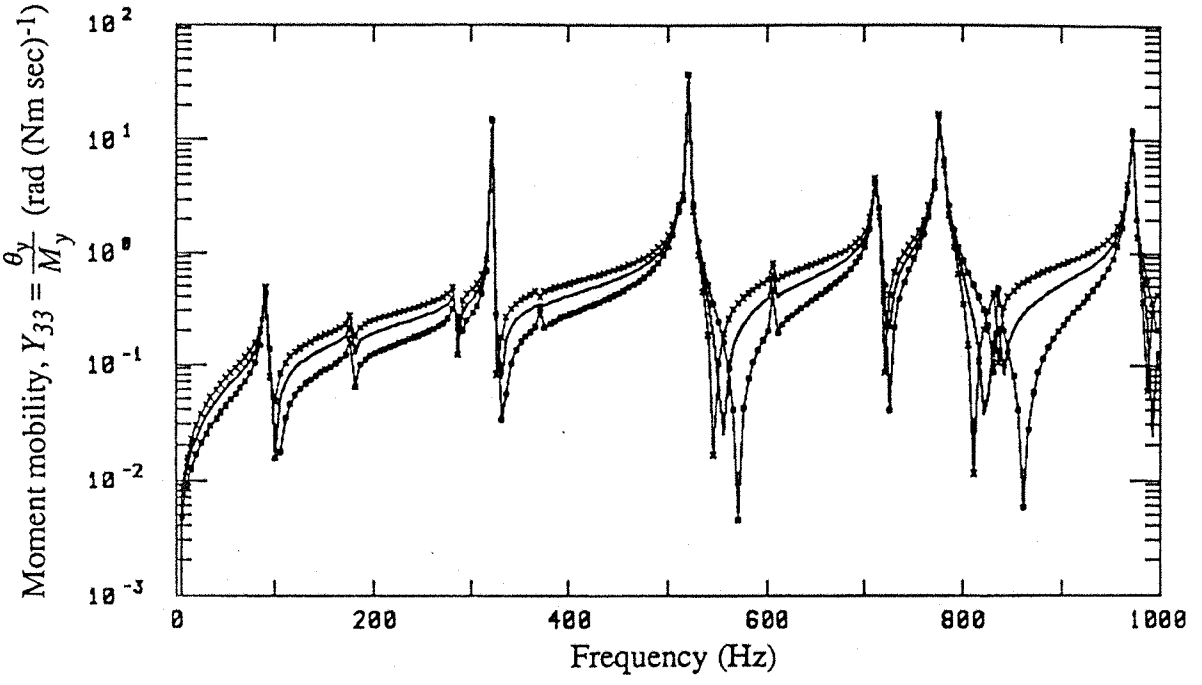

Figure 3.24 : Comparison of the modulus spectra of the moment mobility,Y_{33} for the SSSS plate for various numbers of terms (mxn) :
10x10, —— 25x25 and ✱✱✱✱ 50x50.

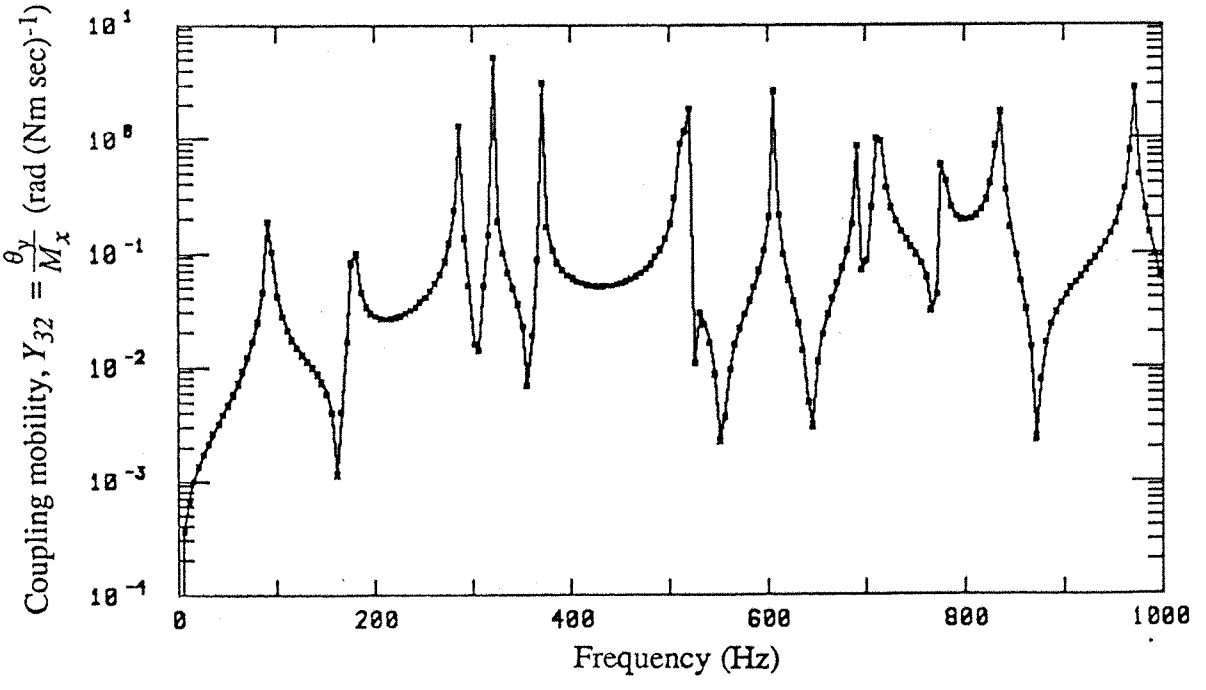

Figure 3.25 : Comparison of the modulus spectra of the coupling mobility,Y_{32} for the SSSS plate for various numbers of terms (mxn) :
10x10, —— 25x25 and ✱✱✱✱ 50x50.

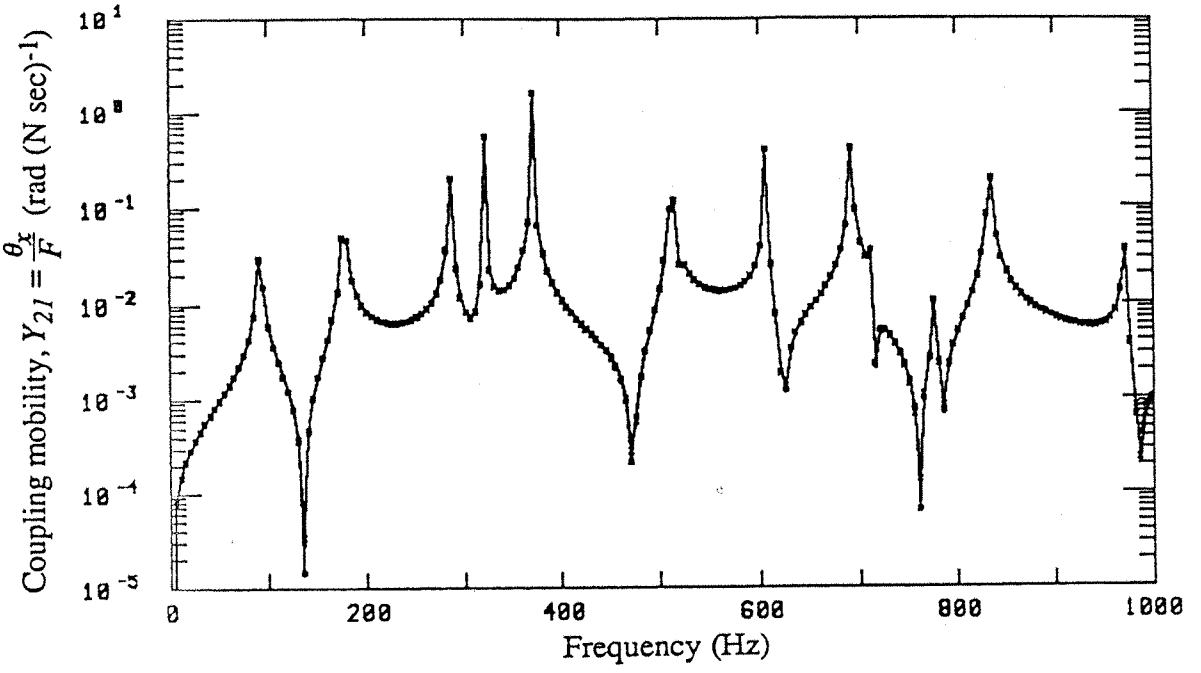

Figure 3.26 : Comparison of the modulus spectra of the coupling mobility, Y_{21} for the SSSS plate for various numbers of terms (mxn) :
-•••- 10x10, —— 25x25 and -**** 50x50.

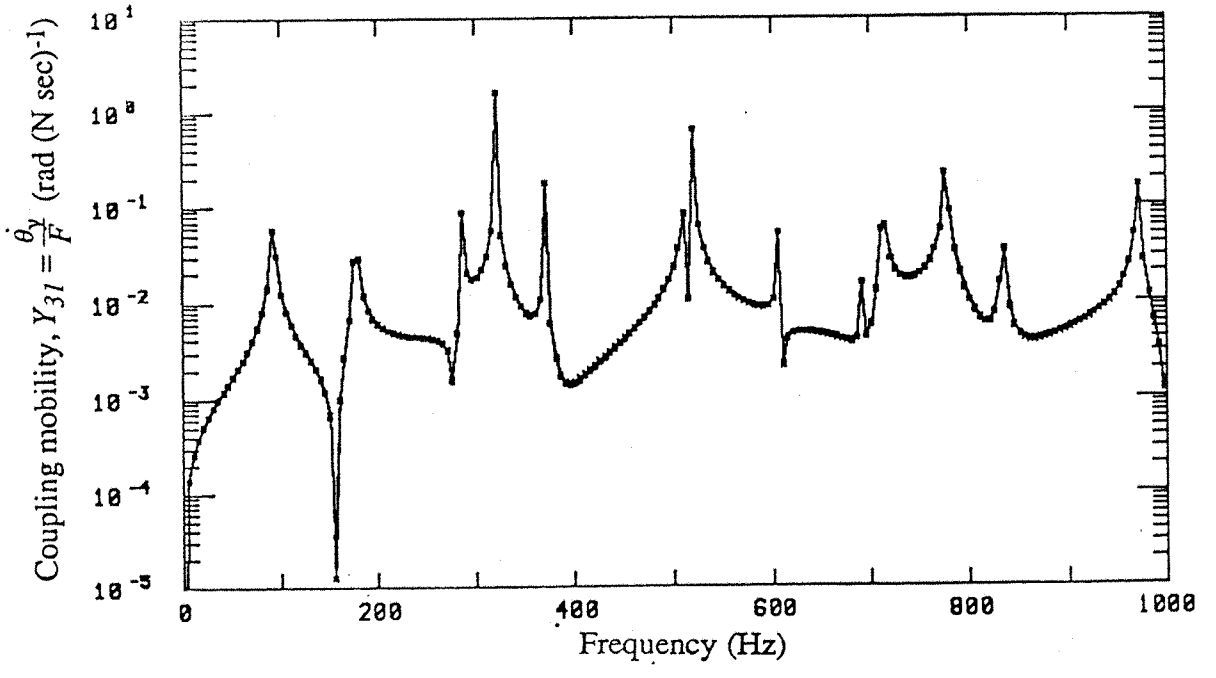

Figure 3.27 : Comparison of the modulus spectra of the coupling mobility, Y_{31} for the SSSS plate for various numbers of terms (mxn) :
-•••- 10x10, —— 25x25 and -**** 50x50.

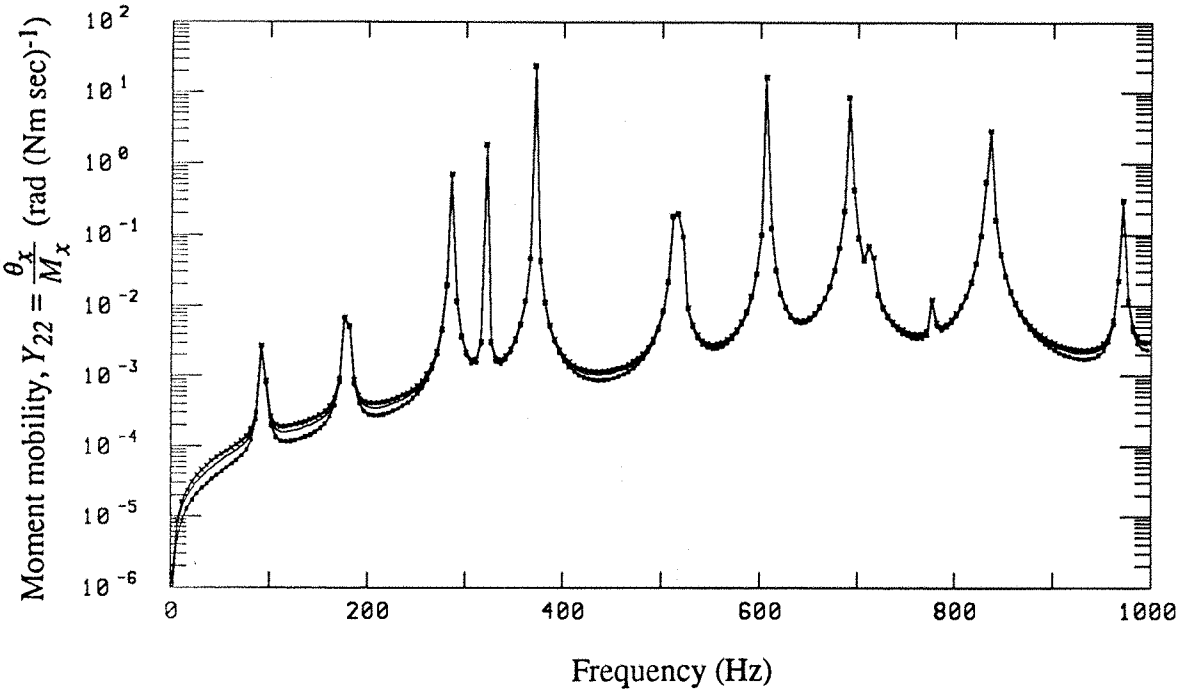

Figure 3.28 : Comparison of the real parts of the moment mobility, Y_{22} for the SSSS plate for various numbers of terms (mxn) :

------ 10x10, ——— 25x25, ***** 50x50.

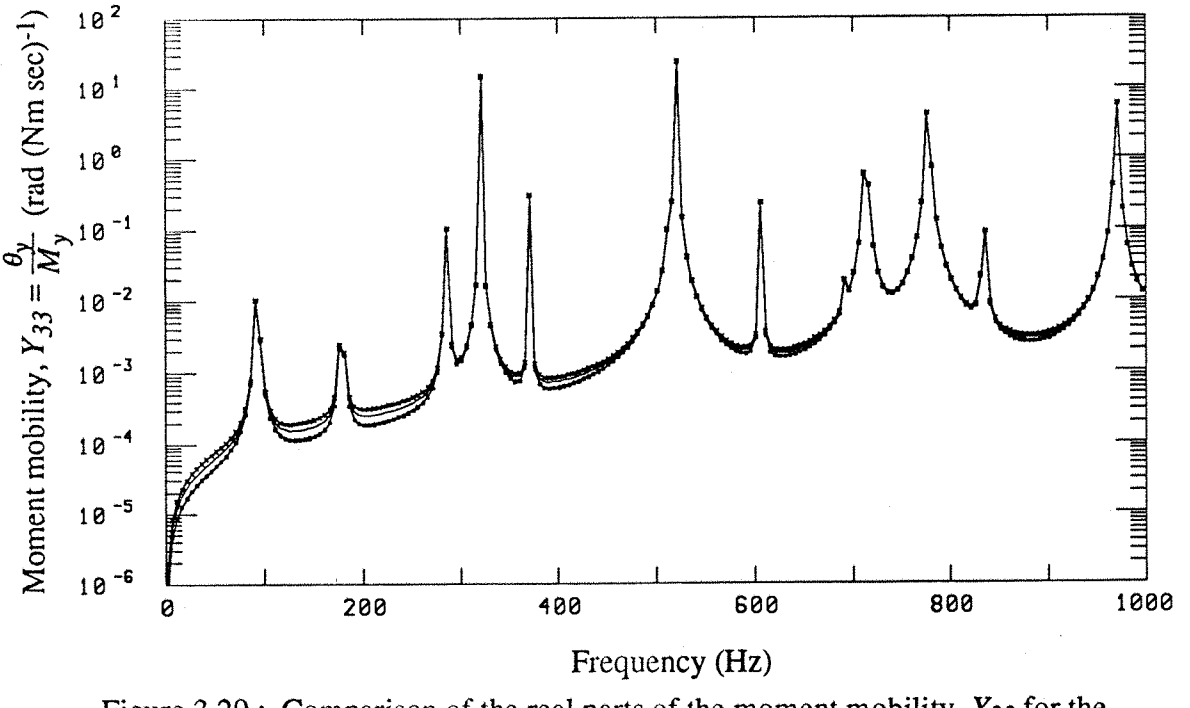

Figure 3.29 : Comparison of the real parts of the moment mobility, Y_{33} for the SSSS plate for various numbers of terms (mxn) :

------ 10x10, ——— 25x25, ***** 50x50.

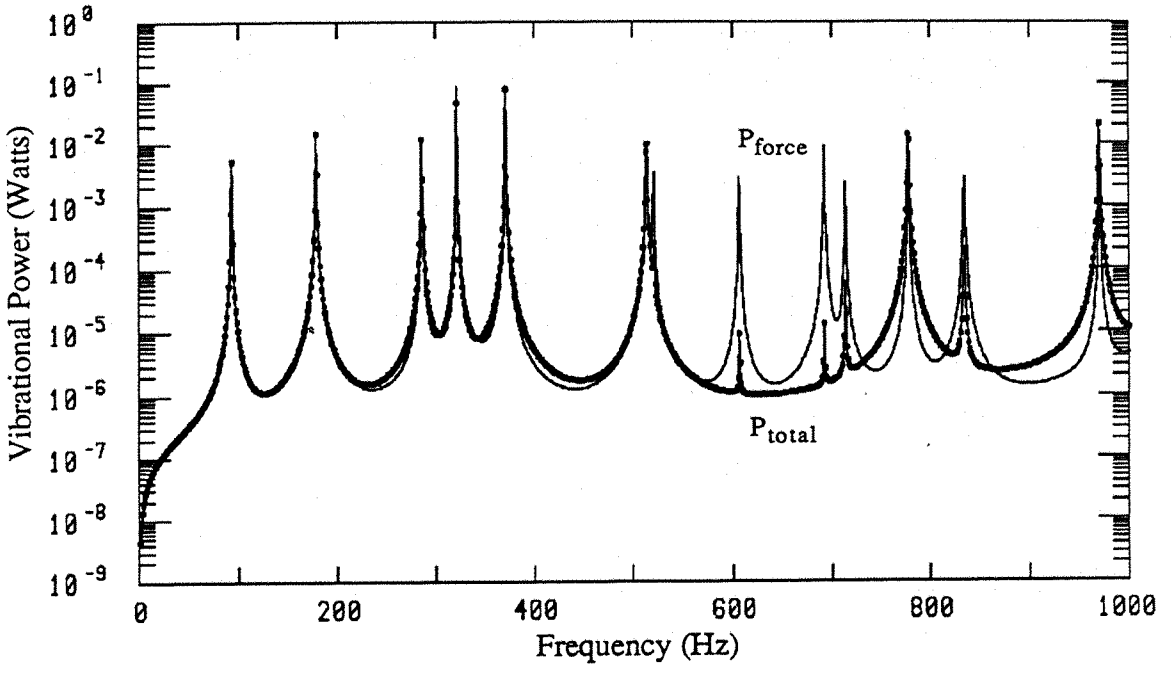

Figure 3.30 : Comparison of P_{force} and P_{total} for the SSSS plate with excitations at an off-centre point : x=0.22*a* , y=0.62*b* (moment arms : a_x = 0.02m, a_y = 0.02m; force amplitude = 1 N, loss factor = 0.001).

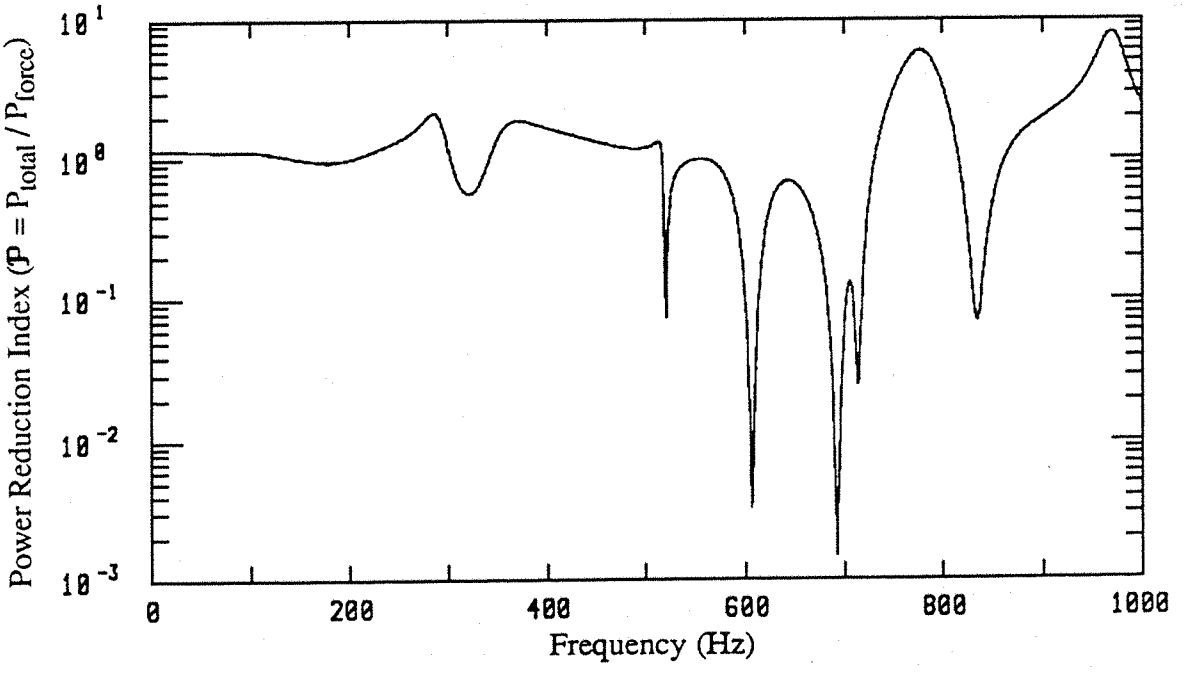

Figure 3.31 : Power reduction index spectrum for the SSSS plate in figure 3.30.

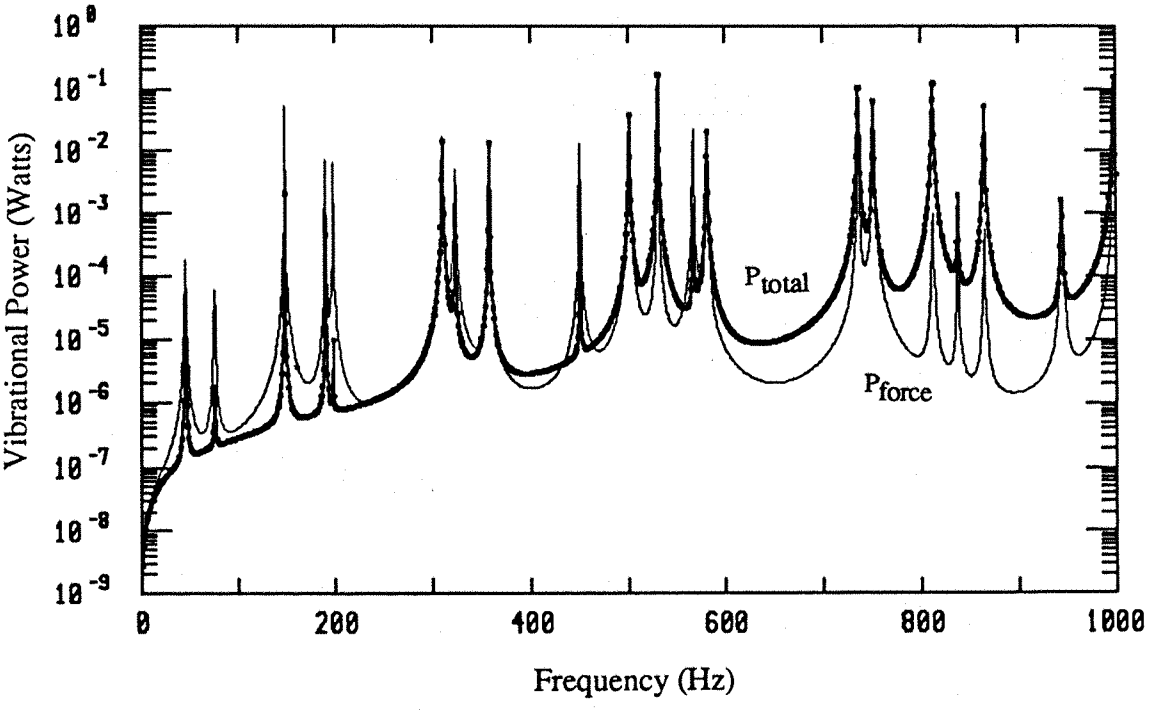

Figure 3.32 : Comparison of P_{force} and P_{total} for the CFSF plate with excitations at an off-centre point : x=0.22*a* , y=0.62*b* (moment arms : $a_x = -0.1$m, $a_y = 0$; force amplitude = 1 N, loss factor = 0.001).

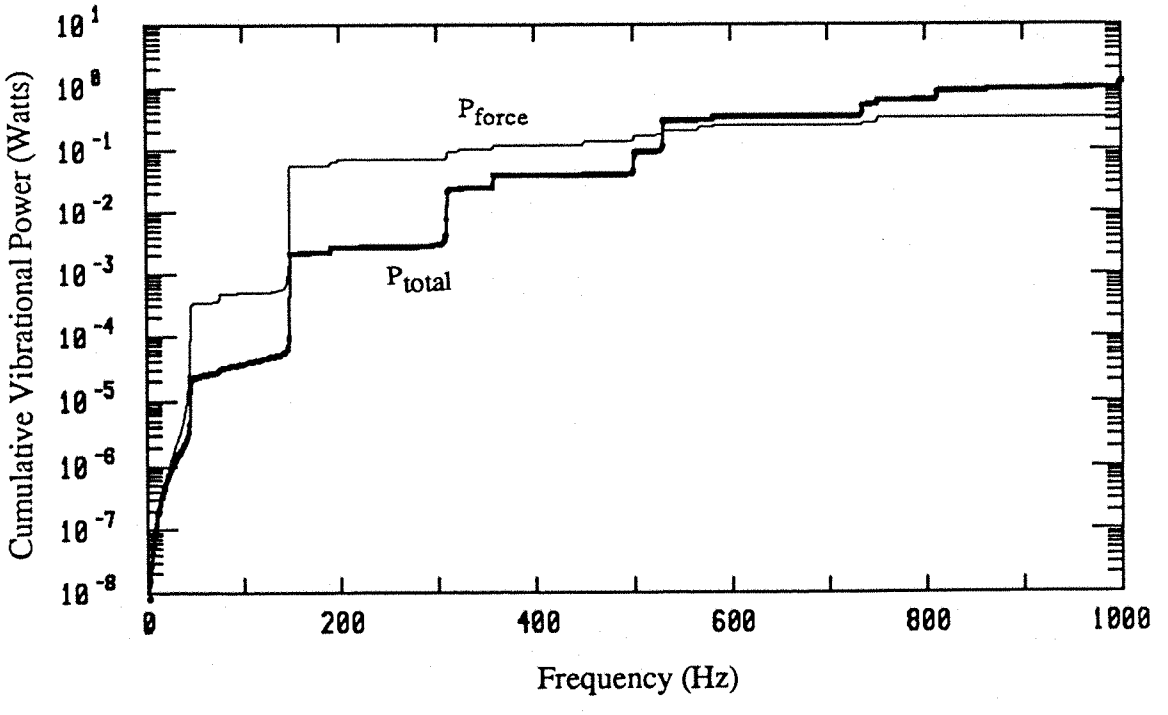

Figure 3.33 : Comparison of the cumulative P_{force} and P_{total} for the CFSF plate in figure 3.32.

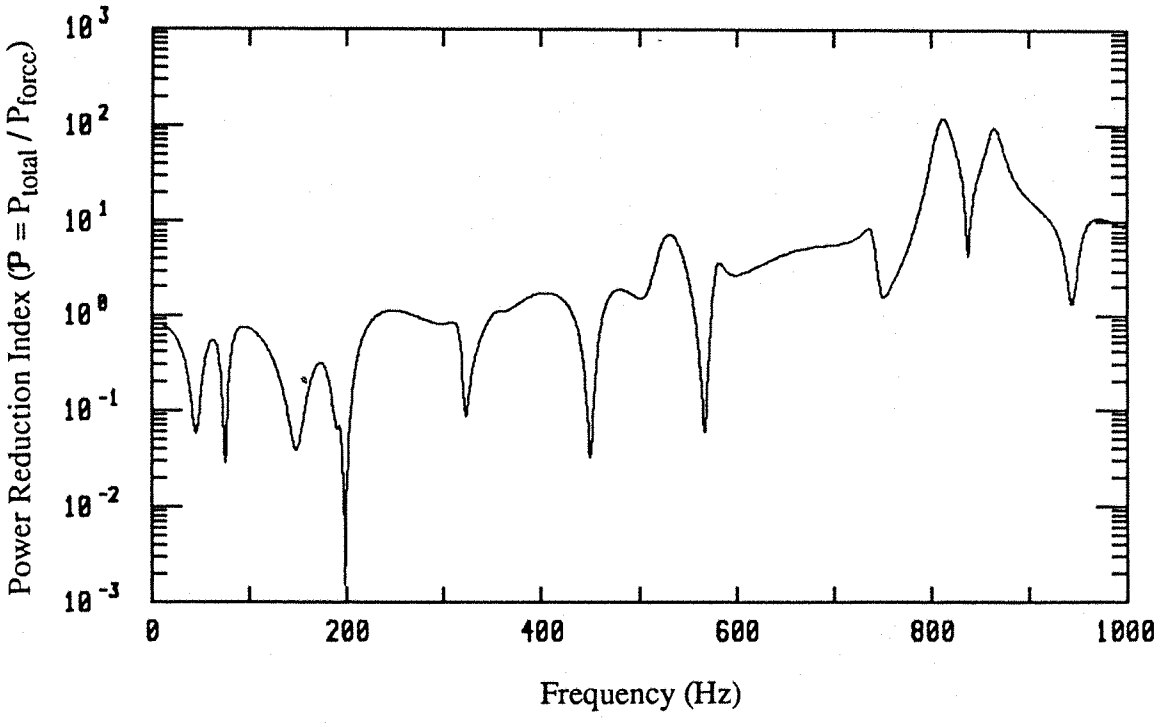

Figure 3.34 : Power reduction index spectrum for the CFSF plate in figure 3.32.

CHAPTER 4

EXPERIMENTAL MEASUREMENTS OF DRIVING POINT MOBILITY FUNCTIONS

4.1 INTRODUCTION

The study of vibrational power input to flexible seating structures subjected to simultaneously acting force and moment excitations requires knowledge of the multi-directional driving point mobility matrix at the excitation point on the structures. The lack of information on moment mobilities, on the coupling mobilities relating linear motions and moments, and rotational motions and forces has been claimed to be a consequence of the lack of commercially available instrumentation for obtaining such data [11,33]. The measurement of rotational responses and excitations and the application of rotational excitation (i.e. moment excitation) are of considerably greater difficulty than measurement of translational responses and force excitation.

This chapter begins with a review of literature concerning various methods for experimental determination of the rotational mobility functions of linear structures. It then continues to describe an experimental arrangement and instrumentation set-up for an approximate method to determine the driving point mobility functions of a CFSF plate via a stiff but light weight carbon fibre reinforced plastic (CFRP) rod. The limitations of the experimental method are discussed and the measured mobility functions are compared with the theoretical predictions.

4.2 REVIEW OF LITERATURE CONCERNING THE MEASUREMENT OF ROTATIONAL MOBILITY FUNCTIONS

The experimental determination of moment mobility functions (i.e. rotational velocities / moments) and the coupling mobility functions (i.e. rotational velocities / forces or translational velocities / moments) has been a subject of considerable interest for the last two decades. Reviews of literature [34-38] show that there are generally two different

approaches of determining these rotational mobility functions by experimental means : the *direct* approach and the *indirect* approach.

The *direct* approach applies forces to measure translational mobility spectra and then extends the results by calculation to obtain the rotational mobility functions. Two different calculation schemes had been reported. The first scheme [34] recognises that the rotational mobility functions are equivalent to spatial derivatives of translational mobility functions (those involving translational velocities and forces). The calculation of these derivatives is performed using conventional translational mobility measurements at discrete locations on the structure and the method of finite differences is adapted to the approximation of these derivatives. The second scheme [35] is the modal constant derivation scheme which makes use of the orthogonality of normal modes and the modal identification technique to derive the rotational mobility functions involving rotational responses from the measured mobility functions involving only the translational responses. However, as was cautioned by Ewins [33], this modal constant derivation process itself gives rise to an inherent error when the frequency range covered does not, of course, include all the natural frequencies of the structure. The performance of this process also depends on the number and locations of the data points used to determine the modal constants.

The *indirect* approach utilises a fixture or exciting block with predetermined dynamic properties to which vibration exciters are attached through force transducers to measure dynamic forces and, indirectly, dynamic moments applied to a point on the structure. The fixture or exciting block also facilitates rotational response measurements on the structure using conventional translational motion transducers [36]. A slightly different approach is the so-called 'scalar fixture method' [37] which employs two calibrated vibration exciters simultaneously to produce accelerometer response measurements which are directly proportional to the elements of the unknown structural mobility matrix. However, in using this method, care must be taken to avoid errors introduced by the fixture. A summary of these measurement methods, except the modal constant derivation scheme, can be found in [38].

In a more recent article, Petersson [39] reviewed the magnetostriction phenomenon and some of the important properties of alloys possessing strong magnetostrictive features which are of interest in experimental structural acoustics. Two versions of the moment exciter which consisted of primarily two giant magnetostrictive rods (Terfenol-D) operating in anti-phase to impart moment excitation to the test structure were described and the performance of the moment exciters was discussed. The work is exploratory,

besides the high cost of the alloy, the performance of the exciter was affected by the inherent non-linearity in the operating characteristics of a giant magnetostrictive sample.

4.3 SPECIMEN AND TEST RIG DESIGN

The test specimen was a 4.1mm thick rectangular steel plate having dimensions of 645mm by 390mm. In order to ensure the flatness of the plate, a high grade ground flat stock was used. The plate was clamped along the edge $x=0$ and simply supported along the opposite edge $x=a$, with the other pairs of edges parallel to the X-axis free. The so-called CFSF configuration. The effective lengths of the plate upon the clamped and simply supported fixtures were : a =585mm and b =390mm as shown in figure 4.1.

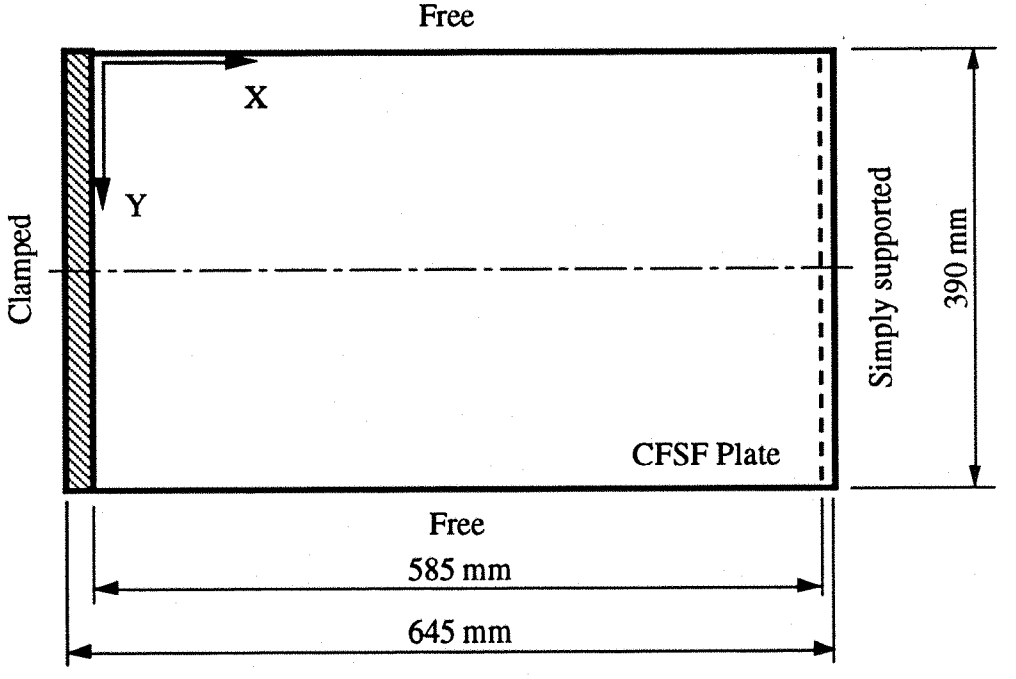

Figure 4.1 : A rectangular flat plate with CFSF configuration.

The clamped fixture consisted of an upper steel bar of dimensions: 400mm length x 50mm width x 25mm thick and a lower steel block of dimensions: 480mm length x 50mm width x 75mm height. The lower steel block was clamped firmly to a vibration isolated test block by six M12 studs. The edge of the steel plate along $x=0$ was clamped between the upper bar and the lower block by nine equally spaced M12 screws and studs. The simply supported fixture along the plate edge $x=a$ consisted of two cylindrical steel shafts of diameter 25.4mm. The ends of the shafts were supported on separate sets of bearing housings which were held in the bearing housing assemblies. The bearing housing assemblies were clamped firmly on the same vibration isolated test

block and the bearing housings were arranged such that the axes of the shafts were horizontal and aligned in a vertical plane. Sectional views of the upper and lower bearing housing assemblies are shown in figure F1 of Appendix F.

4.4 FORCE AND MOMENT EXCITATION ARRANGEMENTS

For measurment of the driving point force mobility function, Y_{11} and the coupling mobility functions between the translational force and the rotational velocities, i.e. Y_{21} and Y_{31}, the force excitation arrangement used is shown in figure 4.2 (a). The excitation force was created by an electro-dynamic exciter which consisted of a fixed permanent magnet and a moving coil. A photograph showing the force excitation arrangement is given in figure F2 of Appendix F.

For measurement of the driving point moment mobility functions, i.e. Y_{22} and Y_{33} and the coupling mobility function between the moment and the rotational velocity about different axes, i.e. Y_{32}, the moment excitation arrangement used is shown in figure 4.2 (b). An electro-dynamic exciter (Ling shaker) was connected to the force transducer by a nylon flexible connector. The force transducer was attached to the carbon fibre reinforced plastic (CFRP) rod which was glued to the plate by a quick setting cyano-acrylate adhesive. The CFRP rod was driven horizontally in the negative X direction for M_y excitation and subsequently in the positive Y direction for M_x excitation. Two photographs showing the M_x and M_y excitation arrangements are given in figures F3 and F4, respectively, of Appendix F. The rod had a cross-sectional area of 9.5mm x 9.5mm and a length of 50mm. The moment arm used to induce the moment excitation about the in-plane X or Y axis was 35mm. This was the shortest possible moment arm available from the Ling shaker without causing interference with the plate. In this moment excitation arrangement, it was assumed that the in-plane translational motions induced by the in-plane force (i.e. F_x or F_y) had negligible influence on the measured transverse motions.

4.5 INSTRUMENTATION SET-UP

The instrumentation set-up used to measure the driving point mobility functions of the CFSF plate at the off-centre location (x=0.22a, y=0.62b) is shown in figure 4.3. A random signal (20Hz to 20kHz white noise) was generated from the signal generator (B&K type 1405) which was connected to a power amplifier to drive the electro-dynamic exciter. An ammeter and a safety fuse were incorporated to prevent overloading of the exciter coil. The excitation force was measured by a force transducer

(B&K type 8200). The responses of the plate at the excitation point were measured by two closely matched accelerometers (B&K type 4375) placed at equal distances (20mm) from the excitation point along the X-direction (for w and θ_y degrees-of-freedom) and subsequently along the Y-direction (for w and θ_x degrees-of-freedom). The lateral translational response (i.e. acceleration) was obtained by averaging the two accelerometer signals. Alternatively, it was also measured by a single accelerometer placed at the excitation point but on the opposite side of the plate. The rotational responses were obtained by subtracting one of the accelerometer signals from the other and dividing the difference by the spacing between the two accelerometers.

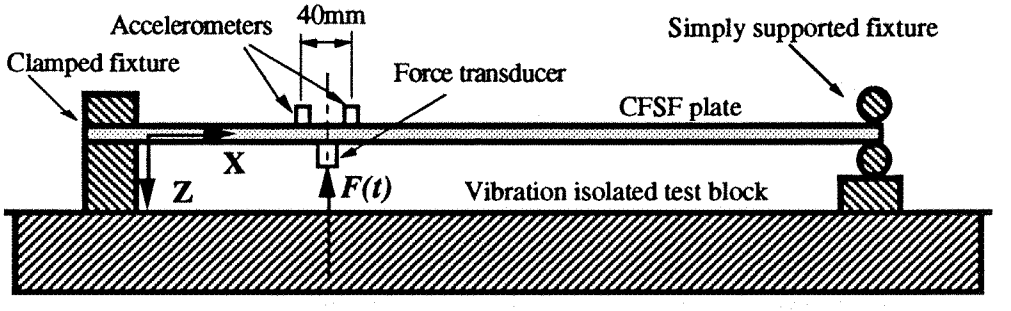

(a) Force excitation arrangement

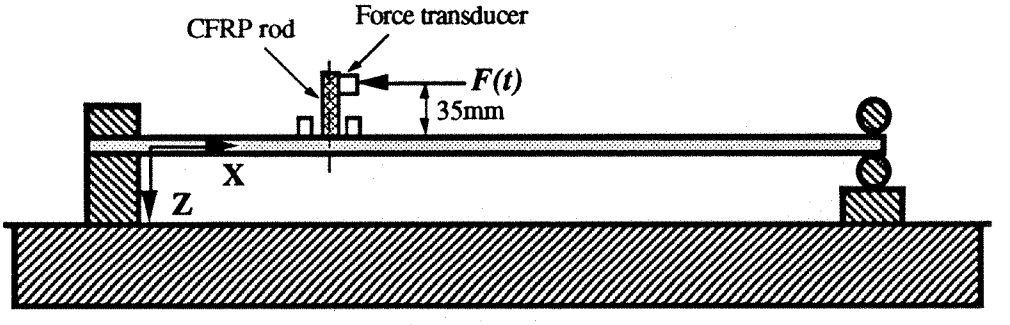

(b) Moment excitation arrangement

Figure 4.2 : Force and moment excitation arrangements for measurement of the driving point mobility functions of the CFSF plate.

The force and acceleration signals were passed through the charge amplifiers (B&K type 2635) and the anti-aliasing (low pass) filters (KEMO Dual Channel Elliptic Filters) and were displayed on an oscilloscope for visual signal monitoring. The analogue signals were then sampled and converted to digital form by a computer controlled data acquisition board (DT 2828) driven by PROSIG PC-DATS data acquisition modules.

The acquired data were then de-multiplexed and stored in a micro-computer for subsequent signal processing using the relevant PC-DATS routines.

The sampling rate used was 4096 samples per second and the number of samples per channel (data length) was 32000. The measured translational and rotational acceleration time histories were first normalised and the respective power spectral and cross spectral density functions were determined to compute the coherence functions and the frequency response functions (i.e accelerances) using the H_1 estimator, which is defined as *the ratio of the cross spectral density function between the input and the response signals to the power spectral density function of the input signal.* The measured driving point accelerances were then converted to the required mobility functions. The frequency resolution of the measured frequency response functions was 2Hz. The job files containing PC-DATS commands used to perform these calculations are listed in Appendix F.

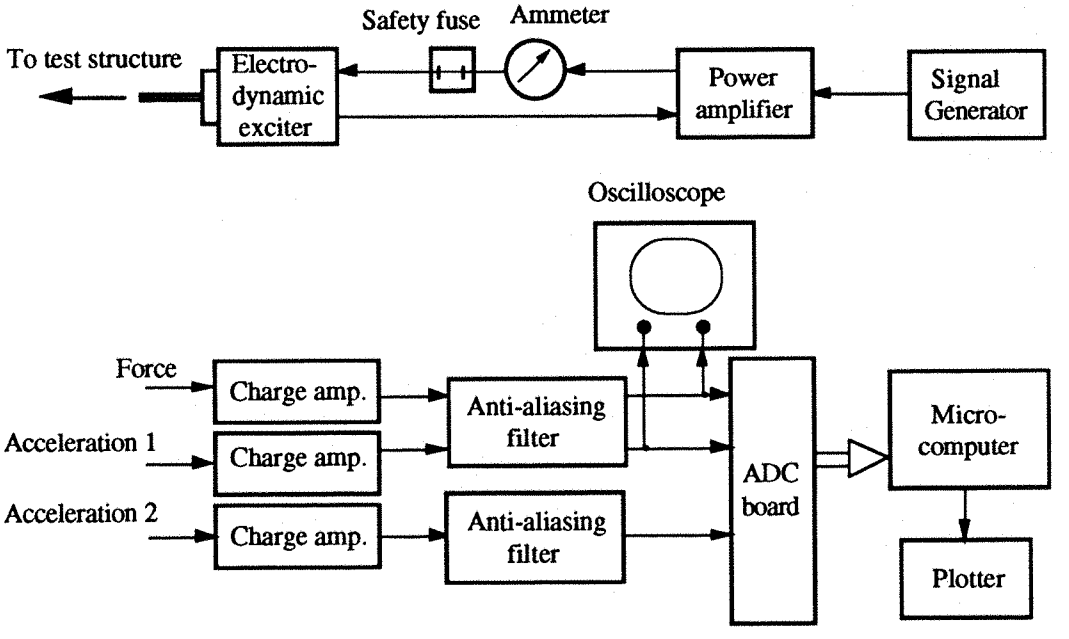

Figure 4.3 : Instrumentation set-up for measurement of the mobility functions.

4.6 EXPERIMENTAL RESULTS AND DISCUSSION

4.6.1 Results of Force Excitation Measurements

The modulus spectra of the driving point force mobility function and the coupling mobility functions between the translational force and the rotational velocities measured with the force excitation arrangement (fig. 4.2(a)) are shown in figures 4.4 to 4.6. The

coherence functions between the force and the response signals calculated for each of these mobility functions are also given in these figures. Comparisons of the modulus spectra of these mobility functions with the theoretical results are shown in figures 4.7 to 4.9. It can be seen that :

(1) there is a good agreement between the measured force, Y_{11} and the Y_{31} coupling mobility functions and the theoretical results.

(2) The agreement between the measured and the theoretical Y_{21} coupling mobility functions is better for the responses around the resonance frequencies than those around the anti-resonance frequencies. This is most likely due to poor signal to noise ratios as suggested by the low coherence region below 300Hz. For the lower order modes, the difference between two accelerometer signals can be very small, especially around the anti-resonance frequencies.

The comparison between the experimental and the theoretical results ends at 800Hz. Above this frequency, the measured mobility functions were likely to be influenced by the rotary inertia of the force transducer and the exciter coil. The coherence functions given in figures 4.4 to 4.6 show a drop in value for frequencies above 850Hz. This effect was also noted in past experimental measurements. Theoretically, it is also possible that the Euler-Bernoulli beam functions used in solving for the plate responses tend to be less accurate at high frequencies due to the effects of shear deformation and rotary inertia of beam sections.

4.6.2 Results of Moment Excitation Measurements

Before looking at the results obtained from the moment excitation measurements and their comparison with the theoretical results, it is important to evaluate the appropriateness of the CFRP rod arrangement as shown in figure 4.2 (b) and its limitations.

a. Evaluation of the Carbon Fibre Reinforced Plastic (CFRP) Rod Arrangement

The configuration as shown in figure 4.2 (b) for moment excitation measurements was selected after a number of trials. The evaluation was performed for the selection between :

(1) the types of electro-dynamic exciter : permanent magnet with two different types of moving coil or the Ling shaker ;
(2) the types of flexible connector for the Ling shaker : nylon threaded stud, steel threaded stud or flexible steel wire ;
(3) the methods of holding the Ling shaker : freely suspended by elastic springs or clamped at the base of the shaker to a shaker support ;
(4) the types of exciting rod : CFRP rod or a steel rod of the same dimensions.

For each of these exciter combinations, the driving point accelerance of the CFRP rod or the steel rod with one end glued to the clamped test fixture was measured. It was found that for the combination of the Ling shaker with the nylon flexible connector and the CFRP rod with a moment arm of 35mm, the first resonance frequency of the cantilevered CFRP rod occured at about 1400Hz which was the highest among all the other types of exciter arrangement investigated. The modulus spectrum of the driving point accelerance and the coherence function of this CFRP rod and exciter arrangement are given in figure F5 of Appendix F. For an ideal set-up, the modulus spectrum of the CFRP rod accelerance, in the Log-Log plot, should be a straight line which increases with increasing frequency, i.e. a constant stiffness configuration. The evaluation also showed that there was no significant difference between the measured accelerances when the Ling shaker was freely suspended or fixed at the base. In all the subsequent measurements, the fixed base configuration was used.

The driving point accelerance of a system consisted of the CFRP rod with one end glued to the CFSF plate at the off-centre location (x=0.22a and y=0.62b) was also measured. A comparison of the modulus spectrum of the accelerance with that measured on the clamped test fixture is given in figure F6 of Appendix F. It can be seen that there are many resonance peaks in the accelerance measured on the plate. These peaks correspond to the resonance responses of the plate. However, the first resonance frequency of the cantilevered CFRP rod on the plate was about 800Hz, a significant reduction compared with the value achieved when attached to the clamped fixture.

b. Reciprocity Check between the Force and Moment Excitation Measurements

For linear systems, the driving point mobility matrix is a symmetric matrix. Hence, the coupling mobility functions between the translational velocity and the moment excitations, i.e. Y_{12} and Y_{13} , should be equal to the coupling mobility functions between the rotational velocities and the force excitation, i.e. Y_{21} and Y_{31} respectively. Figures 4.10 and 4.11 show the comparison between the modulus spectra of these

coupling mobility functions measured with the force excitation and the moment excitation arrangements. The agreement between these two sets of mobility functions is reasonably good, which not only confirms the accuracy of the computer routines used to calculate the mobility functions for the force and the moment excitations, but also suggests that moment excitation via a CFRP rod is appropriate except for frequencies approaching the resonance frequency of the CFRP rod. At frequencies approaching the fundamental resonance frequency of the cantilevered CFRP rod, the measured responses tend to be increased as shown in figure F6.

c. Results for the Driving Point Moment and Coupling Mobility Functions

The modulus spectra of the driving point moment mobility functions, Y_{22} and Y_{33}, and the coupling mobility functions between the moment excitations and the rotational velocities about a different axis, i.e. Y_{32} or Y_{23} together with the respective coherence functions are shown in figures 4.12 to 4.14. The measured mobility functions, in general, are scattered at low frequencies, which is most likely due to poor signal to noise ratios and probably insufficient frequency resolution as was suggested by the 'broad-band' low coherence function for each of these mobility functions. The result for Y_{32} is the worst among the three mobility functions. As this function was measured with a pair of accelerometers which was placed along an axis perpendicular to the excitation direction, the measured response signals were the smallest compared with the response signals in other orientations.

Comparisons of the modulus spectra of these moment and coupling mobility functions with the theoretical results are shown in figures 4.15 to 4.17. It can be seen that the measured resonance frequencies match quite closely with the theoretical results. However, the off-resonance moduli of the measured moment mobility functions are generally greater than the theoretical predictions. This observation is consistent with the discussion on the number of terms used in the solution for plate responses (Section 3.5.4). As only a finite number of terms (9x7) were used to solve for the transverse displacements of the CFSF plate, the resulting moduli of the driving point moment mobility functions would be less than the moduli of the measured mobility functions. It is also likely that for frequencies approaching 800Hz, the responses tend to be amplified by the fundamental resonance of the CFRP rod.

An attempt was made to repeat the measurement of the driving point moment and coupling mobility functions via the moment excitation arrangement with an HP 3566A Spectrum Analyser. The frequency resolution was set at 0.5Hz and a total of 50

averages were used to estimate the frequency response functions. Comparisons of the modulus spectra of this set of mobility functions with the theoretical results are shown in figures F7 to F9 of Appendix F. In spite of the fact that the finer frequency resolution and the smaller statistical variances smoothed the data in the low frequency region, the off-resonance moduli of the moment mobility functions are consistently greater than the theoretical results even at low frequencies, when the flexural wavelengths are much larger than the plate thickness. This suggests that the discrepancy is most likely attributed to the thin-plate theory.

Dyer [40] in his paper, gave an excellent explanation for this discrepancy. In his work of deriving the moment impedance of an infinitely extended plate using higher order plate theory which allows for transverse shear deformation and rotary inertia, it was shown that classical thin-plate theory was inadequate when the distance over which the moment was applied was smaller than plate thickness, a condition which is inherently implied in the derivation of moment mobility functions as given in Chapter 3, Section 3.3.3 (c). Under this condition, a significant part of the plate reaction is in local twist or shear. The infinite transverse shear modulus or negligible transverse shear deformation implicitly assumed in classical thin-plate theory will result in a lower driving point moment mobility functions than the actual or measured results.

4.7 SUMMARY

The driving point mobility functions of a CFSF plate at an off-centre location of $x=0.22a$ and $y=0.62b$ have been measured with conventional electro-dynamic exciter and translational accelerometers. The moment related mobility functions, i.e. Y_{22}, Y_{33} and Y_{32} or Y_{23} were measured via a CFRP rod with one end glued to the plate for inducing the moment excitation to the plate. This approximate method of measurement was found to be adequate in the frequency range below the fundamental resonance frequency of the cantilevered rod with end mass. Within the limits of measuring the rotational motion using two translational accelerometers, the measured driving point mobility functions of the CFSF plate are in good agreement with the theoretical predictions. However, as the predicted moment mobility functions are consistently lower than the measured results even at low frequencies, it confirms that classical thin-plate theory is inadequate for predicting the driving point moment mobility functions. The derivation of the driving point mobility functions of rectangular plates in flexural vibration, as described in Chapter 3, and the experimental determination of these mobility functions have also been reported in [41].

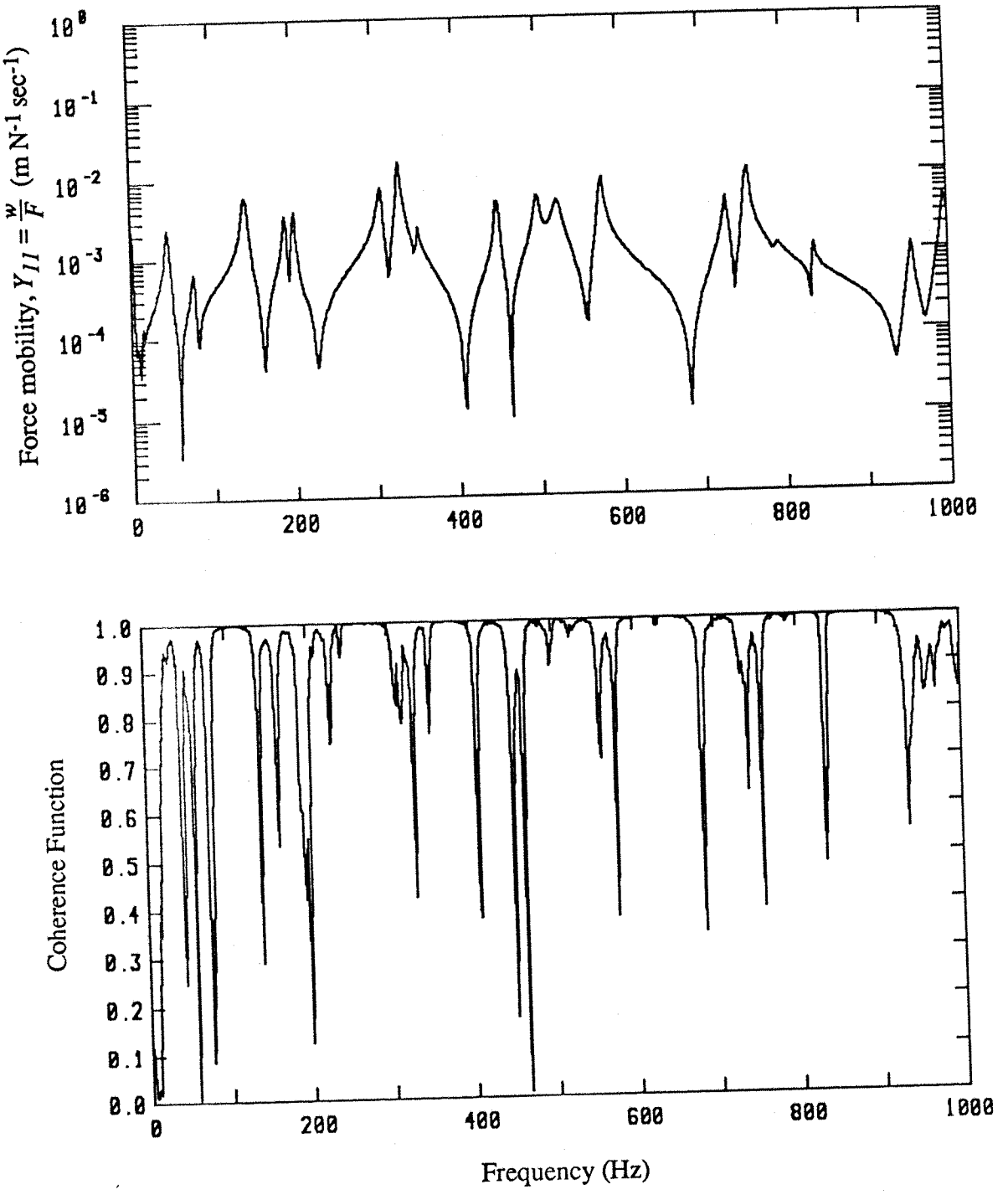

Figure 4.4 : Experimental results : modulus spectrum of the driving point force mobility function, Y_{11} and the coherence function for the CFSF plate at an off-centre point : x=0.22 *a*, y=0.62 *b*.

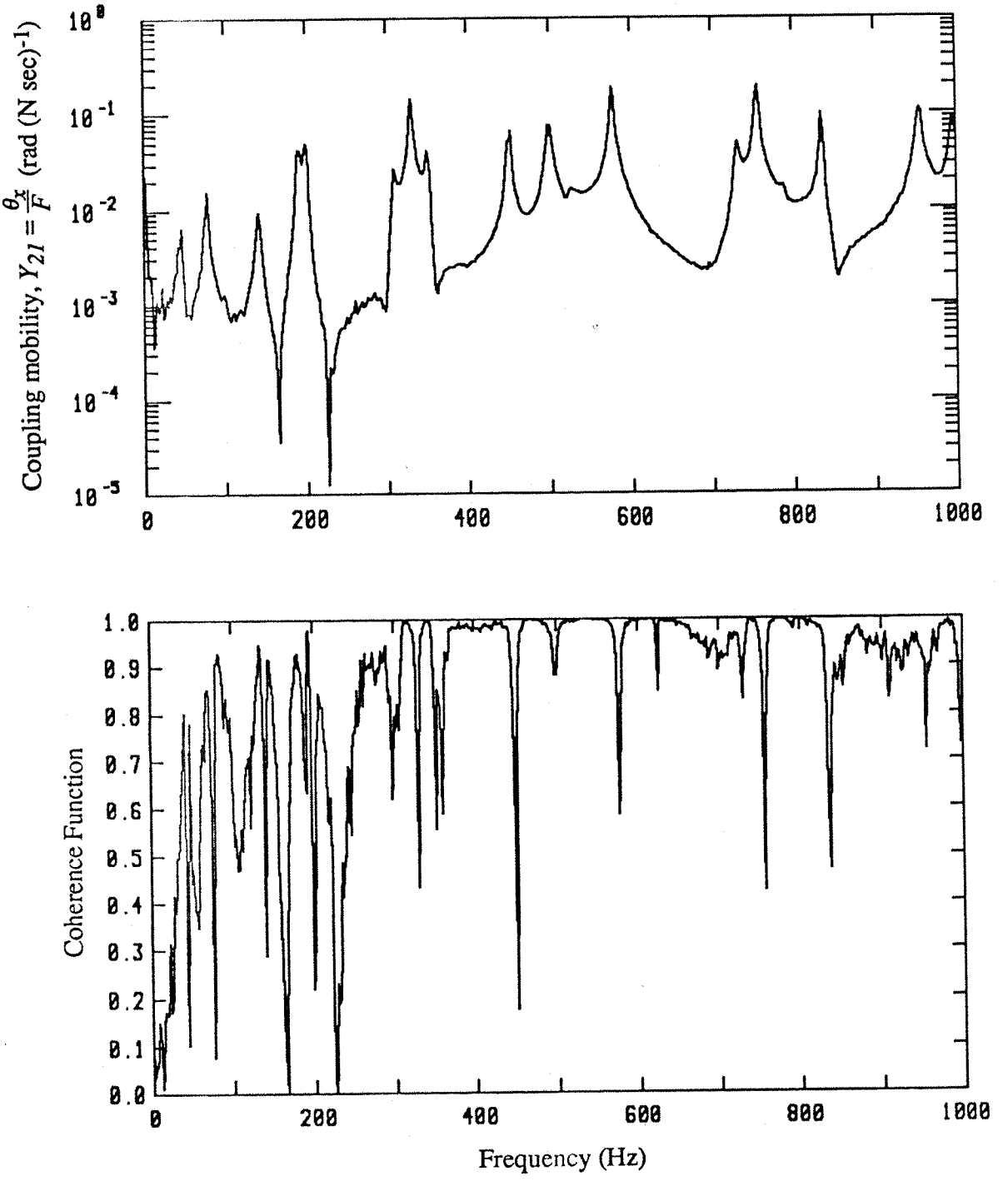

Figure 4.5 : Experimental results : modulus spectrum of the driving point coupling mobility function, Y_{21} and the coherence function for the CFSF plate at an off-centre point : x=0.22 *a*, y=0.62 *b*.

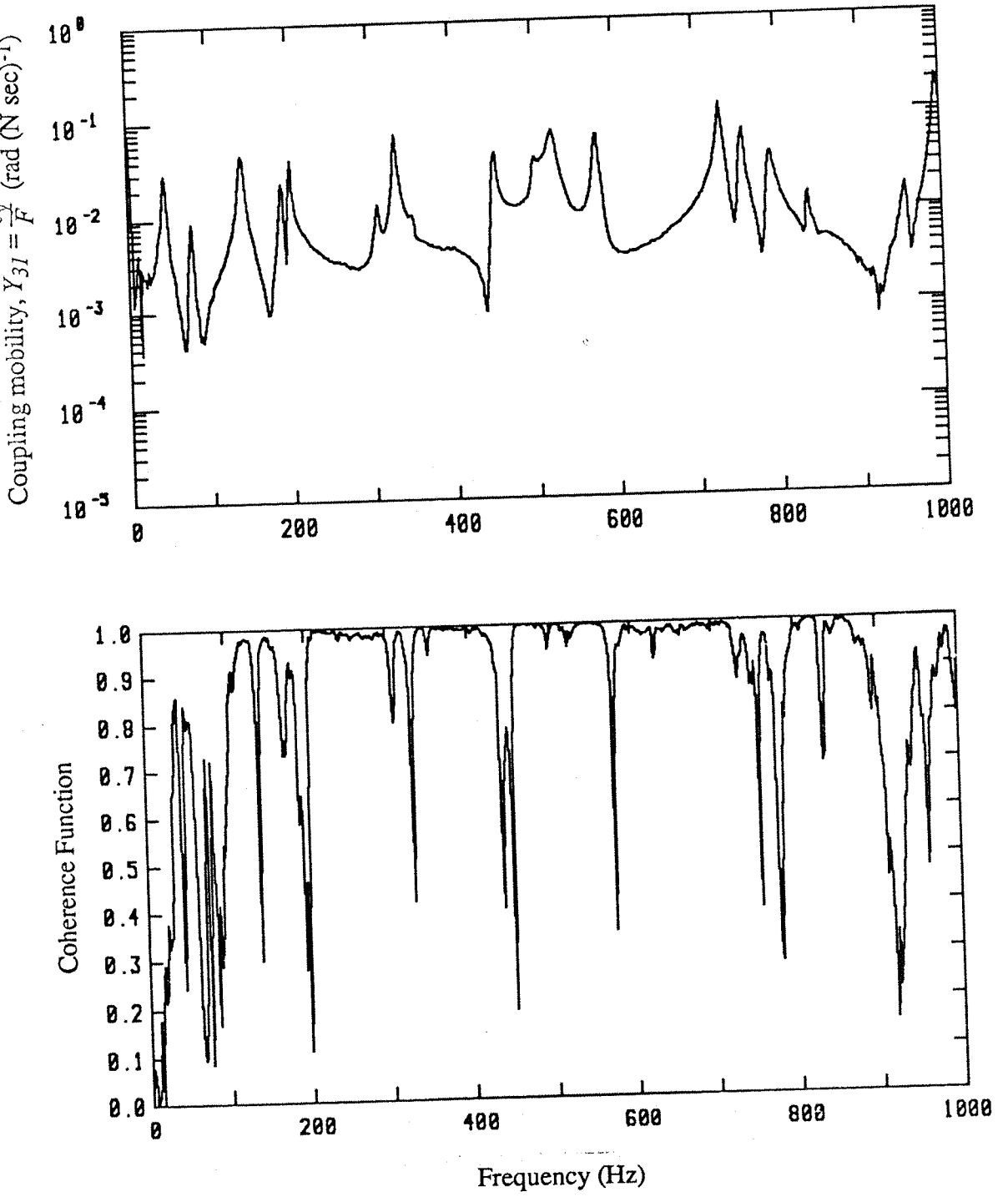

Figure 4.6 : Experimental results : modulus spectrum of the driving point coupling mobility function, Y_{31} and the coherence function for the CFSF plate at an off-centre point : x=0.22 *a*, y=0.62 *b*.

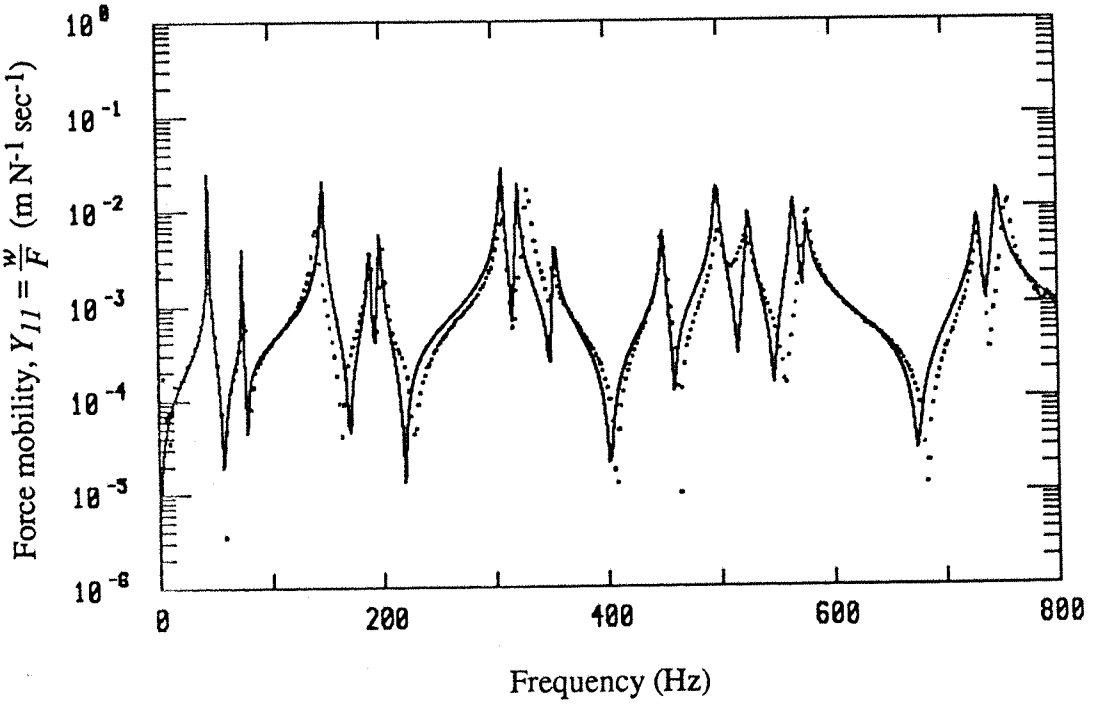

Figure 4.7 : Comparison of the modulus spectra of Y_{11} for the CFSF plate : —— Theoretical result (η = 0.005),····· Experimental result.

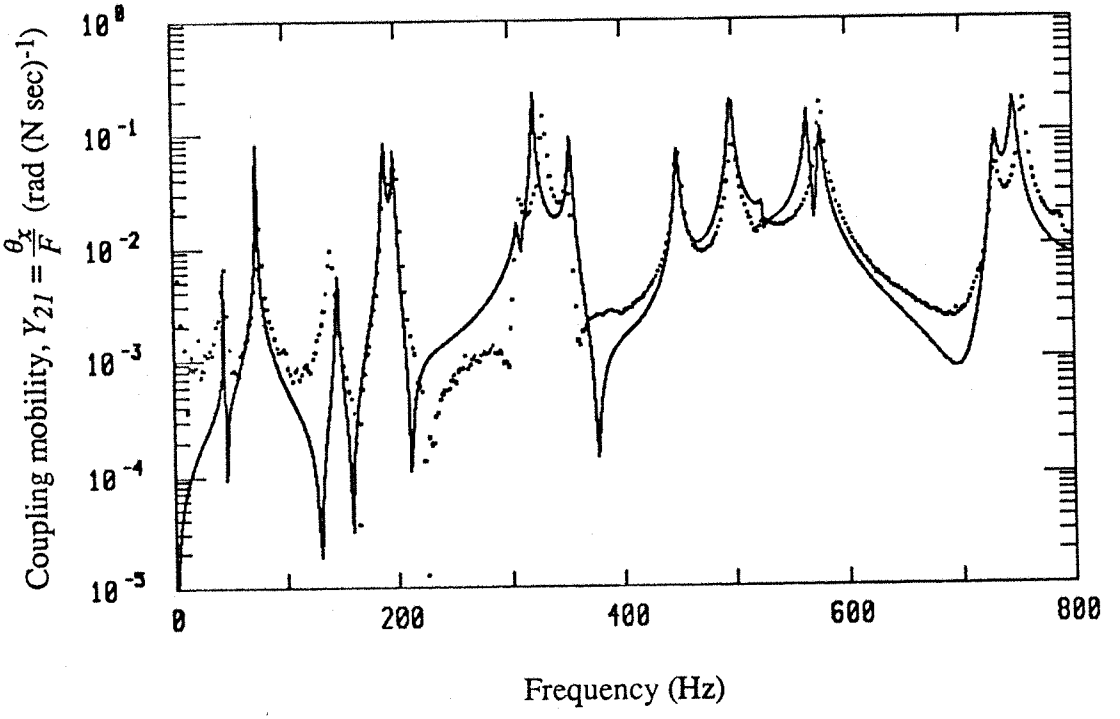

Figure 4.8 : Comparison of the modulus spectra of Y_{21} for the CFSF plate : —— Theoretical result (η = 0.005),····· Experimental result.

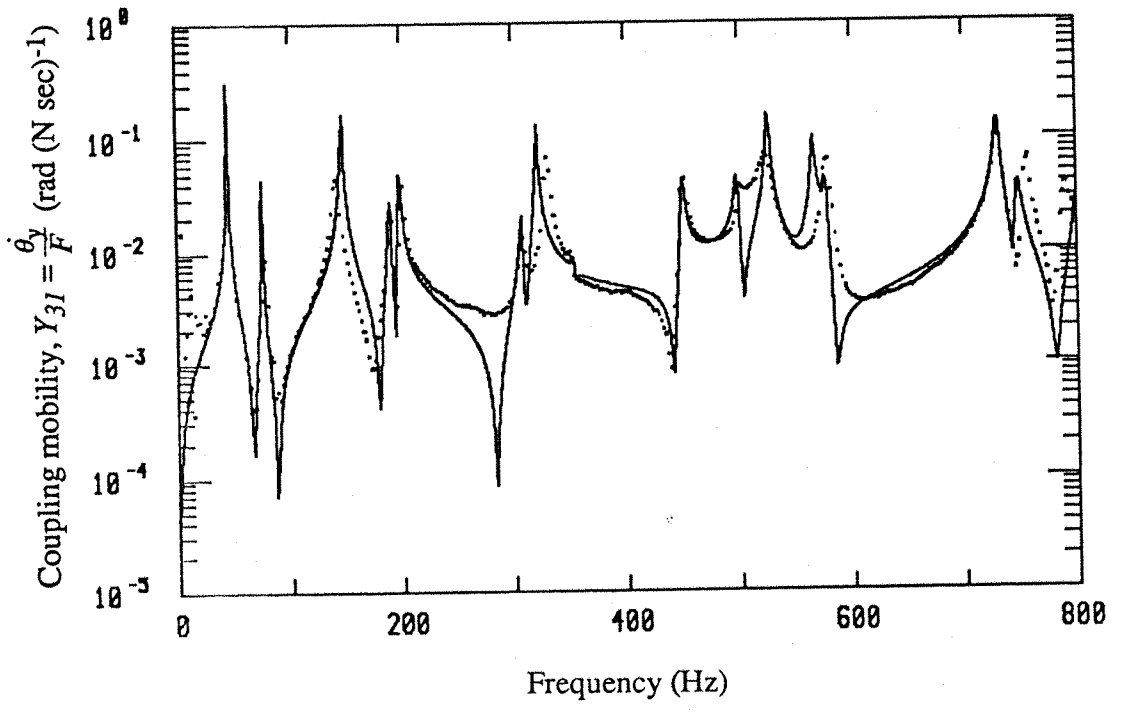

Figure 4.9 : Comparison of the modulus spectra of Y_{31} for the CFSF plate : —— Theoretical result (η = 0.005),····· Experimental result.

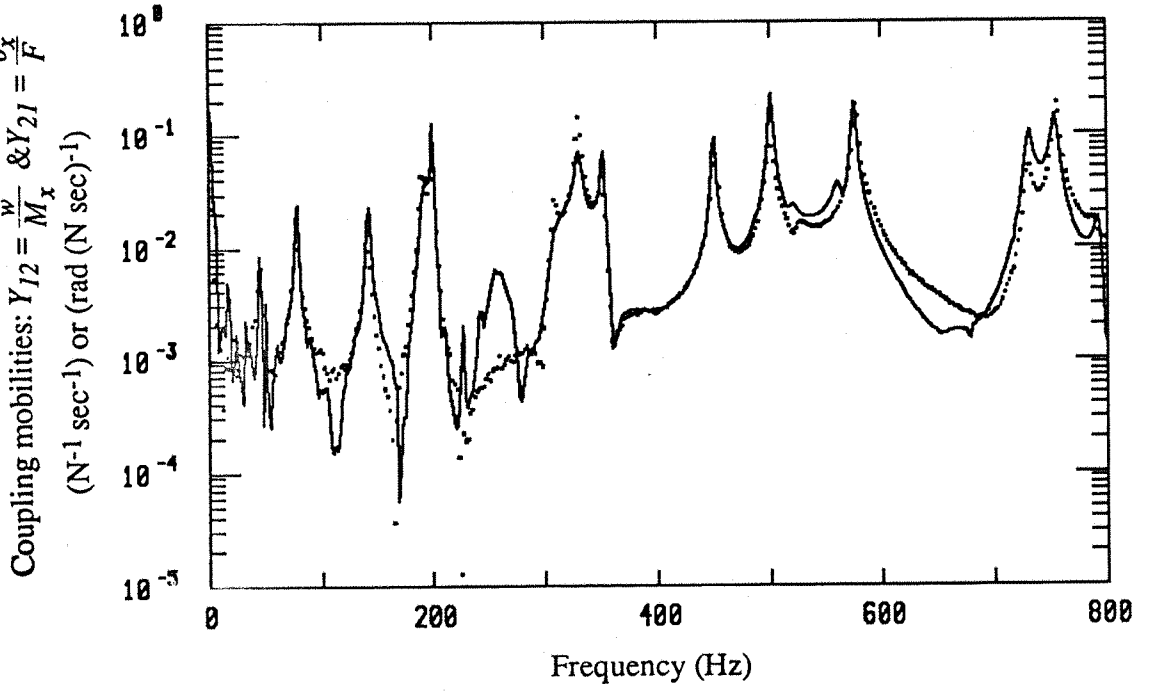

Figure 4.10 : Reciprocity check : comparison of the modulus spectra of Y_{21} and Y_{12} for the CFSF plate : —— Y_{12} ,····· Y_{21}.

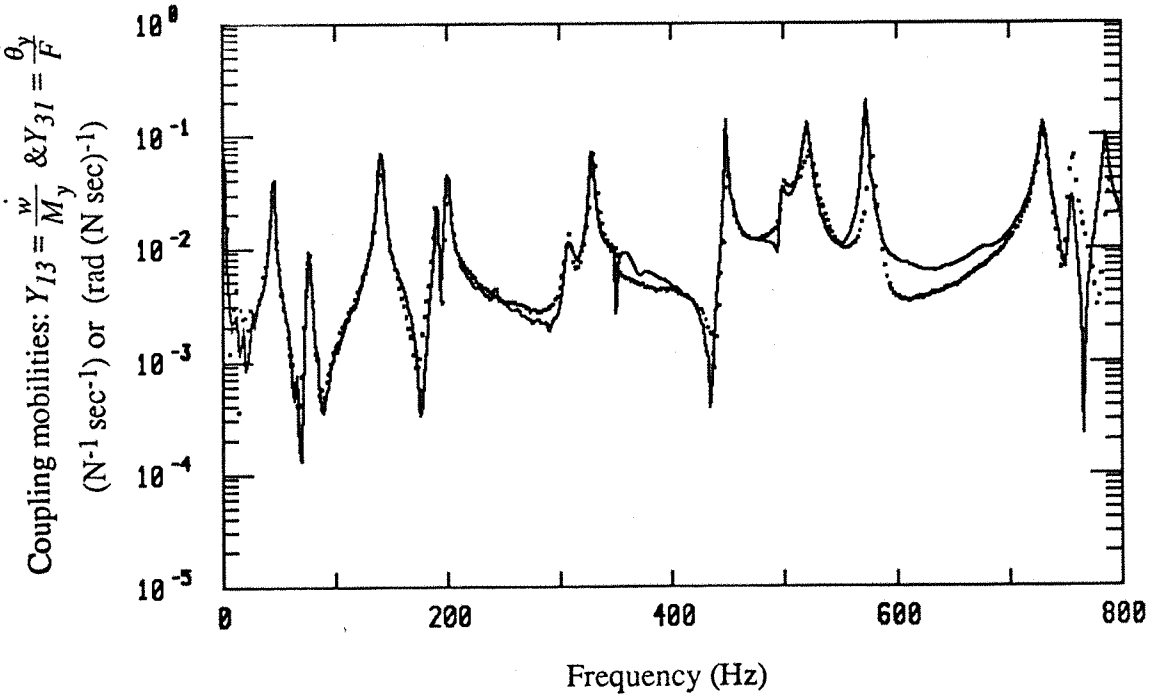

Figure 4.11 : Reciprocity check : comparison of the modulus spectra of Y_{31} and Y_{13} for the CFSF plate : —— Y_{13} ,····· Y_{31}.

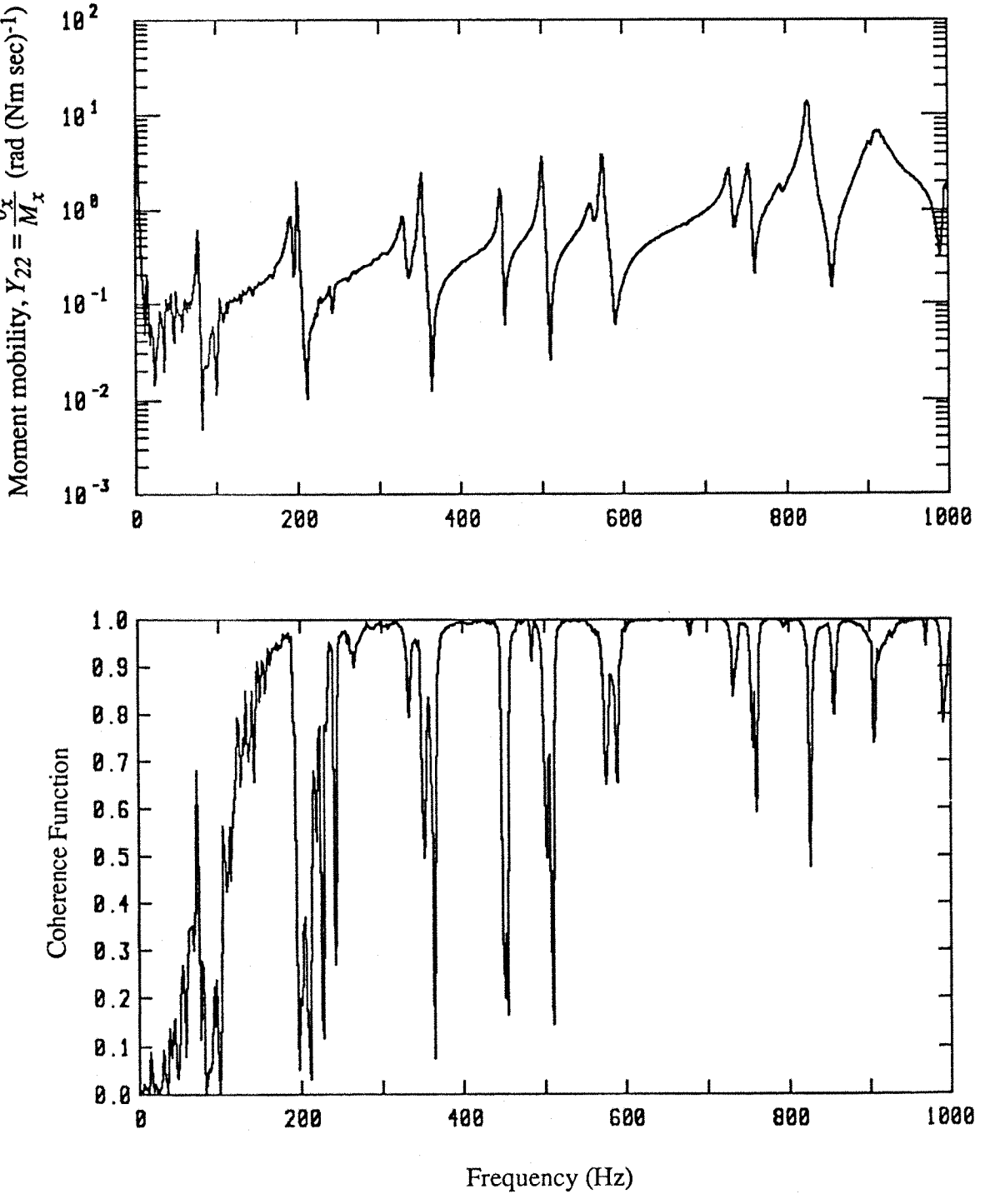

Figure 4.12 : Experimental results : modulus spectrum of the driving point moment mobility function, $\dot{Y}_{22}$ and the coherence function for the CFSF plate at an off-centre point : x=0.22 *a*, y=0.62 *b*.

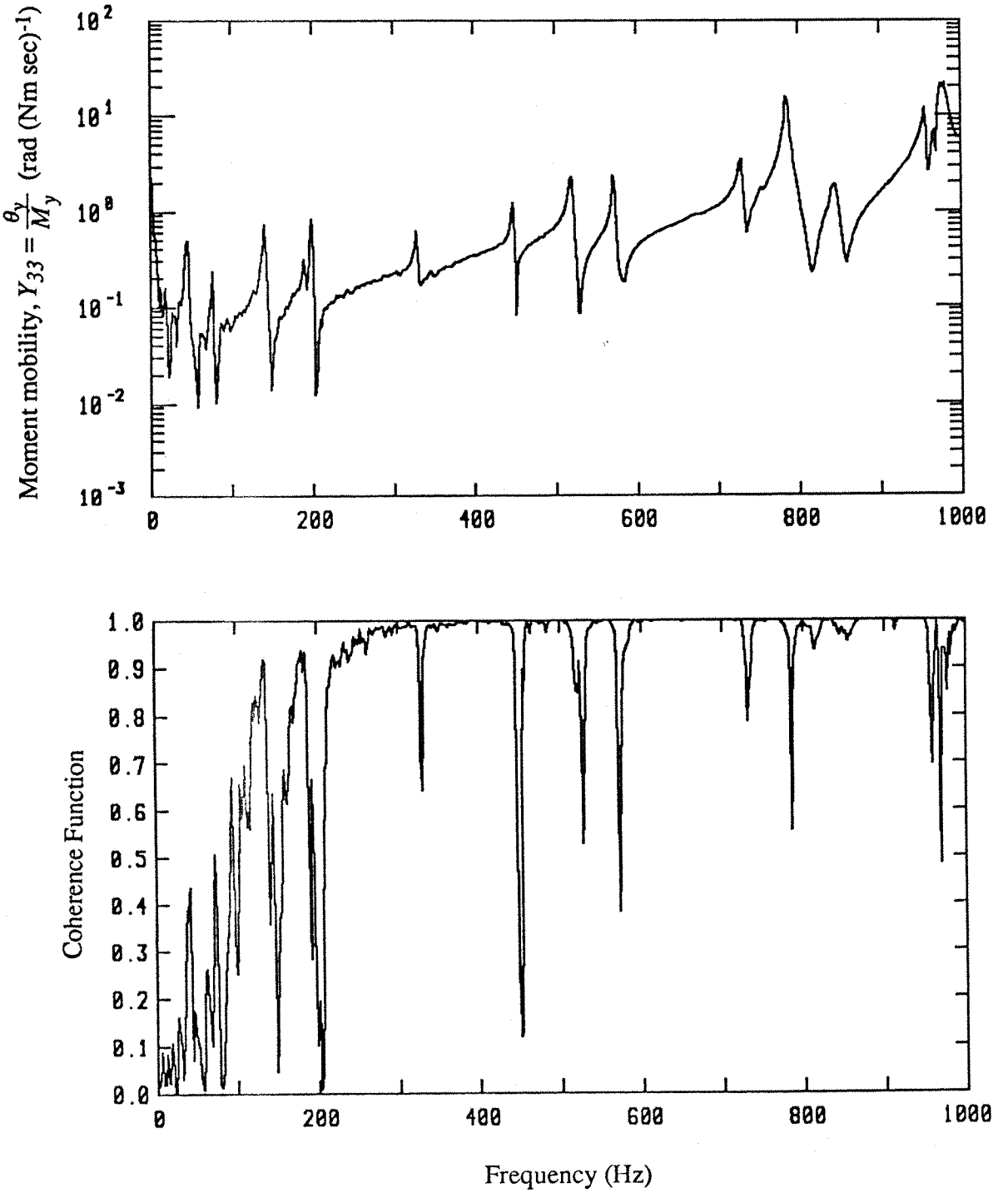

Figure 4.13 : Experimental results : modulus spectrum of the driving point moment mobility function, Y_{33} and the coherence function for the CFSF plate at an off-centre point : x=0.22 *a*, y=0.62 *b*.

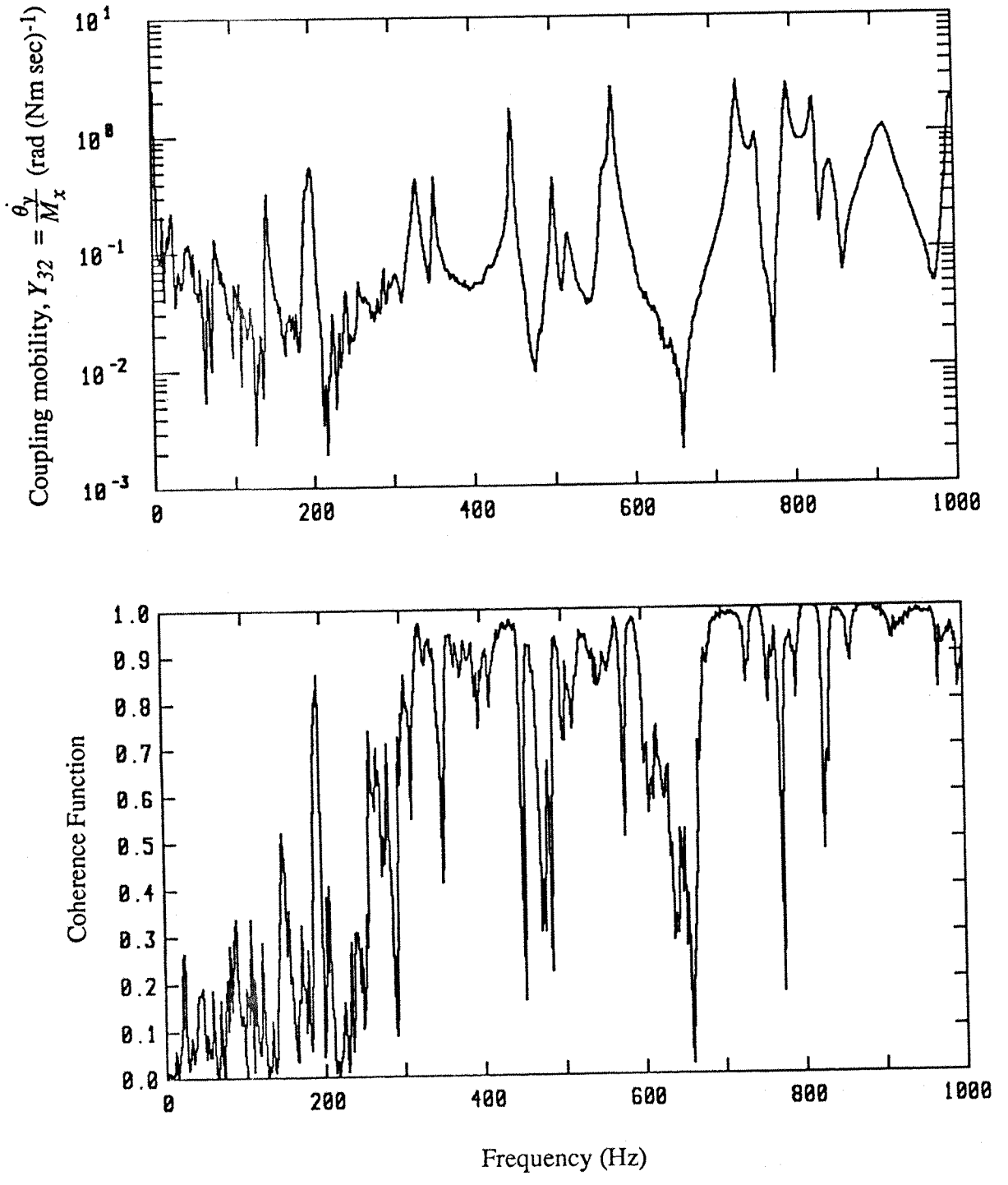

Figure 4.14 : Experimental results : modulus spectrum of the driving point coupling mobility function, Y_{32} and the coherence function for the CFSF plate at an off-centre point : x=0.22 *a*, y=0.62 *b*.

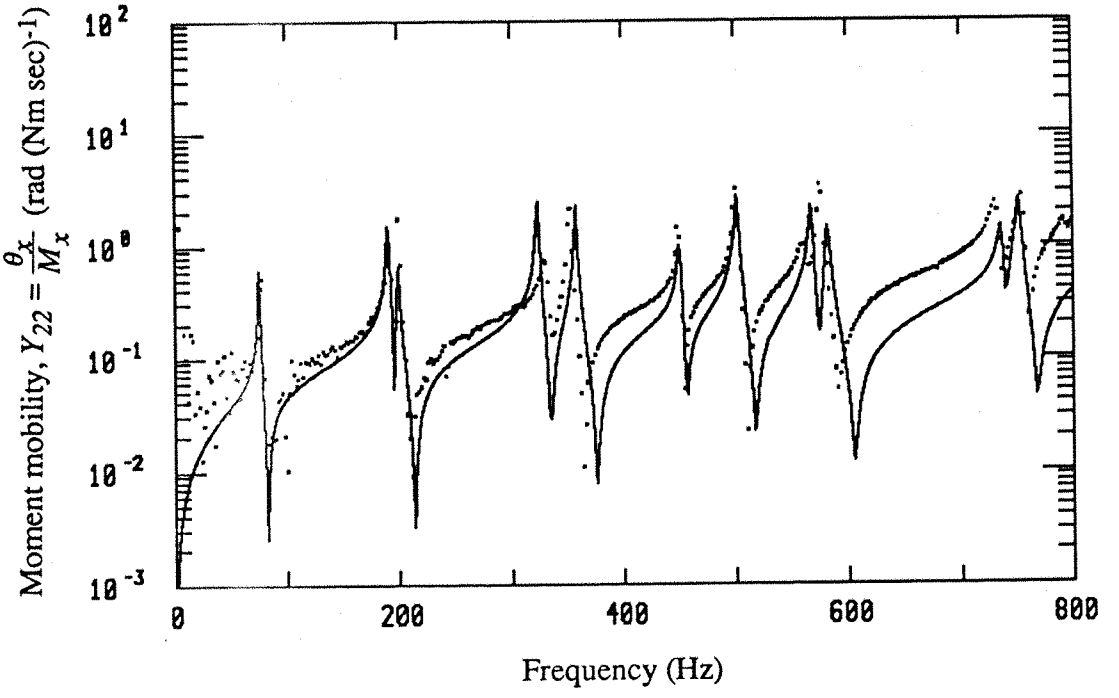

Figure 4.15 : Comparison of the modulus spectra of Y_{22} for the CFSF plate : —— Theoretical result (η = 0.005),····· Experimental result.

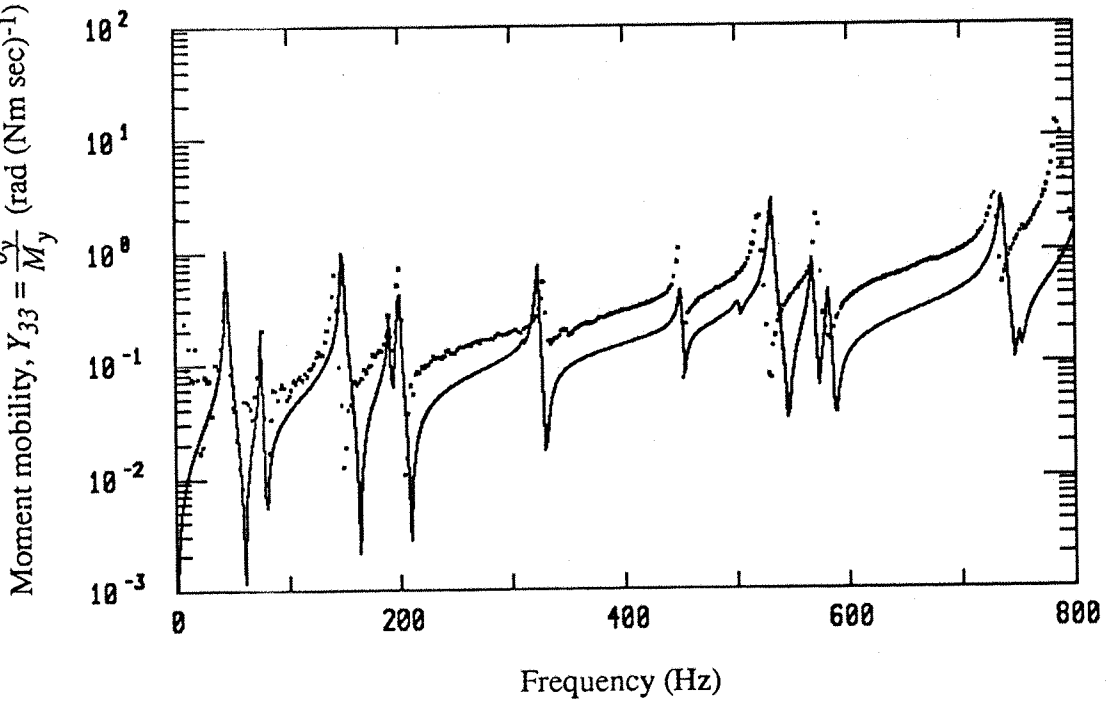

Figure 4.16 : Comparison of the modulus spectra of Y_{33} for the CFSF plate : —— Theoretical result (η = 0.005),····· Experimental result.

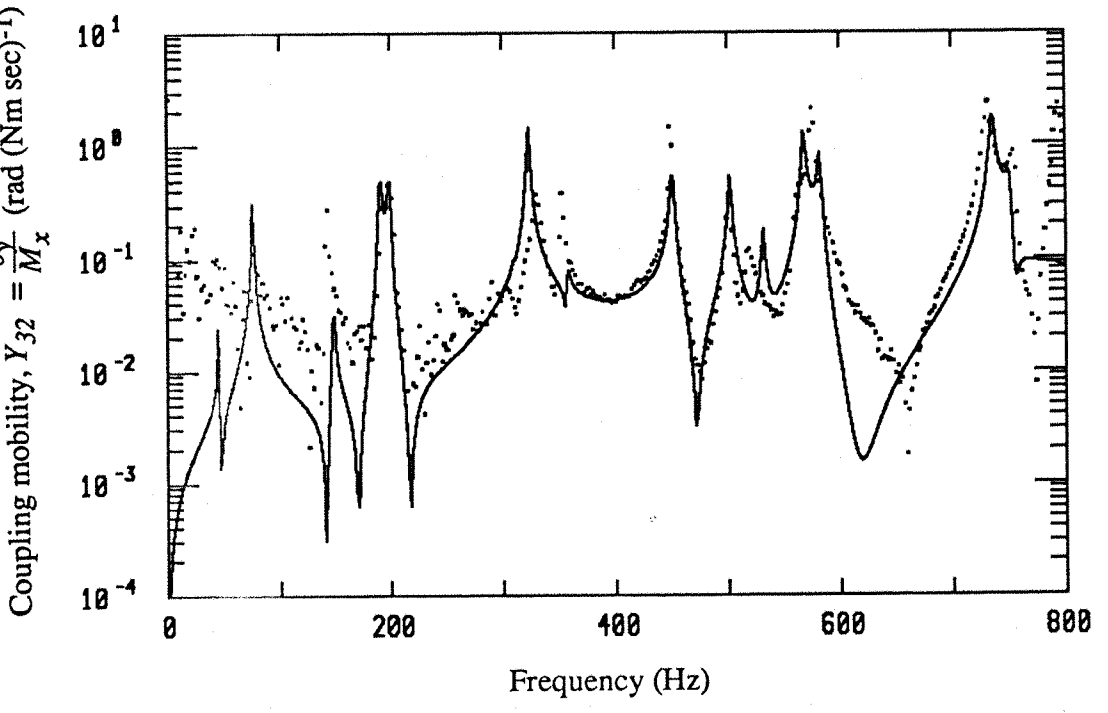

Figure 4.17 : Comparison of the modulus spectra of Y_{32} for the CFSF plate : —— Theoretical result (η = 0.005),····· Experimental result.

PART II

VIBRATIONAL POWER TRANSMISSION BETWEEN COUPLED STRUCTURAL SYSTEMS

CHAPTER 5

VIBRATIONAL POWER TRANSMISSION BETWEEN COUPLED FLEXIBLE SYSTEMS

5.1 INTRODUCTION

The problem of multi-directional vibration transmission between a coupled flexible source - isolator - receiver system has been studied by a number of researchers in the past two decades. In particular, Soliman and Hallam [10] combined the mobility matrices describing the dynamic characteristics of the machine and foundation and the transfer matrix of isolators to calculate the overall response for systems containing any number of isolators when the machine and foundation are both non-rigid.

The study in this chapter extends the work of Soliman and Hallam to include the expressions for the time-averaged vibrational power input to a multi-point mounted machine source and the subsequent vibrational power transmitted to the resilient mounts and a flexible seating structure. The generalised multi-directional model is assumed to have N resilient mounts with six degrees-of-freedom at each mount. The expressions for this generalised model are then compared with the simpliest single degree-of-freedom - single mount model obtained by other researchers. Other simplifications to the generalised model are also discussed.

5.2 A GENERALISED MULTI-DIRECTIONAL MODEL

5.2.1 General Expressions for Vibrational Power Transmission

Consider a machine which is supported on a non-rigid seating structure through N resilient mounts as shown in figure 5.1. The machine is excited by m sinusoidal excitations (consisting of three orthogonal forces and three orthogonal moments). This set of excitations exerts on each resilient mount six components of force and of velocity, i.e. each mounting point requires six degrees-of-freedom (three orthogonal translational and three orthogonal rotational) to define its vibrational motion. Hence the

total number of degrees-of-freedom at the machine mounting points is $n = 6N$. The seating structure is considered to be excited at n degrees-of-freedom through the mounting points.

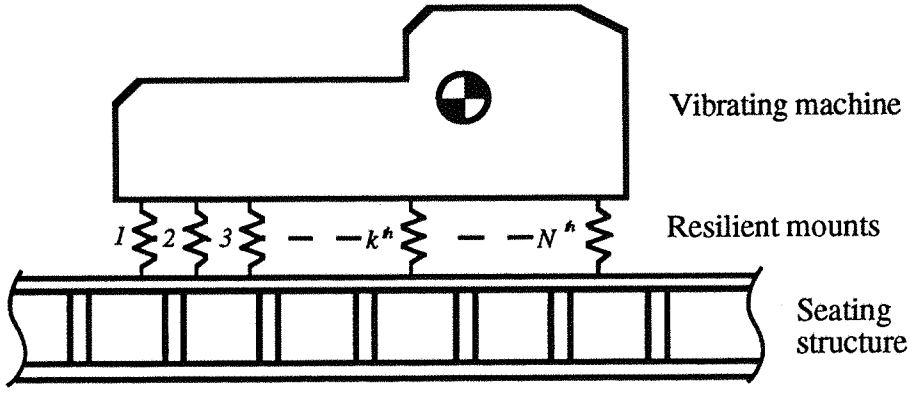

Figure 5.1 : A vibrating machine mounted on a substructure through resilient mounts.

The mathematical representation of this multi-degree-of-freedom coupled system is shown in figure 5.2. The positive sign conventions of the forces and velocity responses are shown in the figure.

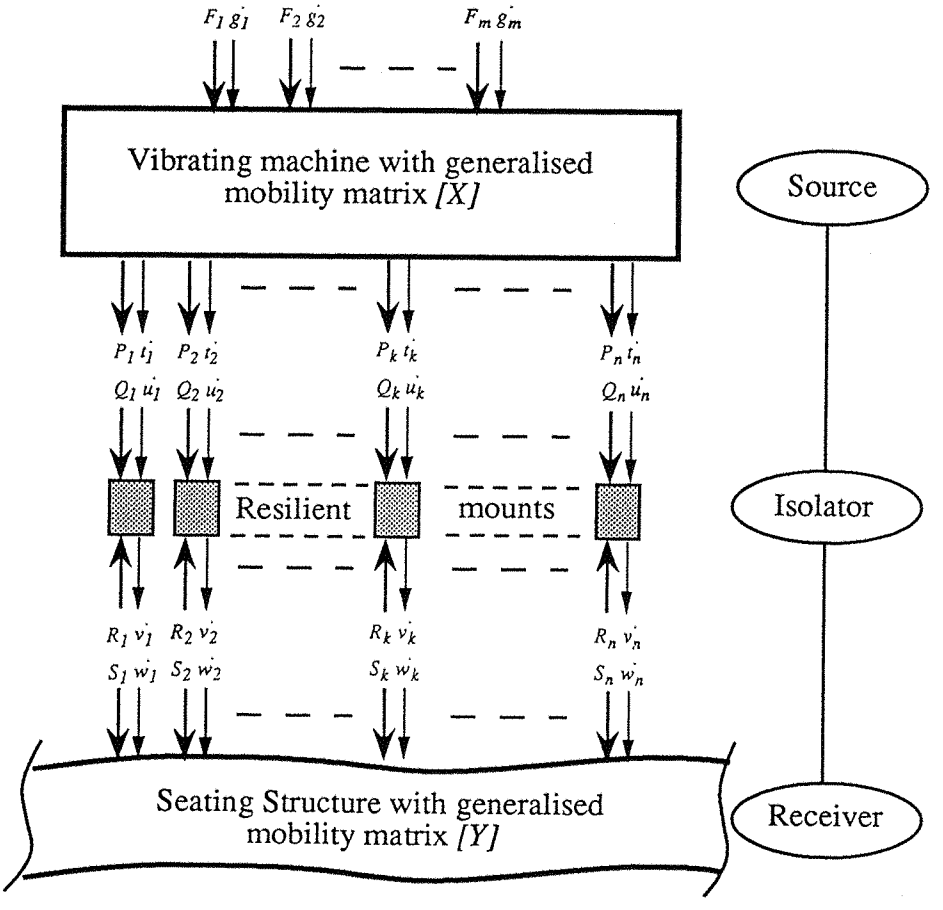

Figure 5.2 : Mathematical model of the coupled source-isolator-receiver system.

The vibrating machine is characterised by its generalised mobility matrix *[X]* which relates the excitation forces and moments F_i *(i=1,2 ... m)* and the resulting transmitted forces and moments P_j *(j =1,2 ...n)* to the translational and rotational velocities $\dot{g}_i$ *(i=1,2...m)* and $\dot{t}_j$ *(j=1,2...n)* at the excitation points and the mounting points respectively.

The seating structure is similarly characterised by the generalised mobility matrix *[Y]* at the mounting points with six degrees-of-freedom at each point. The transmitted forces and moments and the resulting velocities at the mounting points on the seating structure are S_j *(j=1,2 ...n)* and $\dot{w}_j$ *(j=1,2...n)* respectively.

The resilient mounts are characterised by their multi-directional transfer matrix which relates the forces and velocities at one terminal (mounting interface) to the forces and velocities at the other terminal.

The equations of motion governing the vibrating machine can be written in matrix form as :

$$\begin{Bmatrix} \{\dot{t}\} \\ \{\dot{g}\} \end{Bmatrix} = \begin{bmatrix} [X_{11}] & [X_{12}] \\ [X_{21}] & [X_{22}] \end{bmatrix} \begin{Bmatrix} \{P\} \\ \{F\} \end{Bmatrix} \tag{5.1}$$

where $[X_{11}]$ is a *nxn* square matrix representing the point, coupling and transfer mobility functions at the mounting points, $[X_{12}]$ is a *nxm* transfer mobility matrix between the velocity responses at the mounting points and the forces and moments at the excitation points, $[X_{21}]$ is a *mxn* transfer mobility matrix between the velocity responses at the excitation points and the forces and moments at the mounting points, and $[X_{22}]$ is a *mxm* driving point mobility matrix at the excitation points; $\{\dot{t}\}$ and $\{P\}$ are *n* order column vectors of the *n* components of the velocities and the transmitted forces and moments respectively at the mounting interfaces; $\{\dot{g}\}$ and $\{F\}$ are *(n+1)* to *(n+m)* order column vectors of the *m* components of the velocities and excitations respectively acting on the machine. Thus,

$$\{\dot{t}\} = [X_{11}]\{P\} + [X_{12}]\{F\} \tag{5.2}$$

$$\{\dot{g}\} = [X_{21}]\{P\} + [X_{22}]\{F\} \tag{5.3}$$

Similarly, the equations of motion governing the seating structure are :

$$\{ \dot{w} \} = [Y] \{ S \} \tag{5.4}$$

where $[Y]$ is the nxn generalised mobility matrix at the mounting points which consists of the point, coupling and transfer mobility functions between different mounting points and different degrees-of-freedom, $\{\dot{w}\}$ and $\{S\}$ are the n order column vectors of the velocities and the transmitted forces and moments respectively at the mounting points.

For the k^{th} resilient mount, the transmitted forces and moments and the resulting velocities at the input and output interfaces are related by the transfer matrices :

$$\begin{Bmatrix} \{Q_k\} \\ \{\dot{u}_k\} \end{Bmatrix} = \begin{bmatrix} [A_k] & [B_k] \\ [C_k] & [D_k] \end{bmatrix} \begin{Bmatrix} \{R_k\} \\ \{\dot{v}_k\} \end{Bmatrix} \tag{5.5}$$

where $\{Q_k\}$ and $\{R_k\}$ are $6x1$ vectors of the forces and moments acting at the top and bottom interfaces of the mount, $\{\dot{u}_k\}$ and $\{\dot{v}_k\}$ are $6x1$ vectors of the velocities at the top and bottom interfaces of the mount, $[A_k]$, $[B_k]$, $[C_k]$ and $[D_k]$ are the $6x6$ transfer matrices of the mount relating the transmitted forces and moments and the resulting velocities at the two interfacing surfaces.

Since there is no direct link between each pair of adjacent resilient mounts, except through the machine and the seating structure, for all the resilient mounts $(k=1 \text{ to } N)$, one can write :

$$\{Q\} = [A] \{R\} + [B] \{\dot{v}\} \tag{5.6}$$

$$\{\dot{u}\} = [C] \{R\} + [D] \{\dot{v}\} \tag{5.7}$$

where the matrices $[A]$, $[B]$, $[C]$ and $[D]$ are n order diagonal super-matrices (matrices of matrices) [11]:

$$[A] = \begin{bmatrix} [A_1] & 0 & \cdots & 0 & \cdots & 0 \\ 0 & [A_2] & \cdots & 0 & \cdots & 0 \\ \vdots & \vdots & & \vdots & & \vdots \\ 0 & 0 & \cdots & [A_k] & \cdots & 0 \\ \vdots & \vdots & & \vdots & & \vdots \\ 0 & 0 & \cdots & 0 & \cdots & [A_N] \end{bmatrix} \tag{5.8}$$

similarly for super-matrices *[B]*, *[C]* and *[D]*.

Applying the conditions for force equilibrium and motion compatibility (continuity) at each mounting point, we have, for the k^{th} resilient mount :

$$P_k + Q_k = 0 \tag{5.9}$$
$$-R_k + S_k = 0 \tag{5.10}$$
$$\dot{t}_k = \dot{u}_k \tag{5.11}$$
$$\dot{v}_k = \dot{w}_k \tag{5.12}$$

For all the resilient mounts *(k=1 to N)*, we have :

$$\{P\} = -\{Q\} \tag{5.9a}$$
$$\{R\} = \{S\} \tag{5.10a}$$
$$\{\dot{t}\} = \{\dot{u}\} \tag{5.11a}$$
$$\{\dot{v}\} = \{\dot{w}\} \tag{5.12a}$$

The time-averaged vibrational power transmitted via the j^{th} co-ordinate to the seating structure is :

$$P_j = \frac{1}{2} Re \{ S_j \dot{w}_j^* \} \tag{5.13}$$

where $\dot{w}_j^*$ is the complex conjugate of $\dot{w}_j$.

The total time-averaged vibrational power transmitted to the seating structure is the sum of the powers transmitted through each mounting point in each degree-of-freedom. Hence,

$$P_{tr\text{-}plt} = \sum_{j=1}^{n} P_j = \sum_{l=1}^{6} \sum_{k=1}^{N} P_{l\,k}$$

$$= \frac{1}{2} \, Re \, \{ \, \{ S \}^T \, \{ \dot{w} \}^* \} \qquad (5.14)$$

where $\{ S \}^T$ is the transpose of vector $\{ S \}$.

Similarly, the total time-averaged vibrational power input to the machine source is given by:

$$P_{in} = \frac{1}{2} \, Re \, \{ \, \{ F \}^T \, \{ \dot{g} \}^* \} \qquad (5.15)$$

and the total time-averaged vibrational power transmitted to the isolators is :

$$P_{tr\text{-}iso} = \frac{1}{2} \, Re \, \{ \, \{ Q \}^T \, \{ \dot{u} \}^* \} \qquad (5.16)$$

5.2.2 Vibrational Power Transmission Expressed in terms of External Excitations

In theoretical analyses, it is convenient to study the vibrational power transmitted to the seating structure subjected to different combinations of excitations generated by the machine. The transmitted force and moment vector $\{S\}$ and the resulting velocity vector $\{\dot{w}\}$ of the seating structure can be expressed in terms of the excitation vector $\{F\}$ of the vibrating machine.

From the above equations, it can be shown that :

$$\{S\} = \left[\left([C] + [D][Y] \right) + [X_{11}] \left([A] + [B][Y] \right) \right]^{-1} [X_{12}] \{F\} \qquad (5.17)$$

Thus, the transmitted forces and moments, S_j, $j = 1,2 \ldots n$, acting on the seating structure depend on the excitations of the machine, the point and transfer mobility functions of the machine, the dynamic transfer properties of the resilient mounts and the mobility functions of the seating structure.

The velocity responses $\{\dot{g}\}$ at the excitation points of the machine source can be expressed in terms of the transmitted force and moment vector $\{S\}$ and the excitation vector $\{F\}$ as :

$$\{\dot{g}\} = - [X_{21}] \left([A] + [B][Y] \right) \{S\} + [X_{22}] \{F\} \qquad (5.18)$$

The transmitted force and moment vector $\{Q\}$ and the resulting velocity vector $\{\dot{u}\}$ acting at the top surface of the resilient mounts are given as :

$$\{Q\} = ([A] + [B][Y])\{S\} \tag{5.19}$$

$$\{\dot{u}\} = ([C] + [D][Y])\{S\} \tag{5.20}$$

The total vibrational power input to the machine source and transmitted to the resilient mounts and the seating structure can be obtained by substituting eqns. (5.17) to (5.20) into eqns. (5.15), (5.16) and (5.14) respectively.

The vibrational power dissipation in the source and in the resilient mounts is obtained from the following expressions :

$$P_{dis\text{-}bm} = P_{in} - P_{tr\text{-}iso} \tag{5.21}$$

$$P_{dis\text{-}iso} = P_{tr\text{-}iso} - P_{tr\text{-}plt} \tag{5.22}$$

It is interesting to note that eqn. (5.17) also gives the expression for the force transmissibility if the input force vector is a unit force vector. For a single point force excitation with four mounting points and considering only the vertical translational motion, the force transmissibility of the coupled system is defined as :

$$TR = \left| \frac{S_1 + S_2 + S_3 + S_4}{F} \right| \tag{5.23}$$

5.2.3 Vibrational Power Transmission Expressed in terms of Velocity Responses

In practical dynamic measurements, it is easier to measure velocity responses with good accuracy than the force components. For the measurement of the vibrational power transmitted through each of the resilient mounts, the measurable quantities are thus the velocities at the top of the resilient mounts ($\dot{u}_j$, $j = 1,2 \ldots n$) and those at the mounting points of the seating structure ($\dot{w}_j$, $j = 1,2 \ldots n$) (i.e. velocities above and below the isolators).

The transmitted force and moment vector $\{S\}$ can be expressed in terms of these velocity vectors $\{\dot{u}\}$ and $\{\dot{w}\}$ by substituting the equilibrium and continuity conditions (eqns. (5.10a) and (5.12a)) into eqn. (5.7) :

$$\{S\} = [C]^{-1}\{\dot{u}\} - [C]^{-1}[D]\{\dot{w}\} \tag{5.24}$$

where $[C]^{-1}$ is the inverse of matrix $[C]$.

The transpose of the vector $\{S\}$ is :

$$\{S\}^T = \{\dot{u}\}^T[C]^{-1T} - \{\dot{w}\}^T[D]^T[C]^{-1T} \tag{5.25}$$

Thus, the total vibrational power transmitted to the seating structure is given as :

$$P_{tr,plt} = \frac{1}{2} Re\left\{\{\dot{u}\}^T[C]^{-1T}\{\dot{w}\}^* - \{\dot{w}\}^T[D]^T[C]^{-1T}\{\dot{w}\}^*\right\} \tag{5.26}$$

5.3 SIMPLIFICATIONS OF THE GENERALISED MODEL

A qualitative check of the generalised multi-directional linear model for the coupled system can be obtained by simplifying the model to its most simple form, i.e. a single degree-of-freedom - single mount model and comparing with published results.

5.3.1 Single Degree-of-freedom - Single Mount Model

For a single degree-of-freedom - single mount system, the extensional forces, Q and R acting on the top and bottom surfaces of the resilient mount and the resulting velocities $\dot{u}$ and $\dot{v}$ in the direction of the forces, as shown in figure 5.2, can be expressed in the similar matrix form as in eqn. (5.5) :

$$\begin{Bmatrix} Q \\ \dot{u} \end{Bmatrix} = \begin{bmatrix} \alpha_{11} & \alpha_{12} \\ \alpha_{21} & \alpha_{22} \end{bmatrix} \begin{Bmatrix} R \\ \dot{v} \end{Bmatrix} \tag{5.27}$$

where $\alpha_{11}, \alpha_{12}, \alpha_{21}$ and α_{22} are the uni-directional transfer properties (also known as the four-pole parameters) of the resilient mount relating the force and velocity response at one end to those quantities at the other end.

For a linear, massless spring with hysteretic damping and having stiffness, $K(1+j\eta_m)$, where η_m is the loss factor of the spring, we have :

for force equibrium : $Q = R$

from Hooke's law : $Q = K(1+j\eta_m) \left(\frac{\dot{u} - \dot{v}}{j\omega} \right)$

thus, $\dot{u} = \frac{j\omega}{K(1+j\eta_m)} R + \dot{v}$

Hence, $\alpha_{11} = 1$, $\alpha_{12} = 0$, $\alpha_{21} = \frac{j\omega}{K(1+j\eta_m)}$ and $\alpha_{22} = 1$.

The vibrational power transmitted to the seating structure for this simplified model can be obtained from eqn. (5.26) as :

$$P = \frac{1}{2} Re \left\{ \frac{K(1+j\eta_m)}{j\omega} \left(\dot{u}\, \dot{w}^* - \dot{w}\, \dot{w}^* \right) \right\} \qquad (5.28)$$

If one makes an assumption that for a machine isolator, $\dot{u} >> \dot{w}$ as was done in [19], then the vibrational power transmitted to the seating structure is :

$$P \approx -\frac{1}{2\omega} Im \left\{ \frac{K(1+j\eta_m)}{\omega^2} \ddot{u}\, \ddot{w}^* \right\} \qquad (5.29)$$

where $\ddot{u} = j\omega\dot{u}$ and $\ddot{w} = j\omega\dot{w}$ are the accelerations at the top and bottom surfaces of the mount and $Im\ \{\ \}$ denotes the imaginary part of the complex quantities. This expression is similar to that used by Pinnington [19] in the measurement of the vibrational power transmitted through an isolator.

The isolator effectiveness [2], E , of a coupled source-isolator-receiver system is defined as *the ratio of the receiver velocity when directly connected to the source to the receiver velocity when connected through isolators to the source* can be obtained from eqn. (5.17) for this simplified single degree-of-freedom - single mount system as:

$$S = [\, Y + \alpha_{21} + X_{11} \,]^{-1} X_{12} F \qquad (5.30)$$

where $\alpha_{21} = \frac{j\omega}{K(1+j\eta_m)} = \frac{\dot{u}}{R}\Big|_{\dot{v}=0} = \frac{\dot{u}}{Q}$

i.e. the blocked transfer mobility function of the resilient mount which, for the case of a massless damped spring model, is also equal to the point mobility function .

For a rigidly coupled system, K is very large, thus $\alpha_{21} \approx 0$. The transmitted force acting on the receiver is :

$$S_r = [\, Y + X_{11} \,]^{-1} \, X_{12} \, F \tag{5.31}$$

Hence, the isolator effectiveness is :

$$E = \left| \frac{\dot{w}_r}{\dot{w}} \right| = \left| \frac{Y \, S_r}{Y \, S} \right| = \left| 1 + \frac{\alpha_{21}}{Y + X_{11}} \right| \tag{5.32}$$

For a good isolation system, E must be large, thus the point mobility functions, Y and X_{11} of the receiver and the source respectively, must be as small as possible.

5.3.2 Single Degree-of-freedom - Multiple Mount Model

For a single degree-of-freedom - multiple mount system, the total vibrational power transmitted to the seating structure is the sum of the powers transmitted in the specific degree-of-freedom of each mount, i.e.

$$P_{tr\text{-}plt} = \sum_{k=1}^{N} P_k = \frac{1}{2} \, Re \, \{ \, [S]^T \, [\dot{w}]^* \} \tag{5.33}$$

where $[S]$ and $[\dot{w}]$ are the $Nx1$ force and velocity vectors respectively of the mounting points on the seating structure, and N is the number of resilient mounts. The contributions from different mounting points can be accounted for by including the transfer mobility functions in the NxN mobility matrix $[Y]$ of the seating structure.

5.3.3 Multi Degree-of-freedom - Single Mount Model

For a multi degree-of-freedom - single mount system, the total vibrational power transmitted to the seating structure is the sum of the powers transmitted through the mount in each degree-of-freedom, i.e.

$$P_{tr\text{-}plt} = \sum_{l=1}^{L} P_l = \frac{1}{2} \, Re \, \{ \, [S]^T \, [\dot{w}]^* \} \tag{5.34}$$

where $\{S\}$ and $\{\dot{w}\}$ are the $Lx1$ force and velocity vectors respectively of the mounting point on the seating structure, and L (≥ 1 and ≤ 6) is the number of the relevant degrees-of-freedom at the mounting point. The contributions from different degrees-of-freedom at the mounting point can be accounted for by including the coupling mobility functions (i.e. translational velocities / moments and rotational velocities / forces) in the LxL mobility matrix $[Y]$ of the seating structure.

5.4 SUMMARY

In this chapter, expressions for the time-averaged vibrational power input to a machine source and the subsequent powers transmitted to the resilient isolators and a flexible receiver have been derived based on the mobility coupling approach for linear structures. These derivations have been performed for a generalised multi-directional model which consists of N isolators with six degrees-of-freedom for each isolator. Various simplifications to the generalised model are also discussed briefly.

CHAPTER 6

ANALYTICAL MODEL AND COMPONENT DATA

6.1 INTRODUCTION

In the previous chapter, expressions for the time-averaged vibrational power input and transmitted between a coupled source - isolator - receiver system were presented. The generalised model was assumed to have N resilient mounts with a maximum of six degrees-of-freedom at each mounting point. A complete analysis of this model requires a large amount of information : i.e. the point, transfer and coupling mobility functions for all the mounting points and the excitation locations of both the source and the seating structure; and the multi-directional dynamic transfer properties of the resilient mounts. Such an analysis, if possible, will be very complex and time consuming, but often it is impracticable due to computing resources required and the amount of data required to be analysed and measured for practical machinery installations. These difficulties of performing a complete coupling analysis for the case of N mounting points with six degrees-of-freedom at each point had been identified and acknowledged in the past by many researchers [16-22], who eventually made some specific assumptions in order to simplify the problem.

However, in order to have a better understanding of the vibrational power input and transmitted between the coupled source - isolator - receiver system, the influence of the isolator properties on the power transmitted to the seating structure, the contribution of the vibrational power from adjacent mounts and the interaction between translational and rotational degrees-of-freedom at the mounting points, a more refined analytical model compared to previous studies [18,19], has been developed. This model assumed that both the source and the receiver were non-rigid and 'wave effects' might be present in the resilient mounts within the frequency range of interest (between 1 to 1000 Hz). The flexible source was modelled as a free-free beam and the flexible receiver was a clamped-free-simply supported-free rectangular plate. The dynamic transfer properties (four-pole parameters) of the resilient mounts were obtained experimentally based on

the 'Long Rod' model. The governing degrees-of-freedom considered in this study are those associated with flexural vibration of the seating structure.

6.2 DESCRIPTION OF THE ANALYTICAL MODEL

In the analytical model, as shown in figure 6.1, the machine source was simulated by a uniform 'free - free' steel beam of dimensions : 350mm (length) x 120mm (width) x 12.5mm (thickness) and having a fundamental flexural mode of vibration at a natural frequency of 539 Hz. The point, transfer and coupling mobility functions of the beam were obtained from closed form solutions based on the Euler - Bernoulli Beam theory. Detailed procedures for obtaining the driving point mobility functions have been given in Chapter 2. They have also been reported in [27]. The hysteretic loss factor, which accounts for the inherent material damping, used in the calculation was 0.005. More discussion on the point, coupling and transfer mobility functions of the free - free beam will be given in section 6.3.1.

The resilient mounts were made from Sylomer elastomer material of dimensions : 15mm x15mm (square) x 12mm (height). These resilient mounts were firmly glued in between the isolator supports as shown in figure 6.5. The dynamic stiffness and loss factor of the mounts were measured experimentally and Least Squares straight line fitting was employed to generate the dynamic stiffness and loss factor data for the required frequency resolution in the calculations. The dynamic transfer properties of resilient mounts were calculated based on either the 'long rod' model or the massless damped spring model. In calculating the transfer properties, the masses of the isolator supports were taken into consideration. However, as these masses were small compared to the mass of the source beam and the receiver plate, they were neglected in the overall coupled system analysis. Detailed description on the experimental arrangement and the measured and fitted results is given in section 6.3.2.

The receiver or the seating structure was a rectangular flat plate with one edge clamped, the opposite edge simply supported and the other pair of edges free. The dimensions of the plate were : 585mm (length a) x 390mm (length b) x 4.1mm (thickness), which gave a fundamental flexural mode of vibration at a natural frequency of 44.7 Hz. The point, transfer and coupling mobility functions of the plate were obtained by the Rayleigh - Ritz method with appropriate characteristic beam functions in the X- and Y-directions as the assumed functions. The hysteretic loss factor used was 0.005. Detailed description of the method has been given Chapter 3 and also been reported in [41].

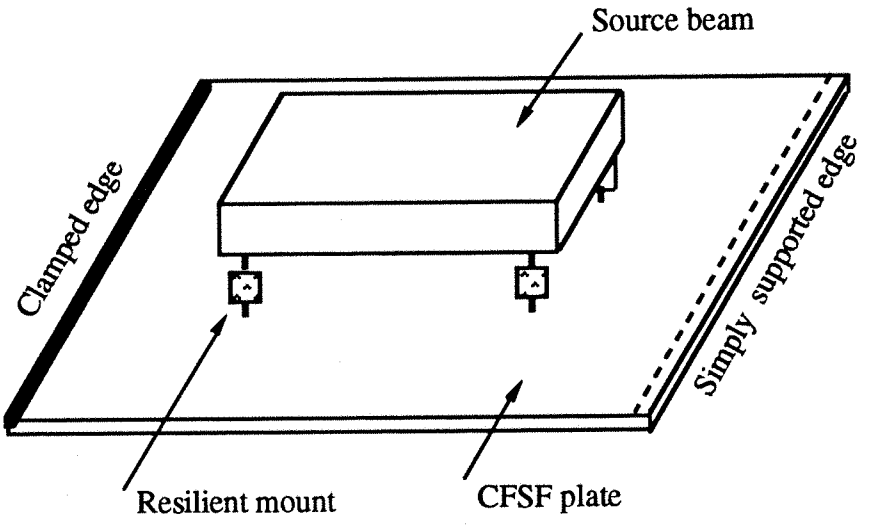

Figure 6.1 : A source - isolator - receiver analytical model.

This theoretical model was analysed for the following conditions :

(1) Four mounting points with only vertical translational motion at each point.

In order to study the influences of the isolator properties on the vibrational power transmission between the coupled source - isolator - receiver system, the vibrational power input to the source beam, and transmitted to the isolator and the receiver were analysed for four different cases of isolator properties : dynamic stiffness and loss factor. These properties are summaried in Table 6.1.

Case No	Dynamic Stiffness	Loss Factor	Remark
C-1	K	η_m	Experimental data
C-2	$K \times 100$	η_m	Stiff isolator, e.g. bolted joint
C-3	K	$\eta_m \times 0.01$	Lightly damped isolator : spring
C-4	$K \times 0.24$	η_m	Longer isolator : 50mm length

Table 6.1 : Dynamic stiffnesses and loss factors of resilient mounts.

Remarks :

1. The dynamic stiffness and hysteretic loss factor of the resilient mount were found to increase linearly with increasing frequency for frequencies below the first 'wave effect' (longitudinal resonance) frequency. Linear Least Squares fitting was employed to fit the

measured data. The Least Squares models for the dynamic stiffness and loss factor are given in eqns. (6.16) and (6.17) respectively.

2. The first 'wave effect' (longitudinal resonance) of the resilient mount was found to occur just beyond the 1kHz range. Thus, in order to study the influence of the 'wave effects', the length of the mount was increased from 12mm to 50mm in the C-4 case.

(2) Four mounting points with a vertical translational motion and a rotational motion at each point.

This model was used to study the influence of the rotational degree-of-freedom on the vertical translational degree-of-freedom for vibrational power transmission between the coupled source - isolator - receiver system. For this model only the measured isolator properties, i.e. case C-1, were used in the analysis.

6.3 DESCRIPTION OF THE COMPONENT DATA

6.3.1 Point , Coupling and Transfer Mobility Functions of a Free - Free Beam

The point, coupling and transfer mobility functions of a free - free beam were derived from consideration of the requirements of motion continuity and force equilibrium conditions at the excitation and isolator mounting points, the 'free' boundary condition at both ends and the use of the receptance matrix for a uniform beam in flexural vibration. The beam was assumed to satisfy the Euler - Bernoulli beam theory.

For driving point mobility functions, a two segment beam model as shown in figure 6.2 was used. The point of interest is located at a distance ℓ_1 from one end of the beam. For transfer mobility functions between the excitations at point C and the velocity responses at point B, a three segment beam model as shown in figure 6.3 was used.

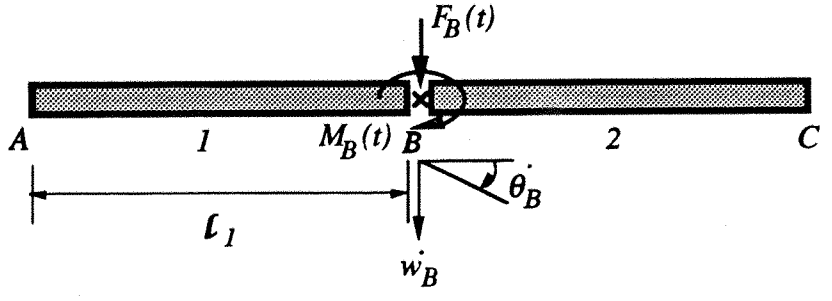

Figure 6.2 : A two segment beam model.

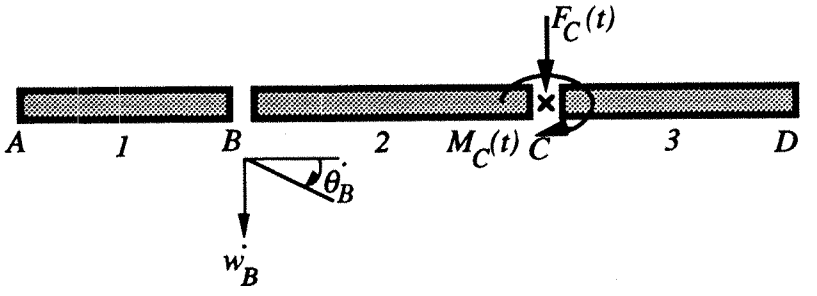

Figure 6.3 : A three segment beam model.

For the source beam, assuming that the excitations are applied at point C, and the resilient mounts are located at points A and B, as shown in figure 6.4, the mobility matrix which defines the motion of the beam can be written as :

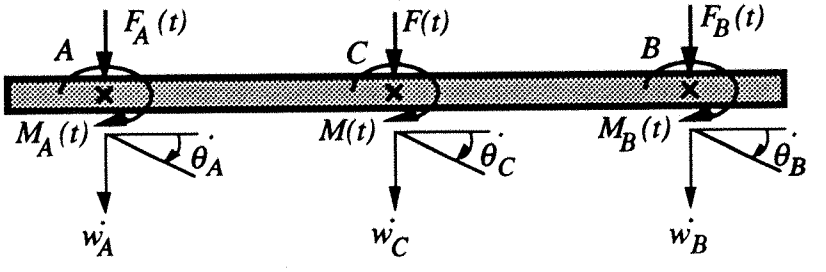

Figure 6.4 : A free - free source beam model.

$$\begin{Bmatrix} \dot{w}_A \\ \dot{\theta}_A \\ \dot{w}_B \\ \dot{\theta}_B \\ \dot{w}_C \\ \dot{\theta}_C \end{Bmatrix} = \begin{bmatrix} X_{11} & X_{12} & X_{13} & X_{14} & X_{15} & X_{16} \\ X_{21} & X_{22} & X_{23} & X_{24} & X_{25} & X_{26} \\ X_{31} & X_{32} & X_{33} & X_{34} & X_{35} & X_{36} \\ X_{41} & X_{42} & X_{43} & X_{44} & X_{45} & X_{46} \\ X_{51} & X_{52} & X_{53} & X_{54} & X_{55} & X_{56} \\ X_{61} & X_{62} & X_{63} & X_{64} & X_{65} & X_{66} \end{bmatrix} \begin{Bmatrix} F_A \\ M_A \\ F_B \\ M_B \\ F \\ M \end{Bmatrix} \tag{6.1}$$

Comparing to eqn. (5.1), the corresponding terms are :

$$\{ \dot{t} \} = \begin{Bmatrix} \dot{w}_A \\ \dot{\theta}_A \\ \dot{w}_B \\ \dot{\theta}_B \end{Bmatrix} \qquad \{ P \} = \begin{Bmatrix} F_A \\ M_A \\ F_B \\ M_B \end{Bmatrix} \tag{6.2, 6.3}$$

$$[\dot{g}] = \begin{Bmatrix} \dot{w}_C \\ \dot{\theta}_C \end{Bmatrix} \qquad [F] = \begin{Bmatrix} F \\ M \end{Bmatrix} \qquad (6.4, 6.5)$$

$$[X_{11}] = [X_{ij}] \qquad i=1,2,3,4\ ;\ j=1,2,3,4. \qquad (6.6)$$

$$[X_{12}] = [X_{ij}] \qquad i=1,2,3,4\ ;\ j=5,6 \qquad (6.7)$$

$$[X_{21}] = [X_{ij}] \qquad i=5,6\ ;\ j=1,2,3,4. \qquad (6.8)$$

$$[X_{22}] = [X_{ij}] \qquad i=5,6\ ;\ j=5,6. \qquad (6.9)$$

As can be seen from this simple illustration, the number of mobility functions required to completely define the dynamic behaviour of the source beam increases rapidly with the numbers of mounting points and the degrees-of-freedom considered, although for linear structures where the Reciprocity principle applies, the mobility matrix is a symmetric matrix. The complexity of the problem will be more intensified by taking into account of the fact that for practical machinery installations, the mobility functions need to be measured or estimated. Measurements in the rotational degrees-of-freedom and applying the moment excitations at the points of interest are also difficult problems to overcome.

Four typical sets of the mobility functions for the source beam (350mm x 120mm x 12.5mm) with the excitations at the centre of the beam and the mounting points at 12.5mm from the ends of the beam are shown in figures G1 to G4 of Appendix G. It can be seen that :

(1) for frequencies below 100Hz, the mobility functions are a straight line which denotes the mass-like nature of the free - free beam, except for two transfer / coupling mobility functions which are spring-like in nature.

(2) These two spring-like mobility functions are X_{25}, the rotational velocity response at mount 'A' due to a unit force excitation at point C, and X_{52}, the translational velocity response at the excitation point to a unit moment excitation at mount 'A'. Clearly, it is the bending stiffness of the beam with governs these transfer / coupling (cross) responses.

(3) X_{56} and X_{65} have numerically very small values, which should be taken as zero. This corresponds to the special case of zero coupling mobility functions

for the symmetric boundary conditions with excitations located at the point of mode shape symmetry. This condition has been noted in the previous chapters.

6.3.2 Dynamic Transfer Properties of Resilient Mounts

The dynamic transfer properties of a resilient mount relates the forces and motions at the top and bottom surfaces (i.e. the input and output terminals) of the mount. The uni-directional transfer properties in the axial direction are commonly known as the four-pole parameters of the mount [6,42-45]. Detailed discussion of the definition and applications of these parameters in relation to vibration isolation can be found in these references. A brief account of the definition and properties of these parameters is given in Appendix H. The following sections describe the experimental arrangement and determination of the dynamic stiffness, loss factor and the transfer properties.

a. Experimental Measurement of the Dynamic Transfer Properties of Resilient Mounts in Axial Vibration

The arrangement for determining the dynamic stiffness, loss factor and the transfer properties of the resilient mount in axial vibration is shown in figure 6.5. The resilient mount was glued to the top and bottom isolator supports which were machined from alumimum alloy for measurement of the translational and rotational motions of the isolator support. The bottom terminal of the isolator rested on a rigid steel block. Axial force excitation, a random signal (20Hz to 20KHz white noise) was generated and applied to the top isolator support by an electrodynamic exciter which consisted of a fixed permament magnet and a moving coil. The top force transducer measured the excitation force and the bottom transducer measured the 'blocked' force at the output terminal. The instrumentation set-up for the measurement is shown in figure 6.6.

The dynamic transfer properties which were measured directly from this arrangement are β_{11} and β_{21} (see Appendix H). The modulus and phase of these two transfer properties are shown in figures H3 and H4 of Appendix H respectively. It can be seen that the plot of β_{11} is the reciprocal of the force transmissibility for a typical mass-spring system. The plot of the modulus of β_{21} is spring-like in nature (increases with increasing frequency) at low frequencies. But this proportional trend tapered off towards the high frequency region. This is because of the frequency dependent nature of the dynamic stiffness of isolators which also increases slightly with increasing frequency.

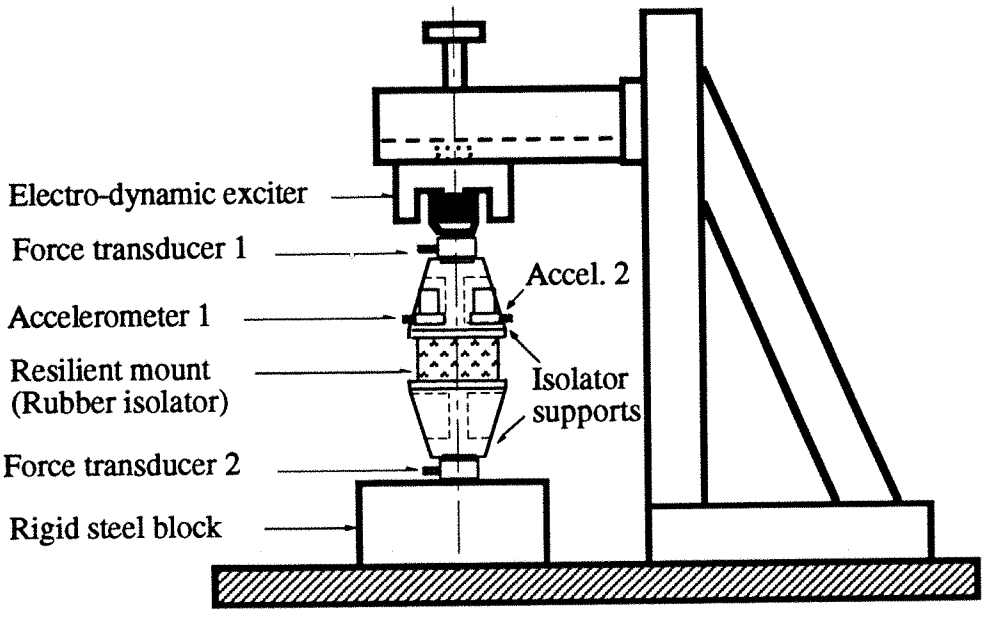

Figure 6.5 : Experimental arrangement for measurement of the dynamic transfer properties of the resilient mount in axial vibration.

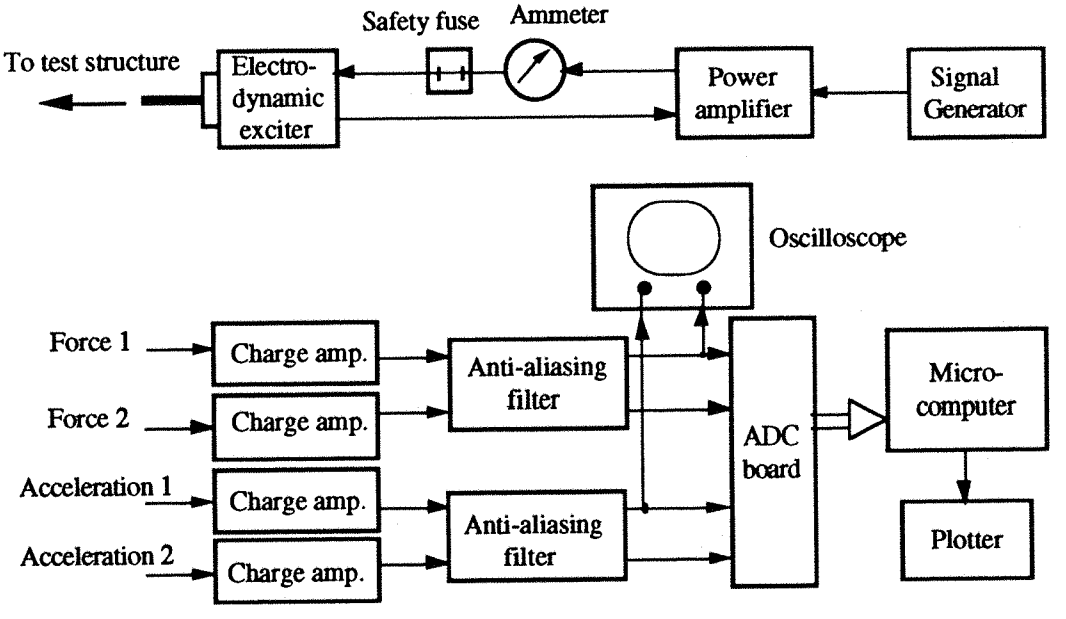

Figure 6.6 : Instrumentation set-up for measurement of the dynamic transfer properties of the resilient mount.

b. Determination of the Dynamic Stiffness and Loss Factor

For the resilient mount with top and bottom isolator supports as shown in figure 6.5, if the isolator supports are sufficiently rigid and stiff in the frequency range of interest, they can be modelled as rigid end plates as shown in figure H2. The transfer mobility

between the velocity response at the top isolator support and the 'blocked' force at the bottom support, β_{21} has been shown [6,43] (and Appendix H) to be independent to the mass of these supports and is given by :

$$\beta_{21} = \alpha_{21} = \frac{j\omega}{E^c A k_l} \sin k_l L \tag{6.10}$$

when considering the isolator as a "long rod".

At low frequencies, i.e. frequencies well below the first longitudinal resonance frequency of the resilient mount :

$$\sin k_l L \approx k_l L$$

Hence,
$$\beta_{21} \approx \frac{j\omega}{E^c A k_l} k_l L = \frac{j\omega L}{E^c A} = \frac{j\omega}{K(1+j\eta_m)} \tag{6.11}$$

where $K^c = K(1+j\eta_m) = \frac{E^c A}{L}$ is the dynamic spring stiffness of the resilient mount. The real and imaginary parts of the reciprocal of β_{21} are :

$$Re\left\{\frac{1}{\beta_{21}}\right\} = \frac{K\eta_m}{2\pi f} \tag{6.12}$$

$$Im\left\{\frac{1}{\beta_{21}}\right\} = -\frac{K}{2\pi f} \tag{6.13}$$

Thus, the dynamic stiffness and loss factor of the resilient mount can be obtained from the real and imaginary parts of β_{21} as :

$$K = -2\pi f \, Im\left\{\frac{1}{\beta_{21}}\right\} \tag{6.14}$$

$$\eta_m = -\frac{Re\left\{\frac{1}{\beta_{21}}\right\}}{Im\left\{\frac{1}{\beta_{21}}\right\}} \tag{6.15}$$

Spectra of the real and imaginary parts of β_{21} are shown in figure H5. It can be seen that above 600Hz, the spectra fluctuate which is most likely caused by the rotary inertia of the top transducer mass and the isolator support, and probably the influence of the

first longitudinal resonance ('wave effect') of the mount which occurred at a frequency slightly above 1000Hz. Nevertheless, for the frequency range from 10 to 500Hz, the dynamic stiffness and loss factor of the mount were determined from the above expressions. Figures H6 and H7 show the spectra of the dynamic stiffness and the loss factor respectively. It can be seen that both the stiffness and the loss factor of the mount increase with increasing frequency. This frequency dependent characteristic for the stiffness or shear modulus and the loss factor have been investigated and reported by Snowdon [46].

In order to represent this frequency dependent characteristic and to generate the dynamic stiffness and loss factor data for the desired frequency resolution for the analysis of the coupled source - isolator - receiver system, a linear regression model based on the Least Squares algorithm was used to fit the experimental data. The linear Least Squares models for the dynamic stiffness and the loss factor are :

$$K = 20090.0 + 23.72 f \tag{6.16}$$

$$\eta_m = 0.2447 + 0.0001173 f \tag{6.17}$$

where f is the frequency in Hertz (Hz). Plots of eqns. (6.16) and (6.17) are shown in figures H6 and H7 respectively.

c. Determination of β_{22} and β_{12}

For linear and symmetrical resilient mounts, relations (H.4) and (H.5) apply. Thus, $\beta_{22}=\beta_{11}$ and β_{12} can be obtained from :

$$\beta_{12} = \frac{\beta_{11}\beta_{22} - 1.0}{\beta_{21}} \tag{6.18}$$

The modulus and phase of β_{12} transfer property are shown in figure H8.

d. Comparison of the Measured and Predicted Dynamic Transfer Properties

Expressions for the dynamic transfer properties of a massless damped spring and a 'Long rod' model for the resilient mount alone are given in Table H-1, and those for the transfer properties of the mount with end plates are given in eqn. (H.6). With these expressions, the dynamic transfer properties of the resilient mount with the isolator

supports have been calculated. In these calculations, the end masses were taken to be 0.0386kg.

Comparisons of the measured and predicted dynamic transfer properties of the resilient mount are shown in figures H9 to H14. It can be seen that both the massless damped spring model and the 'Long rod' model agree quite closely with the measured transfer properties. The exceptions are :

(1) in the low frequency region, from 10 to 50 Hz, which is because of the curve fitted dynamic stiffness model which overestimated the stiffness in this frequency region (see figure H6).

(2) In the high frequency region, from 600 to 1000Hz, which is most likely due to the effects of rotary inertia of added mass and isolator resonances which caused some discrepancies in the estimation of the isolator properties. Strictly speaking, the method given in section 6.3.2 (b) does not take account of the resonances in the resilient mount.

It is also of interest to note that for the transfer property, β_{12} , which was determined experimentally from eqn. (6.18) and analytically from eqn. (H.6), the good agreement between these two sets of results shows that the linearity and reciprocity assumptions for the resilient mount were justified in the frequency range investigated.

6.3.3 Point, Coupling and Transfer Mobility Functions of a CFSF Plate

For a model having multiple mounting points and multi-degrees-of-freedom, the mobility matrix *[Y]* as given in equation (5.4) consists of the point mobility matrix at each mounting point and the transfer mobility matrix between the velocity responses ($\dot{w}$, $\dot{\theta}_x$ and $\dot{\theta}_y$) at one mounting point and the transmitted forces and moments (S, M_x and M_y) at the adjacent mounting points, as illustrated in figure 6.7. These mobility functions for a CFSF plate, i.e. the analytical model of the receiver, have been obtained by the Rayleigh - Ritz method with appropriate characteristic beam functions in the X- and the Y-directions as the assumed functions.

The driving point mobility matrix at each mounting point consists of the driving point force and moment mobility functions and the coupling mobility functions between the responses and excitations in different degrees-of-freedom. The driving point mobility matrix at the mounting point E is given as follows :

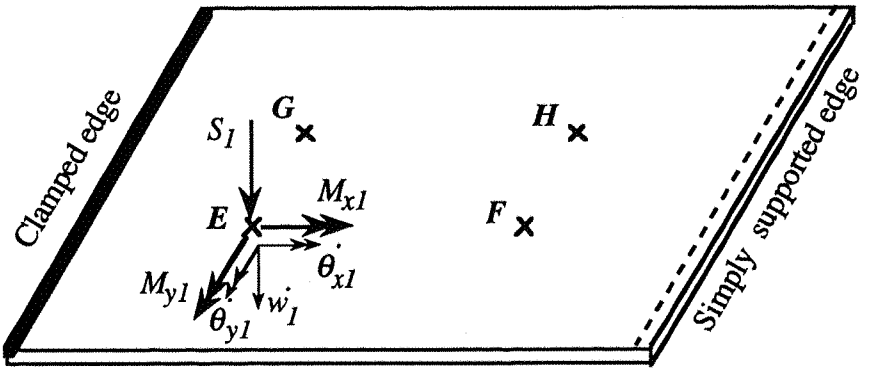

Figure 6.7 : Velocity responses and excitations on the receiver plate.

$$\begin{Bmatrix} \dot{w}_1 \\ \dot{\theta}_{x1} \\ \dot{\theta}_{y1} \end{Bmatrix} = \begin{bmatrix} Y_{11EE} & Y_{12EE} & Y_{13EE} \\ Y_{21EE} & Y_{22EE} & Y_{23EE} \\ Y_{31EE} & Y_{32EE} & Y_{33EE} \end{bmatrix} \begin{Bmatrix} S_1 \\ M_{x1} \\ M_{y1} \end{Bmatrix} \tag{6.19}$$

Similarly, the transfer mobility matrix between two mounting points, say E and F, is :

$$\begin{Bmatrix} \dot{w}_1 \\ \dot{\theta}_{x1} \\ \dot{\theta}_{y1} \end{Bmatrix} = \begin{bmatrix} Y_{11FE} & Y_{12FE} & Y_{13FE} \\ Y_{21FE} & Y_{22FE} & Y_{23FE} \\ Y_{31FE} & Y_{32FE} & Y_{33FE} \end{bmatrix} \begin{Bmatrix} S_2 \\ M_{x2} \\ M_{y2} \end{Bmatrix} \tag{6.20}$$

For the case of four mounting points with a translational $\dot{w}$ and a rotational $\dot{\theta}_y$ degrees-of-freedom, eqn (5.4) is expanded as follows :

$$\begin{Bmatrix} \dot{w}_1 \\ \dot{\theta}_{y1} \\ \dot{w}_2 \\ \dot{\theta}_{y2} \\ \dot{w}_3 \\ \dot{\theta}_{y3} \\ \dot{w}_4 \\ \dot{\theta}_{y4} \end{Bmatrix} = \begin{bmatrix} Y_{11EE} & Y_{13EE} & Y_{11FE} & Y_{13FE} & Y_{11GE} & Y_{13GE} & Y_{11HE} & Y_{13HE} \\ Y_{31EE} & Y_{33EE} & Y_{31FE} & Y_{33FE} & Y_{31GE} & Y_{33GE} & Y_{31HE} & Y_{33HE} \\ Y_{11EF} & Y_{13EF} & Y_{11FF} & Y_{13FF} & Y_{11GF} & Y_{13GF} & Y_{11HF} & Y_{13HF} \\ Y_{31EF} & Y_{33EF} & Y_{31FF} & Y_{33FF} & Y_{31GF} & Y_{33GF} & Y_{31HF} & Y_{33HF} \\ Y_{11EG} & Y_{13EG} & Y_{11FG} & Y_{13FG} & Y_{11GG} & Y_{13GG} & Y_{11HG} & Y_{13HG} \\ Y_{31EG} & Y_{33EG} & Y_{31FG} & Y_{33FG} & Y_{31GG} & Y_{33GG} & Y_{31HG} & Y_{33HG} \\ Y_{11EH} & Y_{13EH} & Y_{11FH} & Y_{13FH} & Y_{11GH} & Y_{13GH} & Y_{11HH} & Y_{13HH} \\ Y_{31EH} & Y_{33EH} & Y_{31FH} & Y_{33FH} & Y_{31GH} & Y_{33GH} & Y_{31HH} & Y_{33HH} \end{bmatrix} \begin{Bmatrix} S_1 \\ M_{y1} \\ S_2 \\ M_{y2} \\ S_3 \\ M_{y3} \\ S_4 \\ M_{y4} \end{Bmatrix} \tag{6.21}$$

Typical sets of the point, coupling and transfer mobility functions for the CFSF plate are given in Appendix I. Figures I1 to I3 show the modulus spectra of the driving point force, moment and coupling mobility functions, respectively, at the mounting points E, F, G and H. These graphs show that there are many resonance peaks in the frequency range of interest. Below the first resonance frequency, the mobility functions are spring-like in nature and because of the symmetical positioning of the mounts, the point mobility functions at mounting points E and G and those at F and H are identical. For mounting points F and H, as they are closer to the simply supported edge, the driving point force mobility at low frequencies (below 100Hz) is greater than that at mounting points E and G which are closer to the clamped edge. The modulus spectra of the force, moment and coupling transfer mobility functions between velocity responses at various mounting points and the force and moment excitations at mounting point E are shown in figures I4 to I6.

6.4 SUMMARY

This chapter describes the analytical model and the component data used in the study of vibrational power transmission between a multi-point mounted flexible source (a free-free beam) - isolators (resilient mounts) - receiver (a rectangular plate) system. The point, transfer and coupling mobility functions of the source beam and the receiver plate are obtained analytically and the dynamic transfer properties of resilient mounts are obtained experimentally. The experimental arrangement for determining the dynamic transfer properties of resilient mounts in axial vibration is also presented. The measured dynamic transfer properties of the mounts agree closely with the predicted results.

CHAPTER 7

VIBRATIONAL POWER TRANSMISSION PREDICTION AND MEASUREMENT

7.1 INTRODUCTION

Based on the theoretical expressions for the vibrational power transmission between a multi-point mounted flexible source-isolator-receiver system and the mobility functions and dynamic transfer properties of the individual components, a FORTRAN computer programme was written to perform the analyses for the coupled system. The vibrational power input to the source beam and transmitted to the resilient mounts and receiver plate as well as the power dissipation in these structures have been examined for four different sets of isolator properties. Contributions of the vibrational power input to the receiver plate from adjacent mounting points and from the rotational motions at the mounting points have also been studied.

This chapter discusses these analytical results and the experimental arrangement of a corresponding coupled laboratory scale system. Velocity responses and vibrational power transmission between the coupled structures subjected to random force excitation on the source beam have also been measured. The measured vibrational powers are compared with the scaled theoretical powers obtained from a unit sinusoidal force excitation.

7.2 FOUR MOUNTING POINT - SINGLE DEGREE-OF-FREEDOM (4M1D) MODEL

7.2.1 Force Transmissibility of Coupled Flexible System

The concept of force transmissibility for a vibration isolation system has been well known and universally accepted. Initially, the force transmissibility of the coupled flexible source (free-free beam), resilient mounts, and flexible receiver (CFSF plate) is compared with the corresponding transmissibility curves of a coupled rigid mass,

viscously damped spring and rigid foundation system with two different damping ratios, $\zeta = 0.1$ and $\zeta = 0.01$, as shown in figure 7.1. It can be seen that the resonance peaks of the source and receiver are clearly shown in the isolation region, which greatly reduce the isolation provided by the resilient mounts. In spite of the relatively soft and highly damped resilient mounts, the resonance peak of the source is very lightly damped. This is most likely, as will be seen later, due to the fact that at high frequencies, the source beam behaves as a 'velocity source' upon the resilient mounts.

The effects of the stiffness and loss factor of resilient mounts on the force transmissibility of the coupled flexible systems are shown in figure 7.2(a). It can be seen that :

(1) increase in the stiffness of resilient mounts greatly changes the response or the force transmissibility of the system and reduces the isolation provided by the resilient mount (i.e. see case C-2 vs case C-1). This would be the case of a bolted joint or 'rigidly coupled' source and receiver system.

(2) Decrease in the damping of resilient mounts increases the resonance peaks of the fundamental mass - spring resonance frequency (22Hz) and the resonance frequencies of the receiver (i.e. see case C-3 vs case C-1).

(3) Reducing the stiffness of resilient mounts by increasing the length of the mounts decreases the fundamental mass-spring frequency, as would be expected. However, in the high frequency region, typically above 400Hz, the isolation provided by the mounts is greatly diminished due to the 'wave effects' or longitudinal resonances of the mounts (see case C-4 vs case C-1).

7.2.2 Effects of Resilient Mount Properties on the Vibrational Power Transmission

The effects of the stiffness and loss factor of the resilient mounts on the vibrational power input to the source beam are shown in figure 7.2(b). In the frequency region (typically below 100Hz) where rigid body motion of the source beam is dominant, there are great differences in the power input to the source beam. Taking the power input for case C-1 properties as the reference, it can be seen that :

(1) for a stiff connection between the source beam and the receiver plate (case C-2), there is relatively small motion of the beam for a given force excitation; thus the power input to the beam is less than for case C-1 for frequencies below the

fundamental mass-spring resonance frequency of the system, although the force transmissibilty is unity at low frequencies for these two cases, as can be seen from figure 7.2(a). Above this resonance frequency, vibrational power input increases due to ineffective isolation provided by the stiff mounts as shown in the force transmissibility curves (figure 7.2(a)).

(2) For lightly damped resilient mounts (case C-3), the power input to the source beam is of the lowest level of the cases considered except around the resonance frequencies. This is most likely due to a much smaller real part of the 'effective' point mobility as suggested from the study on the vibrational power input to rectangular plates (see Chapter 3). (The smaller the loss factors, the smaller are the real parts of the driving point force and moment mobility functions.)

(3) For softer resilient mounts (case C-4), the rigid body motion of the source beam is greater than that of case C-1, hence, results in greater power input to the beam below the first resonance frequency. The power input to the beam increases at high frequencies due to the influence of mount 'wave effects'.

The effects of the stiffness and loss factor of the resilient mounts on the total vibrational power transmitted to the receiver plate (the sum of power transmitted to the plate at the four mounting points) are shown in figure 7.2(c). It can be seen that below the fundamental mass-spring resonance frequency of the system, the power transmitted to the receiver plate is similar in each case, i.e. the effects of the mount properties are not significant. This is due to the unity force transmissibility for the four cases at low frequencies, see figure 7.2(a). Above the fundamental mass-spring resonance frequency, the power transmitted to the plate is dominated by the resonance peaks of the plate and the source beam. For stiff mounts (case C-2), the power transmitted is the greatest due to the largest transmitted forces. For lightly damped mounts (case C-3), the power transmitted at the resonance frequencies increases. For longer or softer mounts (case C-4), the influence of mount 'wave effects' increases the power transmitted to the plate.

The effects of the stiffness and loss factor of the resilient mounts on the total vibrational power transmitted to the resilient mounts (the sum of power transmitted to the four mounts) are shown in figure 7.2(d). It can be seen that for low frequencies when it is dominated by the rigid body motion of the source beam, the power transmitted to the resilient mounts is similar to the power input to the source beam. For high frequencies,

the resonance peaks of the plate modes are more pronounced especially for the case of lightly damped resilient mounts (case C-3).

7.2.3 Vibrational Power Transmission Between the Coupled Systems

Comparisons of the vibrational power input to the source beam and that transmitted to the resilient mounts and the receiver plate for each case of mount properties are shown in figure 7.3. It can be seen that :

(1) in general, due to the rigid body motion of the source beam in the low frequency region, there is no flexural motion in the beam, the vibrational power input to the source beam and the sum of the power transmitted to the resilient mounts are the same. In the high frequency region, when the source beam moves as a 'velocity source' (which can be seen later in that the mobility of the coupled source beam is the same as that of the free-free beam), power is dissipated in the beam as a result of hysteretic losses before transmission to the resilient mounts.

(2) The difference between the sum of the power transmitted to the resilient mounts and the total power transmitted to the receiver plate is the power dissipated in the resilient mounts. The smaller the stiffness and the greater the loss factor of the resilient mounts, the greater is the power dissipation in the mounts.

7.2.4 Dynamic Response of the Source Beam

Figure 7.4 shows comparisons of the modulus and phase spectra of the driving point mobility function at the centre of the source beam and the beam in its 'free-free' boundary conditions. It can be seen clearly that above 100Hz, the resiliently mounted source beam can be regarded as a 'velocity source'. This is because the velocity response of the coupled beam is the same as that of the 'free-free' beam, i.e. the source velocity is not affected by the attachment of resilient mounts.

7.2.5 Force Transmitted to the Receiver Plate

Figure 7.5 shows the modulus spectra of the transmitted forces acting on the receiver plate at the four mounting points. Due to the symmetrical positioning of the mounting points, the transmitted forces acting at points E and G, and those at points F and H are identical (see figure 6.7). The transmitted forces are very similar in nature except close

to the fundamental resonance frequency of the receiver plate. The responses of the plate at these two sets of mounting points are different due to the differences in the boundaries, i.e. clamped edge vs simply supported edge.

7.2.6 Velocity Responses on the Receiver Plate

The modulus spectra of the velocity responses at the four mounting points on the receiver plate are shown in figure 7.6. The velocity responses at mounting points E and G and those at mounting points F and H are identical because of the symmetrical positioning of the mounts. At low frequencies, the velocity responses at points F and H, which are closer to the simply supported edge, are larger than those closer to the clamped edge, i.e. points E and G.

7.2.7 Contribution of Vibrational Power from Adjacent Mounts

For a multiple point mounted machine, the contribution of the vibrational powers from adjacent mounts to a specific mount is accounted for by including the transfer mobility functions between these mounting points. The vibrational power transmitted to the mounting points E and F are shown in figures 7.7 and 7.8 respectively. Both positive and negative powers are shown in the figures. The negative power corresponds to power flow from the plate to the resilient mounts. This is not surprising, as an earlier experimental investigation by Pinnington [21] has shown similar results at the four mounting points. The negative power occurs when the transmitted forces and the resulting velocity responses at the mounting points are in anti-phase. At low frequencies (below 100Hz), when the motion of the source beam is dominated by rigid body translation (no rocking motion as in the analytical model, the force excitation is vertical and acting through the centre of gravity, and the isolators are identical), large negative power is transmitted through mounting points F and H because of the out of phase motion of the plate which corresponds to the second mode of the CFSF plate. Because of the out of phase motion, one pair of the resilient mounts is stretched while the other pair is compressed.

7.3 FOUR MOUNTING POINT - TWO DEGREE-OF-FREEDOM (4M2D) MODEL

The degrees-of-freedom considered in this model were the vertical translational motion and the rotational motion about Y-axis at each mounting point. The resilient mount in

bending (i.e. rotational motion) was approximately modelled as a simple rotational spring [24] with spring constant,

$$K_r = \frac{E I}{L} \tag{7.1}$$

where E is the Young's modulus, I is the second moment of area of the cross-section and L is the length of the resilient mount.

For a resilient mount with square cross-sectional area, A , and length of each side, h, the ratio of K_r to the extensional spring constant, K, is given by :

$$\frac{K_r}{K} = \frac{I}{A} = \frac{h^2}{12} \tag{7.2}$$

The dynamic transfer properties of the resilient mount in bending were then obtained in analogy to an extensional spring as given in section 5.3.1. The loss factor of the resilient mount in bending was assumed to be the same as for the mount in axial vibration.

7.3.1 Vibrational Power Transmission via the Rotational Motion

For the coupled source - isolator - receiver systems subjected to a unit sinusoidal vertical force excitation at the centre (c.g.) of the source beam, vibrational power is transmitted to the isolators via the translational motion and shear force, and the rotational motion and bending moment resulting from flexural vibration of the beam.

Figure 7.9 shows a comparison between the sum of the vibrational power transmitted to the four resilient mounts due to the translational and the rotational motions at the mounting points. The power transmitted to the isolators via the rotational motion and bending moment is much lower than that due to translational motion for this case of force excitation at the centre of the beam. In the rotational power spectrum, an additional rigid body resonance at 36Hz is noted. This corresponds to the rocking mode of the source beam on the resilient mounts. The rocking mode natural frequency can easily be verified from fundamental mechanical vibration theory [47].

7.3.2 Off-centre Force Excitation on the Source Beam

In order to demonstrate the rocking mode of the source beam, velocity responses and vibrational power transmission between the coupled systems subjected to an off-centre

unit sinusoidal force excitation were analysed. The force excitation was applied along the central line of the source beam at a distance of 40mm to the left of the beam centre. The predicted translational and the rotational velocity responses at mounting point E (see figure 6.7) were compared to the corresponding velocity responses induced by central excitation, and are shown in figures 7.10 and 7.11 respectively. It can be seen that the rocking resonance peak is more pronounced in the case of off-centre excitation.

A comparison between the sum of the translational and the rotational vibrational powers transmitted to the four resilient mounts for the off-centre excitation case is shown in figure 7.12. At low frequencies, due to the off-centre force excitation, the rocking motion dominates and thus increases the rotational power transmission to the resilient mounts compared to the case of central excitation (figure 7.9). However, the rotational power decreases with increasing frequency. Above the fundamental mass - spring resonance frequency, especially in the frequency range dominated by flexural vibration of the source beam, there is no significant difference in the power transmission to the resilient mounts for these two cases of excitation.

7.4 EXPERIMENTAL ARRANGEMENT AND INSTRUMENTATION SET-UP

In the experimental arrangement, the source beam was represented by a uniform steel beam which was supported near the four corners by the resilient mounts. These resilient mounts were firmly glued in between the isolator supports as shown in figure 6.5. The isolator supports were then attached to the source beam and the receiver plate by screws and nuts. The receiver plate was clamped along one edge and simply supported along the opposite edge with the other pair of edges free. Detailed dimensions of the beam, resilient mounts and the receiver plate have been described in section 6.2.

A schematic diagram showing the experimental arrangement for measuring the velocity responses and the vibrational power transmission between the coupled source - isolator - receiver systems is shown in figure 7.13. A photograph showing this experimental arrangement is given in figure J1 of Appendix J.

The instrumentation set-up of the experiment is illustrated in figure 7.14. An electro-dynamic exciter which consisted of a fixed permanent magnet and a moving coil was driven by a continuous random signal (10Hz to 1600Hz) generated by an HP 3566A Spectrum Analyser. The random force input to the source beam was measured by a force transducer. The responses of the coupled systems were measured at seven

different locations by accelerometers (B&K type 4375). In order to simplify subsequent signal processing routines, the acceleration signals were converted to velocity signals by the charge amplifiers before being input to the eight channel data acquisition module of the analyser. The frequency response functions obtained from the analyser were then further processed by an on-line microcomputer to calculate the vibrational powers for comparison with the theoretical predictions.

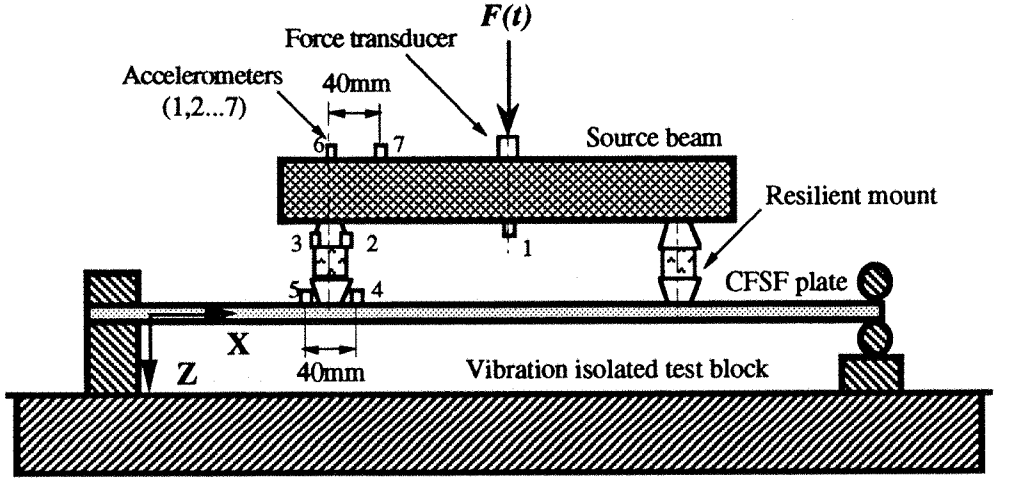

Figure 7.13 : Experimental arrangement for measurement of the vibrational power transmission between the coupled source - isolator - receiver systems.

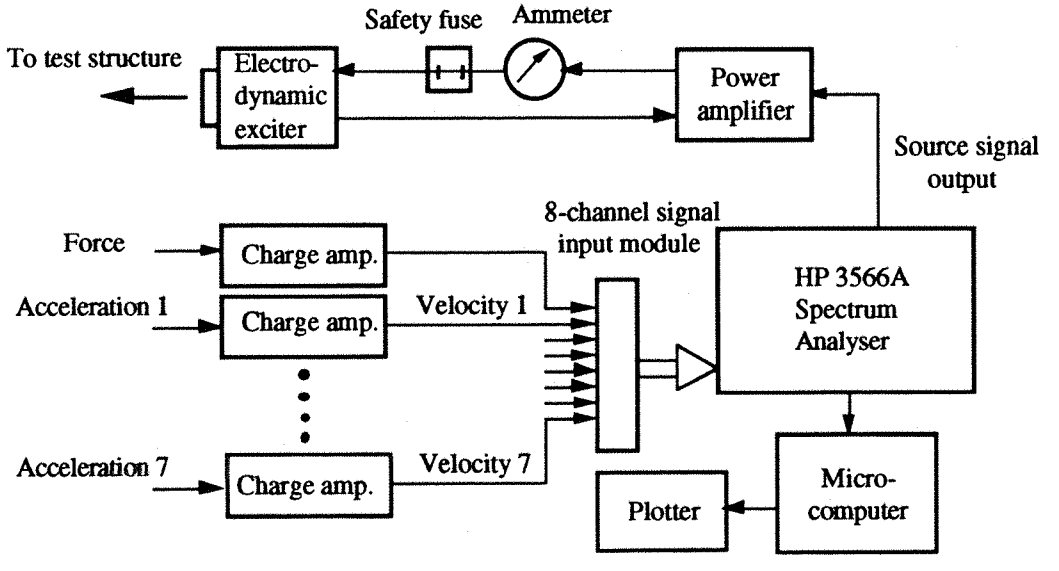

Figure 7.14 : Instrumentation set-up for measurement of the vibrational power transmission between the coupled source - isolator - receiver systems.

7.5 EXPRESSIONS FOR THE VIBRATIONAL POWER ESTIMATION

7.5.1 Vibrational Power Input to the Source Beam

For a linear structure subjected to a point harmonic force, $F(t)$, the time-averaged vibrational power input to the structure is given by the following expression :

$$P_{in} = \frac{1}{2} Re \{ F \dot{w}^* \} \tag{7.3}$$

where $\dot{w}^*$ is the complex conjugate of the velocity response at the excitation point, and $Re\{\ \}$ denotes the real part of the complex quantity. Equivalent expressions for the input power are :

$$P_{in} = \frac{1}{2} |F|^2 Re \{ M \} \tag{7.3a}$$

$$= \frac{1}{2} |\dot{w}|^2 Re \{ \frac{1}{M} \} \tag{7.3b}$$

where M is the driving point mobility function of the structure.

For a linear structure subjected to a random force excitation with spectral density function, G_{ff}, the time-averaged vibrational power per Hz input to the structure can be estimated from the following expressions [48,49].

$$P_{in}|_{Hz} = Re \{ G_{fv} \} \tag{7.4}$$

$$= G_{ff} Re \{ M \} \tag{7.4a}$$

$$= G_{vv} Re \{ \frac{1}{M} \} \tag{7.4b}$$

where G_{fv} is the cross spectral density function between the applied force and the resulting velocity at the excitation point, G_{vv} is the power (auto) spectral density function of the velocity at the excitation point.

7.5.2 Vibrational Power Transmitted to a Resilient Mount

The relationships between the extensional forces, Q and R acting at the top and bottom surfaces of a resilient mount and the resulting velocities, $\dot{u}$ *and* $\dot{v}$, in the direction of the forces are given in eqn.(5.27). The measured quantities in the experiment are the

velocity responses at the top and bottom of the mount. The force, Q, can be expressed in terms of these measured quantities as:

$$Q = \frac{\alpha_{11}}{\alpha_{21}} \dot{u} + \frac{\alpha_{12}\,\alpha_{21} - \alpha_{11}\,\alpha_{22}}{\alpha_{21}} \dot{v} \tag{7.5}$$

For a massless damped spring, $\alpha_{11} = 1.0$, $\alpha_{12} = 0$ and $\alpha_{22} = 1.0$ (table H.1), thus Q can be simplified to :

$$Q = \frac{1}{\alpha_{21}} (\dot{u} - \dot{v}) \tag{7.6}$$

The time-averaged vibrational power transmitted to a resilient mount is :

$$\begin{aligned} P_{iso} &= \frac{1}{2} Re \{ Q \dot{u}^* \} \\ &= \frac{1}{2} Re \{ \frac{1}{\alpha_{21}} (\dot{u} \dot{u}^* - \dot{v} \dot{u}^*) \} \end{aligned} \tag{7.7}$$

For a resilient mount with large loss factor and relatively small dynamic stiffness, the velocity at the bottom of the mount, $\dot{v}$, is much smaller than the velocity at the top surface, $\dot{u}$, especially in the isolation region, then the power transmitted to the mount is approximately given by :

$$P_{iso} \approx \frac{1}{2} | \dot{u} |^2 Re \{ \frac{1}{\alpha_{21}} \} \tag{7.8}$$

Eqn. (7.8) can also be expressed in terms of the applied force, $F(t)$, and the transfer mobility function, M_1, between the velocity at the mounting point and the force at the excitation point, as :

$$P_{iso} \approx \frac{1}{2} | F |^2 | M_1 |^2 Re \{ \frac{1}{\alpha_{21}} \} \tag{7.8a}$$

where $M_1 = \frac{\dot{u}}{F}$.

For random excitation, the equivalent espressions for eqns. (7.8) and (7.8a) are :

$$P_{iso} |_{Hz} = G_{uu} Re \{ \frac{1}{\alpha_{21}} \} \tag{7.9}$$

and

$$P_{iso} |_{Hz} = G_{ff} | M_1 |^2 Re \{ \frac{1}{\alpha_{21}} \} \tag{7.9a}$$

where G_{uu} is the spectral density function of the velocity at the top surface of the resilient mount or at the corresponding mounting point on the source beam.

7.5.3 Vibrational Power Transmitted to the Receiver Plate

The time-averaged vibrational power transmitted to the receiver (seating structure) for the single mount model has been given in eqn. (5.28) which can be re-written as :

$$P_{plt} = \frac{1}{2} Re \left\{ \frac{1}{\alpha_{21}} \left(\dot{u} \dot{v}^* - \dot{v} \dot{v}^* \right) \right\} \tag{7.10}$$

where $\dot{v} = \dot{w}$ from the continuity condition, eqn. (5.12). If $\dot{v} << \dot{u}$ for a machine resilient mount, then the vibrational power transmitted to the receiver plate through one resilient mount can be simplified to :

$$P_{plt} \approx \frac{1}{2} Re \left\{ \frac{1}{\alpha_{21}} \left(\dot{u} \dot{v}^* \right) \right\} \tag{7.11}$$

which can also be expressed as :

$$P_{plt} \approx \frac{1}{2} |F|^2 Re \left\{ \frac{1}{\alpha_{21}} M_1 M_2^* \right\} \tag{7.11a}$$

where $M_1 = \frac{\dot{u}}{F}$ and $M_2 = \frac{\dot{v}}{F}$ are the transfer mobility functions between the velocities at the top and bottom surfaces of the resilient mount, respectively, and the applied excitation force.

For random excitation, the equivalent expressions are :

$$P_{plt}|_{Hz} = Re \left\{ \frac{1}{\alpha_{21}} G_{vu} \right\} \tag{7.12}$$

and

$$P_{plt}|_{Hz} = G_{ff} Re \left\{ \frac{1}{\alpha_{21}} M_1 M_2^* \right\} \tag{7.12a}$$

where G_{vu} is the cross spectral density function between the velocities at the bottom and at the top surfaces of the resilient mount.

It will be seen later that eqns. (7.4a), (7.9a) and (7.12a) are the most useful expressions for estimating the vibrational power transmission between the coupled systems subjected to random force excitation. This is because the point and transfer mobility functions, M, M_1 and M_2 are readily obtained from the spectrum analyser and the applied force spectral density function, G_{ff}, can be used as a scaling factor to adjust the level of the predicted vibrational power from the theoretical model.

7.5.4 Vibrational Power Transmission via Rotational Motion

The time-averaged vibrational power transmitted to a resilient mount and the receiver plate via the rotational motion can be estimated approximately by considering the resilient mount as a damped rotational spring. The rotational spring stiffness , K_r , can be estimated as described in section 7.3. For the coupled systems subjected to random excitation, the rotational vibrational power transmitted to a resilient mount and to the receiver plate can be obtained from previous expressions, eqns (7.9) and (7.12) by replacing α_{21} , M_1 and M_2 by $\alpha_{\theta 21}$, $M_{\theta 1}$ and $M_{\theta 2}$ respectively, where

$$\alpha_{\theta 21} = \frac{j\omega}{K_r(1+j\eta_m)} \tag{7.13}$$

and $M_{\theta 1} = \frac{\dot{\theta}_1}{F}$, $M_{\theta 2} = \frac{\dot{\theta}_2}{F}$ are the transfer mobility functions between the rotational velocities at the top and bottom surfaces of the resilient mount, respectively, and the applied excitation force.

7.6 EXPERIMENTAL RESULTS AND DISCUSSION

7.6.1 Mobility Functions of the Source Beam

Comparison of the measured and predicted moduli and phases of the driving point mobility functions of the source beam is shown in figure 7.15. Similar comparisons for the transfer mobility functions between the vertical translational and the rotational velocities at mounting point E (see figure 6.7) and the input force excitation at the beam centre are shown in figures 7.16 and 7.17 respectively. The predicted mobility functions and the measured results are in good agreement over the freqency range of interest, except for the rotational mobility function (figure 7.17) at frequencies below 40Hz. In this low frequency region, in which the rigid body translational motion of the source beam is dominant, the rotational velocity response measured by taking the

difference between two closely spaced accelerometer signals are less accurate due to the small differences between the measured signals.

Similar comparisons for the transfer translational and rotational mobility functions for the case of a 40mm off-centre excitation are shown in figures 7.18 and 7.19. It can be seen that reasonably good agreement between the measured and predicted results is obtained for frequencies above 40Hz. The discrepancy at low frequencies for the rotational response was most probably due to the limitation of the measurement method.

7.6.2 Real Part of the Driving Point Mobility Function

Whilst figure 7.15 shows a remarkably good agreement between the measured and predicted driving point mobility functions of the source beam, comparison between the measured and predicted real parts of the corresponding driving point mobility functions (figure 7.20) is quite alarming. The real part of the driving point mobility function of a structure is an important function which determines directly the vibrational power input to the structure. Two discrepancies are obvious from the measured result : it fluctuates at low response levels and it becomes negative at certain frequencies.

The fluctuation of the real part of the driving point mobility function at low response levels can be explained by comparing with its phase plot (figure 7.15). As the source beam is very lightly damped, the phase angle in this low response region is very close to -90 degrees. The cosine function of -90 degrees is zero, thus the real part is very small and the noise to signal ratio can be quite high. Increasing the damping of the beam will increase the phase angle (i.e. > -90 degrees), hence increase the real part of the driving point mobility function. Also around 90 or -90 degrees, the rate of change of the cosine function for a small change in the phase angle is the largest, thus causing a relatively large fluctuation in the real part of the mobility function.

From linear structural vibration theory [24,27,41], it is known that the real part of driving point mobility function is always positive. The negative real part of the measured point mobility function occurred because the phase angle was slightly less than -90 degrees. This was most probably due to a small phase mismatch in the measuring instruments, e.g. charge amplifiers, anti-aliasing filters, etc.

As the real part of driving point mobility function is an important component which determines the amount of power input to the structure, the above comparison shows to

certain extent the difficulty of measuring mechanical vibrational power input or transmitted to a structure, compared to the more conventional approach of measuring the modulus and phase of a frequency response function. Nevertheless, as the low level fluctuation of the real part is approximately four decades below the main resonance peaks, it should not pose much of a problem if one is interested in controlling the peak responses of a structure.

7.6.3 Scaling Factor for the Predicted Vibrational Power

The theoretical vibrational powers were calculated based on unit sinusoidal force excitation but the measured powers were obtained from random force excitation at a different level. In order to compare these two sets of results, it is necessary to multiply one of these two sets of results by a scaling factor or scaling spectrum.

From eqns. (7.3a) and (7.4a) the time-averaged vibrational power input to a linear structure by a point harmonic force is : $P_{in} = \frac{1}{2} |F|^2 Re\{M\}$ and that resulted from a random excitation is : $P_{in}|_{Hz} = G_{ff} Re\{M\}$.

If one selects a frequency resolution of 1Hz for the spectra and multiplies eqn. (7.3a) by a scaling factor, γ, such that eqn (7.3a) is equal to (7.4a), i.e.

$$\gamma \frac{1}{2} |F|^2 Re\{M\} = G_{ff} Re\{M'\} \tag{7.14}$$

where M' denotes the measured mobility function. Now, the real part of the driving point mobility function is a structural property, which for linear structures, is independent of the type and level of applied excitations. One can therefore assume that the real parts of the measured and predicted mobility functions are equal (in a 'truely' noise free environment), and for a unit harmonic force, $|F|^2 = 1$, the scaling factor is given by :

$$\gamma = 2 G_{ff} \tag{7.15}$$

A plot of the spectral density function, G_{ff}, of the applied random force excitation is shown in figure 7.21. It can be seen that it fluctuates but maintains a steady average level except near the first resonance frequency of the source beam (539Hz). In order to maintain the 'smoothness' of the theoretical results, a Least Squares straight line was fitted to the G_{ff} spectrum. The Least Squares model of the spectrum, denoted by $\bar{G}_{ff}$

was used in eqn. (7.15) for calculation of the scaled theoretical power. A plot of $\bar{G}_{ff}$ is also shown in figure 7.21.

7.6.4 Comparison of the Measured and Scaled Theoretical Vibrational Powers

After multiplying the theoretical vibrational powers by the scaling spectrum, comparisons of the measured and predicted vibrational power input to the source beam and the power transmitted to the resilient mount at mounting point E (see figure 6.7) are shown in figures 7.22 and 7.23 respectively. The fluctuation in the measured input power spectrum was due to the fluctuation in the real part of the driving point mobility function and the random fluctuation of G_{ff}. The fluctuation in the transmitted power to the resilient mount is purely the random fluctuation of G_{ff}. This random fluctuation of G_{ff} can be rectified by using the Least Squares model, $\bar{G}_{ff}$, of the spectrum. Figures 7.24 and 7.25 show the comparisons between the corresponding measured and predicted powers after removing the random fluctuation of G_{ff}. It can be seen that the agreement between the measured and predicted vibrational powers for these two cases considered is very good. The assumption of $\dot{v} << \dot{u}$ for a resiliently mounted machine is justified in this case.

Figure 7.26 shows a comparison of the measured and predicted vibrational powers transmitted to the resilient mount at mounting point E via the rotational motion.The random fluctuation of G_{ff} has been removed in the measured result, thus the fluctuation in the measured power spectrum is due to the variation of the measured rotational responses at the low response levels. For the predicted power spectrum, the small dips and peaks in the mid-frequency range are due to the anti-resonance dips and resonance peaks of the receiver plate, which have been neglected in the measured power.

A comparison of the measured and predicted vibrational powers transmitted to the receiver plate at mounting point E is shown in figure 7.27. The measured power was smoothed by $\bar{G}_{ff}$ and the predicted power was scaled by the scaling spectrum, eqn.(7.15). It can be seen that, in general, the agreement around the resonance peaks, where the response levels are greater, is good compared to those around the anti-resonance region. This is most probably due to the dynamic range of the measuring transducers as the response levels around the anti-resonance region were approximately six to seven decades below the peak power transmitted to the resilient mount as shown in figure 7.25. In practical situations, vibrational powers at a level of four decades below the resonance peak powers will not be significant.

7.7 SUMMARY

The time-averaged vibrational power transmission in a multi-point mounted flexible source - isolator - receiver system has been studied based on the mobility coupling approach for linear structures. The theoretical model and practical system investigated consisted of a source structure (a free-free beam), resilient isolators and a receiver structure (a rectangular plate). The theoretical model has facilitated study of the influence of the isolator properties on power transmission between the coupled structures, the contribution of the vibrational power from adjacent mounts and the rotational motion at the mounting points.

Experimental measurements of the velocity responses and vibrational power transmission between the coupled structures have also been carried out. Practical expressions for measuring the input and transmitted powers based on the measured mobility functions and the spectral density function of the applied random excitation have been derived. Good agreement was obtained between the measured and predicted vibrational powers. Some of the main theoretical results and their comparisons with the experimental results have also been reported in [50].

The main findings from this study are summarised as follows :

(1) the isolator properties (dynamic stiffness and loss factor) have great influences on the vibrational power input to the source beam and transmitted to the isolators in the low frequency region where it is dominated by the translational rigid body motion of the source beam. In this frequency region, the total power transmitted to the isolators is the same as the power input to the source beam.

(2) In high frequency region, where it is dominated by flexural vibration of the source beam, power is dissipated in the beam due to internal loss before transmission to the resilient mounts. Vibrational power is also dissipated in the resilient mounts before transmission to the receiver. The smaller the stiffness and the greater the loss factor of the resilient mounts, the larger is the power dissipation in the mounts.

(3) The resiliently mounted source beam behaved as a 'velocity source' at frequencies above 100Hz, as the velocity response of the coupled beam was the same as that of a 'free-free' beam.

(4) The vibrational power spectra of different mounting points consist of positive and negative values. Negative power occurs when the transmitted force and the resulting velocity response are in anti-phase.

(5) Whilst it is relatively easy to measure the modulus and phase of a mobility function to a good accuracy, it is very difficult to measure accurately the real part of a mobility function for a lightly damped structure. The low response level of the structure around anti-resonance frequencies is very sensitive to phase mismatch in the measuring instruments.

(6) It is possible to compare the theoretically calculated vibrational powers based on point harmonic force excitation with the measured powers resulting from random excitation. Within the accuracy of the conventional measurement method for rotational degrees-of-freedom, the measured velocity responses and vibrational powers were in good agreement with the theoretical results.

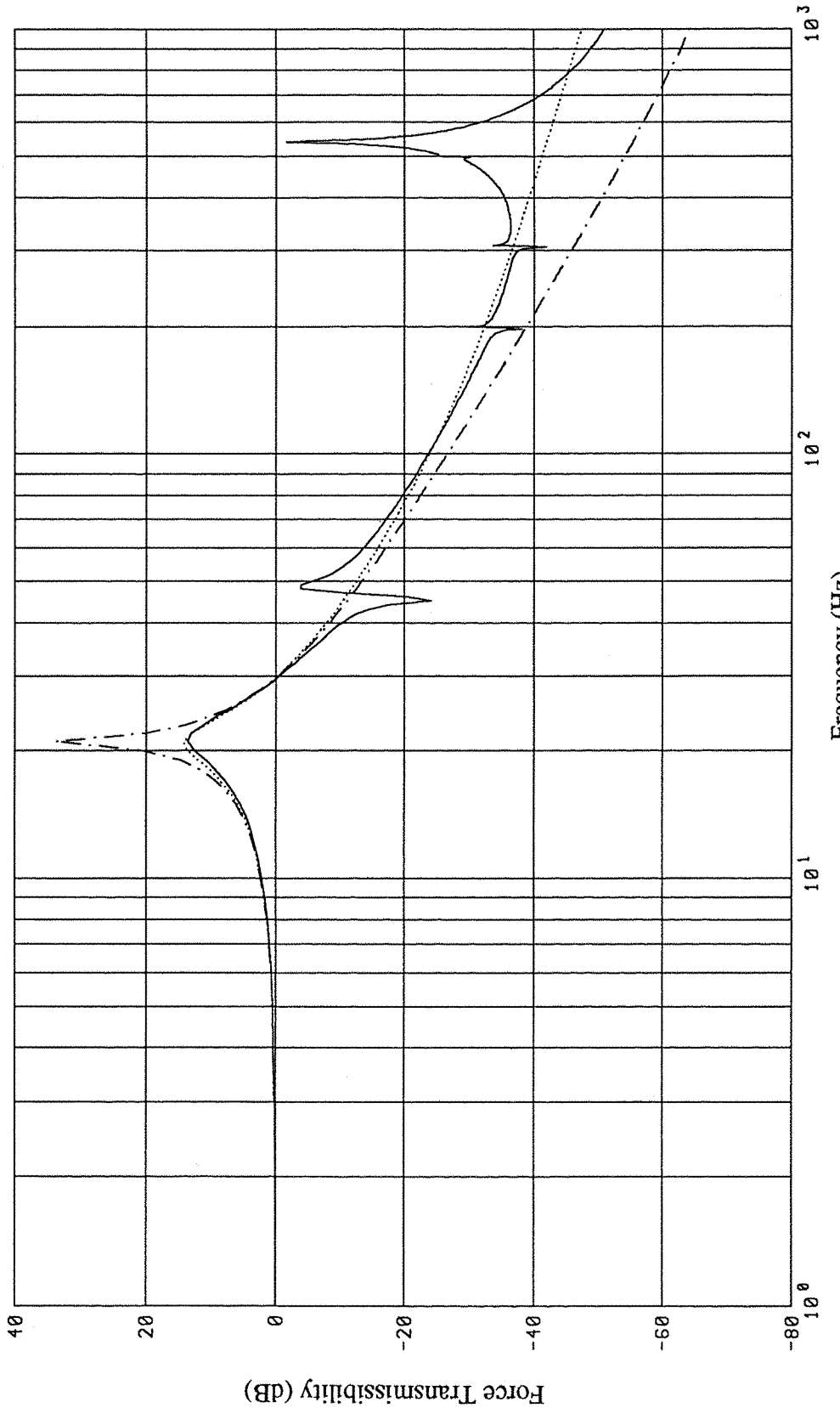

Figure 7.1 : Comparisons of the force transmissibilities of coupled source - isolator -receiver systems : (1) Flexible source (free-free beam) and flexible receiver (CFSF plate) (————), (2) Rigid mass and rigid foundation with viscous damping ratios : $\zeta = 0.1$ (.....), $\zeta = 0.01$ (—·—·—·—).

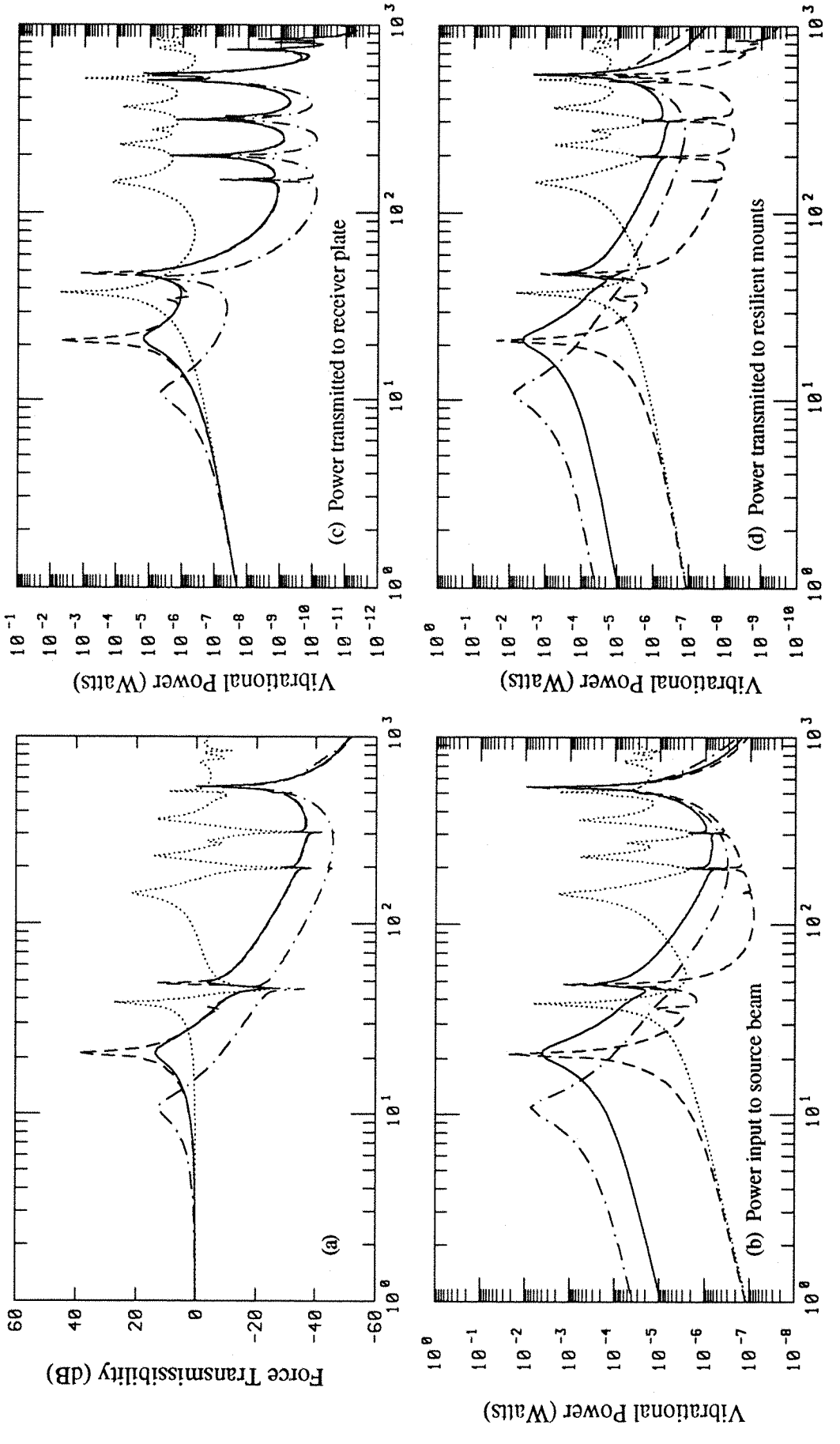

Figure 7.2 : Comparisons of the force transmissibilities and vibrational power transmission between coupled systems for various sets of isolator properties as shown in table 6.1 : ——— case C-1, ... case C-2, - - - - - case C-3 and —·—·— case C-4.

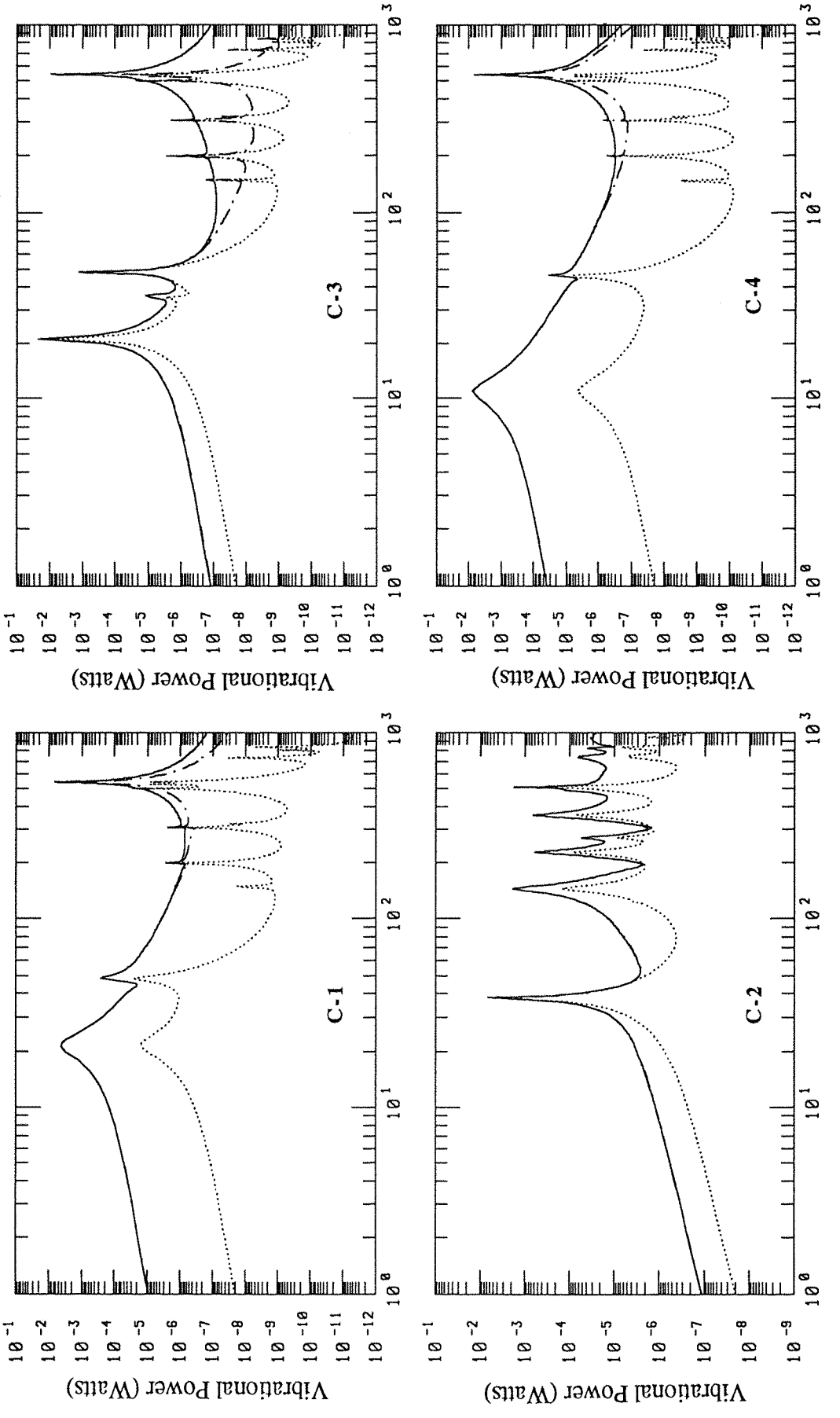

Figure 7.3 : Comparisons of the vibrational power transmission between coupled systems for various sets of isolator properties as shown in table 6.1 : ——— power input to source beam, ... power transmitted to receiver plate, —·—·— power transmitted to resilient mounts.

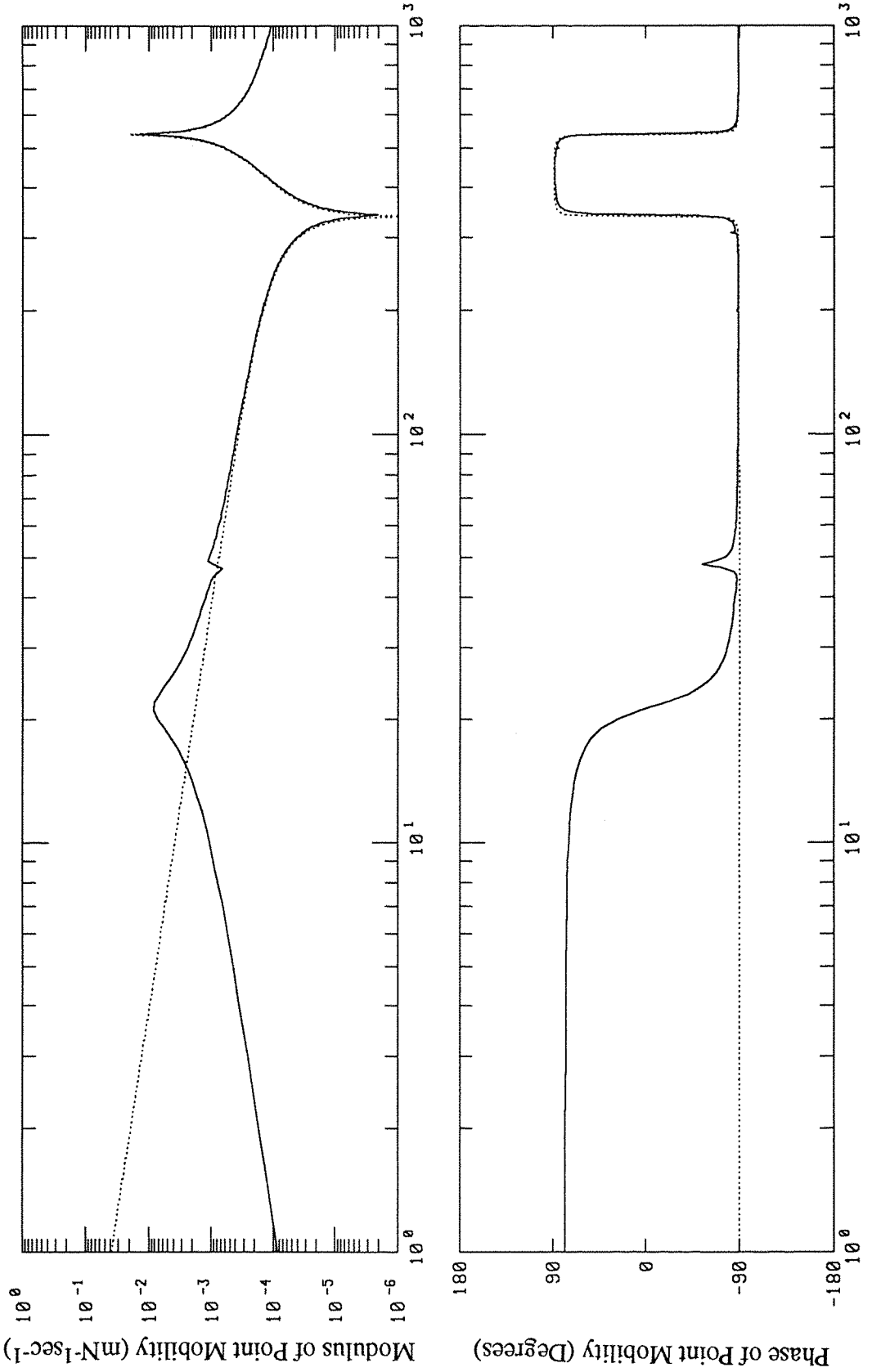

Figure 7.4 : Comparisons of the modulus and phase spectra of the driving point mobility functions at the centre of the beam : —— resiliently mounted beam, ... 'free - free' beam.

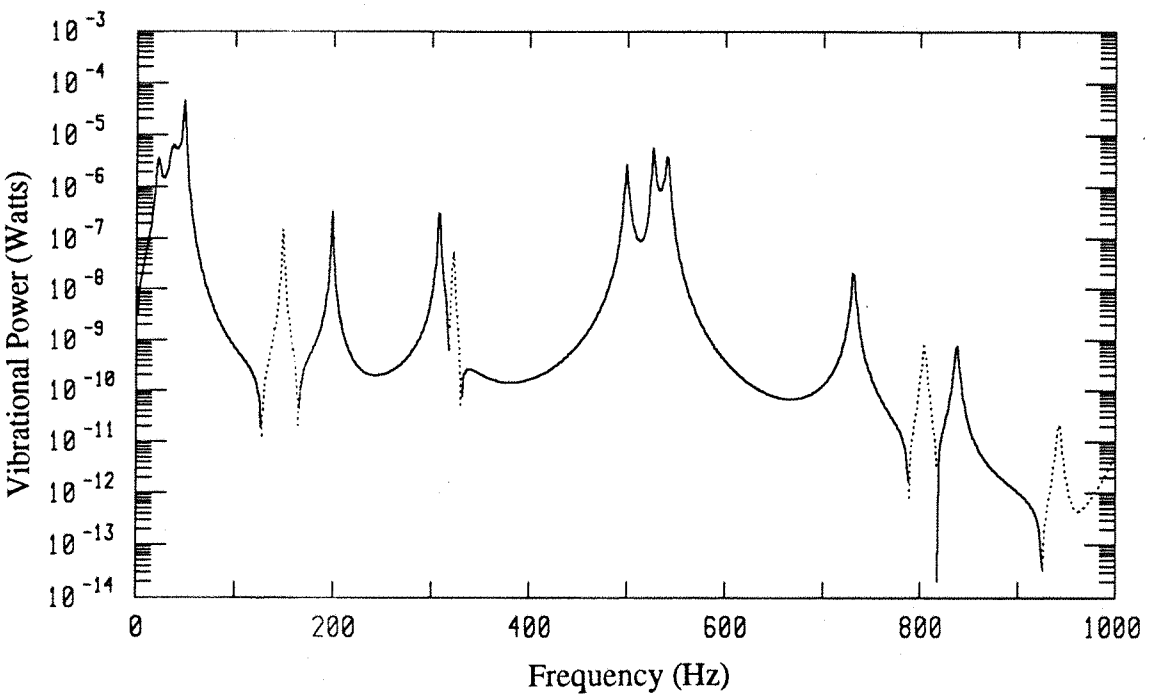

Figure 7.7 : Vibrational power transmitted to the receiver plate at mount E, ——— positive power, ····· negative power.

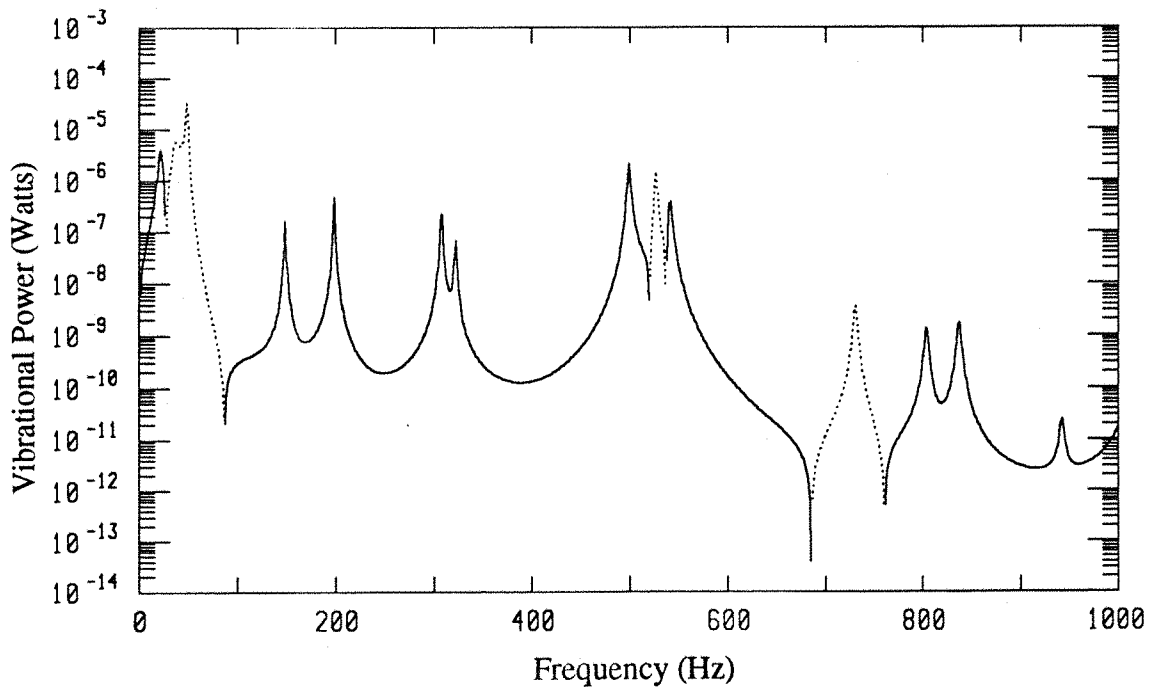

Figure 7.8 : Vibrational power transmitted to the receiver plate at mount F, ——— positive power, ····· negative power.

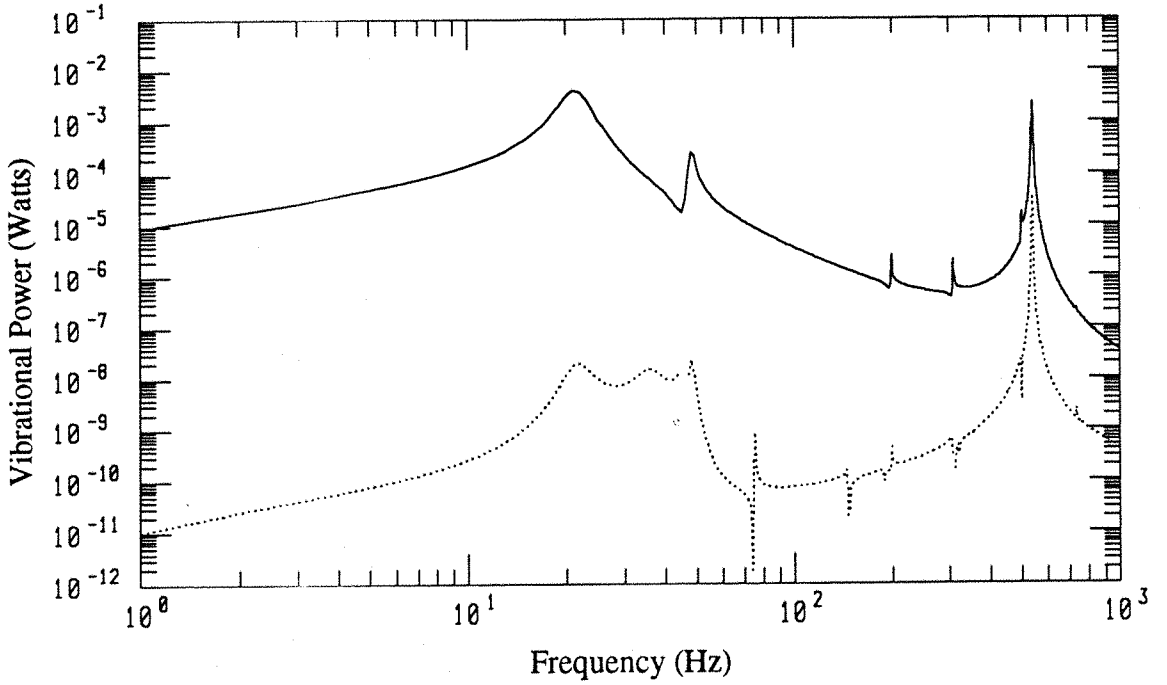

Figure 7.9 : Vibrational power transmitted to the resilient mounts from a point sinusoidal force of 1N applied at the beam centre : ——— translational motion, ····· rotational motion.

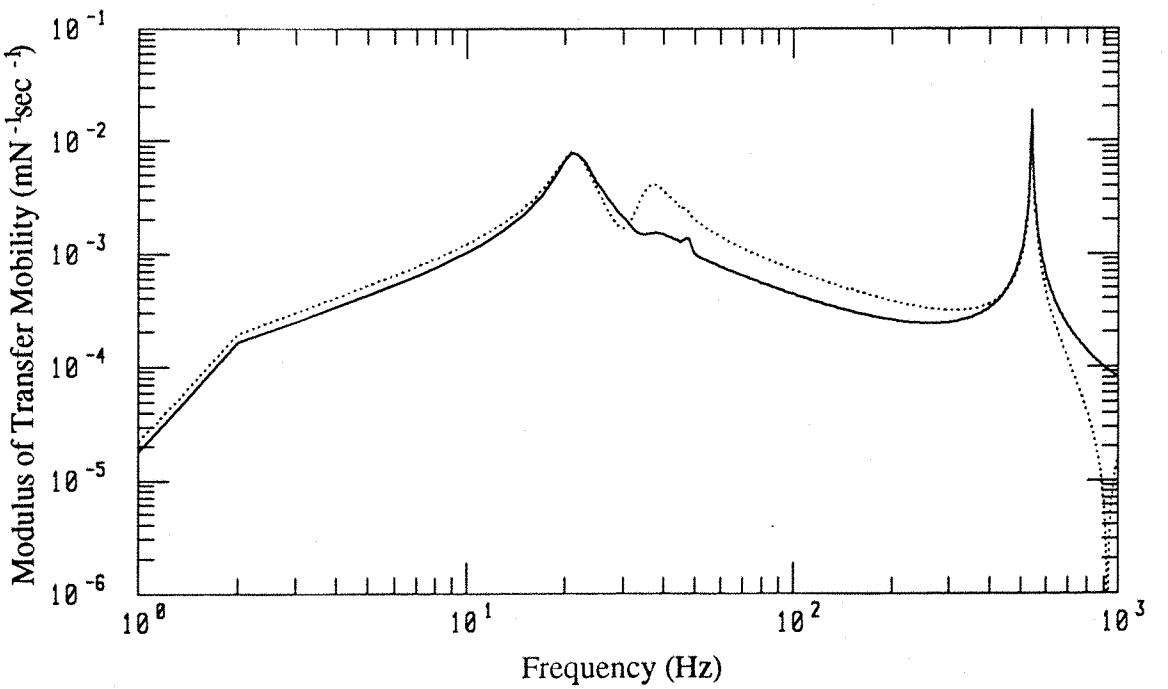

Figure 7.10 : Modulus spectra of the transfer mobility between the translational velocity at mounting point E and applied force : ——— at the centre of the beam, ····· at an off-centre point (40mm left of centre).

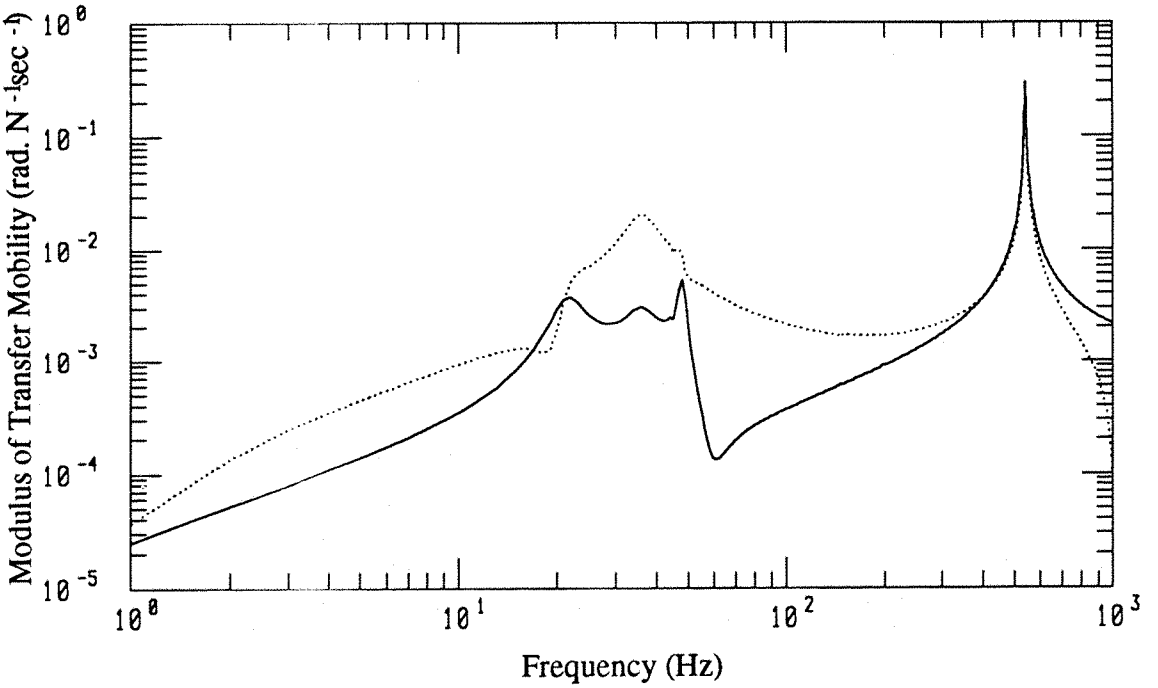

Figure 7.11 : Modulus spectra of the transfer mobility between the rotational velocity at mounting point E and applied force : ——— at the centre of the beam, ····· at an off-centre point (40mm left of centre).

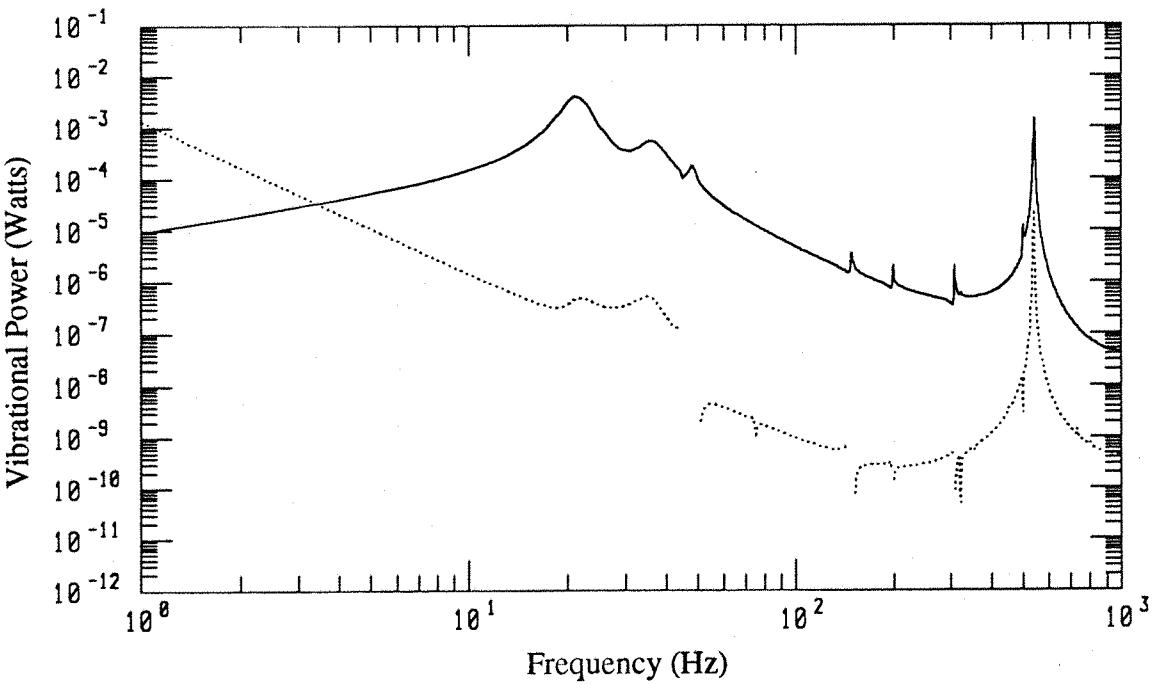

Figure 7.12 : Vibrational power transmitted to the resilient mounts from a point sinusoidal force of 1N applied at an off-centre point (40mm left of centre) : ——— translational motion, ····· rotational motion.

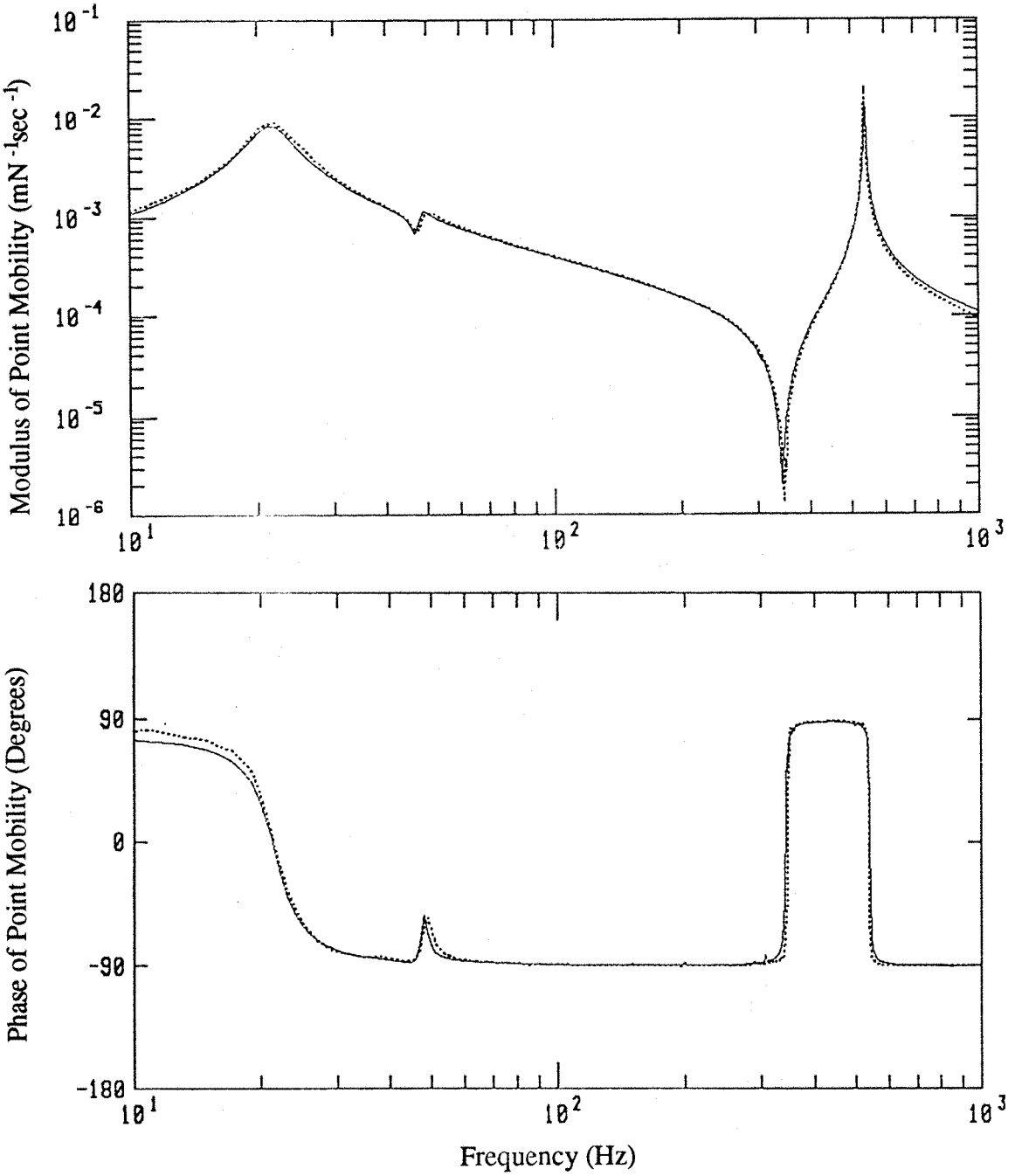

Figure 7.15: Modulus and phase of the driving point mobility function at the centre of the source beam : ——— predicted, ····· measured.

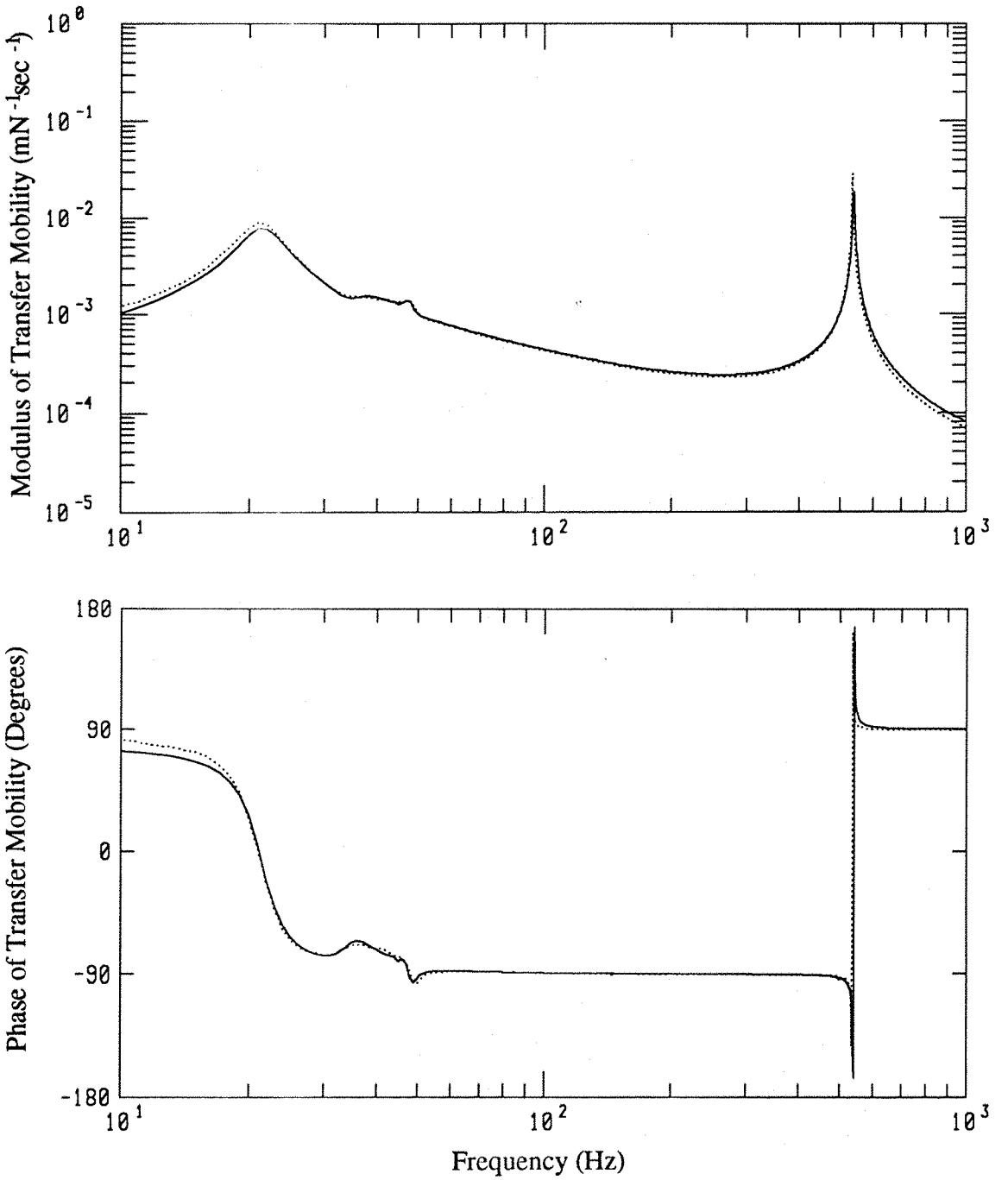

Figure 7.16: Modulus and phase of the transfer mobility function between the translational velocity at mounting point E and the applied force at the beam centre : ——— predicted, ····· measured.

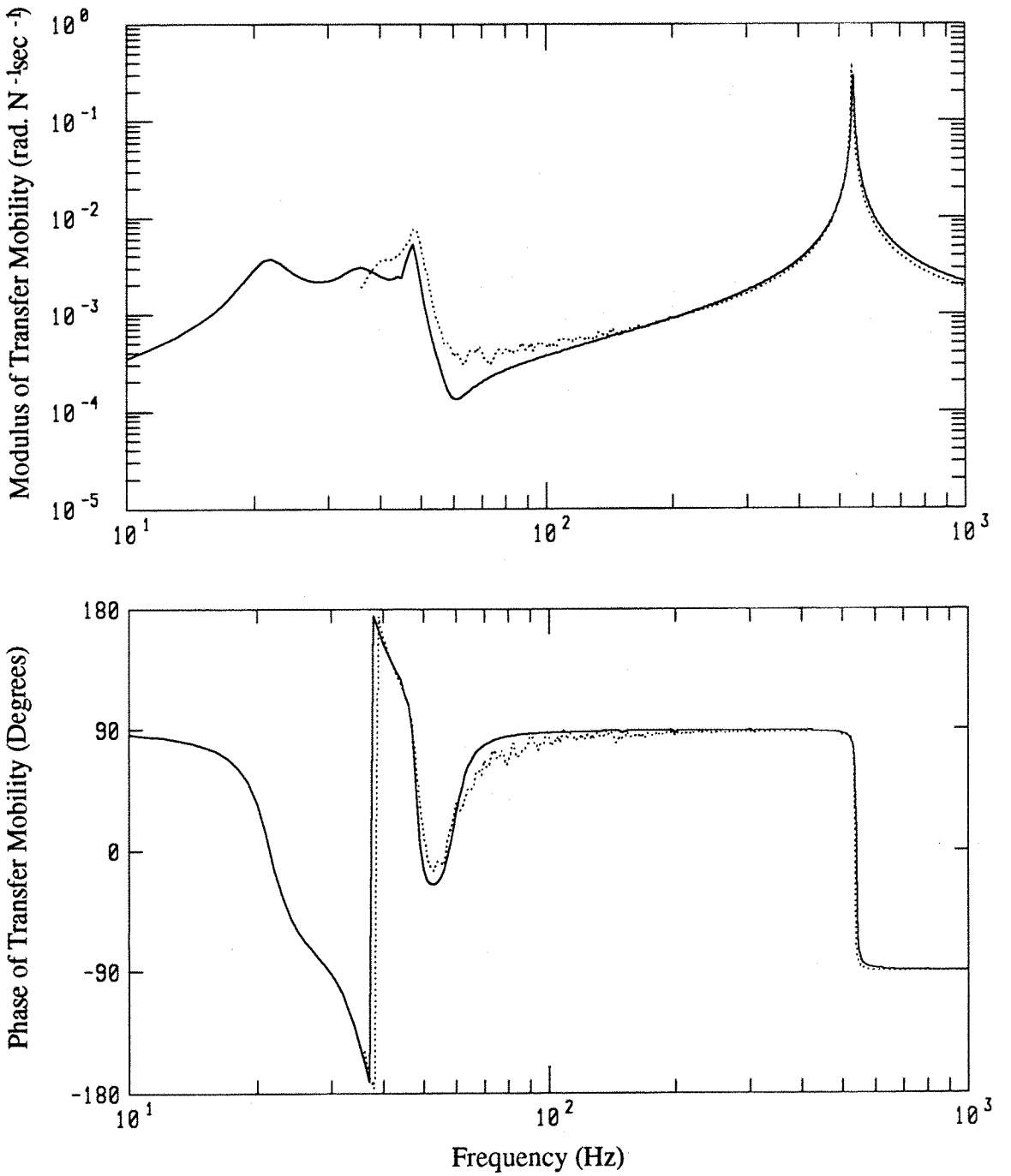

Figure 7.17: Modulus and phase of the transfer mobility function between the rotational velocity at mounting point E and the applied force at the beam centre : ——— predicted, ····· measured.

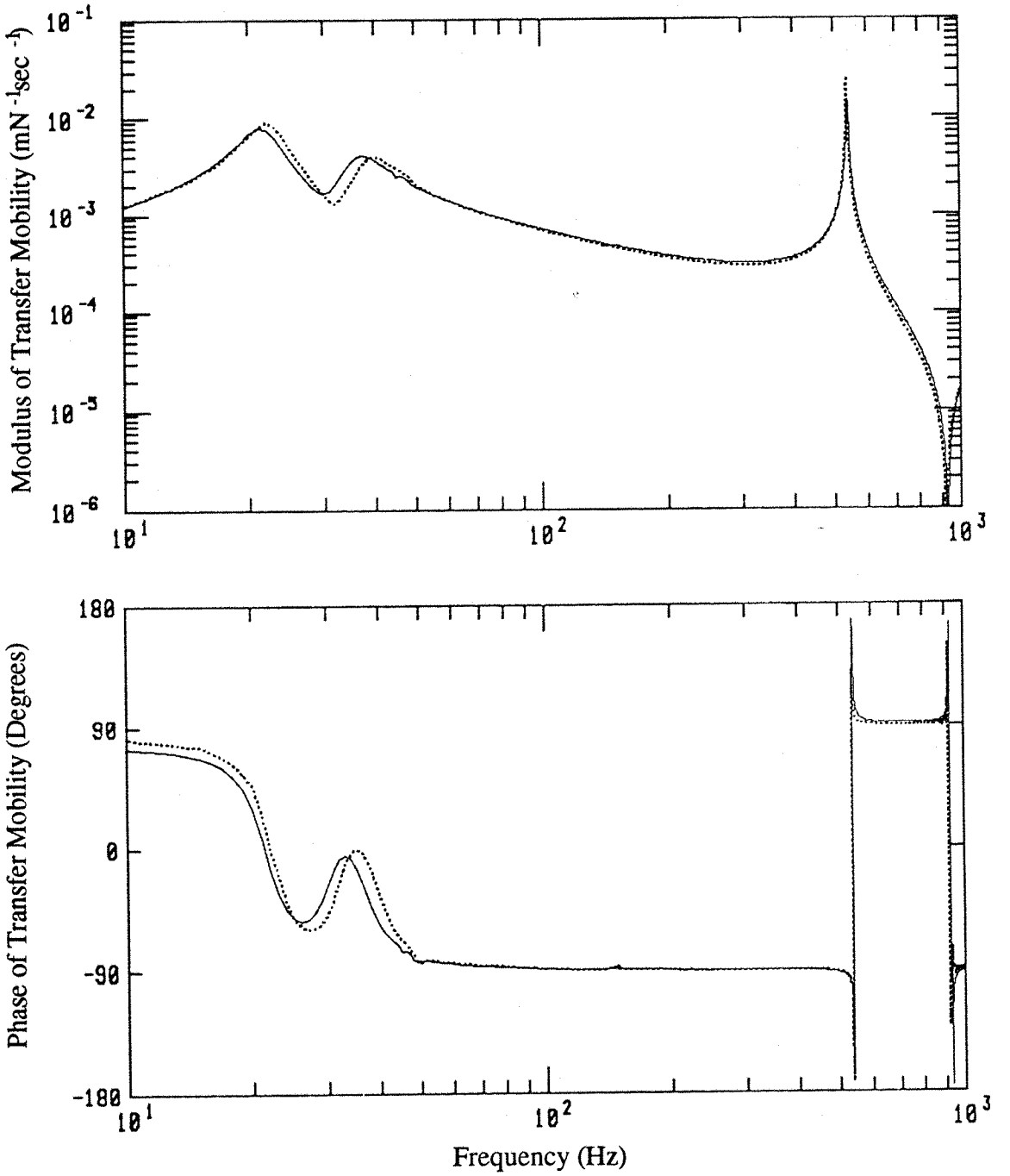

Figure 7.18: Modulus and phase of the transfer mobility function between the translational velocity at mounting point E and the applied force at the off-centre point : ——— predicted, ····· measured.

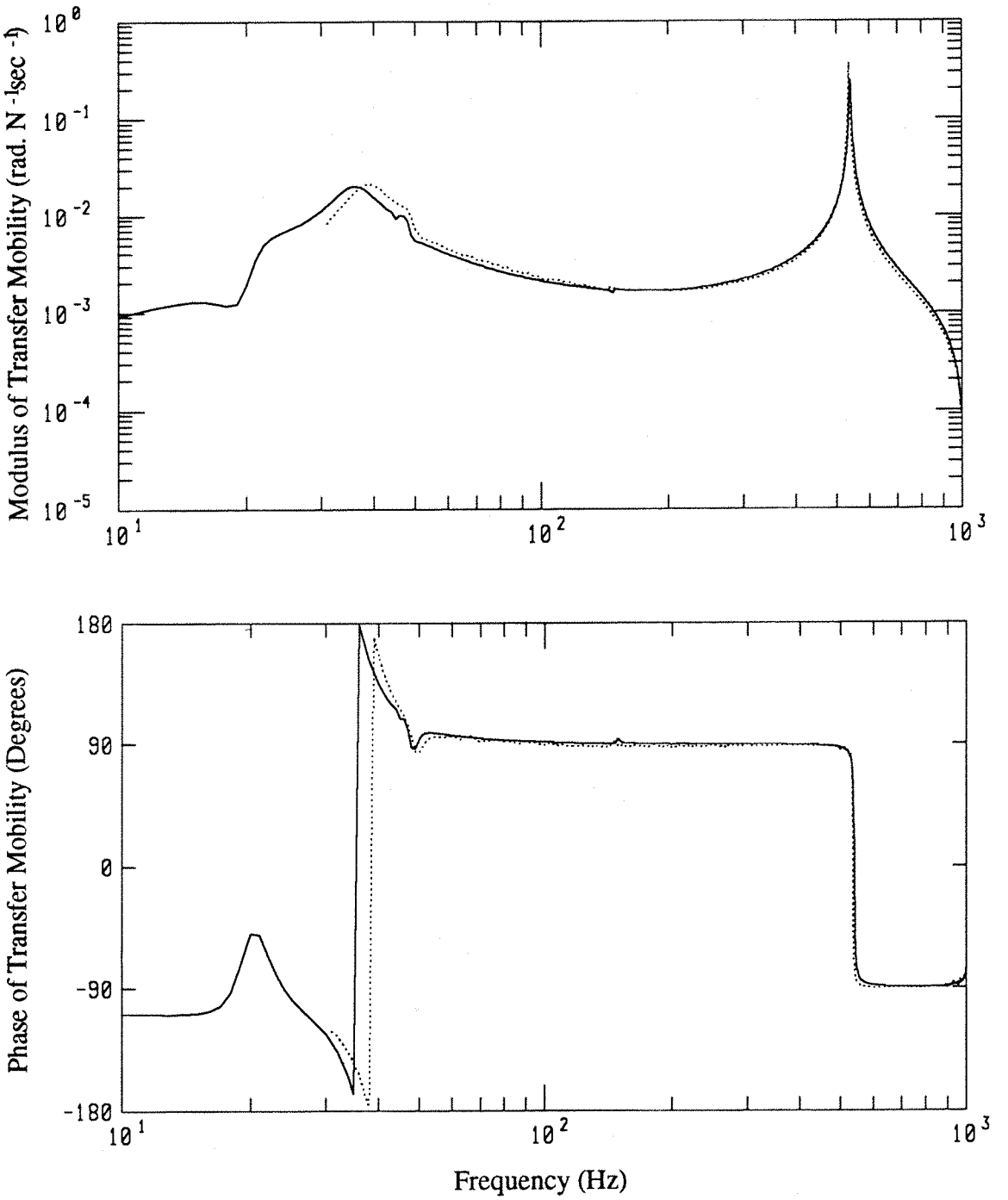

Figure 7.19 : Modulus and phase of the transfer mobility function between the rotational velocity at mounting point E and the applied force at the off-centre point : ——— predicted, ····· measured.

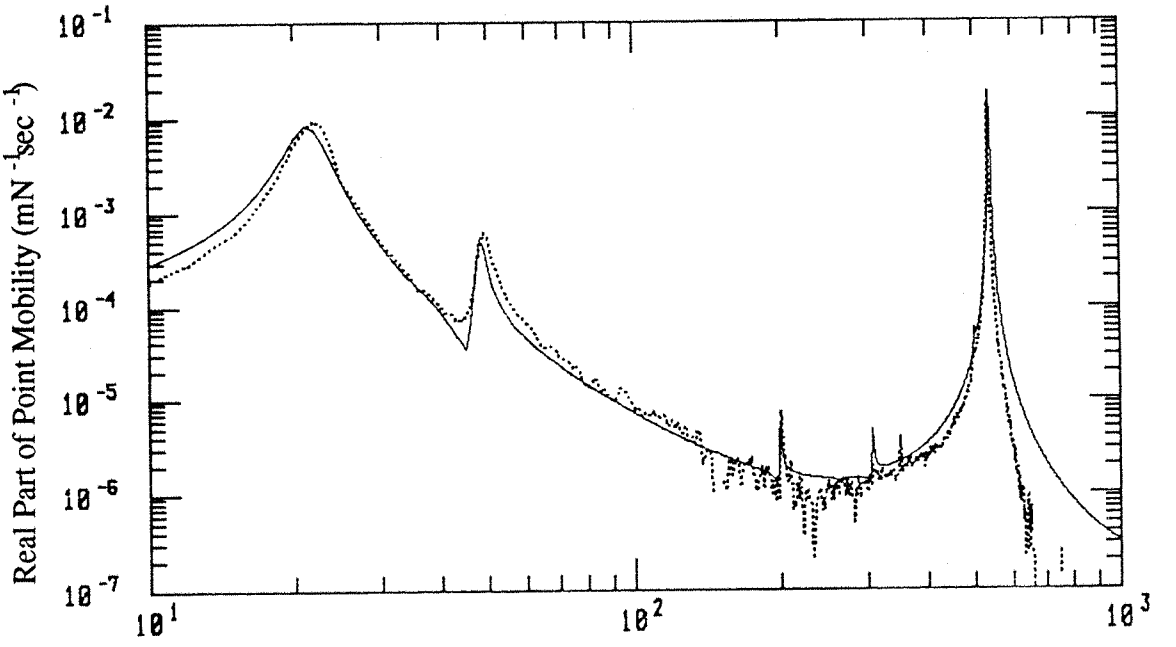

Figure 7.20:Real part of the driving point mobility function at the centre of the source beam : ——— predicted, ····· measured.

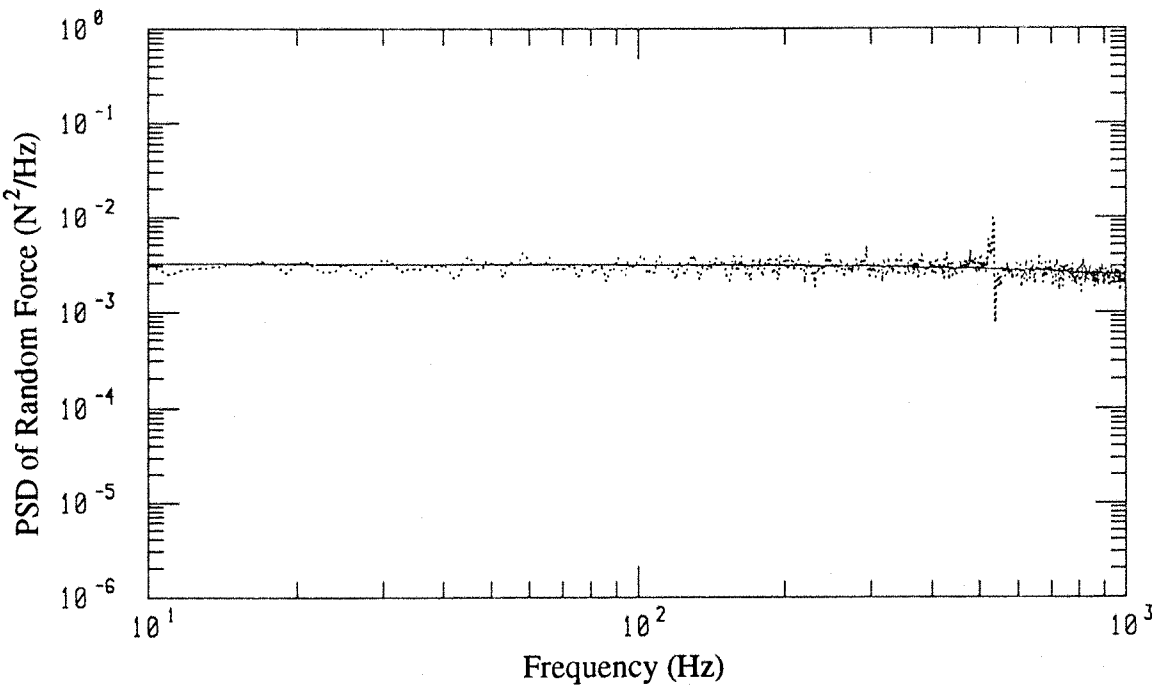

Figure 7.21:Power spectral density function of the random force excitation and its Least Squares straight line model.

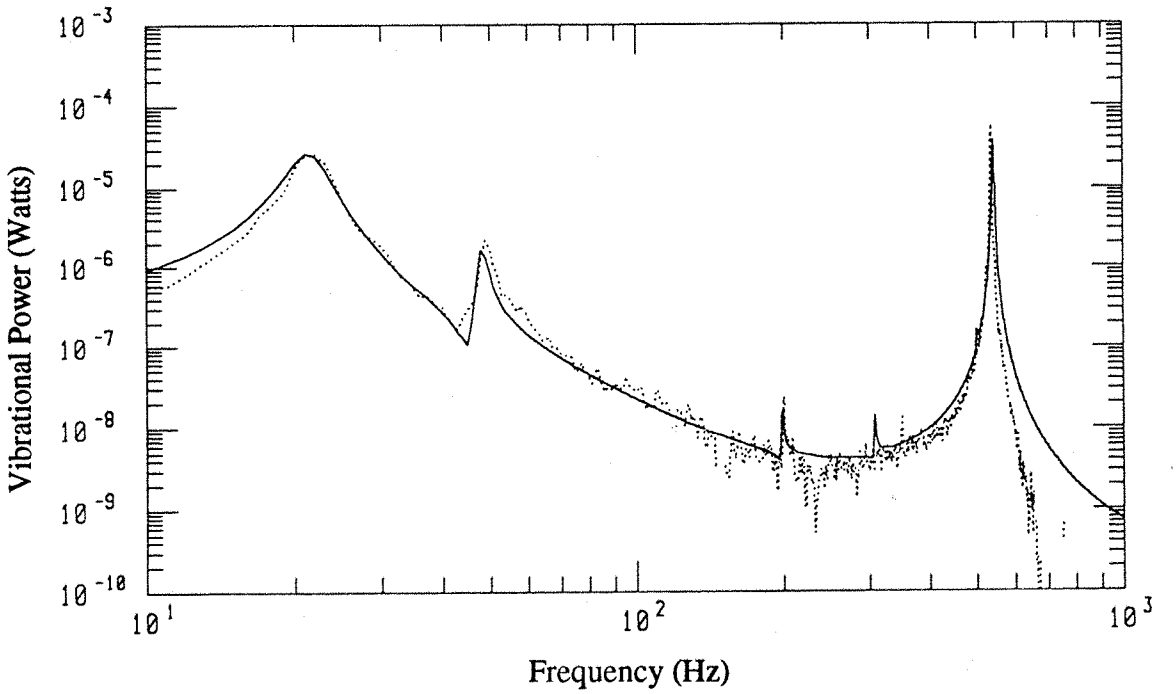

Figure 7.22: Vibrational power input to the source beam at the beam centre :
——— predicted, ····· measured.

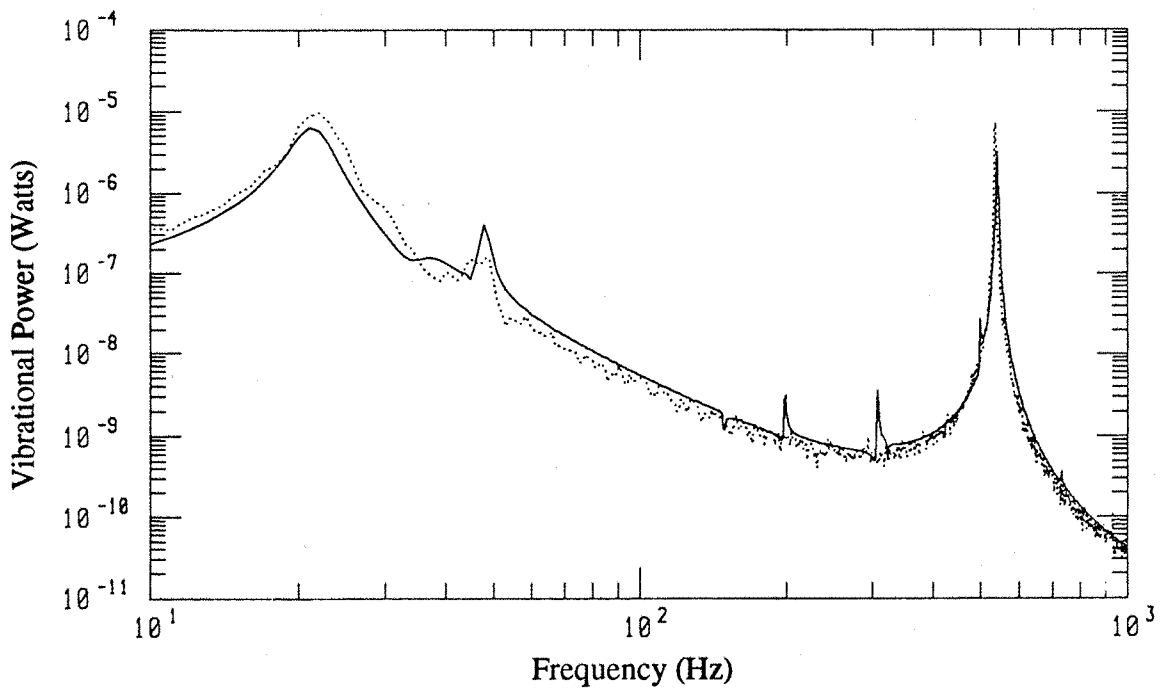

Figure 7.23 : Vibrational power transmitted to the resilient mount at mounting point E
——— predicted, ····· measured.

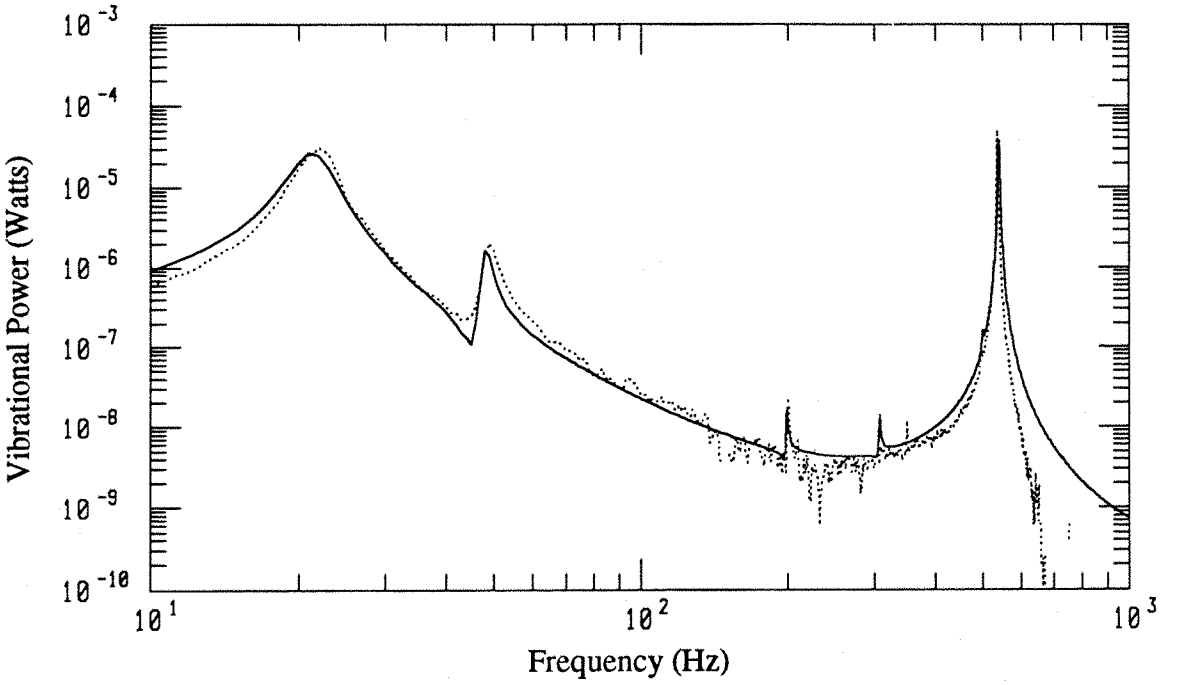

Figure 7.24 : Vibrational power input to the source beam at the beam centre after removing the random fluctuation of G_{ff}: —— predicted, ... measured.

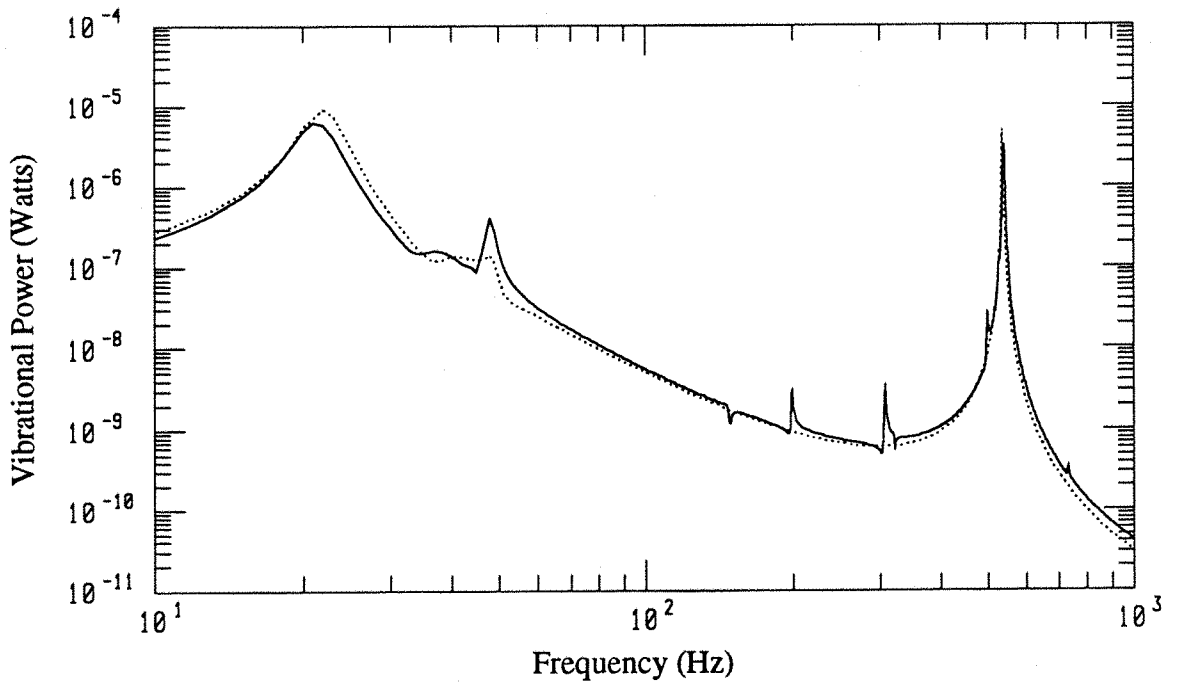

Figure 7.25 : Vibrational power transmitted to the resilient mount at mounting point E after removing the random fluctuation of G_{ff}: —— predicted, ····· measured.

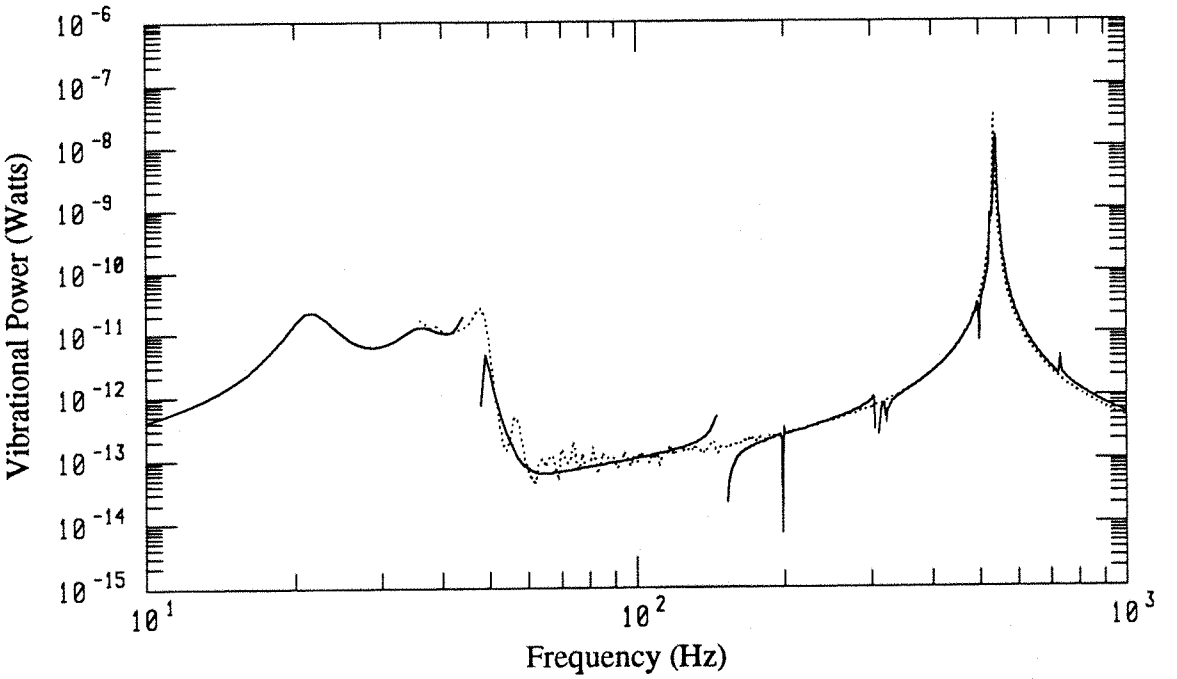

Figure 7.26: Vibrational power transmitted to the resilient mount at mounting point E via the rotational motion after removing the random fluctuation of G_{ff}: —— predicted, ····· measured.

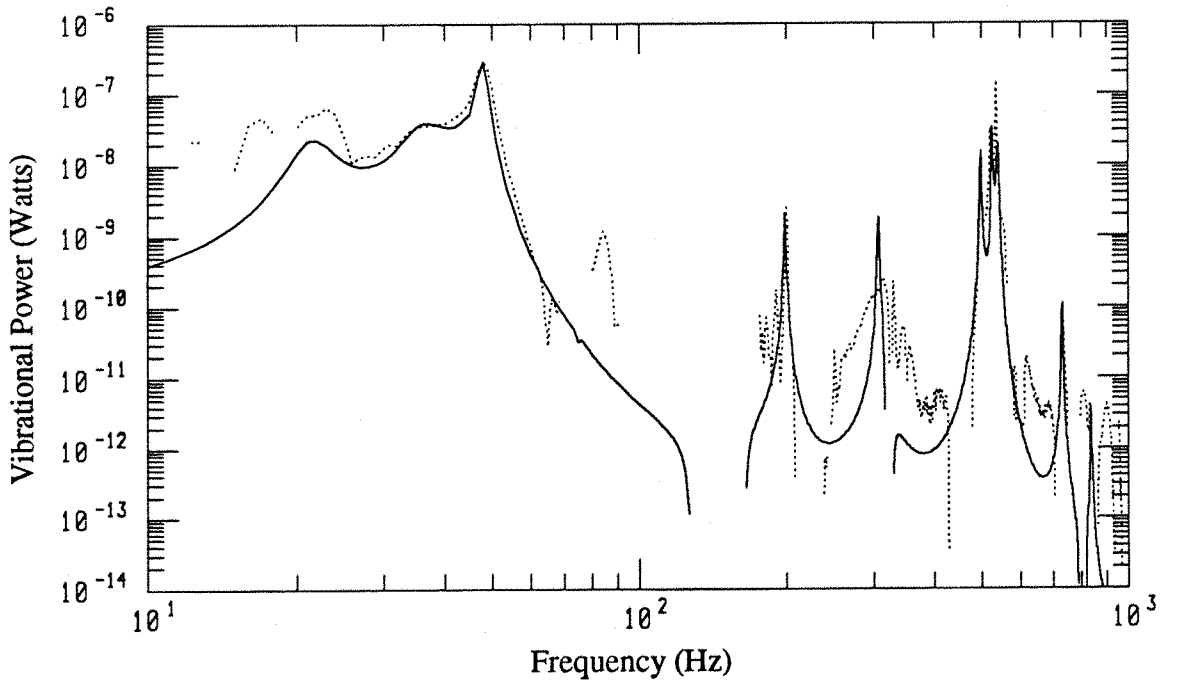

Figure 7.27: Vibrational power transmitted to the receiver plate at mounting point E after removing the random fluctuation of G_{ff}:—— predicted, ····· measured.

PART III

VIBRATION CONTROL VIA POWER INPUT TO FLEXIBLE SEATING STRUCTURES

CHAPTER 8

VIBRATION CONTROL USING THE CONCEPT OF VIBRATIONAL POWER FLOW

8.1 INTRODUCTION

Vibration isolation and control is an important field in modern days of engineering activities. In the case of shipboard machinery, vibration control is always a matter of interest from both the shipbuilder's and the shipowner's point of view. Excessive vibation level not only leads to improper functioning and premature failure of machinery components, annoyance, fatigue and reduced comfort for on-board crews, but also causes a high radiated underwater noise signature.

The results presented in Part I and Part II of the study confirm the importance of resilient mount properties in reducing the vibrational power transmitted to the seating structures. But a more interesting finding is the possibility of reducing the resultant vibrational power input to the seating structures at a specific frequency via a suitably designed force and moment seating. The cancellation of vibrational power components is attributed to the presence of the coupling mobilities.

This chapter examines the cancellation effect in more details, and the various vibration control schemes which utilise the contribution from the coupling mobilities to minimise the resultant time-averaged vibrational power input to flexible seating structures. Both 'active' and passive approaches of vibration control are analysed theoretically. The prerequisites of these control schemes are that :

(1) there must be simultaneously acting force and moment excitations on the flexible seating structure so that the coupling terms in the driving point mobility matrix exist. This condition is likely to be met in practice as the moment arm or the horizontal offset can be designed within a machine mount to generate

simultaneously the applied force and moment at the seating structure when the machine vibrates.

(2) The driving point mobility matrix must be known, either from on site measurements or from analytical solutions (such as the finite element method) because the control schemes make use of the real parts of the force, moment and coupling mobilities to determine the amplitude spectra of the required secondary force or moment and the optimal moment arm spectra. The secondary force and moment are assumed to be in phase with the applied force and moment respectively.

The passive approach of controlling the vibration transmitted from a machine source, at a specific frequency, to flexible beam and plate-like structures via a force and moment seating is also evaluated experimentally.

8.2 VIBRATION CONTROL OF BEAM-LIKE SEATING STRUCTURES

8.2.1 Vibration Control Scheme using a Secondary Force

Consider a typical configuration of a machine mounted on vibration isolators and attached to a beam-like structure. For simplicity, consider the motion at one of the mountings as illustrated in figure 8.1. In order to generate the applied force and moment simultaneously about the mounting point, an intermediate seating block is used in between the vibration mount and the beam-like structure. The primary applied force, $F_a(t)$, is resulted from the resilient mount of a vibrating machine.

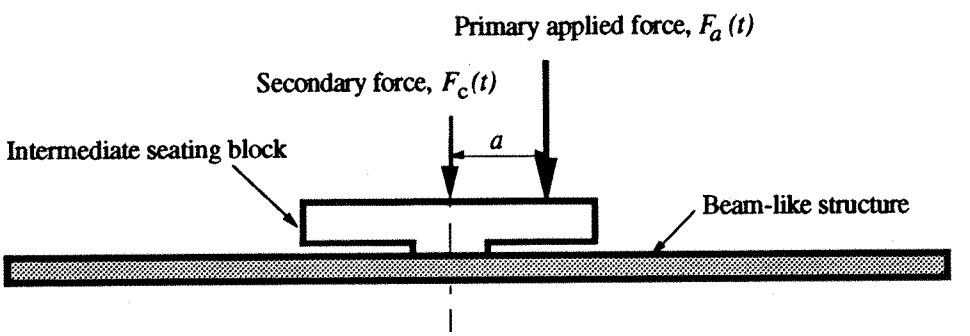

Figure 8.1 : Vibration control mount seating on a beam-like structure with applied and secondary forces (zero moment arm for secondary force).

Consider a secondary force, $F_c(t)$, acting through the mounting axis, which is sinusoidal in nature and is in phase with the applied force. The resultant force acting on the beam-like structure is:

$$F(t) = F_a(t) + F_c(t) \tag{8.1}$$

The expression for the resultant time-averaged vibrational power input to the beam-like structure is given in eqn. (2.69) or (2.73). With the inclusion of a secondary force, the expression becomes:

$$\begin{aligned} P_{total} &= \frac{1}{2} (F_a + F_c)^2 \, Re\{Y_{FF}\} + \frac{1}{2} M_a^2 \, Re\{Y_{MM}\} \\ &\quad + (F_a + F_c) M_a \, Re\{Y_{FM}\} \end{aligned} \tag{8.2}$$

where $M_a(t) = F_a(t) \; a$

Assuming that the moment arm is fixed and the driving point mobility matrix of the beam-like structure is known either from measurements or analytical solutions, then for each frequency value and for a given applied force, the resultant time-averaged vibrational power input is a quadratic function of F_c , which can be written as :

$$P_{total} = \alpha_f F_c^2 + \beta_f F_c + \gamma_f \tag{8.3}$$

where

$$\begin{aligned} \alpha_f &= \frac{1}{2} Re\{Y_{FF}\} \\ \beta_f &= F_a \, Re\{Y_{FF}\} + M_a \, Re\{Y_{FM}\} \\ \gamma_f &= \frac{1}{2} F_a^2 \, Re\{Y_{FF}\} + \frac{1}{2} M_a^2 \, Re\{Y_{MM}\} \\ &\quad + F_a M_a \, Re\{Y_{FM}\} \end{aligned}$$

Differentiating P_{total} with respect to F_c to obtain the expression for the optimal secondary force, $F_{c,opt}$, for the minimum value of P_{total} gives,

$$F_{c,opt} = -\frac{\beta_f}{2 \alpha_f} = -F_a \left[1 + a \frac{Re\{Y_{FM}\}}{Re\{Y_{FF}\}} \right] \tag{8.4}$$

The second derivative of P_{total} with respect to F_c is equal to $2 \alpha_f$ and as $Re\{Y_{FF}\}$ is always positive, α_f is positive and the second derivative is positive. Hence, the condition of $F_{c,opt}$ as given in eqn. (8.4) ensures a minimum value of P_{total} .

The above derivation shows that if the real parts of the force mobility, Y_{FF} and the coupling mobility, Y_{FM} , the magnitude of the applied force, F_a and the moment arm, a, are known, one can determine the amplitude spectrum of the optimal secondary force, $F_{c,opt}$, which minimises the resultant vibrational power input to the beam-like structure.

The practical realisation of this control scheme depends on the ability of applying an in phase secondary force of the required amplitude to the seating along the mounting axis without introducing any additional moment excitation.

8.2.2 Vibration Control Scheme using a Secondary Moment

Consider the same machine - isolator - seating structure arrangement, but with the secondary force replaced by a secondary moment. The secondary moment consists of a force couple having a fixed separation, d, as shown in figure 8.2 :

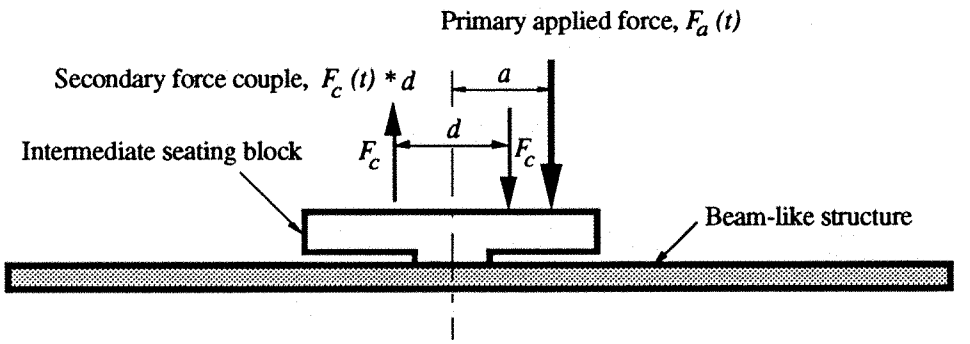

Figure 8.2 : Vibration control mount seating on a beam-like structure with applied force and secondary moment (force couple).

The secondary moment, $M_c(t)$ acting about the mounting axis is given by :

$$M_c(t) = F_c(t)\ d \tag{8.5}$$

which is assumed to be sinusoidal in nature and in phase with the applied moment, $M_a(t)$. The total moment acting on the beam-like structure is :

$$M(t) = M_a(t) + M_c(t) \tag{8.6}$$

The expression for the resultant time-averaged vibrational power input to the beam-like structure becomes:

$$P_{total} = \frac{1}{2} F_a^2 \, Re\{ Y_{FF} \} + \frac{1}{2} (M_a + M_c)^2 \, Re\{ Y_{MM} \} + F_a (M_a + M_c) \, Re\{ Y_{FM} \} \quad (8.7)$$

where $M_a(t) = F_a(t) \, a$

Similarly, for each frequency value and a given applied force level, the resultant time-averaged vibrational power input is a quadratic function of M_c, which can be written as :

$$P_{total} = \alpha_m M_c^2 + \beta_m M_c + \gamma_m \quad (8.8)$$

where

$$\alpha_m = \frac{1}{2} Re\{ Y_{MM} \}$$

$$\beta_m = F_a \, Re\{ Y_{FM} \} + M_a \, Re\{ Y_{MM} \}$$

$$\gamma_m = \frac{1}{2} F_a^2 \, Re\{ Y_{FF} \} + \frac{1}{2} M_a^2 \, Re\{ Y_{MM} \} + F_a M_a \, Re\{ Y_{FM} \}$$

The expression for the optimal secondary moment, $M_{c,opt}$, for the minimum value of P_{total} can similarly be shown to be :

$$M_{c,opt} = -\frac{\beta_m}{2 \alpha_m} = -F_a \left[\frac{Re\{Y_{FM}\}}{Re\{Y_{MM}\}} + a \right] \quad (8.9)$$

Hence, the amplitude spectrum of the optimal secondary moment, $M_{c,opt}$, which minimises the resultant vibrational power input to the beam-like structure can be determined if one knows the real parts of the moment mobility, Y_{MM} and the coupling mobility, Y_{FM}, the magnitude of the applied force, F_a and the moment arm, a.

The potential practical difficulty of this control scheme is the application of an in phase secondary moment about the mounting axis or a force couple of the required amplitude and phase to the seating without introducing any additional force excitation.

In comparison with the control scheme using a secondary force, this moment control scheme is inferior in the following two aspects :

(1) it is more difficult to apply a force couple than to apply a single secondary force;

(2) the α_m and β_m terms (eqns. (8.9)) used in this control scheme consist of the driving point moment mobility, Y_{MM}, which, in practice, is much more

difficult to measure accurately than the driving point force mobility, Y_{FF}, as used in the force control scheme (eqn. (8.4)).

Hence, the vibration control scheme using a secondary force is easier to implement in practice. The feasibility of these two vibration control schemes using a secondary force or a secondary moment has been examined for the clamped - simply supported beam with the excitation located at mid-span and a moment arm of 0.028m. Comparisons of P_{total}, with and without the control schemes are shown in figure 8.3. These comparisons show that :

(1) the reduction in the resultant time-averaged vibrational power input to the beam-like structure using either the force or the moment control scheme is much larger than the reduction one could obtain by simply increasing the damping of the structure as depicted in figures 2.13(a) to 2.13(c). With the control schemes, there is no rise in the resultant power input between any two successive resonance peaks.

(2) There is a difference in the resultant vibrational power input to the beam-like structure using these two control schemes. This is expected as the optimal values of the secondary force and moment depend on the real parts of Y_{FF} and Y_{MM} respectively, which are different in value.

The problem of which control scheme is more effective under different influential parameters, such as the boundary conditions, the excitation location and the excitation moment arm does not merit further attention as the control scheme using the force approach is superior than the moment approach at least from the practical implementation point of view.

The amplitude spectra of the optimal secondary force and moment for minimising the resultant vibrational power input to the beam-like structure are shown in figure 8.4. This figure gives an idea of the 'desirable' secondary force and moment spectra. It must be noted that these spectra may not be perfectly matched in practice due to practical constraints, such as the size and weight of the actuators for applying the secondary force or force couple, and the finite time-lag in sensing the response, computing the required controlling force and activating the actuators to drive the control system. These potential control problems require detailed investigation before the 'active' vibration control scheme can be put in practice.

8.2.3 Vibration Control Scheme using a Combined Secondary Force and Moment

Similar analytical method can be extended to include the vibration control scheme using a combined secondary force and moment, as illustrated in figure 8.5.

However, the analytical expressions for the optimal solution of the secondary force, $F_c(t)$, and moment arm, a_c, are more complex as the resultant time-averaged vibrational power input to the beam-like structure is a quadratic function of two controlling variables, namely $F_c(t)$ and a_c. Mathematical methods are available for finding the minina of functions of two or more variables, such as those given in [51], we shall not devote more time to derive the required expressions but to direct our attention to a more practical, passive approach of vibration control at a specific frequency.

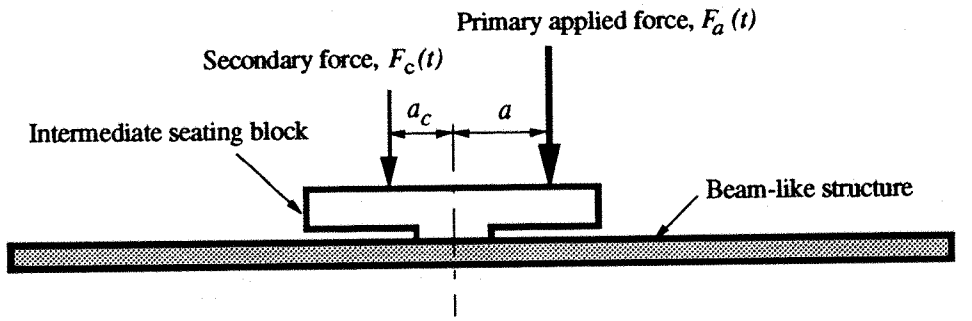

Figure 8.5 : Vibration control mount seating on a beam-like structure with applied and secondary forces (both with moment arms).

8.2.4 Vibration Control at a Specific Frequency - The Passive Approach

The feasibility of using a secondary force or a secondary moment to control the flexural vibration of a beam-like structure subjected to simultaneously acting force and moment excitations has been presented in the previous sections. In spite of the attractive reduction in the resultant time-averaged vibrational power input to the structure, there are some practical difficulties associated with these 'active' vibration control schemes.

In this section, possible vibration control measures which are applied in the passive manner are discussed. Although the passive approach of vibration control is likely to have a limited frequency range of applicability, it is justified by its simplicity and cost effectiveness as compared to the 'active' control scheme. It is also known from past experience that a substantial amount of vibrational power flow is associated with the fundamental firing frequency of a typical shipboard diesel engine. Thus, by controlling the vibrational power flow at this 'troublesome' frequency via a passive method, one

could achieve a considerable amount of reduction in the total vibrational power input to the seating structure.

If the beam-like seating structure is uniform and of sufficient length such that very little flexural wave reflection occurs from the terminating ends or from any geometric discontinuities, and the excitation can be assumed to be located at the free end, then the theory of the semi-infinite beam can be applied.

Under these assumptions, it has been shown that a favourable condition, i.e. $F = k\,M$ (eqn.(2.76)) exists in which minimum vibrational power flow is transmitted in the structure by flexural wave motion. Hence, by knowing the 'troublesome' frequency, the geometric and material properties of the approximately semi-infinite beam-like structure, the optimal moment arm, a_{opt} (or the ratio of the applied moment to the applied force), for the intermediate seating block (or the force and moment seating) can be determined from eqn. (2.77). The power reduction index spectrum of the semi-infinite beam shown in figure 2.15(c) clearly illustrates the potential application of this method.

If the assumptions of the semi-infinite beam condition with the excitation located at one end is not likely to be fulfilled, then the following approach could be adopted.

Consider the typical machine - isolator - seating structure problem, the motion at one of the mountings is illustrated in figure 8.6.

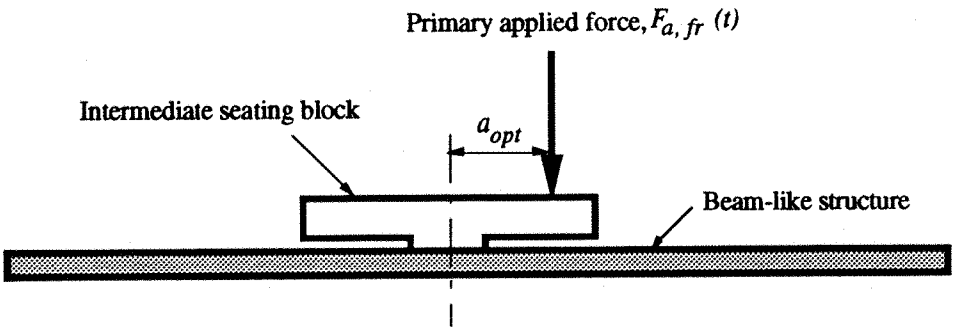

Figure 8.6 : Vibration control mount seating on a beam-like structure with primary applied force and the optimal moment arm (the passive approach).

The passive control measure is to determine the optimal moment arm, a_{opt} from the driving point mobility matrix of the seating structure for the frequency of interest; and then to incorporate this optimal moment arm into the design of the machine seating.

Suppose the frequency of interest is f_r Hz, and by defining $\xi_{p,fr}$ as the ratio of the applied force to the applied moment at this particular frequency, i.e.

$$\xi_{p,fr} = \frac{F_{a\,fr}}{M_{a\,fr}} = \frac{1}{a_{fr}} \tag{8.10}$$

the resultant time-averaged vibrational power input to the beam-like structure at this frequency is :

$$\begin{aligned} P_{total,fr} &= \frac{1}{2} F_{a,fr}^2 \, Re\{ Y_{FF,fr} \} + \frac{1}{2} M_{a,fr}^2 \, Re\{ Y_{MM,fr} \} \\ &\quad + F_{a,fr} M_{a,fr} \, Re\{ Y_{FM,fr} \} \\ &= \frac{1}{2} M_{a,fr}^2 [\xi_{p,fr}^2 \, Re\{ Y_{FF,fr} \} + 2 \xi_{p,fr} \, Re\{ Y_{FM,fr} \} \\ &\quad + Re\{ Y_{MM,fr} \}] \end{aligned} \tag{8.11}$$

which can be rearranged into the usual quadratic form :

$$P_{total,fr} = \alpha_p \xi_{p,fr}^2 + \beta_p \xi_{p,fr} + \gamma_p \tag{8.12}$$

where

$$\begin{aligned} \alpha_p &= \frac{1}{2} M_{a,fr}^2 \, Re\{ Y_{FF,fr} \} \\ \beta_p &= M_{a,fr}^2 \, Re\{ Y_{FM,fr} \} \\ \gamma_p &= \frac{1}{2} M_{a,fr}^2 \, Re\{ Y_{MM,fr} \} \end{aligned}$$

Hence, the optimal ratio of the applied force to the applied moment, $\xi_{p,opt}$, at the frequency of interest, for the minimum value of $P_{total,fr}$ is :

$$\xi_{p,opt} = -\frac{\beta_p}{2 \alpha_p} \tag{8.13}$$

The optimal moment arm which gives rise to the minimum resultant time-averaged vibrational power input to the beam-like structure at the frequency of interest is :

$$a_{opt} = \frac{1}{\xi_{p\,opt}} = -\frac{Re\{ Y_{FF\,fr} \}}{Re\{ Y_{FM\,fr} \}} \tag{8.14}$$

i.e. the negative value of the ratio of the real part of force mobility to the real part of coupling mobility at the frequency of interest. The optimal moment arm is independent of the applied force and is only a function of the seating structure properties, such as

the geometric and material properties of the structure, the boundary conditions and the location of the seating block mounting point along the beam-like structure.

Notice that in calculating the optimal value of the moment arm, the optimal ratio, $\xi_{p,opt}$, is determined first in order to avoid the use of the real part of the moment mobility, which in practice, is more difficult to measure accurately than the force mobility. However, if one could predict the moment mobility of practical seating structures accurately, then the optimal value of the moment arm can be determined directly, instead of the ratio, $\xi_{p,opt}$.

Using this direct approach, the optimal moment arm can be shown to be :

$$a_{opt} = - \frac{Re\{Y_{FM\,fr}\}}{Re\{Y_{MM\,fr}\}} \tag{8.15}$$

If one substitutes the expressions for the real parts of Y_{FF}, Y_{FM} and Y_{MM} of a semi-infinite beam, eqn. (2.16), into eqn. (8.14) or (8.15), one obtains the identical result for the condition of zero resultant time-averaged vibrational power input to an undamped semi-infinite beam, i.e. eqn. (2.77) :

$$k\, a_{opt} = 1 \tag{8.16}$$

8.3 VIBRATION CONTROL OF PLATE-LIKE SEATING STRUCTURES

8.3.1 The Optimal Moment Arms for Rectangular Plates

For a given location on a beam or plate-like seating structure, the driving point mobility functions are frequency dependent. If a moment arm is defined as the ratio of the applied moment to the applied force, which could be achieved, in practice, by a horizontal offset of the line of action of the vertical force from the centre of the mounting, then for a given force level and a given frequency, the resultant vibrational power input to the seating structure from a source, eqns. (2.69), (2.73) or (3.84), is a function of the moment arm. The optimal moment arm, a_{opt} can then be obtained by minimizing the resultant vibrational power input with respect to the moment arm for a specific frequency and location on the structure.

For a rectangular plate having the geometry and co-ordinates as defined in figure 8.7, the positive moment arms parallel to the X- and Y-axes are defined as (note that $F(t)$ is defined as positive if it acts downwards) :

$$a_x = -\frac{M_y}{F} \tag{8.17}$$

$$a_y = \frac{M_x}{F} \tag{8.18}$$

Thus,

$$M_x = F\, a_y \tag{8.19}$$

$$M_y = -F\, a_x \tag{8.20}$$

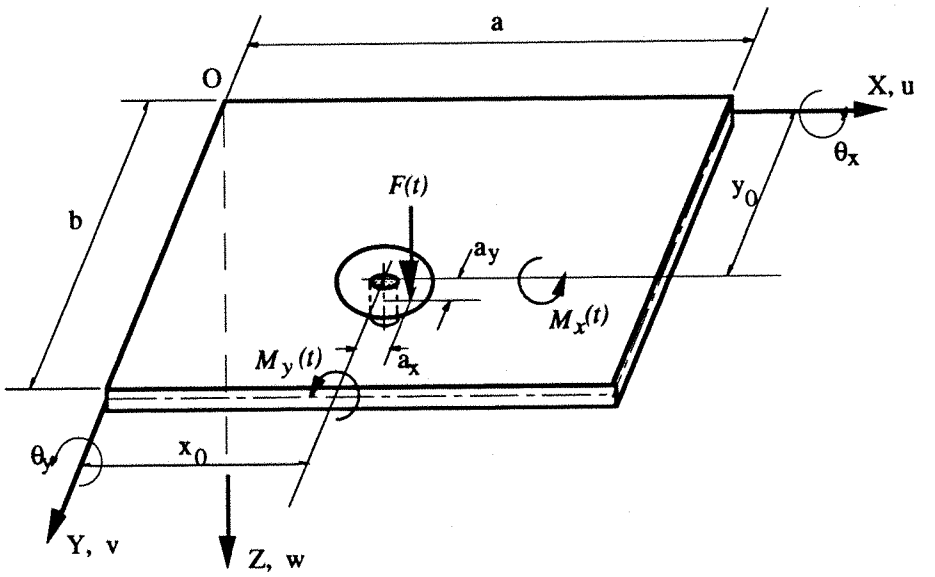

Figure 8.7 : Rectangular plate loaded with simultaneously acting force and moment excitations.

Substituting for M_x and M_y into the expression for the resultant vibrational power, eqn (3.84), one obtains :

$$\begin{aligned} P_T = {} & \frac{1}{2} F^2 Re\{Y_{11}\} + \frac{1}{2} F^2 Re\{Y_{33}\} a_x{}^2 \\ & + \frac{1}{2} F^2 Re\{Y_{22}\} a_y{}^2 - F^2 Re\{Y_{31}\} a_x \\ & + F^2 Re\{Y_{21}\} a_y - F^2 Re\{Y_{32}\} a_x a_y \end{aligned} \tag{8.21}$$

which for a given frequency and applied force amplitude, is a function of a_x and a_y. Minimising P_T with respect to a_x and a_y, one obtains the optimal values for a_x and a_y :

$$a_{x,opt} = \frac{Re\{Y_{21}\} Re\{Y_{32}\} - Re\{Y_{22}\} Re\{Y_{31}\}}{Re\{Y_{32}\} Re\{Y_{32}\} - Re\{Y_{22}\} Re\{Y_{33}\}} \quad (8.22)$$

$$a_{y,opt} = \frac{a_{x\,opt}\, Re\{Y_{33}\} - Re\{Y_{31}\}}{Re\{Y_{32}\}} \quad (8.23)$$

Hence, for a specific location on the plate, the optimal moment arms are governed solely by the dynamic properties of the plate and are independent of the applied force level, as would be expected from linear theory.

8.3.2 Vibration Control Over a Broad Frequency Range - The Ideal Case

The optimal moment arm spectra obtained from eqns. (8.22) and (8.23) for the SSSS plate and the CFSF plate at an off-centre location : x = 0.22a and y = 0.62b , are shown in figures 8.8 and 8.9 respectively. These moment arm spectra were determined solely from the real parts of the driving point mobility functions at the specific point of interest on the plate. By changing the location on the plate, the mobility functions will change and so will the optimal moment arm spectra.

If one can provide some 'active means' to control the moment arms, or the ratios of the applied moment to the applied force, with respect to frequency according to the optimal moment arm spectra, then the 'controlled' resultant vibrational power input to the SSSS plate and the CFSF plate are shown in figures 8.10 and 8.11 respectively. These 'controlled' power spectra give an indication of the maximum power reduction possible at the specific location on the plate.

8.3.3 Vibration Control for a Specific Frequency – The Passive Approach

The above analyses have again confirmed and demonstrated that if one can determine reliably the real parts of the driving point mobility functions of the beam- or plate-like structures, then one can calculate the required moment arms in order to minimise the time-averaged vibrational power input to the structures at a specific frequency. The required moment arms can then be incorporated into the design of the machinery seating. In view of the frequency range of applicability and the input of power components due to moment excitation, especially in the high frequency region, the proposed method for controlling the vibration transmission at a specific frequency is most suitable for the case of a low to medium speed machine operating at a constant speed and mounted on a flexible beam- or plate-like seating structure. The main steps of

the proposed passive approach to vibration control are summarised in the flow diagram given in figure 8.12.

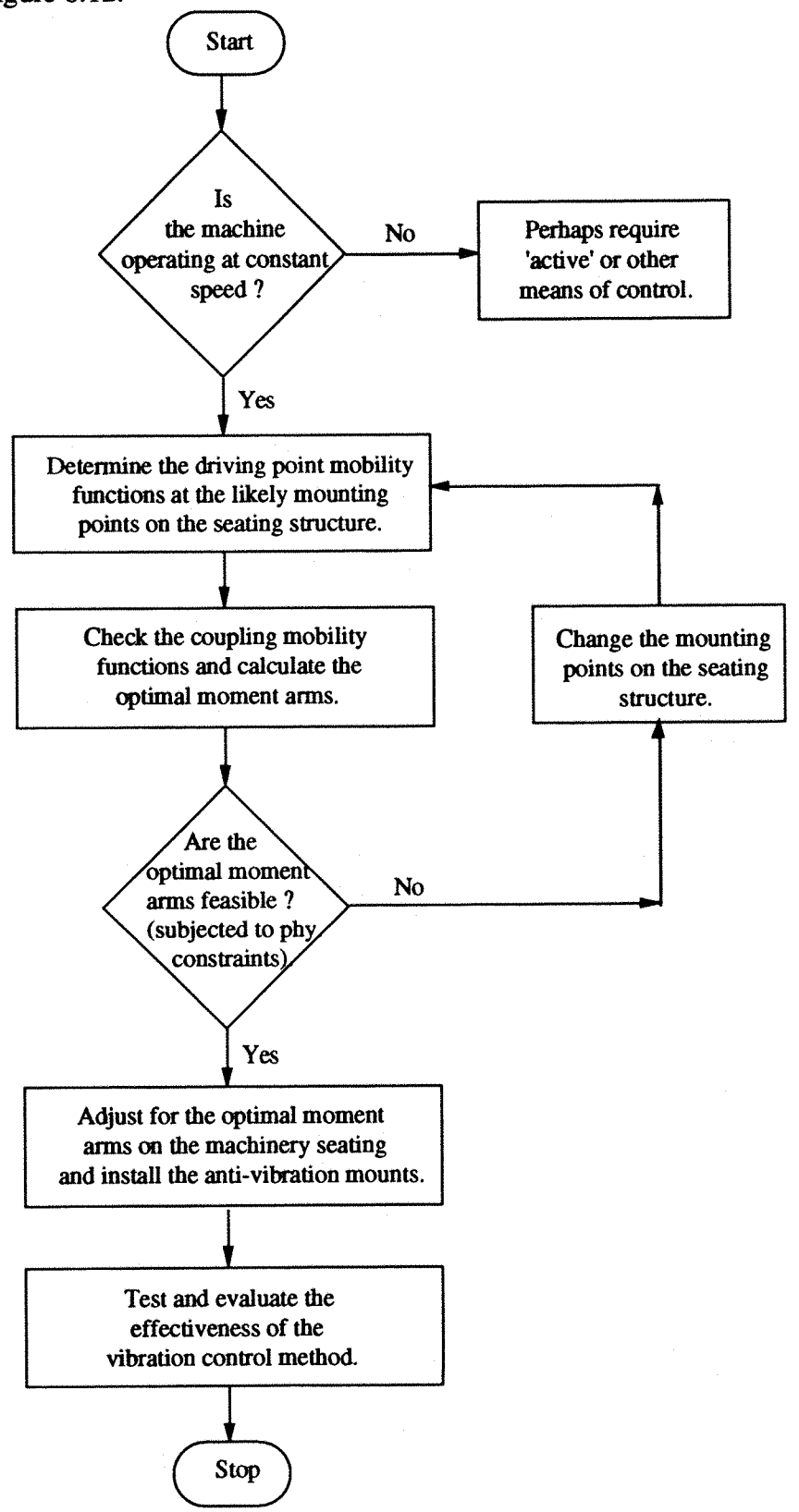

Figure 8.12 : Flow diagram of the passive approach to vibration control of a constant speed machine mounted on a flexible structure.

8.4 EXPERIMENTAL VERIFICATION OF THE PASSIVE APPROACH TO VIBRATION CONTROL

The experimental verification of the passive approach to vibration control was performed for a specific location on a clamped - simply supported beam and the CFSF plate. The objective of the experiment was to reduce the vibrational response of the flexible seating structures around a specific resonance frequency by a force and moment seating design, i.e. by using simultaneously acting force and moment excitations.

8.4.1 The Clamped - Simply Supported Beam Experiment

The experimental apparatus consisted of a uniform steel beam of cross-sectional dimensions : 4mm (thick) x 40mm (width), with one end fully clamped and the other simply-supported. The distance between these two end supports was 585mm. Damping tape was adhered to one side of the beam to increase its damping capacity.

The intermediate seating block as shown in figure 8.6 was made of steel having dimensions of 16mm (width) x 15mm (height) x 72mm (length). The seating block was attached at mid-span of the beam by a quick settling cyano-acrylate adhesive. The moment arm provided by the seating block was plus / minus 0.028m. The predicted power reduction index, $\mathcal{P}$, (eqn. (2.78)), spectrum for a positive moment arm of 0.028m is shown in figure 8.13. It can be seen that a large reduction in the resultant time-averaged vibrational power input to the beam (i.e. $\mathcal{P} < 1$) is predicted in the region of the second resonance frequency and a smaller reduction at the fourth resonance frequency.

The aims of the experiment were to measure the acceleration response at a specific location on the beam with and without the simultaneously acting moment excitation having the required moment arm of 0.028m and to compare the measured transfer accelerances for frequencies around the second resonance of the beam.

The positions of the accelerometer on the beam and the force transducer on the seating block for these two measurements are shown in figure 8.14. The applied moment about the mounting point of the seating block is positive (i.e. clockwise) for a positive downward force. A random signal of bandwidth up to 1000 Hz was used as the excitation. In order to validate the reduction in the response around the second

resonance frequency, the position of the accelerometer was located at a distance of $3\ell/4$ from the clamped end, which is close to an antinode of the second mode.

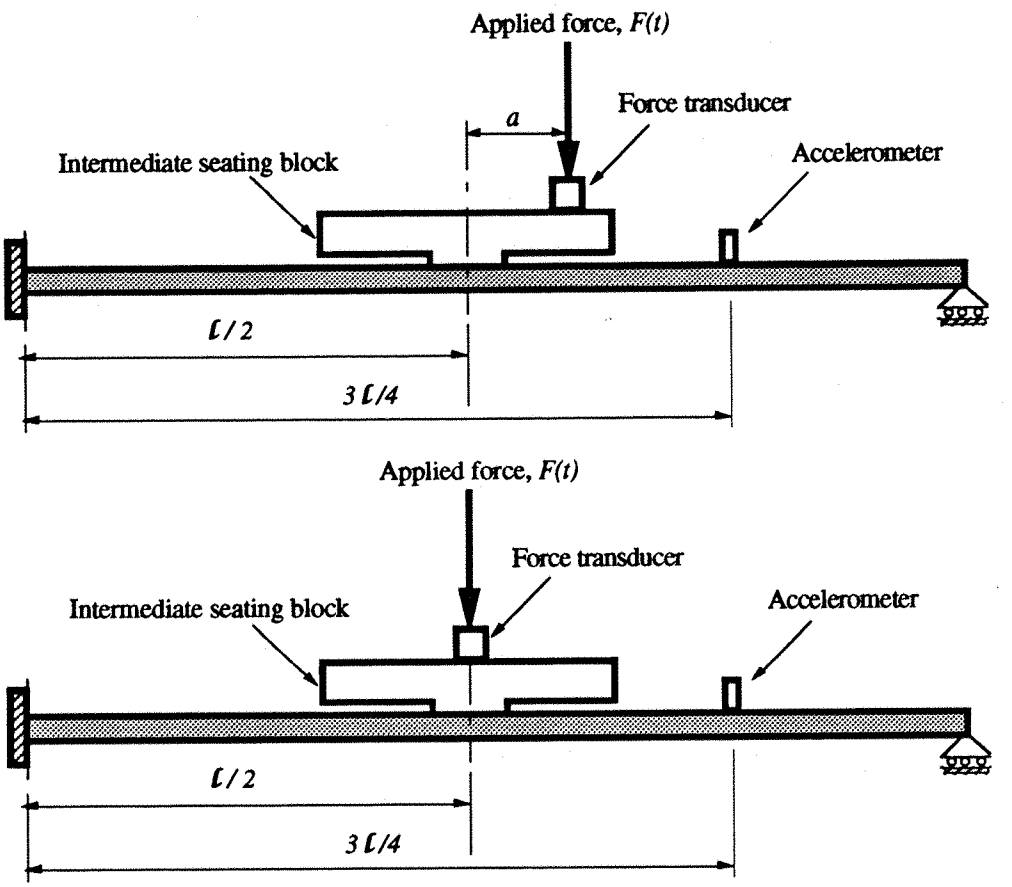

Figure 8.14 : Experimental arrangements on the clamped - simply supported beam for transfer accelerance measurements with and without the moment arm. (a = 0.028m)

A comparison of the moduli of measured transfer accelerances with and without the simultaneously acting moment excitation is shown in figure 8.15. This result shows a remarkable reduction in the acceleration response of the beam around the second resonance frequency for a given applied force when the required positive moment arm is incorporated. A result which agrees closely with the prediction from the power reduction index spectra of figure 8.13.

8.4.2 The CFSF Plate Experiment

The experimental apparatus consisted of the CFSF plate whose dimensions and configuration have been described in Chapter 4, Section 4.3. The intermediate seating block or the force and moment exciting block made of steel and having overall dimensions of 16mm (width) x 20mm (height) x 92mm (length) was attached to an off-

centre location of x = 0.22 *a*, y = 0.62 *b* (i.e. mounting point E of figure 6.7) by a 10-32 UNF screw. The length of the seating block was parallel to the X-axis of the plate providing a moment arm of -80mm. (The negative moment arm means that it extends towards the negative X-axis.) Detailed dimensions of the seating block design is shown in figure K1 of Appendix K.

Two accelerometers were attached to the plate : one close to the mounting point E and the other at the centre of the plate, to measure the velocity response of the plate. A force transducer was attached to the seating block for measurement with the moment arm and directly to mounting point E on the plate for the case without the moment arm. A random signal of bandwidth from 10 to 1600 Hz was used as the excitation. A schematic diagram of the experimental arrangements is shown in figure 8.16. Two photographs showing the experimental arrangements for the cases of with and without the moment arms are attached in figure J2 of Appendix J.

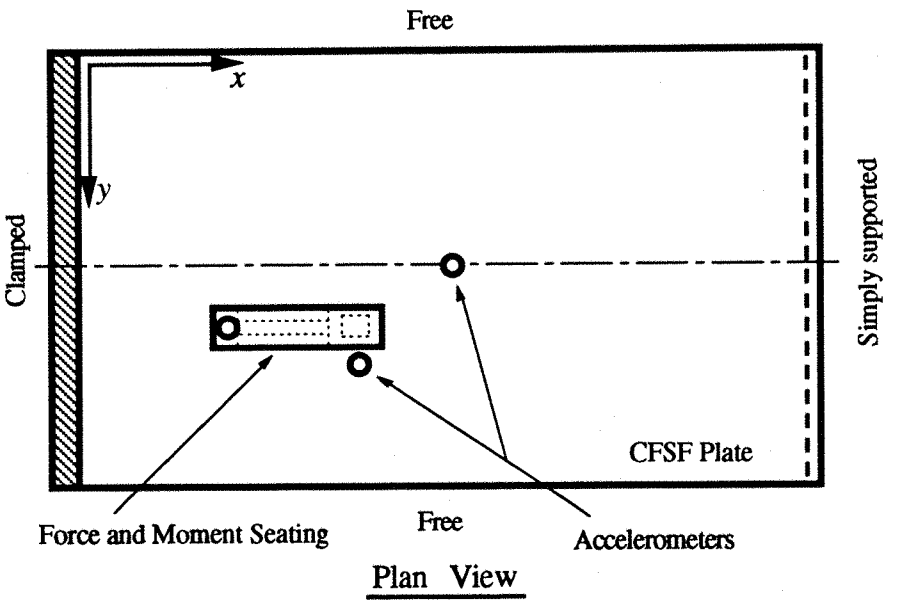

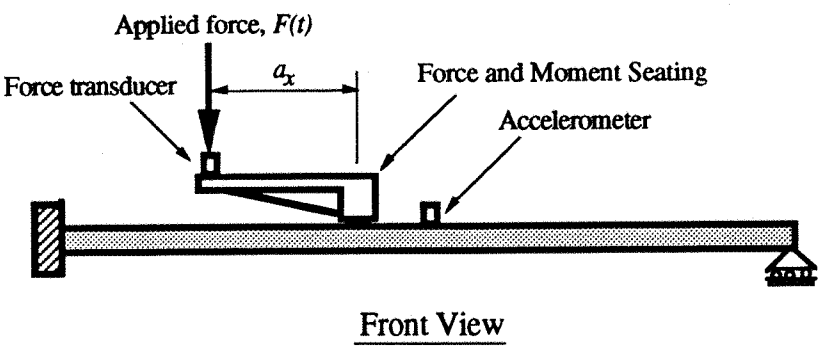

Figure 8.16 : Experimental arrangements on the CFSF plate for point and transfer mobility measurements with and without the moment arm.

The predicted power reduction index, $\mathcal{P}$, spectrum for the CFSF plate with the above set-up (i.e. with moment arm = - 80mm) is shown in figure 8.17 together with the power reduction index spectra of moment arms = - 47mm and - 65mm. It can be seen that all the three moment arms will result in power reduction (i.e. $\mathcal{P} < 1$) for frequencies up to 200 Hz, with the moment arm of - 80mm being the largest reduction. This is because this moment arm is the closest to the optimal moment arm at the fundamental frequency of the plate (44.7 Hz). The optimal moment arm spectra of the CFSF plate at mounting point E is shown in figure 8.18.

Comparison of the moduli of measured point mobility functions at mounting point E with and without the simultaneously acting moment excitation is shown in figure 8.19. The corresponding comparison of the moduli of measured transfer mobility functions between velocity at the plate centre and force excitation at mounting point E is shown in figure 8.20. The remarkable reduction in the velocity response of the plate around the first and second resonance frequencies, for a given applied force when the required moment arm is incorporated, agrees closely with the prediction from the power reduction index as shown in figure 8.17. In fact, all the resonance peak responses are lower than those without the moment arm. This result agrees closely with the 'less than unity' power reduction index spectra at frequencies up to 200Hz.

8.4.3 Practical Implications of Experimental Results

The experimental results presented in the last two sections validate the passive vibration control approach for reducing the vibrational response of flexible seating structures around a specific resonance frequency by applying the required simultaneously acting force and moment excitations via a suitably designed force and moment seating.

The implication of this finding is encouraging : if one can determine reliably the real parts of the driving point mobility functions of a beam or plate-like seating structure at the mounting points, either by a closed form analytical solution, or by the finite element method, or from experimental measurements, then the optimal moment arm for a specific 'troublesome' frequency can be determined. By incorporating this moment arm into the design of an anti-vibration mount seating, it is then possible to reduce the vibrational power transmission from a source at that frequency to the seating structure.

In view of the increase in the vibrational power input to the seating structure due to the additional moment excitation, which is more severe in the high frequency region, and

the limitations imposed by flexural rigidity and mounting stiffness of the force and moment seating (see Chapter 10, Section 10.4), the proposed approach of controlling vibration transmission at a specific frequency is most suitable for the case of a low to medium speed machine or engine running at a constant speed and mounted on a flexible seating structure.

8.5 SUMMARY

The concept of vibration control using the vibrational power terms has been explored in this chapter. Various vibration control schemes using the contribution from the coupling mobilities and a secondary force or moment to minimise the resultant vibrational power input to flexible seating structures were analysed theoretically. The passive approach of controlling vibration transmission from a source to a seating structure, at a specific frequency, by combined force and moment excitations was also validated experimentally. Expressions for the optimal moment arms which minimise the resultant vibrational power input to the flexible seating structures have been obtained for semi-infinite and finite beams and for rectangular plates. The main results described in this chapter have also been summarised and reported in [52]. The important conclusions from this study are :

(1) for flexible beam or plate-like seating structures subjected to simultaneously acting force and moment excitations, reduction in the resultant time-averaged vibrational power input from a source, at a specific frequency, can be achieved by suitably controlling the ratio of the applied moment to the applied force (i.e the moment arm).

(2) The optimal moment arm, for a given frequency and location on the seating structures, is independent of the applied force excitation and is only a function of the dynamic properties of the structures. By incorporating this moment arm into the design of an anti-vibration mount seating, it is possible to reduce the vibrational power transmission at a specific frequency to the seating structure, hence, reducing the vibrational response of the seating structure at the specific frequency.

(3) The proposed method of vibration control at a specific frequency using simultaneously acting force and moment excitations is most suitable for a low to medium, constant speed machine mounted on flexible seating structures.

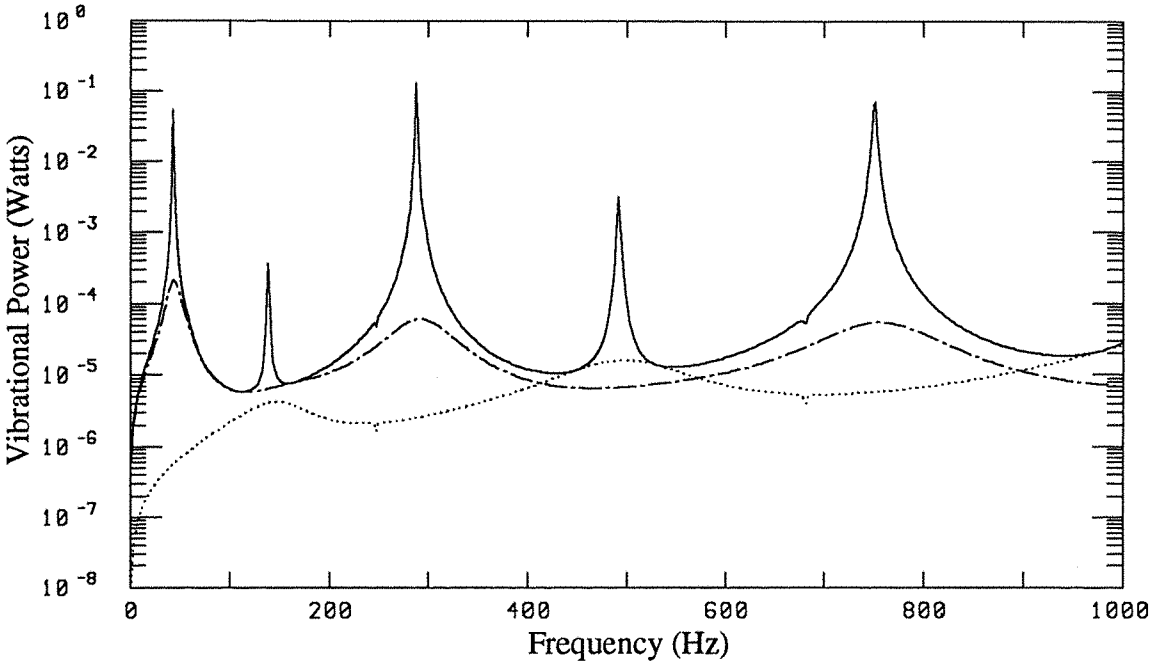

Figure 8.3 : Comparison of P_{total} of the clamped-simply supported beam with and without the control schemes (primary applied force amplitude = 1N, moment arm = 0.028m, loss factor = 0.005) : ——— no control, ····· force control, —·—·— moment control.

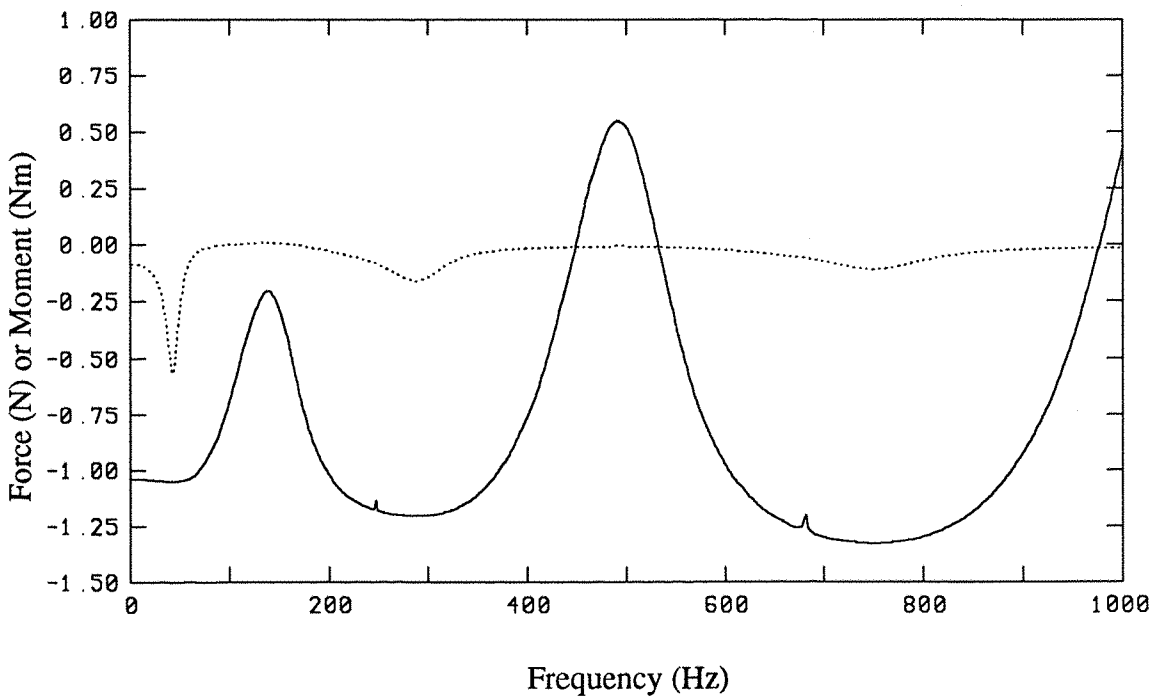

Figure 8.4 : Required amplitude spectra of the optimal secondary force ($F_{c,opt}$, ———) and moment ($M_{c,opt}$, ·····) for the control schemes in figure 8.3.

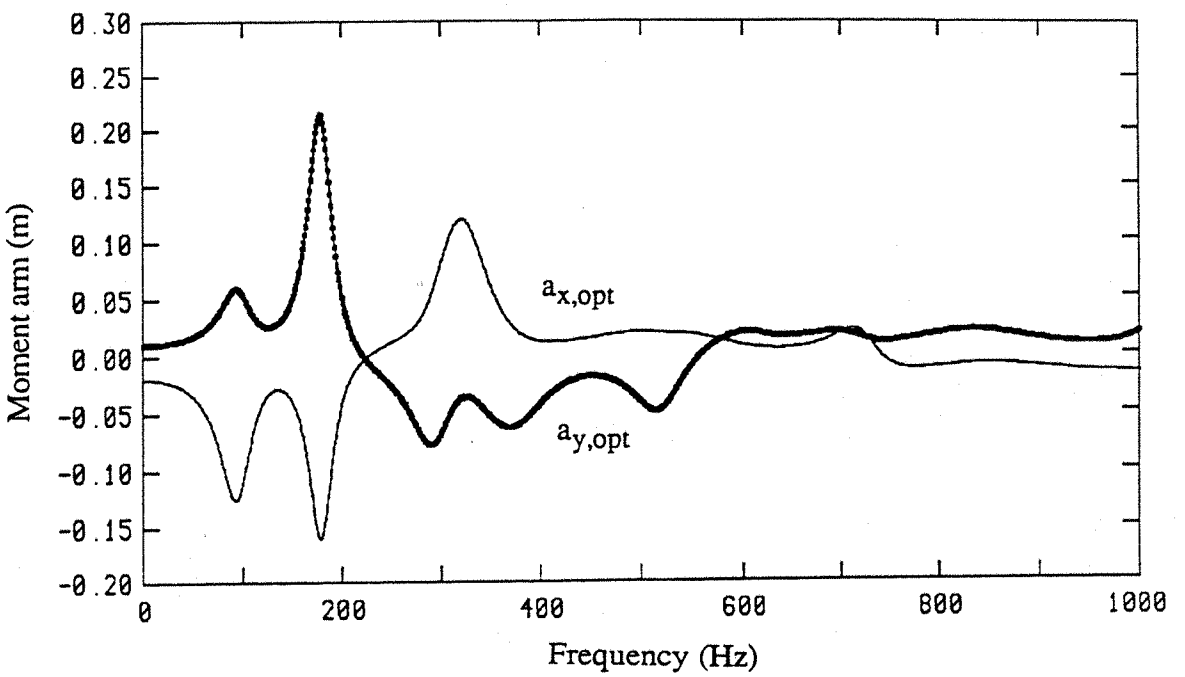

Figure 8.8 : Optimal moment arm spectra for the SSSS plate with excitations at an off-centre point : x=0.22*a* , y=0.62*b* (force amplitude = 1N, loss factor = 0.001).

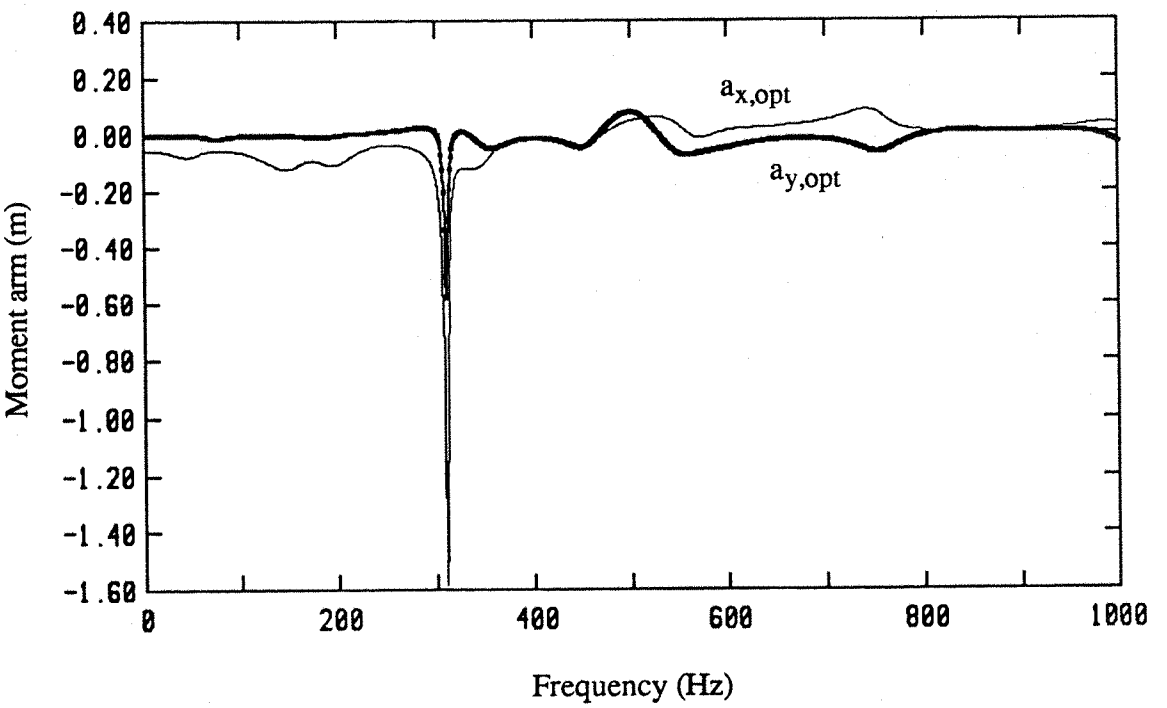

Figure 8.9 : Optimal moment arm spectra for the CFSF plate with excitations at an off-centre point : x=0.22*a* , y=0.62*b* (force amplitude = 1N, loss factor = 0.001).

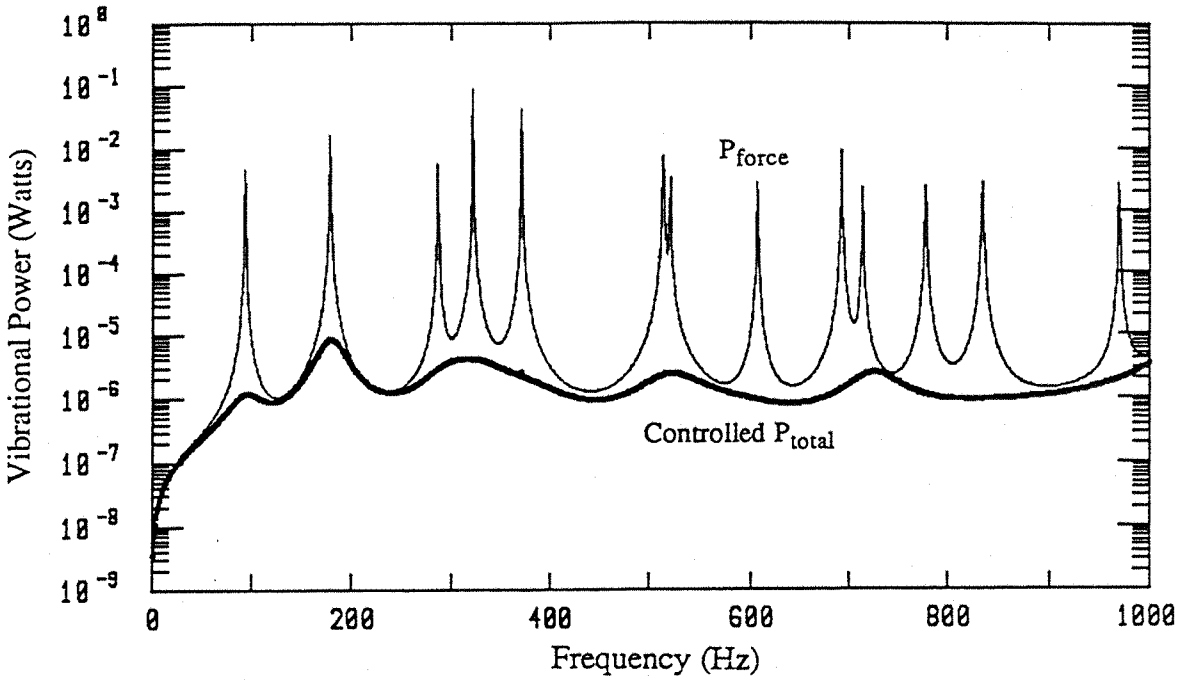

Figure 8.10:Comparison of P_{force} and the controlled P_{total} for the SSSS plate with excitations at an off-centre point : x=0.22*a* , y=0.62*b* (force amplitude = 1N, loss factor = 0.001).

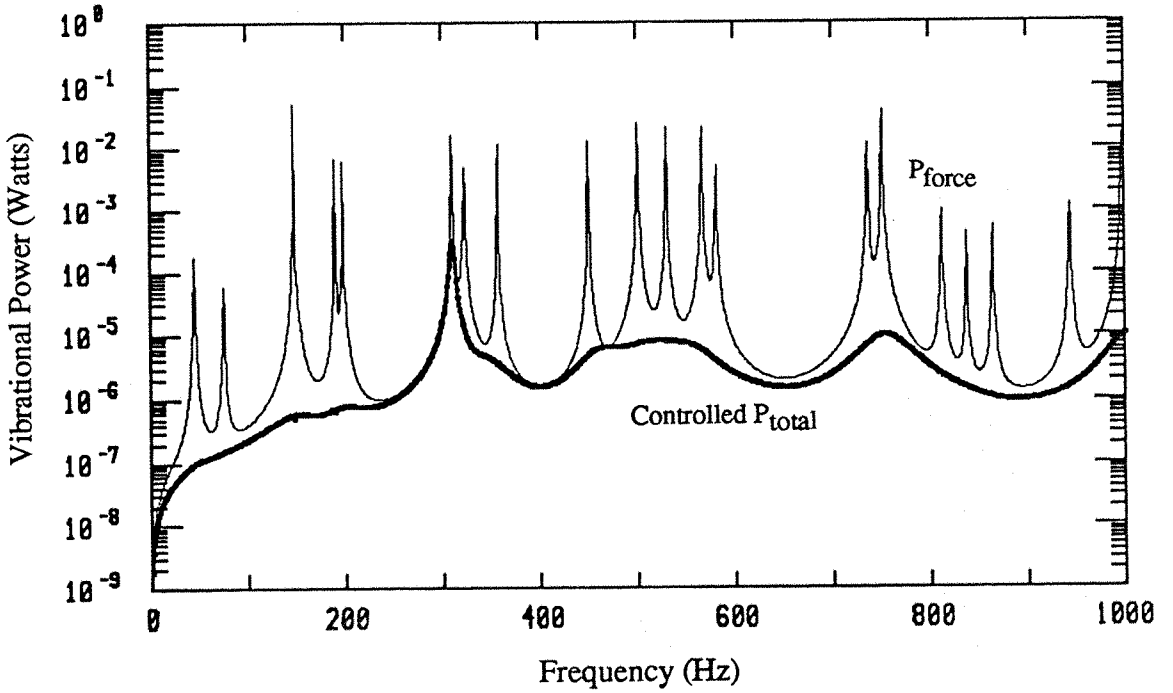

Figure 8.11:Comparison of P_{force} and the controlled P_{total} for the CFSF plate with excitations at an off-centre point : x=0.22*a* , y=0.62*b* (force amplitude = 1N, loss factor = 0.001).

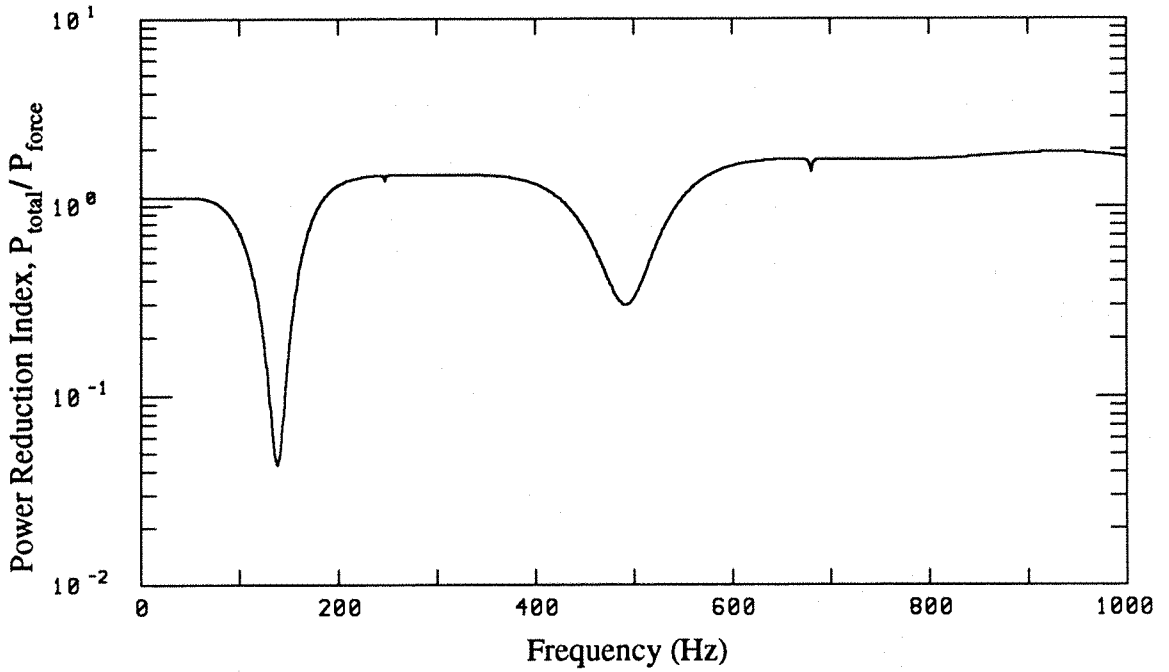

Figure 8.13 : Predicted power reduction index spectrum for the clamped - simply supported beam with moment arm = 0.028m (force amplitude = 1N, loss factor = 0.005).

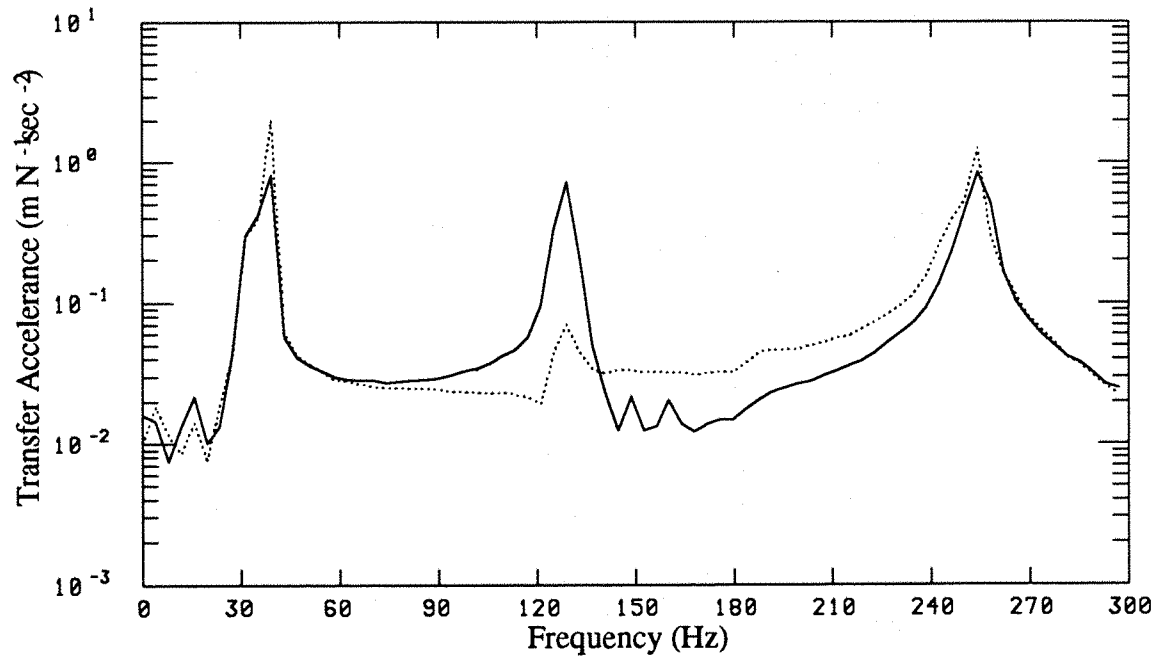

Figure 8.15 : Comparison of the moduli of measured transfer accelerances for the clamped - simply supported beam : ——— no moment arm, ····· with 0.028m moment arm.

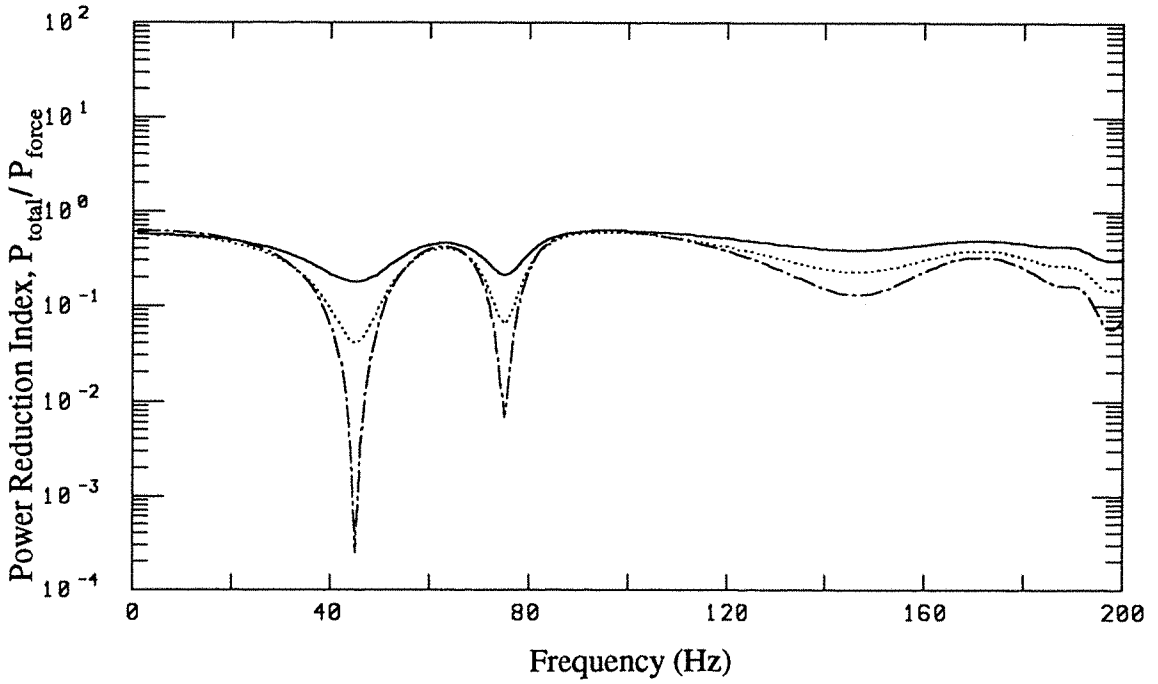

Figure 8.17 : Predicted power reduction index spectra at mounting point E (x=0.22*a*, y=0.62*b*) on the CFSF plate for various moment arms : ——— –47mm, ····· –65mm and —·—·— –80mm.

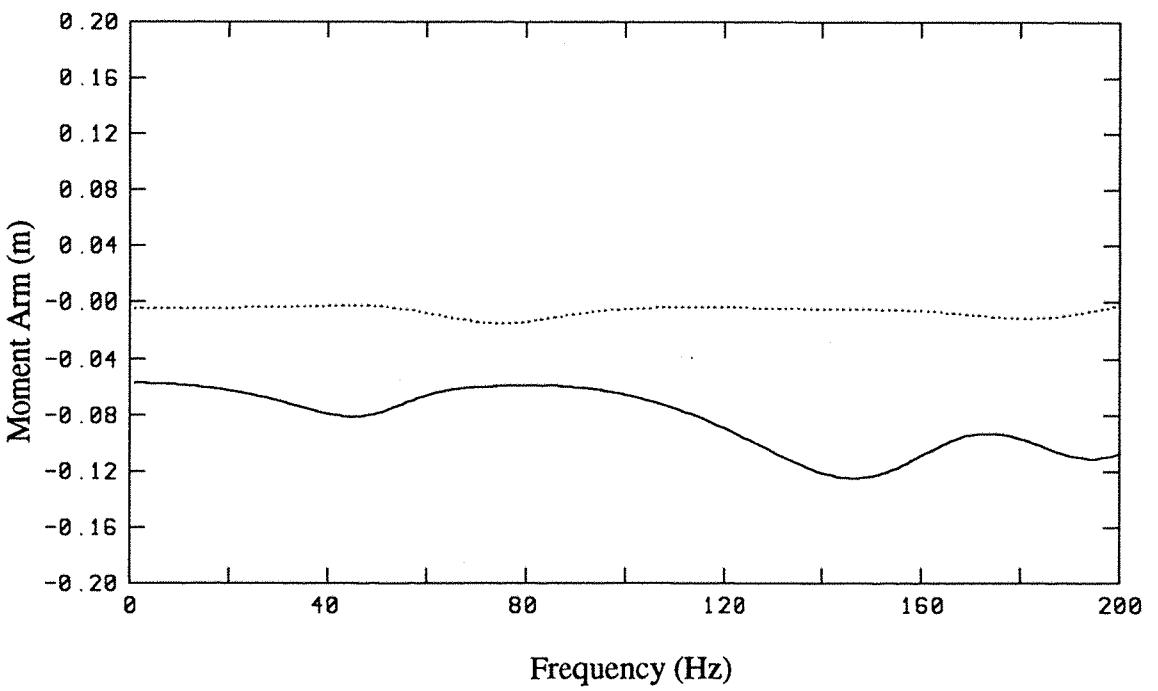

Figure 8.18 : Optimal moment arm spectra at mounting point E (x=0.22*a*, y=0.62*b*) on the CFSF plate : ——— $a_{x,opt}$, ····· $a_{y,opt}$.

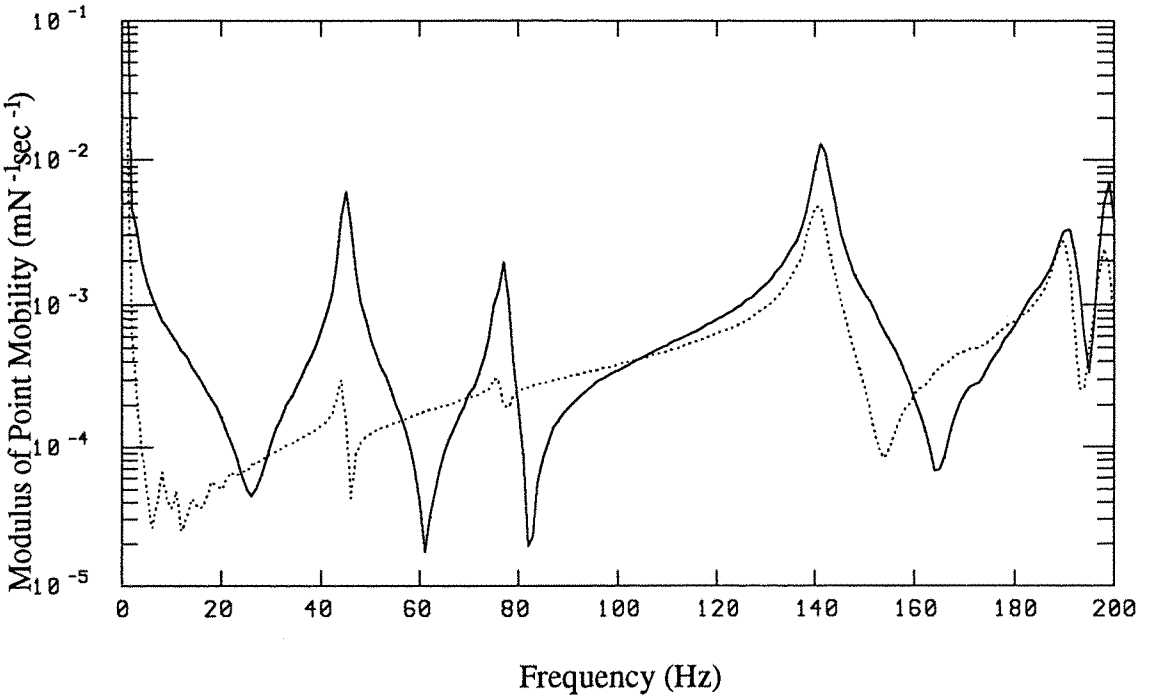

Figure 8.19 : Modulus spectra of the measured point mobility functions at mounting point E (x=0.22*a*, y=0.62*b*) on the CFSF plate : ——— no moment arm, ····· with moment arm of – 80mm.

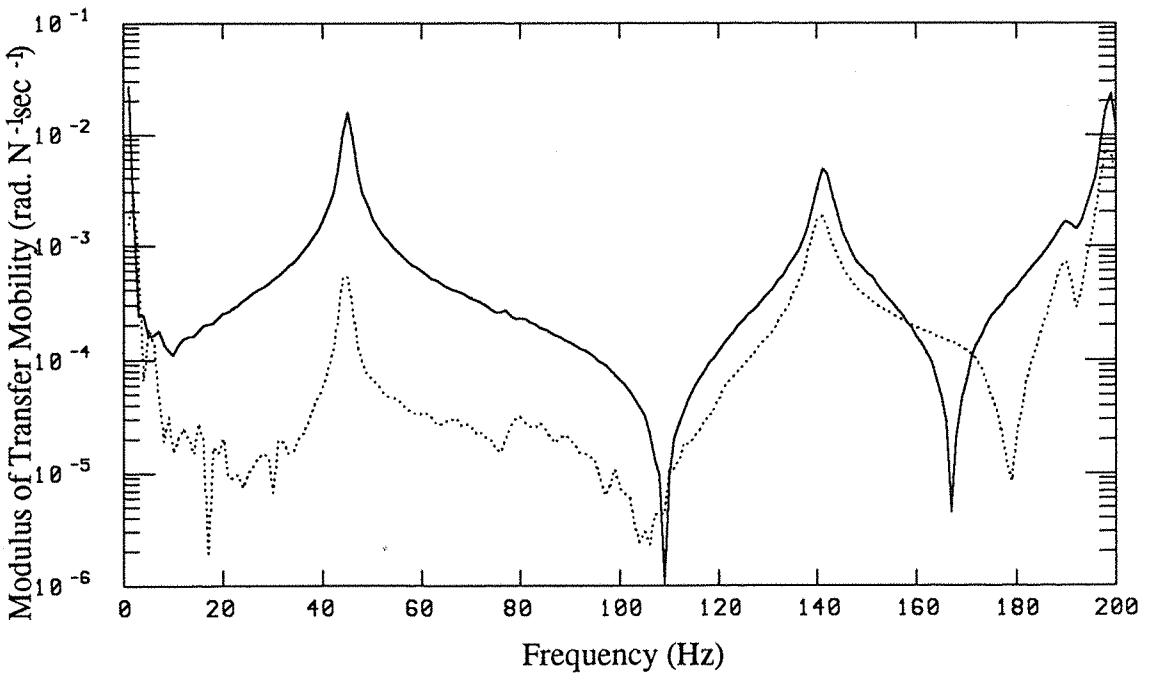

Figure 8.20 : Modulus spectra of the measured transfer mobility functions between velocity at the plate centre and force excitation at mounting point E on the CFSF plate : ——— no moment arm, ····· with moment arm of – 80mm.

CHAPTER 9

VIBRATION CONTROL OF AN UNBALANCED ROTATING MOTOR VIA THE FORCE AND MOMENT SEATING

9.1 INTRODUCTION

In the previous chapter, various vibration control schemes using the contribution from the coupling mobilities to achieve cancellation in the vibrational power components were presented. The passive approach of controlling vibration transmission from a source to a beam and a rectangular plate, at a specific frequency, by combined force and moment excitations was also validated experimentally. The experimental validation was performed for a specially designed force and moment seating (in order to generate simultaneously the required force and moment excitations) mounted at a specific point on the structures.

This chapter describes the design procedures and the experimental arrangement for controlling the vibrational response of the CFSF rectangular plate caused by an unbalanced rotating motor using the so-called 'force and moment seatings'. The motor was mounted on four resilient isolators and supported on the force and moment seatings, which provide the required moment arms at the specific mounting points, in order to reduce vibration transmission around the fundamental flexural mode of vibration of the seating plate.

This experimental study aims at reinforcing the theoretical discussion presented in this thesis, in particular, the cancellation of vibrational power components due to the presence of coupling mobilities, and to demonstrate the applicability of the force and moment seating design to reduce the vibrational response of a flexible seating structure, at a specific frequency, excited by a low to medium constant speed machine resiliently mounted on the structure.

9.2 DESIGN OF THE FORCE AND MOMENT SEATING

The calculation of the optimal moment arms for beam and rectangular plate seating structures based on the real parts of the driving point mobility functions has been described in Chapter 8. The procedures for designing the force and moment seatings to provide the required moment arms are summarised in a more concise form as follows :

9.2.1 The Design Procedures

The design procedures of the force and moment seatings are :

(1) selecting the mounting points on the seating structure. When selecting these mounting points, try to use symmetrical positions on the structure, if available, to simplify the design. Considerations must also be given to the size of the machine, any physical constraints of the seating structure and the predominant mode shape of the structure at the frequency of interest.

(2) Determining the driving point mobility functions for each mounting point, either by a suitable analytical method as described in Chapters 2 and 3 or the finite element method or from experimental measurements. When measuring the mobility functions, attention must be given to the possible phase mismatch in measuring instruments and the difficulties of measuring the rotational motions and applying the moment excitation.

(3) Calculating the optimal moment arms at each mounting point for the specific frequency according to the equations given in Sections 8.2.4 and 8.3.1.

(4) Checking the optimal moment arms against the physical constraints of the seating structure and the machine.

(5) If the optimal moment arms cannot be conveniently incorporated into the design of the force and moment seatings ('cantilevered seatings'), then use them as a guide to design the seatings with the nearest possible moment arm values.

(6) Calculating the power reduction index and comparing the vibrational power input to the seating structure with and without the moment arms, to ensure that sufficient reduction in vibrational power is achieved.

9.2.2 The Optimal Moment Arms

The driving point mobility functions at the selected locations on the CFSF plate were calculated analytically based on the formulation described in Chapter 3. As the fundamental resonance frequency of the CFSF plate in flexure is 44.7Hz, the mobility functions were obtained from 1 to 100Hz with a frequency multiplication factor of 10 (i.e. all characteristic beam functions of up to 1000Hz were used as assumed functions). With this relatively small number of beam functions, the computations of the driving point mobility functions were performed on a microcomputer rather the IBM mainframe as described in Chapter 3.

In order to simplify the design of the force and moment seatings, the mounting points were selected symmetrically with respect to the central line of the plate parallel to the pair of free edges. The locations of the mounting points and the optimal moment arms for the frequency of 45Hz are tabulated in Table 9.1.

Location of Mounting Pt.	Optimal Moment Arms	Designed Moment Arms
Point a : $x_a = 0.1026\,a$ $y_a = 0.6154\,b$	$a_{x,opt}$ = - 0.03265m $a_{y,opt}$ = 0.00049m	a_x = - 0.035m $a_y = 0$
Point b : $x_b = 0.2650\,a$ $y_b = 0.6154\,b$	$a_{x,opt}$ = - 0.10468m $a_{y,opt}$ = - 0.00293m	a_x = - 0.080m $a_y = 0$

Table 9.1 : Locations of mounting points and the optimal and designed moment arms for 45Hz.

Due to the seating arrangement of the force and moment seatings at points a and b, an optimal moment arm of $a_{x,opt}$ = - 0.105m would have caused interference between the seatings. Hence, the nearest possible values for the moment arms were used. These designed values of the moment arms are also given in table 9.1. The arrangement of these two pairs of force and moment seatings is shown in figure 9.1. Figure K1 of Appendix K shows the design of the force and moment seatings with the above designed moment arm values.

The optimal moment arm spectra for mounting points a and b are shown in figures 9.2 and 9.3 respectively. These spectra show that for the frequency range from 1 to 100Hz, the optimal moment arm, $a_{y,opt}$ is very close to zero, as in this frequency range, the flexural mode shapes of the CFSF plate are dominated by the first and second bending modes along the X-wise direction (i.e. similar to the mode shapes of a clamped -

simply supported beam). The coupling in the Y-wise mode shapes is not significant. The optimal moment arm, $a_{x,opt}$ is negative throughout the frequency range for both mounting points. The variation of these moment arms with frequency is quite gradual.

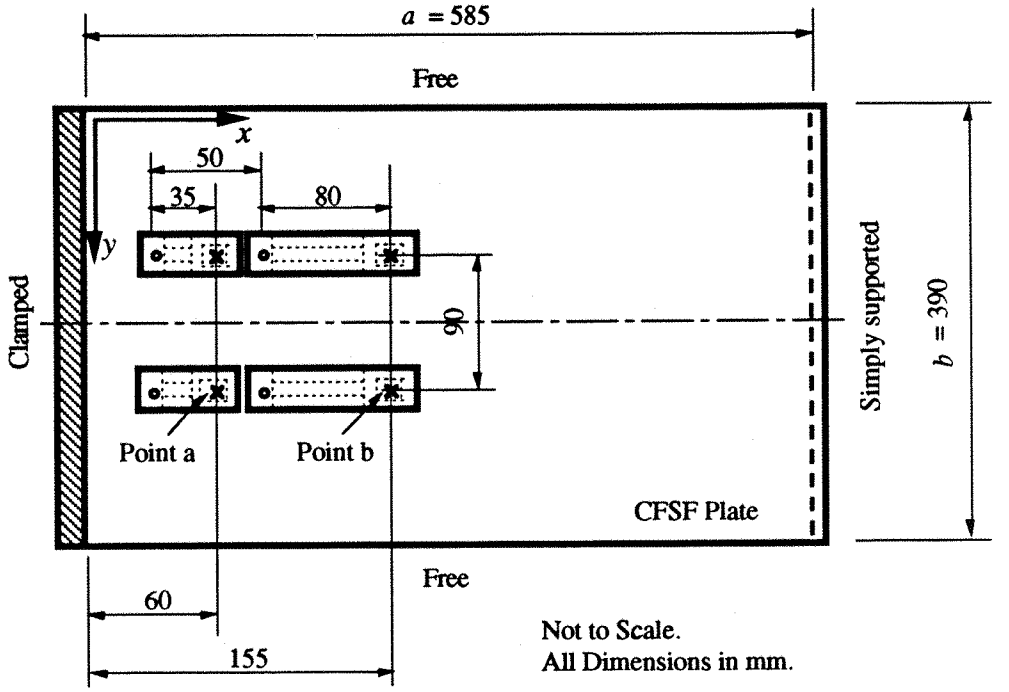

Figure 9.1 : Sketch showing the arrangement of the force and moment seatings on the CFSF plate.

The effectiveness of the force and moment seatings with the designed values of moment arms (see table 9.1) have been predicted using the power reduction index spectra and the vibrational power inputs to the CFSF plate. Figures 9.4 and 9.5 show the power reduction index spectra at mounting points a and b, respectively, for the designed values of the moment arms. Comparisons of P_{force} , i.e. without the moment arms, and P_{total} , i.e. with the moment arms, at mounting points a and b are shown in figures 9.6 and 9.7 respectively. As the moment arm of -0.035m at mounting point a is closer to the optimal value, the reduction in the resultant vibrational power input to the CFSF plate is larger than that of the mounting point b. These four spectra show that there is reduction in the resultant vibrational power throughout the frequency range from 1 to 100Hz and the reduction around the resonance frequencies of the plate is generally larger due to the existence of strong coupling mobilities around these frequencies.

9.3 EXPERIMENTAL ARRANGEMENT FOR UNBALANCED MOTOR MEASUREMENT

9.3.1 Description of the Experimental Apparatus

The experimental apparatus consisted of an electric motor resiliently mounted at four points on the CFSF rectangular plate. The motor had a power rating of 0.125HP (95 Watts) with a maximum speed of 4000RPM. It was manufactured by Parvalux Electric Motors Ltd. The overall dimension of the motor was 140mm in length with a body diameter of 90mm and a mass of 2.6kg.

The four resilient mounts were the same set of isolators used in the experimental measurement of vibrational power transmission between coupled structural systems. The dimensions and properties of the resilient mounts have been described in Chapter 6, Section 6.2. An aluminium alloy plate of approximately 9mm thick was used between the motor and the resilient mounts. The purpose of this plate was to strengthen the motor base plate and for interchangeability between measurements for test cases with and without the force and moment seatings (i.e. moment arms).

The rotational speed of the motor was controlled by a speed controller made from a variable resistor and was calibrated by a Stroboflash, type 1200E, manufactured by DAWE Instruments Ltd. The unbalanced excitation was created by an eccentric mass attached to the end of the motor rotating shaft. The weight of the eccentric mass was chosen so that the motor could maintain a constant speed of rotation in the speed range of interest.

For measurement with moment arms, four force and moment seatings (cantilevered seatings) having the required designed values of moment arms were attached to the CFSF plate at the specific locations as shown in figure 9.1 and table 9.1. The unbalanced motor was then mounted via the resilient isolators to the force and moment seatings. For measurement without the moment arms, the unbalanced motor was mounted on the resilient isolators and attached to the same set of mounting points on the CFSF plate. Two photographs showing the experimental arrangements for the unbalanced motor measurements with and without the force and moment seatings are shown in figure J3 of Appendix J.

9.3.2 The Experimental Procedures

Before conducting the unbalanced motor experiment, it is necessary to ascertain the effectiveness of vibration cancellation provided by this set of force and moment seatings. This is because the optimal moment arms were calculated based on the driving point mobility functions at each mounting point independently, i.e. as if the excitations at each mounting point were independent. The theory presented in Chapter 8 does not take account of the transfer mobility functions between different mounting points. The assumption was that if the vibrational power input at each mounting point was minimised for a specific frequency, then the sum of the power input from a set of mounting points would be smaller than the power input without the moment arms. The contribution from the transfer mobility functions for the case of multiple mounting points was assumed to be less significant.

Of course, the theory presented in Chapter 8 can be extended to include these transfer mobility terms and the minimisation process must consider the moment arms at various mounting points simultaneously. The minimisation process in this case will be much more involved. Hence, it is necessary to validate the force and moment seating design procedures described in Chapter 8 and in Seciton 9.2 for the case of multiple mounting points.

a. The Random Force Experiment

In the random force experiment, the unbalanced motor was replaced by an electro-dynamic exciter which consisted of a permanent magnet and a moving coil. The forcing function was a random signal from 10 to 1600Hz. The applied random signal was measured by a force transducer. Two accelerometers, one placed at the centre of the motor support plate and the other at the centre of the CFSF plate, measured the velocity responses of the structures.

The driving point mobility function of the motor support plate and the transfer mobility function between the velocity response at the centre of CFSF plate and the random force excitation applied at the centre of the motor support plate were calculated for cases with and without the force and moment seatings. Two photographs showing the experimental arrangements for the random force measurements with and without the force and moment seatings are shown in figure J4 of Appendix J.

The objective of this measurement was to compare the driving point and transfer mobility functions with and without the set of force and moment seatings for the cancellation of vibrational power components and hence reducing the vibrational response of the seating plate around the fundamental resonance frequency as predicted in figures 9.4 to 9.7.

b. The Unbalanced Motor Experiment

For a given rotational speed, the response of the motor was measured by an accelerometer placed at the centre of the motor support plate. A second accelerometer was attached to the centre of the CFSF plate to measure the resulting vibrational response of the plate. The first or the reference accelerometer positioned at the centre of the motor support plate in order not to indicate motion caused by rocking of the motor. The second accelerometer was positioned at the centre of the CFSF plate because the objective of the experiment was to reduce motion of the plate in its fundamental flexural mode of vibration, which was expected to have the largest response at the centre of the plate.

In this experiment, the spectral density functions of the acceleration signals measured at these two locations were calculated on an HP 3566A Spectrum Analyser. In order to compare the vibrational responses of the CFSF plate with and without the moment arms in two separate measurements, the spectral density functions of the accelerations measured at the centre of the CFSF plate were divided by the spectral density functions of the reference accelerations, i.e. those measured at the centre of the motor support plate.

The reason of determining and comparing this ratio of the spectral density functions of acceleration signals is that for a given set of resilient mount properties, the power transmitted to a resilient mount, at a given frequency, is proportional to the spectral density function of the velocity (or acceleration) response measured at the top surface of the mount, as shown in eqn. (7.9). The acceleration response measured at the centre of the motor support plate gave an average acceleration transmitted to the top surfaces of the four resilient mounts, at least in the low frequency range of interest as in this experiment. The ratio of spectral density functions used thus gave an approximate measure of the vibrational response of the CFSF plate with respect to the power transmitted to the resilient mounts via the vertical translational motion.

Measurements of the normalised vibrational responses of the CFSF plate with and without the set of force and moment seatings was repeated for a series of rotational speeds of the unbalanced motor ranging from 39Hz to 49Hz in order to cover the fundamental resonance frequency of the plate at 44.7Hz.

c. The Square Wave Simulation Experiment

In conducting the unbalanced motor experiment, it was noticed that the resulting excitation on the resilient mounts was, by no means, a single sinusoidal vertical force. Other components of forces and moments were also present. Although a single sinusoidal vertical out-of-balance force can be achieved theoretically by incorporating two identical unbalanced masses rotating in opposite direction to each end of the motor, this arrangement was not used. Instead a square wave signal exciting an electro-dynamic exciter, similar to the arrangement for the random force experiment (see photographs shown in figure J4 of Appendix J for the experimental arrangement), was used to simulate a single sinusoidal vertical out-of-balance force with higher harmonics.

The Fourier series of a square wave signal is a series of sine waves with reducing amplitudes for higher harmonics. The fundamental frequency of the sine wave is the reciprocal of the period of the square wave. The second sine wave has a frequency which is three times the fundamental frequency and an amplitude which is one-third that of the first sine wave. Hence, a square wave signal is an ideal simulation of a sinusoidal out-of-balance force with odd numbered higher harmonics.

For a given square wave excitation, the normalised vibrational responses of the CFSF plate, with and without the force and moment seatings, were determined and compared. The measurement was then repeated for a series of square waves with different periods covering a range of frequencies from 40 to 48 Hz.

The objective of this square wave simulation experiment was to compare the effectiveness of reducing the vibrational responses around the fundamental resonance frequency of the CFSF seating plate, using the force and moment seatings when subjected to a single sinusoidal out-of-balance force, to the results obtained from the unbalanced motor experiment.

9.4 EXPERIMENTAL RESULTS AND DISCUSSION

9.4.1 Validation for a Set of Force and Moment Seatings

The effectiveness of vibration cancellation around the fundamental resonance frequency of the CFSF plate by using a set of force and moment seatings can be seen from the results obtained from the random force experiment. Figure 9.8 shows the modulus spectra of the driving point mobility functions at the centre of the motor support plate for the cases of with and without moment arms. The fundamental resonance peak of the CFSF plate at 44.7Hz occurred for the case of no moment arms (i.e. without the set of force and moment seatings). With the force and moment seatings, this resonance peak was suppressed. The resonance peak at 76Hz appeared in both the mobility spectra was the mass-spring resonance frequency of the system.

Comparison of the modulus spectra of the transfer mobility functions between velocity at the centre of the CFSF plate and applied random excitation at the centre of the motor support plate is shown in figure 9.9. It can be seen that with the set of force and moment seatings, there was reduction in vibrational response at the centre of the CFSF plate for frequencies up to 100Hz.

These experimental results support the assumption mentioned in Section 9.3.2, that in the low frequency region, the contribution from the transfer mobility functions, for the case of multiple mounting points, is not significant. The design procedures described in Section 9.2 are appropriate for the case of a machine, resiliently mounted through a set of points, on a flexible seating structure.

9.4.2 Vibration Characteristics of the Motor and the CFSF Plate Responses

The spectral density functions of the acceleration signals measured at the centres of the motor support plate and the CFSF plate, with and without the force and moment seatings, are shown in figures 9.10 and 9.11. The fundamental unbalance frequencies of the motor in figures 9.10 and 9.11 were 40Hz and 45Hz respectively. These two figures show typical experimental results for the unbalanced motor at frequencies close to and at the resonance frequency of the seating plate.

From the upper spectra of these two figures, it can be seen that majority of the vibrational power transmitted from the motor through the resilient mounts to the seating plate is at the fundamental unbalanced frequency, a typical phenomenon for rotational

machines. The rise in the spectral density functions with increasing frequency is due to the nature of acceleration signals.

The four spectral density functions of acceleration signals measured at the centre of the CFSF plate, as shown in the lower spectra of figures 9.10 and 9.11, indicate the presence of resonance responses of the plate at high frequencies. Comparisons of these spectral density functions at the centre of the CFSF plate, with and without the moment arms, are shown in figures 9.12 and 9.13 for unbalanced motor frequencies of 40Hz and 45Hz respectively. The 'trade off' of the force and moment seatings, i.e. the additional power input to the plate due to moment excitation as well as from the coupling terms, resulting in stronger resonance response of the plate, is obvious at high frequencies as depicted in these two figures. Nevertheless, these resonance peaks at high frequencies are approximately two to three decades below the fundamental unbalance frequency peaks. Hence, the control of vibration transmission from a low to medium constant speed rotating machine to a flexible seating structure, using a set of force and moment seatings, is still possible as the higher harmonics or subharmonics are much smaller than the fundamental unbalance frequency peak.

9.4.3 The Normalised Vibrational Response of the CFSF Plate

Comparisons of the spectral density functions of acceleration signals measured at the centres of the motor supported plate and the CFSF seating plate are shown in figure 9.14 for the cases with and without the force and moment seatings and for unbalance frequencies of 40Hz and 45Hz. The comparison was performed for a bandwidth from 0 to 100Hz. Two important observations from these comparisons are noted.

(1) For unbalanced motor frequency close to the resonance frequency of the CFSF plate, such as 40Hz, the resonance response of the plate at 44.7Hz is more obvious for the case of no moment arms than that with the moment arms (compare figures 9.14(a) and 9.14(b)).

(2) For unbalanced motor frequency at or very close to the resonance frequency of the CFSF plate, such as 45Hz, the resonance response of the plate is very obvious resulting in a broader and higher resonance peak.

The normalised vibrational response of the CFSF plate was obtained by dividing the spectral density function of the acceleration signal measured at the centre of the CFSF plate to that at the centre of the motor support plate, i.e. the dotted line spectra divided

by the full line spectra in figure 9.14. Comparisons of these responses with and without the force and moment seatings and for unbalanced motor frequencies of 40, 42, 44, 45, 46 and 48Hz are shown in figure 9.15. It can be seen from these comparisons that :

(3) with the incorporation of the force and moment seatings, the normalised vibrational responses around the fundamental resonance frequency of the plate were consistently lower than those without the seatings.

(4) The greatest reduction in the vibrational responses was at the fundamental resonance frequency of the plate even though the unbalanced motor frequency was not at the fundamental resonance frequency of the plate.

(5) The reduction in the vibrational responses was the greatest when the unbalanced motor frequency coincided with the fundamental resonance frequency of the plate. The is most likely due to the fact that stronger coupling mobility functions existed at the fundamental resonance frequency of the plate.

(6) The normalised vibrational responses depicted a broader peak when the unbalanced motor frequency approached the fundamental resonance frequency of the plate. This is because of a broader and higher resonance peak of the CFSF plate as noted in figure 9.14.

9.4.4 Results from the Square Wave Simulation Experiment

In the square wave simulation experiment, the spectral density functions of the velocity signals measured at the centres of the motor support plate and the CFSF plate were determined for the cases with and without the force and moment seatings. Comparisons of these spectral density functions for fundamental sinusoidal frequencies of 40 and 45Hz are shown in figure 9.16. Similar results are observed in these comparisons as in the unbalanced motor experiment, i.e. at 40Hz, the resonance response of the CFSF plate at 44.7Hz was excited resulting in a second resonance peak as shown in figure 9.16(a) and (b). When the fundamental sinusoidal frequency coincided or was very close to the resonance frequency of the plate, the resonance peak was more pronounced. These plots also show that there was reduction in the vibrational response of the CFSF plate when the force and moment seatings were installed.

Comparisons of the normalised vibrational responses at the centre of the CFSF plate with and without the force and moment seatings and for fundamental sinusoidal frequencies of 40, 42, 44, 45, 46 and 48Hz are shown in figure 9.17. These comparisons show similar results as noted for the unbalanced motor experiment described in Section 9.4.3 (3) to (6). The fluctuation in the normalised responses at low frequencies, typically below 20Hz, are most probably due to limitations of instrumentation.

9.5 SUMMARY

In this chapter, the procedures and considerations for designing a set of four force and moment seatings, which consists of two identical pairs, have been demonstrated. These force and moment seatings have been designed for specific mounting points on the CFSF plate in order to reduce the vibrational response of the plate around its fundamental resonance frequency, caused by the unbalanced excitation of an electric motor. The effectiveness of this set of force and moment seatings, though they were not designed at the optimal values due to physical constraints, has been demonstrated from the experimental results. With the incorporation of the force and moment seatings, the normalised vibrational responses around the fundamental resonance frequency of the plate were consistently lower than those without the seatings.

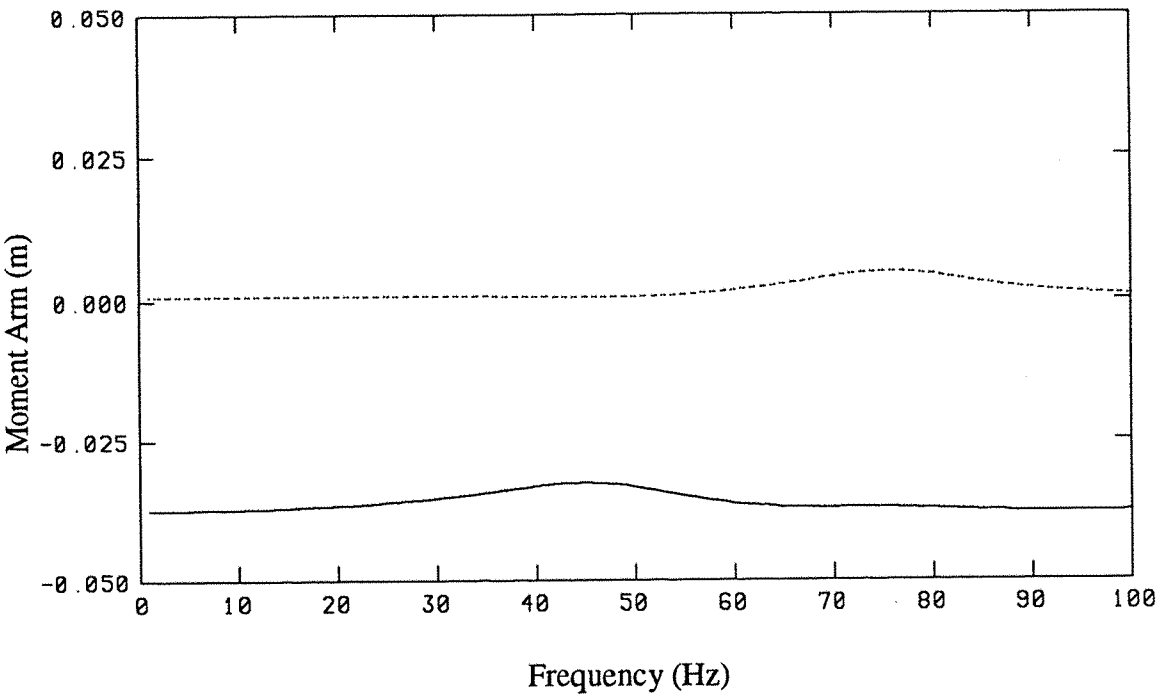

Figure 9.2 : Optimal moment arm spectra at mounting point a (x_a=0.1026*a*, y_a=0.6154*b*) on the CFSF plate : ——— $a_{x,opt}$, ····· $a_{y,opt}$.

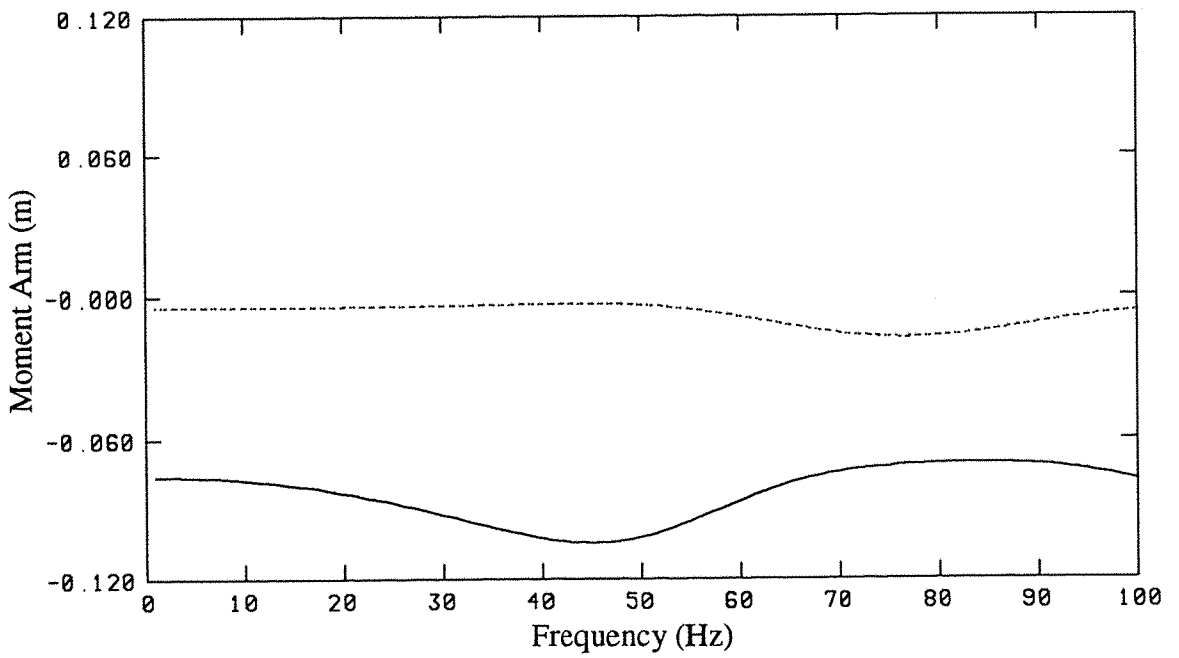

Figure 9.3 : Optimal moment arm spectra at mounting point b (x_b=0.2650*a*, y_b=0.6154*b*) on the CFSF plate : ——— $a_{x,opt}$, ····· $a_{y,opt}$.

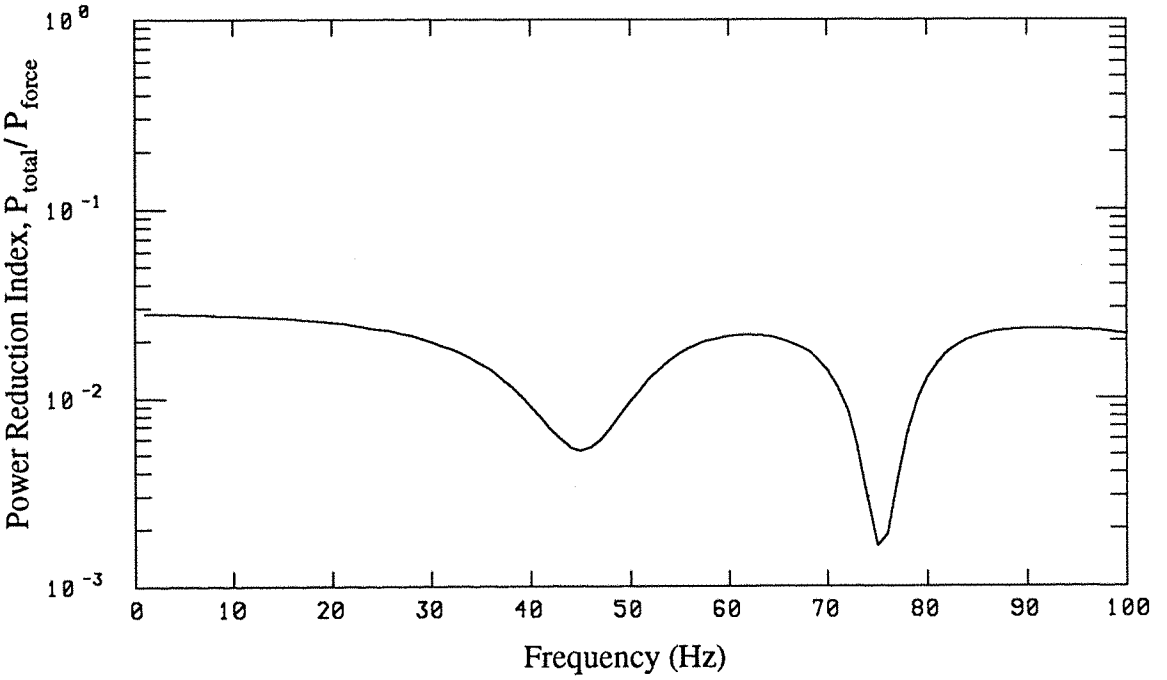

Figure 9.4 : Predicted power reduction index spectrum at mounting point a on the CFSF plate for moment arms : $a_x = -0.035$m, $a_y = 0$.

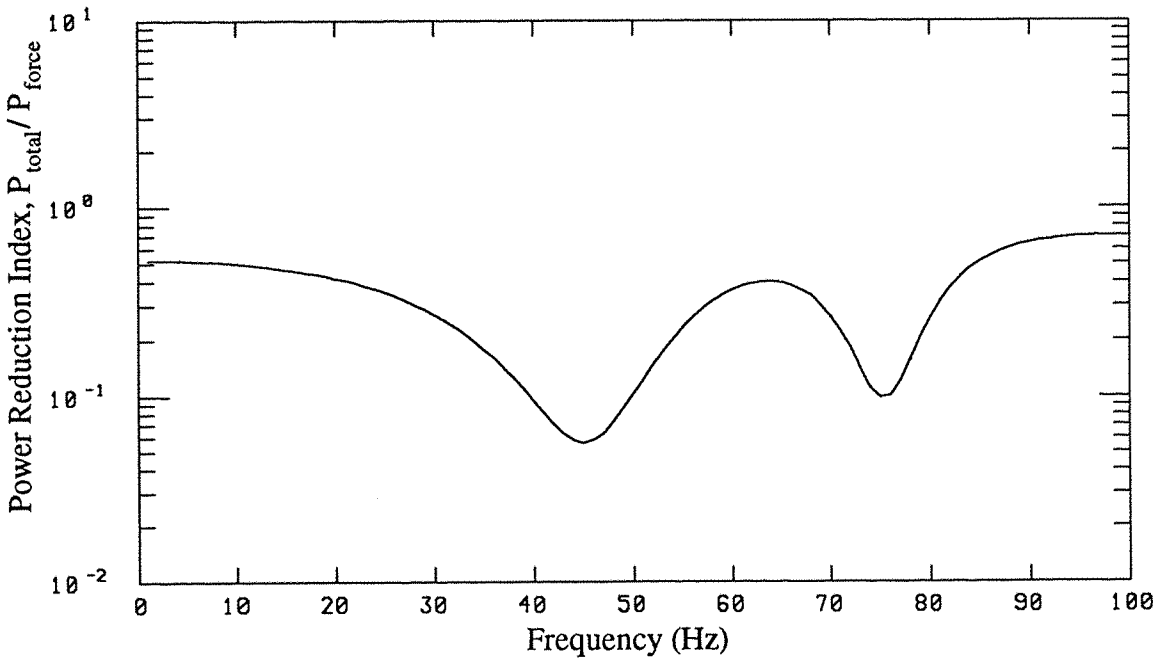

Figure 9.5 : Predicted power reduction index spectrum at mounting point b on the CFSF plate for moment arms : $a_x = -0.080$m, $a_y = 0$.

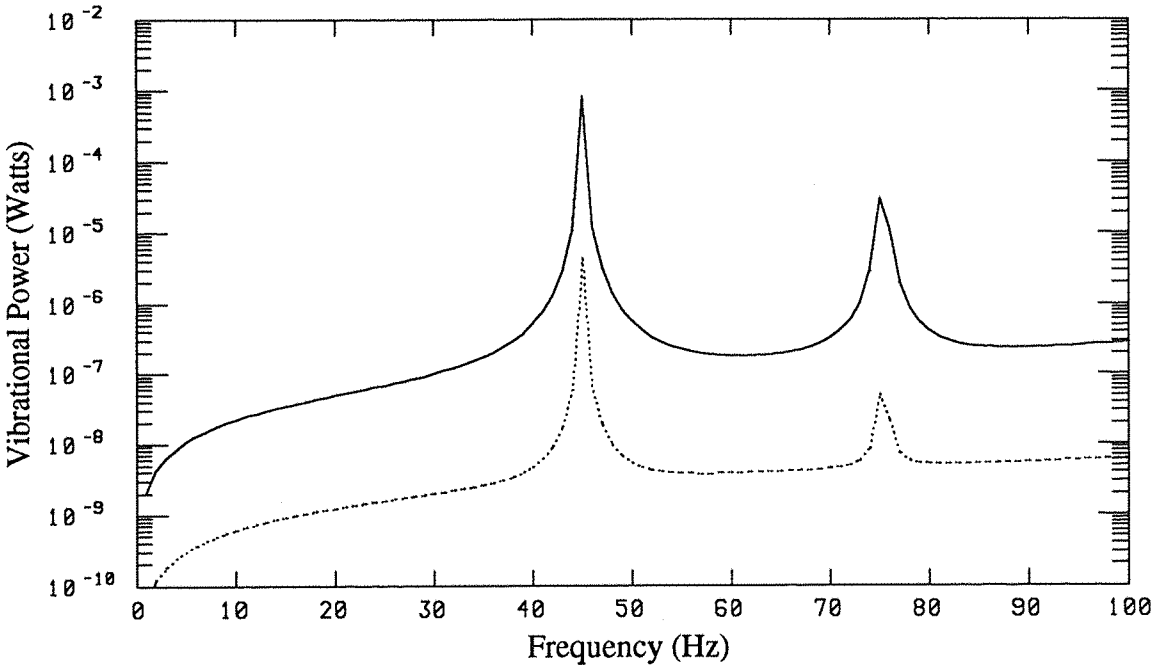

Figure 9.6 : Comparison of the vibrational power inputs to the CFSF plate at mounting point a with (·····, P_{total}) and without (———, P_{force}) the moment arms : $a_x = -0.035$m , $a_y = 0$.

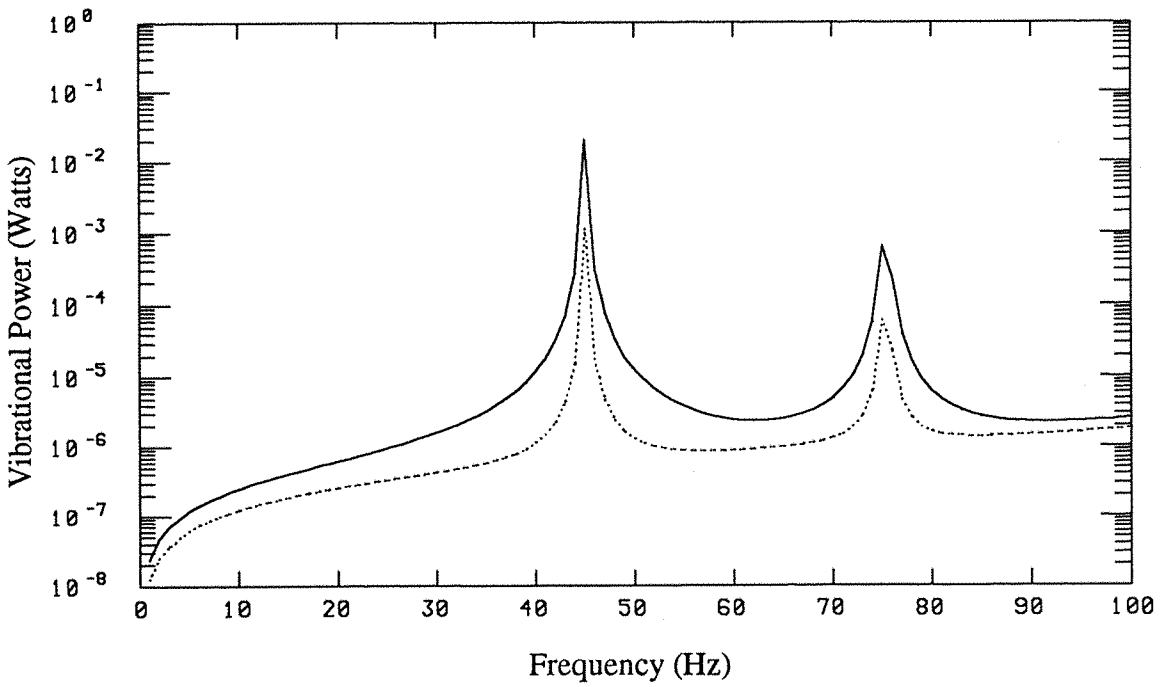

Figure 9.7 : Comparison of the vibrational power inputs to the CFSF plate at mounting point b with (·····, P_{total}) and without (———, P_{force}) the moment arms : $a_x = -0.080$m , $a_y = 0$.

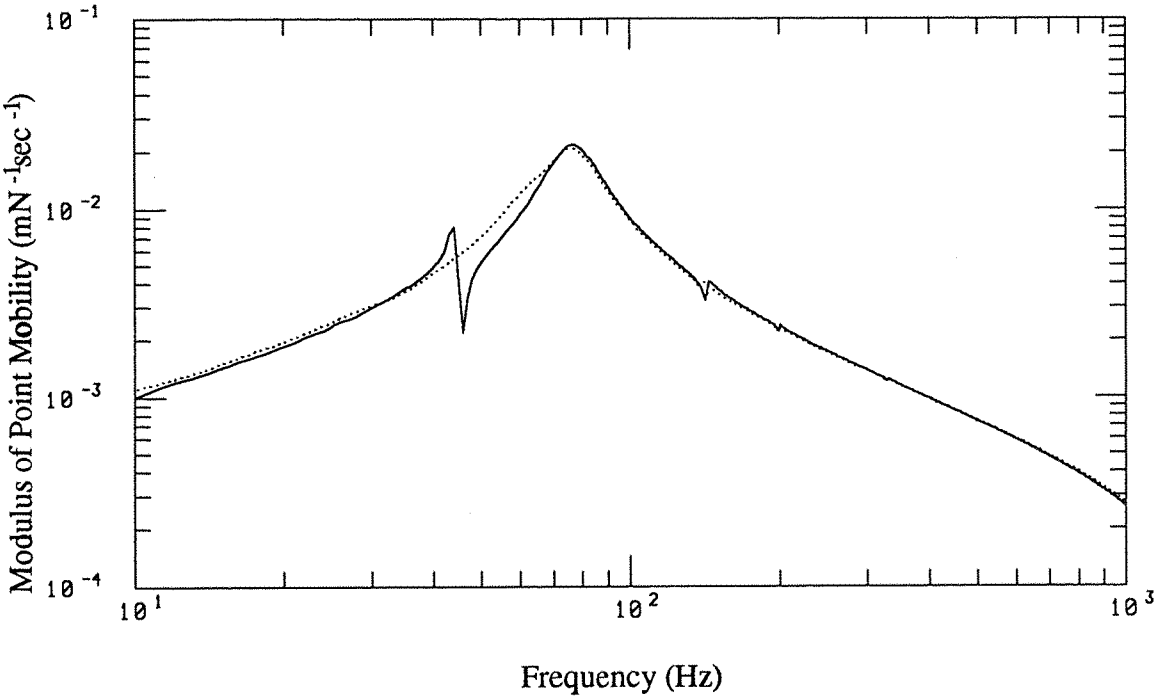

Figure 9.8 : Modulus spectra of the measured point mobility functions at the centre of motor support plate : ——— no moment arm, ····· with moment arms.

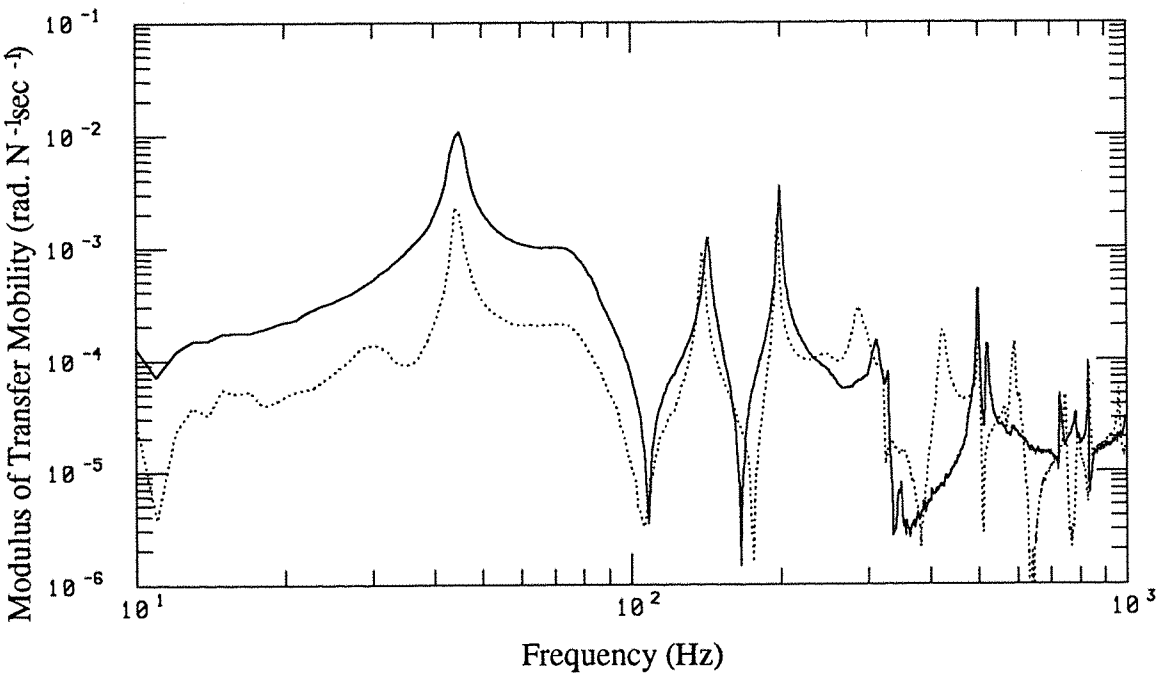

Figure 9.9 : Modulus spectra of the measured transfer mobility functions between velocity at the centre of CFSF plate and applied random excitation at the centre of motor support plate : ——— no moment arm, ····· with moment arms.

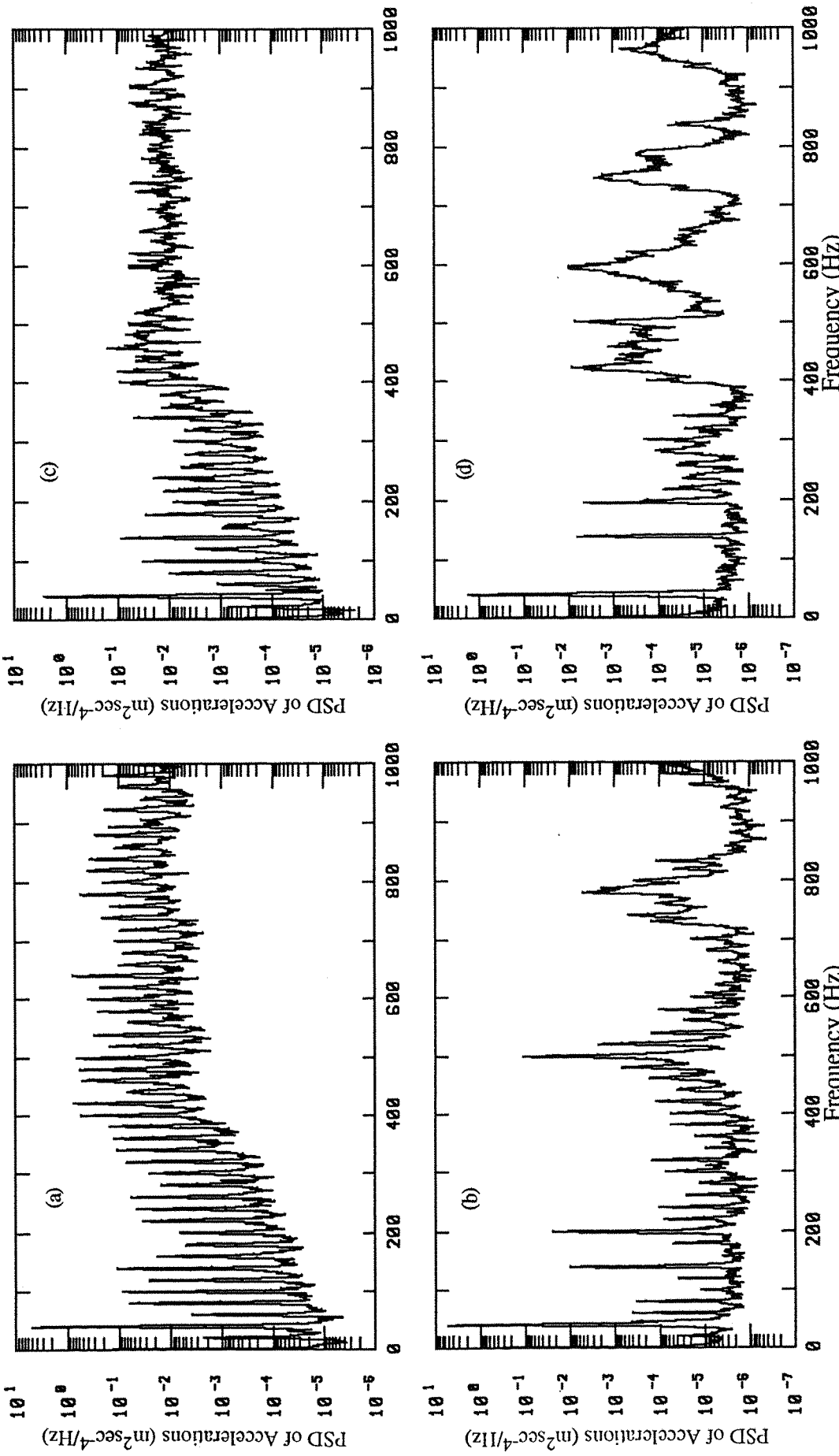

Figure 9.10 : Spectral density functions of the acceleration signals with fundamental unbalanced motor frequency of 40Hz:
(a): at the centre of motor support plate, no moment arm, (b): at the centre of CFSF plate, no moment arm,
(c): at the centre of motor support plate, with moment arms, (d): at the centre of CFSF plate, with moment arms.

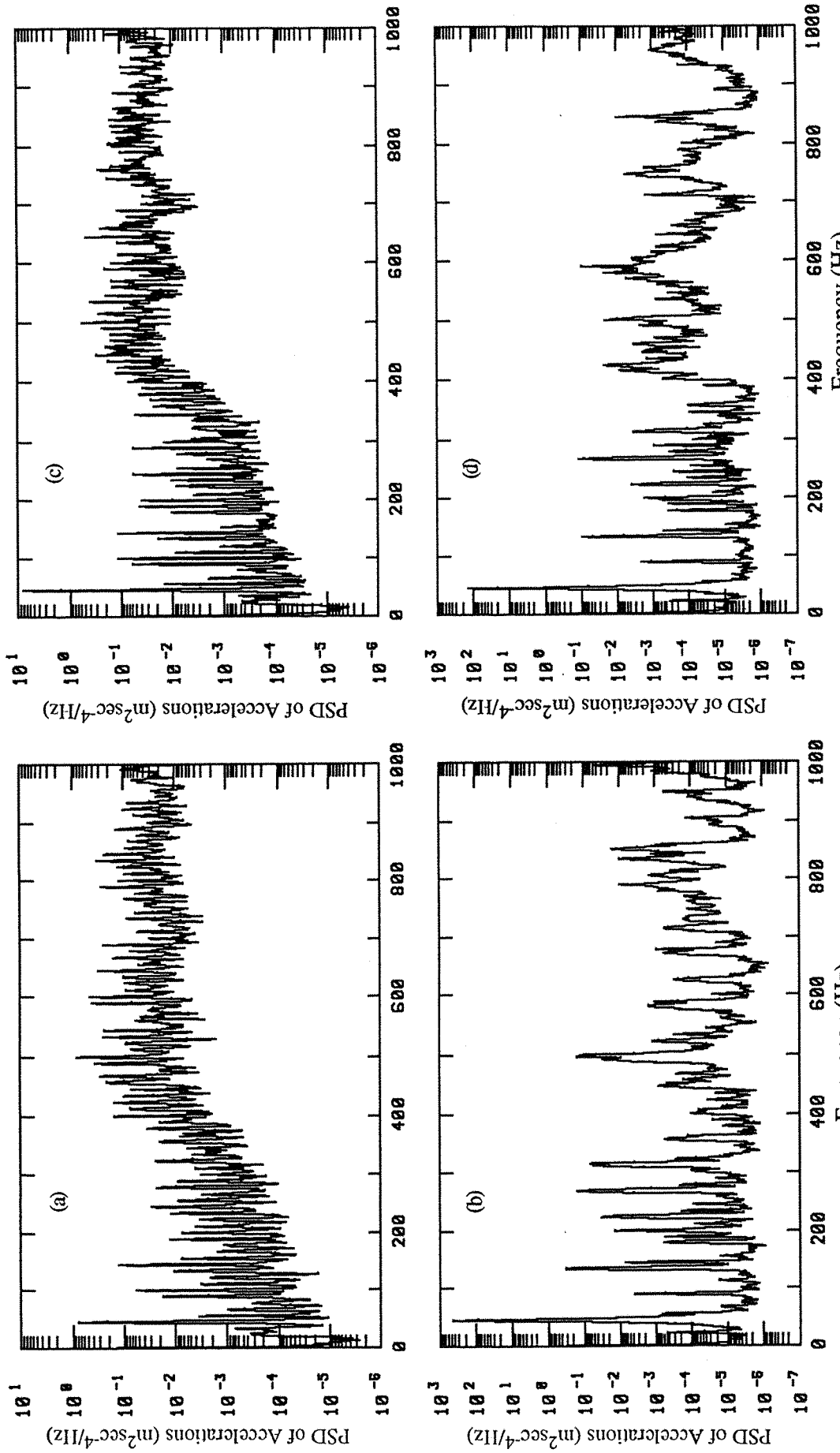

Figure 9.11 : Spectral density functions of the acceleration signals with fundamental unbalanced motor frequency of 45Hz:
(a): at the centre of motor support plate, no moment arm, (b): at the centre of CFSF plate, no moment arm,
(c): at the centre of motor support plate, with moment arms, (d): at the centre of CFSF plate, with moment arms.

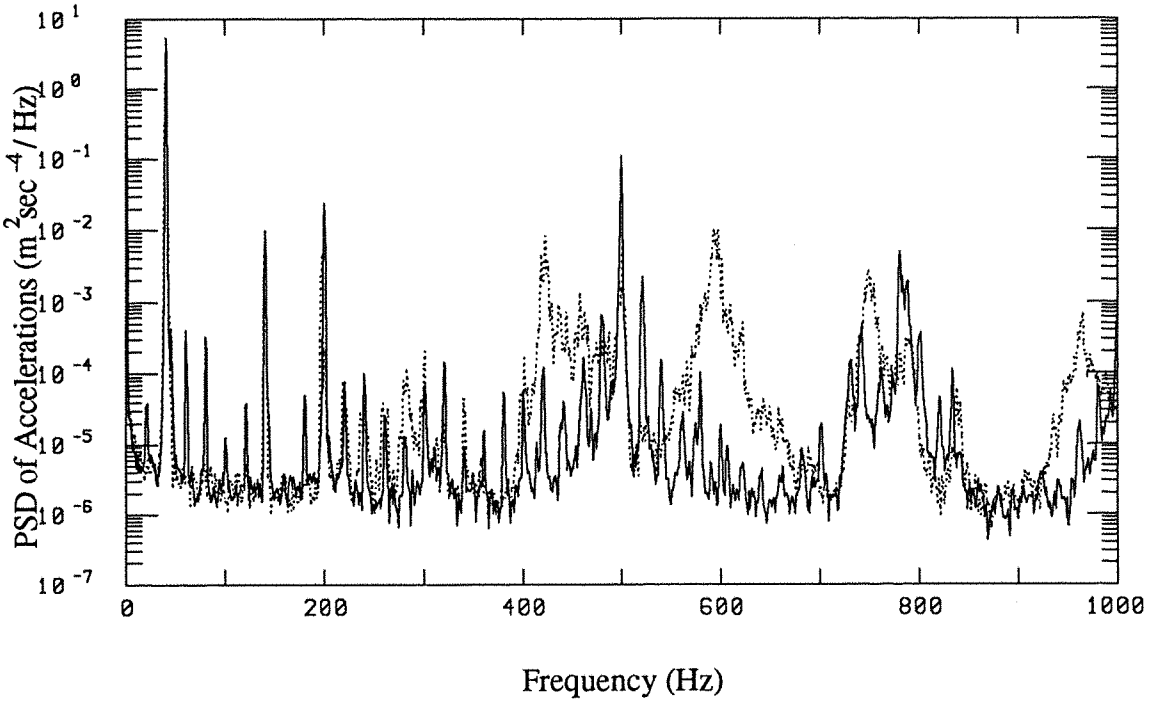

Figure 9.12 : Comparison of the measured spectral density functions of acceleration signals at the centre of CFSF plate with the fundamental unbalanced motor frequency of 40Hz: ——— no moment arm, ····· with moment arms.

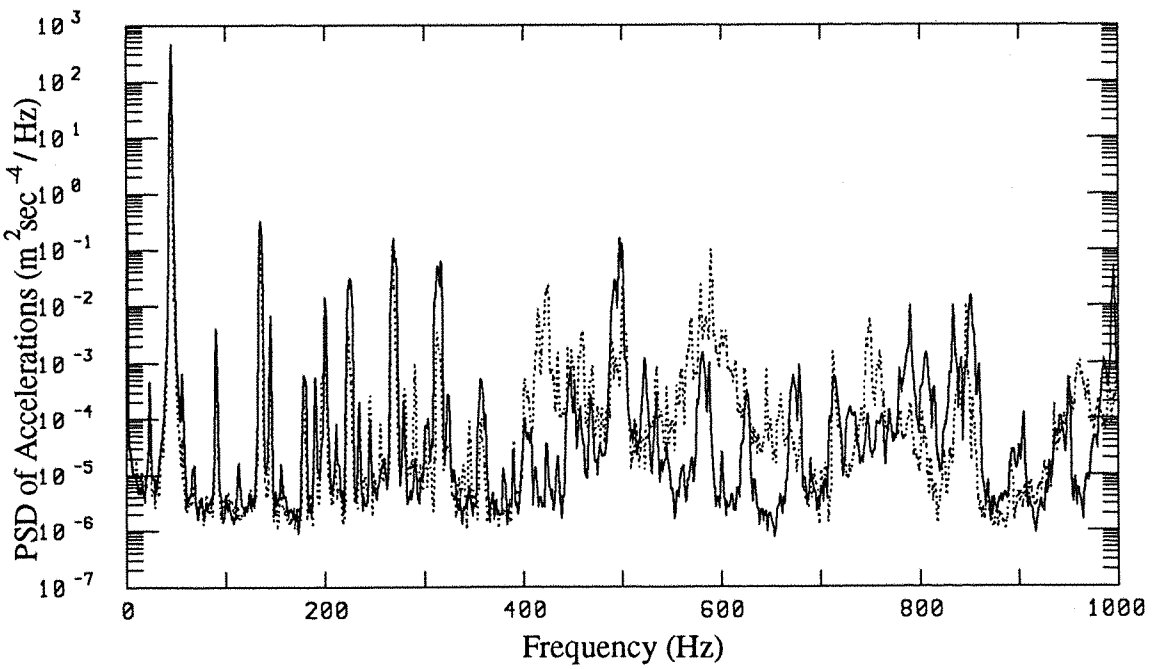

Figure 9.13 : Comparison of the measured spectral density functions of acceleration signals at the centre of CFSF plate with the fundamental unbalanced motor frequency of 45Hz: ——— no moment arm, ····· with moment arms.

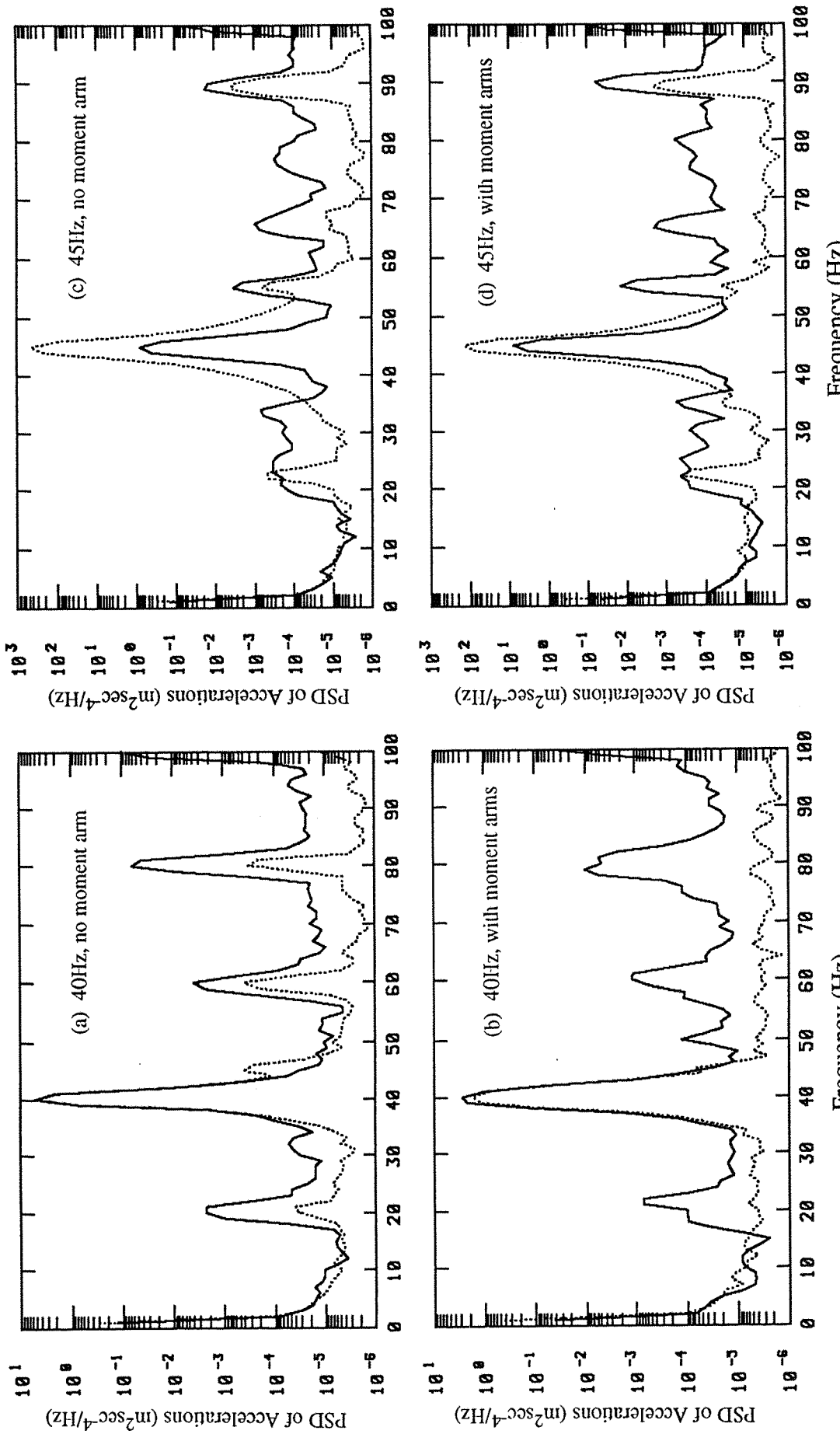

Figure 9.14 : Comparisons of the measured spectral density functions of acceleration signals at the centre of motor support plate (——) and at the centre of CFSF plate (.....) for fundamental unbalanced motor frequencies of 40 and 45Hz.

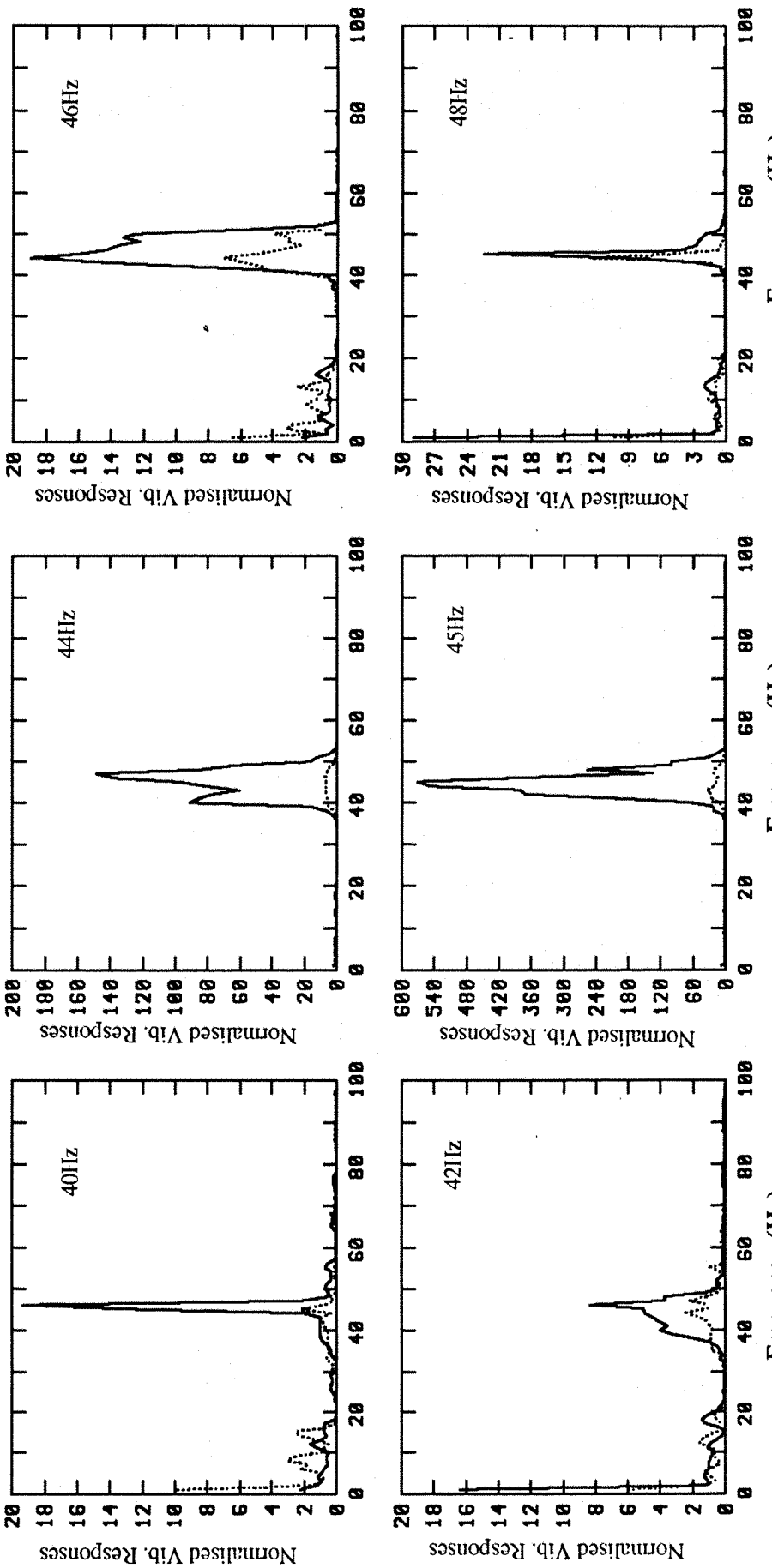

Figure 9.15 : Comparisons of the normalised vibrational responses at the centre of CFSF plate for various unbalanced motor frequencies : ——— no moment arm, ... with moment arms.

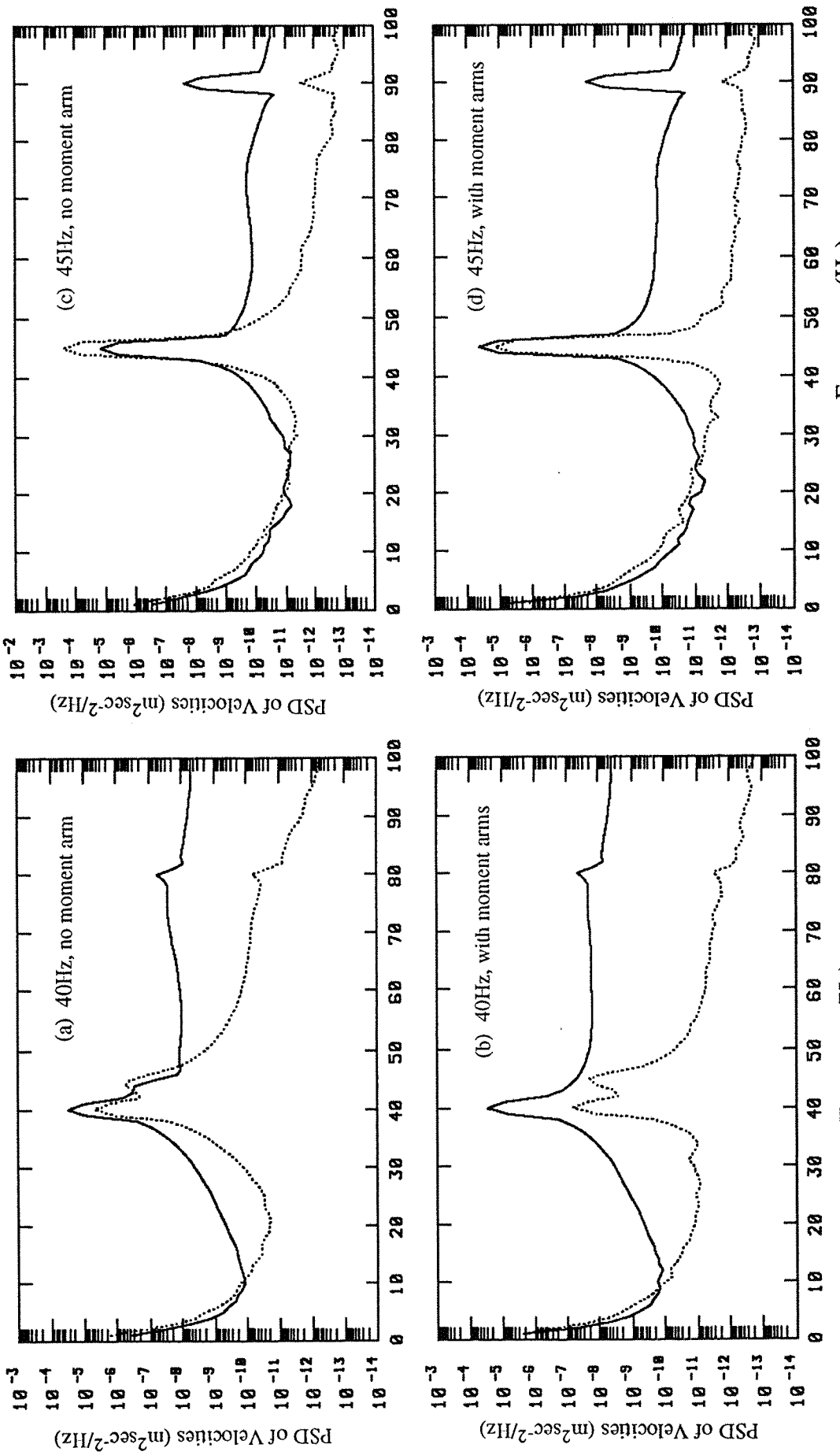

Figure 9.16 : Comparisons of the measured spectral density functions of velocity signals at the centre of motor support plate (——) and at the centre of CFSF plate (·····) for fundamental sinusoidal frequencies of 40 and 45Hz.

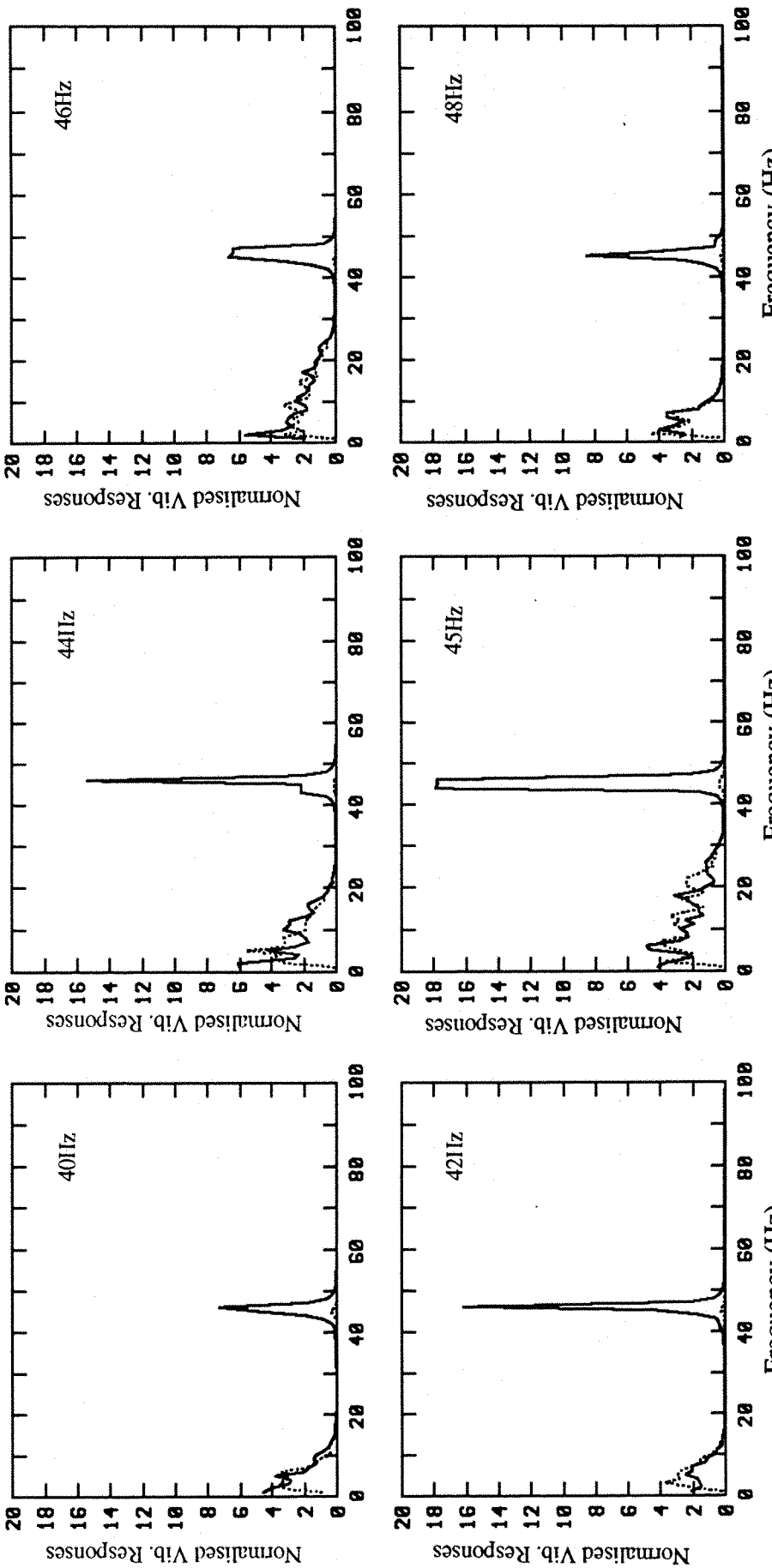

Figure 9.17 : Comparisons of the normalised vibrational responses at the centre of CFSF plate from the square wave simulation experiment with various fundamental sinusoidal frequencies : ——— no moment arm, ... with moment arms.

CHAPTER 10

PARAMETRIC STUDY OF THE FORCE AND MOMENT SEATING DESIGN

10.1 INTRODUCTION

The concept of using a force and moment seating to reduce the vibrational power transmitted to a flexible beam or plate-like structure has been discussed in the previous chapters. The cancellation effect of the vibrational power components resulting from the simultaneously acting force and moment excitations has also been validated by experiments. The analytical studies assumed that the mass and rotary inertia of the force and moment seating had negligible influence on the dynamic responses of the seating structures, i.e. the force and moment seating was modelled as a massless but infinitely stiff structure. No account of the resonance effect of the force and moment seating was considered. This is probably true in the low frequency range and for the case of a small but relatively rigid force and moment seating.

However, in practical machinery installations, due to the weight of the machines and the size of the receivers (seating structures), the weight and size of the force and moment seatings may alter significantly the dynamic responses of the seating structures. Furthermore, the force and moment seatings may have resonances close to the frequency of interest. Hence, it is important from the designer's viewpoint to know the minimium permissible resonance frequency of the force and moment seating with respect to the fundamental unbalance frequency of a rotating machine.

The optimal moment arm spectra are obtained from the driving point mobility functions of the receiver at a specified location and having a specified damping value (i.e. hysteretic loss factor). It is also in the designer's interests to establish to what extent the optimal moment arms and hence the resulting reduction in the vibrational power components will be affected by additional damping treatment of the receiver, changes in structural thickness and thus the flexural rigidity of the receiver, as well as variations of

the mounting points due to manufacturing tolerances or unforeseen design discrepancies.

Another practical question from the designer's viewpoint is, can the optimal moment arm for vibration control at a specific frequency be obtained from simplified design formula which gives a reasonable estimate of the required moment arm for design guidelines, without the endeavour of finding the detailed driving point mobility functions of the receiver. It is the aims of this chapter to try to answer these practical questions.

10.2 DESIGN OF A FORCE AND MOMENT SEATING FOR A TYPICAL SHIPBOARD FOUNDATION

A typical shipboard foundation supporting a rotating machine consists of a 0.1016m (4in) thick steel plate with one edge fully clamped and the other three edges free (i.e. a CFFF plate). The length and width of the plate are 0.9144m (3ft) each. The machine is operating at a speed of 3600 RPM which gives rise to a fundamental unbalance frequency of 60Hz.

In order to evaluate the feasibility of designing a force and moment seating to reduce the vibrational power transmitted to the seating CFFF plate at the rotational frequency of 60Hz, the optimal moment arm spectra at a location of $x_0 = 0.9a$, $y_0 = 0.5b$ (where $a = b = 0.9144$m (3ft), i.e. at a distance of nine-tenths of the length along the line of symmetry parallel to the pair of free edges) were calculated based on the driving point mobility functions at the point.

The optimal moment arms at 60Hz are : $a_x = -0.49$m and $a_y = 0$. The negative sign of the moment arm means that it extends towards the negative X-direction. The orientation of the force and moment seating with respect to the CFFF plate is illustrated in figure 10.1, which appears to be feasible as it is possible to support the machine within the original 0.9144m x 0.9144m (3ft x 3ft) base area.

The vibrational power inputs to the CFFF plate at the specified location for the cases with (i.e. P_{total}) and without (i.e. P_{force}) the optimal moment arms at 60Hz have been calculated. Figure 10.2 shows a comparison of these vibrational powers. The corresponding power reduction index spectrum is shown in figure 10.3. These two figures show that with the optimal moment arms at 60Hz, the resultant power input to the plate is lower than the power due to the force excitation alone (i.e. without moment

arms) for frequencies up to 185Hz. At 60Hz, there is slightly less than a decade of reduction in the vibrational power input to the plate.

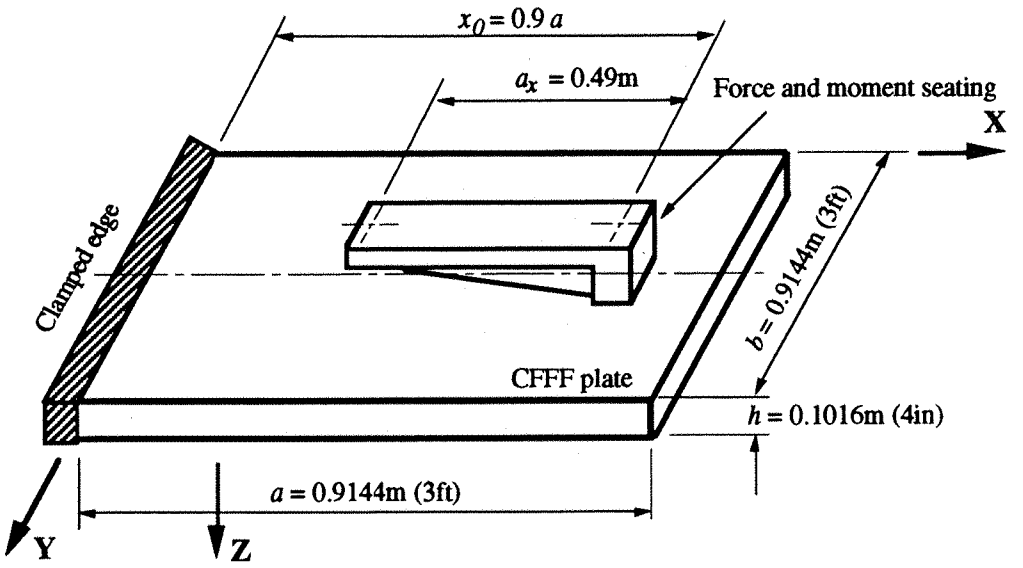

Figure 10.1 : Arrangement of the force and moment seating on the CFFF plate.

10.3 DESIGN SENSITIVITY STUDY

The influences on the optimal moment arms and the resulting vibrational power reduction at 60Hz by changing some of the seating CFFF plate properties have been examined for the following sets of parameters summarised in table 10.1.

Case No:	Dimensions	Loss Factor	Excitation Location	
	$a \times b \times h$ (m^3)	η	x_0	y_0
C-1	0.9144 x 0.9144 x 0.1016	0.005	0.9a	0.5b
C-2	0.9144 x 0.9144 x 0.1016	0.1	0.9a	0.5b
C-3	0.9144 x 0.9144 x 0.0254	0.005	0.9a	0.5b
C-4	0.9144 x 0.9144 x 0.1016	0.005	0.75a	0.5b
C-5	0.9144 x 0.9144 x 0.1016	0.005	0.9a	0.4b

Table 10.1 : Dimensions and properties of CFFF plate for the design sensitivity study.

Case C-1 consists of the original set of design data for the CFFF plate which also serves as the reference set of data. In case C-2, the hysteretic loss factor was increased from 0.005 to 0.1, which would simulate the effect on the optimal moment arms of

applying an additional damping treatment to the seating plate and would show the change in the resulting vibrational power input to the structure. In case C-3, the thickness of the seating plate was reduced from 0.1016m (4in) to 0.0254m (1in), thus reducing the flexural rigidity and the fundamental resonance frequency of the plate to below the rotational frequency of 60Hz.

The effect of variations in the mounting locations due to manufacturing tolerances or unforeseen design discrepancies was simulated in cases C-4 and C-5. In case C-4, the mounting point was located along the line of symmetry (central line) but at a distance of $0.75a$ instead of $0.9a$. In case C-5, the mounting point was off-centred to a location of $x_0 = 0.9a$, $y_0 = 0.4b$.

For each of these sets of parameters, the driving point mobility functions of the CFFF plate at the excitation point are shown in figures 10.4 and 10.5. Figures 10.4 (a) to 10.4 (d) show the comparisons of the driving point force, Y_{11}, moment, Y_{22} and Y_{33}, and the coupling, Y_{31}, mobility functions respectively. As the excitation location was along the line of mode shape symmetry for the pair of free edges, except for case C-5, the other two coupling mobility functions, $Y_{21} = \dot{\theta}_x / F$ and $Y_{32} = \dot{\theta}_y / M_x$ are numerically very small (i.e. no significant coupling in these degrees-of-freedom). The Y_{21} and Y_{32} coupling mobility functions of the off-central excitation, case C-5, are shown in figures 10.5(a) and 10.5(b) respectively.

Comparisons of the optimal moment arms for cases C-2, C-3, C-4 and C-5 with that of case C-1 are shown in figures 10.6(a) to 10.6(d) respectively. It can be seen that :

(1) additional damping treatment of the CFFF plate does not change the optimal moment arm spectra as shown in figure 10.6(a).

(2) The flexural rigidity of the plate has a significant influence on the optimal moment arm spectra as shown in figure 10.6(b). This is because the driving point mobility functions at the excitation location for these two cases (C-1 and C-3) are entirely different (see figures 10.4(a) to (d)).

(3) Variation of the mounting locations on the plate only have very small influence on the optimal moment arm spectra if the variation is kept within reasonable manufacturing tolerances. For a mounting point off-set from the symmetry line (i.e. case C-5), as shown in figure 10.6(d), the moment arm, $a_{y,opt}$ is no longer zero.

Comparisons of P_{force} and P_{total} for cases of C-2, C-3, C-4 and C-5 with those of case C-1 are shown in figures 10.7(a) to 10.7(d) respectively. The corresponding comparisons of the power reduction index spectra are shown in figures 10.8(a) to 10.8(d). The P_{total} and P_{force} vibrational power components are the power inputs to the CFFF plate for cases with and without the force and moment seating having moment arms of $a_x = -0.49$m , $a_y = 0$. It can be seen that with higher damping, the real parts of the mobility functions increase, except around the resonance frequencies, thus the power inputs to the plate also proportionally increase. However, the ratio of P_{total} to P_{force} , i.e. the power reduction index, at 60Hz remains essentially constant as shown in figure 10.8(a). Reducing the flexural rigidity of the plate affects significantly the vibrational power inputs to the plate as depicted in figures 10.7(b) and 10.8(b). Variations of the mounting point locations have only a small influence on the power components as shown in figures 10.7(c), (d) and 10.8(c), (d). For the two cases considered (C-4 and C-5), there is no significant change in the vibrational power inputs at 60Hz.

In conclusion, these comparisons show that addition of damping treatment on the receiver plate, or slight variation of the mounting points in a practical machinery installation will have insignificant effects on the optimal moment arm spectra and hence the resulting reduction of vibrational power input to the plate. In contrast, changing the flexural rigidity of the plate, either by changing the plate thickness or adding stiffeners, may cause significant changes in the optimal moment arm spectra and the resulting power reduction. It is recommended to re-calculate the optimal moment arm required if there is significant change in the flexural rigidity of the receiver plate.

10.4 RESONANCES OF FORCE AND MOMENT SEATING

In practical machinery installations, the required force and moment seatings to reduce the vibrational power input to the receiver at a specific frequency may be too large and will therefore have its fundamental resonance frequency close to the frequency of interest. The effect of the force and moment seating resonance phenomena on the cancellation of the vibrational power components input to the receiver is analysed in this section. The study aims to establish the permissible lowest resonance frequency of the force and moment seating with respect to the frequency of interest.

10.4.1 Description of the Theoretical Model

The coupling of the force and moment seating to the receiver (i.e. the CFFF plate), as shown schematically in figure 10.1, is similar to that described in Chapter 5. Two analytical models for the force and moment seating were used. The first model was a uniform beam model which possesses both mass and stiffness. The second model was a lumped mass model in which the force and moment seating was represented by a rigid mass with appropriate mass and mass moment of inertia. The receiver was the CFFF rectangular plate whose driving point mobility functions at the mounting location have been obtained analytically (see figure 10.4).

a. Uniform Beam Model

The force and moment seating is modelled as a uniform beam segment with the applied force acting at the end A. The beam segment is coupled to the CFFF plate through the end B. The coupling at end B is assumed to be rigid in the frequency range of interest (from 0 to 1000Hz). A schematic diagram of the beam segment is shown in figure 10.9, in which $F_A = F(t)$, the applied force excitation, and $M_A = 0$. The receptance matrix for the uniform beam segment in flexural vibration is given in eqn. (2.25) or (2.34).

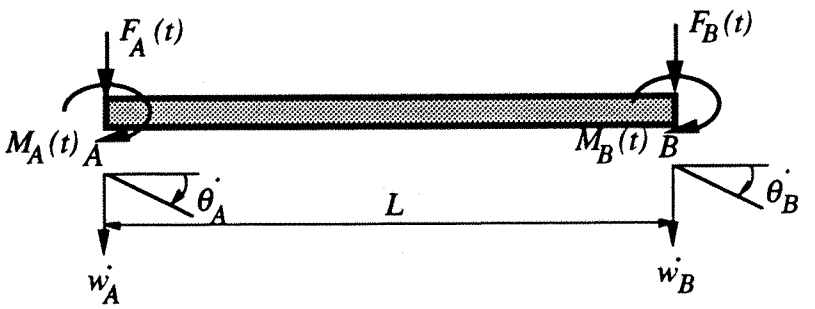

Figure 10.9 : Uniform beam model of the force and moment seating.

The driving point mobility matrix of the CFFF plate, considering only the w and θ_y degrees-of-freedom for coupling with the beam model is :

$$\begin{Bmatrix} \dot{w}_C \\ \dot{\theta}_C \end{Bmatrix} = \begin{bmatrix} Y_{11} & Y_{13} \\ Y_{31} & Y_{33} \end{bmatrix} \begin{Bmatrix} F_C \\ M_C \end{Bmatrix} \tag{10.1}$$

where F_C and M_C are the transmitted force and moment, $\dot{w}_C$ and $\dot{\theta}_C$ are the resulting

translational and rotational velocities, respectively, at the coupling point on the CFFF plate as shown in figure 10.10.

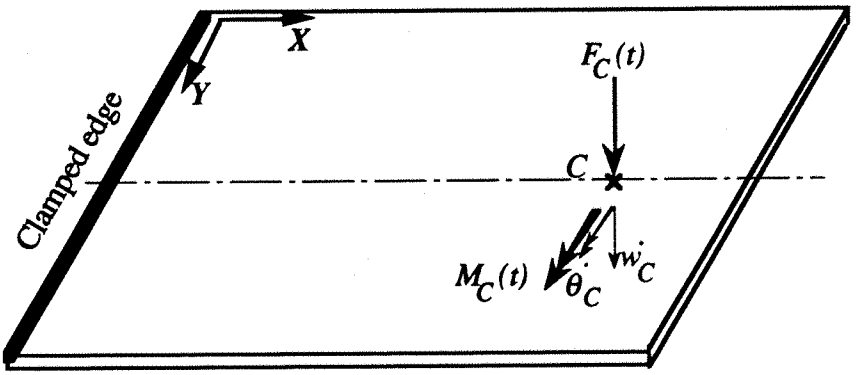

Figure 10.10 : Transmitted force and moment and the resulting velocity responses on the CFFF plate.

For sinusoidal excitation, the equivalent receptance matrix *[R]* at the coupling point on the plate is :

$$\begin{Bmatrix} w_C \\ \theta_C \end{Bmatrix} = \begin{bmatrix} R_{11} & R_{13} \\ R_{31} & R_{33} \end{bmatrix} \begin{Bmatrix} F_C \\ M_C \end{Bmatrix} \tag{10.2}$$

in which, $R_{ik} = \dfrac{Y_{ik}}{j\omega}$ $\quad i = 1,3 \; ; \; k = 1,3.$

and j is the complex operator, ω is the excitation frequency in radians per second.

The sign conventions of a rectangular plate in flexural vibration have been defined in figure 3.1. It is noted that the Y axis of the plate and the beam segment are in opposite directions. Taking this into consideration and applying the equilibrium and continuity conditions at the coupling point, one obtains the following relations :

$$F_C = -F_B \tag{10.3}$$
$$M_C = M_B \tag{10.4}$$
$$w_C = w_B \tag{10.5}$$
$$\theta_C = -\theta_B \tag{10.6}$$

Using these relationships and from eqn. (10.2) and the receptance matrix of the beam segment, eqn.(2.25), it can be shown that :

$$\begin{Bmatrix} F_B \\ M_B \end{Bmatrix} = \begin{bmatrix} A_{11} & A_{12} \\ A_{21} & A_{22} \end{bmatrix} \begin{bmatrix} -R_b & R_d \\ -R_d & -R_f \end{bmatrix} \begin{Bmatrix} F_A \\ M_A \end{Bmatrix} \tag{10.7}$$

where

$$A_{11} = \frac{1}{\Delta_1} [\, R_{33} + R_e \,]$$

$$A_{12} = \frac{1}{\Delta_1} [\, R_{13} + R_c \,]$$

$$A_{21} = \frac{1}{\Delta_1} [\, R_{31} + R_c \,]$$

$$A_{22} = \frac{1}{\Delta_1} [\, R_{11} + R_a \,]$$

$$\Delta_1 = (R_{11} + R_a)(R_{33} + R_e) - (R_{13} + R_c)(R_{31} + R_c)$$

The transmitted force and moment acting at the coupling point on the plate can then be obtained from eqns. (10.3), (10.4) and (10.7). The resultant vibrational power input to the plate is :

$$P_{total} = \frac{1}{2} Re \{ F_C \times \dot{w}_C{}^* \} + \frac{1}{2} Re \{ M_C \times \dot{\theta}_C{}^* \} \tag{10.8}$$

where $\dot{w}_C{}^*$ and $\dot{\theta}_C{}^*$ are the complex conjugates of the resulting translational and rotational velocities respectively at the coupling point on the plate.

b. Lumped Mass Model

By modelling the force and moment seating as a rigid mass having the appropriate mass, m, and the mass moment of inertia, I_m, as shown in figure 10.11, the expressions for the transmitted force and moment at the coupling point on the CFFF plate can be similarly derived as :

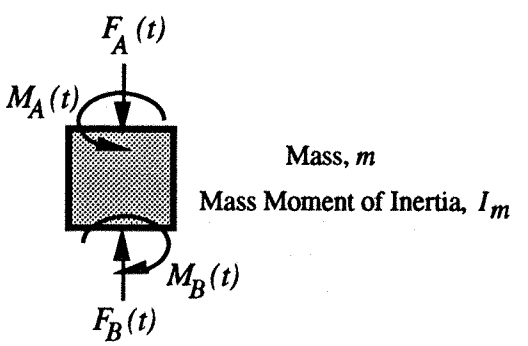

Figure 10.11 : Lumped mass model of the force and moment seating.

$$\begin{Bmatrix} F_C \\ M_C \end{Bmatrix} = \begin{bmatrix} B_{11} & B_{12} \\ B_{21} & B_{22} \end{bmatrix} \begin{bmatrix} -\frac{1}{m\omega^2} & 0 \\ 0 & -\frac{1}{I_m\omega^2} \end{bmatrix} \begin{Bmatrix} F_A \\ M_A \end{Bmatrix} \qquad (10.9)$$

where
$$B_{11} = \frac{1}{\Delta_2}\left[R_{33} - \frac{1}{I_m\omega^2} \right]$$
$$B_{12} = \frac{1}{\Delta_2}\left[-R_{13} \right]$$
$$B_{21} = \frac{1}{\Delta_2}\left[-R_{31} \right]$$
$$B_{22} = \frac{1}{\Delta_2}\left[R_{11} - \frac{1}{m\omega^2} \right]$$
$$\Delta_2 = \left(R_{11} - \frac{1}{m\omega^2} \right)\left(R_{33} - \frac{1}{I_m\omega^2} \right) - R_{13}\, R_{31}$$

The applied force and moment excitations are : $F_A = F(t)$ and $M_A = F(t) \times |a|$, where $|a|$ is the amplitude of the moment arm provided by the force and moment seating.

10.4.2 Analytical Results and Discussion

a. Effects on the Transmitted Force and Moment

The effects on the transmitted force and moment caused by resonances of the force and moment seating have been studied using the uniform beam model. In this model, the force and moment seating was a 0.1016m (4in) thick steel beam with a rectangular cross-section. The length and width of the beam were 0.49m and 0.1m respectively. The hysteretic loss factor of the beam was assumed to be 0.005. For simplicity, the moment arm was assumed to be 0.49m and the applied force amplitude was 1N.

In the lumped mass model, the rigid mass, m, was equal to that of the above steel beam. The mass moment of inertia, I_m, was taken to be equal to $\left[\frac{1}{3} m L^2 + \frac{1}{12} m h^2 \right]$, where L and h are the length and thickness of the beam. (i.e.the mass moment of inertia of a rectangular block about a perpendicular axis through one end).

Two sets of the driving point mobility functions of the CFFF plate which correspond to cases C-1 (i.e. $\eta = 0.005$) and C-2 (i.e. $\eta = 0.1$) of table 10.1 were used for the coupling analysis. Comparisons of the moduli and phases of the transmitted force and moment between the uniform beam and the lumped mass models are shown in figures 10.12 and 10.13. Figure 10.12 shows the comparisons for the case of CFFF plate loss

factor equal to 0.005, and figure 10.13 is for loss factor equal to 0.1.

It can be seen that the transmitted force and moment maintain the correct amplitude and phase only at low frequencies of up to 80Hz. Above 80Hz, the amplitude and phase are significantly affected by resonance responses of the CFFF plate and the force and moment seating. The resonance peak due to the fundamental flexural mode of vibration of the force and moment seating at a frequency of 325Hz is clearly shown in the spectra for the case of uniform beam model. Increase the damping of the CFFF plate does not reduce this resonance peak significantly.

b. Effects on the Resultant Vibrational Power Input

In addition to the above combinations of CFFF plate parameters (i.e. loss factor = 0.005 and 0.1), the uniform beam and the lumped mass models for the force and moment seating, the study of the effects of force and moment seating resonances on the resultant vibrational power input to the CFFF plate has also been carried out for two additional thicknesses of the seating. These thicknesses were 0.0508m (2in) and 0.0254m (1in), which correspond to the fundamental resonance frequency of the seating at 175.5Hz and 87.7Hz respectively. For these two thicknesses, only the driving point mobility functions of the CFFF plate with loss factor of 0.1 were used in the analysis.

Comparisons of the resultant vibrational power input to the CFFF plate for both the uniform beam and the lumped mass models with those obtained from the idealised model (i.e. without considering the mass and inertia effects of the force and moment seating) are shown in figures 10.14 and 10.15. Figure 10.14(a) shows the comparison of P_{force} (without the force and moment seating) and P_{total} (with the force and moment seating) for the case of CFFF plate with 0.005 loss factor. Figures 10.14(b), (c) and (d) are for CFFF plate with 0.1 loss factor and for the force and moment seating thicknesses of 0.1016m (4in), 0.0508m (2in) and 0.0254m (1in) respectively. Figures 10.15(a) to (d) are the similar set of plots but with a linear frequency scale from 0 to 200Hz. In these plots, the differences between the P_{force} and P_{total} spectra are the power reduction due to the cancellation effect.

It can be seen that the resonance response of the force and moment seating has negated the cancellation effect provided by the seating, as would be expected. The worst case was when the resonance occurred at a frequency of 87.7Hz, as shown in figures 10.14(d) and 10.15(d), where the reduction in the vibrational power at 60Hz was

overcome by the resonance response of the force and moment seating. For a 0.0508m (2in) thick seating, where the resonance response is at 175.5Hz, as shown in figures 10.14(c) and 10.15(c), there is a small reduction in the cancellation effect. However, for a 0.1016m (4in) thick seating, the reduction in the cancellation effect is not significant.

This comparative study suggests that in order to maintain the cancellation effect of the vibrational power components from a force and moment seating, the fundamental resonance frequency of the seating should be at least three times higher than the frequency of interest. The fundamental resonance frequency of a force and moment seating can also be raised by reducing the length of the moment arm but with a sacrifice of the power reduction, as the moment arm is no longer at its optimal value. A compromise may have to be made, in practice, among the length of moment arms, the flexural rigidity (i.e. the fundamental resonance frequency) of the seatings, the physical constraints on the seatings and the amount of power reduction achieved.

The effect of a damping treatment on the force and moment seating on the cancellation effect has also been studied. Figure 10.16 shows the comparison of P_{total} for two loss factors of the force and moment seating : η = 0.005 and 0.1, based on the uniform beam model. The P_{force} and P_{total} spectra from the idealised model were also included for comparison purposes. It can be seen that although the added damping has reduced the resonance response of the force and moment seating, the cancellation effect at 60Hz remains unchanged. Hence, if the above design criterion for force and moment seating resonance frequency is fulfilled, additional damping on the seating does not improve the cancellation effect.

10.5 SIMPLIFIED DESIGN FORMULA

10.5.1 Rectangular Plates with a Pair of Free Edges

For rectangular plates with a pair of free edges, such as the CFFF and CFSF plates, it has been noticed that the fundamental flexural mode shape of the plates is similar to that of a uniform beam having the boundary conditions of the other pair of edges (i..e C-F or C-SS boundary conditions). Furthermore, if the mounting locations are close to the central line parallel to the pair of free edges, the contributions from two of the three coupling mobility functions, such as Y_{21} and Y_{32} are small (see Section 10.3). Hence, if the fundamental unbalance frequency of a rotating machine is close to the fundamental resonance frequency of the seating plate, then as a first approximation, the

expressions for the optimal moment arms, eqns. (8.22) and (8.23) can be simplified to:

$$a_{x,opt} \approx \frac{Re\{Y_{31}\}}{Re\{Y_{33}\}} \tag{10.10}$$

$$a_{y,opt} \approx 0 \tag{10.11}$$

The real parts of the mobility functions : $Re\{Y_{31}\}$ and $Re\{Y_{33}\}$ can be approximated by those of a unit width (i.e. 1m) uniform beam having the same thickness, length and the appropriate boundary conditions.

Comparisons of the real parts of the force, moment and coupling mobility functions between a CFFF plate of case C-1 dimensions (table 10.1) and an equivalent unit width cantilevered beam are shown in figures 10.17(a), (b) and (c) respectively. It can be seen that other than a slight difference in the fundmental resonance frequencies, the real parts of the mobility functions below and around the fundamental resonance frequencies are very close to each other, which supports the approximation formula given above. The third resonance peak of the CFFF plate is mainly contributed by the second free-free flexural mode governed by the pair of free edges. The real part of the coupling mobility function of the plate is negative due to the sign conventions and has been multiplied by –1.0 for comparison purposes.

10.5.2 Expressions from Elastic Deflection of Beams

For a constrained structure, such as a cantilevered beam or a CFFF plate, the driving point mobility functions are stiffness controlled or spring-like in nature (i.e. increase with increasing frequency) for frequencies well below the fundamental resonance frequency. If a machine is operating at a speed well below the fundamental resonance frequency of the receiver (seating structure), which follows common engineering practice, then a further simplification can be obtained by estimating these dynamic stiffnesses from the theory of Elastic Deflection of Beams.

From the elementary theory of Strength of Materials [53,54], the static deflection and angular rotation of a beam at a specific point along the beam depend on the type of loading and the geometric and material properties of the beam. The elastic deflection and rotation can be obtained from the knowledge of the resulting bending moment diagram.

For a uniform cantilevered beam of length, L, subjected to a concentrated force, F, at a distance, d, from the fixed end, the equations for the deflection curve can be shown to be :

$$w(x) = \frac{1}{EI}\left[\frac{F}{6}(d-x)^3 + \frac{F d^2}{2}x - \frac{F d^3}{6}\right] \quad \text{for } 0 < x < d;$$

$$w(x) = \frac{1}{EI}\left[\frac{F d^2}{2}x - \frac{F d^3}{6}\right] \quad \text{for } d < x < L \qquad (10.12)$$

For a concentrated couple or moment, M, acting at a distance, d, the equations for the deflection curve are :

$$w(x) = \frac{1}{EI}\left[-\frac{M x^2}{2}\right] \quad \text{for } 0 < x < d;$$

$$w(x) = \frac{1}{EI}\left[-M d x + \frac{M d^2}{2}\right] \quad \text{for } d < x < L \qquad (10.13)$$

The equations for the angular rotation or slope of deflection, θ_y, are obtained by differentiating the deflection curve with respect to the co-ordinate x. For a rectangular plate with the sign conventions as shown in figure 3.1, the relation between the deflection, w, and angular rotation, θ_y, has been defined in eqn. (3.25).

The static translational stiffness or the reciprocal of the deflection per unit force at a point very close to the loading point (i.e. x is smaller but very close to d) can be obtained by substituting $x \approx d$ in the first equation of eqn. (10.12). (Note that beam deflection at the point of loading is not defined as the bending moment diagram is discontinuous at this point.) Similar comments apply to the deflection per unit moment and the angular rotation per unit force or moment. These static translational and rotational stiffnesses and the 'coupling' stiffness are given as follows :

$$K_{t,stat} = \left[\frac{w}{F}\right]^{-1} = \left[\frac{d^3}{3EI}\right]^{-1} \qquad (10.14)$$

$$K_{r,stat} = \left[\frac{\theta_y}{M}\right]^{-1} = \left[\frac{d}{EI}\right]^{-1} \qquad (10.15)$$

$$K_{c,stat} = \left[\frac{\theta_y}{F}\right]^{-1} = \left[\frac{w}{M}\right]^{-1} = \left[-\frac{d^2}{2EI}\right]^{-1} \qquad (10.16)$$

where the subscripts t, r and c denote the translational, rotational and coupling stiffnesses respectively. The complex static stiffnesses can be obtained by replacing the Young' Modulus, E, by its complex form.

The reciprocal of these complex stiffnesses for a cantilevered beam of dimensions : 0.9144m (3ft) length x 1m width and 0.1016m (4in) thick and a loss factor of 0.005 have been calculated for a point close to a location which is nine-tenths of the length from the clamped end. Comparisons of the equivalent of the real parts of these translational, rotational and coupling compliances (reciprocal of stiffnesses) with the real parts of the driving point force, moment and coupling mobility funcitons of the CFFF plate and a unit width cantilevered beam are shown in figures 10.18 (a), (b) and (c) respectively. It can be seen that these static values are in good agreement with the mobility functions for frequencies well below the fundamental resonance frequency of the plate and beam.

Hence, by substituting the equivalent static values for the real parts of the coupling and moment mobility functions as given in eqns. (10.16) and (10.15) into eqn. (10.10), one obtains the simplified design formula for the optimal moment arm for frequencies within the stiffness controlled region as :

$$a_{x,opt} = -0.5\,d \tag{10.17}$$

where d is the distance of the excitation point from the clamped end.

For a cantilevered beam having a length of 0.9144m (3ft) and at a location of nine-tenths of the length from the clamped end, the optimal moment arm, based on eqn. (10.17) is –0.41m, which is numerically 16% smaller than the optimal value of –0.49m at 60Hz. However, the agreement will be closer if the frequency of interest is further away from the fundamental resonance frequency of the seating plate, as shown in figures 10.18 (b) and (c).

For beams and plates with other boundary conditions, simplified design formulae for the optimal moment arm within the stiffness controlled region can be similarly derived from the deflection curves of elastic beams with appropriate boundary conditions.

10.6 SUMMARY

The analyses described in this chapter attempt to answer many practical questions which are of great interest to designers. In particular, the effects on the optimal moment arms and the reduction in the vibrational power components input to the receiver caused by additional damping treatment, the change in flexural rigidity of the receiver and the variation of the mounting locations on the receiver have been analysed. The adverse effect due to resonances of the force and moment seating has also been investigated. It is proposed that the fundamental resonance frequency of the force and moment seating should be at least three times higher than the frequency of interest (i.e. the fundamental unbalance frequency of the machine). Finally, simplified design formulae for the optimal moment arms have been obtained for frequency ranges well below and also around the fundamental resonance frequency of the seating structures, which are plate-like and having a pair of free edges.

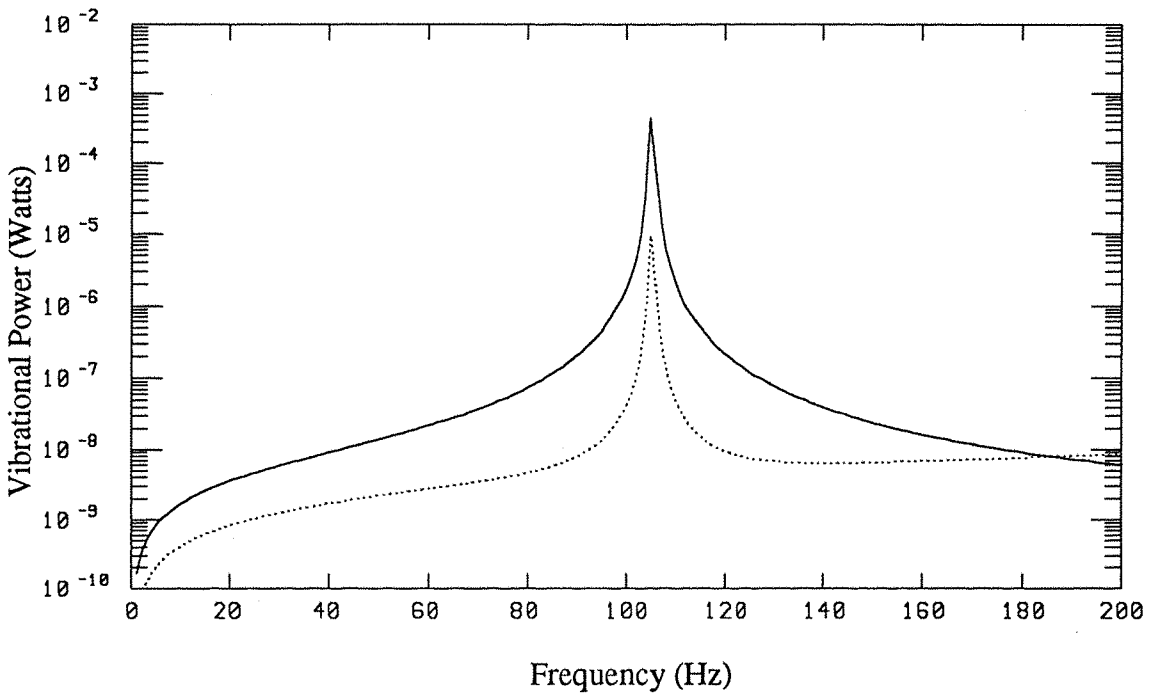

Figure 10.2 : Comparison of P_{force} (———) and P_{total} (·····) for the CFFF plate with excitations at an location of $x_0 = 0.9a$ and $y_0 = 0.5b$, moment arms : $a_x = -0.49$m, $a_y = 0$, force amplitude = 1N, loss factor = 0.005.

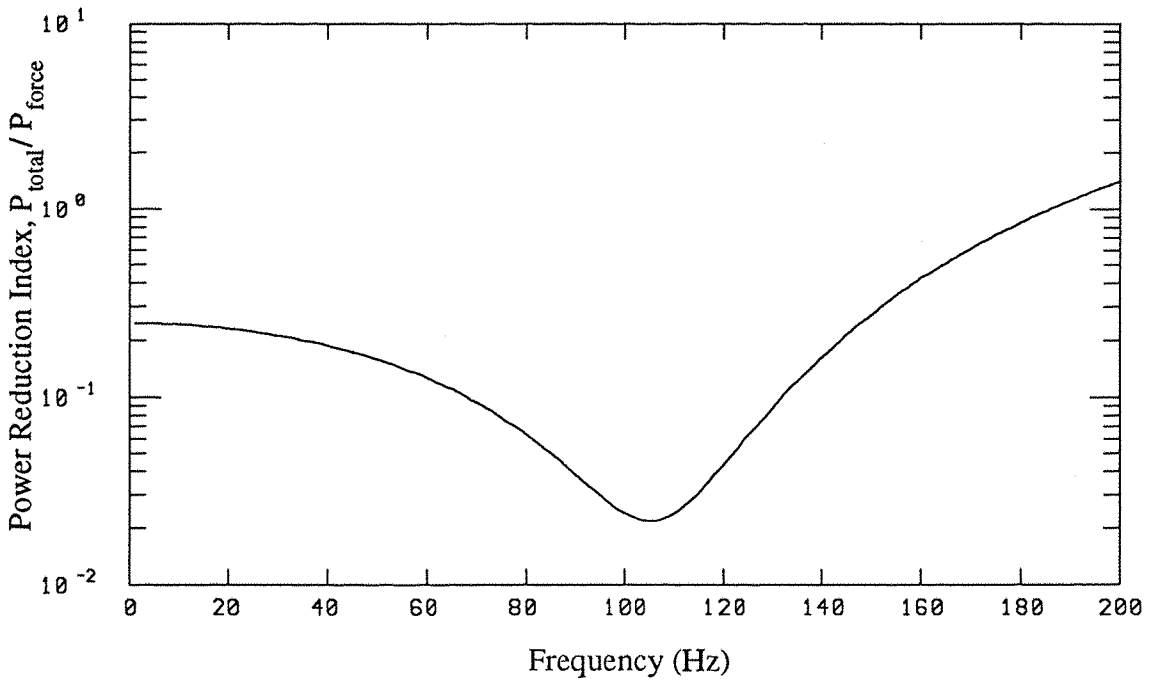

Figure 10.3 : Predicted power reduction index spectrum for the corresponding CFFF plate in figure 10.2.

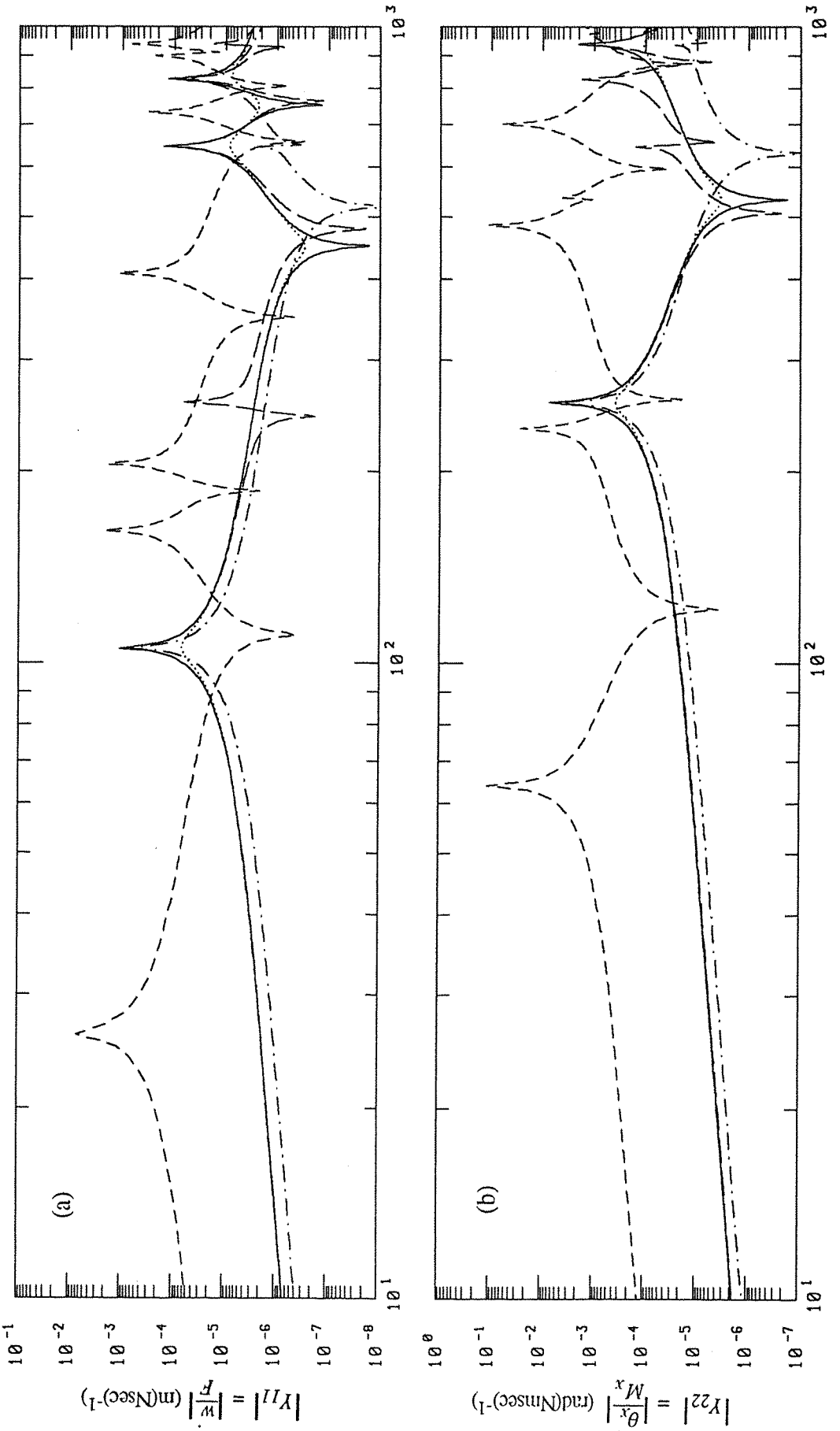

Figure 10.4 : Comparisons of the modulus spectra of the driving point mobility functions for the CFFF plate with various parameters as shown in table 10.1: ——— case C-1, ... case C-2, - - - - - case C-3, —·—·— case C-4 and — — — case C-5.

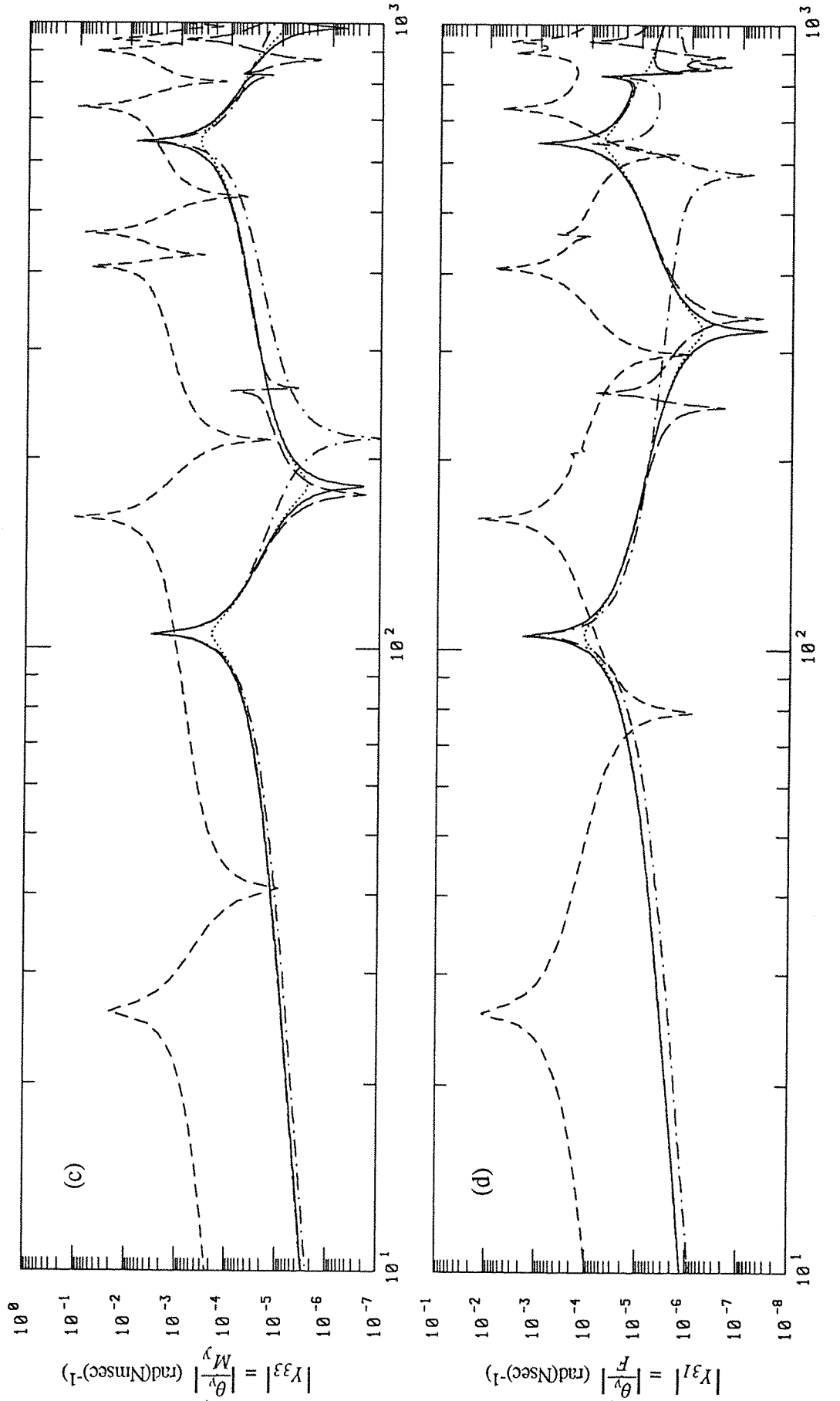

Figure 10.4 (contd.): Comparisons of the modulus spectra of the driving point mobility functions for the CFFF plate with various parameters as shown in table 10.1: ——— case C-1, ····· case C-2, - - - - case C-3, —·—·— case C-4 and ——— case C-5.

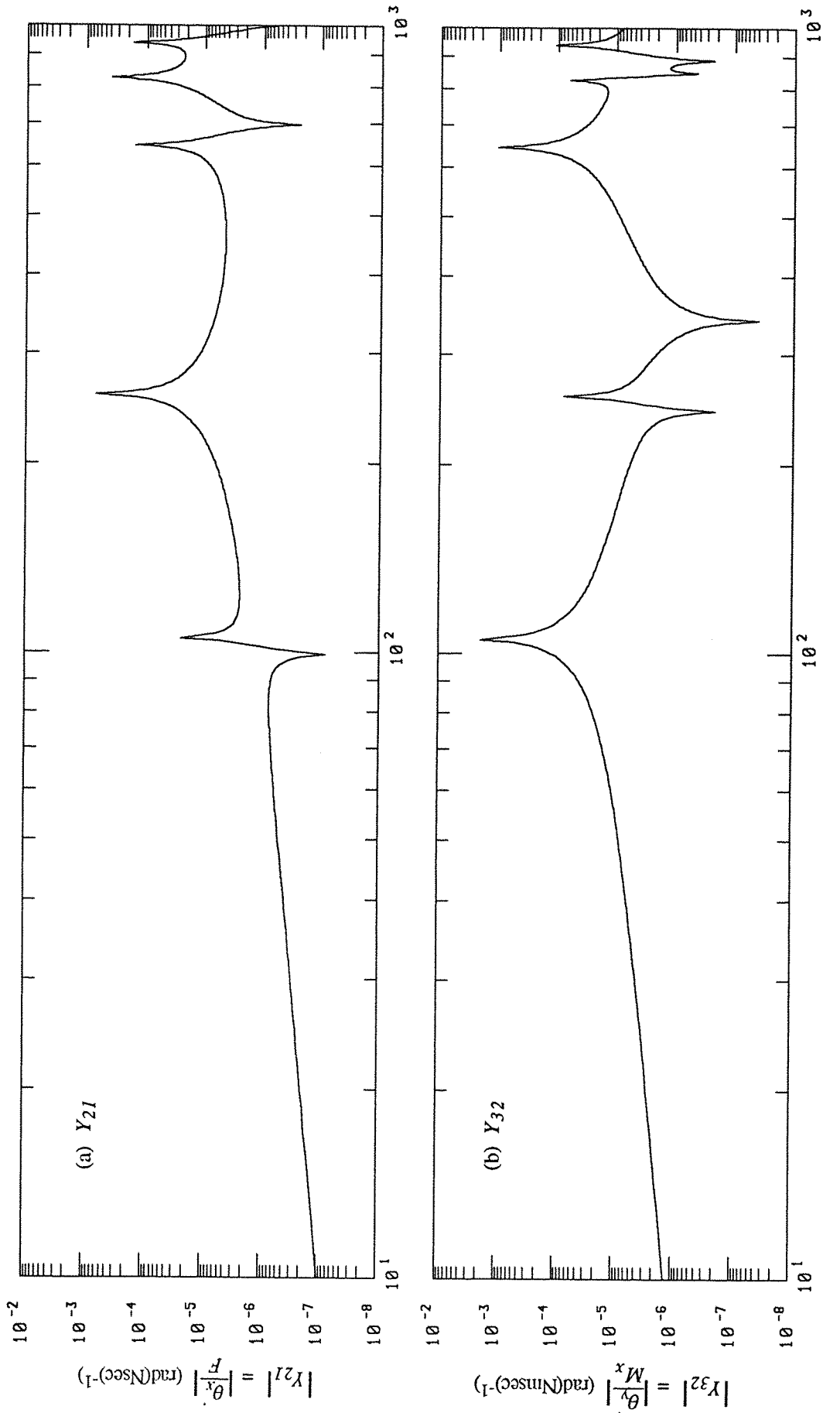

Figure 10.5 : Modulus spectra of the driving point coupling mobility functions for the CFFF plate with excitations at an off-centre location : $x_0 = 0.9a, y_0 = 0.4b$ (case C-5) : (a) : Y_{21} , (b) : Y_{32} .

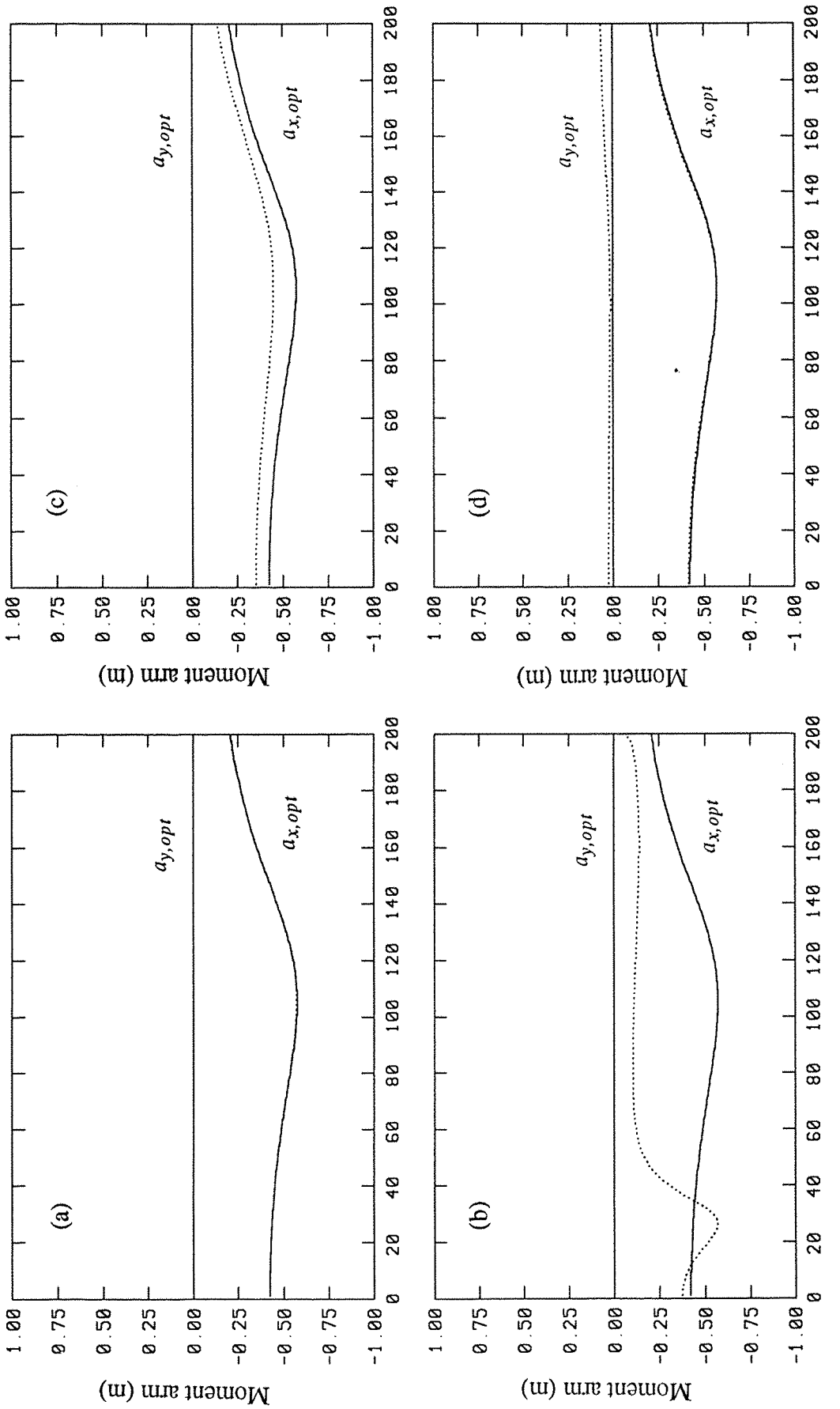

Figure 10.6 : Comparisons of the optimal moment arm spectra for various sets of CFFF plate parameters as shown in table 10.1 :
——— case C-1, ... various cases : (a) : C-2, (b) : C-3, (c) : C-4 and (d) : C-5.

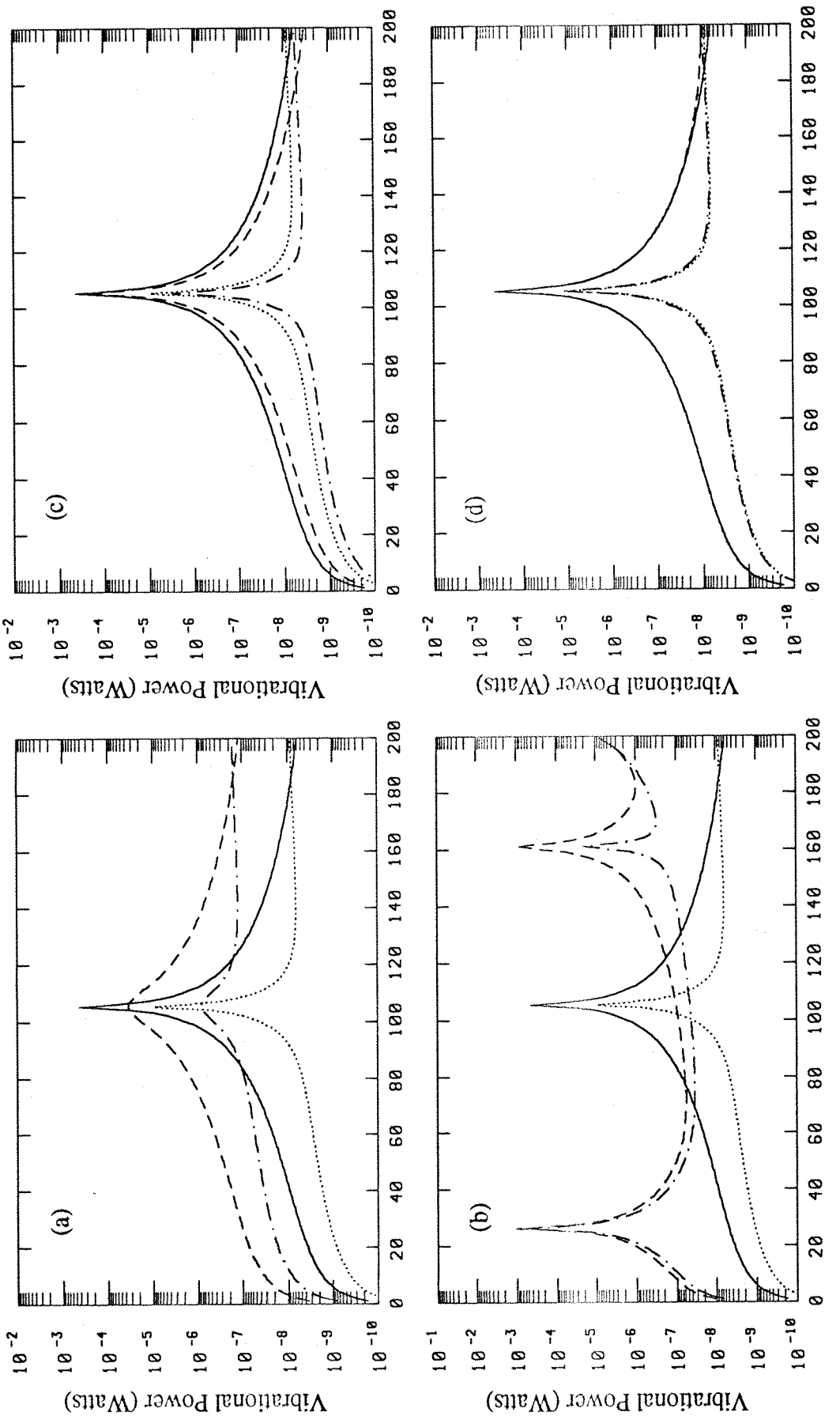

Figure 10.7 : Comparisons of P_{force} and P_{total} for various sets of CFFF plate parameters as shown in table 10.1 : ——— P_{force} and ..... P_{total} of case C-1, - - - - P_{force} and —·—·— P_{total} of various cases : (a) : C-2, (b) : C-3, (c) : C-4 and (d) : C-5.

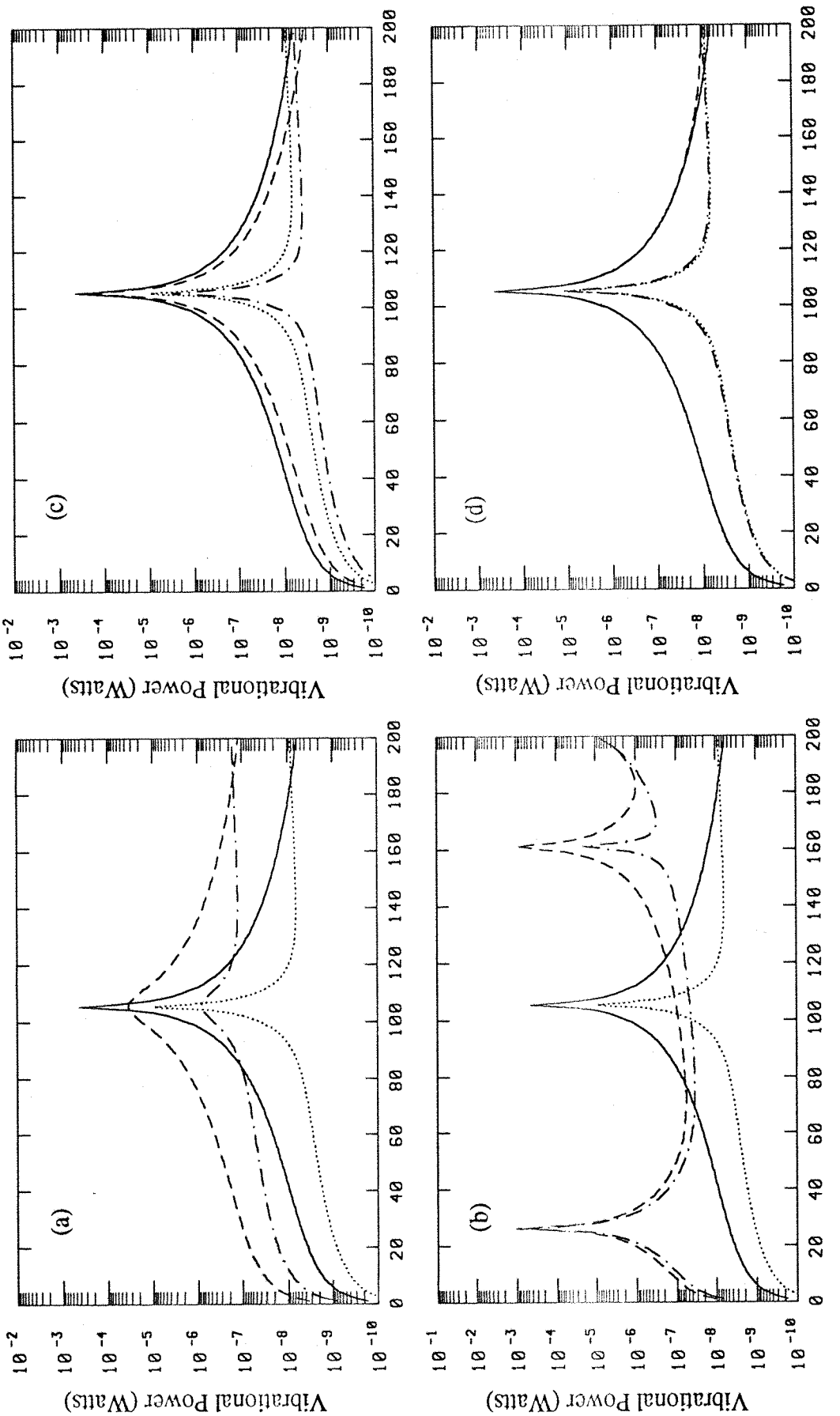

Figure 10.7 : Comparisons of P_{force} and P_{total} for various sets of CFFF plate parameters as shown in table 10.1 : ——— P_{force} and ..... P_{total} of case C-1, - - - - P_{force} and —·—·— P_{total} of various cases : (a) : C-2, (b) : C-3, (c) : C-4 and (d) : C-5.

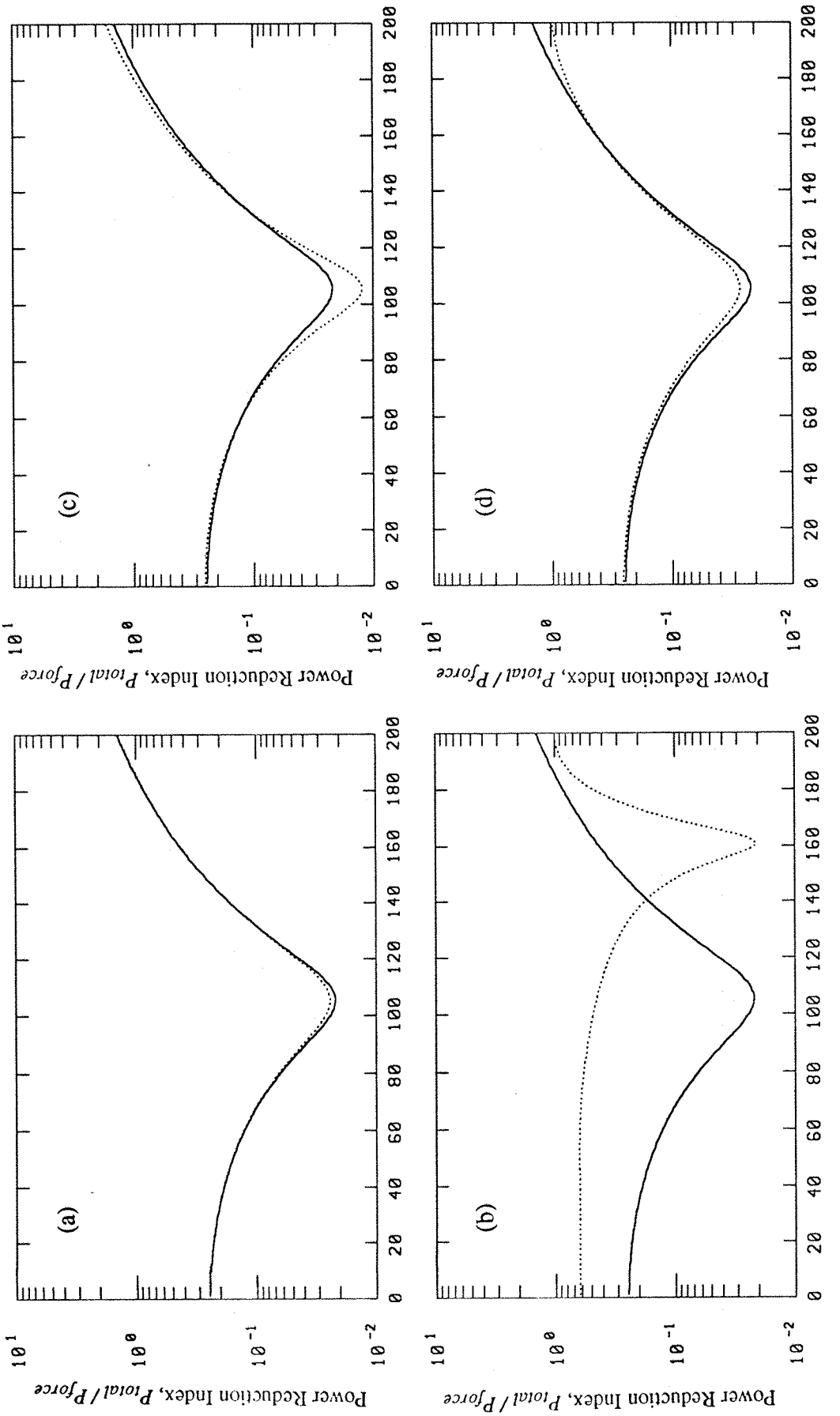

Figure 10.8 : Comparisons of the power reduction index spectra for various sets of CFFF plate parameters as shown in table 10.1 : —— case C-1, ... various cases : (a) : C-2, (b) : C-3, (c) : C-4 and (d) : C-5.

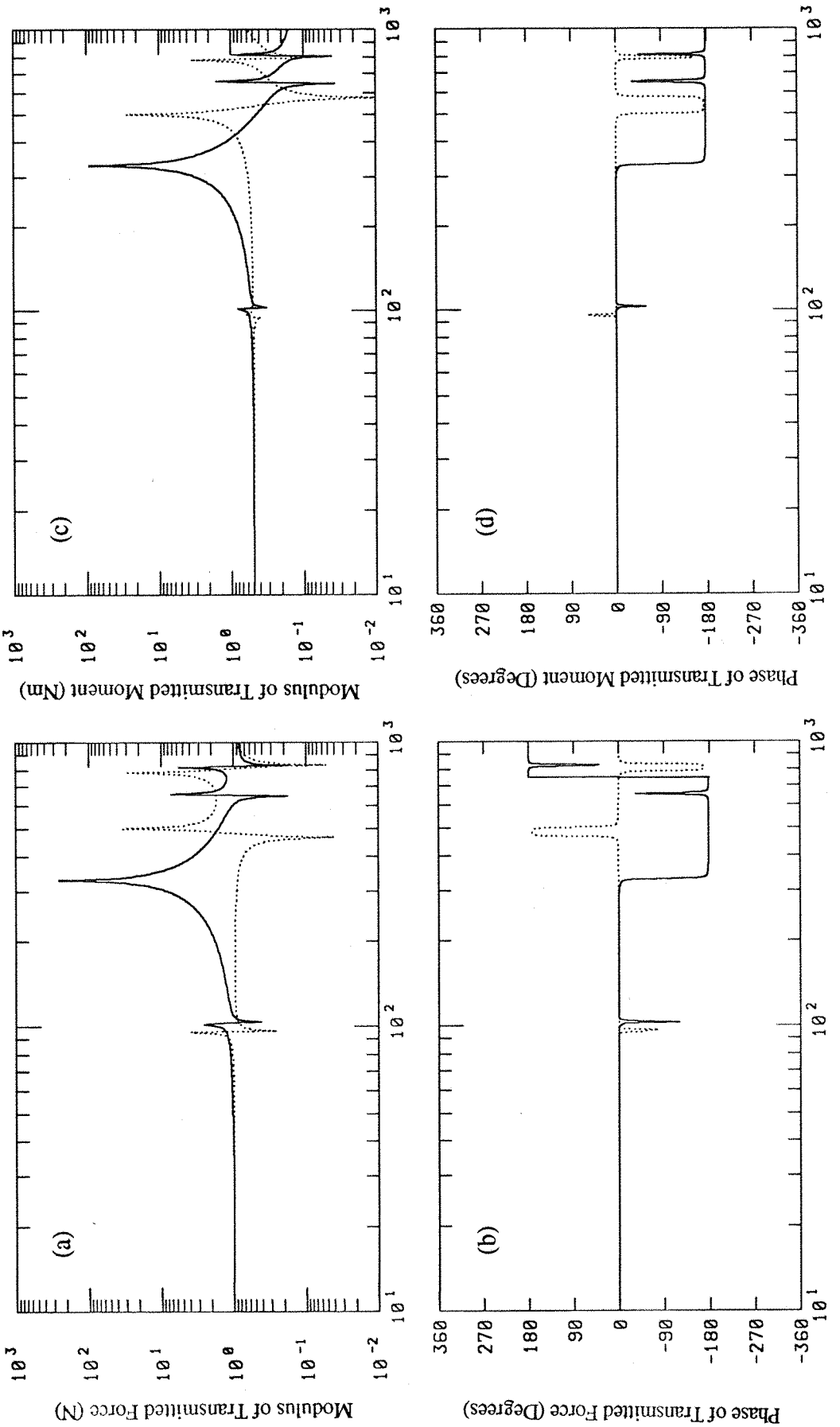

Figure 10.12 : Comparisons of the transmitted force and moment for two different models of the force and moment seating (plate $\eta = 0.005$): ——— uniform beam model, ... lumped mass model : (a) and (b) : transmitted force, (c) and (d) : transmitted moment.

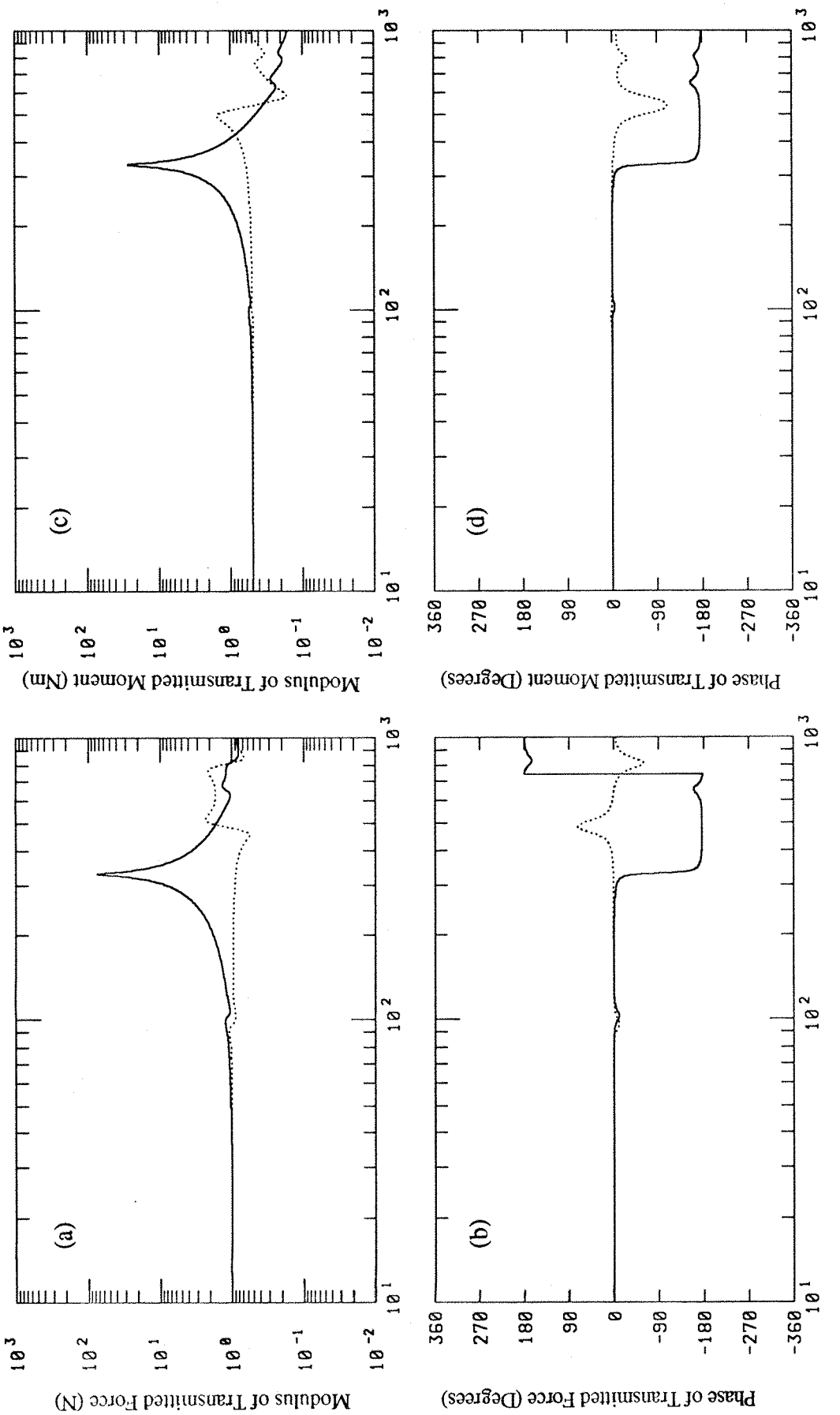

Figure 10.13 : Comparisons of the transmitted force and moment for two different models of the force and moment seating (plate $\eta = 0.1$): ——— uniform beam model, ... lumped mass model : (a) and (b) : transmitted force, (c) and (d) : transmitted moment.

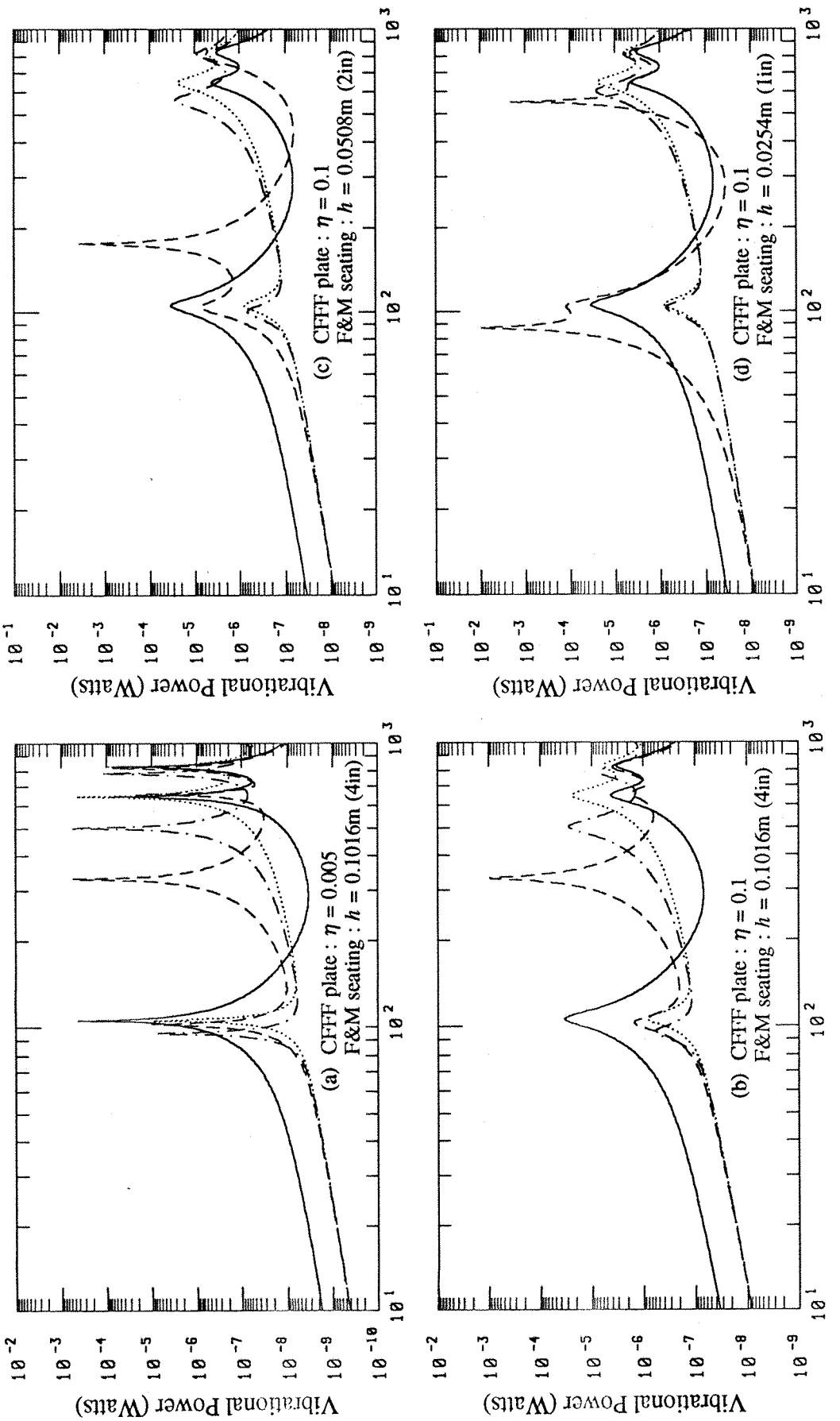

Figure 10.14 : Comparisons of P_{force} and P_{total} for various sets of force and moment seating parameters : ——— P_{force} and ..... P_{total} of the idealised model, - - - - P_{total}, uniform beam model and —·—·— P_{total}, lumped mass model.

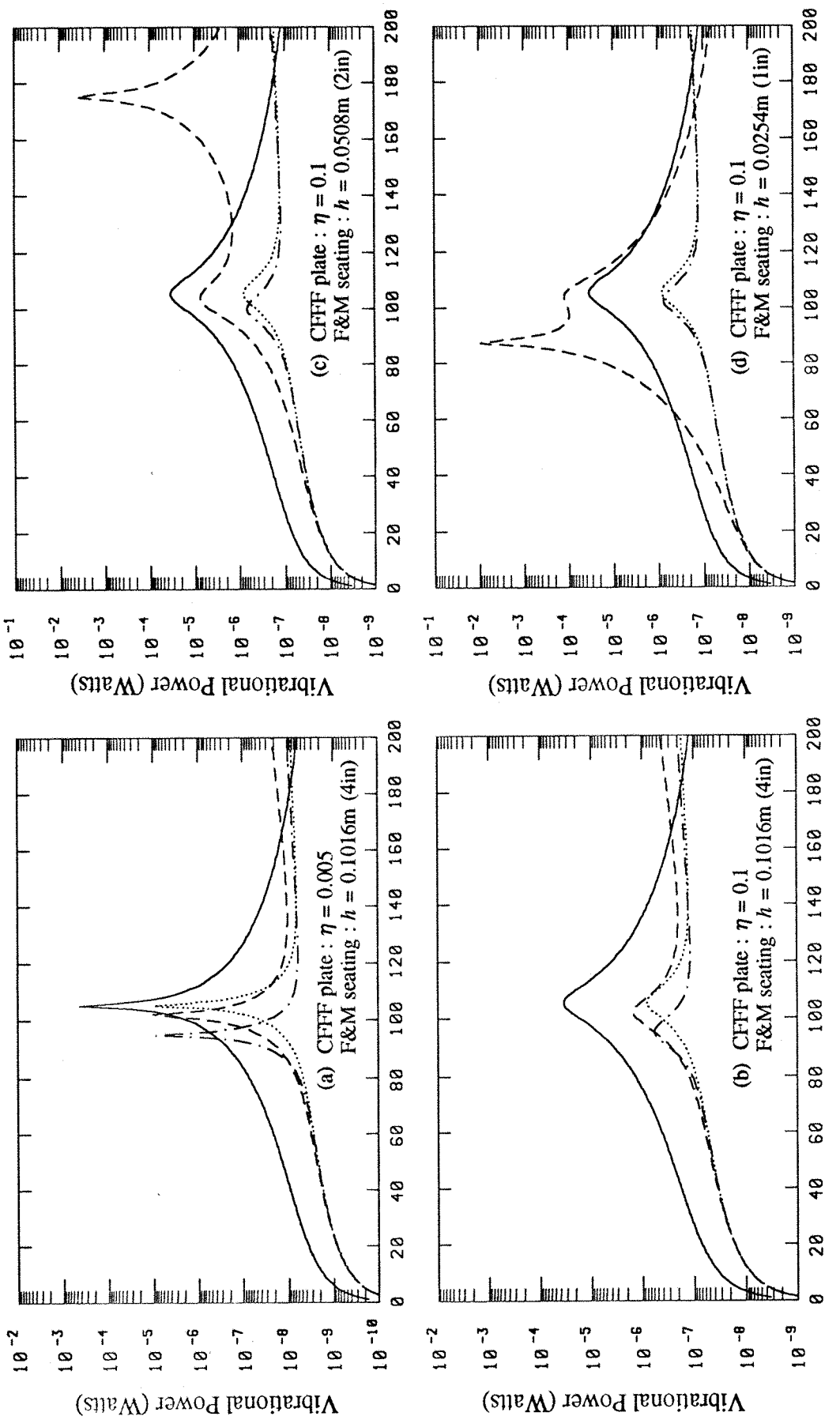

Figure 10.15 : Comparisons of P_{force} and P_{total} for various sets of force and moment seating parameters : ——— P_{force} and ····· P_{total} of the idealised model, - - - - P_{total}, uniform beam model and –·–·– P_{total}, lumped mass model.

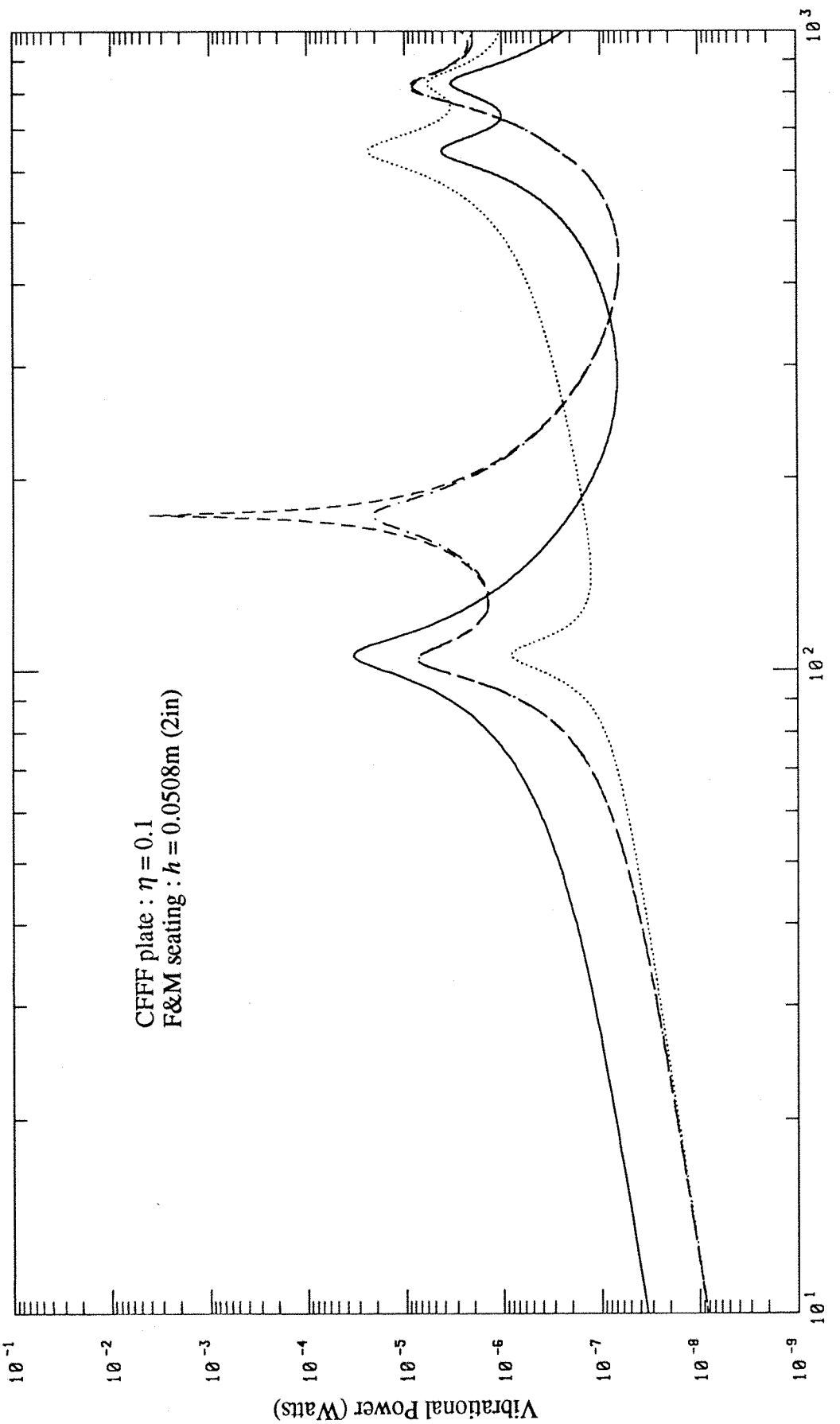

Figure 10.16 : Comparisons of P_{force} and P_{total} for various sets of force and moment seating parameters : ——— P_{force} and ..... P_{total} of the idealised model, - - - - P_{total}, $\eta = 0.005$ and –·–·– P_{total}, $\eta = 0.1$ of the uniform beam model.

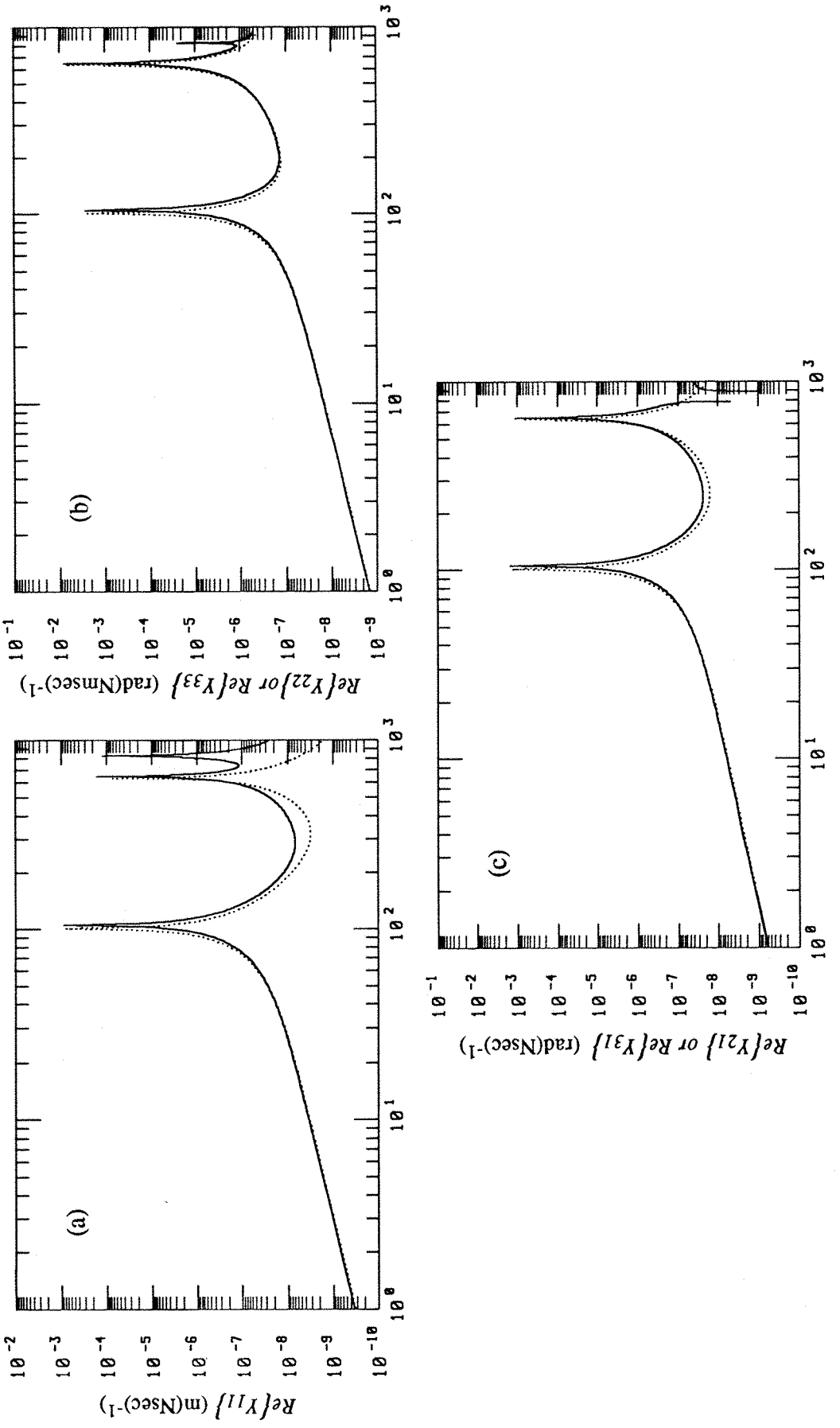

Figure 10.17 : Comparisons of the real parts of the driving point mobility functions between the CFFF plate and a unit width cantilevered beam : ——— CFFF plate, ... C-F beam, (a) : force mobility, (b) : moment mobility and (c) : coupling mobility.

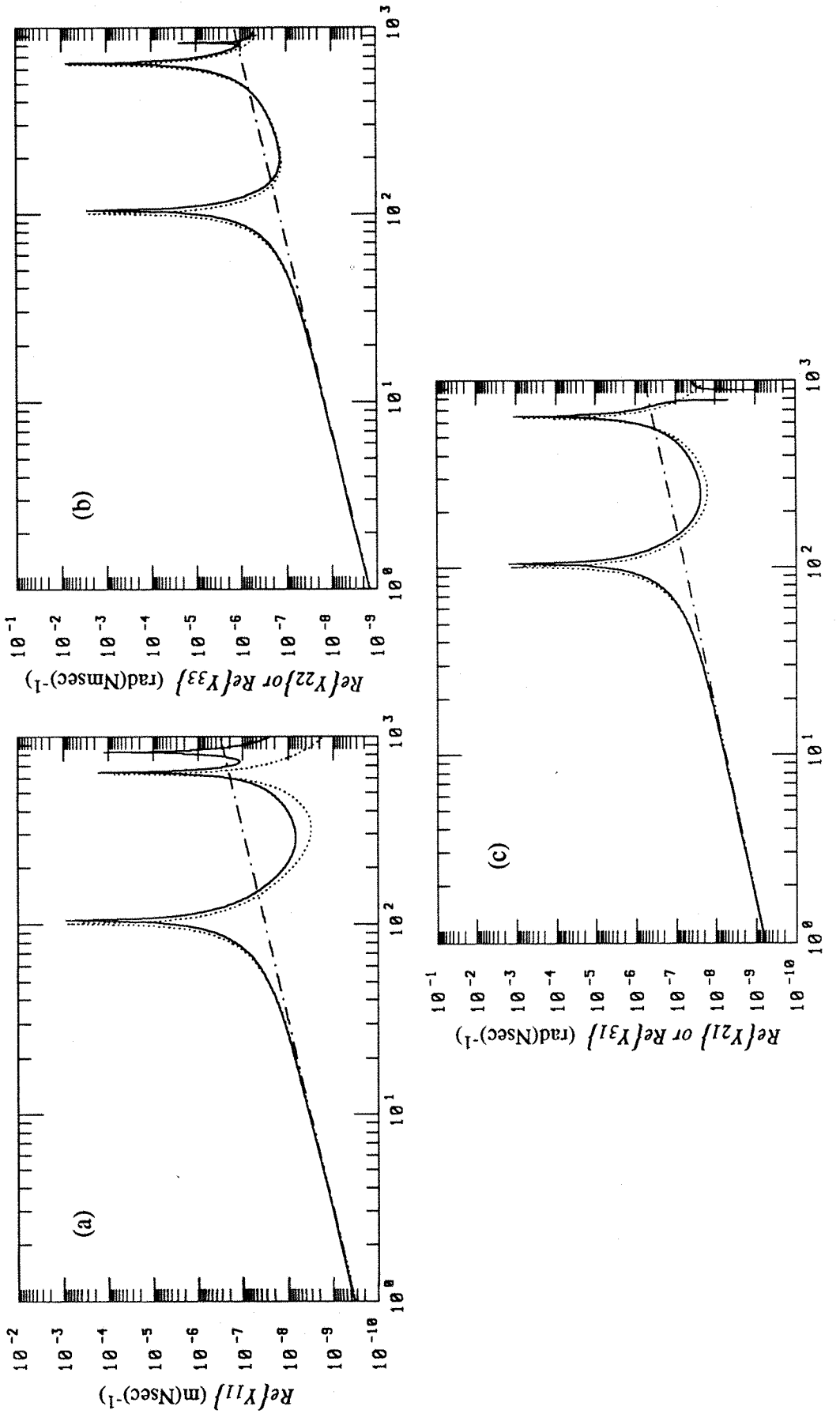

Figure 10.18 : Comparisons of the real parts of the driving point mobility functions : ——— CFFF plate, ... unit width C-F beam, —·—·— equivalent static values, (a) : force mobility, (b) : moment mobility and (c) : coupling mobility.

CHAPTER 11

CONCLUSIONS

The overall objective of this study has been to predict and control vibration transmission from resiliently mounted shipboard machinery to flexible seating structures by using the concept of vibrational power flow. The unifying concept of vibrational power has been identified to be the only approach which can overcome the difficulty arising from incompatible units of the transfer functions when one attempts to compare the effects of multi-directional vibration transmission in a machine isolation system. In order to apply the vibrational power terms for comparison, one needs to know, in general, the applied force and/or moment excitations and the resulting velocity responses at the point of interest on the structure. Alternatively and more appropriately, one needs to know either the excitations or the velocity responses and the driving point mobility functions at the excitation point on the structure which govern the dynamic characteristics of the structure. Hence, a detailed description of the force, moment and coupling mobility functions at the point of interest on the structure is essential in this type of study.

Based on classical theories of beams and rectangular plates in flexural vibration, the driving point force, moment and coupling mobility functions have been derived for beam and plate-like seating structures when subjected to co-located simultaneously acting sinusoidal force and moment excitations, i.e. for a multi-excitation system. The vibrational power components input to these seating structures resulting from the applied force excitation and the translational motion or the moment excitation and the rotational motion or in particular, the contribution from the couplings between these components for a multi-excitation system were investigated in detailed. The problem of vibration transmission between a multi-point mounted flexible source - isolator - receiver system has also been studied in terms of the vibrational power input, transmitted and dissipated in the structures using the mobility coupling approach. From study of the vibrational power components resulting from a multi-excitation system, various novel vibration control schemes, both active and passive approaches, based on minimisation of the resultant vibrational power input to the seating structures were then proposed and evaluated. The procedures for a passive approach to vibration control of a rotating machine installation with a predominant excitation at low frequency mounted on a flexible seating structure were evaluated in detail, as the passive approach is a

more robust and less expensive than the active approach to vibration control. Several laboratory scale experimental measurements were conducted to validate the theoretical predictions. The experimental results, in general, are in good agreement with the theoretical predictions. The optimal moment arm concept for the reduction of vibration levels by combined force and moment excitations was validated experimentally. The reduction of the vibrational response around the fundamental resonance frequency of a rectangular plate seating structure caused by unbalanced motor excitations was also demonstrated. The main findings and conclusions from this study are given in the following sections. It should be noted that although the study was carried out in relation to shipboard machinery installations,the results are applicable to machinery installations generally.

The Use of Vibrational Power for Vibration Studies : The advantages of applying the unifying concept of time-averaged vibrational power to study the problem of multi-directional vibration transmission in a machine isolation system have been demonstrated. The common unit of power (in Watts) facilitates comparison of the vibrational powers resulting from the translational and the rotational motions as well as the coupling between these motions for a multi-excitation system. It is from this analysis that cancellation of vibrational power components resulting from the coupling mobility functions for finite beam and rectangular plate seating structures subjected to simultaneously acting force and moment excitations is obvious.This result subsequently leads to the development of a novel approach to vibration control and hence the reduction of unwanted machine-induced vibration levels on flexible seating structures, which will be discussed in more detail later.

Vibrational power, being a single quantity which embodies both the force and velocity at the point of concern on the structure, offers a better insight into the study of vibration transmission in a machine isolation system. It is not just the transmitted force or the transmitted velocity is of concern but rather the transmitted force and the resulting velocity response are combined in the vibrational power transmitted to the isolators and the seating structure. The classical force transmissibility or motion transmissibility approach to vibration study is conventionally applied to a single degree-of-freedom system. For a multi-directional, multi-excitation, source-isolator-receiver system, couplings between different degrees-of-freedom of the system occur and the concept of vibrational power transmissibility appears to be the only means to compare these coupling effects, such as the transmitted force resulting from an applied moment excitation component. This vibrational power transmissibility concept remains to be a subject of interest for further study.

In the study of vibration transmission between a coupled system (Chapters 6 and 7), the theoretical model and practical system investigated consisted of a flexible source structure (a free-free beam) mounted on four resilient isolators and attached to a flexible receiver structure (a rectangular plate). The dynamic transfer properties (four-pole parameters) of the isolators, which were obtained experimentally and modelled either as a 'Long Rod' longitudinal vibration model or a massless damped spring model, were used to couple the driving point and transfer mobility functions of the source beam and the receiver plate at the mounting points. The measured dynamic stiffnesses and loss factors of the rubber isolators were found to increase slightly with increasing frequency. These frequency dependent characteristic were incorporated in the analyses by means of Least Squares straight line relationships. The dynamic stiffness and loss factor of the resilient isolators, as would be expected, were found to have significant influences on the vibrational power input, transmission and dissipation in the coupled structures. The smaller the stiffness and the greater the loss factor of the isolators, the larger is the power dissipation in the isolators, hence, resulting in smaller vibrational power transmitted to the receiver. However, 'wave effects' or longitudinal resonances in the isolators increase the power transmitted to the receiver. In the low frequency region where it was dominated by the translational rigid body motion of the source beam, the total power transmitted to the isolators was the same as the power input to the source beam. However, in the high frequency region, dominated by flexural vibration of the source beam, a small amount of power was dissipated in the beam due to internal losses (damping) before transmission to the resilient mounts.The 'velocity source' response characteristic at high frequencies exhibited by the source beam was attributed to a relatively large mobility (or impedance) mismatch between the source beam mounting points and the resilient isolators. However, one has to realise that in many practical situations, machines are large and heavy and the mounting flanges of machines can be relatively 'soft' at high frequencies; the 'velocity source' concept is strictly not applicable to such situations. The vibrational power spectra of different mounting points consist of positive and negative values. Negative power occurs when the transmitted force and the resulting velocity response are in anti-phase, which in this study corresponds to power flow from the supporting plate to the resilient mounts. This confirms past experimental results obtained by other researchers that for multiple point mounted machines, circulation of vibrational power may occur among the mounting points due to the phase relationships between the transmitted force and the resulting velocity response at different mounting points, a phenomenon which is not easily accounted for by conventional transmissibility analysis.

The vibrational power transmitted to the resilient mounts via the rotational motion and bending moment resulting from flexural vibration of the source beam was investigated for two specific cases of a unit sinusoidal vertical force excitation : one applied at the centre of the beam and the other at a distance of approximately one-ninth of the beam length from the beam centre. In these two cases, the rotational vibrational power is much smaller than the power transmitted via the translational motion and shear force, except for the second case where the rocking motion of the source beam dominates at low frequencies. However, these two cases studied are too restrictive to arrive at a general conclusion of whether or not the rotational motion can be neglected compared with the translational motion in a machine isolation system. More combinations of force and moment excitations must be investigated before one can arrive at general conclusions. Nevertheless, the present study provides the basis for more general further study. As the number of component mobility data files increase rapidly with the number of multi-directional excitations as well as the number of degrees-of-freedom required, one essential task is to develop a more efficient way of handling a large set of input data files.

In Chapter 7, expressions for measuring the input and transmitted vibrational powers between the coupled structures based on the measured mobility functions and the spectral density function of the applied random force excitation were derived. With the definition of a scaling spectrum, the measured powers resulting from random force excitation, compared favourably with the theoretically calculated vibrational powers based on a point harmonic force excitation. The measurements conducted in this study and many other power flow or structural intensity measurements have shown that the real part of the driving point mobility functions plays a vital role in the accuracy of the measured vibrational power. For lightly damped structures, the real parts of the driving point mobility functions are very small. The low response levels of structures around anti-resonance frequencies are very sensitive to phase mismatch in the measuring instruments. In spite of the fact that significant advances have been achieved in the development of signal processing software and experimental instrumentation over the past two decades, the problem of phase mismatch in modern measuring instruments still remains to be a challenging problem for experimentalists. Hence, the development of a 'perfect' phase matched system is essential for wider applications of vibrational power techniques in practical measurements.

Contributions from the Coupling Mobility Functions : For finite beams and rectangular plates subjected to co-located simultaneously acting sinusoidal force and moment excitations, the driving point coupling mobility functions always exist, except for the

special situation when the excitation location coincides with a point of mode shape symmetry for beams and plates with symmetric boundary conditions, which corresponds to a condition of decoupling between the different degrees-of-freedom concerned. Eichler [55] in his work on the admittances (i.e. the driving point mobility functions) of a semi-infinite plate bounded by a straight edge and excited harmonically by simultaneously acting force and moment excitations at the edge also came to the conclusion that the transverse translation and the tangential rotation about an axis parallel to the plate edge were coupled with each other. However, there is no such coupling for an infinite plate, i.e. coupling mobility functions do not exist for an infinite plate subjected to simultaneously acting force and moment excitations. The physical explanation for the existence of the driving point coupling mobility functions is that for beams and plates in flexural vibration caused by simultaneously acting force and moment excitations, the resulting translational response at the excitation point is partly due to the force excitation and partly due to the moment excitation. The part resulting from the moment excitation constitutes the coupling mobility function. Similar observations can be made concerning the resulting rotational response due to the simultaneously acting force excitation. However, one has to caution that these coupling mobility functions cannot exist on their own, which means that a point force excitation acting on a linear structure will not result in a rotational motion without translational motion in the direction of the force. This remark also applies to a point moment excitation and the resulting translational motion without rotational motion.

For those situations when the driving point coupling mobility functions exist, they contribute to vibrational power components input to the structures as importantly as the direct force and/or moment mobility functions. The real parts of the driving point force and moment mobility functions of linear structures are always positive, but the real parts of the driving point coupling mobility functions can be positive or negative depending on the particular mode shapes. Hence, for positive force and moment excitations, negative real parts of the coupling mobility functions give rise to cancellation of vibrational power components input to the structures. This cancellation effect forms the basis of the novel vibration control technique proposed and investigated in this study. The cancellation effect can be explained physically that for the case of simultaneously acting force and moment excitations acting on an undamped semi-infinite beam, the propagating waves induced by the force and moment excitations, respectively, are equal in magnitude but opposite in phase, hence resulting in a complete cancellation of the propagating waves. For damped finite structures, it can be visualised that the driving point displacement caused by the force excitation is

counter-acted upon by the displacement caused by the moment excitation, hence the nett displacement is smaller than the displacement caused by the force alone.

The analytical results show that the high frequency trends of the real parts of force and moment mobility functions of beams and plates are in good agreement with the corresponding mobility functions obtained from the 'equivalent' infinite structures. Increase in hysteretic loss factor (i.e. internal damping) of the structures clearly demonstrates the convergence of the real parts of these mobility functions to the infinite structure values. The physical explanation is that for highly damped finite structures, the flexural waves propagating from the excitation point are being heavily attenuated before reaching the boundaries, and in the limits, virtually no reflected waves are available to form standing waves, which is the physical phenomenon of an infinitely extended structure. The loss factor used in this study was introduced through the complex Modulus of Elasticity, which according to Cremer, Heckl and Ungar [24] would facilitate a simple representation of otherwise very complex physical processes associated with damping (i.e. processes in which mechanical energy is converted into heat). One could then argue that by increasing the loss factor of the structure and from the above comparison of the real parts of mobility functions with those of infinite structures, one could model the effect of external dissipation of vibrational energy to surrounding fluid media or sand, as was done by Sun and Richards [56]. Thus the damping model used in this study has practical significance in connection to shipboard structures where external dissipation of energy to surrounding fluid media usually occurs. In this aspect, the assumption of a 'closed system',i.e. no dissipation of energy across the boundaries, in order for the orthogonality relationship to hold, seems to be violated. (The othogonality relationship was used in Chapter 3 to arrive at the expression for forced response of finite systems.) Nevertheless, if external dissipation of vibrational energy to surrounding fluid media can be modelled by an internal loss factor of a system, then the orthogonality relationship is not critically violated.

Vibration Control Applications : The most significant contribution from this study is the development of various vibration control schemes using a multi-excitation system to minimise the resultant vibrational power input to the supporting structure and thus to reduce the unwanted machine-induced vibration levels on the structure. In particular, the passive approach to vibration control is to attach a set of force and moment seatings with predetermined moment arms to the machine mounting points in order to reduce the predominant vibration component at a specific frequency, such as the fundamental unbalance frequency of a rotating machine, transmitted to the seating structure. Expressions for the optimal moment arms for attachment to beams and rectangular

plates were obtained by minimising the resultant vibrational power input to these structures under a multi-excitation system. For beam-like seating structures, the optimal moment arm can be obtained from the negative ratio of the real part of the driving point force mobility function to the real part of the driving point coupling mobility function (eqn (8.14)). This simple expression enables the optimal moment arm to be obtained from direct measurements for machine seating structures which can be considered to be beam-like in the frequency range of interest (usually in the low frequency range due to low fundamental unbalance frequency of rotating machines). Simplified design formulae for the optimal moment arm in the stiffness controlled region and around the fundamental resonance frequency of seating structures of the plate type with a pair of free edges were also obtained for design-guide purposes (eqns (10.10) and (10.17)). Design sensitivity studies were also performed for the design of the force and moment seating as this type of vibration control procedure has been shown to be possible. It was found that the optimal moment arms and the reduction in the vibrational power components input to the seating structure were relatively insensitive to use of an additional damping treatment on the structure or to slight variation of the position of the mounting points in a practical machinery installation but were affected significantly by changing the flexural rigidity of the seating structure. The adverse effects of force and moment seating resonances have also been investigated. The study showed that the fundamental resonance frequency of the force and moment seating should be at least three times higher than the frequency of interest (such as the fundamental unbalance frequency of a rotating machine) in order to maintain the required reduction of vibrational power input to the seating structure.

The passive approach to vibration control for a specific frequency is most suitable for the case of a low to medium constant speed machine mounted on flexible seating structures. This is because this type of machine usually has predominant excitation associated with the fundamental rotation frequency and the excitation levels associated with the higher harmonics decrease with increasing frequency. The proposed method may not be of benefit at high frequencies because of finite mounting stiffness of the force and moment seating which will inevitably reduce the fundamental resonance frequency of the force and moment seating. Also, the real part of the driving point moment mobility function of supporting structures generally increases with increasing frequency; when combined with machines having dominant high frequency excitation components, will cause large amounts of vibrational power to be injected into the supporting structure at high frequencies. In practice, one may also encounter situations in which the large or highly damped seating structure behaves as an infinite structure in the frequency range of interest. In this condition the coupling mobility function is

known to be very small and the proposed vibration control technique may offer little, if not an adverse, effect on the reduction of vibration transmitted to the seating structure. It is also possible that in the frequency range of interest, vibrational power circulation occurs among the mounting feet of a machine, as the passive vibration control technique is based on power minimisation at each mounting point as if it were independent from the other, the interaction among the mounting points may reduce the benefit offered by the force and moment seating. The theoretical development of the vibration control technique is based on the linearity assumption. In practice, nonlinear behaviour of a machine isolation system may occur which may also affect the effectiveness of the technique. Concerning horizontal force excitation from a machine, which may result in moment excitation at the mounting points on the seating structure, the magnitude of the induced moment excitation will be small if the length of the resilient mount is short, which is in-line with the normal practice of preventing 'wave effects' from occuring in the mounts at low frequencies. For resilient rubber mounts, the shear modulus is typically one-third of the modulus in the axial direction [46], which would help to reduce the transmitted horizontal components to the seating structure.

Various active vibration control schemes using the contribution from the coupling mobility functions resulting from primary simultaneously acting force and moment excitations and a secondary controlled force or moment were analysed theoretically for beam-like seating structures. The potential use of the active schemes did not however receive detailed investigation in this study mainly due to time constraints. This should be explored if further funding is possible. Although the proposed vibration control technique was developed for use in shipboard machinery installations, it is also applicable to general machinery installations in factory workshops or plant rooms and engine mountings in cars, aircraft, etc. The claim of novelty for the passive and active vibration control schemes proposed in this study is for the design procedures of the force and moment seating which have arisen from the study of the vibrational power input to flexible seating structures for a multi-excitation system.

Measurements of Rotational Mobility Functions : These measurements were performed with conventional piezoelectric force transducers and translational accelerometers, the electro-dynamic exciter and the commercially available multi-channel (up to eight channels) spectrum analyser. The moment related (or rotational) mobility functions of a rectangular plate having CFSF boundary conditions were measured via a carbon fibre reinforced plastic rod with one end glued to the plate for inducing moment excitation to the plate. From reciprocity checks for the driving point coupling mobility functions

between the conventional force excitation and this moment excitation arrangements, it can be seen that the approximate method for measuring moment related mobility functions is adequate in the frequency range below the fundamental resonance frequency of the cantilevered rod with end mass. The measured moment mobility modulus spectra were found to be consistently higher than the theoretical results which confirmed the inadequacy of thin-plate theory for prediction of driving point moment mobility functions. The infinite transverse shear modulus assumption underestimated the rotational responses of the plate under the action of a closely spaced force couple. The use of higher order plate theory which includes rotary inertia and finite transverse shear modulus, no doubt, would be of benefit in this type of study, but the greater computational effort may not warrant this because the study carried out made use of the real parts of moment mobility functions which for lightly damped structures are much smaller than the imaginary parts of the functions. The imaginary parts of moment mobility functions relate directly to the local stiffness of the structure and thus suffer more severe consequences from the inadequency of thin-plate theory. Also in practical situations, a force and moment seating with a very small connecting area to the seating structure has little practical significance. Two main difficulties associated with measurements of rotational mobility functions are the measurement of rotational response at low frequencies and the application and measurement of moment excitation. The latter is the most difficult of all mobility function measurements. The rotational responses at low frequencies measured by taking the difference between two closely spaced accelerometer signals is inaccurate due to small differences between the measured signals. The attachment of accelerometers to the test structure may also mass-load the structure and alter the rotational inertia property of the structure, especially for delicate, light weight structures. Hence it is necessary to develop a more robust experimental method for measuring the rotational responses. The use of a pair of laser beams or other non-contacting devices for determination of the rotational responses for delicate, light weight structures is worth exploiting. For moment excitation and measurement, the development of a moment exciter using giant magnetostrictive rods by Petersson [39] is very encouraging. Measurements of moment mobility functions using the moment exciter have also been reported in [57]. Further refinement of the moment exciter should be carried out.

To conclude this chapter, it is proposed that the passive vibration control technique should be applied via a set of force and moment seatings to practical machinery seatings having relatively simple configurations and the possibility should be investigated of developing simplified design-guide formulae for the optimal moment arms of more complicated, practical structures.

REFERENCES

1. White R.G., Chapter 26: Vibration Control II in *Noise and Vibration*, ed. White R.G. and Walker J.G., Ellis Horwood, 1982.
2. Ungar E.E. and Dietrich C.W., *High - frequency Vibration Isolation*, J. Sound and Vib. (1966) 4(2), 224-241.
3. Sykes A.O., *Isolation of Vibration : When Machine and Foundation are Resilient and When Wave Effects Occur in the Mount*, Noise Control, May / June 1960, 23-38.
4. Muster D., *Predicting the Vibratory Interaction between a Simple Substructure and Nonrigid Foundation*, Noise Control, May / June 1961, 39-44.
5. Snowdon J.C., *Resilient Mounting of Machinery on Platelike and Modified Platelike Substructures*, J. Acoust. Soc. Am., 61(4), April 1977, 986-994.
6. Snowdon J.C., *Vibration Isolation : Use and Characterization*, J. Acoust. Soc. Am., 66(5), November 1979, 1245-1274.
7. White R.G. *Vibration Control of Machinery Installations and Structures : Some Design Procedures and Experimental Diagnostic Techniques*, The Institution of Engineers Australia, Vibration and Noise Conference, Melbourne, 18-20 September 1990, 1-9.
8. Petersson B.A.T. & Gibbs B.M., *The Influence of Source Location with Respect to Vibrational Energy Transmission*, International Congress on Intensity Techniques, CETIM, Senlis (France) 27-29 August 1990, 449-456.
9. Petersson B.A.T., *Moment and Force Excitation at Edges and Corners of Beam and Plate-like Structures*, 4th International Conference on Recent Advances in Structural Dynamics, ISVR, Southampton , 15-18 July 1991, 148-157.
10. Soliman J.I. and Hallam M.G., *Vibration Isolation Between Non-rigid Machines and Non-rigid Foundations*, J. Sound and Vib. (1968) 8 (2), 329-351.
11. Sykes A.O., *Characterising the Vibratory Output of a Multi-terminal Machine and Predicting the Vibration of the Supporting Structure*, Paper No. 831433, Aerospace Congress and Exposition, Long Beach, CA1983, Society of Automotive Engineers.
12. Verheij J.W., Section 2 : Multi-Directional Structureborne Sound Transfer Through Resilient Mountings in *Multi-path Sound Transfer from Resiliently Mounted Shipboard Machinery*, Institute of Applied Physics TNO-TH Delft, 1986 (Ph. D. Thesis, 1982).
13. Verheij J.W., *Measuring Sound Transfer from Resilient Mountings for Separate Excitation with Orthogonal Translations and Rotations*, Proceedings, INTER-NOISE 80, 723-726.
14. Verheij J.W., Chapter 7: Isolators. In Course Notes for *Noise Reduction of Machinery Installations by Vibration Isolation*, Jointly organised by ISVR, Metravib, and TPD-TNO, 1990.
15. Dobson B.J., Horner J.L. and Pinnington R.J., *Study of Machinery Induced Vibration of Ships' Structures Using the Concept of Vibrational Power*, Undersea Defence Technology Conference, October 1988, London, 289-296.
16. Petersson B. and Plunt J., *Structrue-Borne Sound Transmission from Machinery to Foundations*, Final report, Report 80-19, Department of Building Acoustics, Chalmers University of Technology, Gothenburg, October 1980.
17. Popkov V.I., *Vibroacoustic Diagnosis and the Reduction of the Vibration of Shipboard Machinery*, JPRS Translation No. 64931, Arlington, VA, 1975.
18. Goyder H.G.D. and White R.G., *Vibrational Power Flow from Machines into Built-up Structures, Part III : Power Flow through Isolation Systems*, J. Sound and Vib., (1980) 68(1), 97-117.

19. Pinnington R. J. and White R. G., *Power Flow Through Machine Isolators to Resonant and Non-resonant Beams*, J. Sound and Vib., (1981) 75(2), 179-197.
20. Pinnington R.J., *Vibrational Power Transmission Between Sources and Substructures*, University of Southampton, Ph.D. Thesis, 1982.
21. Pinnington R. J., *Vibrational Power Transmission to a Seating of a Vibration Isolated Motor*, J. Sound and Vib., (1987) 118(3), 515-530.
22. Jacobsen F. and Ohlrich M., *Vibrational Power Transmission from Multipoint Mounted Machinery to Supporting Structure*, The Acoustics Laboratory, Technical University of Denmark, Report No. 35, 1986.
23. Lyon R. H., *Machinery Noise and Diagnostics*, Butterworths, 1987.
24. Cremer L., Heckl M. and Ungar E.E., *Structure - Borne Sound,* (2nd Edition) Springer - Verlag, 1988.
25. Lyon R. H., *In-plane Contribution to Structural Noise Transmission*, Noise Control Engineering Journal, Vol.26, No.1, Jan-Feb. 1986, 22-27.
26. Warburton G.B. *The Dynamical Behaviour of Structures*, (2nd Edition), Pergamon Press, 1976.
27. Koh Y.K., *A Study of the Vibrational Power Input to Beam-like Structures Subjected to Simultaneously Acting Force and Moment Excitations*, ISVR Technical Report No: 190, Aug 1990.
28. Szilard R., *Theory and Analysis of Plates: Classical and Numerical Methods*, Prentice-Hall, Inc., Englewood Cliffs, New Jersey, 1974.
29. Warburton G.B. *Response Using The Rayleigh - Ritz Method*, Earthquake Engineering and Structural Dynamics, Vol. 7, 1979, 327-334.
30. Leissa A. W., Clausen W. E., Hulbert L. E. & Hopper A. T. *A Comparison of Approximate Methods for the Solution of Plate Bending Problems,* AIAA Journal, Vol. 7, No. 5, May 1969, 920-928.
31. Bishop R.E.D. & Johnson D.C. *The Mechanics of Vibration*, (1st Edition) 1960, Cambridge University Press.
32. Gladwell G.M.L., Bishop R.E.D. & Johnson D.C. *Receptance Series for Systems Possessing "Rigid Body" Modes*, Journal of the Royal Aeronautical Society, Vol. 66, June 1962, 394-397.
33. Ewins D.J., *Modal Testing : Theory and Practice*, Research Studies Press Ltd., 1986.
34. Sattinger S.S., *A Method for Experimentally Determining Rotational Mobilities of Structures*, The Shock and Vibration Bulletin, 50(2), Sep 1980, 17-28.
35. Ewins D.J. and Gleeson P.T., *Experimental Determination of Multidirectional Mobility Data for Beams*, The Shock and Vibration Bulletin, 45(5), June 1975, 153-173.
36. Ewins D.J. and Sainsbury M.G., *Mobility Measurements for the Vibration Analysis of Connected Structures*, The Shock and Vibration Bulletin, 42(1), 1972, 105-122.
37. Smith J.E., *Measurement of the Total Structural Mobility Matrix*, The Shock and Vibration Bulletin, 40(7), Dec 1969, 51-84.
38. ANSI S2.34-1984, (ASA 34-1984), American National Standard, *Guide to the Experimental Determination of Rotational Mobility Properties and The Complete Mobility Matrix.*
39. Petersson B.A.T., *Giant Magnetostrictive Devices in Structural Acoustics*, 3rd International Conference on Recent Advances in Structural Dynamics, ISVR, Southampton, 18-22 July 1988, 397-405.
40. Dyer I., *Moment Impedance of Plates*, J. Acoust. Soc. Am. 32(10), October 1960, 1290-1297.
41. Koh Y.K. and White R.G., *On the Driving Point Mobility Functions of Rectangular Plates in Flexural Vibration,* 10th International Modal Analysis Conference, San Diego, CA, 3-7 February 1992, 912-921.
42. Molloy C. T., *Use of Four-Pole Parameters in Vibration Calculations*, J. Acoust. Soc. Am. 29(7), July 1957, 842-853.

43. Snowdon J.C., *Mechanical Four-Pole Parameters and Their Application*, J. Sound and Vib., (1971) 15(3), 307-323.
44. Schloss F., *Recent Advances in Mechanical Impedance Instrumentation and Applications*, The Shock and Vibration Bulletin, 34(3), 1964, 3-14.
45. Meltzer G. and Melzig-Thiel R., *Experimental Determination and Practical Application of the Four-pole Parameters of Structure-borne Sound Isolators*, Archives of Acoustics 5,4, (1980), 315-336.
46. Snowdon J.C., *Vibration and Shock in Damped Mechanical Systems*, New York : John Wiley & Sons, Inc., 1968.
47. Tse F.S., Morse I.E. and Hinkle R.T., *Mechanical Vibrations Theory and Applications*, (2nd Edition), Allyn and Bacon, Inc., 1978.
48. Fahy F.J., *Application of Cross-Spectral Density to a Measurement of Vibration Power Flow between Connected Plates*, J. Acoust. Soc. Am., 62(5), November 1977, 1297-1298.
49. Verheij J.W., *Cross Spectral Density Methods for Measuring Structure Borne Power Flow on Beams and Pipes*, J. Sound and Vib., (1980) 70(1), 133-139.
50. Koh Y.K. and White R.G., *Vibrational Power Transmission Between Coupled Flexible Source - Isolator - Receiver Systems*, 17th International Seminar on Modal Analysis, Leuven, Belgium, 23-25 September 1992, 175-191.
51. Weltner K., Grosjean J., Schuster P. & Weber W. J., *Mathematics for Engineers and Scientists* , (1st edition) Stanley Thornes (Publishers) Ltd, 1986.
52. Koh Y.K. and White R.G., *Prediction and Control of Vibrational Power Transmission Between Coupled Structural Systems*, 4th International Conference on Recent Advances in Structural Dynamics, (Work In Progress Paper), ISVR, Southampton, 15-18 July 1991, 48-60.
53. Nash W.A., *Strength of Materials*, (2nd Edition), Schaum's Outline Series, McGraw - Hill Book Co., 1972.
54. Popov E.P., *Introduction to Mechanics of Solids*, Prentice-Hall, Inc., Englewood Cliffs, New Jersey, 1968.
55. Eichler E., *Plate - Edge Admittances*, J. Acoust. Soc. Am., 36(2), February 1964, 344-348.
56. Sun J.C. and Richards E.J., *Prediction of Total Loss Factors of Structures, I : Theory and Experiments*, J. Sound and Vib. (1985) 103(1), 109-117.
57. Gibbs B.M., Petersson B.A.T. and Qiu S., *The Characterization of Structure-borne Emission of Building Services Machinery Using the Source Descriptor Concept*, Noise Control Engineering Journal, Vol.37, No.2, Sep-Oct. 1991, 53-61.

APPENDIX A

EXPRESSIONS FOR Q_{ij}

Expressions for the terms (Q_{ij}) relating the integration constants (B_i, $i = 1,2,3,4$) and the applied end forces and moments (F_A, F_B, M_A and M_B) in eqn.(2.23) are :

$$\begin{Bmatrix} B_1 \\ B_2 \\ B_3 \\ B_4 \end{Bmatrix} = \begin{bmatrix} Q_{11} & Q_{12} & Q_{13} & Q_{14} \\ Q_{21} & Q_{22} & Q_{23} & Q_{24} \\ Q_{31} & Q_{32} & Q_{33} & Q_{34} \\ Q_{41} & Q_{42} & Q_{43} & Q_{44} \end{bmatrix} \begin{Bmatrix} F_A \\ F_B \\ M_A \\ M_B \end{Bmatrix}$$

in which

$$\begin{aligned}
Q_{11} &= H_1 (1 - \cos k\ell \cosh k\ell - \sin k\ell \sinh k\ell) \\
Q_{12} &= H_1 (\cosh k\ell - \cos k\ell) \\
Q_{13} &= H_1 k (\sin k\ell \cosh k\ell + \cos k\ell \sinh k\ell) \\
Q_{14} &= H_1 k (\sin k\ell + \sinh k\ell) \\
Q_{21} &= H_1 (\sin k\ell \cosh k\ell - \cos k\ell \sinh k\ell) \\
Q_{22} &= H_1 (\sin k\ell - \sinh k\ell) \\
Q_{23} &= H_1 k (\cos k\ell \cosh k\ell - \sin k\ell \sinh k\ell) \\
Q_{24} &= H_1 k(\cos k\ell - \cosh k\ell) \\
Q_{31} &= H_1 (\cos k\ell \cosh k\ell - \sin k\ell \sinh k\ell - 1) \\
Q_{32} &= H_1 (\cosh k\ell - \cos k\ell) \\
Q_{33} &= H_1 k (\sin k\ell \cosh k\ell + \cos k\ell \sinh k\ell) \\
Q_{34} &= H_1 k (\sinh k\ell + \sin k\ell) \\
Q_{41} &= H_1 (\sin k\ell \cosh k\ell - \cos k\ell \sinh k\ell) \\
Q_{42} &= H_1 (\sin k\ell - \sinh k\ell) \\
Q_{43} &= H_1 k (1 - \cos k\ell \cosh k\ell - \sin k\ell \sinh k\ell) \\
Q_{44} &= H_1 k (\cos k\ell - \cosh k\ell) \\
H_1 &= \frac{1}{2 E I k^3 (\cos k\ell \cosh k\ell - 1)}
\end{aligned}$$

APPENDIX B

EXPRESSIONS FOR THE DEFINITE INTEGRALS

$$JJ_{mr} = \int_0^a {}_2X_m \; X_r \; dx$$

$$= \int_0^a \left[- B_{1m} e^{jk_{xm}x} - B_{2m} e^{-jk_{xm}x} + B_{3m} e^{k_{xm}x} + B_{4m} e^{-k_{xm}x} \right] \left[B_{1r} e^{jk_{xr}x} + B_{2r} e^{-jk_{xr}x} + B_{3r} e^{k_{xr}x} + B_{4r} e^{-k_{xr}x} \right] dx$$

$$= \frac{-B_{1m} B_{1r}}{j(k_{xm}+k_{xr})} \left[e^{j(k_{xm}+k_{xr})a} - 1 \right] + \frac{-B_{1m} B_{2r}}{j(k_{xm}-k_{xr})} \left[e^{j(k_{xm}-k_{xr})a} - 1 \right]$$

$$+ \frac{-B_{1m} B_{3r}}{jk_{xm}+k_{xr}} \left[e^{(jk_{xm}+k_{xr})a} - 1 \right] + \frac{-B_{1m} B_{4r}}{jk_{xm}-k_{xr}} \left[e^{(jk_{xm}-k_{xr})a} - 1 \right]$$

$$+ \frac{-B_{2m} B_{1r}}{j(-k_{xm}+k_{xr})} \left[e^{j(-k_{xm}+k_{xr})a} - 1 \right] + \frac{-B_{2m} B_{2r}}{j(-k_{xm}-k_{xr})} \left[e^{j(-k_{xm}-k_{xr})a} - 1 \right]$$

$$+ \frac{-B_{2m} B_{3r}}{-jk_{xm}+k_{xr}} \left[e^{(-jk_{xm}+k_{xr})a} - 1 \right] + \frac{-B_{2m} B_{4r}}{-jk_{xm}-k_{xr}} \left[e^{(-jk_{xm}-k_{xr})a} - 1 \right]$$

$$+ \frac{B_{3m} B_{1r}}{k_{xm}+jk_{xr}} \left[e^{(k_{xm}+jk_{xr})a} - 1 \right] + \frac{B_{3m} B_{2r}}{k_{xm}-jk_{xr}} \left[e^{(k_{xm}-jk_{xr})a} - 1 \right]$$

$$+ \frac{B_{3m} B_{3r}}{k_{xm}+k_{xr}} \left[e^{(k_{xm}+k_{xr})a} - 1 \right] + \frac{B_{3m} B_{4r}}{k_{xm}-k_{xr}} \left[e^{(k_{xm}-k_{xr})a} - 1 \right]$$

$$+ \frac{B_{4m} B_{1r}}{-k_{xm}+jk_{xr}} \left[e^{(-k_{xm}+jk_{xr})a} - 1 \right] + \frac{B_{4m} B_{2r}}{-k_{xm}-jk_{xr}} \left[e^{(-k_{xm}-jk_{xr})a} - 1 \right]$$

$$+ \frac{B_{4m} B_{3r}}{-k_{xm}+k_{xr}} \left[e^{(-k_{xm}+k_{xr})a} - 1 \right] + \frac{B_{4m} B_{4r}}{-k_{xm}-k_{xr}} \left[e^{(-k_{xm}-k_{xr})a} - 1 \right]$$

The integrals of J_{mm}, JJJ_{mr}, J_{nn}, JJ_{ns} and JJJ_{ns} are similarly obtained.

APPENDIX C

EXPRESSIONS FOR THE DEFINITE INTEGRALS INVOLVING 'RIGID-BODY' BEAM FUNCTIONS

The expressions for the elements of the mass *[M]* and stiffness *[K]* matrices are given in eqns. (3.53), (3.54) and (3.55). In the following expressions, the translational 'rigid-body' beam function is denoted by $m = -1$ or $r = -1$ and the rotational 'rigid-body' beam function is denoted by $n = -2$ or $s = -2$.

For the diagonal terms ($r = m$ and $s = n$) :

$$K_{m-1m-1} = D\, b\, k_{xm}^{\,4} J_{mm}$$

$$K_{m-2m-2} = D\left[b\, k_{xm}^{\,4} J_{mm} + \frac{24\,(1-\nu)}{b}\, k_{xm}^{\,2}\, JJJ_{mm} \right]$$

$$M_{m-1m-1} = M_{m-2m-2} = \rho\, h\, a\, b$$

For the off-diagonal terms ($r \neq m$ and $s \neq n$) and $n \geq 1, s \geq 1$ (i.e. flexural beam functions):

$$K_{m-1m-2} = K_{m-2m-1} = K_{r-1m-2} = K_{r-2m-1} = K_{r-1m-1} = 0$$

$$K_{r-2m-2} = D\left[\frac{24\,(1-\nu)}{b}\, k_{xr}\, k_{xm}\, JJJ_{rm} \right]$$

$$K_{m-1mn} = D\left[k_{xm}^{\,4} J_{mm} \int_0^b Y_n\, dy + \nu\, k_{xm}^{\,2} k_{yn}^{\,2} JJ_{mm} \int_0^b {}_2Y_n\, dy \right]$$

$$K_{m-2mn} = D\left[k_{xm}^{\,4} J_{mm} \int_0^b Y_{-2}\, Y_n\, dy + \nu\, k_{xm}^{\,2} k_{yn}^{\,2} JJ_{mm} \int_0^b Y_{-2\,2} Y_n\, dy + \frac{4\sqrt{3}\,(1-\nu)}{b}\, k_{xm}^{\,2} k_{yn}\, JJJ_{mm} \int_0^b {}_1Y_n\, dy \right]$$

$$K_{msm\text{-}1} = D\left[k_{xm}^{4} J_{mm} \int_0^b Y_s \, dy + \nu \, k_{xm}^{2} k_{ys}^{2} JJ_{mm} \int_0^b {}_2Y_s \, dy \right]$$

$$K_{msm\text{-}2} = D\left[k_{xm}^{4} J_{mm} \int_0^b Y_{-2} \, Y_s \, dy + \nu \, k_{xm}^{2} k_{ys}^{2} JJ_{mm} \int_0^b Y_{-2} \, {}_2Y_s \, dy + \frac{4\sqrt{3}\,(1-\nu)}{b} k_{xm}^{2} k_{ys} \, JJJ_{mm} \int_0^b {}_1Y_s \, dy \right]$$

$$K_{r\text{-}1mn} = D\left[\nu \, k_{xr}^{2} \, k_{yn}^{2} \, JJ_{rm} \int_0^b {}_2Y_n \, dy \right]$$

$$K_{r\text{-}2mn} = D\left[\nu \, k_{xr}^{2} k_{yn}^{2} \, JJ_{rm} \int_0^b Y_{-2} \, {}_2Y_n \, dy + \frac{4\sqrt{3}\,(1-\nu)}{b} k_{xr} \, k_{xm} \, k_{yn} \, JJJ_{rm} \int_0^b {}_1Y_n \, dy \right]$$

$$K_{rsm\text{-}1} = D\left[\nu \, k_{xm}^{2} k_{ys}^{2} \, JJ_{rm} \int_0^b {}_2Y_s \, dy \right]$$

$$K_{rsm\text{-}2} = D\left[\nu \, k_{xm}^{2} k_{ys}^{2} \, JJ_{rm} \int_0^b Y_{-2} \, {}_2Y_s \, dy + \frac{4\sqrt{3}\,(1-\nu)}{b} k_{xr} \, k_{xm} \, k_{ys} \, JJJ_{rm} \int_0^b {}_1Y_s \, dy \right]$$

$$M_{m\text{-}1m\text{-}2} = M_{m\text{-}2m\text{-}1} = M_{r\text{-}1m\text{-}1} = M_{r\text{-}1m\text{-}2} = M_{r\text{-}2m\text{-}1} = 0$$

$$M_{r\text{-}2m\text{-}2} = M_{r\text{-}1mn} = M_{r\text{-}2mn} = M_{rsm\text{-}1} = M_{rsm\text{-}2} = 0$$

$$M_{m\text{-}1mn} = \rho \, h \, a \int_0^b Y_n \, dy$$

$$M_{m\text{-}2mn} = \rho h a \int_0^b Y_{-2}\, Y_n \, dy$$

$$M_{msm\text{-}1} = \rho h a \int_0^b Y_s \, dy$$

$$M_{msm\text{-}2} = \rho h a \int_0^b Y_{-2}\, Y_s \, dy$$

$$\int_0^b Y_n \, dy = \frac{C_{1n}}{jk_{yn}}\left[e^{jk_{yn}b} - 1\right] + \frac{C_{2n}}{-jk_{yn}}\left[e^{-jk_{yn}b} - 1\right]$$

$$+ \frac{C_{3n}}{k_{yn}}\left[e^{k_{yn}b} - 1\right] + \frac{C_{4n}}{-k_{yn}}\left[e^{-k_{yn}b} - 1\right]$$

$$\int_0^b y\, Y_n \, dy = \frac{C_{1n}}{jk_{yn}}\left[\, b\, e^{jk_{yn}b} - \frac{e^{jk_{yn}b} - 1}{jk_{yn}}\right]$$

$$+ \frac{C_{2n}}{-jk_{yn}}\left[\, b\, e^{-jk_{yn}b} - \frac{e^{-jk_{yn}b} - 1}{-jk_{yn}}\right]$$

$$+ \frac{C_{3n}}{k_{yn}}\left[\, b\, e^{k_{yn}b} - \frac{e^{k_{yn}b} - 1}{k_{yn}}\right]$$

$$+ \frac{C_{4n}}{-k_{yn}}\left[\, b\, e^{-k_{yn}b} - \frac{e^{-k_{yn}b} - 1}{-k_{yn}}\right]$$

$$\int_0^b Y_{-2}\, Y_n \, dy = \frac{2\sqrt{3}}{b}\int_0^b y\, Y_n \, dy - \sqrt{3}\int_0^b Y_n \, dy$$

The expressions for other integrals can be obtained by simply replacing the coefficients of the function Y_n by those of ${}_1Y_n$ and ${}_2Y_n$.

APPENDIX D

FLOW DIAGRAM OF THE COMPUTATION ALGORITHMS FOR THE ANALYTICAL SOLUTIONS OF THE MOBILITY FUNCTIONS OF RECTANGULAR PLATES

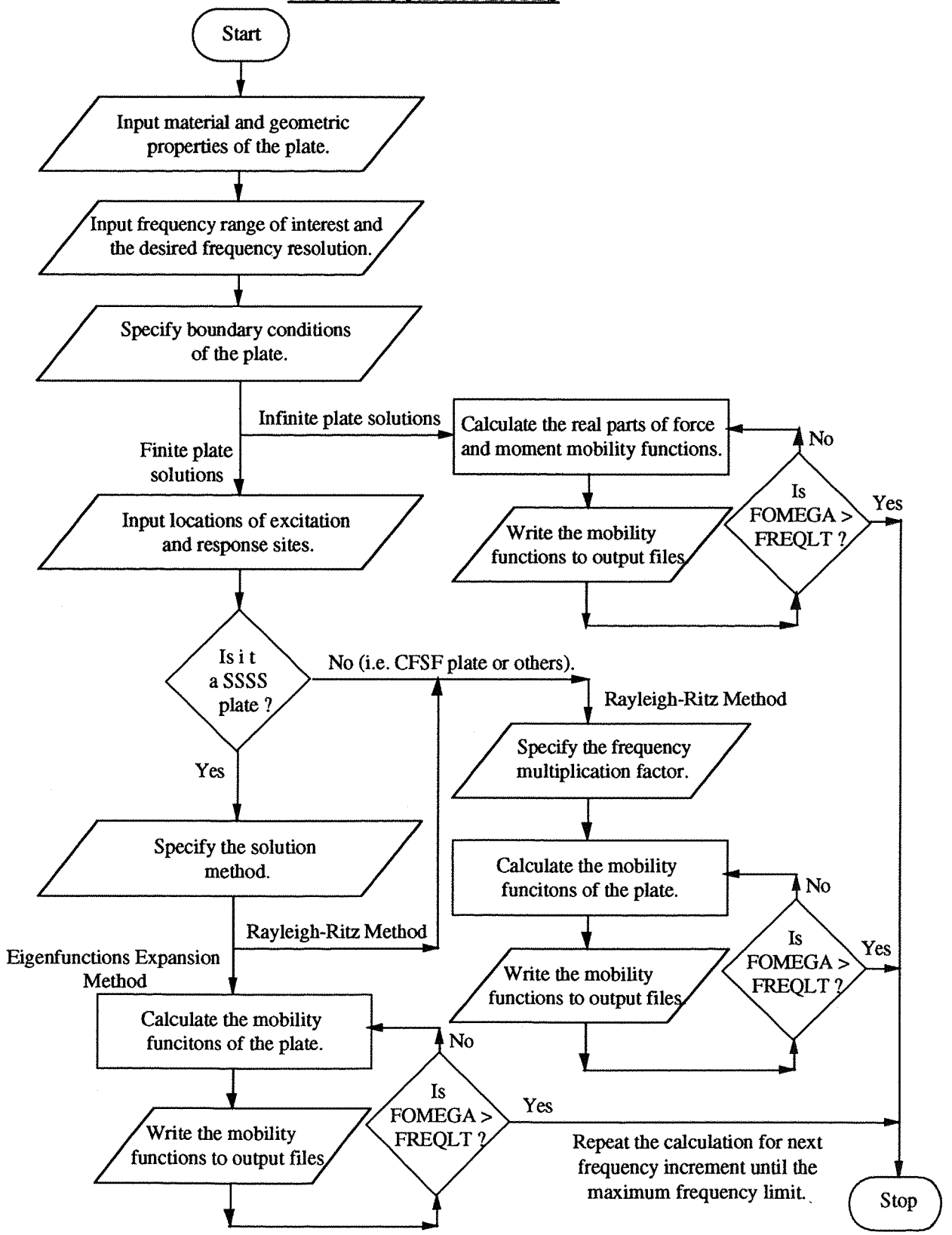

Record No :	Description	Sample Value
1	Type of material : [1 : aluminum ; 2 : steel.]	2
2	Hysteretic loss factor :	0.005
3	Length of edge parallel to X-axis [m] :	0.585
4	Length of edge parallel to Y-axis [m] :	0.390
5	Thickness of plate [m] :	0.0041
6	Lower frequency limit [Hz] :	1.0
7	Upper frequency limit [Hz] :	1000.0
8	Frequency resolution [Hz] :	1.0
9	Type of boundary conditions : * (e.g. CFSF)	13
10	Location of excitation - X-coord. [0 to 1 ratio]:	0.22
11	Location of excitation - Y-coord. [0 to 1 ratio]:	0.62
12	Location of response site - X-coord. [0 to 1 ratio]:	0.22
13	Location of response site - Y-coord. [0 to 1 ratio]:	0.62
14	Frequency multiplication factor :	2.5

Table D-1 : Input Parameters for the Analytical Solution of the Mobility Functions of Rectangular Plates

Note :

* The types of boundary conditions available for selection are :

(11) infinite homogeneous plate
(12) SSSS plate
(13) CFSF plate
(14) CCCC plate
(15) CSCS plate
(16) CCSS plate
(17) CCFF plate
(18) CFCF plate
(19) CFFF plate
(20) CCFC plate
(21) CSFS plate

APPENDIX E

DERIVATION OF THE SSSS PLATE DISPLACEMENT AMPLITUDE FUNCTION USING THE RAYLEIGH - RITZ METHOD

When applying the Rayleigh - Ritz method to a rectangular plate with all edges simply supported, the assumed functions $X_m(x)$ and $Y_n(y)$ of the displacement function (eqn (3.44)) are the characteristic functions of a beam with both ends simply supported. These beam functions are :

$$X_m(x) = \sin k_{xm} x = \sin \frac{m\pi}{a} x \qquad m = 1,2,...,M$$

$$Y_n(y) = \sin k_{yn} y = \sin \frac{n\pi}{b} y \qquad n = 1,2,...,N$$

where $k_{xm} = \frac{m\pi}{a}$ and $k_{yn} = \frac{n\pi}{b}$ are the flexural wavenumbers associated with the beam functions. These functions have the same orthogonal property but normalised to half the values given in eqns (3.47) and (3.48) , i.e. :

$$\int_0^a X_m(x)\, X_r(x)\, dx = \begin{cases} 0 & \text{if } m \neq r \\ \frac{a}{2} & \text{if } m = r \end{cases}$$

$$\int_0^b Y_n(y)\, Y_s(y)\, dy = \begin{cases} 0 & \text{if } n \neq s \\ \frac{b}{2} & \text{if } n = s \end{cases}$$

Substituting these beam functions into the expressions for the elements of the mass and stiffness matrices in eqns (3.53), (3.54) and (3.55), and replacing a and b by $\frac{a}{2}$ and $\frac{b}{2}$ respectively in eqn (3.54), one obtains :

$$M_{mnmn} = \frac{1}{4} \rho h a b$$

$$K_{mnmn} = \frac{1}{4} D a b \left[\left(\frac{m\pi}{a}\right)^2 + \left(\frac{n\pi}{b}\right)^2 \right]^2$$

and $\qquad M_{rsmn} = K_{rsmn} = 0 \qquad$ for $r \neq m$ and $s \neq n$

Hence, the coefficient matrix $[\chi_{rsmn}]$ of the unknown functions ζ_{mn} is a diagonal matrix. The diagonal elements are :

$$\chi_{mnmn} = K_{mnmn}\,(1 + j\,\eta) - \omega^2 M_{mnmn}$$

$$= \frac{\rho hab}{4}\left[\ \omega_{mn}{}^2\,(1+j\,\eta) - \omega^2\ \right]$$

where ω_{mn} are the eigenfrequencies as given in eqn (3.32).

The inverse of the matrix $[\chi_{rsmn}]$ is also a diagonal matrix with the diagonal elements equal to the reciprocal of χ_{mnmn}.

Thus from eqn (3.66), one obtains the transverse displacement amplitude function of the SSSS plate :

$$w(x,y) = F \sum_{m=1}^{M} \sum_{n=1}^{N} \frac{4}{\rho hab} \frac{\sin\frac{m\pi}{a}x_0 \sin\frac{n\pi}{b}y_0 \ \sin\frac{m\pi}{a}x \ \sin\frac{n\pi}{b}y}{\left[\ \omega_{mn}{}^2\,(1+j\eta) - \omega^2\ \right]}$$

which yields the identical expression for the driving point force mobility function of the plate as given in eqn (3.33), and hence the other moment and coupling mobility functions, if M and N are sufficiently large.

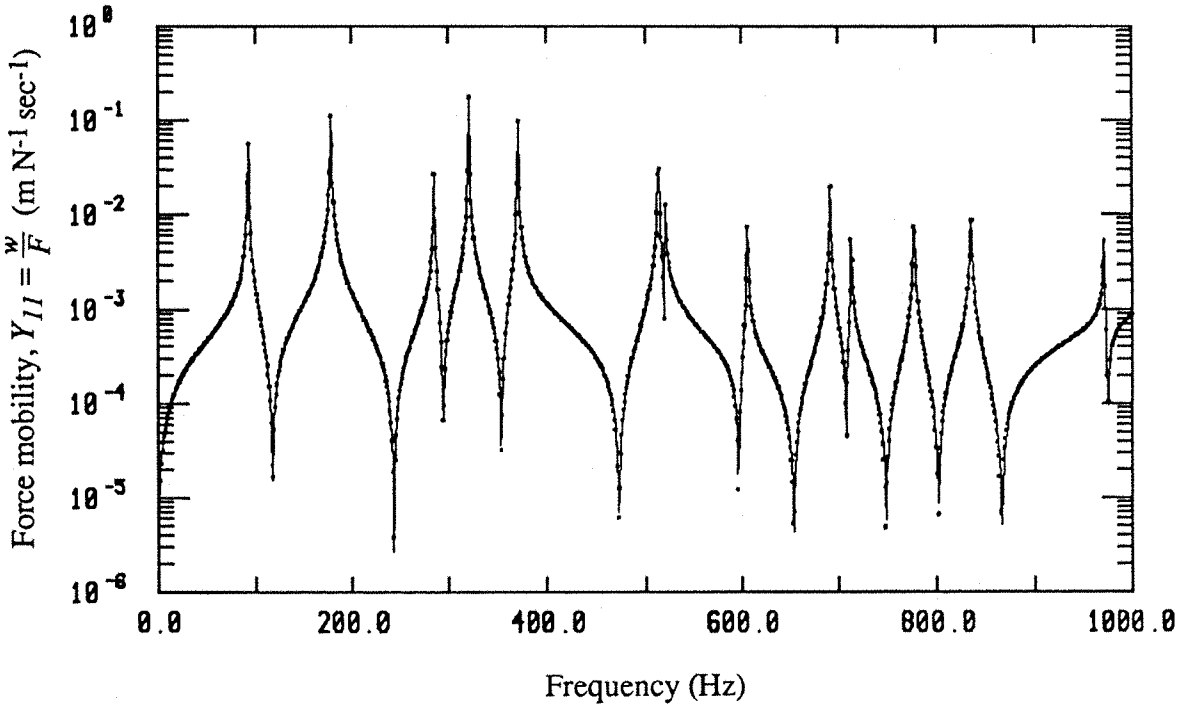

Figure E1 : Comparison of the modulus spectra of Y_{11} for the SSSS plate : —— Rayleigh-Ritz method,····· Eigenfunction Expansion Theorem.

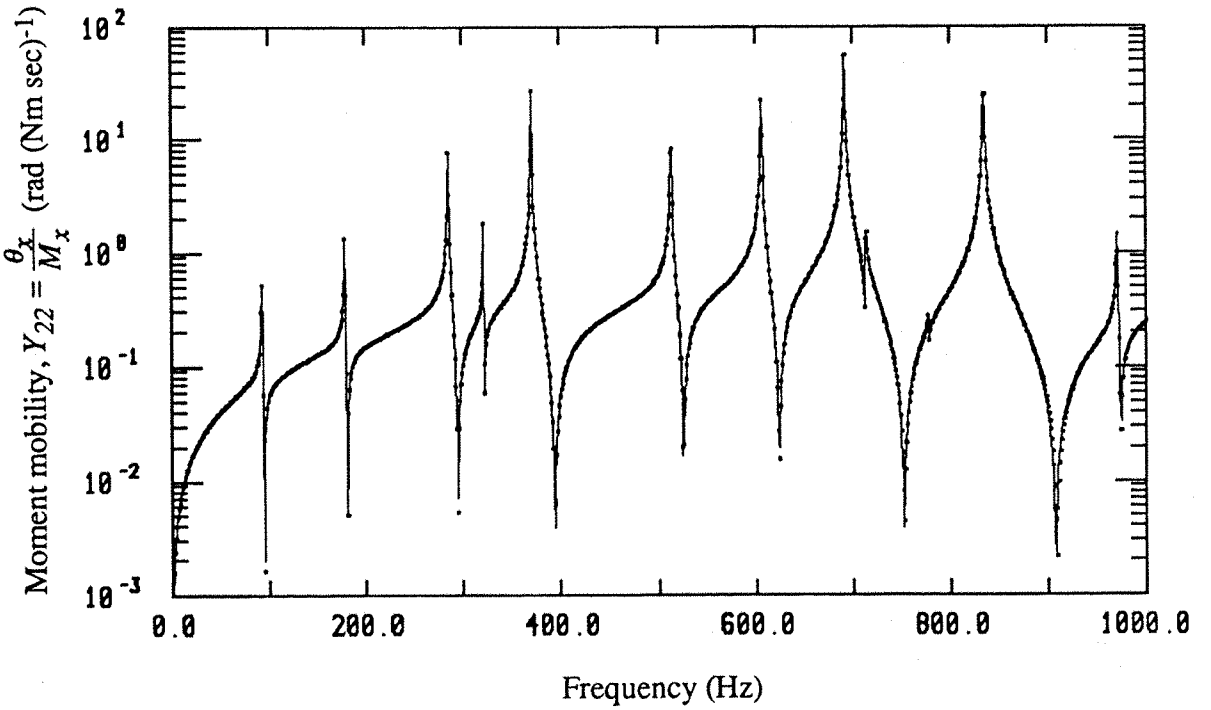

Figure E2 : Comparison of the modulus spectra of Y_{22} for the SSSS plate : —— Rayleigh-Ritz method,····· Eigenfunction Expansion Theorem.

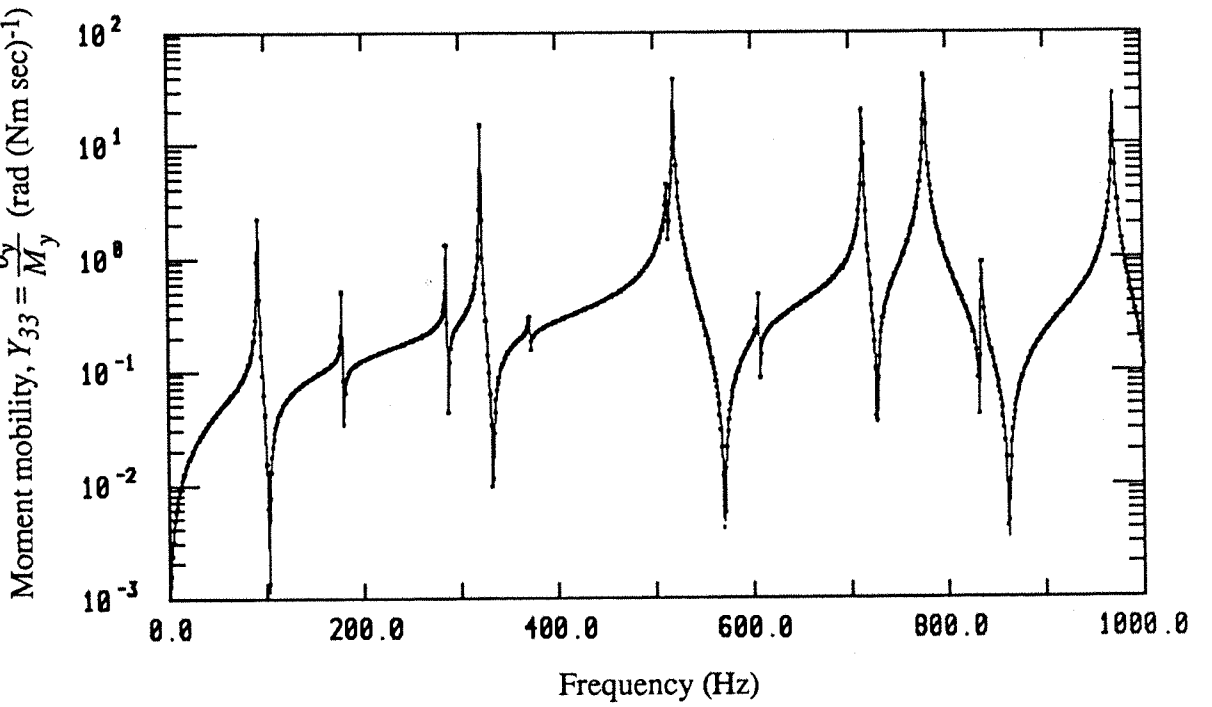

Figure E3 : Comparison of the modulus spectra of Y_{33} for the SSSS plate :
—— Rayleigh-Ritz method,····· Eigenfunction Expansion Theorem.

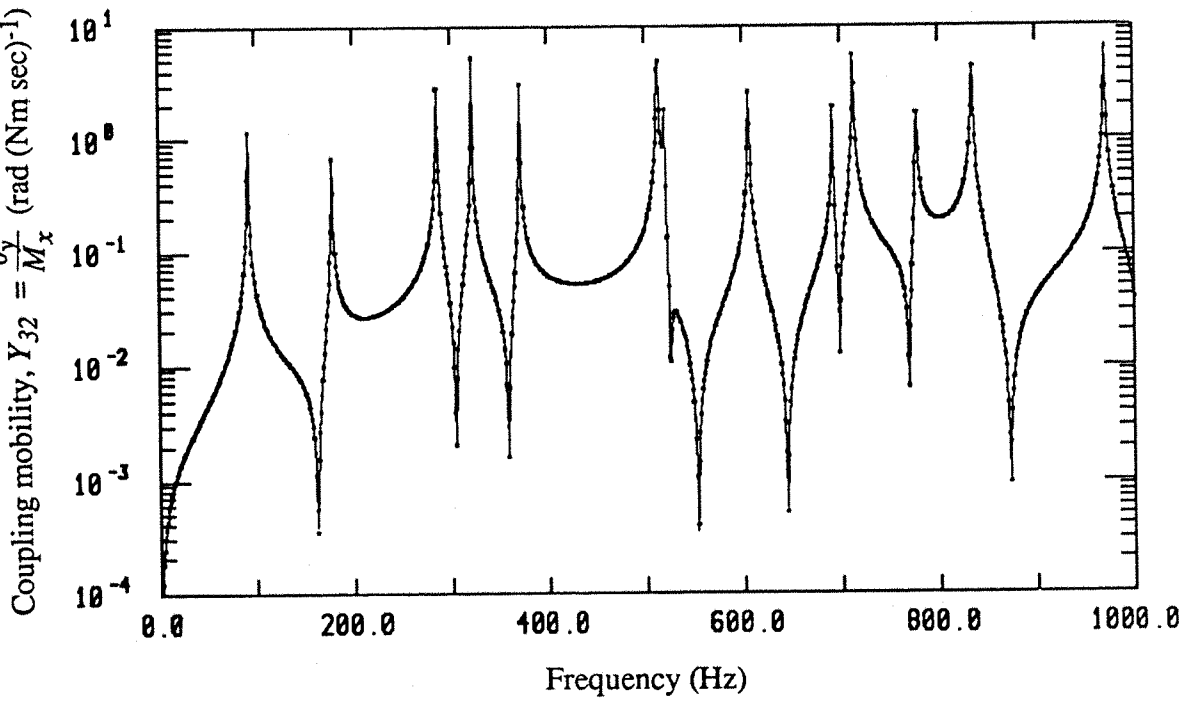

Figure E4 : Comparison of the modulus spectra of Y_{32} for the SSSS plate :
—— Rayleigh-Ritz method,····· Eigenfunction Expansion Theorem.

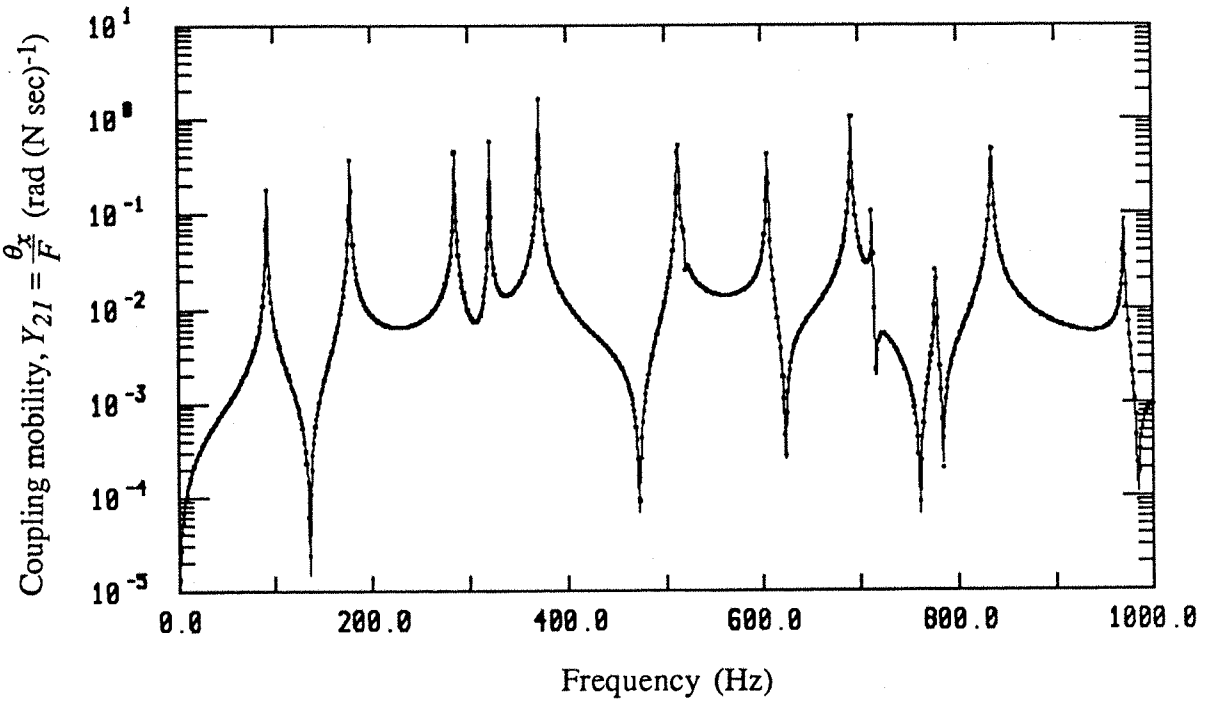

Figure E5 : Comparison of the modulus spectra of Y_{21} for the SSSS plate : —— Rayleigh-Ritz method,····· Eigenfunction Expansion Theorem.

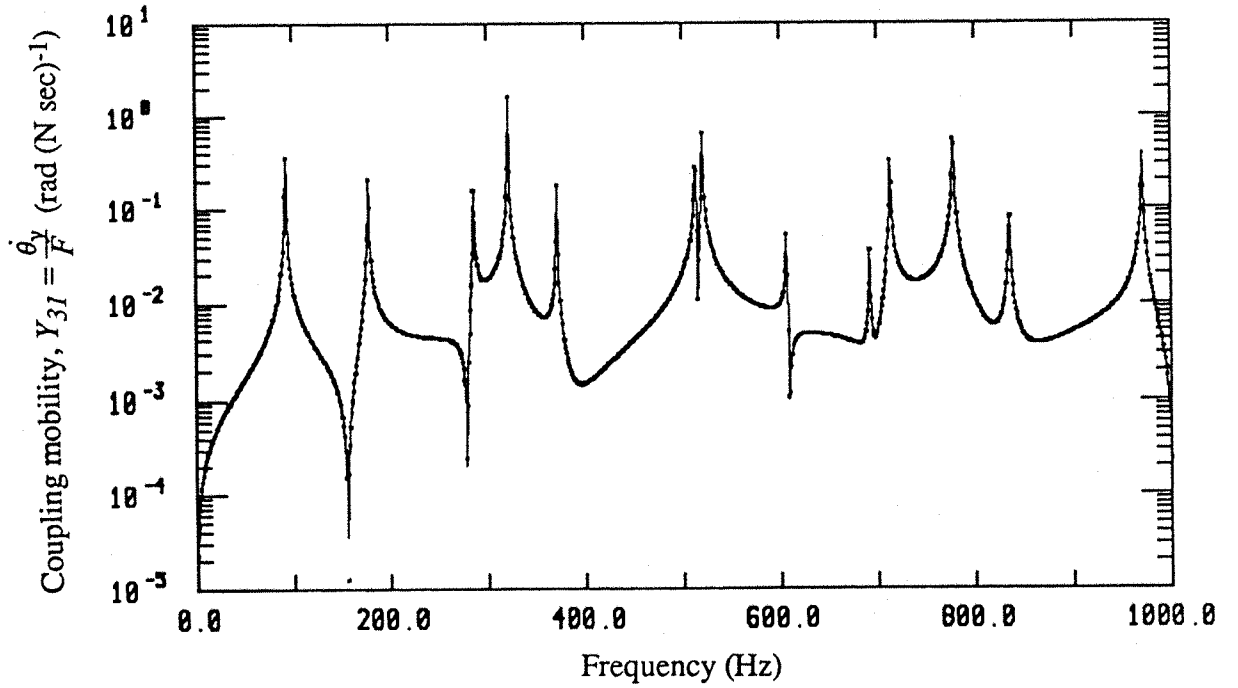

Figure E6 : Comparison of the modulus spectra of Y_{31} for the SSSS plate : —— Rayleigh-Ritz method,····· Eigenfunction Expansion Theorem.

APPENDIX F

DRAWING, PHOTOGRAPHS, PROGRAM LISTINGS AND FIGURES FOR EXPERIMENTALLY DETERMINATION OF THE DRIVING POINT MOBILITY FUNCTIONS

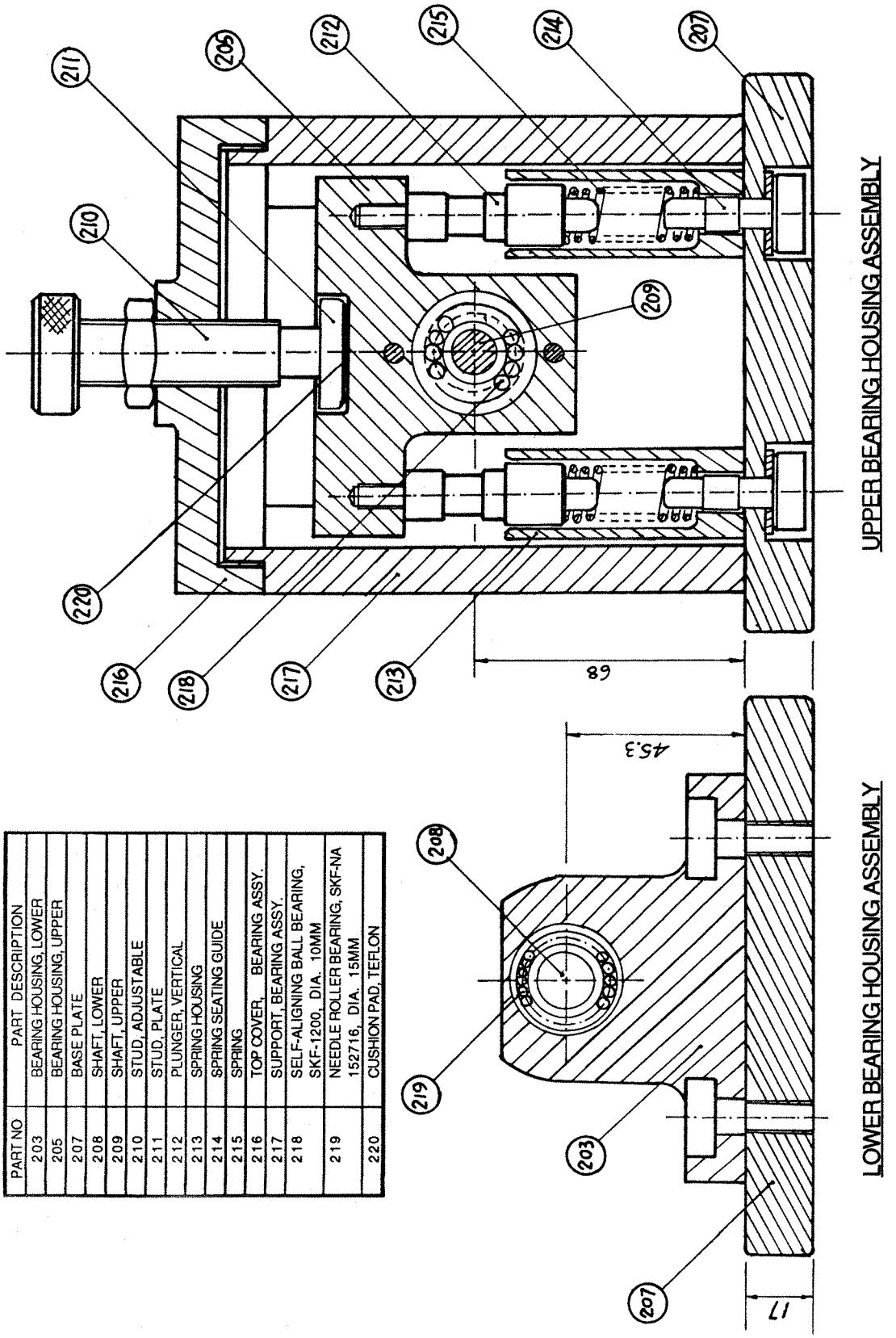

PART NO	PART DESCRIPTION
203	BEARING HOUSING, LOWER
205	BEARING HOUSING, UPPER
207	BASE PLATE
208	SHAFT, LOWER
209	SHAFT, UPPER
210	STUD, ADJUSTABLE
211	STUD, PLATE
212	PLUNGER, VERTICAL
213	SPRING HOUSING
214	SPRING SEATING GUIDE
215	SPRING
216	TOP COVER, BEARING ASSY.
217	SUPPORT, BEARING ASSY.
218	SELF-ALIGNING BALL BEARING, SKF-1200, DIA. 10MM
219	NEEDLE ROLLER BEARING, SKF-NA 152716, DIA. 15MM
220	CUSHION PAD, TEFLON

Figure F1 : Sectional views of the upper and lower bearing housing assemblies.

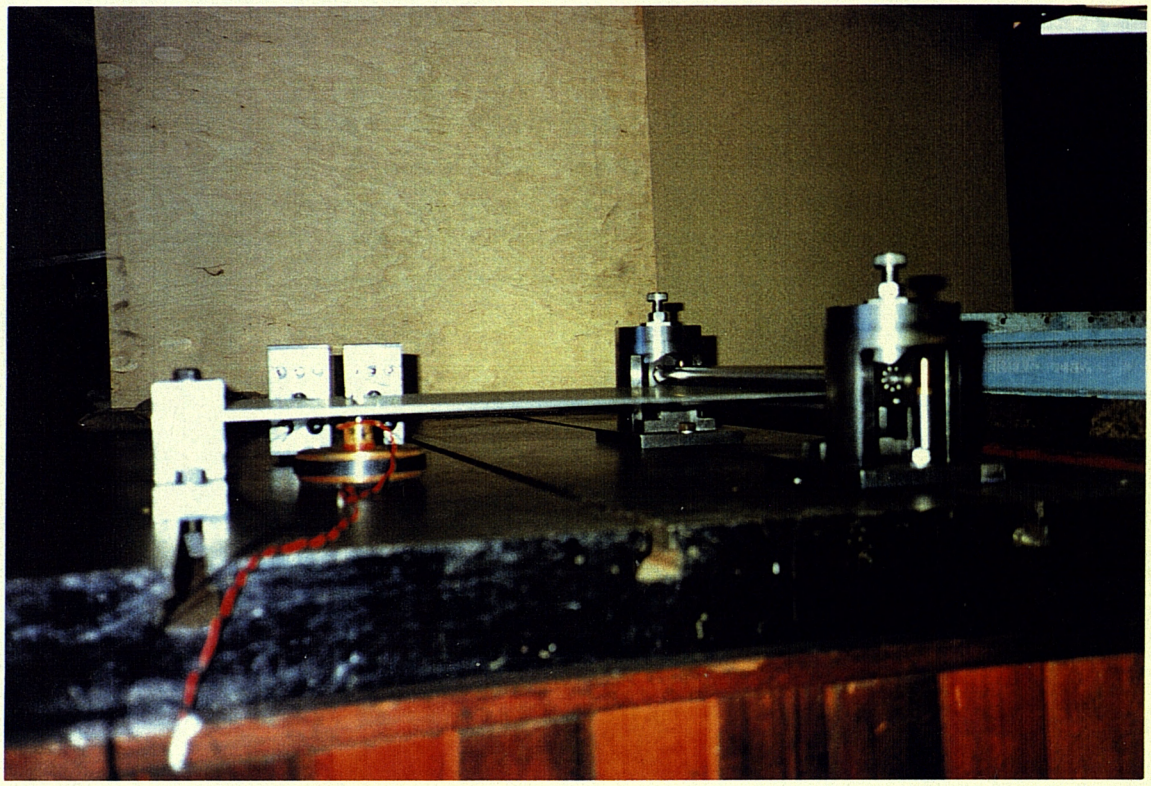

Figure F2 : Experimental arrangement for the force excitation experiment

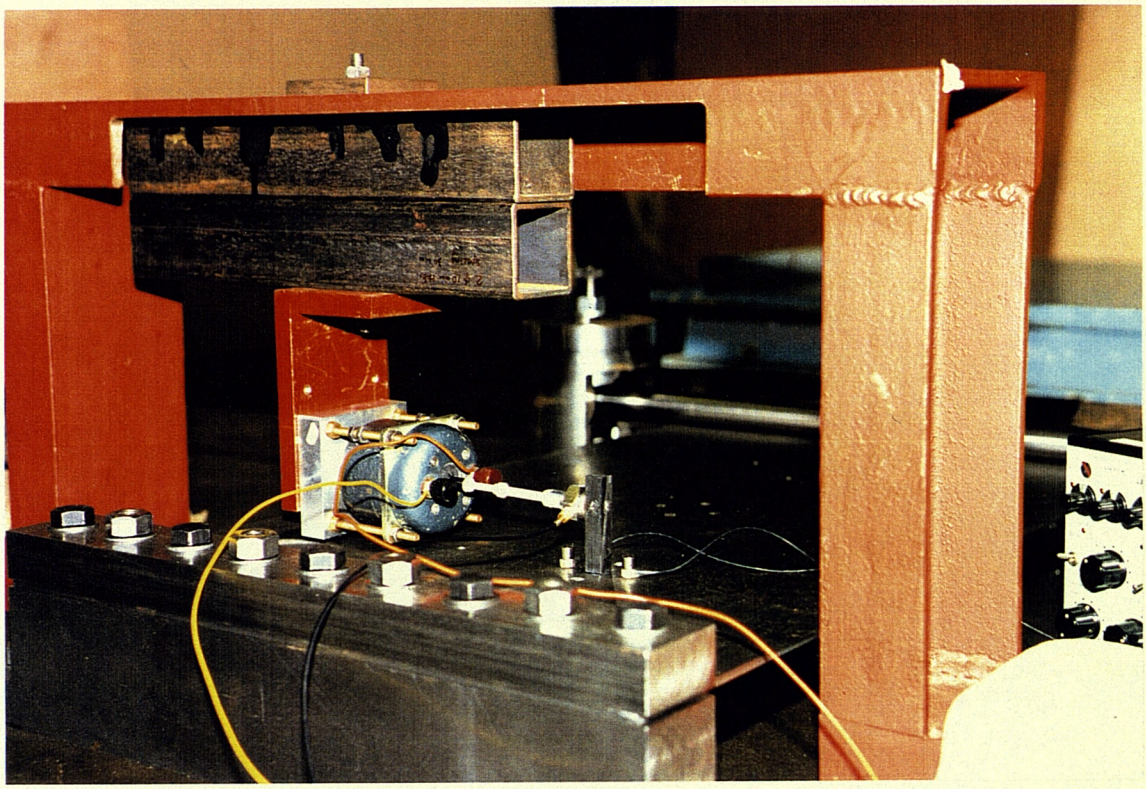

Figure F3 : Experimental arrangement for M_x excitation experiment.

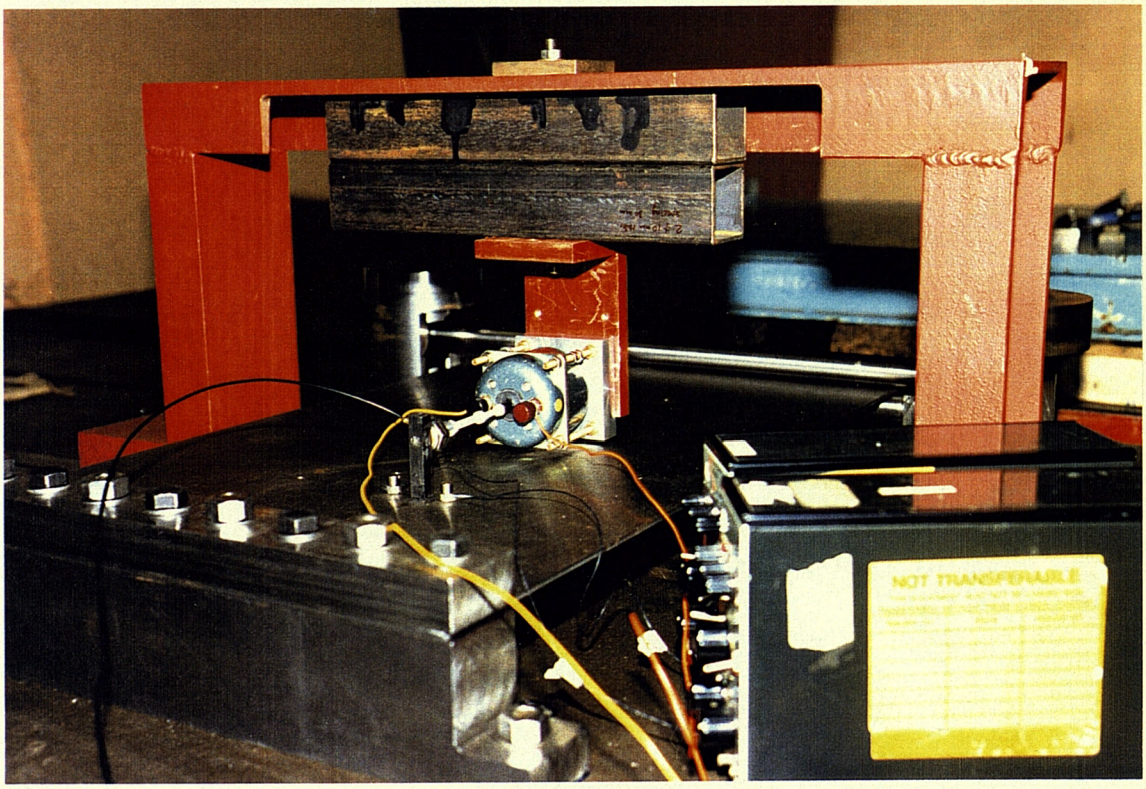

Figure F4 : Experimental arrangement for M_y excitation experiment.

Listings of PC-DATS Job Files for Experimentally Determination of the Driving Point Mobility Functions

1. The Force Excitation Scheme

```
!   K3FORCE.JOB    (PROSIG / PC-DATS DATA ANALYSIS JOB FILE)
!
!  ======================================================================
!     Y.K.KOH                        ISVR                        June 1991
!
!     This JOB file calculates the following frequency response
!     functions using PROSIG / PC-DATS software :
!
!     (1) Driving point force mobility [ Y11 ]
!         (translational velocity / force)
!     (2) Driving point coupling mobility [ Y21 or Y31 ]
!         (rotational velocity about X or Y-axis / force)
!
!     The experimental data are acquired via DT2828 data acquisition
!     board and the PC-DATS command : [/ACQD21]. The acquired data in
!     the DATA.ACQ file are de-multiplexed into its individual data
!     channels using the /DEMUX command :
!
!      - channel 1:   1.DAC : measured force signal, [F1.DAC]
!      - channel 2:   2.DAC : acceleration signal 1, [V1.DAC]
!      - channel 3:   3.DAC : acceleration signal 2. [V2.DAC]
!
!     The frequency response functions are estimated using the H1
!     estimator.
!  ======================================================================
!
/WRITE(' Compute the average translational acceleration : ')
!
/ARITH("V1",104,1,"V2")
/ARITH(104,105,7,0.5)
/KILL(104)
!
/WRITE(' Compute the angular acceleration : ')
!
/ARITH("V2",106,2,"V1")
/WRITE('     Input spacing between accelerometers : ')
/ARITH(106,107,8,*)
/KILL(106)
!
/WRITE(' Normalise the force and response signals: ')
!
/NORM("F1",111,1)
/NORM(105,122,1)
/NORM(107,124,1)
/KILL(102,105,107)
!
```

1. The Force Excitation Scheme (Continued)

```
/WRITE(' Compute the PSD of force and response signals: ')
!
/ASD(111,"FPSD")
/ASD(122,"APSD")
/ASD(124,"RPSD")
!
/WRITE(' Compute the CSD of force and response signals: ')
!
/CSD(111,122,"FACSD")
/CSD(111,124,"FRCSD")
!
/KILL(111,122,124)
!
/WRITE(' Compute the frequency response function: ')
!
!        *** H1 Estimator ***
!
/ARITH("FACSD","A11",4,"FPSD")
/ARITH("FRCSD","A21",4,"FPSD")
!
!   Compute the coherance functions.
!
/COHER("FACSD","FPSD","APSD","CA11",0)
/COHER("FRCSD","FPSD","RPSD","CA21",0)
!
/KILL("FPSD","APSD","RPSD","FACSD","FRCSD")
!
/WRITE(' Convert accelerances to mobilities :')
!
/OMAR("A11","Y11R",3,2)
/OMAR("A21","Y21R",3,2)
!
/WRITE(' Compute the modulus and phase of the transfer functions: ')
!
/MOPH("Y11R","Y11M",0,1)
/MOPH("Y21R","Y21M",0,1)
!
/KILL("A11","A21")
END
```

2. *The Moment Excitation Scheme*

```
!   K3MOMENT.JOB       (PROSIG / PC-DATS DATA ANALYSIS JOB FILE)
!
!  ======================================================================
!     Y.K.KOH                          ISVR                        July 1991
!
!     This JOB file calculates the following frequency response
!     functions using PROSIG / PC-DATS software :
!
!     (1) Driving point moment mobility [ Y22 or Y33 ]
!         (rotational vel. about X or Y-axis / moment of the same axis)
!     (2) Driving point coupling mobility [ Y32 ]
!         (rotational vel. about Y-axis / moment about X-axis)
!     (3) Driving point coupling mobility [ Y12 or Y13 ]
!         (translational vel. / moment about X or Y-axis)
!
!     The experimental data are acquired via DT2828 data acquisition
!     board and the PC-DATS command : [/ACQD21]. The acquired data in the
!     DATA.ACQ file are de-multiplexed into its individual data channels
!     using the /DEMUX command :
!
!       - channel 1:     1.DAC : measured force signal, [F1.DAC]
!       - channel 2:     2.DAC : acceleration signal 1, [V1.DAC]
!       - channel 3:     3.DAC : acceleration signal 2. [V2.DAC]
!
!     The frequency response functions are estimated using the H1
!     estimator.
!  ======================================================================
!
/WRITE(' Compute the average translational acceleration : ')
!
/ARITH("V1",104,1,"V2")
/ARITH(104,105,7,0.5)
/KILL(104)
!
/WRITE(' Compute the angular acceleration : ')
!
/ARITH("V2",106,2,"V1")
/WRITE('     Input spacing between accelerometers : ')
/ARITH(106,107,8,*)
/KILL(106)
!
/WRITE(' Compute the applied moment excitation : ')
/WRITE('     Input the value of moment arm : ')
/ARITH("F1",103,7,*)
!
/WRITE(' Normalise the force and response signals: ')
!
/NORM(103,111,1)
/NORM(105,122,1)
/NORM(107,124,1)
/KILL(103,105,107)
!
```

2. *The Moment Excitation Scheme (Continued)*

```
/WRITE(' Compute the PSD of force and response signals: ')
!
/ASD(111,"FPSD")
/ASD(122,"APSD")
/ASD(124,"RPSD")
!
/WRITE(' Compute the CSD of force and response signals: ')
!
/CSD(111,122,"FACSD")
/CSD(111,124,"FRCSD")
!
/KILL(111,122,124)
!
/WRITE(' Compute the frequency response function: ')
!
!     *** H1 Estimator ***
!
/ARITH("FACSD","A11",4,"FPSD")
/ARITH("FRCSD","A21",4,"FPSD")
!
!   Compute the coherance functions.
!
/COHER("FACSD","FPSD","APSD","CA11",0)
/COHER("FRCSD","FPSD","RPSD","CA21",0)
!
/KILL("FPSD","APSD","RPSD","FACSD","FRCSD")
!
/WRITE(' Convert accelerances to mobilities :')
!
/OMAR("A11","Y12R",3,2)
/OMAR("A21","Y22R",3,2)
!
/WRITE(' Compute the modulus and phase of the transfer functions: ')
!
/MOPH("Y12R","Y12M",0,1)
/MOPH("Y22R","Y22M",0,1)
!
/KILL("A11","A21")
END
```

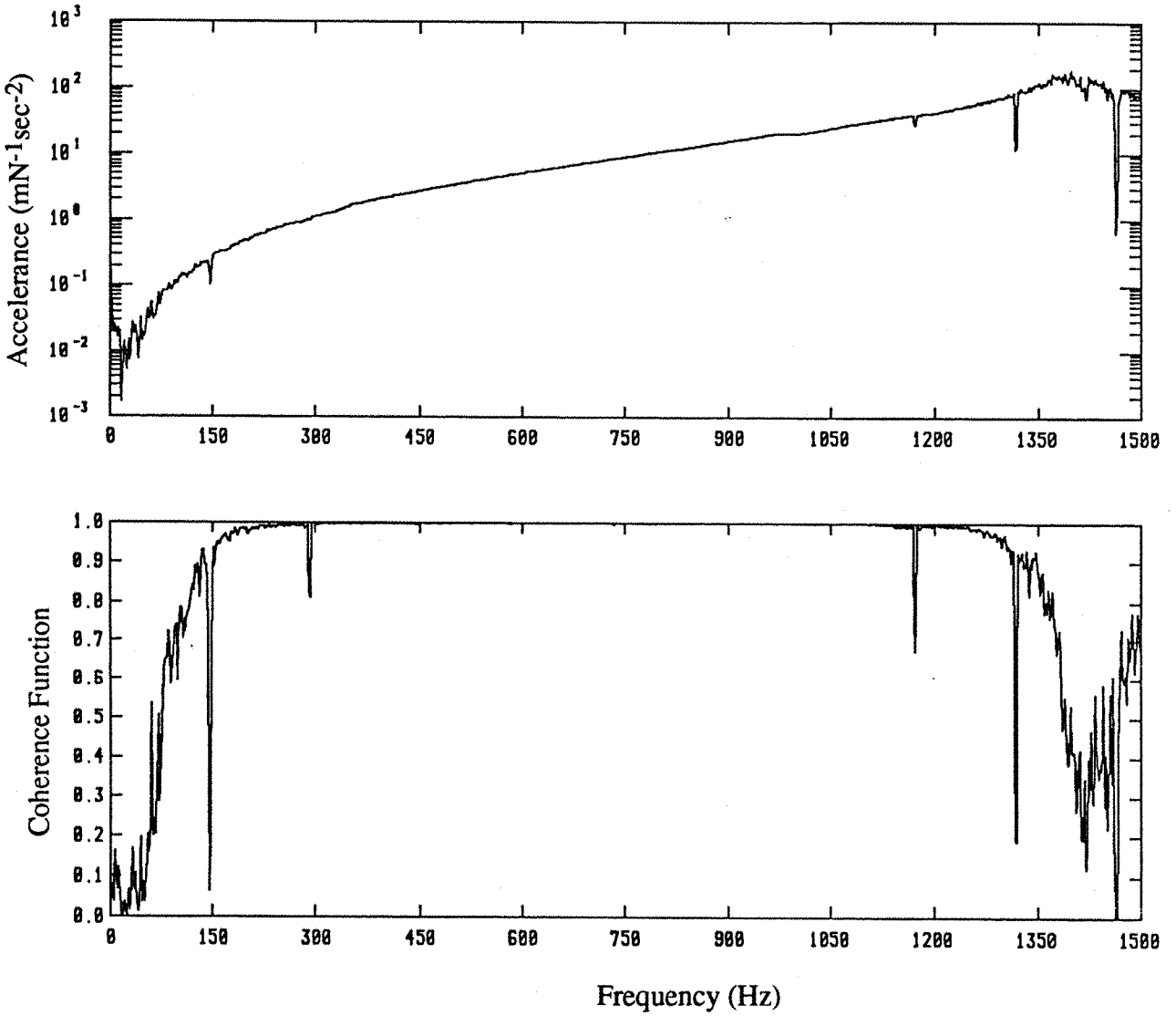

Figure F5 : Experimental results : modulus spectrum of the driving point accelerance and the coherence function for the carbon fibre reinforced plastic rod with one end glued to the clamped test fixture.

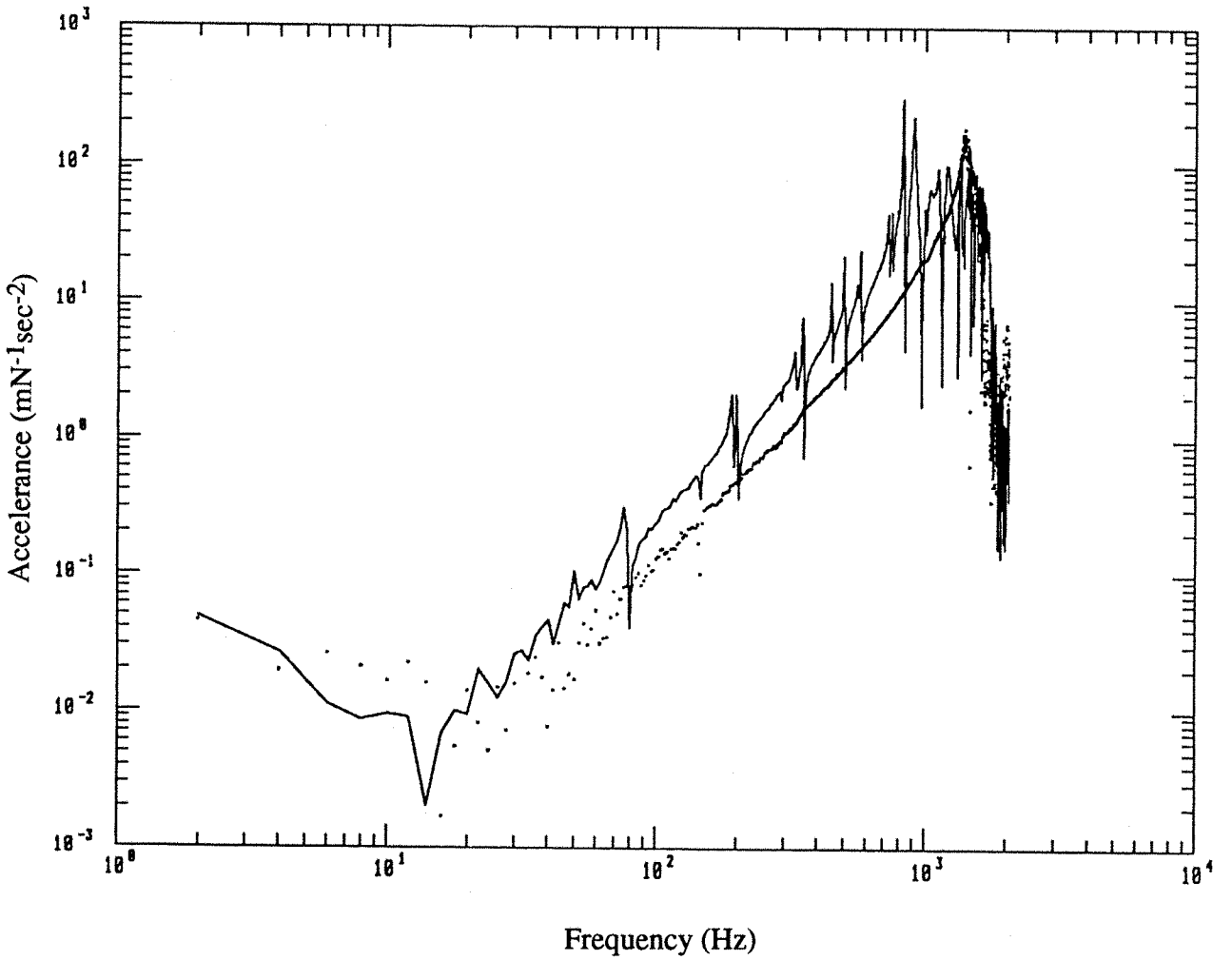

Figure F6 : Comparison of the modulus spectra of the driving point accelerance for the carbon fibre reinforced plastic rod with one end glued to the clamped test fixture (·····) and to the CFSF plate (———).

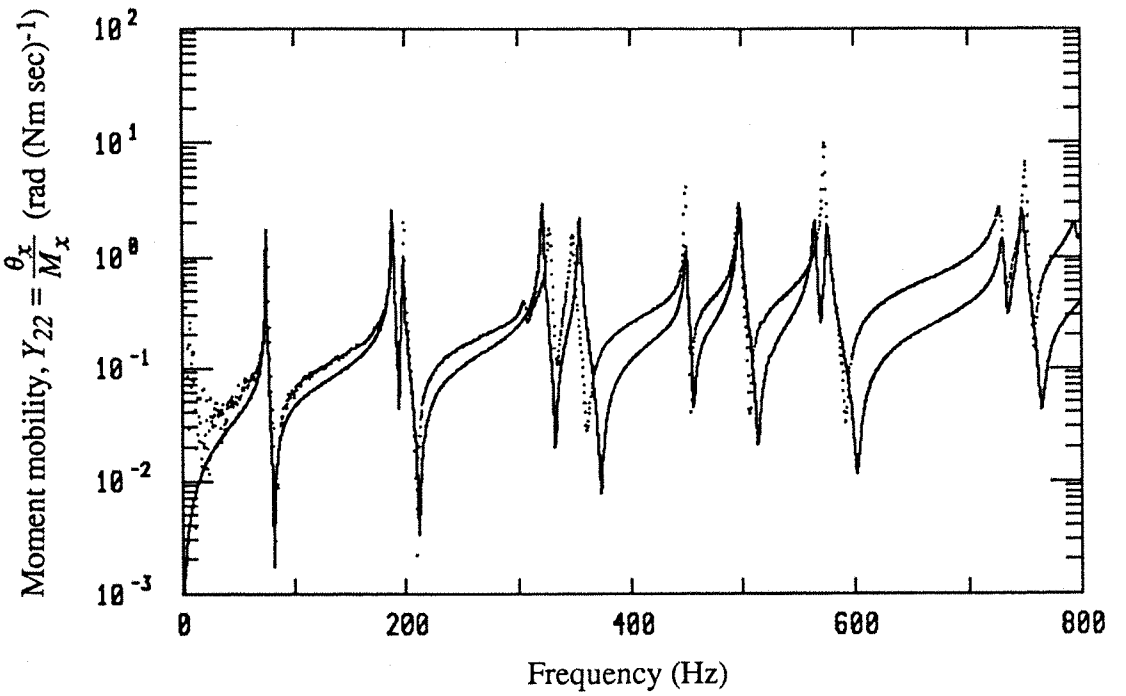

Figure F7 : Comparison of the modulus spectra of Y_{22} for the CFSF plate :
—— Theoretical result (η = 0.005, freq. resolution : 1Hz),
····· Experimental result (freq. resolution : 0.5Hz).

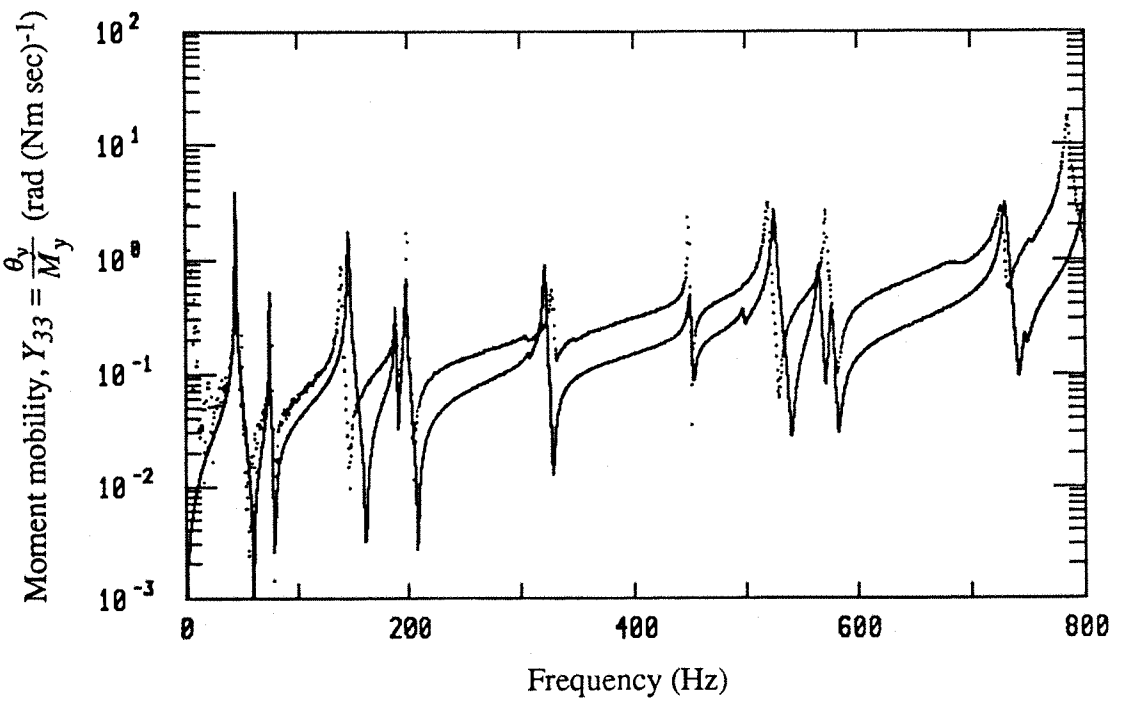

Figure F8 : Comparison of the modulus spectra of Y_{33} for the CFSF plate :
—— Theoretical result (η = 0.005, freq. resolution : 1Hz),
····· Experimental result (freq. resolution : 0.5Hz).

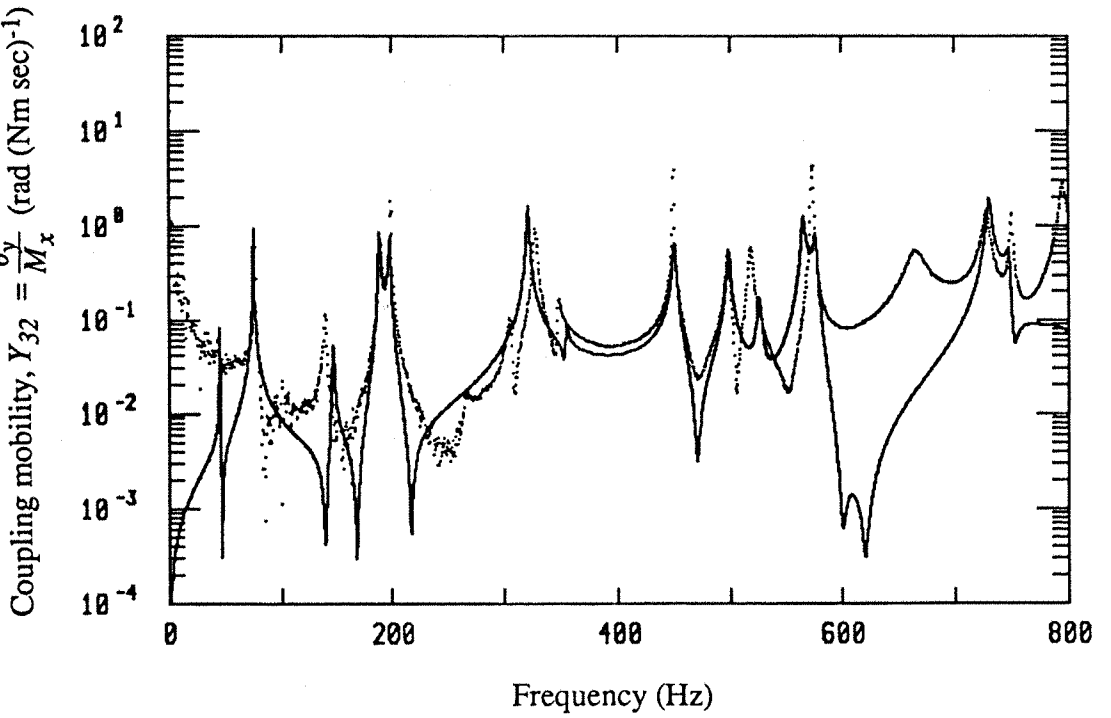

Figure F9 : Comparison of the modulus spectra of Y_{32} for the CFSF plate :
—— Theoretical result (η = 0.005, freq. resolution : 1Hz),
····· Experimental result (freq. resolution : 0.5Hz).

APPENDIX G

POINT, COUPLING AND TRANSFER MOBILITY FUNCTIONS OF A FREE - FREE BEAM

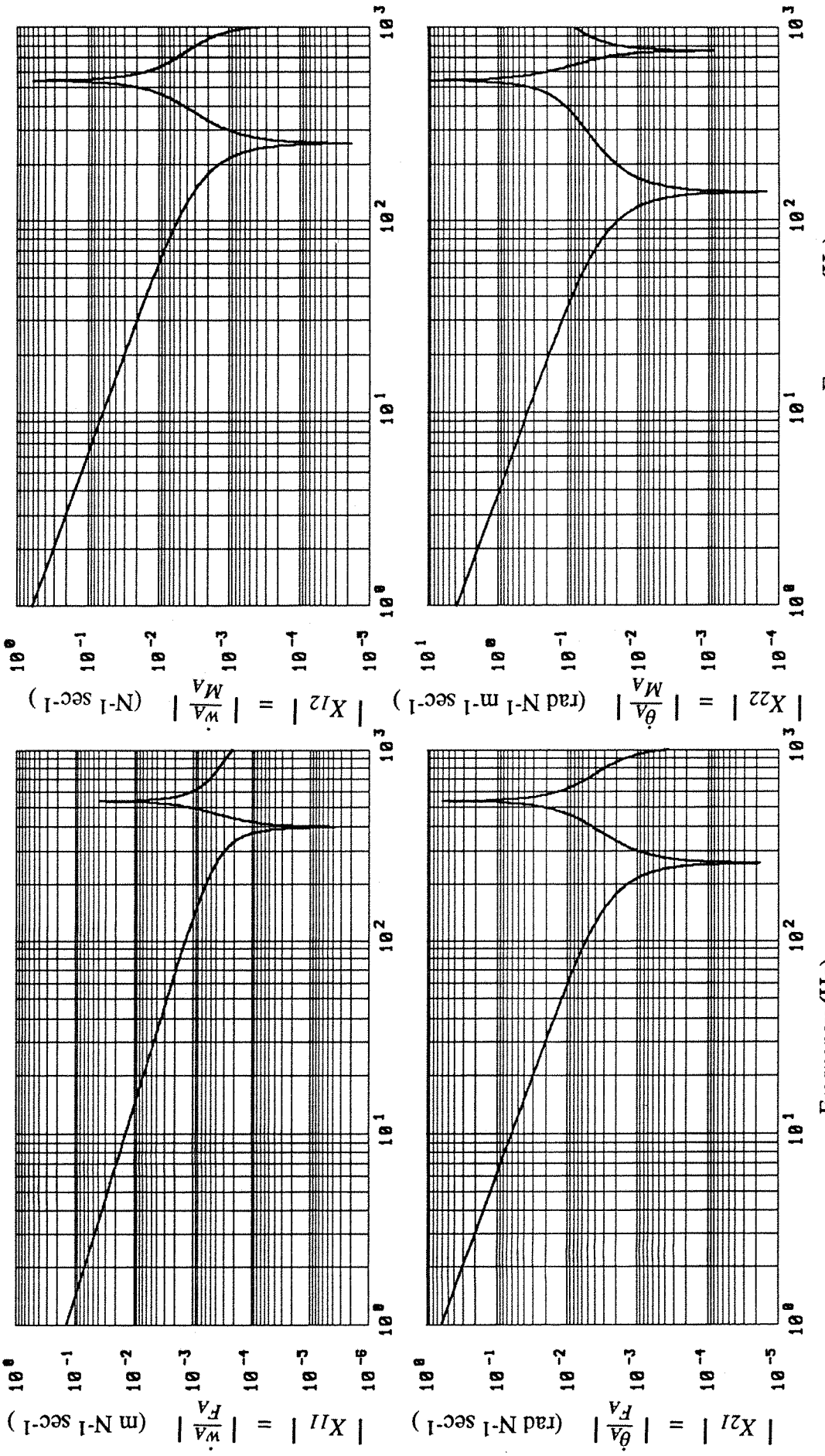

Figure G1 : Modulus spectra of the driving point mobility functions of the free-free beam at mounting point A.

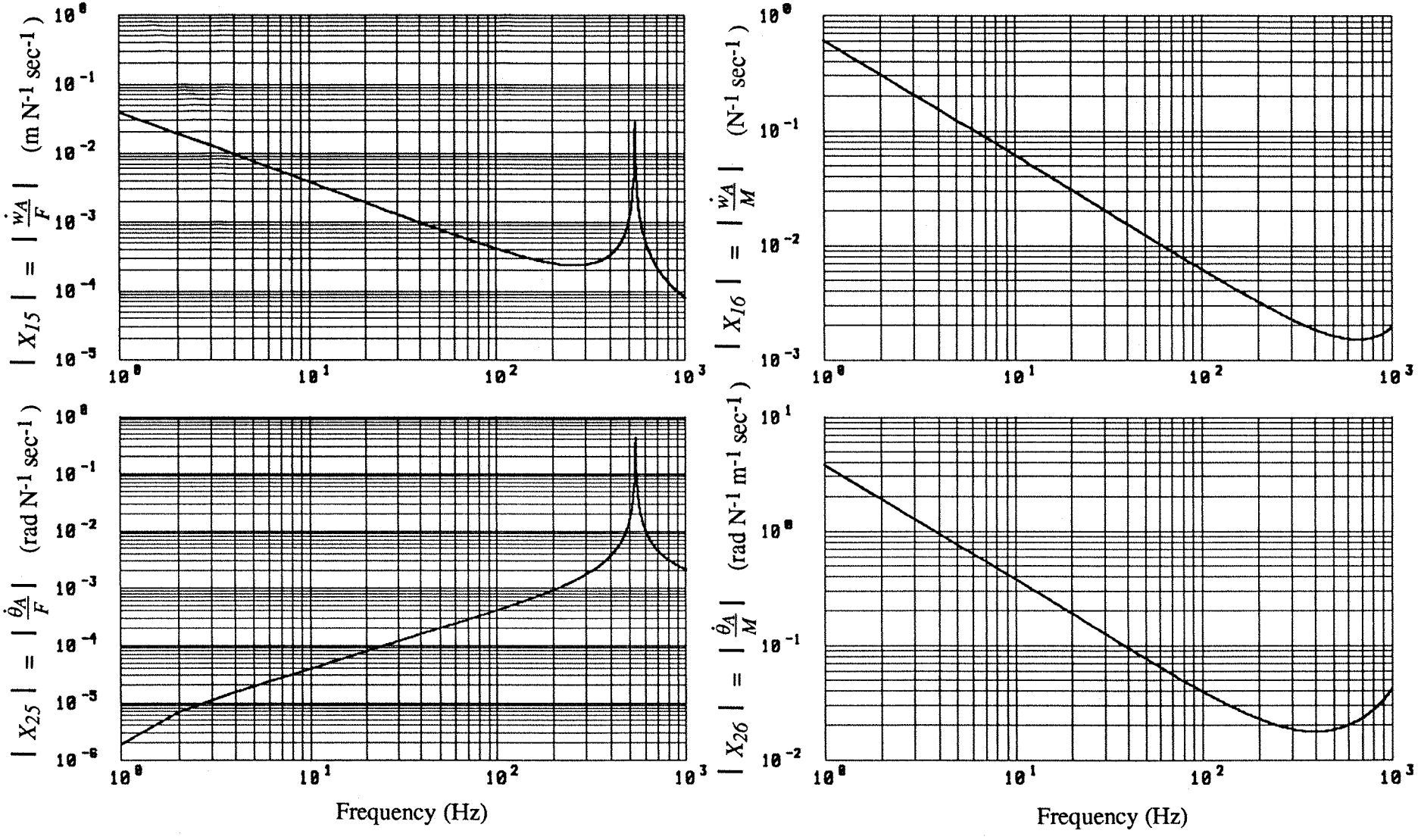

Figure G2: Modulus spectra of the transfer mobility functions between responses at point A and excitations at point C.

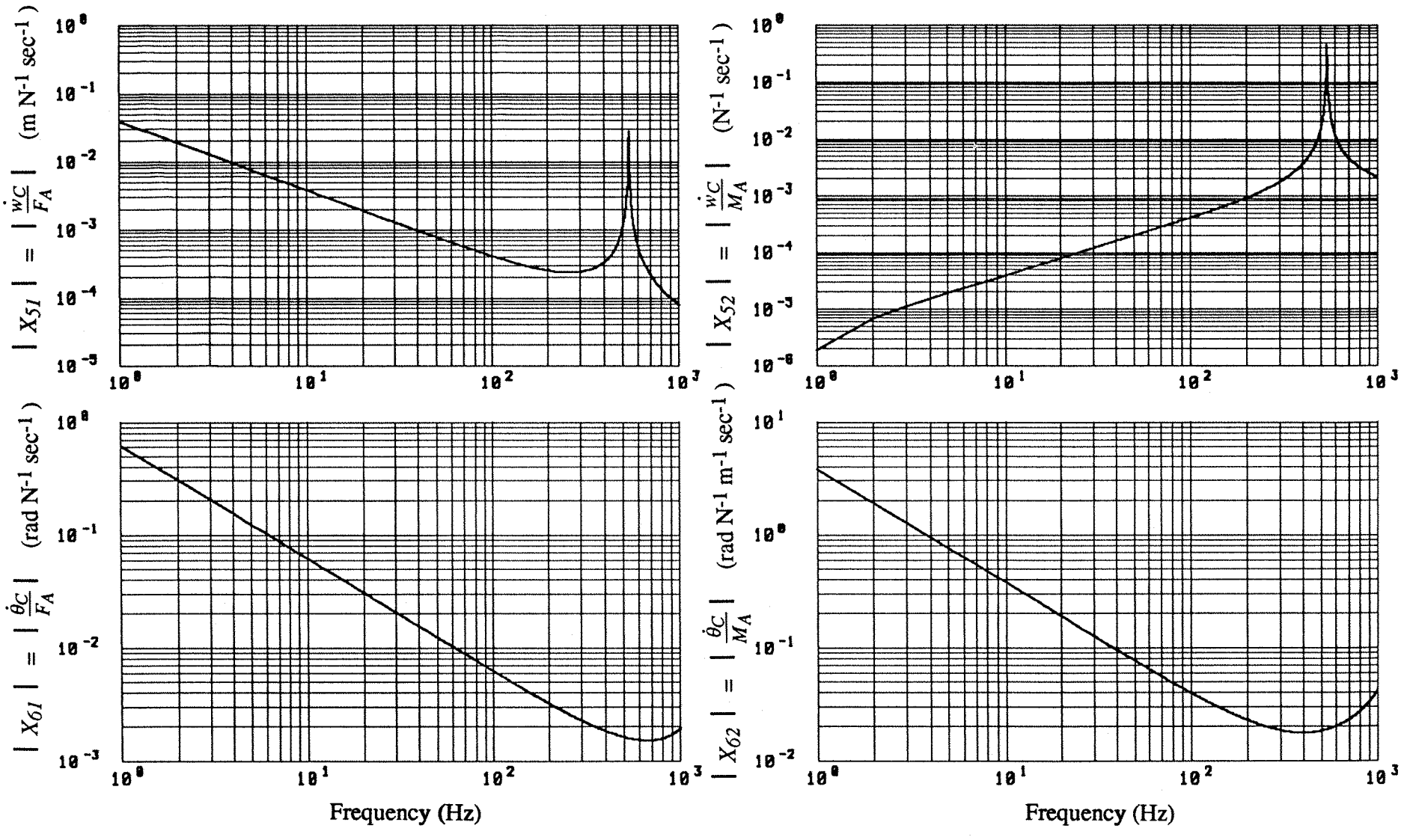

Figure G3 : Modulus spectra of the transfer mobility functions between responses at point C and excitations at point A.

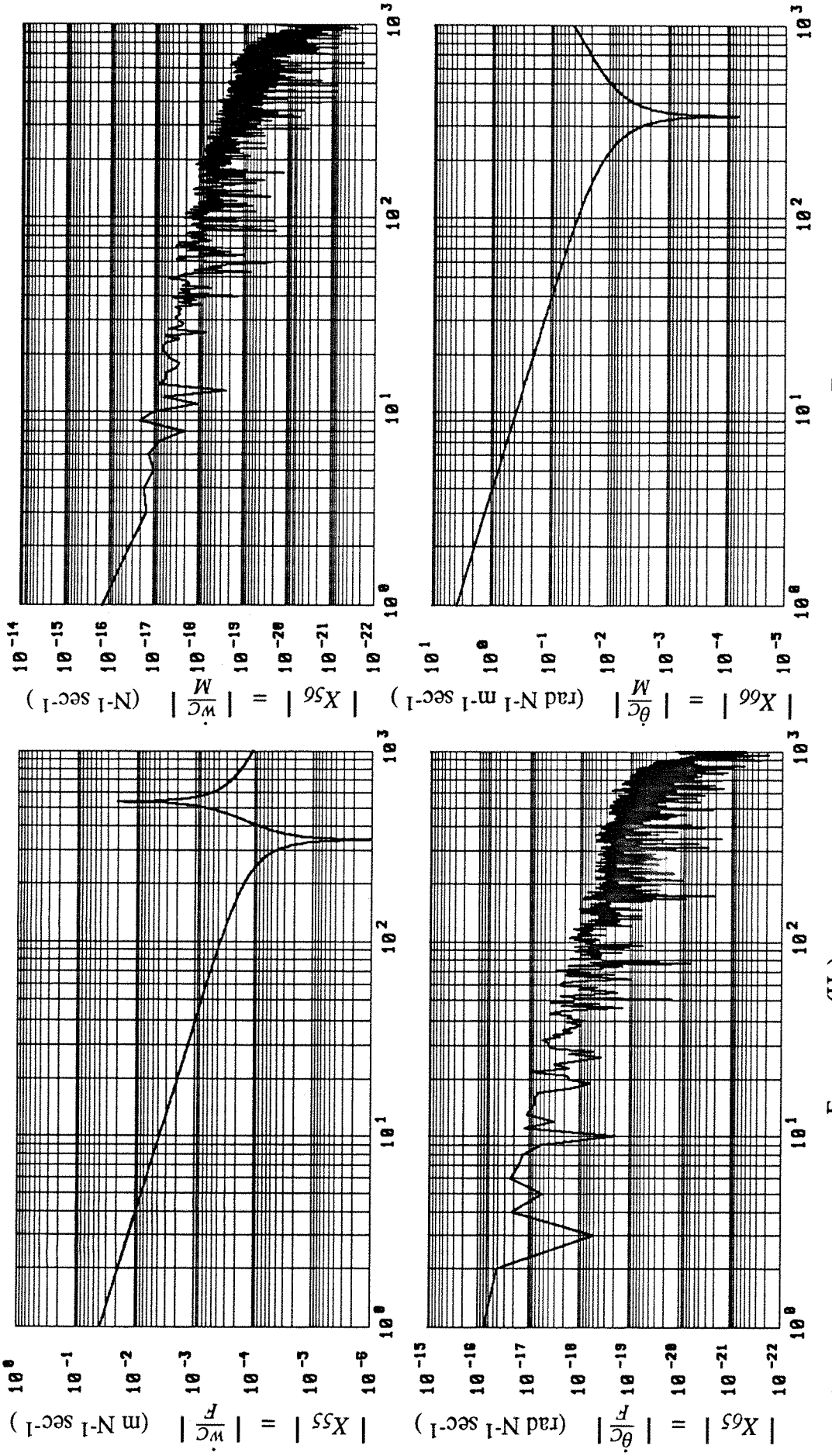

Figure G4 : Modulus spectra of the driving point mobility functions of the free-free beam at excitation point C.

APPENDIX H

DYNAMIC TRANSFER PROPERTIES OF RESILIENT MOUNTS

H.1 EXPRESSIONS FOR DYNAMIC TRANSFER PROPERTIES (FOUR-POLE PARAMETERS)

For a linear mechanical system, as shown in figure H.1, the input terminal of the system vibrates sinusoidally with a velocity, $\dot{v}_1$ in response to an applied force F_1. The output terminal of the system exerts a force F_2 on the input terminal of some further system, sharing with it a common velocity, $\dot{v}_2$. Thus, there is an equal and opposite force F_2 acting on the system at the output terminal.

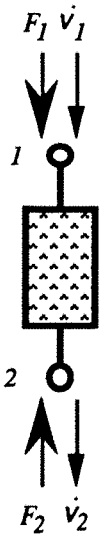

Figure H1 : An arbitrary linear mechanical system.

The dynamic transfer properties relating the forces and velocities at the input and output terminals of the system can be expressed in the following matrix form :

$$\begin{Bmatrix} F_1 \\ \dot{v}_1 \end{Bmatrix} = \begin{bmatrix} \alpha_{11} & \alpha_{12} \\ \alpha_{21} & \alpha_{22} \end{bmatrix} \begin{Bmatrix} F_2 \\ \dot{v}_2 \end{Bmatrix} \qquad \text{(H.1)}$$

where α_{11}, α_{12}, α_{21} and α_{22} are the dynamic transfer properties, which are also known as the four-pole parameters and are defined as follows :

For a blocked output terminal (i.e. no motion at '2') :

$$\alpha_{11} = \left.\frac{F_1}{F_2}\right|_{\dot{v}_2=0} \quad , \quad \alpha_{21} = \left.\frac{\dot{v}_1}{F_2}\right|_{\dot{v}_2=0} \tag{H.2}$$

For a free output terminal (i.e. no reaction at '2') :

$$\alpha_{12} = \left.\frac{F_1}{\dot{v}_2}\right|_{F_2=0} \quad , \quad \alpha_{22} = \left.\frac{\dot{v}_1}{\dot{v}_2}\right|_{F_2=0} \tag{H.3}$$

These parameters, in general, are frequency dependent complex quantities. Two important relations are generally applicable in simplifying the determination of these parameters :

(1) If the system is symmetrical, i.e. it does not matter which terminal is input or output, then

$$\alpha_{11} = \alpha_{22} \tag{H.4}$$

(2) If the system is linear where the Reciprocity principle applies, then

$$\alpha_{11}\,\alpha_{22} - \alpha_{12}\,\alpha_{21} = 1 \tag{H.5}$$

Hence, for a system which satisfies the above two conditions, only two of the four-pole parameters are sufficient to specify the performance of the system completely. The derivation and proof of these relationships can be found in [43].

Expressions for the dynamic transfer properties in the axial direction for a rigid mass, a massless damped spring, a resilient mount subjected to axial sinusoidal vibration can easily be derived (see eqn. (5.27)) and found in the literature [6,42,43]. These expressions are summarised in Table H.1. In the table : M is the rigid mass, K is the spring stiffness, η_m is the loss factor of the spring, ω is the circular frequency in radians per second, $E^c = E(1+j\,\eta_m)$ is the complex Young's modulus, A is the cross-sectional area, L is the length and k_l is the longitudinal wave number of the rod.

Types of Models	Dynamic Transfer Properties			
	α_{11}	α_{12}	α_{21}	α_{22}
Rigid mass	*1.0*	$j\omega M$	*0*	*1.0*
Massless damped spring	*1.0*	*0*	$\frac{j\omega}{K(1+j\eta_m)}$	*1.0*
'Long rod' model	$\cos k_l L$	$\frac{jE^cAk_l}{\omega} \sin k_l L$	$\frac{j\omega}{E^cAk_l} \sin k_l L$	$\cos k_l L$

Table H.1 : Dynamic transfer properties of simple mechanical systems.

H.2 DYNAMIC TRANSFER PROPERTIES OF A RESILIENT MOUNT WITH END PLATES

For a resilient mount bonded to metal end plates of masses M_1 and M_2 as shown in figure H.2, the output terminal of the upper plate is assumed to be rigidly connected to the input terminal of the mount, so that the output from the upper plate is the input to the mount. The same is assumed for the output terminal of the mount and the input terminal of the lower plate. These plates and mount are said to be connected in series.

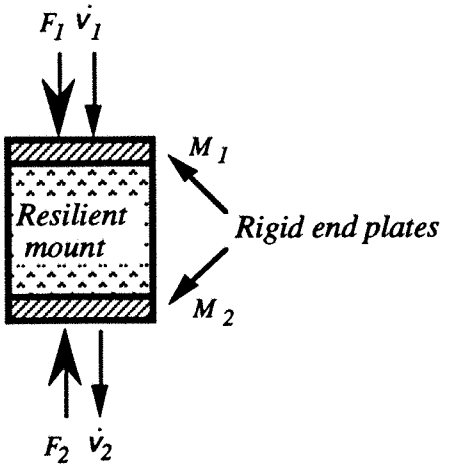

Figure H2 : A resilient mount with rigid end plates.

The dynamic transfer properties of the combined system in axial vibration can be written as :

$$\begin{bmatrix} \beta_{11} & \beta_{12} \\ \beta_{21} & \beta_{22} \end{bmatrix} = \begin{bmatrix} 1.0 & j\omega M_1 \\ 0 & 1.0 \end{bmatrix} \begin{bmatrix} \alpha_{11} & \alpha_{12} \\ \alpha_{21} & \alpha_{22} \end{bmatrix} \begin{bmatrix} 1.0 & j\omega M_2 \\ 0 & 1.0 \end{bmatrix} \quad \text{(H.6)}$$

in which

$$\beta_{11} = \alpha_{11} + j\omega M_1 \alpha_{21}$$

$$\beta_{12} = \alpha_{12} - \omega^2 M_1 M_2 \alpha_{21} + j\omega [M_2 \alpha_{11} + M_1 \alpha_{22}]$$

$$\beta_{21} = \alpha_{21}$$

$$\beta_{22} = \alpha_{22} + j\omega M_2 \alpha_{21}$$

where α_{11}, α_{12}, α_{21} and α_{22} are the dynamic transfer propreties of the mount alone. It is interesting to note that the dynamic transfer property, β_{21} : the transfer mobility between the velocity response at the input terminal and the blocked force at the output terminal of the combined system is the same as that of the resilient mount alone, i.e. it is not affected by the presence of the end plates. This property will be used in the determination of the dynamic stiffness and loss factor of the resilient mounts.

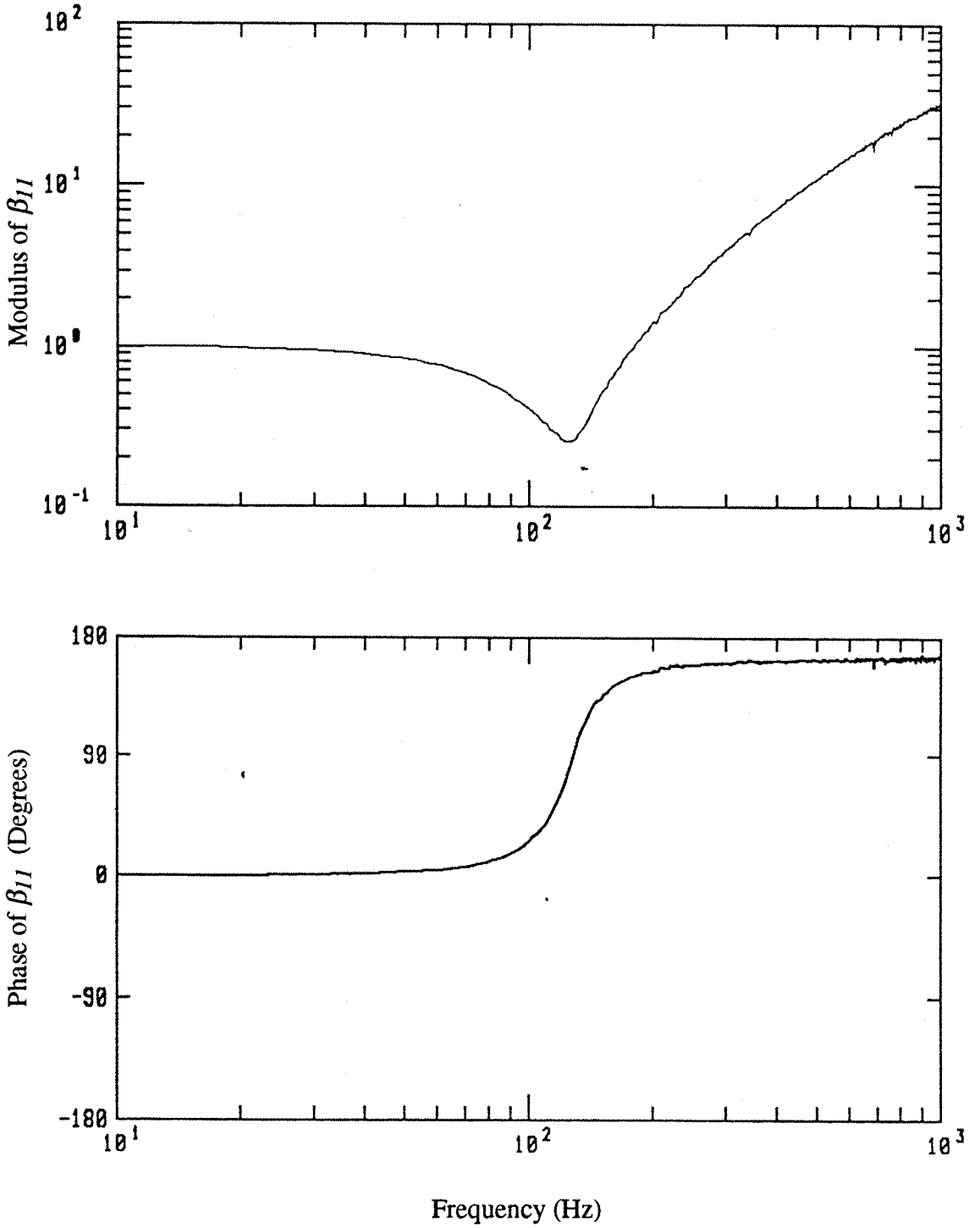

Figure H3: Modulus and phase of the measured β_{11} transfer function.

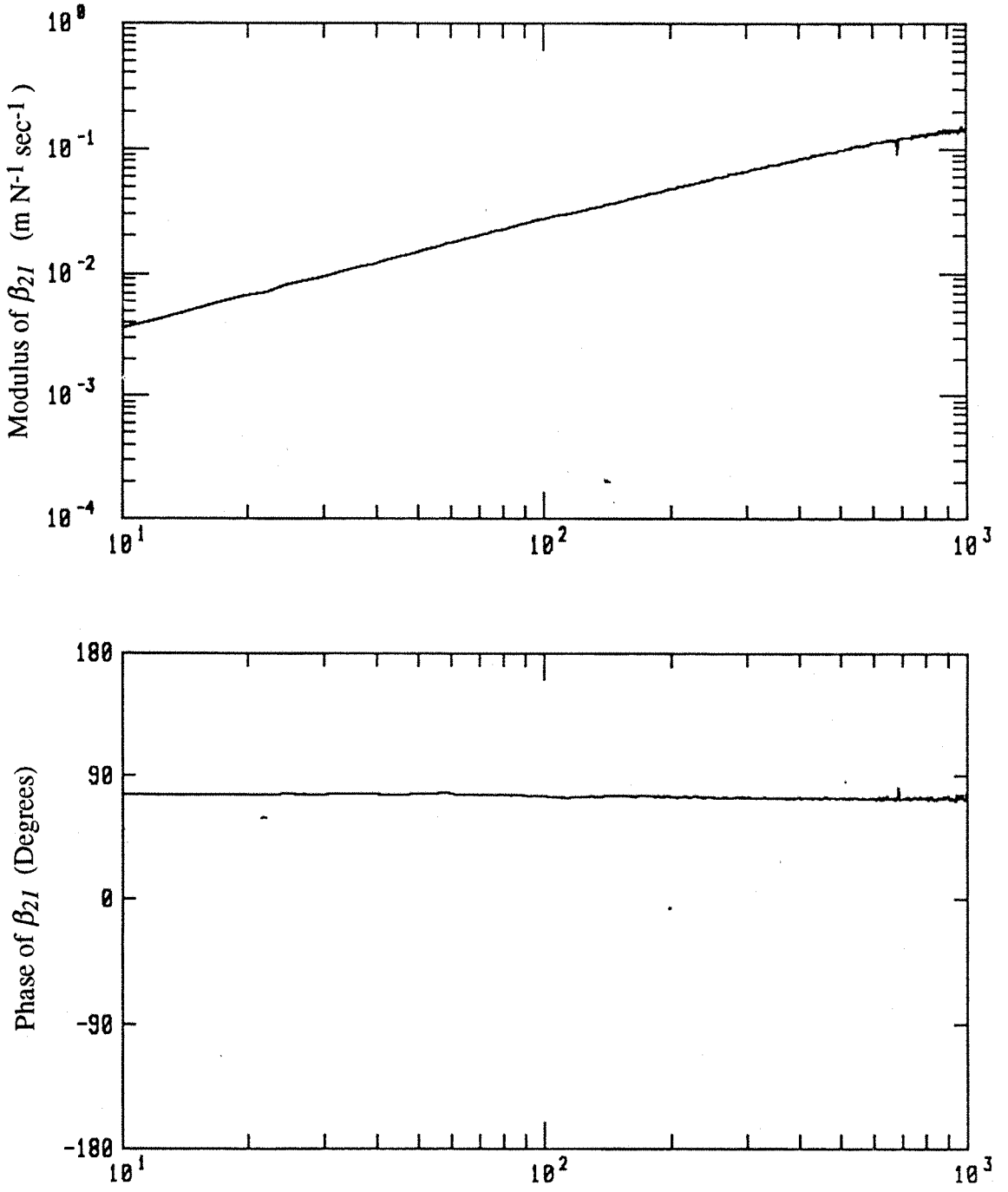

Figure H4 : Modulus and phase of the measured β_{21} transfer function.

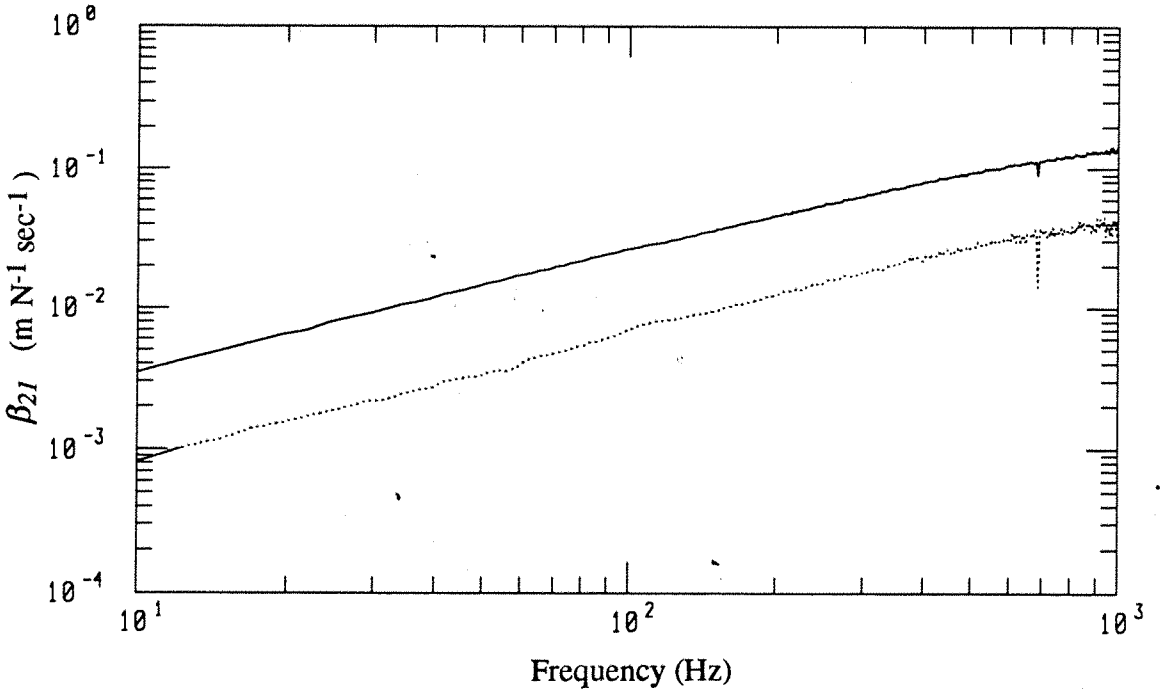

Figure H5 : Real (·····) and imaginary (———) parts of the measured β_{21} transfer function.

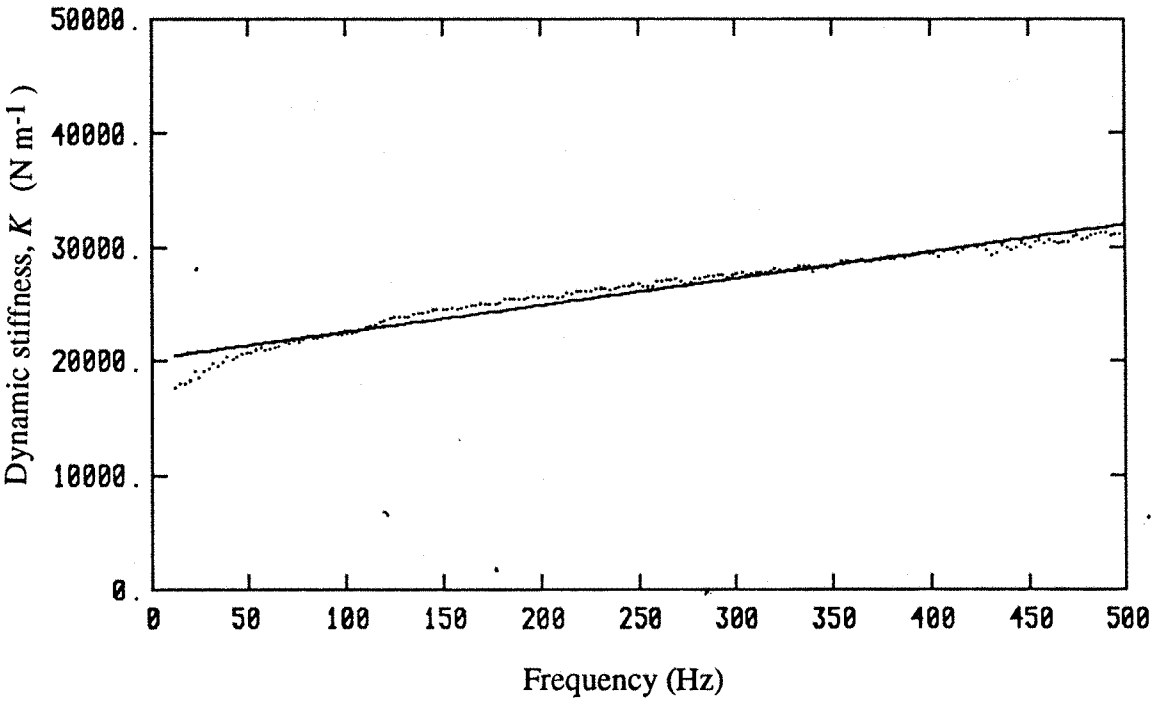

Figure H6: Spectrum of the measured dynamic stiffness and the Least Squares fit line,

$K = 20090.0 + 23.72 f$

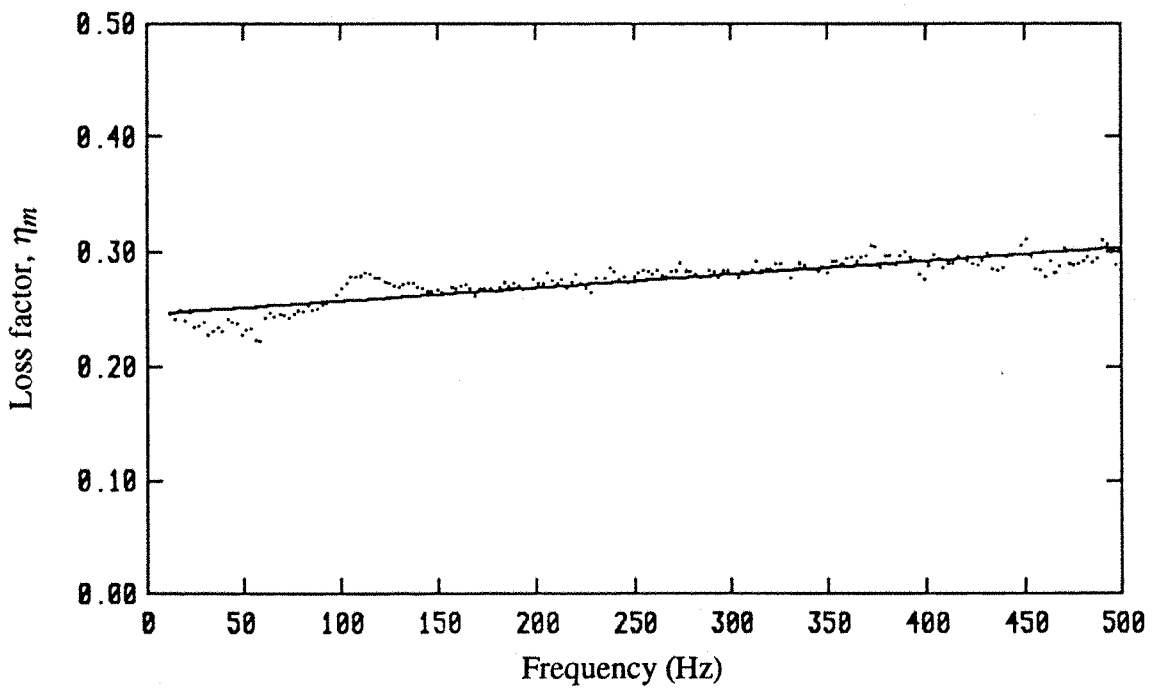

Figure H7 : Spectrum of the measured loss factor and the Least Squares fit line,

$\eta_m = 0.2447 + 0.0001173 f$

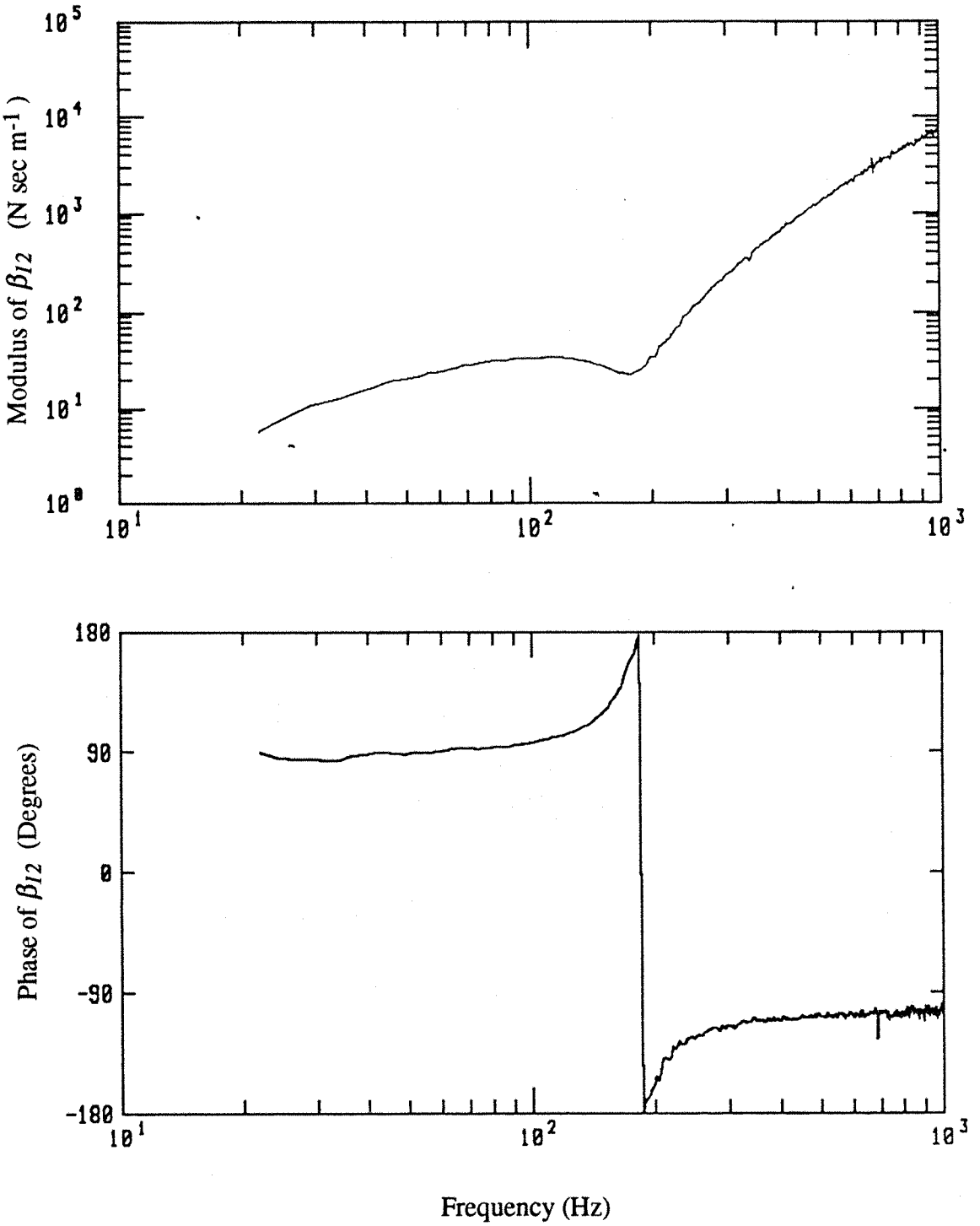

Figure H8 : Modulus and phase of the derived β_{12} transfer function.

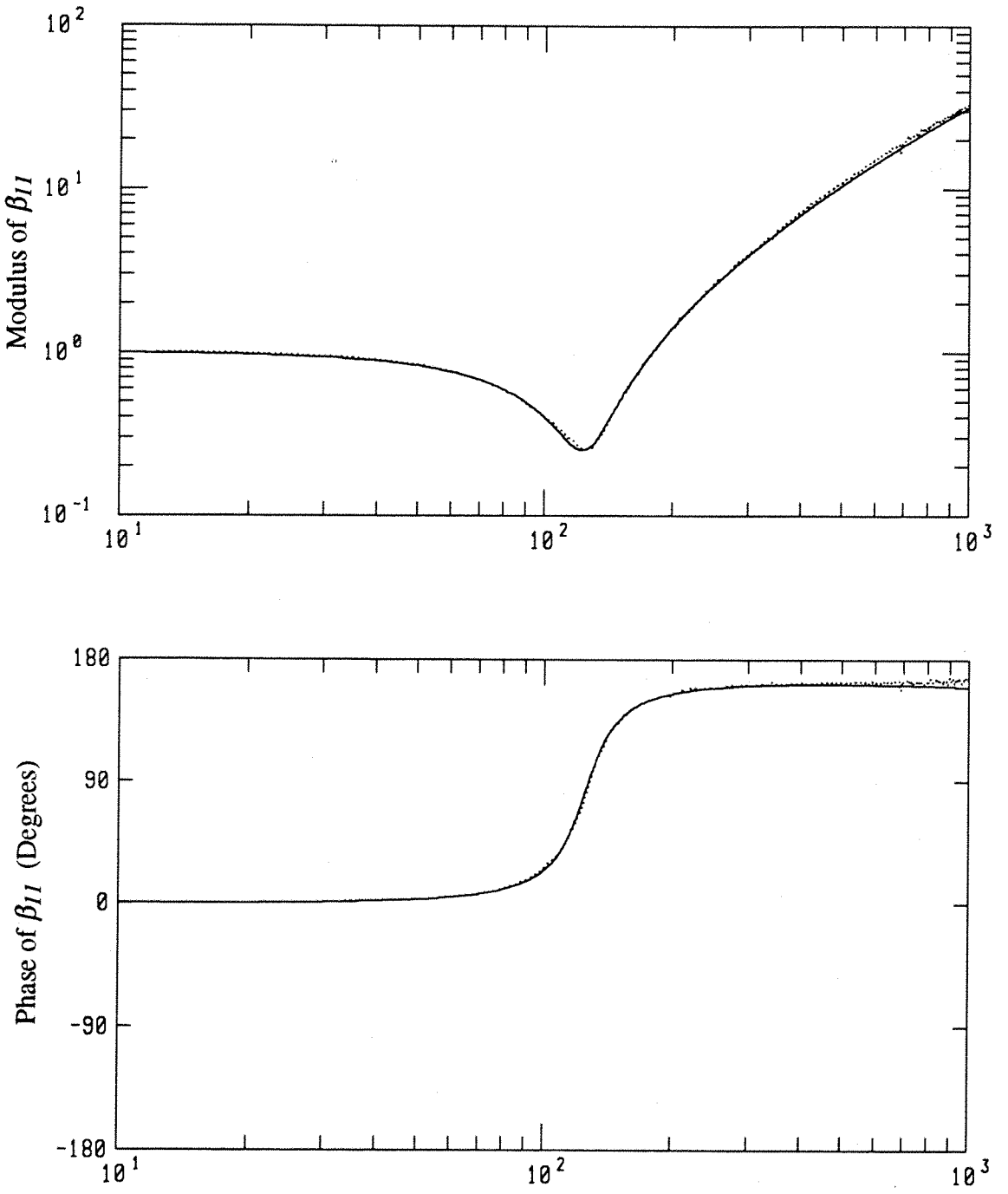

Figure H9: Comparison of the measured (·····) and predicted (———)β_{11} transfer function using the massless spring model.

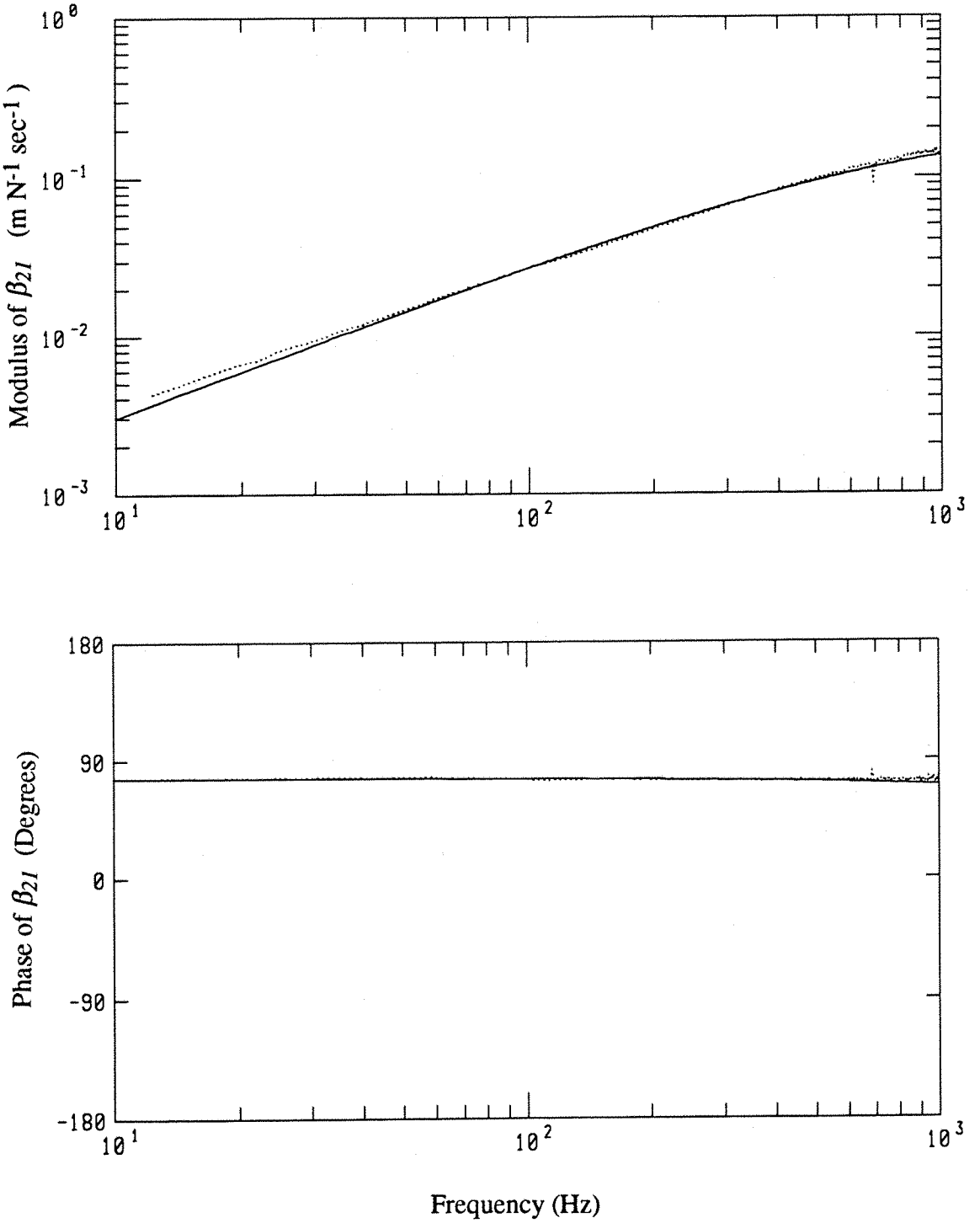

Figure H10 : Comparison of the measured (·····) and predicted (———)β_{21} transfer function using the massless spring model.

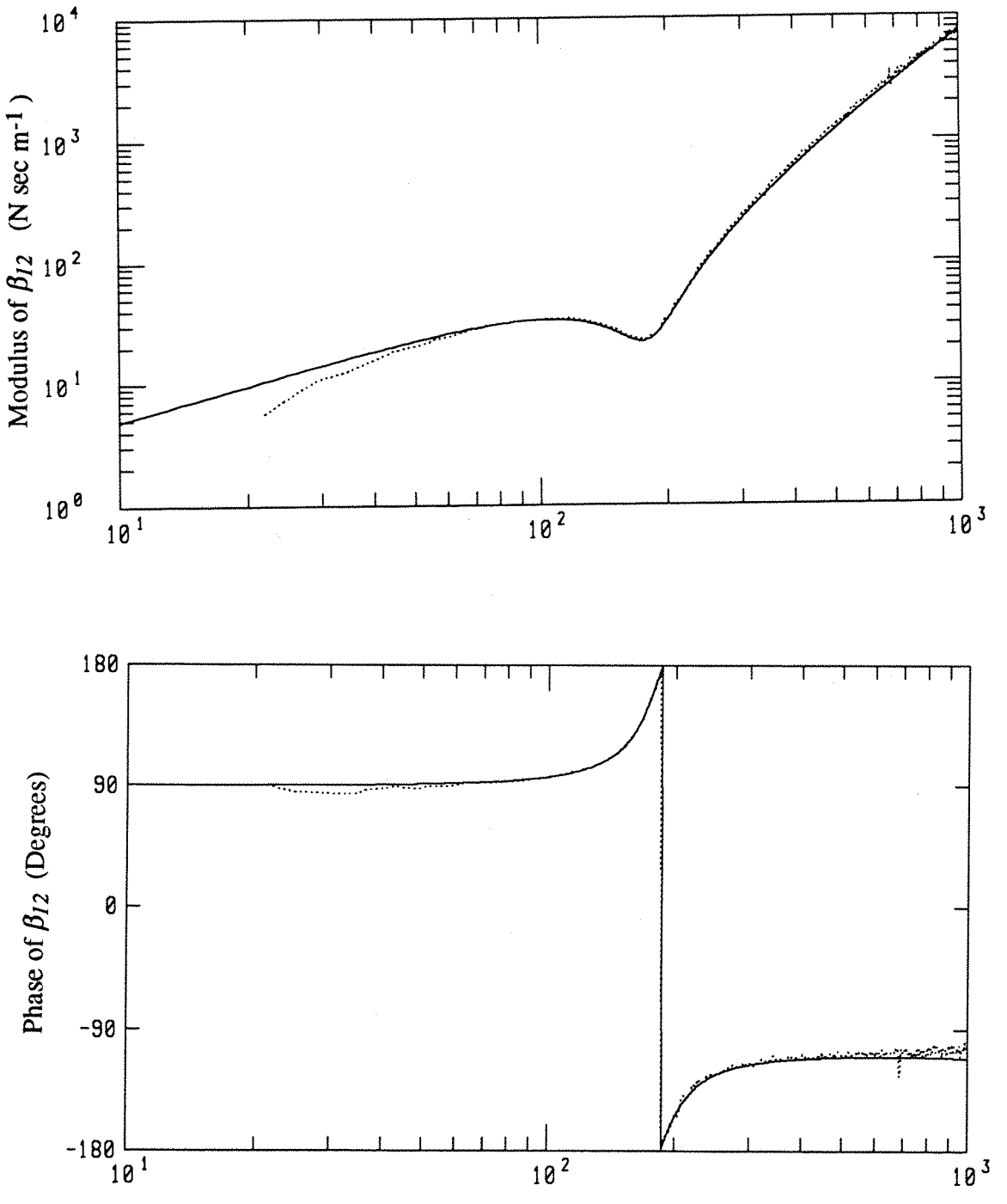

Figure H11: Comparison of the measured (·····) and predicted (———)β_{12} transfer function using the massless spring model.

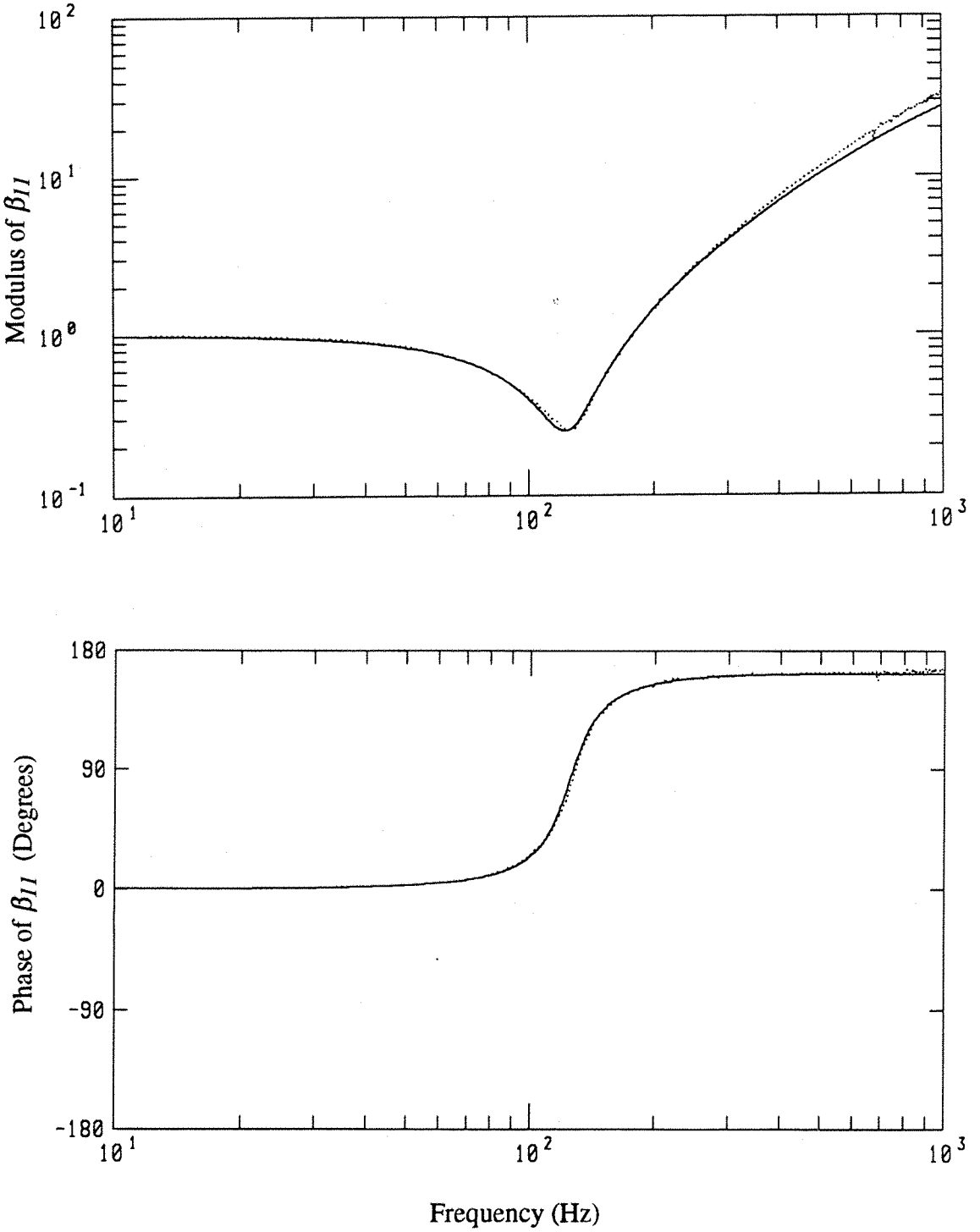

Figure H12 : Comparison of the measured (·····) and predicted (———)β_{11} transfer function using the 'Long rod' model.

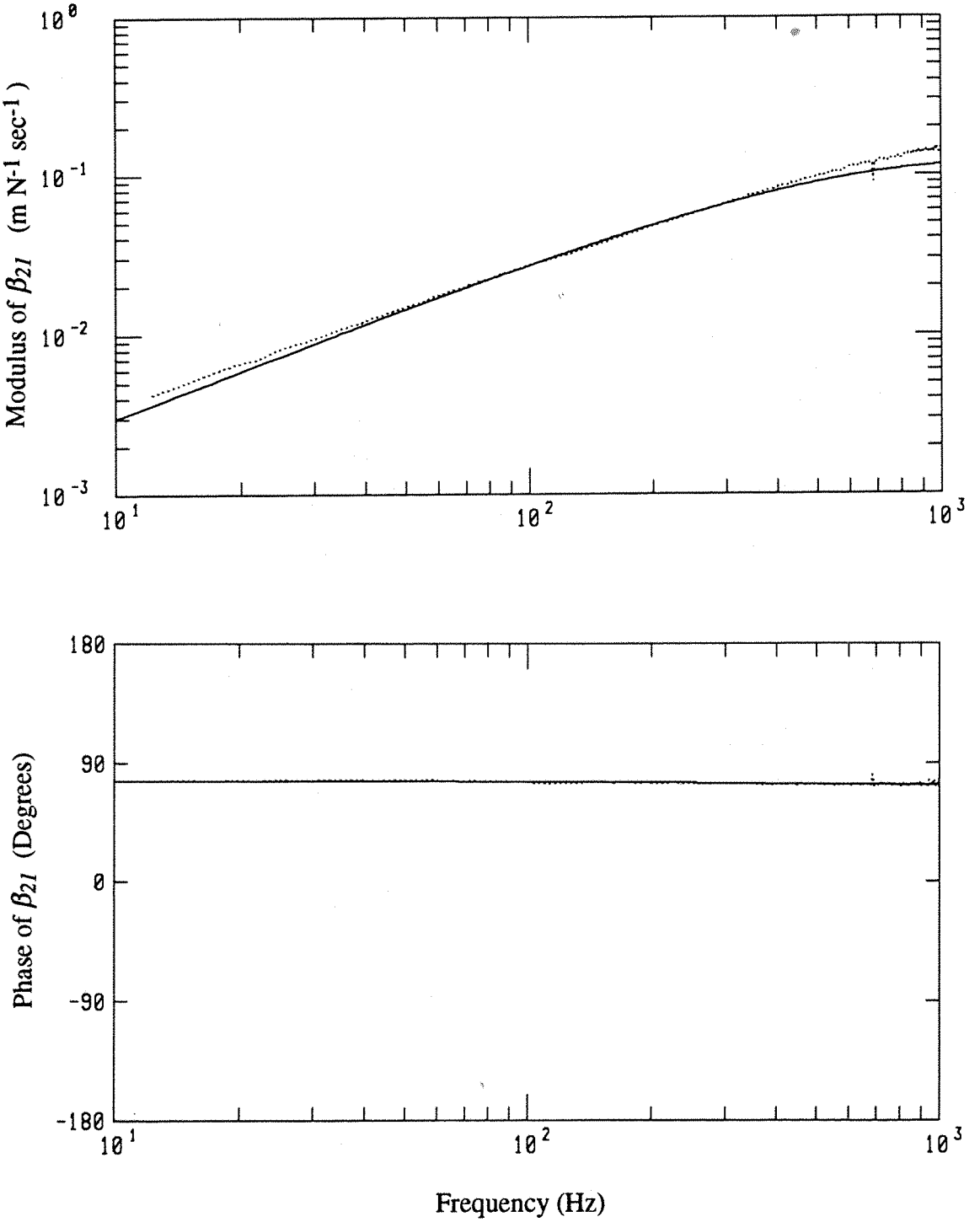

Figure H13 : Comparison of the measured (·····) and predicted (———)β_{21} transfer function using the 'Long rod' model.

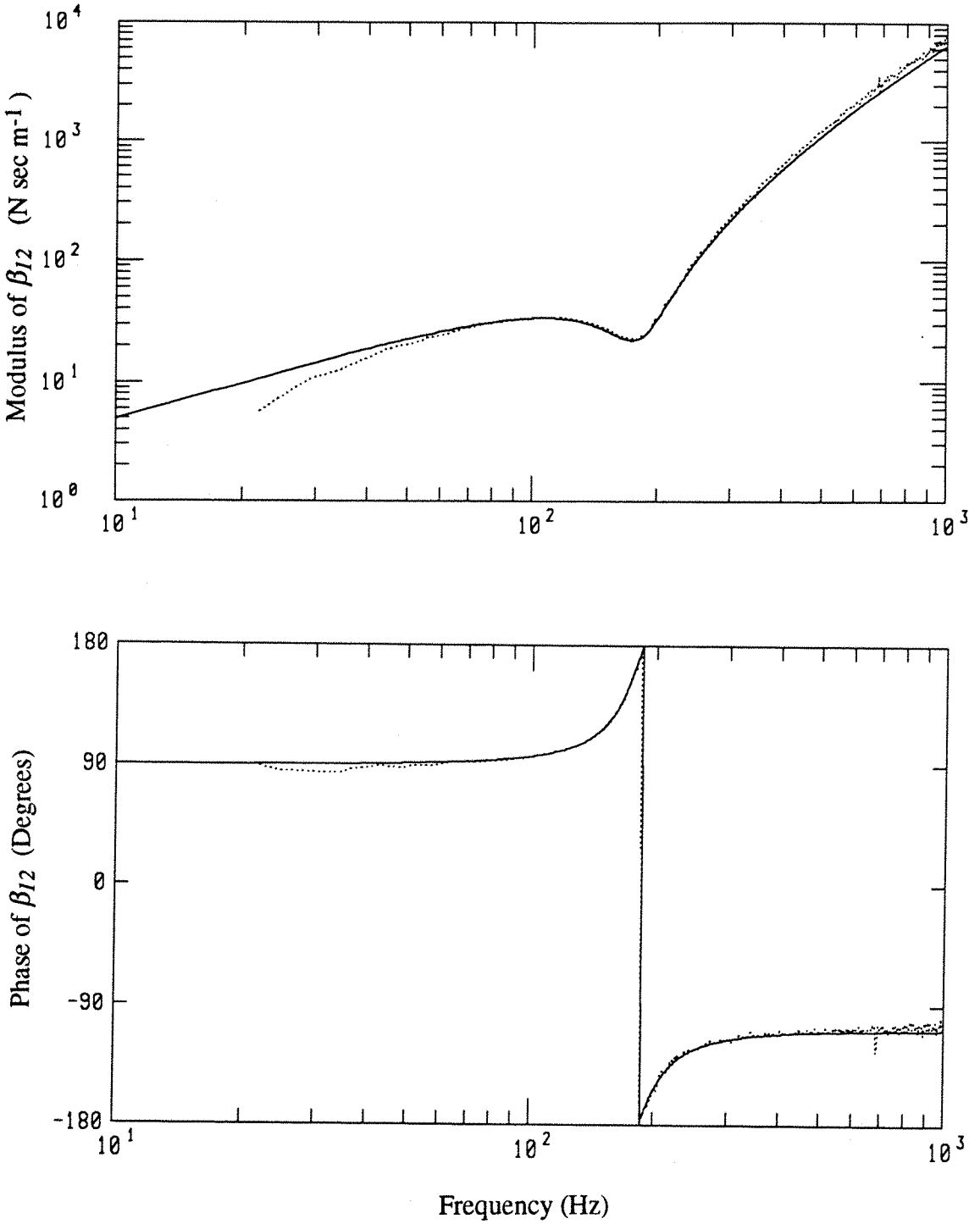

Figure H14: Comparison of the measured (·····) and predicted (———)β_{12} transfer function using the 'Long rod' model.

APPENDIX I

POINT, COUPLING AND TRANSFER MOBILITY FUNCTIONS OF A CFSF PLATE

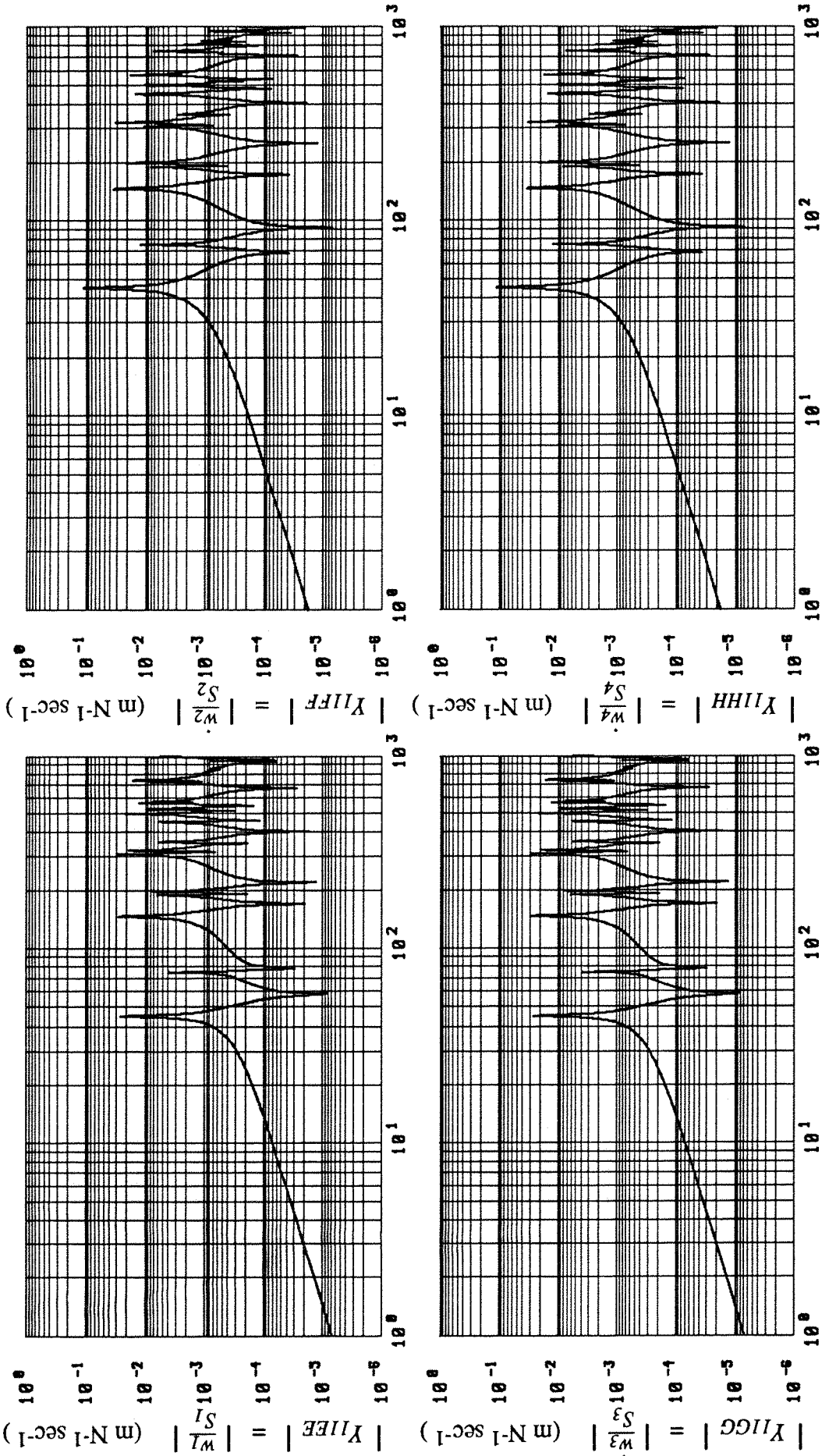

Figure I1 : Modulus Spectra of the driving point force mobility functions, Y_{11} at the four mounting points.

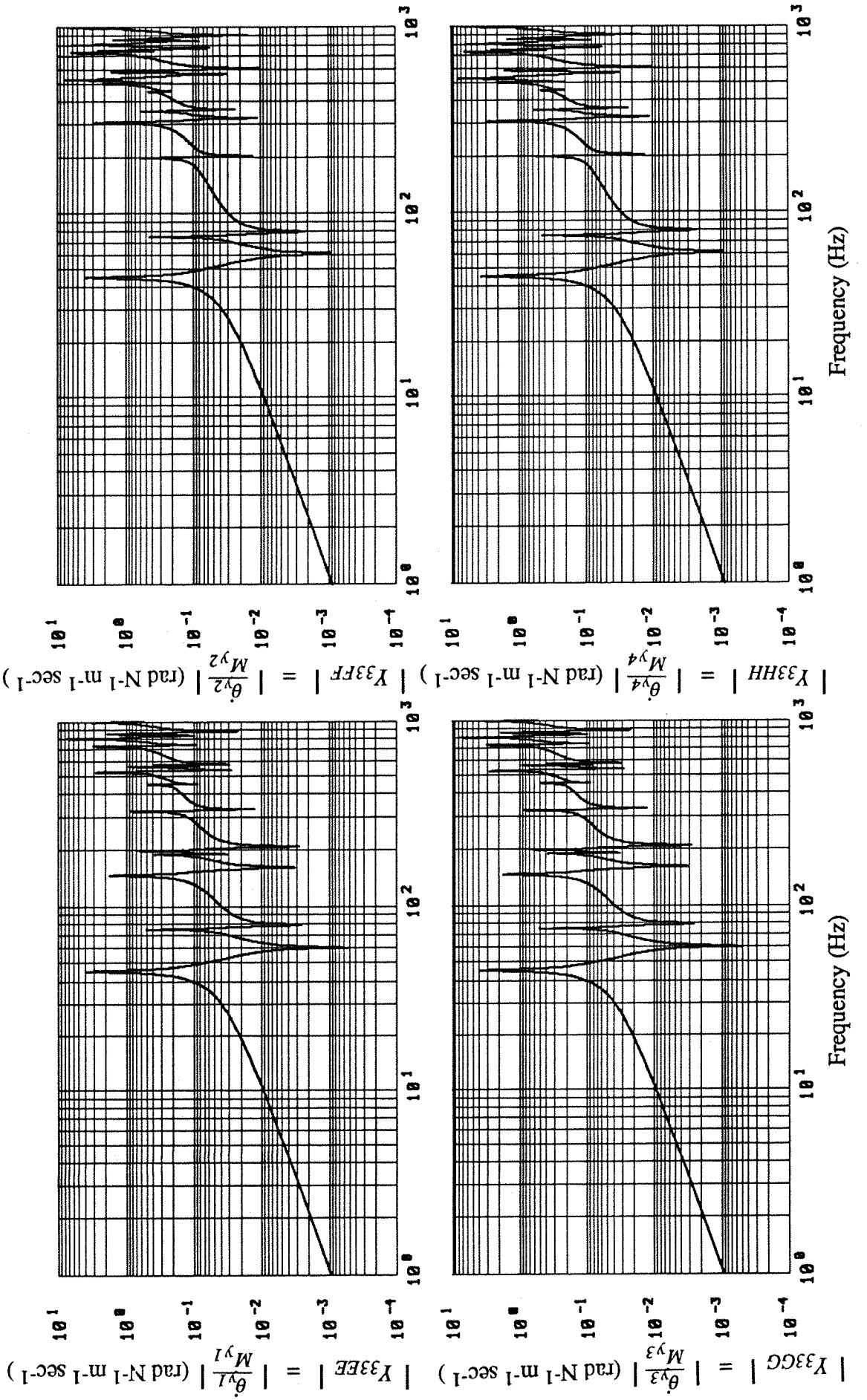

Figure I2 : Modulus Spectra of the driving point moment mobility functions, Y_{33} at the four mounting points.

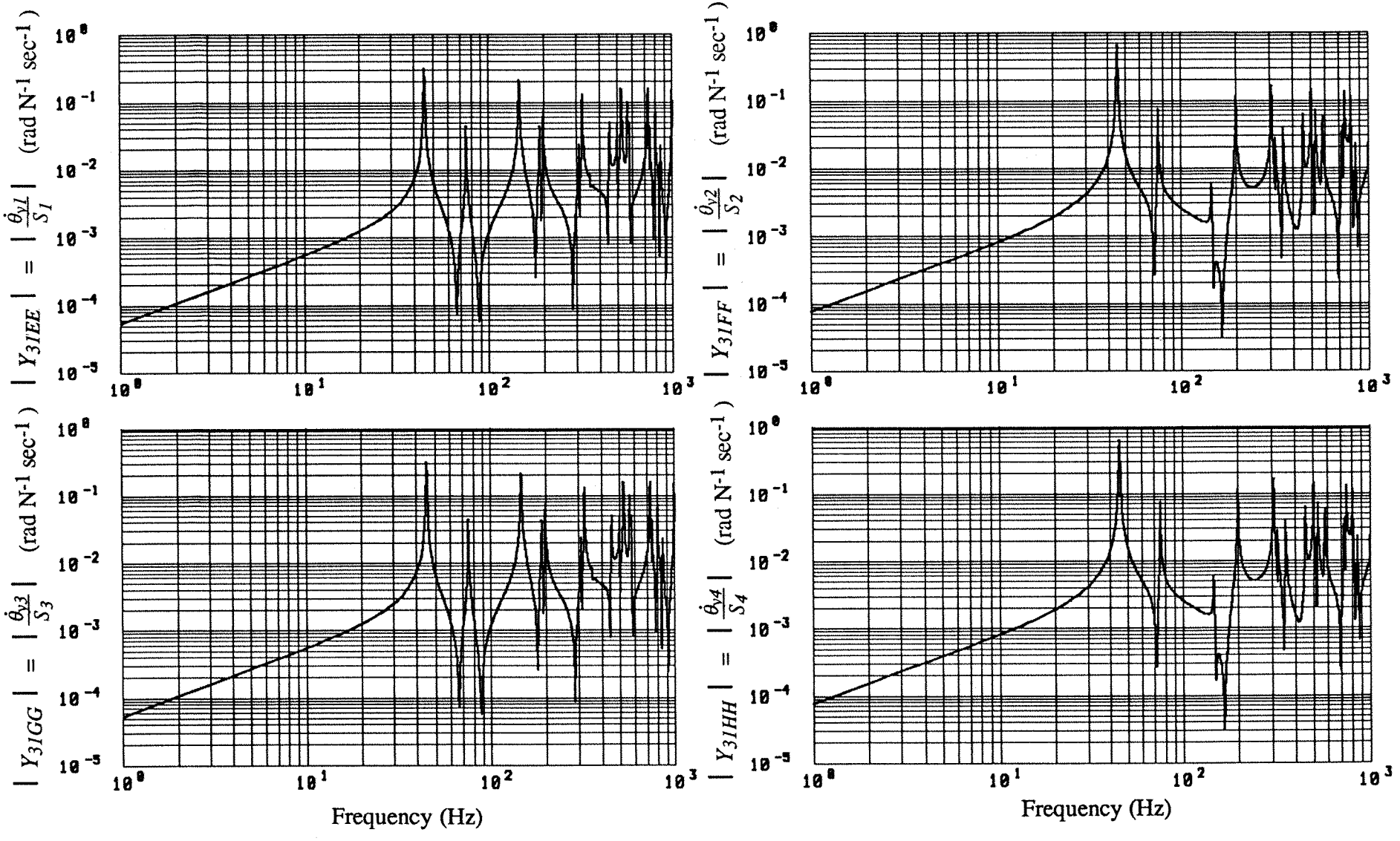

Figure I3 : Modulus Spectra of the driving point coupling mobility functions, Y_{31} at the four mounting points.

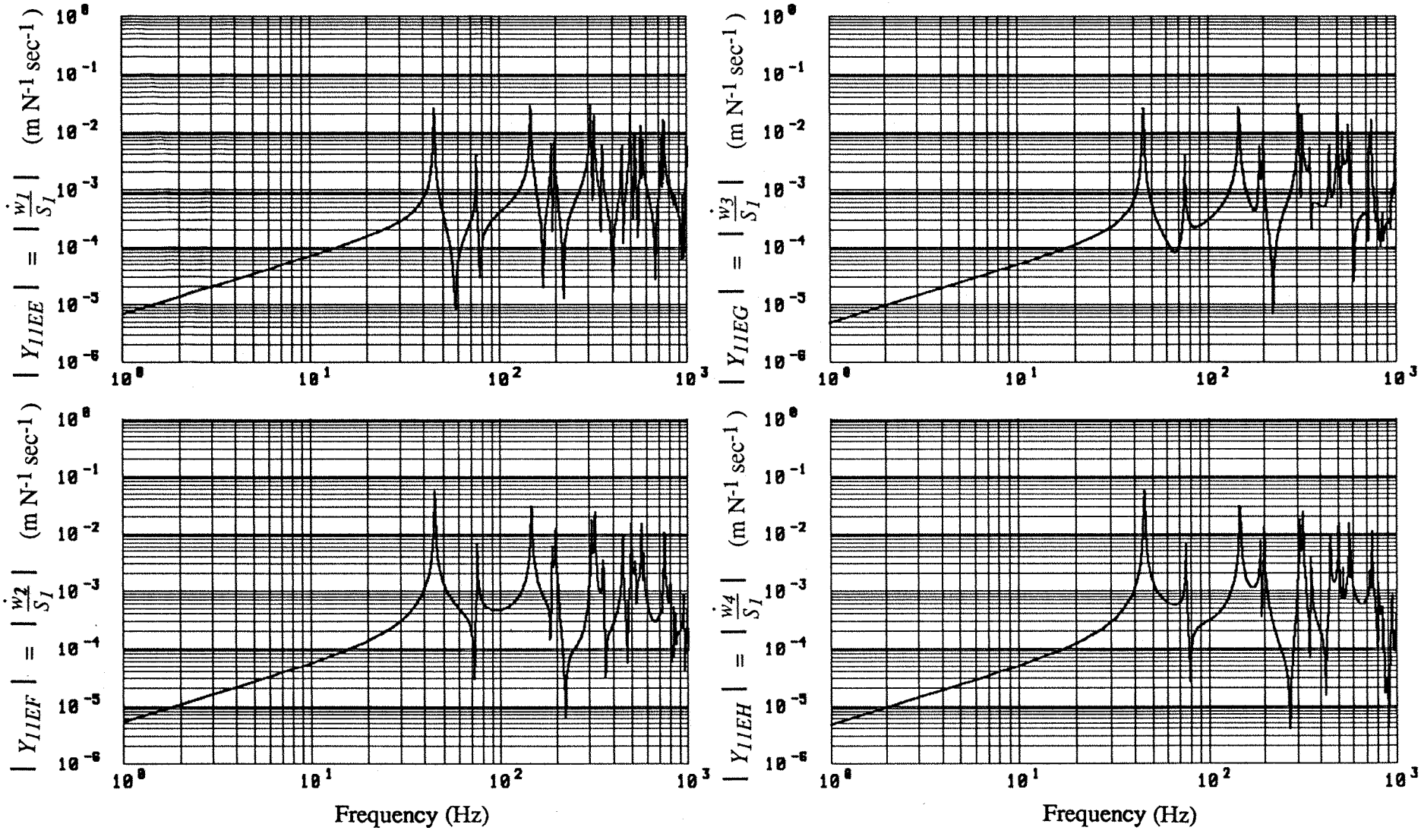

Figure I4 : Modulus Spectra of the point and transfer force mobility functions, Y_{11} at the four mounting points with the force excitation at point E.

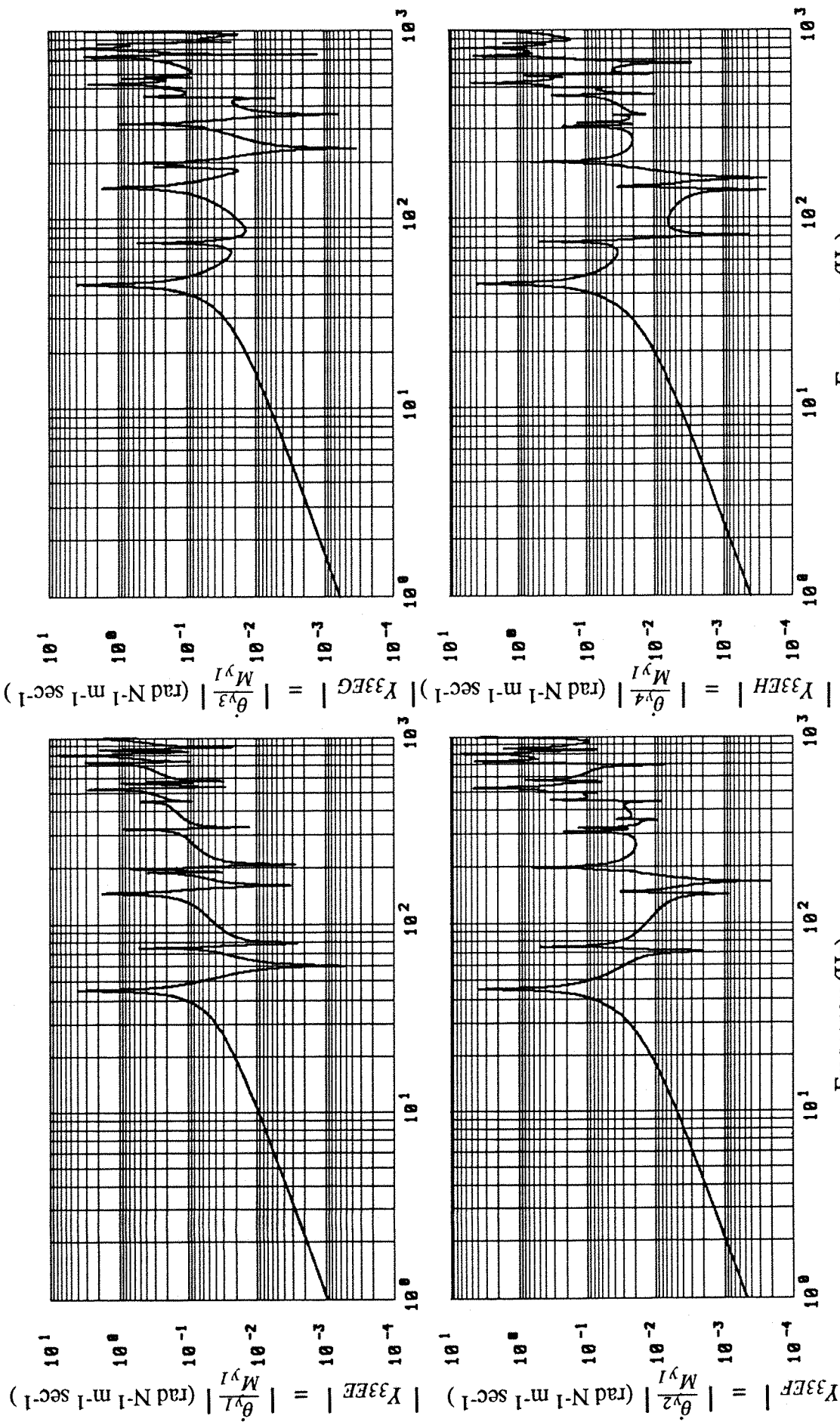

Figure I5 : Modulus Spectra of the point and transfer moment mobility functions, Y_{33} at the four mounting points with the moment excitation at point E.

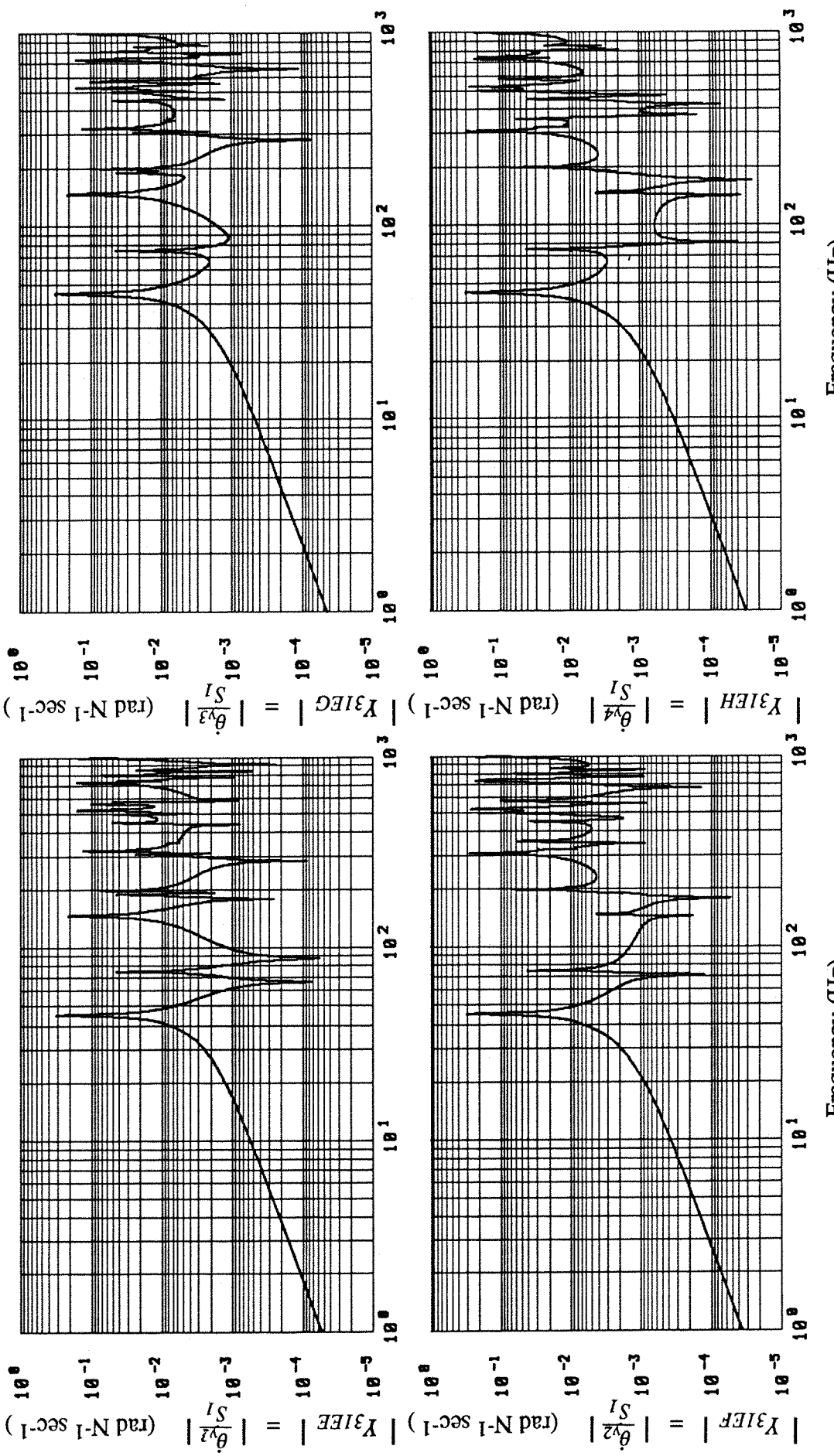

Figure I6 : Modulus Spectra of the point and transfer coupling mobility functions, Y_{31} at the four mounting points with the force excitation at point E.

APPENDIX J

PHOTOGRAPHS OF VARIOUS EXPERIMENTAL ARRANGEMENTS

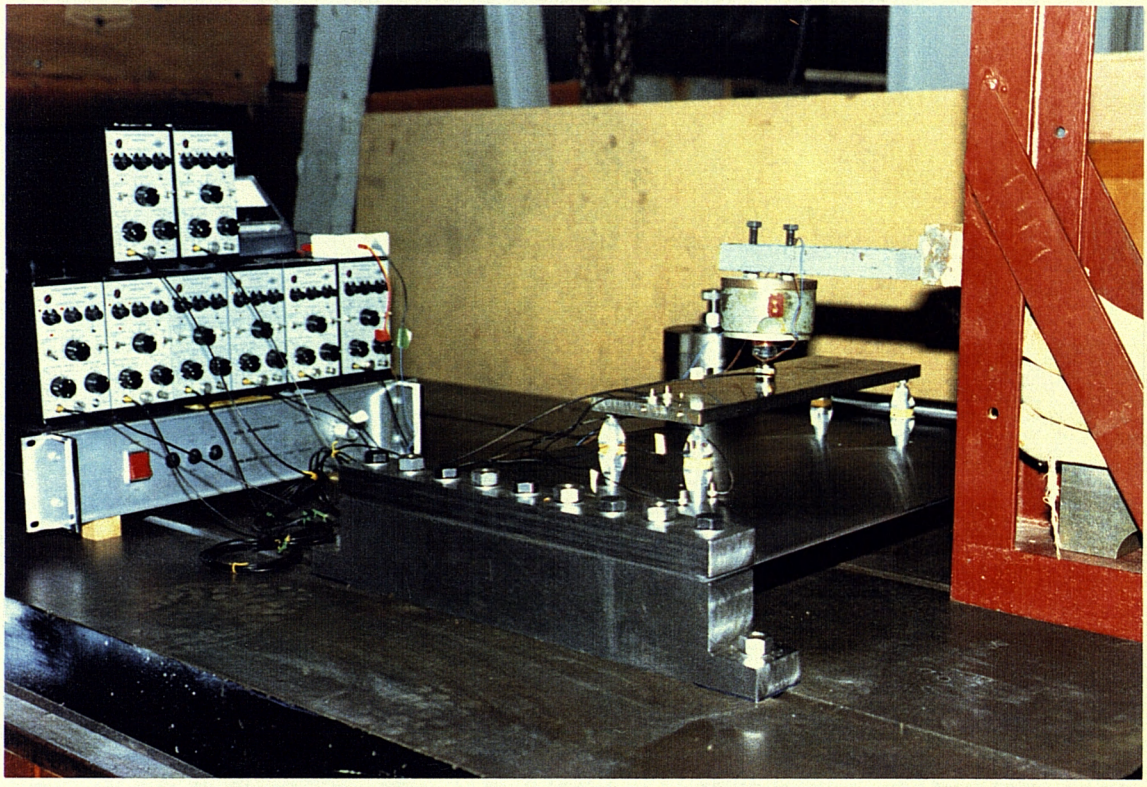

Figure J1 : Experimental arrangement for measuring the velocity responses and vibrational power transmission between a coupled source beam - resilient isolator - receiver plate system.

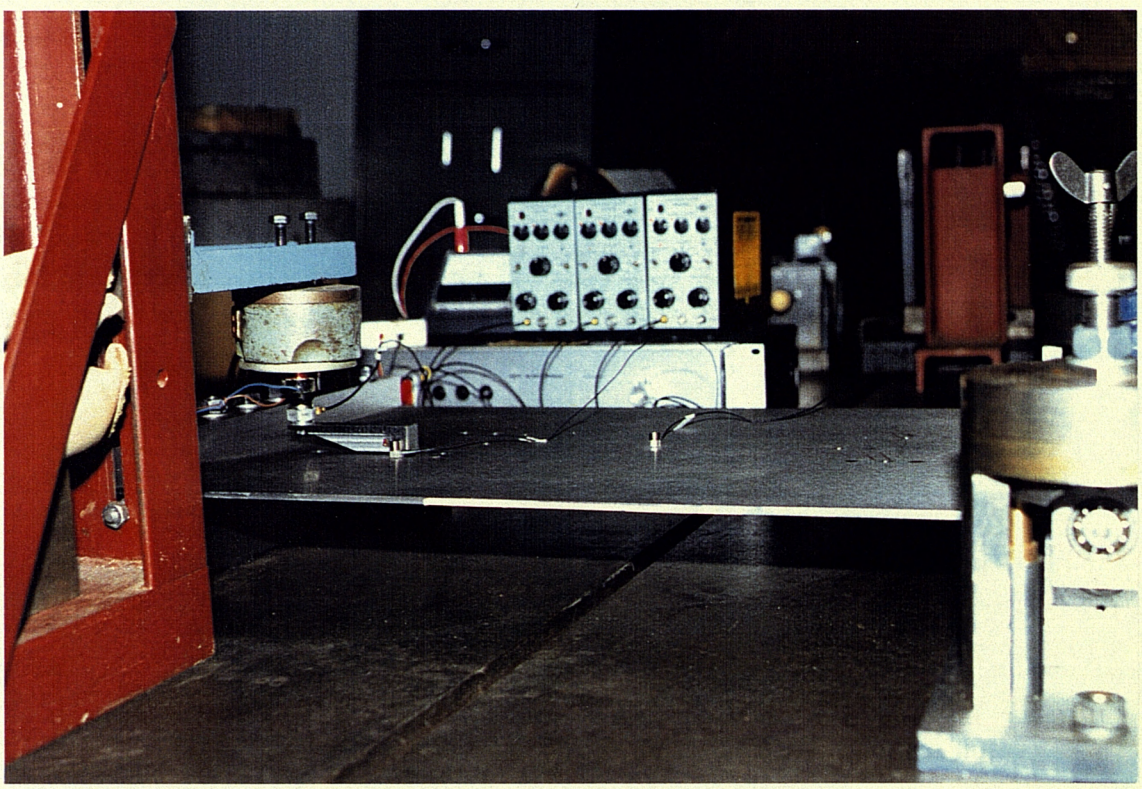

(a)

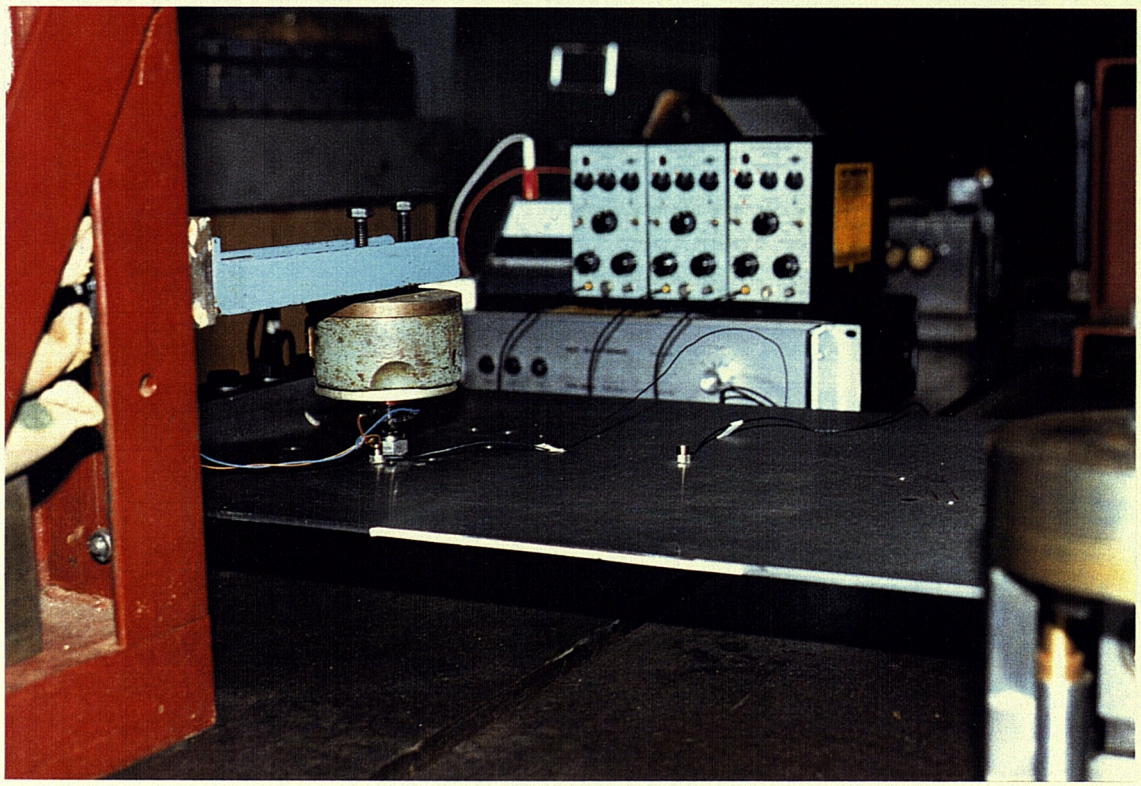

(b)

Figure J2 : Experimental arrangements for measuring the velocity responses of the CFSF plate : (a) with a force and moment seating having a moment arm of -80mm, (b) no moment arm.

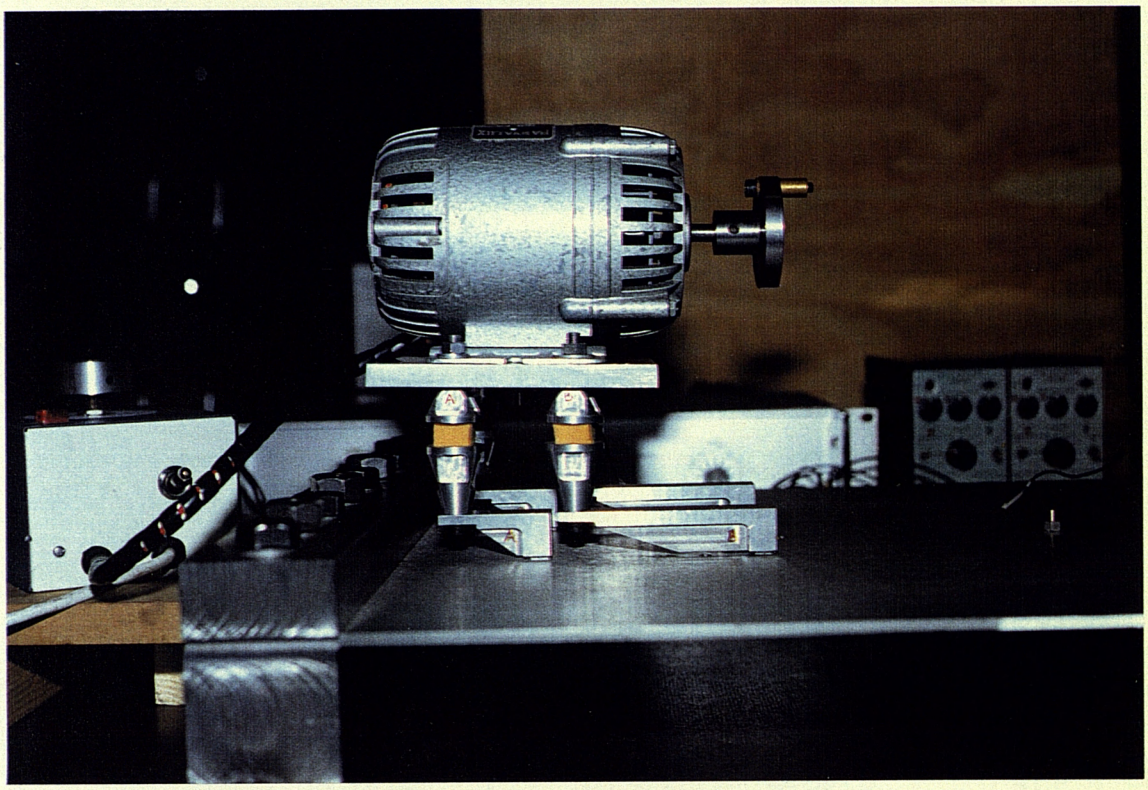

(a)

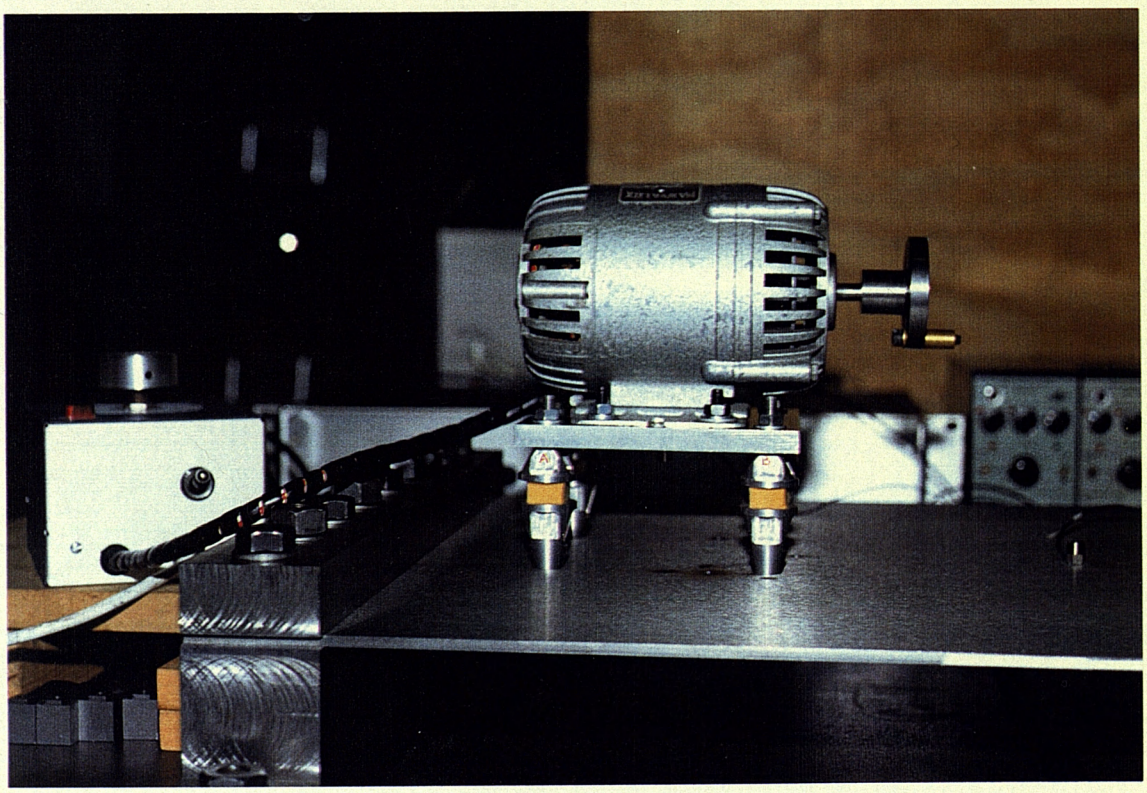

(b)

Figure J3 : Experimental arrangements for the unbalanced motor experiment : (a) with a set of force and moment seatings, (b) without the force and moment seating.

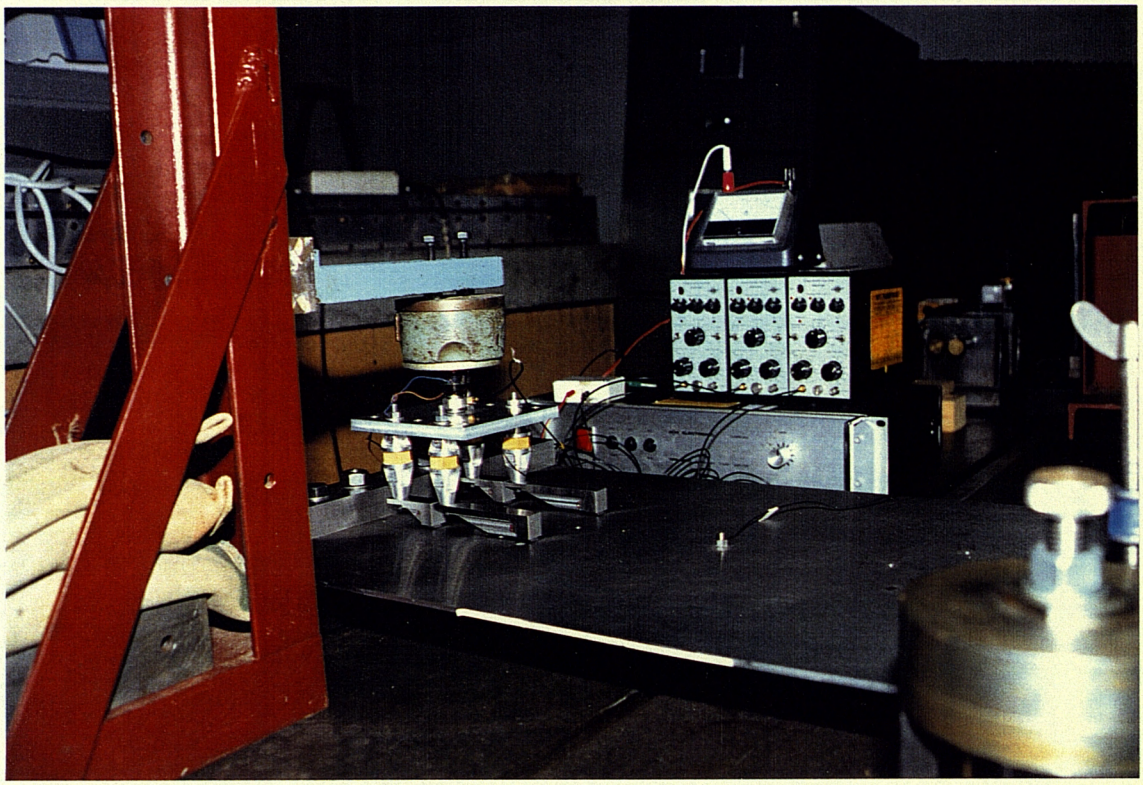

(a)

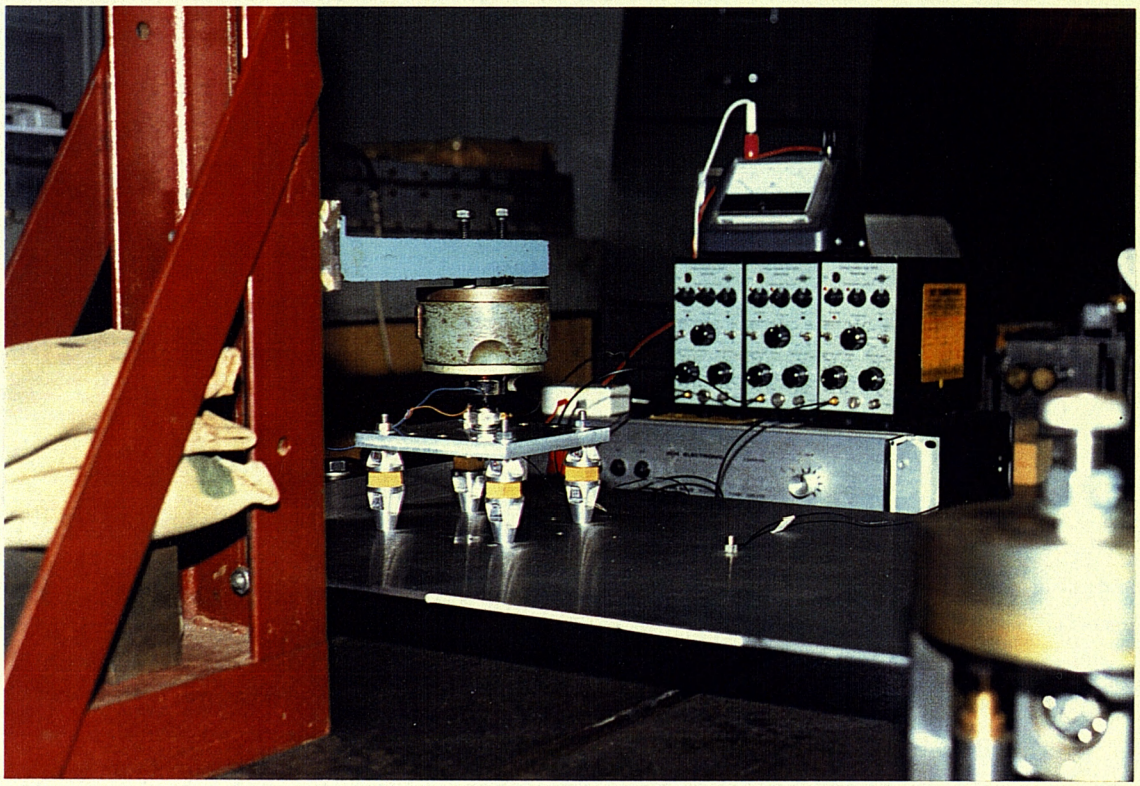

(b)

Figure J4 : Experimental arrangements for the random force experiment : (a) with a set of force and moment seatings, (b) without the force and moment seating.

APPENDIX K

DRAWING OF THE FORCE AND MOMENT SEATING

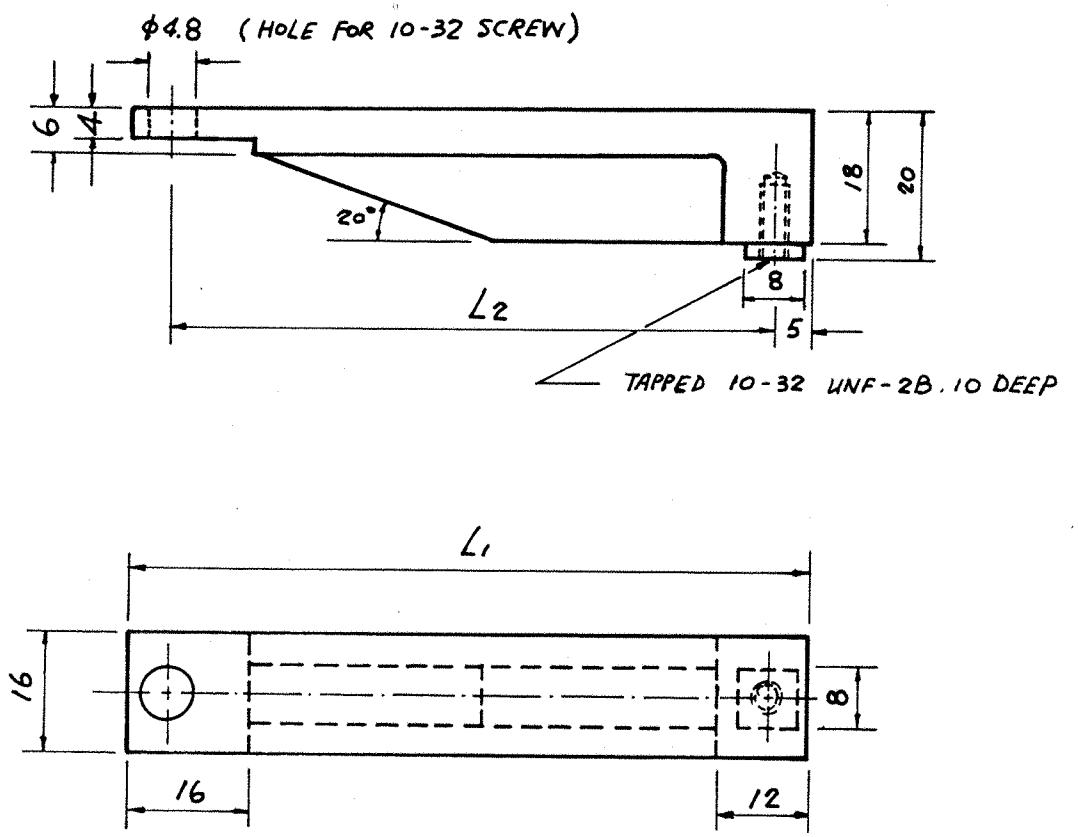

DIMENSIONS		QTY.
L_1	L_2	
92	80	2
47	35	2

MATERIAL : STEEL

ALL DIMENSIONS IN MM.

Figure K1 : Drawing of the force and moment seating.